# Investigations into Antibody Conjugation by Cysteine-to-Lysine Transfer

Muhammed Haque

A thesis submitted in partial fulfilment of the requirements for the degree of Doctor of Philosophy

Supervisor: Prof. James R. Baker

March 2023

# Declaration

I, Muhammed Haque, confirm that the work presented in this thesis is my own. Where information has been derived from other sources, I can confirm that this has been indicated in the thesis.

Muhammed Haque
March 2023

# Abstract

Protein modification is a powerful and important tool for the generation of bioconjugates of immense diagnostic and therapeutic utility. Strategies towards achieving efficient, selective, and accessible bioconjugation are widely studied and sought after, particularly for the development of antibody-drug conjugates (ADCs). However, existing approaches towards synthesising ADCs on native antibodies suffer from numerous limitations, resulting in heterogeneous mixtures of unpredictable tolerability, pharmacokinetics, and efficacy. Whilst engineering antibodies can overcome some of these limitations, these technologies are expensive, time-consuming, and complex.

The cysteine-to-lysine transfer (CLT) approach enables an accessible way of synthesising homogeneous ADCs, modified site-selectively at lysine residues to generate stable amide products. This strategy utilises cysteine residues as initial ligating hooks before an acyl transfer enables modification of proximal lysine residues. Whilst CLT enables site-selective lysine conjugation on off-the-shelf antibodies utilising easily accessible alkyl thioesters, currently, it is a time-consuming process, and competing hydrolysis inhibits quantitative product formation.

This work concerns the development of the next generation of CLT reagents. To enable CLT to become a more widely accessible strategy, chemical synthesis is conducted to develop several novel reagents with unique reactivity. Electron-deficient thioesters were developed to improve thioester reactivity, and these represent the fastest currently available reagents for CLT. Of particular interest is a tetrazine thioester that demonstrates rapid reactivity and click chemistry on *N*-terminal cysteine, with complete modification observed within minutes. Additionally, a plethora of carbonyl-related functional groups were investigated for their potential as Fab and protein modification reagents. These studies represent the first attempt of the exploration of many of these functional groups for stable and controlled antibody modification, and some particularly promising and useful chemistry is demonstrated. Finally, early works into the expansion of thioesters is discussed, involving dual-reactive thioester reagents that offer two sites of protein reactivity.

# Impact Statement

The development of bioconjugation methods have enabled extensive progress in the development of bioconjugates utilised for diagnostic and therapeutic purposes, such as antibody-drug conjugates (ADCs). ADCs combine two biologically relevant moieties – a monoclonal antibody and a payload. Monoclonal antibodies have shown significant success as cancer therapies due to their exquisite selectivity for diseased cells, resulting from their highly specific antigen-binding sites. However, their large sizes have limited tumour penetration. Extremely potent cytotoxins are excellent at killing cells, but they lack selectivity for diseased cells. Thus, ADCs combine the specificity of antibodies with the cell-killing ability of potent payloads. As a result, ADCs have become effective anti-cancer treatments, with eight approved in the last six years.

However, current technologies used to synthesise ADCs limit their efficacy. Earlier generations of ADCs modified lysine residues, but the large number of accessible lysine residues resulted in heterogeneity, causing poor tolerability, unpredictable pharmacokinetics, and increased costs. Recent strategies have focused on modification of cysteine residues to achieve greater homogeneity, but lose the stabilisation effect of native disulfide bonds, suffer from payload loss, and can form antibody isomers. Whilst engineering antibodies to integrate a non-canonical site can improve conjugation, these techniques are expensive and not readily accessible.

Recent work has developed the cysteine-to-lysine transfer (CLT) strategy, whereby a cysteine residue is used as an initial ligating hook, modified by an alkyl thioester. Proximal lysine residues can then trigger an *S*-to-*N* acyl transfer, which transfers the acyl group from the cysteine onto the lysine, generating an amide bond. CLT enables the generation of lysine-modified antibodies in a more homogeneous manner. This methodology provides an exciting and accessible way of generating homogeneous ADCs on off-the-shelf antibodies. However, the time needed to generate conjugates is long, and existing thioesters suffer from hydrolytic instability, lowering efficiency.

This research identifies novel thioesters of superior reactivity to those previously explored in the literature for protein modification. Of particular interest are electron-deficient thioesters that show faster transthioesterification and CLT to those alkyl reagents previously explored. In particular, a tetrazine thioester demonstrates rapid

*N*-terminal cysteine modification and click chemistry and represents one of the most reactive tetrazine rings available in existing literature. This reagent is widely applicable in chemical biology investigations for the rapid functionalisation and modification of *N*-terminal cysteine-containing peptides.

Further work has demonstrated the applicability of alternative carbonyl-related functional groups for antibody conjugation. These reagents may present new opportunities and alternative chemistry for the controlled modification of proteins. Many of these reagents demonstrate exceptional stability under physiologically relevant conditions and could be of interest as part of the wider chemical biology toolbox. Early attempts into the expansion of thioesters with dual-reactive handles may also prove of interest as an alternate method of achieving affinity-guided protein modification, utilising simple small molecules instead.

Overall, this work introduces multiple novel compounds and demonstrates their effectiveness as protein modification reagents, exploring their unique and variable chemistry. The reagents and strategies developed within could be of use in a variety of chemical biology applications.

*Bismillah*

*“In the name of Allah”*

# Acknowledgements

It is simply not possible to summarise my time at UCL with mere words. But to try, these past few years have been nothing short of eventful, unpredictable, frustrating, enjoyable, difficult, rewarding, demanding, and fascinating. I have gone through the entire range of imaginable emotions within a single day of work, possibly even within a single hour at times. A PhD is no easy endeavour – I will admit that there were times where I had doubts, but at the end of it all, I have not a single regret about my decision to pursue this PhD. I have grown immensely as a researcher and, more importantly, as a person, and I am so grateful for this entire experience.

Science should simply work how you would like it to work, but we are not that fortunate. It is with the support of everyone at the KLB that I could overcome the range of issues one might face over the course of a PhD. Leaving UCL therefore leaves me with mixed feelings – happiness and relief, with a strong sense of accomplishment. But also, sadness and regret that I leave an incredible cohort. I am certain that I would not have enjoyed my PhD as much as I would have with any other group of people, at any other place in the world. We have overcome a pandemic, we have experienced climates ranging from the tropics to the arctics, and we have dealt with some particularly obnoxious smells. So, to everyone at the KLB – thank you for the memories, the laughs, the shared pain, the NMR trips, the Mass Spec discussions, and the food.

I must start by thanking my brilliant supervisor Prof. Jamie Baker. Jamie has been the best supervisor possible, and I am thankful for the opportunity to study under his guidance. It is no understatement to say none of this would have been possible without his unwavering support, encouragement, and advice. Jamie's passion for science is infectious, and I am eternally inspired by his dedication to his students – he truly wants the best, in all aspects of life. I have learnt an incredible amount over my time with Jamie, and I have grown tremendously as a scientist and as a person thanks to him. I will miss all the scientific and non-scientific discussions. I wish Jamie the absolute best in everything he pursues, including in his footballing career!

I would also like to thank Prof. Vijay Chudasama. Vijay has had just as much involvement and interest in my research and progress as anyone else. His scientific brain is simply amazing, and I have benefitted a lot from his suggestions and advice.

Vijay has always been a fantastic person to have around in our labs, and I will miss his sense of humour and energy. I look forward to hearing about the next big thing from the Chudasama group.

Dr Nafsika Forte, the star of the KLB. I came into the KLB lab with no chemical biology experience. I barely knew how to use a pipette properly, and I had never worked on reaction scales where a literal drop is the entire sample. Nafsika spent her time and effort in teaching me everything I needed to know, from making gels to my very first column on the Biotage. Nafsika's work rate is astonishing, and her dedication to her research is something I have tried to maintain throughout my PhD, although it is not always possible to match her energy levels.

Another star I must talk about is Dr Archie Wall. Archie is somehow the hardest working person and yet the most chilled person I have met. I admired his ability to be calm about everything and provide grounded advice. I have very fond memories of his first ever ELISA. His banter and wittiness is top tier and is something I miss daily.

Life in the KLB would not have been the same without the Senior Bakers, Dr Alina Chrzastek and Yanbo Zhao.

Alina, for being a staple throughout my KLB life. It has been some journey. From the balance room during the very first days of our rotation projects, to finally reaching the end. Alina has been there since day 1. And it only took me 1000 days to learn how to spell her surname. I will forever be grateful for the gossips, the secrets, the laughs, the anxieties, the stresses, the snacks, and the financial advice. I will always appreciate that there was someone just as tidy as me in labs, and there is no one else I would rather have shared a fume hood or desk area with than Alina.

Yanbo, for being the influencer we all need. Yanbo has been another constant throughout my PhD. Although she seemed innocent at first, I quickly realised there is an entirely different side of Yanbo, and I am glad that I did – the witty and chaotic side. I will miss the tasty snacks, the talks, the walks, the banter, and the practical pranks. Yanbo has always been willing to help me with whatever I need, and I would probably be stuck doing the maths if it wasn't for her human calculator abilities. I have tried so many different snacks thanks to Yanbo, and those are experiences I will never forget.

Next up is the Burger Boys, Mikesh Patel and Usman Shabbir.

Mikesh, for being a fellow boss man enthusiast. We have studied cars, the science of designing the perfect chicken burger, and a little bit of chemistry alongside that. I will be forever grateful for Mikesh's music on the lab speakers, his enthusiasm for motives, and his colourful terminology. The Korean shop trips, the countless cheat meals, the random assortment of sweets. Mikesh's help throughout my research has been invaluable, and his expertise in chemistry is not too bad. As the man himself says, it is what it is – an excellent proverb for dealing with experimental hardship.

Usman, for being the ultimate guide. From events unfolding in the lab, to the best places to eat, Usman knows it all. His chemical stash is on another level, and I very much appreciate the unrestricted access... Usman is the guy for chemistry and is one of the sharpest people I have ever met. I am also very grateful for that generous helping of biryani, the fudge, and the various other baked goods. I will miss Usman's sense of humour and quick speed of thought. I will also need to hire a new investigator.

Dr Roshni Malde, the lightbulb. Sorry, or should I say Roshini. Sorry, or should I say Rashini. I will forever appreciate that cheesecake, the Bollywood music, and the general ideas about where to eat next. Like her research, Roshni was always a bright person to have in labs, and I am grateful that she was so appreciative of my many pranks. Next time, save some awards for the rest of us please.

Lula, the mother of Voldemort. Without Lula, perhaps I would not appreciate cats in the manner I do today, and perhaps I would always feel like something is missing. I am thankful for Lula's choice of music, her passion for Italian food, and her openness. Lula's always been a colourful person around the KLB – both in her choice of words, but also in her hairstyles, which is a massive contrast to the grey skies of London.

Charlie, the boy born in the year X. Simply, I refuse to acknowledge Charlie's year of birth, as there is no way a person born in the year 2000 is a fully functioning member of society. Charlie is a very talented student – when things 'don't chicken' in his research, I am sure Charlie will be able to figure things out. I will miss snack time.

Nehaal, for perhaps being the trendiest person to ever walk the corridors of the KLB. I wish him good luck in all the future raffles he may decide to take part in. Nehaal's

chemistry knowledge is incredible, and I always enjoyed listening to his talks – scientific or otherwise. It is a shame that he is a Manchester United fan.

I must also thank all past and current members of the KLB lab, starting with the sages of knowledge: Dr Dave Chisholm, for his big boy reactions, Dr Steven Yap, for all the things related to LCMS and Brompton bicycles; Dr Matthew Penny, for the all-round pleasantness and being my waste management partner; Dr Richard Spears, for all the small molecule assistance; Dr Peter Szijj, for the Mass Spec help and trivia; Dr Faiza Javaid, for the helpful summaries of all gossip; Dr Fabien Thoreau, for the fou de ball; Dr Andre Shamsabadi, for his chemistry help, Dr Calise Bahou, for being an expert in chemical biology; Dr Antoine Maruani, for his incredible knowledge of just about everything; Dr Richard Proctor, for the *p*-toluenesulfonic acid which I must have borrowed about ten times; and Dr Sahra St. John-Campbell, for getting the lab in order and fixing that Kardex.

Finally, the next generation of soon-to-be KLB graduates: Lea Rochet, for her sense of humour, friendliness, and her passion for France; Ioanna Thanasi, for not leaving me alone with the nitrogen dewar, and the shared Mass Spec frustrations; Phyllida Britton, for saving so much electricity by turning the fume hood lights off, but also for the fun talks; Cliona McMahon, for the incredible defensive skills at football; Toby Butcher, for being a lovely person to work with. You will all do fine, you are all unbelievably talented, smart, and hardworking individuals. I am looking forward to seeing what you all achieve in the future.

Of course, I would like to thank my parents and my family for their unwavering support, even if they don’t quite understand what exactly I have done over these last few years.

I would also like to thank MRC for funding my PhD and giving me the freedom to pursue a PhD in such an interesting field, and in particular Kim Duffy for her relentless work in making sure everything runs smoothly. I also would like to thank Dr Abil Aliev for his work in ensuring the most consistent and reliable NMR service in the world, and Dr Kersti Karu for helping with Mass Spec.

# Table of contents

# Abbreviations

| | |
|---|---|
| **3G** | Third-generation |
| **AcOH** | Acetic acid |
| **ADC** | Antibody-drug conjugate |
| **ADCC** | Antibody-dependent cell cytotoxicity |
| **AJICAP** | Affinity peptide mediated regiodivergent functionalisation |
| **APG** | Azidophenylglyoxal |
| **APN** | Arylpropionitriles |
| **BCMA** | anti-B-cell maturation antibody |
| **BCN** | Bicyclononyne |
| **BCR** | B-cell receptors |
| **BTG** | Bacterial transglutaminase |
| **BVP** | Bis(vinylsulfonyl)piperazines |
| **CAR** | Cluster-to-antibody ratio |
| **cat.** | Catalytic |
| **CDR** | Complementarity-determining region |
| **$C_H$** | Heavy constant domain |
| **Cit** | Citrulline |
| **$C_L$** | Light constant domain |
| **CLT** | Cysteine-to-lysine transfer |
| **$Cs_2CO_3$** | Caesium carbonate |
| **CuAAC** | Copper-catalysed azide-alkyne cycloaddition |
| **DAR** | Drug-to-antibody ratio |
| **DCM** | Dichloromethane |
| **DIAD** | Diisopropyl azodicarboxylate |
| **DM1** | Mertansine |
| **DMF** | Dimethylformamide |
| **DMP** | Dess-Martin Periodinane |
| **DMSO** | Dimethyl sulfoxide |
| **Dox** | Doxorubicin |
| **DPR** | Diaminopropionic acid |
| **DSC** | *N*,*N*'-disuccinimidyl carbonate |

| | |
|---|---|
| **DTT** | Dithiothreitol |
| **DVP** | Divinylpyrimidines |
| **EBX** | Ethynylbenziodoxolone |
| **EDC** | 1-Ethyl-3-(3-dimethylaminopropyl)carbodiimide |
| **EEDQ** | N-Ethoxycarbonyl-2-ethoxy-1,2-dihydroquinoline |
| **eq.** | Equivalents |
| **EtOH** | Ethanol |
| **FAR** | Fluorophore-to-antibody ratio |
| **FDNB** | 5-fluoro-2,4-dinitrobenzene |
| **$FeBr_2$** | Iron (II) bromide |
| **FGE** | Formaldehyde-generating enzyme |
| **$F_v$** | Variable fragment |
| **g** | Gram |
| **GSH** | Glutathione |
| **h** | Hour |
| **HAMA** | Human anti-mouse antibody |
| **HC** | Heavy chain |
| **HCl** | Hydrochloric acid |
| **HHLL** | Heavy-heavy light-light |
| **HIPS** | Hydrazino-*Iso*-Pictet-Spengler |
| **HL** | Heavy-light |
| **HSA** | Human serum albumin |
| **IBA** | Indole-3-butyric acid |
| **iEDDA** | Inverse electron-demand Diels Alder |
| **$K_2S_2O_8$** | Potassium persulfate |
| **KOH** | Potassium hydroxide |
| **LC** | Light chain |
| **LCMS** | Liquid-chromatography mass spectroscopy |
| **mAb** | Monoclonal antibody |
| **MC** | Maleimidocaproyl |
| **MDR1** | Multi-drug resistance protein |
| **MeCN** | Acetonitrile |
| **MeOH** | Methanol |

| | |
|---|---|
| **MeSH** | Methanethiol |
| **MESNa** | Sodium 2-mercaptosulfonate |
| **mg** | Milligram |
| **min** | Minute |
| **mM** | Millimolar |
| **MMAE** | Monomethyl auristatin E |
| **MMAF** | Monomethyl auristatin F |
| **mmol** | Millimoles |
| **MPAA** | 4-mercaptophenylacetic |
| **MS** | Mass spectroscopy |
| **$NaN_3$** | Sodium azide |
| **$NaNO_2$** | Sodium nitrite |
| **NBD** | Nucleotide-binding domain |
| **nCAA** | Non-canonical amino acids |
| **NCL** | Native chemical ligation |
| **NGM** | Next-generation maleimide |
| **nHL** | non-Hodgkin's lymphoma |
| **NHS** | *N*-hydroxysuccinimide |
| **NK** | Natural killer |
| **NMM** | *N*-methyl morpholine |
| **NMR** | Nuclear magnetic resonance |
| ***p*-TSOH** | *p*-toluenesulfonic acid |
| **PABC** | *p*-Aminobenzylcarbonyl |
| **pAcPhe** | *p*-acetylphenylalanine |
| **PBD** | Pyrrolobenzodiazepine |
| **PDI** | Protein disulfide isomerases |
| **PDI** | Pyridazinediones |
| **PhSH** | Thiophenol |
| **PTM** | Post-translational modification |
| **ReACT** | Redox-activated chemical tagging |
| **SAR** | Structure-activity relationship |
| **$scF_v$** | Single chain variable fragment |
| **SDS-PAGE** | Sodium dodecyl sulfate–polyacrylamide gel electrophoresis |

| | |
|---|---|
| **SMCC** | Succinimidyl-4-(*N*-maleimidomethyl) cyclohexane-1-carboxylate |
| **SPAAC** | Strain-promoted azide-alkyne cycloaddition |
| ***t*-BHP** | *t*ert-Butyl hydroperoxide |
| **TCEP** | Tris(2-carboxyethyl)phosphine |
| **TCO** | *trans*-cyclooctene |
| **TEAB** | Tetraethylammonium bromide |
| **TEMPO** | (2,2,6,6-Tetramethylpiperidin-1-yl)oxyl |
| **THF** | Tetrahydrofuran |
| **TLC** | Thin-later chromatography |
| **µM** | Micromolar |
| **µmol** | Micromole |
| **Val** | Valine |
| **$V_H$** | Heavy variable domain |
| **$V_L$** | Light variable domain |

# 1. Introduction

## 1.1. Protein modifications

Protein modifications are controlled changes that increase protein functional and structural diversity, and these are critical in both natural biological processes and in chemical biology research. Completed in 2003, the human genome project identified approximately 25,000 protein coding genes; however, human proteomes are vastly more complex, featuring proteins of varying structural and functional diversity.[1] Nature utilises an enzymatic toolbox to achieve such variety, through post-translational modifications (PTMs) of proteins. Such modifications, when driven by natural processes, are highly chemoselective and site-selective. Notable examples of PTMs include phosphorylation, acetylation, and ubiquitination, amongst many others. PTMs are critical to all phases of biochemical processes in humans, responsible for mediating biological actions ranging from apoptosis to cell signalling.[2] As a result of their importance in proper biological functioning, it is therefore unsurprising that dysregulation of PTMs can cause significant disease development.[3] Thus, there is much interest in tracking PTMs, labelling relevant proteins, understanding their specific roles in biological conditions, and developing strategies to mediate various disease progressions.

In addition to studying PTMs themselves, chemical biology research has been inspired by nature's endogenous modifications. There is much work in developing techniques that can enable protein modification in a site-selective, chemoselective manner that mimics the precise enzymatic control seen in PTMs.[4] Modification of proteins has enabled the synthesis of protein bioconjugates with potential diagnostic and therapeutic applications. For example, protein-drug bioconjugates are proving to be very effective drugs in the treatment of previously unmet diseases and are rapidly becoming first-line therapy options. An emerging pharmaceutical of increasing therapeutic interest are antibody-drug conjugates (ADCs).

## 1.2. Antibody-drug conjugates

Modern chemical biology approaches have enabled extensive chemical modification of proteins, leading to chemical probes and the development of therapeutic conjugates such as ADCs (**FIG. 1**).[5] ADCs consist of a monoclonal antibody (mAb) covalently bound through a chemical linker (cleavable or non-cleavable) to a cytotoxic drug.

These immunoconjugates are therefore capable of combining the specificity of mAbs for an antigen with drug cytotoxicity; minimising off-site toxicities related to these normally intolerable, promiscuous chemotherapies, and enabling increased payload delivery to target sites. This makes ADCs therapies with expanded therapeutic windows that can take advantage of even the most potent drugs, such as toxic natural products, and thus fulfil the requirements of Paul Ehrlich's 'magic bullet' – a therapy that selectively targets diseased cells, over healthy neighbours.[6]

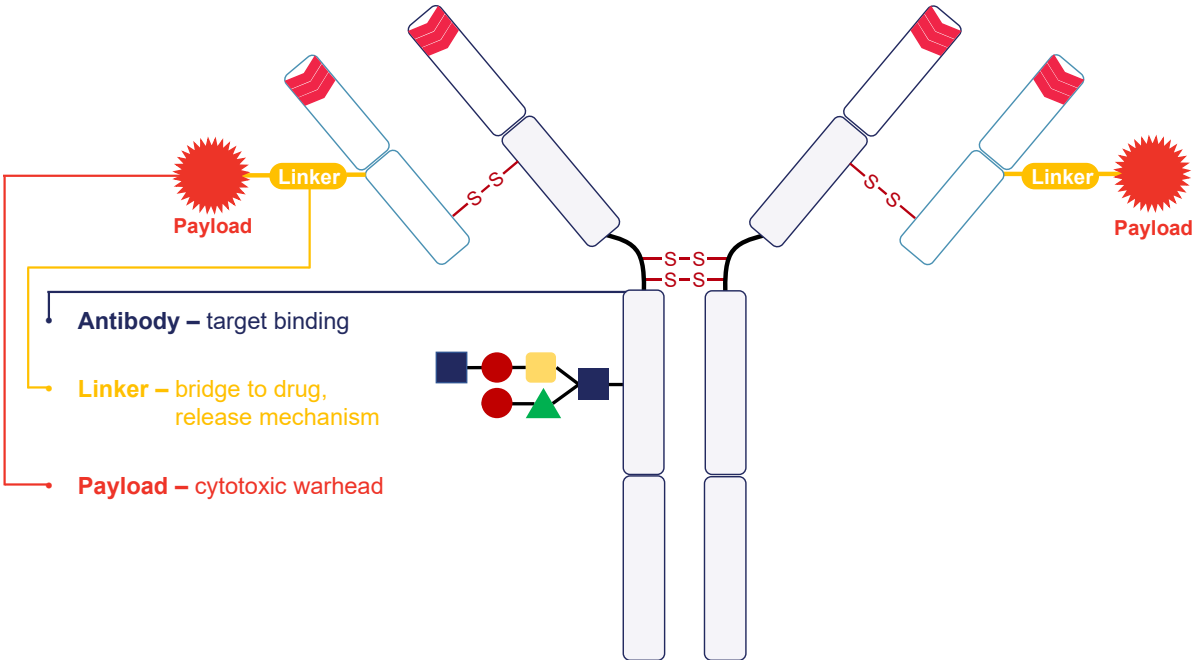


**FIGURE 1.** Schematic representation of an antibody-drug conjugate (ADC).

Antibodies typically consist of a hydrophilic surface with internal hydrophobic regions; however, due to the increased size and hydrophobicity, resulting from the attachment of a payload, ADCs are cleared more rapidly than their parent naked mAb (**FIG. 2**).[7] Dosage is crucial, as is ensuring that the selected payload is capable of demonstrating potent cytotoxicity at low concentrations. Examples of strategies to overcome rapid ADC clearance include linker technology,[8] payload characteristics,[9] and improving ADC homogeneity.[10]

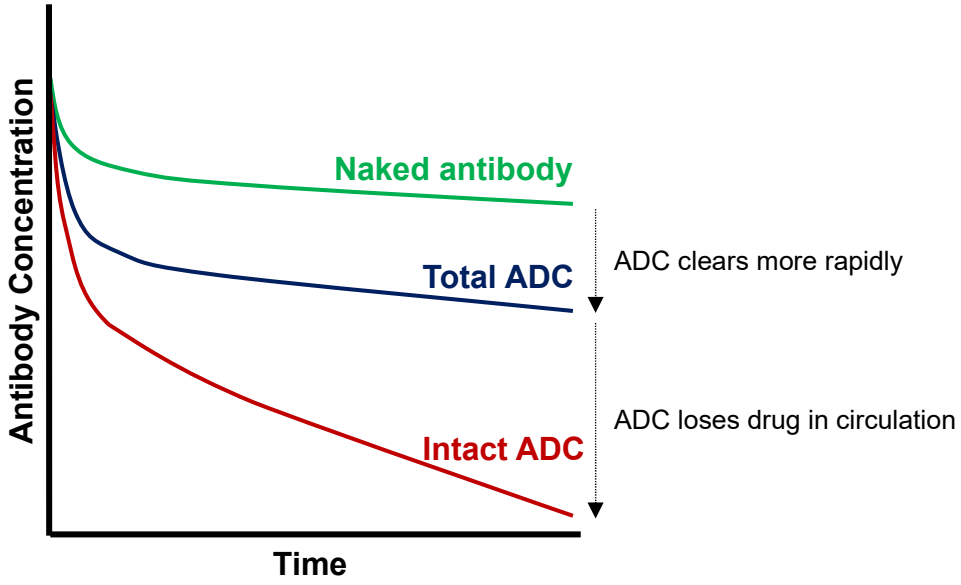


**FIGURE 2.** Illustration of antibody concentration over time, comparing a naked mAb, the initial ADC dose, and the intact ADC.

ADCs are commonly internalised to execute their intended biological effect (**FIG. 3**). The ADC binds to the target antigen and is internalised *via* receptor-mediated endocytosis. Following this, it is trafficked around the cytoplasm in endosomes. Depending on the linker release mechanism, the cytotoxic payload is released, enabling cell death. It is also possible for deconjugation of the ADC drug to occur near the tumour microenvironment. Thus, the ADC components dictate the exact mechanism of inducing cellular death – the linker type, the payload's mechanism of action, and the antibody for the target antigen.

A 'bystander effect' may also be desirable. The bystander effect is mostly limited to cleavable linkers, where the unloaded payload can bypass the cellular membrane to leave the initial target cell and penetrate nearby cells which may or may not express the target antigen. This can be beneficial in tumour types which express the antigen heterogeneously, as the ADC can kill antigen-positive and antigen-negative tumour cells.[11] When the target antigen is expressed in a high and homogeneous manner on the cancer region, the bystander effect can instead cause unwanted off-site toxicity by killing healthy neighbouring cells. The type of linker used is often responsible for bystander effect. Nonetheless, it is crucial for proper linker stability, to ensure the exposure of this toxicity towards healthy cells is minimised.

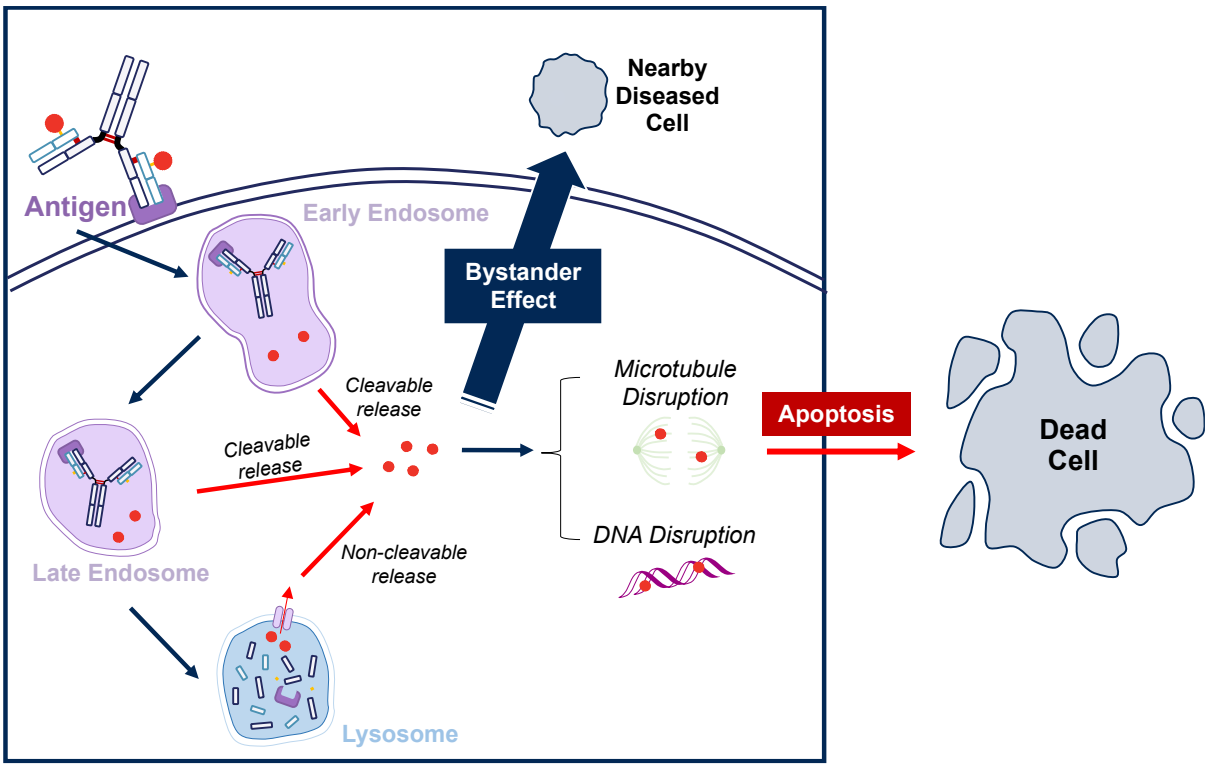


**FIGURE 3.** Simplified mechanism of action of a typical ADC.

As a result of their targeted drug delivery approach, ADCs are successful anti-cancer therapies (**FIG. 4**). The first ADC, Mylotarg, was approved in 2000 for the treatment of acute myeloid leukaemia. Since then, another 10 ADCs have joined the cancer therapy market, with 8 of these approved after 2017 (**TABLE 1**).

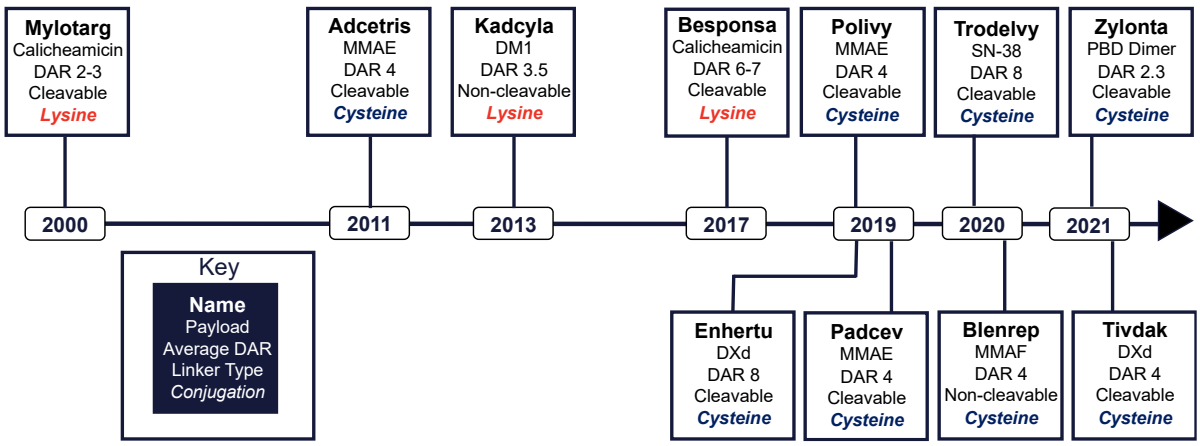


**FIGURE 4.** Timeline of ADCs approved for clinical use, and their key biochemical properties.

**TABLE 1.** ADCs currently approved for clinical use. AML – acute myeloid leukaemia, HL – Hodgkin's lymphoma, ALCL – anaplastic large-cell lymphoma, HER2+ BC – human epidermal growth factor receptor-2 positive breast cancer, ALL – acute lymphoblastic leukaemia, DLBCL – diffuse large B-cell lymphoma, TNBC – triple-negative breast cancer, MM – multiple myeloma.

| ADC | Target | mAb | Linker | Release, Mechanism | Payload, Mechanism | DAR | Indication | Approval Year | Ref |
|---|---|---|---|---|---|---|---|---|---|
| **Mylotarg** | CD33 | IgG4 | Hydrazone+ Disulfide | Cleavable, Acidic | Ozogamicin, DNA cleavage | 2-3 | CD33+ AML | 2000 | [12] |
| **Adcetris** | CD30 | IgG1 | Dipeptide | Cleavable, Enzyme | MMAE, Microtubule inhibitor | 4 | HL, ALCL | 2011 | [13] |
| **Kadcyla** | HER2 | IgG1 | Thioether | Non-cleavable, Lysosome | Ozogamicin, DNA cleavage | 3.5 | HER2+ BC | 2013 | [14] |
| **Besponsa** | CD22 | IgG1 | Hydrazone+ Disulfide | Cleavable, Acidic | Ozogamicin, DNA cleavage | 6 | B-ALL | 2017 | [15] |
| **Polivy** | CD79b | IgG1 | Dipeptide | Cleavable, Enzyme | MMAE, Microtubule inhibitor | 3.5 | DLBCL | 2019 | [16] |
| **Padcev** | Nectin4 | IgG1 | Dipeptide | Cleavable, Enzyme | MMAE, Microtubule inhibitor | 3.8 | Urothelial Cancer | 2019 | [17] |
| **Enhertu** | HER2 | IgG1 | Tetrapeptide | Cleavable, Enzyme | Dxd, TOP1 inhibitor | 8 | HER2+ BC | 2020 | [18] |
| **Trodelvy** | TROP2 | IgG1 | SMCC | Cleavable, Enzyme | SN-38, TOP1 inhibitor | 7.6 | TNBC | 2020 | [19] |
| **Blenrep** | BCMA | IgG1 | MC | Non-cleavable, Lysosome | MMAF, Microtubule inhibitor | 4 | MM | 2020 | [20] |
| **Zynlonta** | CDC19 | IgG1 | Dipeptide | Cleavable, Enzyme | SG319 PDB dimer, DNA cleavage | 2.3 | DLBCL | 2021 | [21] |
| **Tivdak** | Tissue Factor | IgG1 | Dipeptide | Cleavable, Enzyme | MMAE, Microtubule inhibitor | 4 | Cervical Cancer | 2021 | [22] |

It is evident that recent years have demonstrated the potential of ADCs as cancer therapies. Additionally, there have been significant improvements in understanding ADCs – their mechanisms of actions, their distribution within the body, and the properties of the targeted antigen. Importantly, selecting the correct antibody, linker, and drug combination for the targeted antigen is crucial for the therapeutic effectiveness and stability of an ADC.

### 1.2.1. The antibody

Antibodies are Y-shaped glycoproteins synthesised entirely by B cells as part of the adaptive immune system. B cells produce a single, specific species of antibody with defined antigen-binding sites. Initially, these antibodies are found inserted into the cell surface membrane of B cells, forming B-cell receptors (BCRs).[23] Upon detection and binding of an antigen, the adaptive immune response is triggered. These B cells proliferate rapidly and differentiate into effector B-cells, which are capable of secreting significant amounts of soluble antibodies into the blood. The soluble antibodies then initiate further immune responses that ultimately eliminate the foreign pathogen from the body (**FIG. 5**).

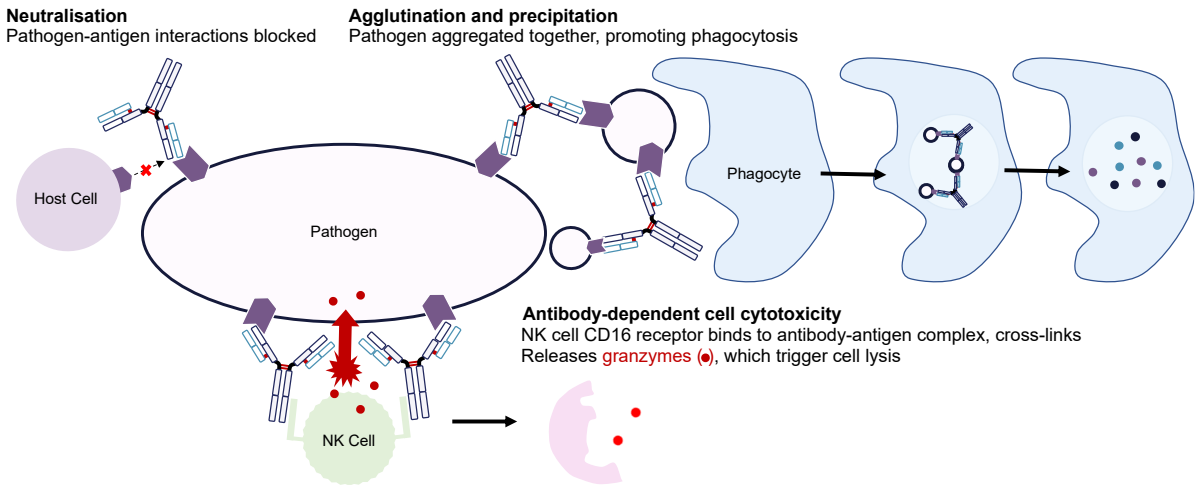


**FIGURE 5.** Simplified mechanisms of antibody-mediated immune responses.

These processes include: 1) neutralisation, preventing the pathogenic antigen from binding with host cells; 2) promotion of phagocytosis, by linking together antigens and enabling phagocytotic cells to consume, digest, and eliminate the pathogen; and 3) antibody-dependent cellular cytotoxicity (ADCC), where the antibody-antigen complex is recognised by natural killer (NK) cells, which secrete granzymes that initiate cell lysis.[24] Whilst free antibody concentration declines after elimination of an infection,

some memory B cells, that can provide an accelerated antibody-mediated immune response as part of the secondary immune response, remain.[25]

Antibodies are composed of pairs of identical light (LC) and heavy chains (HC). The individual LC and HC are linked together by a disulfide bond, with LC and HC pairs strongly held together by a combination of non-covalent protein interactions and by disulfide bonds in the flexible hinge region. Each individual chain contains a single amino-terminal variable domain ($V_L$ or $V_H$) and one or more carboxylic-terminal constant domains ($C_L$, $C_H1$, $C_H2$, $C_H3$) (**FIG. 6**).

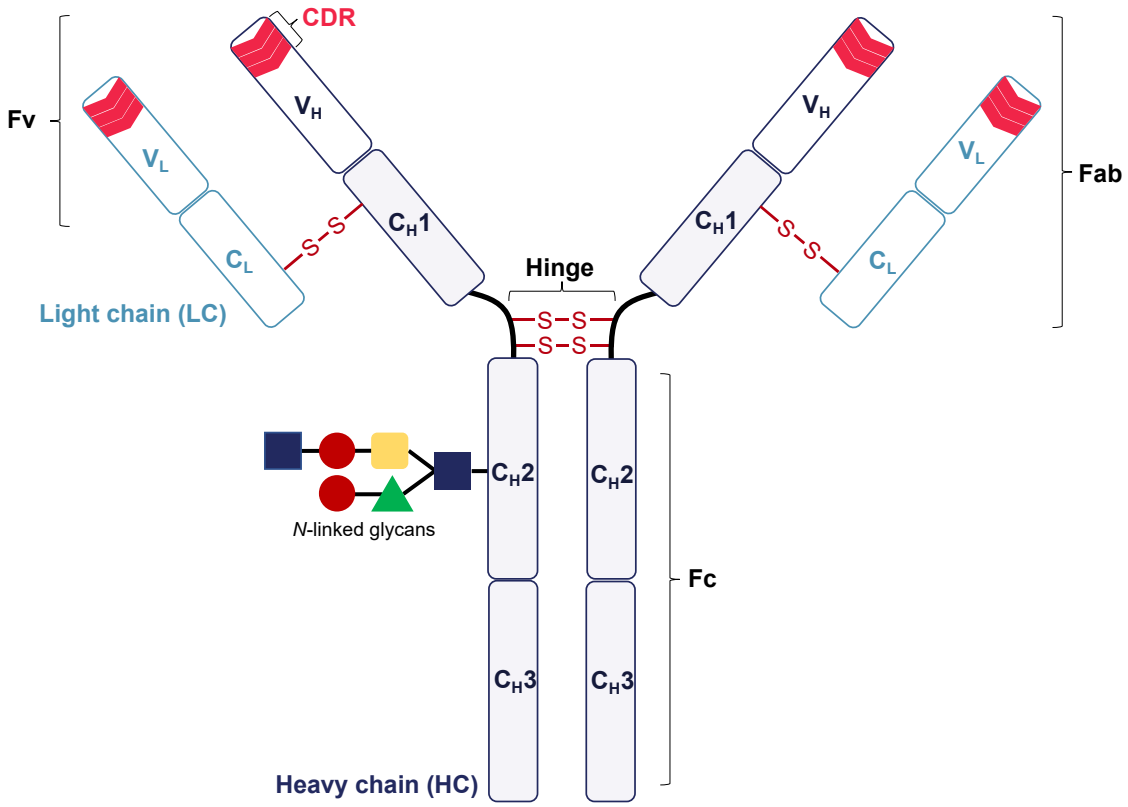


**FIGURE 6.** Schematic illustration of the structure of a human $IgG_1$ antibody.

Classification of human antibodies is achieved according to properties of the HC into five isotypes, which have differing effector functions – IgG, IgA, IgD, IgE, and IgM.[26] IgG antibodies consist of γ HCs and are the most abundant isotype in human blood serum responsible for much of the secondary immune response, thus are amongst the most studied isotype in therapeutic antibody research. Within the IgG isotype itself, there exist four subclasses termed $IgG_1$, $IgG_2$, $IgG_3$, and $IgG_4$, in descending order of abundance. These subclasses differ slightly in properties such as molecular weight, number of inter-chain disulfide bonds, half-life, and antigen response. For example,

$IgG_1$ has a molecular weight of 146 kDa, 60% relative abundance, 4 inter-chain disulfide bonds, a half-life of 21 days, and responds to soluble protein antigens.

By the action of proteases such as pepsin, $IgG_1$ antibodies can be further split into a single dimeric $(Fab)_2$ and single Fc species. The Fab region is responsible for the cross-linking and binding of antigens, while the Fc region activates receptors on effector cells. Fab contains a single complete LC ($V_L$ and $C_L$), as well as parts of the HC ($V_H$ and $C_H1$).[27] Furthermore, Fab can be divided into a variable fragment (Fv) composed only of $V_H$ and $V_L$. The Fv contains the antigen recognition site which is mediated through six complementarity-determining regions (CDRs). The CDRs are hypervariable domains that enable antibodies to respond and recognise limitless numbers of very diverse antigens. These structural features enable antibodies to demonstrate highly selective and robust binding to their antigen.

The high specificity and affinity for particular antigens offered by antibodies makes them very useful therapeutic tools. Köhler and Milstein's hybridoma technology enabled the first instances of large-scale mAb production with predetermined antigen specificity, opening the possibility for mAbs with clinical usefulness.[28] Muromonab-CD3, in 1985, was the first approved mAb drug treatment, used as an immunosuppressant.[29] However, the use of foreign protein sequences from non-human species resulted in high immunogenicity, limiting efficacy of these treatments. The human anti-mouse antibody (HAMA) is one such example of advancements in methods, where human antibodies are produced in response to a mouse-derived mAb.[30] Humanisation of mAbs enabled exceptional advances in their clinical approvals. The Nobel Prize in Chemistry (2018) was awarded to George P. Smith and Sir Gregory P. Winter for their work on phage display of peptides and antibodies.[31] Further work in genetic engineering enabled the generation of chimeric, humanised, and fully human mAbs that overcame previous immunogenicity issues. Trastuzumab, a humanised mAb, and Humira, a fully human mAb, are examples of two of the most clinically utilised mAb drugs worldwide. There are currently 79 approved mAbs, 30 of which are used in cancer treatments.[32]

#### 1.2.1.1. Antibody fragments

Despite the undoubted therapeutic usefulness of full mAbs, they still have shortcomings, particularly in cancer treatments. Often, manufacturing large quantities

of mAbs for prolonged treatments of chronic diseases is expensive, especially since post-translational modification (e.g., glycosylation) is necessary. Additionally, the primary form of transport into tumours is by diffusion, with diffusive properties of the antibody determined by size and antigen availability. The reduced size of antibody fragments improves diffusive capabilities and so results in greater tumour uptake and improved intratumoural distribution.[33] Additionally, the smaller size of antibody fragments also enables binding to more obscure 'immunosilent' antigen sites.[34, 35] These fragments can retain antigen specificity while offering high levels of efficacy. The loss of the Fc region can be disadvantageous since effector cells cannot be activated, propensity for aggregation increases, and thermostability decreases; however this also prevents Fc-mediated immunogenicity and toxicity.[36]

Protease digestion is commonly used for the generation of Fab fragments, while smaller single chain (scFv) and third-generation (3G) antibody fragments are generated through expression systems.[37] Fab consists of solely the Fab region of a full mAb, the scFv fragments consist of a flexible peptide linker joining the $V_L$ and $V_H$ domains together, while the 3G fragments consist of single-domain, miniature antibody components (**FIG. 7**).

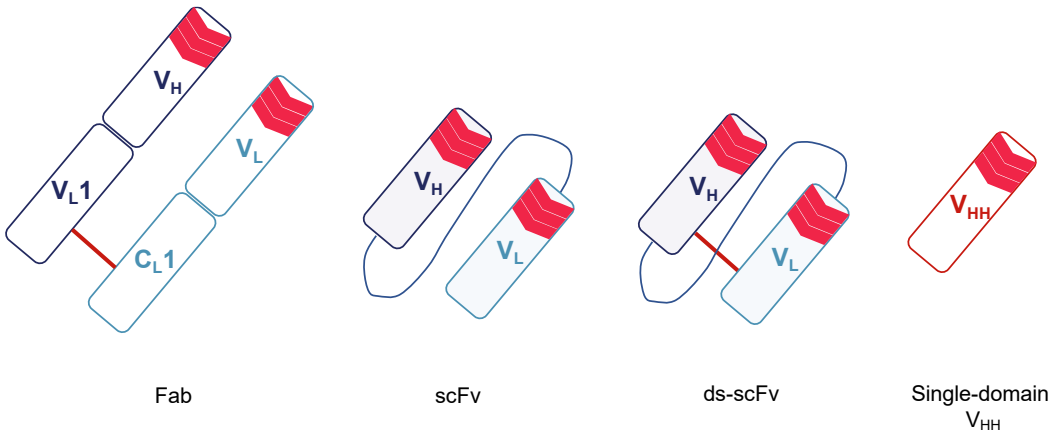


**FIGURE 7.** Schematic illustration of antibody fragments. Red line = disulfide bond.

Currently, only five fragment antibody therapies have achieved clinical approval, four of which are Fab constructs – Abciximab for angioplasty; ranibizumab for macular degeneration; idarucizumab as an anticoagulant; and certolizumab pegol for Crohn's disease.[38] scFv therapies show somewhat promising pre-clinical results,[39] but have largely failed to demonstrate benefit in large-scale clinical studies.[40] Only Lumoxiti, an Fv fragment of an anti-CD22 antibody conjugated to a large toxin, has achieved clinical

approval.[41] Single-domain antibody fragments are earlier yet in their development, however there is already one clinically approved therapy – caplacizumab, for thrombosis treatment. These single-domain antibodies make use of camelid antibodies, which contain unique $V_{HH}$ domains capable of high affinity antigen binding. The incredibly small size of these single-domain fragments means they are rarely immunogenic, possess good solubility, demonstrate an ability to bind to obscure epitopes, which are parts of antigens that bind to specific antibodies, and are more easily manufactured, since inter-domain interactions do not need to be considered.[42]

However, the smaller size of all types of antibody fragments mean they are well below the renal threshold, so often suffer from very rapid clearance from circulation. Therefore, despite possessing increased penetration potential, the dose reaching tumour sites is low. Fragment antibodies have not demonstrated any meaningful improvements in cancer indications than their mAb counterparts and have often struggled in clinical trials. Work to lengthen the half-life of fragments continues, with strategies involving PEGylation,[43] albumin conjugation,[44] fusion to immunoglobulin-binding domains,[45] and many others.[46]

While mAbs have clinical benefits, for some indications they still do not demonstrate sufficiently high efficacy. The attachment of cytotoxic moieties, and the generation of ADCs, aims to resolve this lack of potency. In addition to the antibody-mediated effects, the attached drug can also contribute towards increasing cytotoxicity at the target site. This method of approach is particularly useful for the treatment of cancer.

### 1.2.2. The linker

In cleavable and non-cleavable linkers used in clinically approved ADCs, internalisation of the ADC initiates the cell-killing process, thus they must be stable enough to survive blood circulation until reaching the target site.[47] ADC linkers consist of two attachment sites – a linker-mAb unit, and a linker-drug unit. Release mechanisms responsible for payload delivery are often found at the linker-drug site.

#### 1.2.2.1. Cleavable linkers

In ADCs containing cleavable linkers, there are a variety of release mechanisms for enabling controlled drug release at the target site, including i) acid-initiated cleavage, ii) reducible disulfides, or iii) enzyme-mediated cleavage in lysosomes. Changes in

cytosolic pH or concentrations of metabolites can also behave as chemical triggers and may be characteristics distinctive to target cells, such as tumour cells.[48]

Hydrazones were the first developed acid-labile linkers to be successfully used in ADCs (**FIG. 8**). The earliest example of its use is BR96-Doxorubicin (Dox), where eight Dox equivalents are linked to a chimeric mAb BR96, forming one of the earliest ADCs.[49] The study provided evidence of reduced toxicity and less off-site Dox binding, owing to the initial stability of the hydrazone linker. Mylotarg, used for the treatment of CD-33+ acute myeloid leukaemia, also features a hydrazone linker, and was the first ADC approved to utilise acid-labile cleavage for payload release.[50] Initial early-phase studies confirmed the effectiveness of Mylotarg – patients showed good recoveries whilst adverse effects appeared to be minimised, leading to accelerated approval. However, longer-term Phase 3 studies did not show any meaningful improvement over standalone chemotherapy, and, in fact, patients did suffer from Mylotarg-related fatal adverse effects, including haemorrhage, infection, and acute respiratory distress syndrome, leading to temporary clinical withdrawal. This is likely due to the insufficient blood plasma stability of the hydrazone linker.[51] Later studies investigating hydrazone linkers in ADCs showed that while buffer stability at pH 7.4 was good, blood plasma stability at the same pH was significantly lower. *In vitro* stabilities were lower and *in vivo* toxicities were significantly higher in hydrazone-linked conjugates than the corresponding non-acid labile conjugates.[52] More recently developed derivatives include aromatic hydrazones, which showed good buffer stability, but poor plasma stability, leading to lower clinical responses than originally predicted.[53] Discrimination between acidic and neutral pH is difficult for the linker to achieve, especially since much time is spent in circulation in blood plasma.

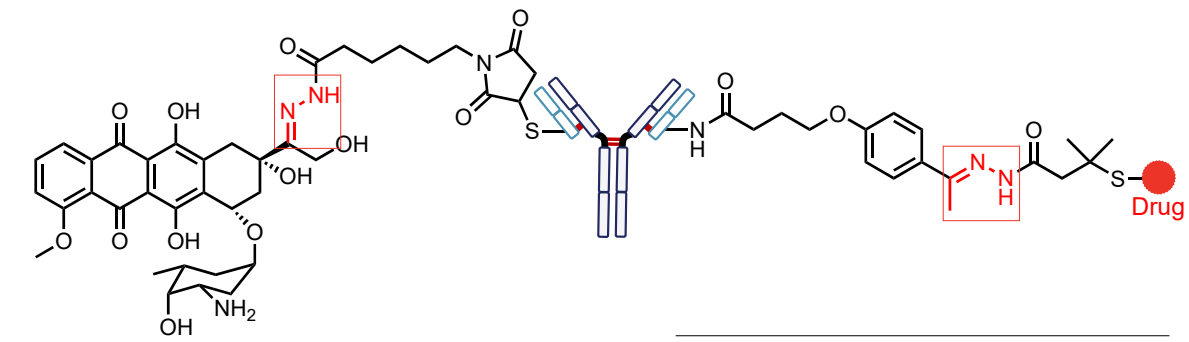

**FIGURE 8.** Hydrazone-cleavable linkers used in BR96-Dox and Mylotarg, hydrazone in red.

Nonetheless, the continued use of Mylotarg, and Besponsa, another ADC for leukaemia treatment, prove the viability of an acid-sensitive linker strategy. In 2020, Trodelvy for triple-negative breast cancer treatment was approved, featuring an acid-labile carbonate linker (**FIG. 9**).[54] The carbonate moiety was found to possess a cleavage half-life of 18 h in neutral pH, blood serum conditions, and resultantly the free payload is capable of initiating a bystander effect on neighbouring cancer cells within the tumour microenvironment.[55,56] Thus, Trodelvy has demonstrated efficacy against both Trop2-positive cancer cells and those with considerably less Trop2 expression, with no clear dependence on antigen expression.[57] Here, the selective targeting of the antibody towards target sites is crucial, enhancing delivery of the Trodelvy payload to tumour microenvironments, where the majority of carbonate linker hydrolysis occurs. Prior to this delivery, the carbonate linker is somewhat protected by being bound to the parent mAb, limiting early payload loss.

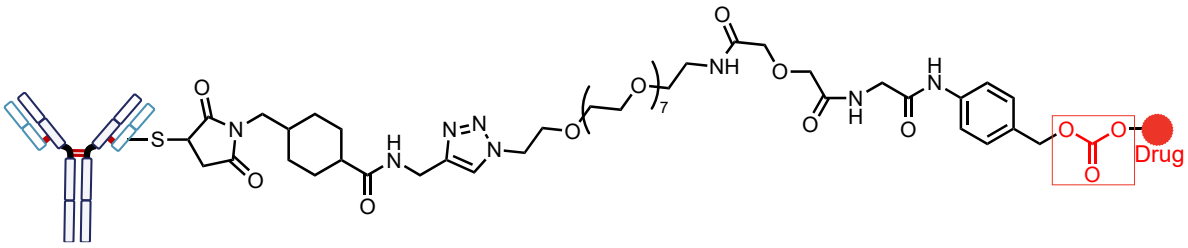


**FIGURE 9.** Full structure of carbonate linker used in Trodelvy, carbonate in red.

Advances in acid-cleavable linker technology include the use of novel acid-sensitive groups, though these are yet to be explored in clinical settings. Silyl ethers have demonstrated stability over 7 days at pH 7.0, however readily degrade at pH 5.0 after a few hours (80% release after 72 h).[58] More recently, cyclic acetals have been explored.[59] Again, in blood plasma conditions, these acetals prove stable, and degradation occurs mostly in acidic conditions. *In vivo* and *in vitro* efficacy studies in mouse xenografts demonstrate an ADC made *via* this linker technology to show comparable efficacies to Kadcyla.

Reducible disulfides (**FIG. 10**) are another commonly employed type of cleavable linker, used in many clinically approved ADCs. Unlike acid-cleavable linkers, disulfides are stable towards most pH conditions encountered in physiological environments.

They can be reduced to release their payloads in the presence of thiol nucleophiles, such as human serum albumin (HSA), which has a buried cysteine thiol, thioredoxin, or cytoplasmic glutathione (GSH). While HSA-induced release is possible, the position of the cysteine residue – within an enclosed hydrophobic pocket with limited solvent exposure – means unspecific blood plasma reduction is unlikely.[60] Meanwhile, GSH concentration in the blood plasma is notably lower than in cell cytoplasm. GSH concentration in healthy cell cytoplasm is within the 1-10 mM range, with tumour cell cytoplasm demonstrating even higher concentrations (up to 1000-fold) due to oxidative stress.[61] Also, there is evidence that protein disulfide isomerases (PDIs) are of importance in tumour proliferation, survival, and metastasis. One of the functions of these enzymes is to catalyse the formation and breakage of disulfide bonds, so these enzymes could also assist in selective disulfide reduction at tumour sites.[62] However, currently there is no evidence showing PDIs assist drug release of reducible disulfide-linked ADCs. Nonetheless, there is a significant difference between the reductive potential of the blood plasma, healthy cells, and tumour microenvironment, meaning selective drug release at tumour sites, through disulfide reduction, is possible. The first literature example of reducible disulfide for ADC synthesis involved a huC242 conjugate, where an investigation into steric hindrance around the disulfide was conducted.[63] Steric hindrance on the payload side of the disulfide demonstrated greater efficacy, whilst less steric hindrance on the linker side was found to be more effective. Increased methylation on the payload side increases hydrophobicity, cell membrane penetration, and decreases reactivity with free metabolite thiols, which enables the payload to pursue the bystander effect more successfully.

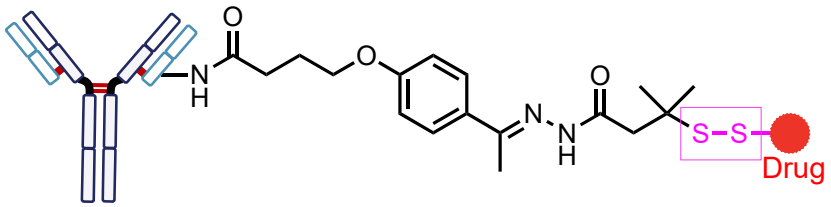


**FIGURE 10.** Linker used in Mylotarg and Besponsa, reducible disulfide in pink.

Both Mylotarg and Besponsa, approved ADCs for leukaemia treatment, both feature the dual-sensitive linker containing acid-labile and reducible disulfide elements. Interestingly, both ADCs have disulfides where methylation occurs on the linker side of the disulfide, though the acid-cleavable hydrazone is also responsible for drug

release in this case. Lorvotuzumab mertansine is currently undergoing clinical trials against a variety of cancer types, featuring a disulfide-cleavable linker as its primary drug release mechanism.[64] In general, much work is being done in using reducible disulfides for targeted drug delivery.[65]

Enzyme-cleavable linkers are the most applied linkers used in current ADCs, with five of the nine currently approved ADCs employing this type of linker – Adcetris, Polivy, Padcev, Enhertu, Zynlonta and Tivdak, all used in the treatment of various types of cancer.

In particular, the Valine-Citrulline (Val-Cit) linker is a widely popularised enzyme-cleavable linker, used in Adcetris, Polivy, Padcev, and Tivdak (**FIG. 11**). These dipeptide linkers target cathepsin B, an intracellular, lysosomal cysteine protease. Cathepsin B has been shown to be overexpressed and overregulated at tumours sites. Tumour cells also release cathepsin B into the extracellular tumour microenvironment, enabling it to exert its proteolysis onto healthy, neighbouring sites. This mode of activity is believed to enable tumours to invade and metastasise more effectively.[66] Val-Cit linkers use the abnormally high cathepsin B levels in tumour sites to their advantage, achieving selective drug release through cathepsin B-mediated linker proteolysis. The first example of a Val-Cit linker in use conjugated Dox to BR96, showing stability in human serum yet release in cathepsin B environments – a 550-fold potency increase was seen in overexpressing cells.[67] The BR96-Dox conjugate developed using the Val-Cit linker also showed superior selectivity and potency than the corresponding hydrazone linked conjugate, further demonstrating the reliable release mechanism mediated by cathepsin B. Due to the steric bulk of the linker and Dox, it was necessary to add a spacer in the form of *p*-aminobenzylcarbonyl (PABC) for efficient Dox release. Thus, conjugates utilising a Val-Cit linker require more careful design consideration in terms of linker and drug size to efficiently fit within the cathepsin B active site. Despite the overall superior systemic stability of these dipeptide linkers, other extracellular enzymes are still capable of eliciting premature drug release, leading to a loss of ADC potency.[68] In addition to cathepsin B, carboxylesterase 1C is capable of proteolysing the Val-Cit linker, though modifying conjugate site and slightly altering the chemical structure of groups neighbouring the Val-Cit moiety can resolve this.[69]

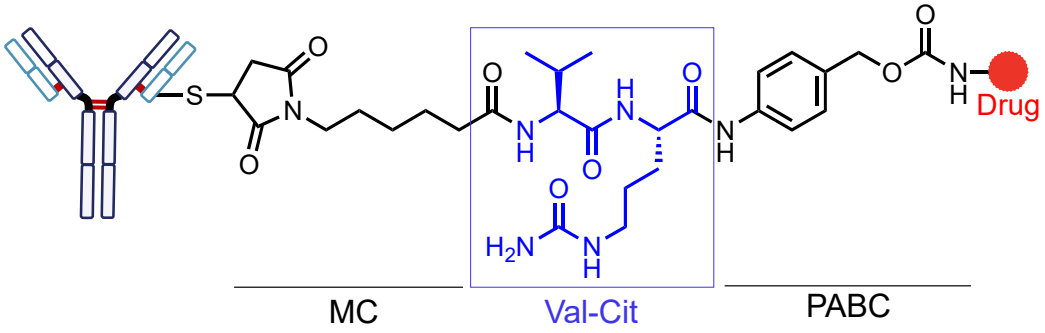


**FIGURE 11.** Val-Cit linker used in Adcetris, Polivy, Padcev and Tivdak.

Other commonly used peptide linkers include Val-Ala, as seen in Zynlonta,[70] and a novel tetrapeptide linker used in Enhertu.[71] These peptide linkers all demonstrate different *in vivo* stabilities and cleavage sites. More recent work has successfully demonstrated the use of arylsulfate motifs as an alternative enzyme-cleavable linkers, focusing instead on targeting lysosomal sulfatases.[72] The primary advantage of these linkers is their increased hydrophilicity, which prevents aggregation, requires no spacer, and enables recruitment of lipophilic payloads. There are also a number of other linker systems utilising the various proteolytic functionalities of the lysosomes,[73] whilst other systems of interest include copper-triggered,[74] near-IR light-mediated,[75] and iron-cleavable linkers.[76] Overall, enzyme-cleavable linkers provide highly effective linkers capable of offering systemic stability partnered with an effective and precise drug release mechanism. These properties mean they will likely remain very popular cleavable linkers in ADCs for the foreseeable future.

#### 1.2.2.2. Non-cleavable linkers

In ADCs composed of non-cleavable linkers, lysosomal proteolytic machinery degrades the mAb and linker to then release the cytotoxic payload. Since non-cleavable linkers have no defined release mechanisms, their stability during circulation is usually very good, and off-site toxicities are reduced in comparison to cleavable linkers. This has been reflected in studies that target the CD70 antigen – ADCs with non-cleavable linkers show better tolerability in comparison to a cleavable Vat-Cit linked counterpart.[77] Other investigations have shown that non-cleavable linkers cannot exert the bystander effect – the resultant linker-payload construct is zwitterionic, so cannot bypass the plasma membrane. In cases where the antigen is expressed heterogeneously, non-cleavable linkers show lower efficacy compared to cleavable linkers. Anti-tumour activity in those heterogeneous cancer types requires

the bystander effect to kill antigen-positive and antigen-negative tumour cells nearby.[78] However, in tumour cells that express the antigen in a more homogeneous manner, this can instead kill nearby healthy cells, causing off-site toxicity. Thus, non-cleavable linkers are more suitable for cancer indications that demonstrate clear disparities in antigen expression between diseased and healthy cells, such as breast cancer.[79]

Hetero-bifunctional crosslinkers commonly used as non-cleavable linkers include maleimidocaproyl (MC), and *N*-succinimidyl-4-(*N*-maleimidomethyl) cyclohexane-1-carboxylate (SMCC) (**FIG. 12**). The reagents consist of a protein-reactive moiety which conjugates onto the antibody, and an attached payload. Whilst MC linkers are thiol reactive at the maleimide moiety, SMCC linkers are commonly supplied as NHS esters, which form amide bonds upon reactions with free amine residues.

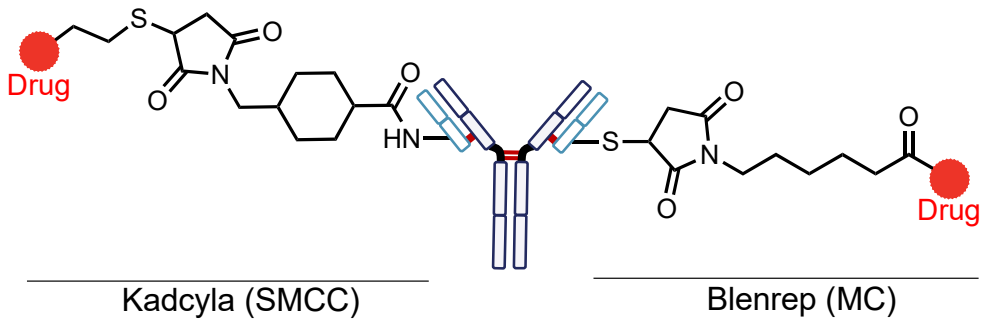


**FIGURE 12.** SMCC and MC linkers used in Kadcyla and Blenrep respectively.

Kadcyla, used for HER2+ breast cancer treatment, uses an SMCC linker to conjugate trastuzumab to a maytansinoid payload.[80] In 2020, Blenrep was approved for the treatment of refractory multiple myeloma, utilising a MC linker to conjugate an auristatin payload onto an anti-B-cell maturation antibody (BCMA) belantamab.[81] Blenrep is the world's first anti-BCMA antibody approved for therapy. Both ADCs do cause reversible vision loss due to unspecific ADC uptake in the eye, however this is a problem shared by the linker-payload combination, rather than the linker or payload individually. Regardless, dose modification appears to prevent or resolve this toxicity, thus the increased therapeutic window of ADCs is of benefit in this indication.

Most ADCs currently in clinical usage or development rely on cleavable linkers due the wider range of applications resulting from their in-built release trigger. It is critical these cleavable linkers are carefully designed to remain stable while in circulation, yet still be capable of effectively releasing their cytotoxic warheads at intended target

sites. Site-dependent induction of chemical release can be difficult to achieve. Only cleavable linkers are capable of the bystander effect, which can be beneficial or detrimental depending on the tumour. Non-cleavable linkers have also resulted in highly efficacious clinically approved ADCs, though it is crucial for the attached pharmacophore to remain unchanged during the lysosome-induced degradation. Thus, antigen and payload selection are crucial factors to consider when deciding on the type of linker to incorporate within an ADC, and the interplay between all three components is hugely responsible for the effectiveness and safety profiles of ADCs.

### 1.2.3. The payload

Extremely toxic payloads can be utilised by ADCs, since the specificity attained by the mAb means off-site binding is less common. These include some of nature's most powerful toxins that would otherwise be too hazardous to use. Additionally, the rate of mAb uptake is only 0.003%–0.008% of injected dose per gram of tumour, so these payloads must be capable of effectively eliciting cell death at very low concentrations.[82] It is also important these payloads are stable in storage, during ADC preparation, and in circulation. Aqueous solubility is also key, to ensure the drug can exhibit its intended biological effects in the cellular environment. Most ADC payloads currently in clinical use have a mechanism of action that blocks cell proliferation, either by affecting mitosis or DNA synthesis.

#### 1.2.3.1. Microtubule inhibitors

Auristatin derivatives are the most popular payloads used in clinically approved ADC design – featuring in Adcetris, Padcev, Polivy, Tivdak, and Blenrep. The first four feature the monomethyl auristatin E (MMAE), whilst the latter uses monomethyl auristatin F (MMAF) (**FIG. 13**). Auristatins are derived from the natural product Dolastatin 10, an anti-mitotic toxin found in the sea hare *Dolabella auricularia*.[83] Initially, Dolastatin 10 itself was used in clinical trials; however significant off-site toxicity limited its use.[84] Structure-activity relationship (SAR) studies revealed modifications to the C-terminal and N-terminal are capable of modulating cytotoxicity and incorporating a linker for mAb attachment, leading to the synthesis of MMAE and MMAF.[85] These two derivatives are largely similar, however MMAE is more membrane permeable, while MMAF is more hydrophilic and less prone to aggregation.[86] Studies have found that free MMAE is more cytotoxic than free MMAF, while conjugated

MMAF shows greater cytotoxicity.[87] MMAE may be favourable for ADCs targeted towards tumours with heterogeneously expressed antigens, where the superior bystander effect of MMAE can exhibit cytotoxicity, whereas ADCs targeting tumours with internalising antigens may benefit from more potent MMAF conjugates. The auristatins cause microtubule aggregation and prevent nucleotide exchanges to inhibit tubulin polymerisation, arresting mitosis and causing apoptosis.[88] Despite the continued clinical use of the auristatins, MMAE and MMAF are still imperfect payloads. In solution, half of the free drug is locked in an inactive conformation, severely limiting cytotoxicity towards tumour cells.[89] MMAE and MMAF are also substrates of multi-drug resistance protein 1 (MDR1), which mediates the efflux of toxins from the tumour cell, increasing resistance to ADCs.[90]

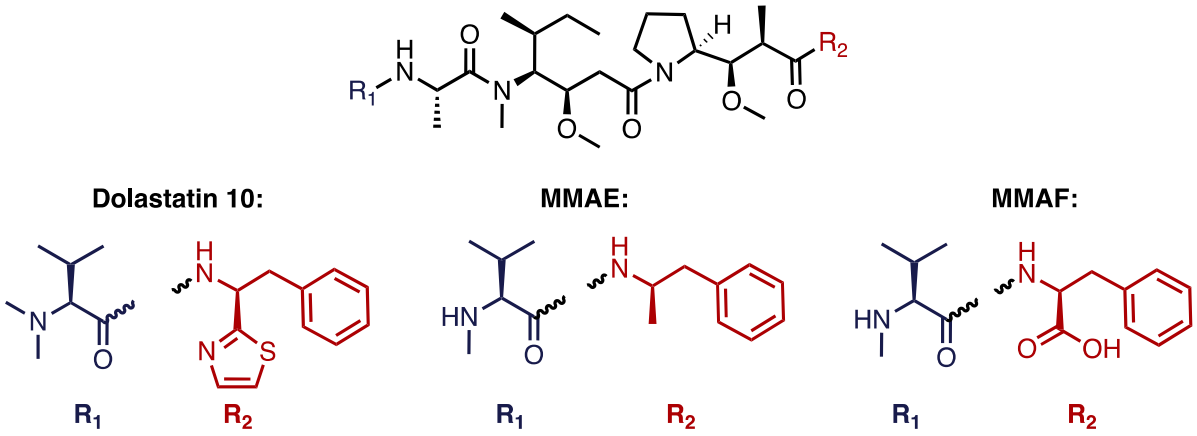


**FIGURE 13.** Chemical structures of dolastatin 10, and the derived payloads MMAE (used in Adcetris, Padcev, Polivy, and Tivdak) and MMAF (used in Blenrep).

Maytansinoids are another class of microtubule inhibitor used as ADC payloads. Like the auristatins, the maytansinoids are extremely potent natural toxins, derived from maytansine isolated from the plant *Maytenus ovutus*. Conjugation of maytansine analogues to mAbs increased specificity, reduced side-effects, and revived clinical interest (**FIG. 14**).

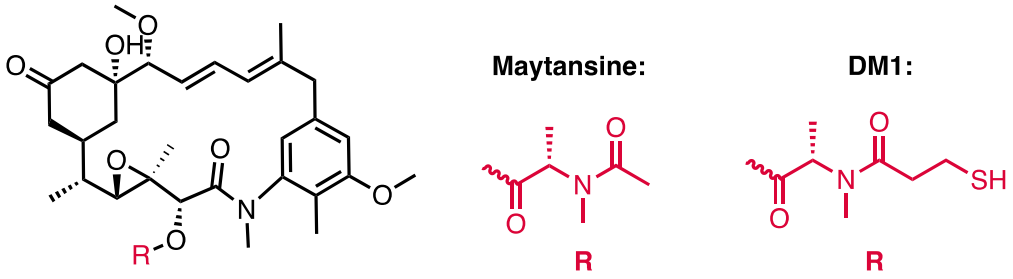


**FIGURE 14.** Chemical structures of maytansine, and DM1 used in Kadcyla.

The derivative mertansine (DM1) was employed as the payload in Kadcyla. DM1 is often metabolised by the liver to *S*-methyl DM1, which may be the active drug form.[91] The maytansinoids operate by suppressing the dynamic instability of microtubules by binding to the microtubule ends, which prevents the growing and shrinking of these polymers necessary to initiate mitosis.[92] The addition of DM1 in Kadcyla also disrupts intracellular trafficking in breast cancer cells, which does not occur when only the parent mAb is used.[93] Problematically, DM1 is also a substrate of MDR1 which mediates the efflux of DM1 from the tumour cell. MDR1 overexpression is a common resistance mechanism in many types of cancers, with Kadcyla no exception.[94] DM1 conjugated to trastuzumab *via* more hydrophilic PEG linkers have been shown to somewhat overcome MDR1-mediated resistance, though remain substrates of MDR1 and remain vulnerable to this resistance mechanism.[95]

#### 1.2.3.2. DNA inhibitors

Calicheamicin are DNA disruptors isolated from the bacterium *Micromonospora echinospora*, employed in the ADCs Mylotarg and Besponsa. The calicheamicin are extremely promiscuous toxins that do not differentiate even between different organisms.[96] Attachment to a mAb attenuated this toxicity to make it suitable for anti-cancer purposes. Binding of the ADC to its target antigen delivers the payload intracellularly, where it moves into the nucleus. The calicheamicin binds to the minor DNA groove, generating a 1,4-dehydrobenzene-diradical species. This species is capable of breaking the double-stranded structure of DNA, arresting the cell cycle, and leading to apoptosis.[97] Like the microtubule inhibitors, calicheamicin is also susceptible to MDR1-mediated resistance, reducing efficacy of ADCs including these payloads.[98] This could be associated with the initial poor benefit-risk ratio of Mylotarg, which led to its temporary withdrawal from the clinical market.

#### 1.2.3.3. DNA cross-linkers

The pyrrolobenzodiazepine (PBD) class of cytotoxins were initially discovered in *Streptomyces*, with anthramycin, the first identified PBD antibiotic, shown to possess antitumour properties.[99] Subsequent investigations demonstrated that the PBD compound binds to the minor groove of DNA, selectively binding to 5'-purine-guanine-purine sequences. Mechanistically, this binding occurs by forming a covalent bond between the exocyclic amino group of the guanine base, and an electrophilic position

on the PBD.[100] Cross-linked DNA then triggers a cascade of processes leading to cellular death. Whilst anthramycin itself is too toxic to be used therapeutically, synthetic PBD dimers have demonstrated more suitability as ADC payloads, such as tesirine utilised by Zynlonta (**FIG. 15**).[101,102]

PBD dimers consist of two monomeric PBD units connected *via* a flexible propyldioxy linker. These dimers span six base pairs and can covalently cross-link guanine residues on opposing strands of the DNA.[103] Importantly for overcoming resistance mechanisms, PBD dimers do not significant distort the structure of DNA, and so are not easily detected by DNA repair mechanisms.[104] Thus, PBD dimers can persist and kill proliferating cells, whilst evading excision resistance mechanisms seen in tumour cells against other cross-linking agents, such as *cis*-platin.[105] Tesirine also cross-links DNA faster than other traditional DNA cross-linker agents such as *cis*-platin and is effective against tumours with low antigen counts due to its significant potency. Additionally, tesirine demonstrated activity against both solid and haematological cancers, which is beneficial for its versatility as an ADC warhead, and it also has a short half-life. Whilst this somewhat impacts its ability to engage in bystander killing, it does help to limit off-site toxicity and prevent accumulation of the drug due to systemic loss. PBD dimers continue to be of significant interest as one of the newest class of ADC warheads, with multiple other PBD-containing ADCs under active clinical investigation.[106,107]

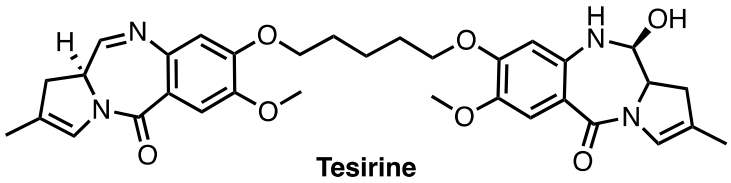

**Tesirine**

**FIGURE 15.** Chemical structure of the PBD dimer tesirine used in Zynlonta.

### 1.2.3.4. Topoisomerase inhibitors

Rather than directly targeting DNA, other payloads aim to inhibit enzymes required for successful DNA replication, such as Topoisomerase I. The topoisomerases work synergistically on DNA supercoils to enable processes leading to replication and transcription. Topoisomerase I cleaves a single strand, and covalently binds it, forming an enzyme-DNA intermediate. The free, non-cleaved strand is held by non-covalent bonds near the enzyme, which then passes this non-cleaved strand through the

introduced single-strand break. Topoisomerase I then ligates the two strands to reseal the DNA, removing negative supercoils, releasing tension, and enabling DNA or RNA polymerase to execute their functions.[108] Therefore, targeting topoisomerase I could enable tumour cell death by causing excessive DNA supercoiling and preventing normal cellular functions. Enhertu and Trodelvy all use topoisomerase I inhibitors as their payloads (**FIG. 16**) and have found use as ADCs suitable for treatment of cancers that other therapies have failed to successfully treat.

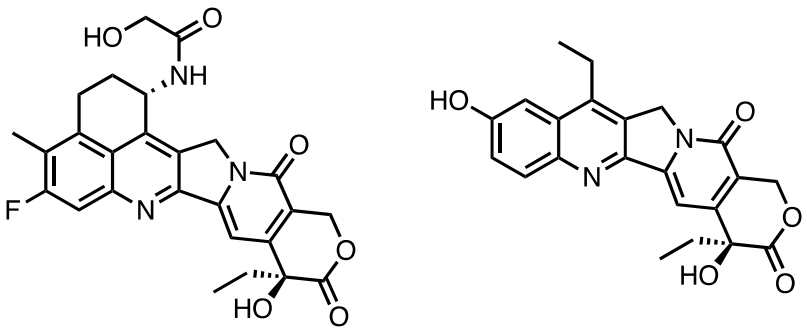


**DXd** **SN-38**

**FIGURE 16.** Chemical structures of DXd (used in Enhertu and Tivdak) and SN-38 (used in Trodelvy).

Enhertu is an anti-HER2 ADC similar to Kadcyla, featuring the same mAb trastuzumab. However, there is significantly less tumour resistance against Enhertu, and, unlike Kadcyla, Enhertu is even effective at treating HER2+ gastric cancer. It is believed the exatecan-derived payload DXd is not a suitable substrate for MDR1, preventing efflux and tumour resistance.[109] DXd is also less hydrophobic than the DM1 payload used in Kadcyla, meaning it was possible to equip Enhertu with more equivalents of DXd (DAR of 8.0), which leads to more effective enzyme inhibition and more apoptosis. Thus, Enhertu offers a new avenue of treatment to patients that have developed resistance against other forms of therapies.

Other topoisomerase I inhibitors include prodrugs. Irinotecan has shown efficacy against a wide range of cancers, with metabolism by human carboxylesterases producing a highly active, potent metabolite SN-38. SN-38 is several magnitudes more cytotoxic than its parent irinotecan, even at lower concentrations.[110] Trodelvy targets the Trop-2 antigen located on a wide variety of solid tumours and delivers SN-38 as the cytotoxic payload.[111] Like Enhertu's DXd, the lower hydrophobicity of SN-38 meant

higher equivalents of drug could be added onto the mAb without negatively affecting pharmacokinetic properties. Thus, topoisomerase I inhibitors offer increased scope of payloads in comparison to the traditional targets, and this is only more recently being fully exploited in ADC development.

## 1.3. Bioconjugation strategies

mAbs, linkers, and payloads have undergone investigations which have helped select components suitable for use in ADCs. However, site-selective strategies to attach the linker-payload construct onto the mAb itself remain relatively unoptimised. Bioconjugation techniques should aim to produce ADCs with an average drug-to-antibody ratio (DAR) between two-to-four – lower DARs provide poor cytotoxicity, whilst higher DARs tend to lead to hydrophobicity, rapid clearance, and lowered efficacy.[112] Heterogeneity is a significant challenge, affecting pharmacological profiles, safety, and batch-to-batch reproducibility. Thus, the next generation of ADCs must utilise improved site-selective conjugation to create homogeneous constructs with greater potential for clinical advancement.

### 1.3.1. Native antibody modification

A conjugation process which can be conducted on native mAbs is the most desirable approach. Methodologies must be developed to act within the accessibility, polarity, or surrounding environment of the desired conjugation site on the native mAb.

#### 1.3.1.1. Cysteine modification

The low abundance of cysteines (~1.7%) in mAbs means selective conjugation to these residues is often possible. Cysteine residues are commonly found within hydrophobic environments and play crucial roles in many catalytic processes.[113] As a result, cysteine residues are popular target sites for protein modification in general. Cysteine residues, crucially, contain a highly nucleophilic thiol sidechain with a pKa of ~8. Thus, in typical physiological conditions (pH 7), approximately 10% of the thiol exists as a thiolate, increasing its nucleophilicity. Most cysteine residues in mAbs natively exist within disulfide bonds, contributing towards stabilising the structure of the antibody, so reduction of accessible disulfide bonds is necessary prior to conjugation. Commonly used reagents to achieve this include tris(2-carboxyethyl)phosphine (TCEP) or dithiothreitol (DTT). Following reduction, the addition of electrophilic reagents can achieve modification. Eight of the current eleven

approved ADCs utilise cysteine conjugation, exemplifying its usefulness as a target site.

Maleimides have been widely used for cysteine conjugation since their conception in the 1950s (**FIG. 17A**).[114] Maleimides have been shown to demonstrate fast kinetics and exceptional cysteine-selectivity. In particular, the structural features of the maleimide make it ideal for thiol-specific reactions *via* a Michael-type addition – the two carbonyls are electron-withdrawing, increasing susceptibility towards nucleophiles, and the 5-membered ring structure induces ring strain, which is released upon thiol addition.[115] The succinimide ring also contains a point of attachment on the nitrogen. These useful properties have made maleimides used in all current cysteine-conjugated ADCs, where the maleimide binds directly to the cysteine residue, and a linker-payload moiety is attached to the succinimide nitrogen. Another popular thiol-reactive reagent, iodoacetamide, has also been commonly used for cysteine modification, irreversibly forming a thioether; however, these reagents suffer from cross-reactivity with other residues such as histidine, methionine, lysine, glutamic acid, and tyrosine,[116] which limits its suitability for usage in ADC applications.

Despite widespread use in ADCs, maleimides have shown to be somewhat unstable *in vivo*, as the thiosuccinimide linkage can undergo retro-Michael addition that causes drug loss, increasing off-site toxicities and decreasing efficacy.[117] Despite this, Adcetris, approved for non-Hodgkin's lymphoma (nHL), successfully used the first maleimide conjugation strategy in clinical settings,[118] and multiple other ADCs have followed since. Strategies to improve upon this instability have been extensively explored in literature. Self-hydrolysing maleimides introduce a basic diaminopropionic acid (DPR) neighbouring the maleimide ring, so intramolecular catalysis of the thiosuccinimide ring hydrolysis is possible.[119] The hydrolysed product is not susceptible to elimination seen in conventional maleimides, increasing serum stability. However, in murine models, efficacy varied amongst different mouse strains; no treatments were durable enough to prevent tumour recurrence, and the DPR-maleimide ADC was not initially homogeneous, requiring purification to isolate species with a DAR of 4.0. Later work showed that protonation of the amine can also accelerate hydrolysis through inductive electron-withdrawal, and it is this feature that primarily drives increased self-hydrolysing rates.[120] Stronger electron-withdrawing

groups such as sulfones, trifluoromethyls, and alcohols increase the rate of ring-hydrolysis over retro-Michael β-elimination. Maleimides remain interesting compounds due to their ease of synthesis, thiol reactivity, and stability in bioconjugation conditions.

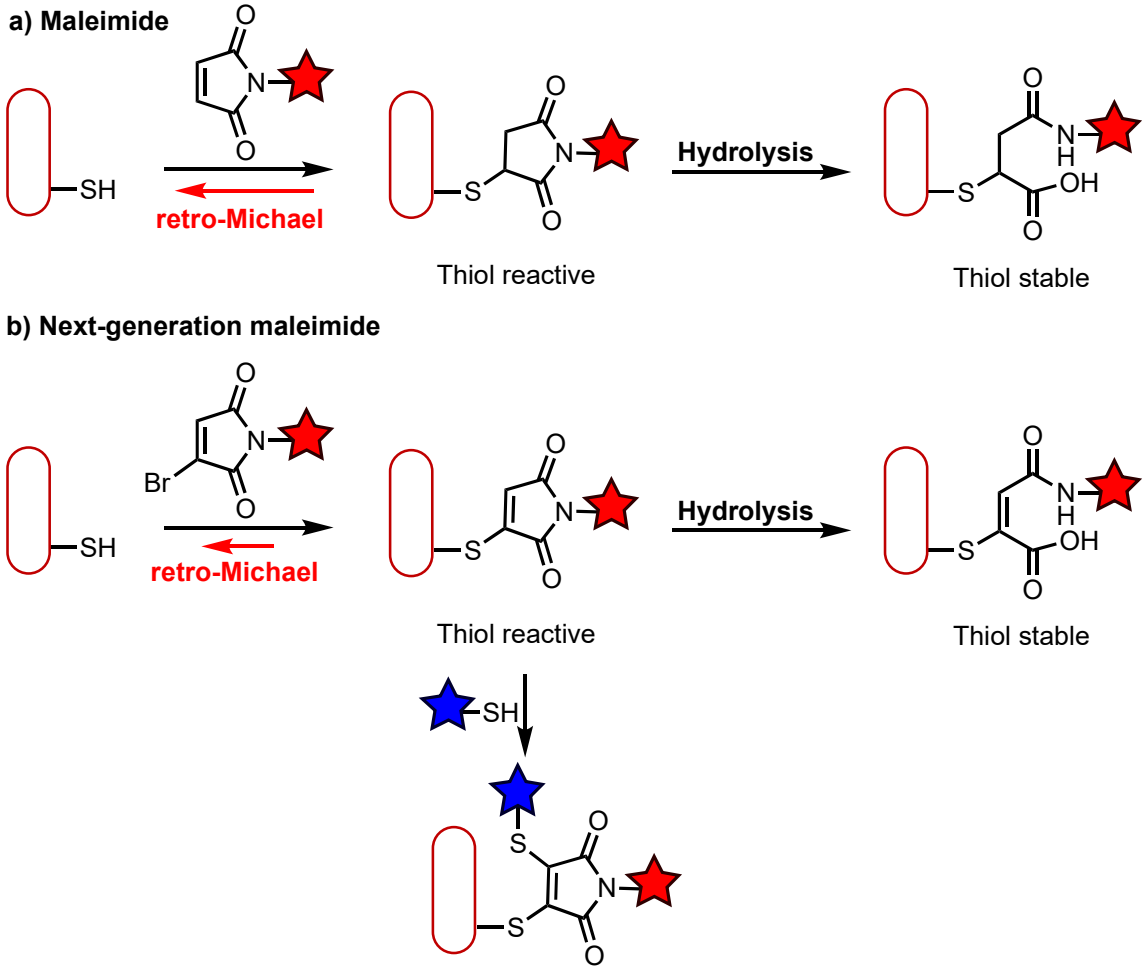


**FIGURE 17. A)** Cysteine modification with traditional maleimide**. B)** Next-generation bromomaleimide for cysteine modification.

Other developments include the Baker, Caddick, and co-workers reports on next-generation maleimides (NGMs) (**FIG. 17B**),[121] which include an additional bromine leaving group across the maleimide double-bond. These NGMs enabled a highly selective modification of cysteine thiol in a rapid and efficient manner, undergoing completion in 1 h with as little as 1 equivalent of NGM.[122] A second bromine on the maleimide double-bond enables substitution with a second thiol for further modification. Addition of a large excess of thiol enables reversible covalent cysteine modification,[123] whilst hydrolysis of the thiomaleimide to the maleamic acid, by incubating the conjugate at elevated pH and temperature, prevents reversibility, and

hence prevents retro-Michael addition.[124] NGMs have shown more success in ADC applications as re-bridging agents, discussed later.

Bernardes *et al.* investigated the use of carbonylacrylic reagents for irreversible cysteine bioconjugation, where conjugation on reduced trastuzumab produced thioether conjugates with a DAR of 8.0 (**FIG. 18**).[125] Similarly to maleimides, their mechanism of action involves a Michael addition to an acrylic group to form a thioether bond. Antigen recognition for breast cancer receptor HER2+ remained, however no *in vivo* studies were conducted. High DARs can lead to poor efficacy *in vivo* due to increased hydrophobicity and propensity for aggregation, resulting in rapid clearance rates and less payload delivery. However, hydrophilic linkers have shown higher DARs can maintain efficacy.[126]

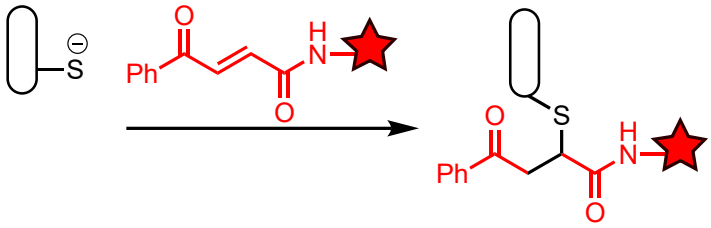


**FIGURE 18.** Carbonylacrylic reagents for cysteine modification.

3-arylpropionitriles (APN) were reported by Wagner and co-workers as another cysteine-selective reagent for ADC synthesis (**FIG. 19**).[127] The reagent contains an internal alkyne group, which selectively reacts with cysteine thiol to form an acrylonitrile product. DARs of 3.8 were possible. The attachment between the cysteine residue and the APN was found to be stable in human serum, and in the presence of excess thiol only 8% degradation was observed over 120 h. The APN platform demonstrates properties suitable for cysteine bioconjugation on mAbs, with good selectivity, stability, and functionalisation possible.

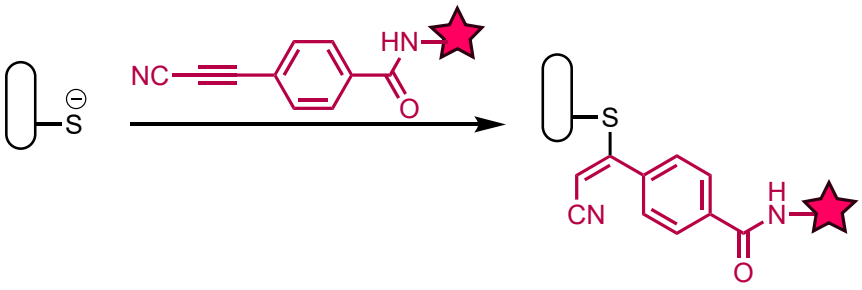


**FIGURE 19.** 3-arylpropionitrile reagents for cysteine modification.

Hypervalent iodine reagents have also been of interest for cysteine modification, as they enable selective attachment in short timeframes, whilst enabling the direct installing of a terminal alkyne for subsequent functionalisation. Waser and co-workers explored ethynylation as a strategy for modification of cysteine thiol, using ethynylbenziodoxolone (EBX) reagents (**FIG. 20**).[128] In small molecule studies, optimised EBX derivatives could achieve complete labelling with cysteine in 15 minutes at 37 ºC, in impressive 99% yields. Some side-reactivity with tyrosine and arginine residues were seen in these studies and were also seen in small amounts on non-reduced trastuzumab. Nonetheless, the major product on reduced trastuzumab involved a cysteine-modified species, with 97% conversion and a DAR of 4.4 seen when using 16 equivalents of reagent. The inserted terminal alkyne then underwent successful click chemistry to introduce a fluorophore.

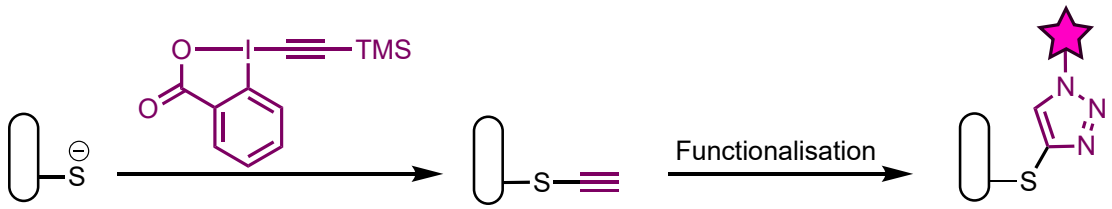


**FIGURE 20.** EBX reagents for cysteine modification.

Transition metals have rarely been used for bioconjugation purposes, due to problems with handling, storage, and stability, however work by Buchwald and co-workers reported the use of stable, benchtop palladium (II) complexes for selective cysteine bioconjugation (**FIG. 21**).[129] Reagent synthesis is straightforward, and their application on trastuzumab produced *S*-arylated products in just 0.5 h, with a DAR of 4.4. The aryl component included the drug vandetanib, thus the strategy enabled the rapid generation of functional, cytotoxic ADCs in a rapid manner. It is important to carefully design these Pd complexes, as ligand choice impacts reactivity, C-S reductive elimination, selectivity, and stability. Additionally, purification of any resultant conjugates should be thorough, as leftover Pd cause unwanted effects in biological settings – the group managed to remove 94% of excess Pd.

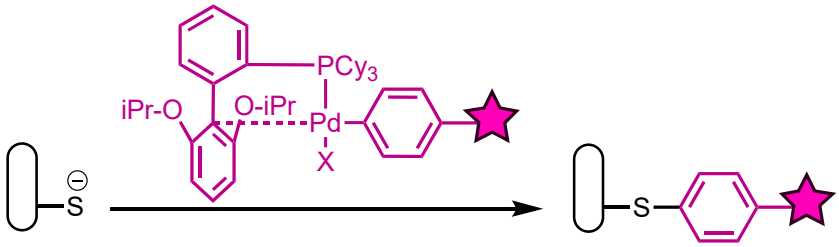


**FIGURE 21.** Pd(II) complexes for cysteine modification.

In efforts to improve water solubility of cysteine bioconjugates, phosphonamidite-based reagents were more recently developed and Hackenberger and co-workers (**FIG. 22**).[130] These reagents consisted of an ethynyl alkyne handle for thiol labelling, an easily modifiable alcohol, and an amine connected to a linker. Staudinger-phosphonite reactions enabled one-pot synthesis of ethynylphosphonamidite derivatives where hydrophilicity could be easily controlled by the addition of PEG groups on the alcohol position. Using Adcetris as a comparison ADC, the group used an ethynlphosphonamidite compound with diethylene glycol and vedotin to selectively modify cysteine residues on brentuximab. The phosphonamidite demonstrated far superior solubility, almost 2-fold improved due to the glycol moiety, compared to the maleimide-vedotin construct. Additionally, the resultant ADC showed similar cytotoxicity effects as Adcetris, however, crucially 90% of the phosphonamidite-linked ADC was still connected to the MMAE payload after seven days in serum, compared to just 30% in Adcetris after three days.

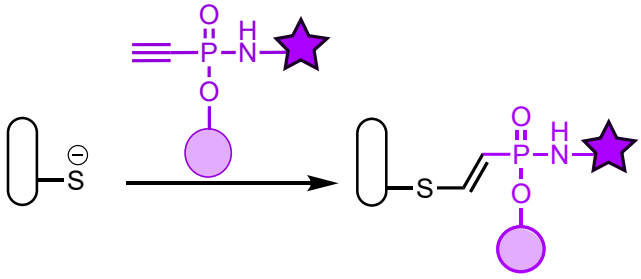


**FIGURE 22.** Phosphonamidite reagents for cysteine modification.

In addition to those discussed, other notable native cysteine modification reagents include allenamides,[131] bicyclobutane amides,[132] Ellman's reagent with subsequent thiol addition,[133] heteroaromatic sulfones,[134] and vinyl sulfones.[135] Though the application of these particular modification strategies for ADC synthesis have not been fully explored *in vivo*, they regardless demonstrate interesting properties and mechanisms of actions (**FIG. 23**).

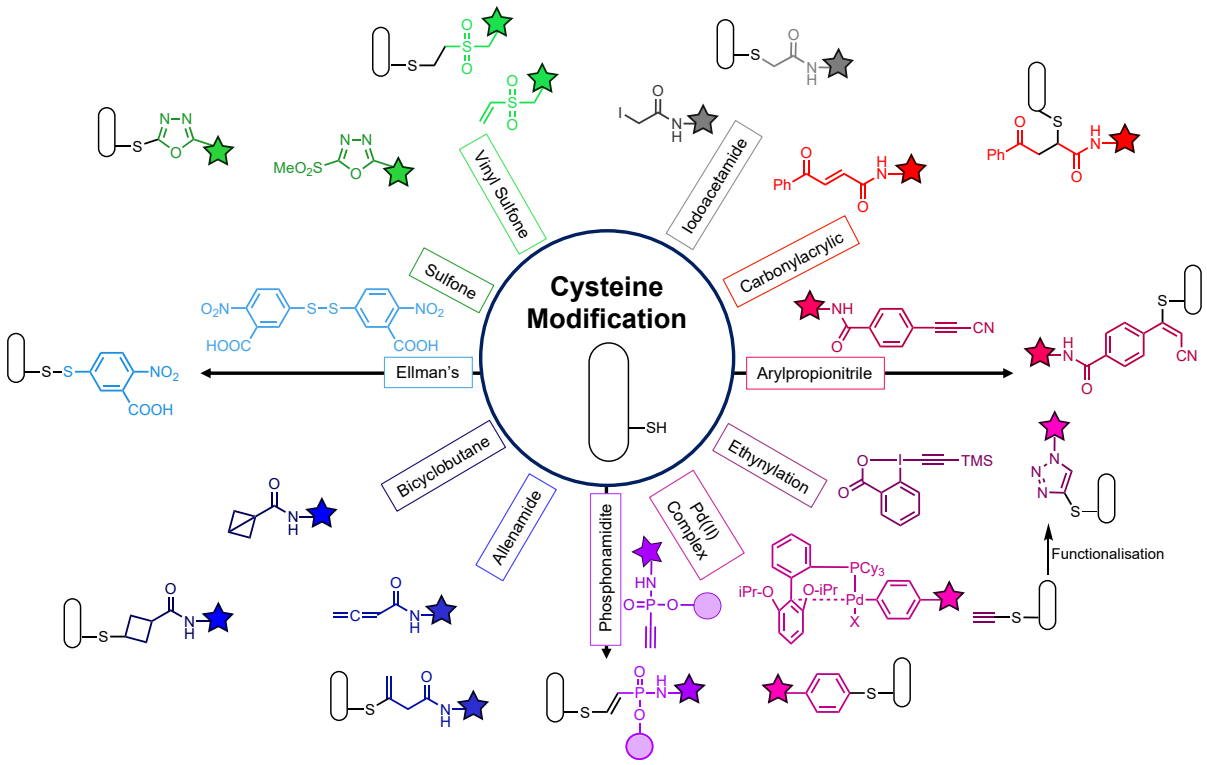


**FIGURE 23.** Summary of cysteine conjugation reagents.

Despite the undoubted selectivity benefits, current cysteine conjugations remove the structural stabilising effect provided by native disulfide bonds. While selectivity can be controlled, homogeneity is not guaranteed, since drug loadings can vary depending on the extent of disulfide reduction and reagent reactivity – as shown, many current strategies do not completely modify all available eight cysteine residues in a typical mAb and produce varying DARs. Stability in the presence thiol-containing metabolites found in serum can also significantly vary, and such instability may only present itself in patient clinical trials.

### 1.3.1.2. Disulfide re-bridging

Disulfide re-bridging can provide homogeneous constructs whilst retaining the stabilising effect of interchain disulfide bridges. These reagents work on the same principle as cysteine modification – selective targeting of cysteine residues, with the reagent containing two electrophilic, thiol reactive groups to enable re-bridging of the disulfide. Whilst not completely replicating the structural features of a native disulfide bond due to differences in size and bridge length, re-bridging does help stabilise the tertiary structure in comparison to mono-cysteine modification. Non-covalent interactions are also crucial in maintaining structure.

Bis-sulfones are one of the earliest examples of disulfide re-bridging reagents, introduced first in the 1990s for this purpose.[136] Mechanistically, the bis-sulfone undergoes an *in situ* elimination of one sulfone leaving group to produce an $\alpha,\beta$-unsaturated carbonyl, which then undergoes Michael addition with a thiol nucleophile, forming a thioether bond. The addition-elimination process repeats for the addition of the second thiol, thus re-bridging the adjacent cysteine residues. Godwin and co-workers were the first to explore the use of bis-sulfones for ADC synthesis (**FIG. 24**).[137] They successfully generated bis-alkylated, MMAE-loaded ADCs with an average DAR of 2.8, which they investigated in *in vitro* and *in vivo* experiments. These bis-sulfone reagents demonstrated good stability against HSA, a common thiol-containing metabolite responsible for payload loss in maleimide-conjugated ADCs and maintain the same DAR over 120 h of incubation. Interestingly, the group also explored a Fab conjugate with a DAR 1.0 alongside the DAR 2.8 full ADC – both showed good tumour-cell killing, however the conjugates showed less potency than the free MMAE drug and required high dosage (three 20 mg/kg doses). Later work showed that the MMAE was lost in circulation due to poor linker stability – PEGylation of the linker was necessary to protect from early loss, and the resultant bis-sulfone ADCs showed greater potency than Adcetris.[138]

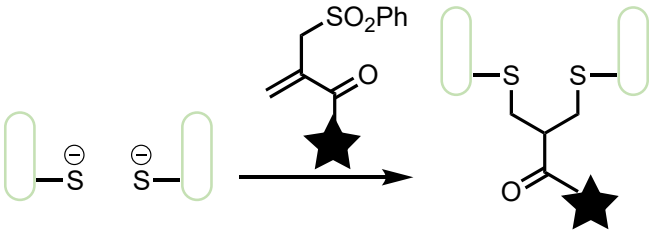


**FIGURE 24.** Bis-sulfone intermediate reagent for disulfide re-bridging.

As discussed previously, NGMs enable selective thiol modification, and disubstituted derivatives enable conjugating re-bridging.[139] Whilst they demonstrate improved efficacy compared to classical maleimides, thiol exchange reactions can still reduce serum stability, as seen in bromomaleimides (**FIG. 25**).[140] The addition of a second leaving group across the maleimide double bond in dibromomaleimides is necessary for this re-bridging action. A relevant ADC was synthesised using dithiomaleimides with a PEG linker attached to MMAE. Stabilisation of the maleimide by hydrolysis to the maleamic was achieved by hydrolysis in pH 8.4 for 72 h, a time-consuming step. The resultant ADC produced DARs of 3.9, and demonstrated *in vitro* and *in vivo*

antiproliferative effects in only HER2+ cell lines.[141] Later work introduced electron-withdrawing C-2 linkers onto the maleimide nitrogen, and this optimised the post-conjugation hydrolysis step to 1 h at pH 8.5, with stability seen in physiological and lysosomal pH.[142] Similar work by Jackson and co-workers compared maleimide conjugates to those prepared with NGMs, using identical payloads and linkers, and found NGM-prepared ADCs demonstrated a more sustained tumour suppression than conventional maleimide counterparts. These re-bridged NGM ADCs also showed improved pharmacokinetics, efficacy, and lower toxicity, underlining the benefit of homogeneity.[143]

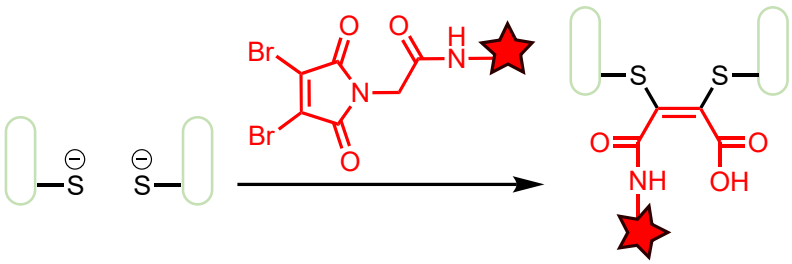


**FIGURE 25.** NGMs for disulfide re-bridging.

Chudasama, Baker *et al.* also investigated pyridazinediones (PDs) (**FIG. 26**).[144] PDs work in a similar manner to NGMs, where two addition-elimination reactions lead to re-bridging of the disulfide bond. PDs are stable towards hydrolysis and are less susceptible to retro-Michael additions. Additionally, PDs have four possible sites for modification, including the electrophilic attachment sites and two additional sites on the two nitrogen atoms. This enables the synthesis of dual-functionalised PDs. Sequential click modifications offered a 4-loaded ADC containing Dox and a fluorophore.[144] Similar reductions in cell viability were observed *in vitro* for the ADC to that of trastuzumab for HER2+ cells, however slightly more off-site toxicity against HER2- cells was also observed. The PD scaffold later produced a homogeneous, 4-loaded PD- (MMAE), and this conjugate found very good blood serum stability, and a selective and sustained *in vivo* tumour reduction against HER2+ cells, however significantly high doses (20 mg/kg) are used in comparison to typical studies.[145] Wang and co-workers also developed more hydrophilic linker-payload constructs, by functionalising a PD with a branched PEG structure and a DM1 toxin, reducing the need for the addition of an organic co-solvent during ADC preparation.[146] Additionally,

PDs were incorporated with TCEP, to enable a one-pot reduction-re-bridging conjugation strategy with a single reagent.[147]

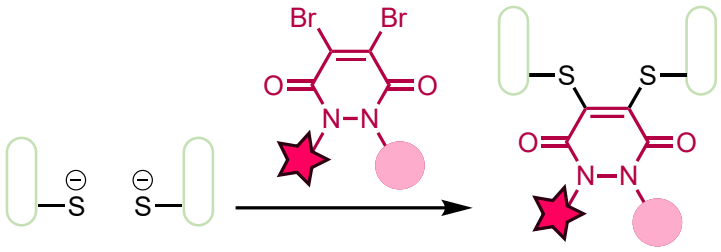


**FIGURE 26.** PDs for disulfide re-bridging.

The C-Lock disulfide bridge developed by Shi *et al.* has also shown promise (**FIG. 27**).[148] A disubstituted quinoxaline core and a MMAF derivative are conjugated to a 5T4-targeting mAb (ZV05).[149] Electrophilic bromine sites enable substitution by thiols to form thioethers. An adjacent pyridine ring acts as an electron-withdrawing group, and the inductive effects enables increased reactivity of the C-Lock reagents towards cysteine residues. Distribution of C-Lock-ADC demonstrated localisation mostly at tumour sites. ADC internalisation and *in vivo* efficacy was significant more pronounced in highly expressing 5T4 cell lines, particularly breast (3 mg/kg dose) and pancreatic (5 mg/kg dose) cancers.

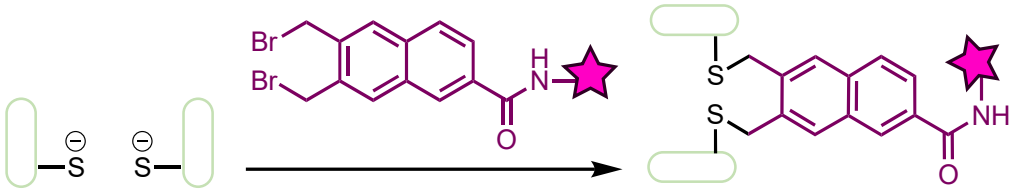


**FIGURE 27.** C-Lock for disulfide re-bridging.

More recent work includes the bis(vinylsulfonyl)piperazines (BVP), developed by Jiang and co-workers (**FIG. 28**).[150] There are two vinylsulfonyl groups attached on opposite ends of a piperazine scaffold. Similarly to vinylsulfones, a site-selective Michael addition of a cysteine thiol enables thioether formation. These BVP reagents were shown to enable re-bridging of trastuzumab with species of average DAR 2.0 produced. The BVP ADC showed similar internalisation, cytotoxicity, and antigen affinity in HER2+ cells as Kadcyla at lower drug loadings. Importantly, they demonstrated less cytotoxicity towards HER2- cells than Kadcyla.

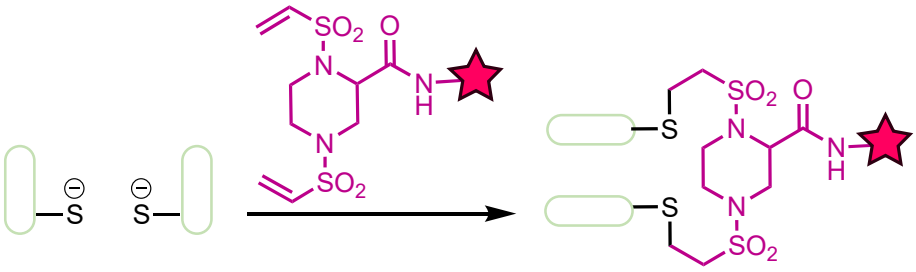

**FIGURE 28.** BVPs for disulfide re-bridging.

Divinylpyrimidines (DVP) synthesised by Spring and co-workers also utilise a Michael addition to a vinyl group. Initial work showed these reagents could re-bridge trastuzumab within 2 h at 37 ºC (**FIG. 29**).[151] The major product was the re-bridged DAR 4.0 antibody species, however small amount of half-antibody formation was also observed. Lower concentrations and equivalents of DVP addition could reduce this unwanted formation. Biological evaluation against HER2+ cell lines showed the DVP ADC maintained antigen affinity and later *in vivo* studies showed a tolerable and efficacious response in breast cancer models.[152]

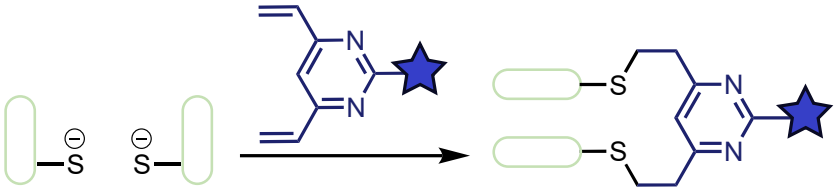

**FIGURE 29.** DVPs for disulfide re-bridging.

Other novel approaches include using platinum (II) complexes (**FIG. 30**).[153] These form strong Pt-S bonds with the cysteine thiols, preventing instability issues seen in C-S bond forming re-bridging reagents. On Fab, DARs of 1.9 were achieved, with 95% conjugation efficiency in 2 h at 37 ºC. Unlike other re-bridging agents, which are typically limited to four attachments, these Pt(II)-linked ADCs could have up to eight attachments – aggregation due to drug hydrophobicity could be controlled by inserting longer PEG chains, or by using more hydrophilic drugs. Various anti-cancer mAbs were used to synthesise ADCs using these Pt(II) linkers, and all demonstrated improved cytotoxicity and retained all binding affinity.

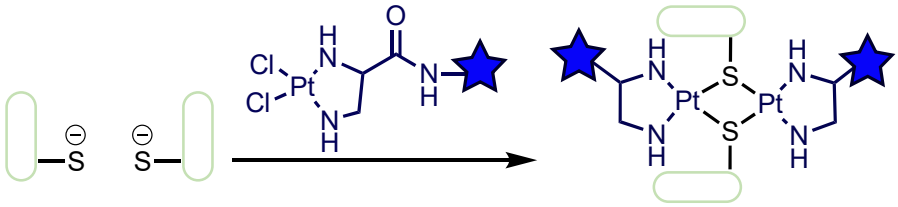

**FIGURE 30.** Pt(II) complexes for disulfide re-bridging.

Emerging strategies that demonstrate potential for the synthesis of future ADCs include Baker and co-workers dual-reactivity disulfide bridging reagents (**FIG. 31**).[154] This method uses a halothioester to form an initial bridging moiety on a Fab fragment. The resultant bridge consists of a stable thioether linkage, and a labile thioester group. The authors explored the use of hydrazine as a ligating nucleophile, which can then be functionalised with an aldehyde; and introduced a fluorophore-labelled disulfide on the freed thiol using a disulfide reagent.

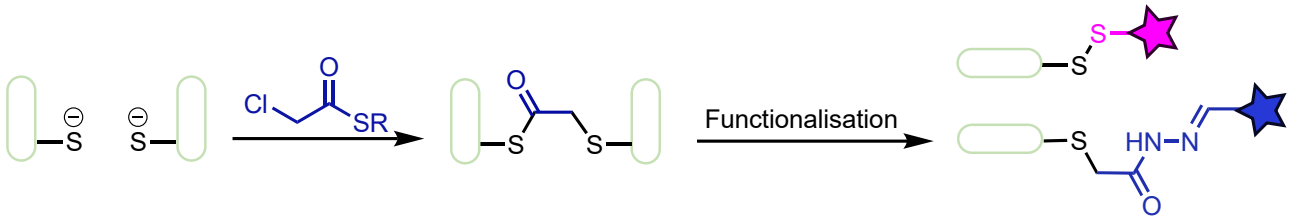


**FIGURE 31.** Halothioester for disulfide re-bridging and functionalisation.

In addition, Wagner and colleagues also developed a re-bridging variation of their APN compounds,[155] whilst other strategies that are yet to undergo further biological evaluation for ADC contexts include thiol-ynes,[156] and azirines.[157] Whilst no approved ADC utilises disulfide bridging, it is undoubtedly an area of immense interest due to selectivity, stability, and functionalisation (**FIG. 32**).

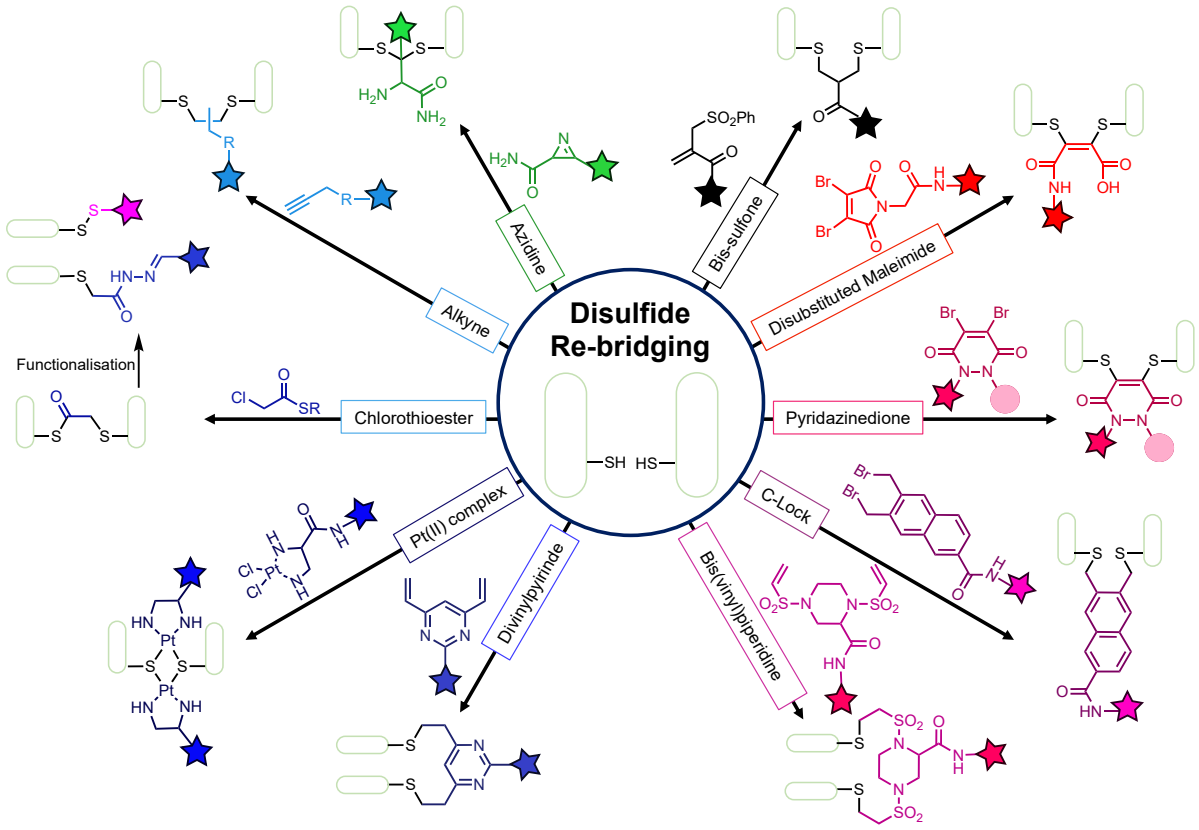


**FIGURE 32.** Summary of relevant disulfide re-bridging strategies.

However, disulfide scrambling and half-antibody formation commonly affects homogeneity of disulfide-conjugated ADCs,[158,159] increasing difficulties of preparation through disulfide modification. Whilst the impact of a non-native re-bridge can be minimised, it still ultimately perturbs the tertiary structure in comparison to native disulfides.

### 1.3.1.3. Lysine modification

Lysine conjugation is a very popular strategy for protein conjugate synthesis. Lysine contains a nucleophilic, primary amine sidechain, with pKa ~10.5. In physiological conditions, lysine is commonly protonated as the ammonium form. Common reagents for lysine modification include acylating agents, which can form stable amide bonds, resulting in stable bioconjugates. Such reagents include iminoboronates,[160,161] sulfonyl fluorides,[162] isothiocyanates,[163] diazonium salts,[164] and aldehydes.[165] For ADC synthesis however, lysine modification with these reagents can result in heterogeneous mixtures. A typical $IgG_1$ mAb has ~80 solvent accessible lysine residues,[166] 90% of all conjugation occurs on 8-10 lysine residues that demonstrate preferrable kinetics for reactivity – it is difficult to achieve selective and controlled

modification of identical lysine sites.[167] ADC heterogeneity could contribute towards poor pharmacokinetics, efficacy, and safety profiles. Thus, whilst there are plentiful lysine modification reagents for general protein bioconjugation, site-selective strategies successfully explored for ADC synthesis are more limited, demonstrated by the lack of recently approved lysine-conjugated ADCs.

*N*-hydroxysuccinimide (NHS) esters were developed in the 1960s for acylation of proteins, and have widespread use and commercial availability (**FIG. 33**).[168]. They contain an activated acyl group that readily reacts with amines to generate stable amide bonds, between pH 7.0-9.0, in short timeframes. Notably, Mylotarg, Kadcyla, and Besponsa utilise lysine conjugation, and all utilise NHS esters. However, all three of these ADCs are heterogeneous. Mylotarg was temporarily withdrawn from the market due to significant off-site toxicity, and this could be related to its heterogenous preparation.[169] Kadcyla preparations contain species with DARs varying between 0-8, with ~40 different lysine residues modified.[170,171] NHS esters also exhibit cross-reactivity with other nucleophilic amino acid residues, including histidine, serine, threonine, and tyrosine, and are prone to hydrolysis.[172]

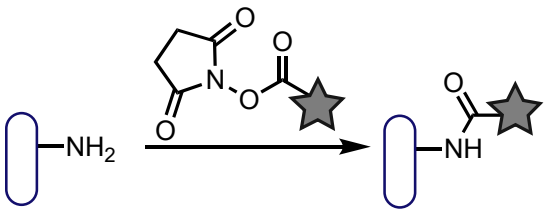


**FIGURE 33.** NHS esters for unselective lysine acylation.

Despite NHS ester shortcomings, recent work by Mendelsohn and co-workers used NHS esters to generate more homogeneous, lysine-modified ADCs. Their strategy focused on using an IgG affinity peptide containing an NHS ester.[173,174] Through non-covalent interactions, the peptide localises towards a particular region of the mAb. This brings the NHS ester closer to specific lysine residues, which can then enable amide formation by NHS substitution. Their affinity peptide mediated regiodivergent functionalisation (AJICAP) platform generated ADCs with DARs of 1.9 in 91% conversion. Crucially, the conjugation method was conducted at pH 5.5, for 1 h at 22 ºC. Lower pH's can minimise hydrolysis and the reactivity of other nucleophilic amino acid sidechains by ensuring they remain protonated. In addition to this work, other

affinity-guided modifications have proved promising for controlling lysine site-selectivity (**FIG. 34**).

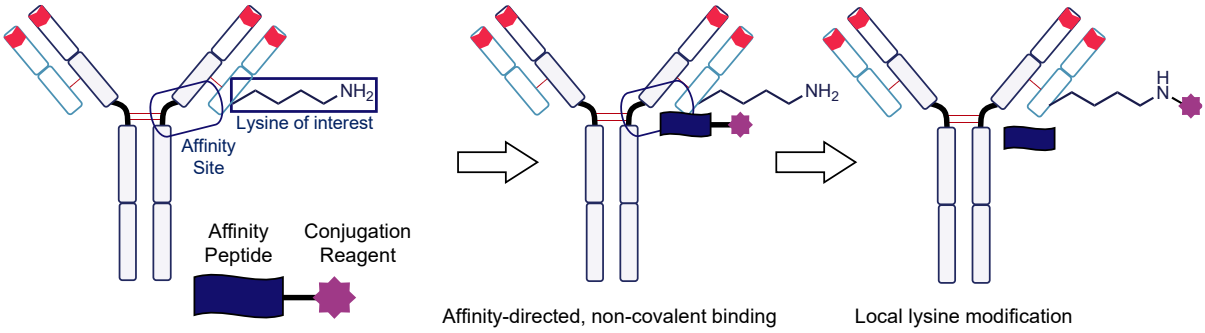


**FIGURE 34.** Simplified schematic of affinity-guided lysine modification.

Xiao and co-workers developed their own peptide-based protocol, where they inserted 4-fluorophenyl carbamate onto their peptide sequence (**FIG. 35**).[175] Upon bringing carbamate and targeted lysine residues in proximity, cross-linking occurs to form a stable urea bond. A trastuzumab-fluorophore conjugate could be generated in this manner, requiring 48 h at 37 ºC, pH 8.5 for 98% conversion, and modification of a single lysine residue.

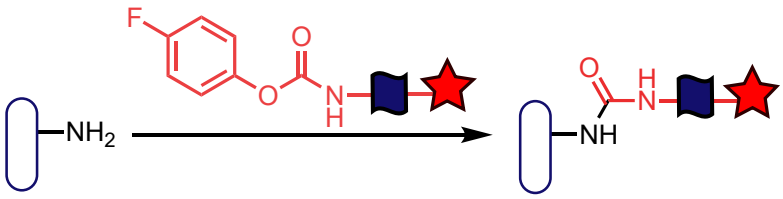


**FIGURE 35.** 4-fluorophenyl carbamate reagent for affinity-guided lysine modification. Blue flag = affinity peptide.

Bilgicer and co-workers discovered that indole-3-butyric acid (IBA) binds to a nucleotide-binding domain (NBD) on the Fab fragment, with high affinity.[176,177] Lam *et al*. explored this on a mAb by developing 5-fluoro-2,4-dinitrobenzene (FDNB) peptide with bioorthogonal functionalities (**FIG. 36**).[178] SnAr occurs between the lysine primary amine and a fluorine leaving group on the FDNB peptide, forming an amine bond. An ADC could be synthesised using 2.5 equivalents of the FDNB peptide, in 15 minutes at 22 ºC. An NHS strategy produced 6.2 lysine modifications, whereas this affinity-based method modified 1.6 lysine residues – whilst site-selectivity could not be guaranteed due to a small number of lysine residues neighbouring the NBD, it was possible to control the extent and the region of modification.

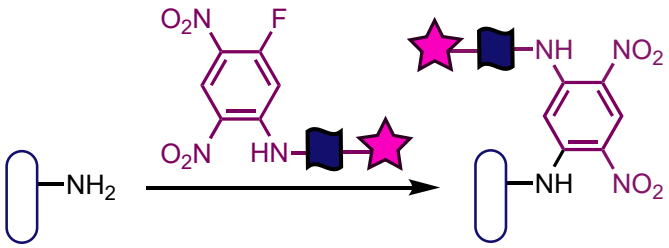


**FIGURE 36.** 5-fluoro-2,4-dinitrobenzene reagent for affinity-guided lysine modification. Blue flag = affinity peptide.

Small molecule approaches towards achieving similar controlled and selective lysine modification often rely upon finding exceptionally reactive lysine residues with activated reagents of matching reactivity. Cellitti and co-workers discovered that nearby histidine and aspartic acid residues could help distinguish lysine residues from each other.[179] On trastuzumab Fab, a fluorophenyl ester (**FIG. 37**) could selectively modify a single lysine residue located close to histidine and aspartic acid residues – mutation of any of these residues resulted in a loss of modification. Flow chemistry could be used to minimise any leftover selectivity issues, and they observed complete conversion to the singly modified species. Analogous NHS esters continued to produce heterogeneous mixtures.

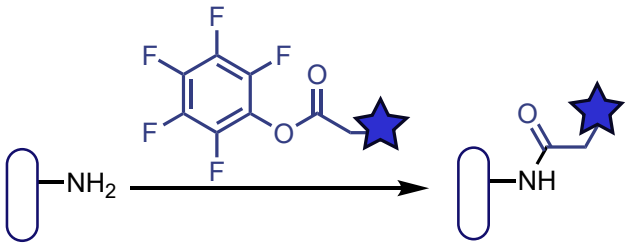


**FIGURE 37.** Fluorophenyl esters for lysine modification.

Lysines in hydrophobic pockets show unique properties, with a lower pKa (~6.0) compared to solvent-exposed lysines. The mAb h38C2 contains one such hydrophobic pocket,[180] and Rader and co-workers utilised $\beta$-lactam handles for modification of a lysine residue located within this pocket (**FIG. 38**).[181] Firstly, they developed dual-variable domains by combining the Fv of h38C2 with trastuzumab. MMAF attached to a $\beta$-lactam was introduced, with the lysine amine breaking the $\beta$-lactam ring structure to form an amide bond. A single lysine residue – the h38C2 lysine – was modified, giving species of DAR 2.0, after 4 h at 22 ºC, pH 7.4. The group also

used methylsulfonyls for modification of the same residue in separate investigations, providing the hydrophobic pocket lysine to be uniquely reactive.[182]

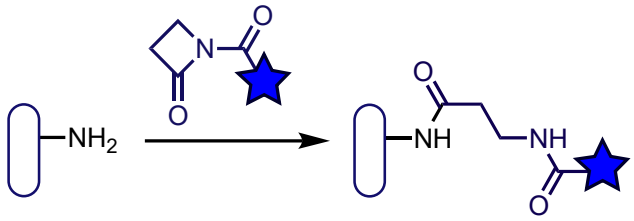


**FIGURE 38.** $\beta$-lactam handles for lysine modification.

Computer-assisted design identified a sulfonyl acrylate that forms a favourable chair-like conformation with lysine on trastuzumab (**FIG. 39**).[183]. This enabled selective addition to a single lysine on the LC, in 2 h at 37 ºC, pH 8.0. On smaller proteins with free cysteine residues, the sulfonyl acrylate favoured lysine modification. Residue-selectivity on trastuzumab was not determined, and only 1 eq. of reagent was added which could lead to incomplete conversion. Following amine formation, an alkene functional group could be further modified *via* the aza-Michael addition of nucleophiles.

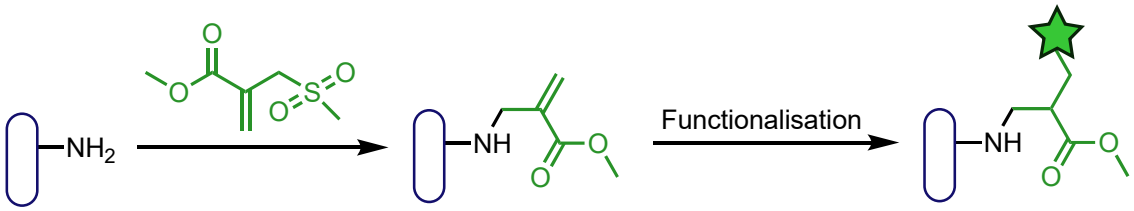


**FIGURE 39.** Sulfonyl acrylates for lysine modification, followed by functionalisation.

Aldehydes are popular bioconjugation reagents due to their electrophilicity, and ability to engage in a wide range of bioorthogonal reactions.[184] Their reactions with amines produce imines. Rai and co-workers utilised aldehydes in a similar manner for ADC synthesis.[185] They developed a phospha-Mannich reaction with benzaldehyde and triethylphosphite (**FIG. 40**) – first, reversible imine formation occurred on the lysine residues, and this is followed by irreversible and chemoselective substitution by nucleophilic alkylphosphites. On trastuzumab, the resultant aminophosphites are stable and formed over 8 h at pH 7.8. Late-stage functionalisation by oxime ligation occurred over 14 h, requiring a total of 22 h to achieve a functional ADC with DAR 0.92. It is worth noting that low DARs are unfavourable for effective ADCs *in vivo*, as insufficient payloads are delivered.[186] The phospha-Mannich ADC does provide greater cytotoxicity than trastuzumab, and greater selectivity than free Dox.

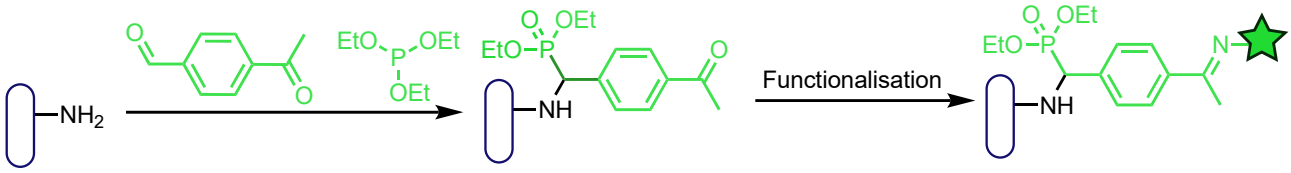


**FIGURE 40.** phospha-Mannich strategy for lysine modification, using aldehydes.

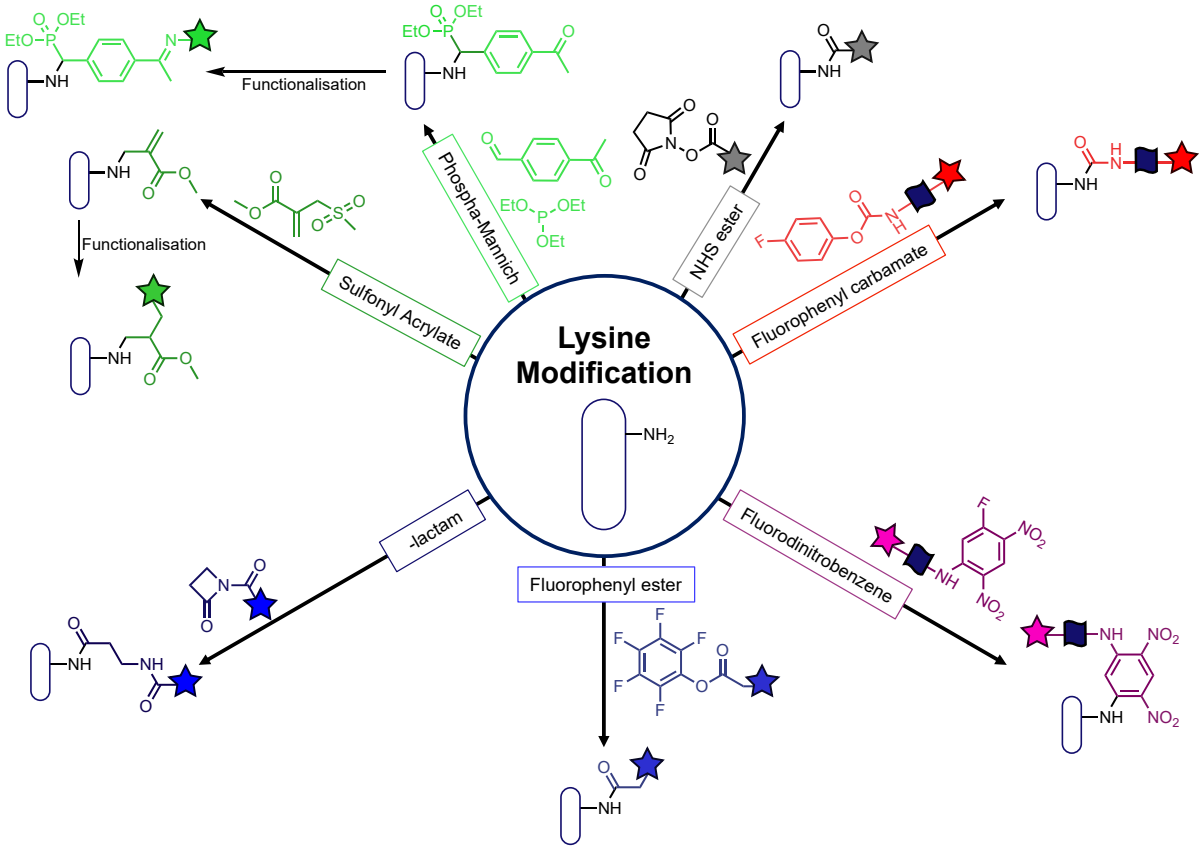


**FIGURE 41.** Summary of relevant lysine modification reagents. Blue flag = affinity-peptide.

In addition to those discussed (**FIG. 41**), we have covered multiple other site-selective lysine modification strategies in a review of the area.[187] Due to the difficulty of modulating reagent reactivity, many existing procedures on native mAbs depend upon the protein environment and identifying lysine residues with unique behaviour. Small molecule strategies to achieve similar conjugation efficiency, convenience, and homogeneity to that of cysteine conjugation are still widely sought after for the generation of homogeneous lysine-modified ADCs.

### 1.3.1.4. Residues of emerging interest

While cysteine and lysine are the most modified residues for protein bioconjugation in general, there has been work in modifying other native mAb residues, such as

tyrosine, arginine, histidine, and tryptophan. Bioconjugation of these residues for ADC synthesis is in early stages, but they represent new chemical modification opportunities.

Tyrosine contains an amphipathic phenol sidechain. The bulky aromatic ring is hydrophobic, but there is also a polar, nucleophilic alcohol.[188] Tyrosine residues are not typically solvent exposed, which can make targeting them more difficult, however this could enable good homogeneity. Barbas and co-workers reported the use of 4-formylbenzene diazonium hexafluorophosphate (FDBP) for tyrosine modification. Initially, the work was done on model proteins,[189] and the group later explored this technique for an ADC (**FIG. 42**).[190] Diazo coupling occurs between the phenol and the diazonium salt on the *ortho* position of the phenol ring, forming a diazo bond. FDNP contains a free aldehyde, which can then be functionalised – Barbas *et al.* used oxime addition to insert an aplaviroc drug. They tested the protocol on various $IgG_1$ mAbs and found DARs varying between 0.5-2.0. The major modification site was the same tyrosine residue in these ADCs, indicating good site-selectivity, but drug loading varied between different mAbs. Whilst low DARs are unfavourable for anti-cancer ADCs, Barbas and co-workers' tyrosine-conjugated ADCs were successful for the neutralisation of HIV-1 virus, and the ADCs were generally more potent than the naked, parent mAbs.

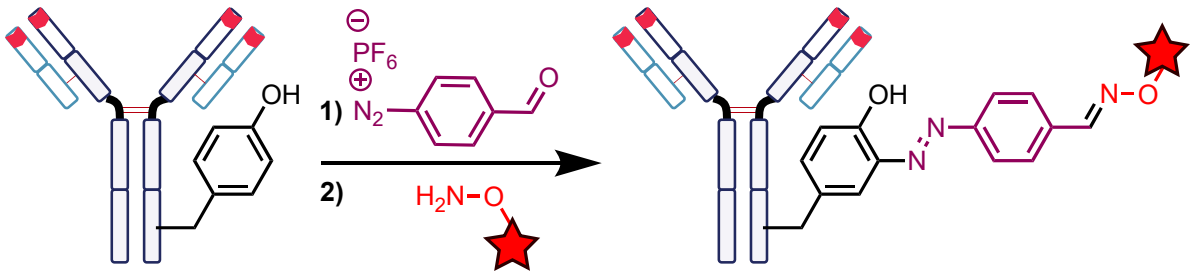


**FIGURE 42.** Tyrosine conjugation *via* diazonium salts.

Wagner and co-workers investigated arginine as a potential modification site, which is a residue not commonly explored for protein bioconjugation since there are often more tractable sites (**FIG. 43**).[191] Arginine residues are quite common the mAb surfaces, second only to lysine in terms of solvent accessibility.[192] The lower number of arginine residues (~40 compared to ~80 lysine) could enable better control of homogeneity. The Maillard reaction between the guanidine group of arginine and 4-azidophenylglyoxal (APG) formed an imidazole ring in 6 h, enabling later

bioorthogonal functionalisation through the introduced azide group. It is worth noting that up to eight different arginine sites were modified, though peptide mapping analysis confirms arginine modification over lysine modification. The resultant Maillard products were stable in blood serum for five days. As equivalents of APG added was increased, the DAR also increased, with 20 equivalents resulting in DARs of 5.3 – in this study, different conjugate preparations used different APG equivalents, producing varying DARs. Whilst not homogeneous or site-selective, APG-mediated arginine modification nonetheless demonstrates the possibility of arginine modification for ADCs.

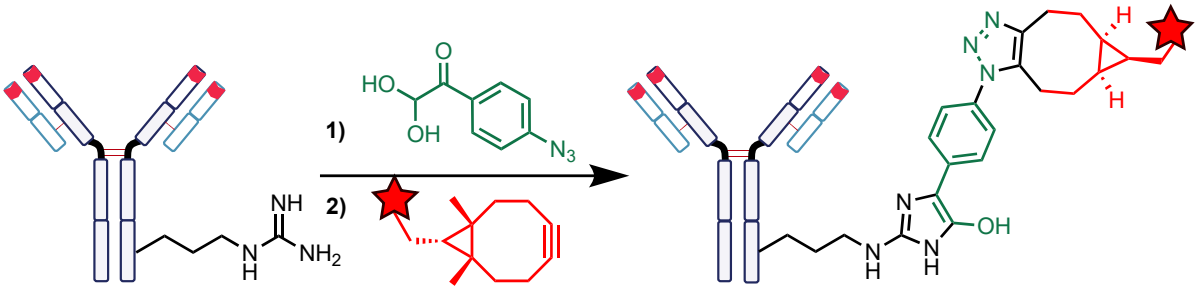


**FIGURE 43.** Arginine conjugation *via* the Maillard reaction with a glyoxal compound.

Epoxide-based reagents have shown themselves to be useful for the modification of histidine residues. Histidine residues are interesting for protein modification, as they contain an electron-deficient heteroatomic imidazole sidechain with nucleophilic properties. This sidechain has a low pKa (~6.0), so at acidic and physiological pH, the imidazole may be more reactive than other nucleophilic sidechains such as cysteine or lysine.[193] Rai and co-workers reported a linchpin-directed modification strategy, where they synthesised linchpin probes, containing an epoxide, a spacer, and an aldehyde (**FIG. 44**).[194] The aldehyde forms reversible imines with various lysine amine groups – when the epoxide is brought close to a targetable histidine residue, an irreversible nucleophilic substitution occurs, opening the epoxide ring and forming a C-N bond. Once bound to the target site, the aldehyde can then be functionalised by oxime addition. Studies on trastuzumab Fab and MS/MS analysis confirmed modification of histidine over lysine, occurring in 16 h in a 37% conversion. A trastuzumab-DM1 ADC was synthesised, and this ADC offered similar cytotoxicity to Kadcyla. The HER2+ selectivity of the more homogeneous histidine-conjugated ADC was improved, with less toxicity seen in HER2- cells compared to Kadcyla.

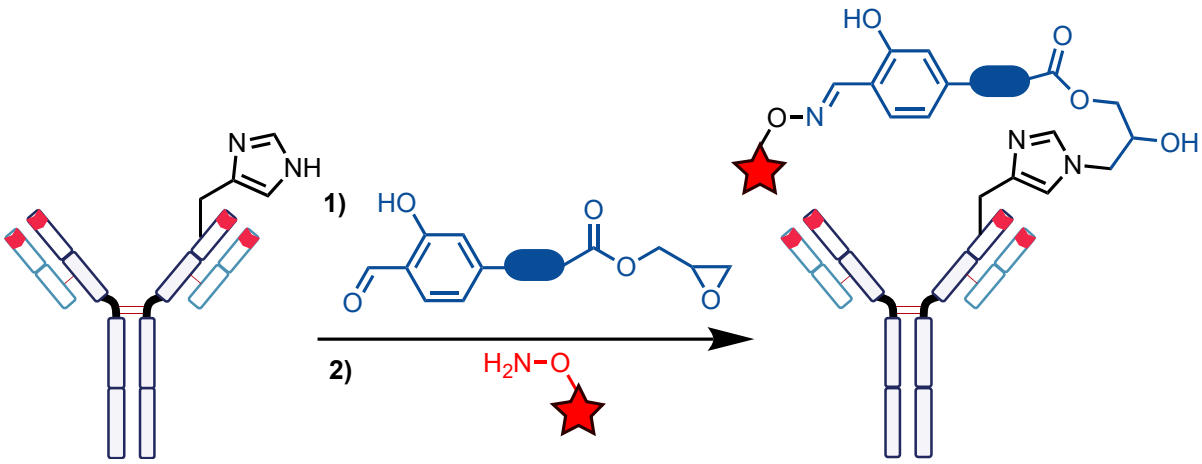


**FIGURE 44.** Histidine conjugation *via* epoxide ring opening, with a linchpin compound.

Finally, tryptophan presents an intriguing site for modification. Tryptophan is the least expressed residue on typical proteins (~1% abundance), and is often found buried within the protein structure, exhibiting little surface accessibility. The indole moiety offers unique reactivity as it is less reactive than typical nucleophilic residues, so the primary method to achieve modification includes C-H activations.[195] One such example includes Kanai and co-workers work on using a radical-based strategy for the conjugation of gold nanoclusters onto trastuzumab's tryptophan residues (**FIG. 45**).[196] They used a 9-azibicyclo[3.3.1]nonan-3-one derived radical, keto-ABNOH, alongside TEMPO+ for activation. Compared to their previous work, this novel strategy prevented over-oxidation and nitrosylation, whilst also improving upon aqueous stability and storability of the conjugation reagents.[197] They synthesised a keto-ABNOH derivative with an azide handle, and successfully conjugated on the tryptophan indole within 1 h at 22 ºC in pH 6.8 buffer. An overnight SPAAC reaction could then introduce their gold nanocluster. An analogous lysine-modified conjugate was also synthesised – the tryptophan conjugate produced cluster-to-antibody ratio (CAR) of 0.66, whilst the lysine conjugate produced CARs of 2.75. Problematically, the HER2+ binding affinity of the tryptophan conjugate was 4-times lower than naked trastuzumab, as the modified tryptophan residue is near the CDR. A similar issue was seen on the lysine conjugate due to promiscuous modification, though this conjugate had a greater tendency for aggregation too. Whilst suitable for imaging purposes the authors are aiming towards, loss of any HER2+ affinity would be detrimental to ADCs.

Nonetheless, their work provides the potential benefits of chemistry not previously explored on antibodies, namely C-H activation chemistry.

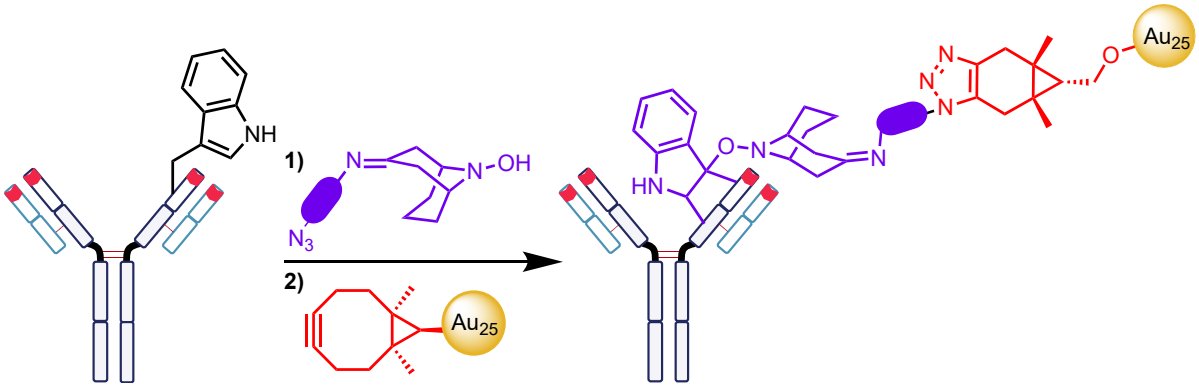


**FIGURE 45.** Tryptophan conjugation *via* C-H activation with a ABNOH compound.

### 1.3.2. Engineered antibody modification

Recombinant antibody engineering has become a common technique for producing ADCs of increased homogeneity, involving the insertion of a targetable moiety onto mAbs (**FIG. 46**). Insertion sites are chosen to enable accessibility and efficient expression of the engineered mAb and ensure no structural or functional impairments. Antigen binding, internalisation, and structural integrity remain unchanged.[198]

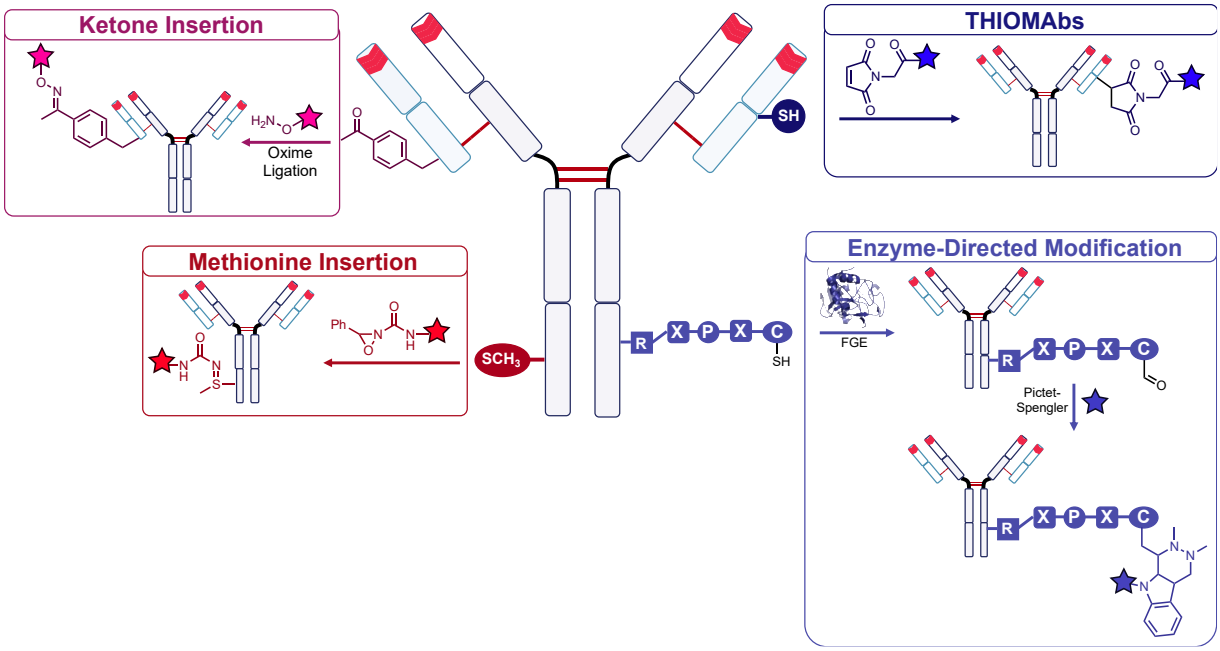


**FIGURE 46.** Scheme of antibody engineering strategies, including introduction of cysteine residues (THIOMAB), insertion of methionine, insertion of non-canonical moieties such as aldehydes, and enzyme-directed modification.

#### 1.3.2.1. Cysteine engineering

Site-selective conjugation onto engineered cysteines can provide homogeneous constructs, since these residues are already low in natural abundance in therapeutic $IgG_1$ mAbs.[199] Junutula *et al.* developed the THIOMABs, which engineered two additional cysteines onto trastuzumab.[200,201]

The non-cleavable maleimide linker selectively reacts with cysteine, conjugating together MMAE or drug maytansinoid 1 (DM1) onto the mAb – a positively charged, partially accessible environment was optimal to ensure linker stability and maximise efficacy for both drugs. An average DAR 2.0 was observed, with a homogeneity of 92.1%. The THIOMABs showed greater HER+ selectivity, tumour-killing potency, and less immunogenicity compared to a heterogenous model. Tolerability is also improved in the THIOMABs, likely because of increased conjugate stability, less free cytotoxic payload, and less off-target binding. However, there is still some retro-Michael addition which causes payload transfer to thiol-containing metabolites, somewhat decreasing serum stability.[38] This was largely due to the highly solvent accessible site, which enabled maleimide-thiol exchange. Future generations of THIOMABs utilised a different engineering site, which surrounded the inserted cysteine into the LC, into an environment with positively charged amino acid residues. This environment enables a faster succinimide ring hydrolysis, thus increasing stability.[198]

More recent THIOMABs form cysteine conjugates through disulfide linkages or NGMs, which have improved upon serum stability.[202,203] Lehar *et al.* developed a THIOMAB-AAC composed of a *S. aureus* mAb and a protease-cleavable linker to rifamycin.[204] This AAC has proceeded into Phase 1 clinical trials – *in vivo*, a single dose demonstrated a reduction in bacterial load comparable to three days of vancomycin treatment.[205]

Whilst they are not as nucleophilic as cysteine residues, methionine residues offer other interesting properties as potential conjugation sites. They are uncommon, hydrophobic, and are often buried within proteins. At physiological pH, methionine residues are therefore difficult to modify with traditional electrophiles, which could offer avenues for more site-selective modification, especially if engineering can introduce more available methionine sites. Chang and co-workers reported a redox-activated chemical tagging (ReACT) method for methionine modification, using oxaziridine

compounds.[206] The methionine sulfur engages in a nucleophilic attack of the oxygen or nitrogen atom of the oxaziridine, which then triggers N-O bond cleavage. Intramolecular rearrangement produces a sulfimide linkage with inactivated by-products released. By generating trastuzumab Fab conjugates with inserted methionine residues *via* the THIOMAB platform, Chang and co-workers could selectively and quantitively modify these residues within 10 minutes, using an oxaziridine carrying a click handle. The click handle could engage in bioorthogonal click chemistry, enabling loading of the cytotoxin Dox with DAR 1.0 or 2.0, depending on number of methionine insertions.

#### 1.3.2.2. Non-canonical amino acids

Non-canonical amino acids (nCAAs) are non-proteogenic insertions used to achieve site-selectivity, offering functionality orthogonal to the canonical residues. These insertions are genetically encoded through the development and use of bespoke antibody expression systems. Axup *et al.* investigated the mutagenesis of alanine into *p*-acetylphenylalanine (pAcPhe) on trastuzumab.[207]

An oxime click ligation attaches a non-cleavable MMAE payload, in a >95% yield with a DAR 2.0. *In vitro* cytotoxicity demonstrated the ADC has similar cytotoxicity against HER2+ cells to unconjugated DM1, but less toxicity against HER- cells, confirming conjugate stability, since DM1 release now only occurs upon internalisation to HER2+ target cells.

Jackson *et al.*[208] compared the oxime-ADC and the Junutula and co-workers THIOMAB, demonstrating the stable oxime bond had improved *in vitro* stability, with minimal payload transfer to HSA over 10 days, though *in vivo* efficacy remains similar and more recent THIOMABs have improved serum stability. Also, azide insertions enable strain-promoted (SPAAC) or copper-catalysed (CuAAC) azide-alkyne cycloaddition, and these ligated-ADCs have demonstrated potent anti-cancer activity.[209, 210]

Selenocysteine is widely regarded as the 21$^{st}$ naturally occurring amino acid and is analogous to cysteine in many ways; however, selenocysteine features a selenol sidechain with a lower pKa (~5.0), where the sulfur atom seen in cysteine thiol is replaced by selenium.[211] As a result, selenols are more likely to be deprotonated at

physiological and acidic pH than thiols, and thus selenocysteine can offer a uniquely reactive nucleophilic site for modification. Additionally, there are no natural mAbs expressing selenocysteine, which can help establish good site-selectivity too. Rader and co-workers inserted a selenocysteine into a mAb to develop the selenomabs, working on a similar principle to the previously discussed THIOMabs.[212] Initial work produced selenomabs with only one inserted selenocysteine due to problems experienced during protein expression, however second-generation selenomabs in a follow-up study overcame these issues to successfully insert two selenocysteines.[213] The group generated selenomab-based ADCs, where they investigated the use of functionalised iodoacetamides or maleimides for site-selective conjugation at the selenol sidechain. The selenoether bond from iodoacetamide conjugation proved vastly more stable in human plasma than the corresponding maleimide, due to previously discussed issues with maleimides. Since selenocysteines are reactive at low pH, the conjugation experiments were carried out at pH 5.2, which minimises interfering nucleophilicity from other sidechains which limits the promiscuous reactivity of iodoacetamide. The selenomab-ADC demonstrated homogeneous DARs of 2.0 and demonstrated superior *in vivo* efficacy to heterogeneous Kadcyla. The selenomab-ADC is also significantly more selective towards HER2+ cells than Kadcyla.

#### 1.3.2.3. Enzyme-directed modification

Enzyme-directed modifications can generate site-selective orthogonal chemistry – the Hydrazino-*Iso*-Pictet-Spengler (HIPS) ligation between an aldehyde and a hydrazine has been commonly used to achieve selective protein modification.[214] The SMARTag technology developed by Rabuka *et al.* enzymatically oxidises a cysteine residue in a CXPXR sequence into an aldehyde-bearing formaglycine using the formaldehyde-generating enzyme (FGE).[215] Site-selective conjugation occurs on the only two aldehyde-bearing formaglycine moieties, via HIPS ligation. SMARTag helped synthesise an ADC used for the treatment of nHL, using an anti-CD22 antibody, inotuzumab, conjugated to a non-cleavable maytansine payload, with a DAR 1.8.[216] Upregulation of efflux pumps such as MDR1 is often responsible for cancer relapse, however the ADC provided resistance against MDR1, reducing payload loss through this resistance mechanism, and provided improved efficacy when compared with maytansine in MDR1+ cell lines. The ADC, TRPH-222 (Triphase), has since entered Phase 1 clinical trials.[217]

Other enzyme-directed mAb modifications include bacterial transglutaminase (BTG), an acyl transfer enzyme (glutamine to amine-containing acceptor) which has been used to generate DBCO-containing ADCs, coupled onto polymers as immune cell activators.[218, 219] Mushroom tyrosinase has been used to site-selectively modify tyrosine residues on native mAbs.[220] Most enzyme-directed approaches towards ADCs utilise biological enzymatic transformations to achieve very impressive site-selectivity, which are not otherwise possible *via* small molecule chemical approaches.

Engineered mAbs can provide homogeneous ADCs superior to heterogenous, native competitors; however, engineering mAbs is complex, expensive, inefficient, and impractical. Developing and optimising procedures towards affinity-peptides and engineered antibodies are intensive, requiring a significant amount of time, resources, and expenses. A combination of the selectivity and homogeneity offered by engineered mAbs with the convenience of native mAbs is highly desired. Small molecule approaches to achieving this are highly sought after, as they enable accessible strategies with lower burden of costs and resources.

### 1.3.3. Native chemical ligation

Native chemical ligation (NCL) was developed by Kent and co-workers in the early 1990s for the synthesis of proteins and has become a fundamental chemical biology approach (**FIG. 47**).[221] The initial utility of NCL involved the generation of longer peptides through the attachment of two smaller peptides in a site-selective and chemoselective manner,[222,223] however it has since been used for the total synthesis of far more complex synthetic protein targets.[224] The NCL reaction involves an initial reversible transthioesterification between the thiol sidechain of a *N*-terminal cysteine and an electrophilic *C*-terminal thioester. This forms a new thioester linkage between the two peptides. A spontaneous, intramolecular *S*-to-*N* acyl transfer rearranges the acyl group to form a stable, irreversible amide linkage. The NCL process can occur in mild conditions, such as 22 ºC at pH 7.0, making it easily accessible.

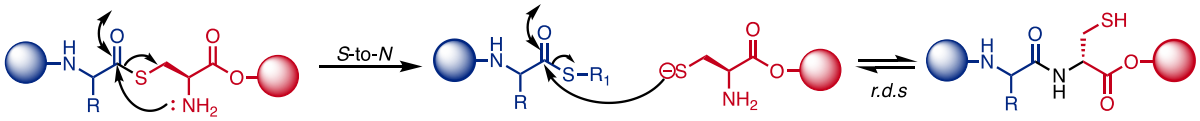


**FIGURE 47.** Mechanism of a NCL reaction.

The initial transthioesterification is often the rate-determining step. Investigations into increasing the rate of this step have mostly involved the use of catalytic thiols,[225] such as sodium 2-mercaptosulfonate (MESNa) and 4-mercaptophenylacetic acid (MPAA), which both feature excellent water solubility. Thiophenol is another thiol sometimes used for NCL catalysis; however, its poor water solubility, toxicity, and odour make it undesirable for use. In general, aryl thiols are found to increase the rate of transthioesterification more than corresponding alkyl thiols, with MPAA demonstrating impressive rate enhancement effects – reaction times can be optimised to enable complete ligation within 1 h. Aryl thiols enable the generation of more reactive thioesters *in situ*, for nucleophilic attack by the cysteine thiol sidechain. Crucially, the aryl thiols possess lower pKa which corresponds to better leaving group ability, with MPAA having a pKa of ~6.5 compared to MESNa with a pKa of ~9.2. Whilst aryl thioesters could be prepared in advance to avoid the addition of additives, these thioesters may be too reactive and engage in unselective nucleophilic substitutions by lysine residues or undergo competing hydrolysis.

Internal cysteines can also affect ligation rates,[226] enabling faster transfer onto the *N*-terminal amine. Whilst smaller ring structures generally allow a faster shift, NCL has also been used for the synthesis of macrocyclic structures with large intermediate ring systems.[227] Reports into ring size influence on NCL rates find that 17- to 20-membered intermediate ring sizes were optimal, whilst acyl transfer in 8-, 11-, or 14- membered intermediate rings were far more difficult to drive towards amide formation.[226] Formation of NCL products *via* such unfavourable ring sizes requires more forcing conditions to drive towards completion, such as applying heat or microwave radiation.[217, 218] Finally, amino acid residues adjacent to the *C*-terminal thioester have also shown to somewhat influence the rate of NCL – more sterically hindered, bulky sidechains increase steric hindrance and thus slow down the rate of NCL. For example, glycine residues adjacent to the *C*-terminal can undergo faster NCLs than *C*-terminal thioesters with a valine residue, which feature a bulkier isopropyl sidechain.[230]

NCL therefore provides a convenient and chemoselective method of synthesising amide bonds on proteins. Thioesters are readily synthesised through coupling procedures from commercially available starting materials such as carboxylic acids.

The regioselectivity of NCL is attractive for ADC synthesis, as it enables the site-selective modification of lysine residues, as Baker and co-workers reported in their cysteine-to-lysine (CLT) protocol.[231]

### 1.3.3.1. Cysteine-to-lysine transfer

The CLT protocol utilises the concept of NCL for strategies leading to the synthesis of more homogeneous, lysine-conjugated ADCs (**FIG. 48**). The work was conducted on trastuzumab Fab, which has diagnostic and therapeutic relevance, so presents an ideal platform. Trastuzumab Fab has 26 lysine residues, and two cysteine residues within a disulfide bond.

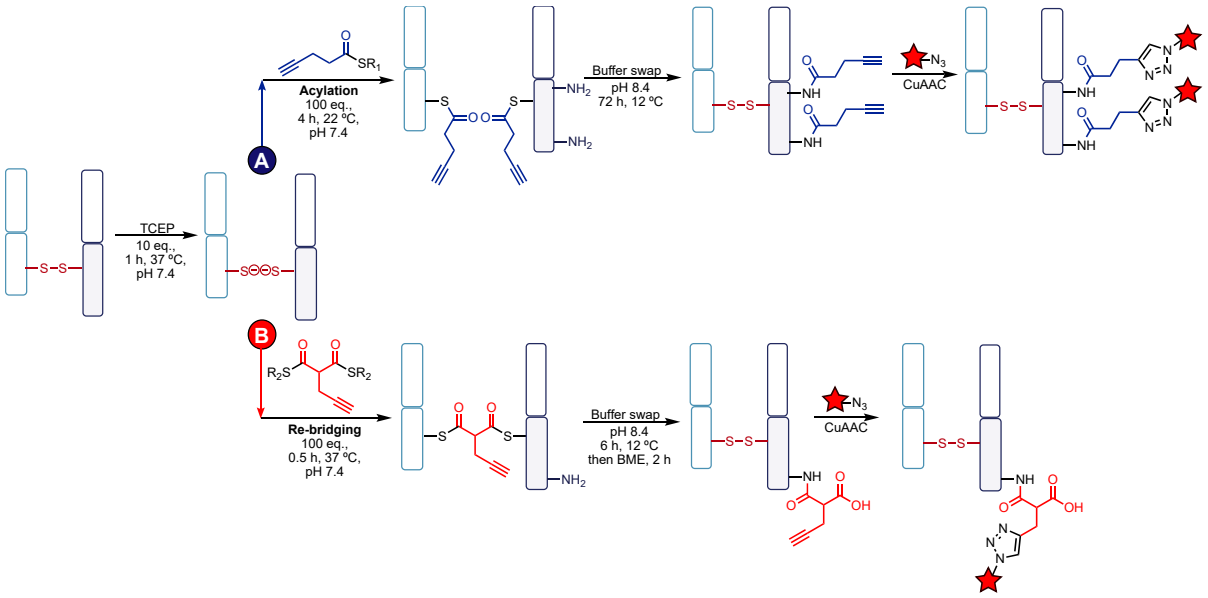


**FIGURE 48.** General CLT scheme. **A)** Alkyl mono-thioester. **B)** Alkyl bis-thioester.

The crystal structure of trastuzumab Fab identifies three lysine residues near the single disulfide bond, distant from the CDRs – K136, K221, and K225 (**FIG. 49**). The distance of these residues varies between the HC cysteine (C223) and the LC cysteine (C214). The proximal lysine residues, K221 and K225, are close to both cysteine residues, with a distance between 6-8 Å. K136 is slightly further away, with a distance between 11-12 Å, however it is within reasonable proximity. Due to the shorter distance between the sidechains of the participating cysteine and lysine sidechains, K221 and K225 are expected to be the major sites of modification. Thus, these lysine residues present an opportunity to achieve site-selective modification, utilising the cysteine residues as an initial ligating site, bringing reactive acyl groups near the lysine residues, which can then enable nucleophilic substitution in the *S*-to-*N* acyl transfer.

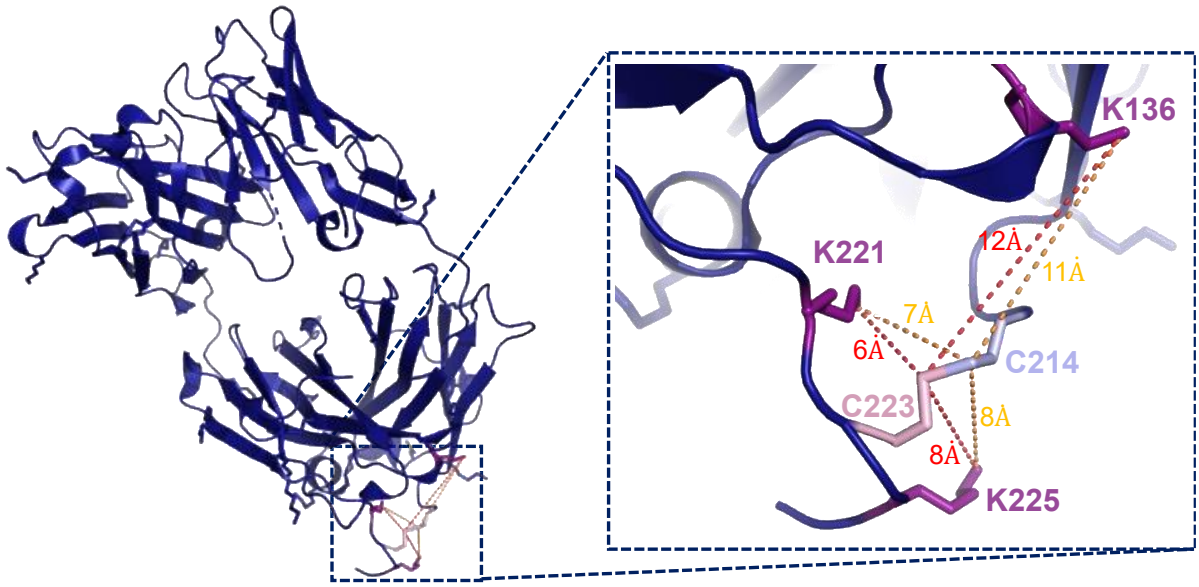


**FIGURE 49.** Crystal structure of trastuzumab Fab and a closer perspective of the disulfide bond region, containing the cysteine residues and the proximal lysine residues. Relevant residue distances are labelled. PDB 6BAE.

Thioesters were found to possess ideal reactivity profiles for CLT. They demonstrate good stability in aqueous conditions, but importantly they also demonstrate good chemoselectivity for cysteine residues and can engage in relatively quick transthioesterification reactions. Aryl thioesters were found to be too reactive and caused unselective lysine modification. By tuning down reactivity and synthesising alkyl thioesters, it was possible to achieve selective cysteine modification in 4 h, at 22 ºC, pH 7.4. A re-bridging bis-thioester was also synthesised, and this showed complete re-bridging in 0.5 h at 37 ºC, pH 7.4. The increased rigidity of the bis-thioester may improve reaction rates. Additionally, the bis-thioester has electron-withdrawing $\beta$-carbonyl groups, which increase electrophilicity of the thioester and thus make it more reactive towards incoming nucleophiles. Both thioesters contained click handles for late-stage functionalisation *via* CuAAC.

Cysteine selectivity is possible for the thioesters at pH 7.4, as the lysine residues, with an amine sidechain of pKa 10.5, are mostly protonated and hence less reactive. However, to enable the acyl transfer to occur, and increase the probability of the proximal lysines engaging in a nucleophilic substitution of the cysteine thioesters, it is necessary to increase pH. A pH of 8.4 was found to be sufficient in enhancing lysine reactivity, and the proximal lysine residues could initiate a spontaneous *S*-to-*N* acyl transfer, forming stable amide bonds. For the mono-thioester, a 72 h reaction at 12 ºC

was conducted – other conditions resulted in more competing hydrolysis cleaving the thioester, forming the carboxylic acid, and thus limited the number of acyl groups leftover for transfer. So, whilst reaction rates could be increased, conversions would decrease. Upon acyl transfer, the native disulfide bond spontaneously reforms. Peptide digestion and MS/MS analysis of the CLT conjugate confirmed site-selective modification of the three proximal lysine residues with two acyl groups.

The re-bridging bis-thioester also demonstrated site-selective modification of a single lysine residue (K136). Due to the rigidity of the re-bridging reagent and its increased reactivity, CLT of the bis-thioester occurred at a faster rate, completing in 6 h. However, the native disulfide bonds were not reformed in this example, and the CLT conjugate was incubated with excess thiol for 2 h to enable re-oxidation of the cysteine thiol sidechains to the native disulfide bond. Hydrolysis of the thioester occurred here too. Whilst in traditional NCL the rate-determining step is the initial transthioesterification, the CLT protocol's rate-determining step is instead the acyl transfer – this is likely due to the large ring size of the formed macrocyclic intermediate between the cysteine residues and the proximal lysine residues.

Both mono-thioester and bis-thioester were then functionalised with a fluorophore through CuAAC click chemistry on the alkyne handle. The mono-thioester showed fluorophore-antibody ratios (FAR) of 1.5, whilst the bis-thioester demonstrated a FAR of 0.8. These CLT conjugates retained full HER2 binding relative to native trastuzumab Fab, confirmed through an ELISA. The average conversion was around 75%, which is lower compared to cysteine engineered methods, such as the THIOMABs which typically obtain 90% conversion.

However, this conversion is significantly greater than other similar transfer strategies. Another advantage of the CLT protocol is that it can be utilised on native, 'off-the-shelf' mAbs, using small molecule thioesters which are readily synthesised through simple organic chemistry procedures. This removes the technical complexity involved with other non-chemical strategies such as protein engineering, affinity-peptides, or enzyme-directed transformations. The CLT protocol enables site-selective lysine-modified Fab species through simple chemistry and a straightforward bioconjugation protocol, so it presents a promising method towards more homogeneous Fab conjugates and ADCs.

## 1.4. Aims and Objectives

This work aims to investigate and design new reagents to achieve site-selective antibody conjugation, as achieving homogeneous ADC synthesis is highly sought in chemical biology research. The key focus of this research work involves CLT, and the development of reagents and strategies to improve upon the existing CLT foundations and introduce convenient and successful methods of synthesising ADCs.

Prior research demonstrated the suitability of thioesters as CLT reagents, as they possess an ideal reactivity profile that preferentially reacted with cysteine residues *via* transthioesterification at pH 7.4. A core aim of this project is to expand upon the thioesters and investigate tuning their reactivity to further explore CLT. More reactive thioesters are desirable, as they may engage in faster acyl transfer reactions which is particularly relevant for the synthesis of ADCs. The design and synthesis of electron-deficient thioesters included incorporating nitrogen-containing heterocycles, as these are effective electron-withdrawing groups. A novel tetrazine thioester was envisioned to be of utmost interest, as it will possess a very strong electron-withdrawing effect on the thioester carbonyl whilst also introducing the capability of inverse-electron demand Diels-Alder (iEDDA). Upon successful synthesis, these electron-deficient thioesters will then be explored on antibody fragments, optimising the transthioesterification and acyl transfer steps of these reagents (**FIG. 50**).

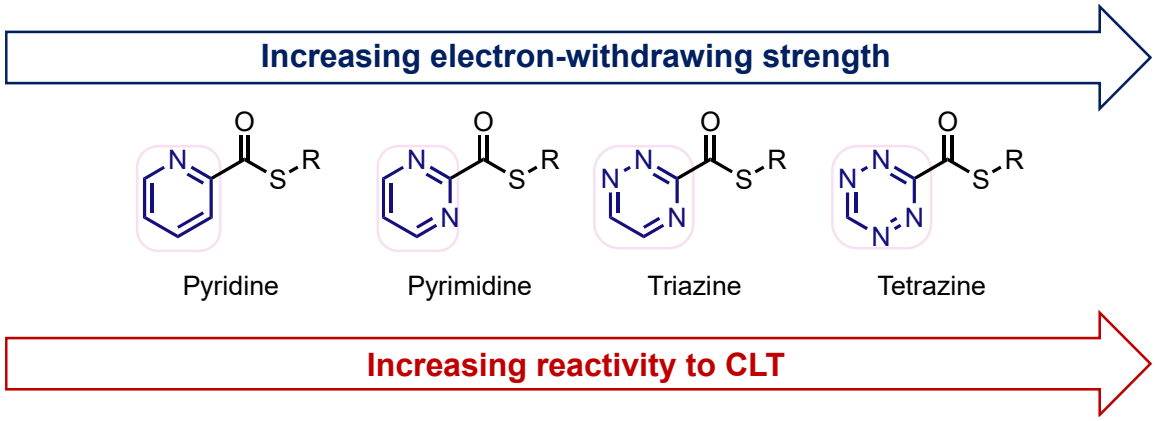


**FIGURE 50.** Structures of proposed target electron-deficient thioesters.

Another aim of this project concerns the investigation of alternative functional groups for the modification of proteins. CLT has only previously been explored using thioesters, however there are several carbonyl-related reagents that could prove to be of significant interest as CLT reagents or as general protein modification reagents.

Examples include thiocarbonates, thiocarbamates, dithiocarbonates, and carbonimidodithioates (**FIG. 51**). Whilst these compounds do exist in literature, they are relatively less well understood, and have not been explored for protein modification and may offer novel chemistry of significant usefulness for chemical biology applications. This work will also aim to develop accessible synthetic routes towards these compounds and investigate their potential as protein modification reagents on an antibody fragment.

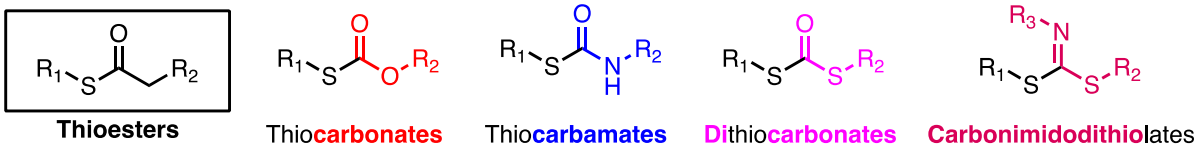


**FIGURE 51.** Structures of proposed novel functional groups to explore on antibody.

Finally, this work also investigates the use of thioesters as guided-labelling reagents in dual-reactive reagent designs. It is already well established that thioesters demonstrate good selectivity for cysteine modification. Thioesters with aldehyde moieties will be synthesised to investigate their potential protein modification applications – the aldehyde-thioester could enable selective amine formation in a controlled manner, which provides a more site-selective way of achieving amine-modified conjugates. This strategy utilises the site-selectivity of thioesters to enable proximity-driven reactions with other reactive functional groups.

# 2. Electron-deficient thioesters

Thioesters were shown to demonstrate excellent selectivity for cysteine thiols over other nucleophilic amino acids present on trastuzumab Fab. Whilst the initial transthioesterification step is reasonably fast, the acyl transfer step is slow, requiring 72 h to achieve complete transfer. In addition, some hydrolysis is experienced over time due to the elevated pH, necessary for lysine reactivity due to the amine sidechain pKa (10.5), which leads to the loss of the acyl group. Faster reactions could overcome the limitations of CLT with the alkyl thioesters. If the thioester can undergo transthioesterification and quickly transfer onto the proximal lysine to form a stable amide, this could prevent unwanted acyl group loss, maximising modification efficiency. Thioesters engaging in protein reactions at lower pH may also experience less competing hydrolysis, which could also increase the efficiency of CLT. Additionally, it is more convenient to have a protocol that enables the generation of site-selectively modified conjugates within shorter timeframes.

Whilst the rate of the transthioesterification step can in-part be controlled by the nature of the thiol leaving group, the rate of CLT is exclusively determined by the thioester electrophilicity. This chapter investigates the development of electron-deficient thioesters, and their use as CLT reagents on trastuzumab Fab. A focus of this work involves the incorporation of electron-withdrawing groups onto these thioesters, which aim to withdraw electrons from the thioester carbonyl, and make the thioester more reactive towards nucleophiles. Whilst there are a range of electron-withdrawing groups available, nitrogen heterocycles were chosen as the focus of this work – their different levels of electron-withdrawing strength, commercial availability and potential for further functionalisation makes them attractive and suitable reagents as starting points.

## 2.1. Chemical synthesis

### 2.1.1. Synthesis of nitrogen heterocycle thioesters

For initial investigations, pyridine, quinoline, and pyrimidine carboxylic acids were selected. A greater number of nitrogen atoms on the ring would produce a greater electron-withdrawing effect on the thioester carbonyl through the inductive and mesomeric effect. This is also reflected in the pKa of these nitrogen heterocycles – the greater the number of nitrogens, the greater the electron-deficiency of the ring system. This leads to less favourable protonation, increased acidity due to a more

easily donated proton, and a lower pKa. The predicted reactivity of the heterocycles is as follows: pyrimidine (pKaH 1.3) > quinoline (pKaH 4.9) > pyridine (pKaH 5.2). Like the alkyl thioesters explored in early CLT studies, MESNa was chosen as the thiol leaving group, due to its excellent water solubility and good leaving group ability.

Initial attempts to synthesise the pyridine-MESNa thioester **1** from pyridine-2-carboxylic acid were unsuccessful (**SCHEME 1, TABLE 2**). A wide variety of coupling agents and conditions were tested, but many returned starting material or resulted in complex mixtures. A number of these strategies utilise an activating agent, relying on the carboxylic acid acting as a nucleophile to form a reactive intermediate, which can then be substituted by a nucleophile to form the desired coupled product. However, in the case of these electron-deficient carboxylic acids, the carboxylic acid itself is not a good nucleophile due to its lower electron-density. Additionally, the coupling intermediate is likely very reactive, again due to the electron-withdrawing effect of the adjacent ring system, and thus may be prone towards degradation (**FIG. 52**).

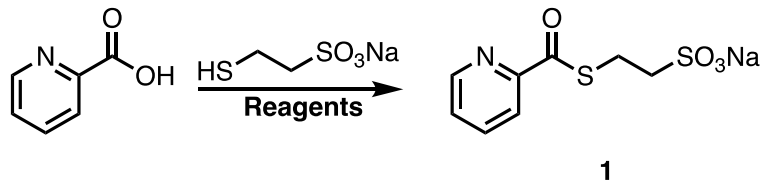


**1**

**SCHEME 1.** Screening reagents for the synthesis of pyridine MESNa thioester **1**.

**TABLE 2.** Coupling conditions for the synthesis of pyridine-MESNa thioester **1**.

| Reagent | Additive | Solvent | T (ºC) | Time (h) | Yield (%) |
|---|---|---|---|---|---|
| EDC+NHS | TEA | DMF | RT | 16 | 0 |
| HATU | DIPEA | DMF | RT | 16 | 0 |
| EDC | DMAP | DMF | RT | 16 | 0 |
| Oxalyl Chloride | DMF (cat.) | DCM | RT | 16 | 0 |
| Thionyl Chloride | TEA | DCM | RT | 16 | 0 |

| | | | | | |
|---|---|---|---|---|---|
| EEDQ | / | DMF | 80 | 16 | 31 |

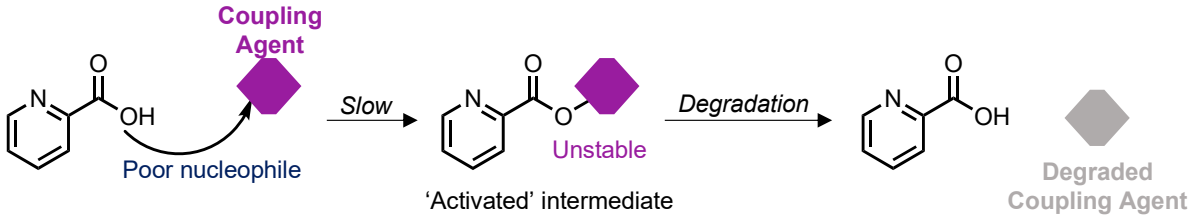


**FIGURE 52.** Outcomes of coupling conditions using pyridine 2-carboxylic acid.

NHS ester formation, HATU, and EDC all suffered from limited carboxylic acid nucleophilicity and instability of activated intermediates. Using chlorinating reagents such as oxalyl chloride or thionyl chloride formed chlorinated by-products and were incompatible with MESNa due to poor solubility in non-polar organic solvents. EEDQ was the most suitable coupling reagent for the synthesis of pyridine-MESNa thioester **1**, requiring heating at 80 ºC to obtain the desired product in 31% yield.

Having identified a synthetic route for the synthesis of pyridine-MESNa thioester **1**, the route was next applied for the synthesis of quinoline-MESNa thioester **2** and pyrimidine-MESNa thioester **3** (**SCHEME 2**). The thioesters could be successfully synthesised, though the yields were low, in-part due to the high polarity of MESNa, which often co-eluted during column chromatography.

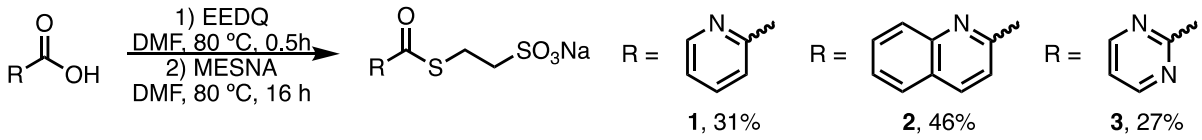


**SCHEME 2.** Synthesis of electron-deficient thioesters **1**, **2**, and **3**.

### 2.1.2. Synthesis of diene thioesters

In addition to the simpler nitrogen heterocyclic systems, thioesters with dienes such as triazine and tetrazine were pursued. The triazine and tetrazine ring possess more nitrogens so have a stronger inductive and mesomeric electron-withdrawing effect, increasing reactivity of the thioesters towards nucleophiles even more. Additionally, these diene rings are compatible with inverse electron-demand Diels Alder (iEDDA) reactions (**FIG. 53A**). iEDDA with triazine or tetrazine dienes is one of the fastest currently available bioorthogonal reactions, surpassing the rates of other click chemistries such as CuAAC cycloadditions.[232] iEDDA reactions occur in aqueous

conditions and complete within minutes. Also, they do not require a catalyst, such as the toxic Cu(II) species used in CuAAC. A [4+2] cycloaddition occurs between the diene (triazine or tetrazine) HOMO and the LUMO of a dienophile, such as bicyclononyne- (BCN) or *trans*-cyclooctene- (TCO) reagents (**FIG. 53B**).

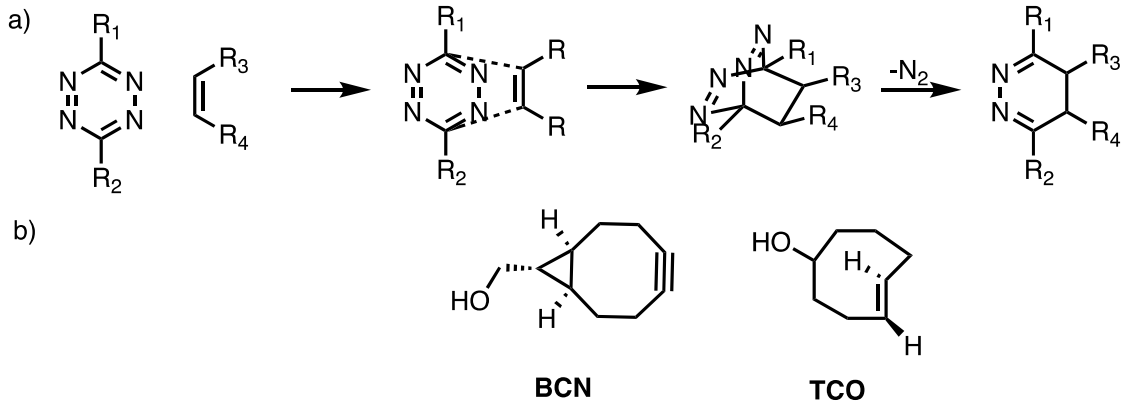


**FIGURE 53.** iEDDA. **A**) Mechanism on tetrazine rings as dienes. **B)** Structures of commonly used dienophiles.

A thioester taking advantage of these dienes would benefit from very fast reactions with protein residues and have a convenient reactive handle for further functionalisation. Additionally, the presence of a carbonyl group from the thioester moiety would make these dienes even more reactive towards dienophiles. So, the two components would synergise well with each other to increase respective reactivities.

A 1,2,4-triazine carboxylic acid **4** was synthesised *via* a literature protocol, starting from commercially available ethyl oxamate (**SCHEME 3**).[233]

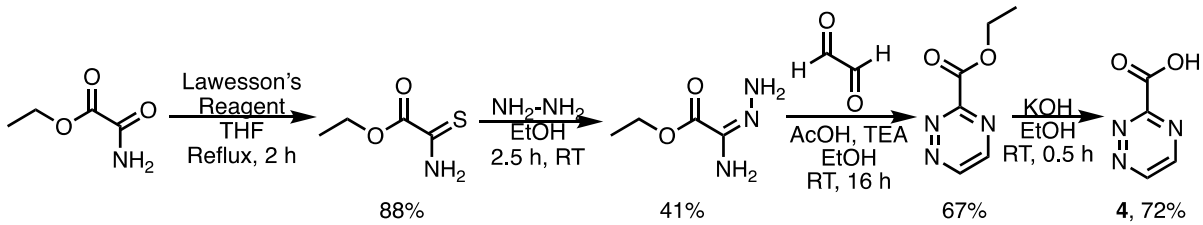


**SCHEME 3.** Synthesis of 1,2,4-triazine-3-carboxylic acid **4**.

Lawesson's reagent converted the amide into the thioamide ethyl thiooxamate in very good yields. This was followed by substitution of the thioamide with excess hydrazine, forming ethyl oxalamidrazonate which was purified by recrystallisation. Glyoxal was added in addition with catalytic AcOH to form the triazine ring, and lastly the ester was hydrolysed to form 1,2,4-triazine-3-carboxylic acid **4** in good yields.

However, synthesis of triazine-MESNa thioester **5** was not possible under the EEDQ synthetic route. Other coupling agents such as HATU and thionyl chloride were also investigated, but they also did not yield any product. Only complex mixtures were observed by TLC. NMR analysis of the crude mixture suggested loss of the triazine aromatic hydrogen atoms, whilst the carboxylic acid itself remained unmodified.

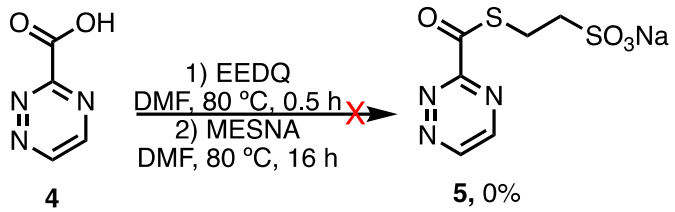


**4** **5,** 0%

**SCHEME 4.** Addition of thiol to 1,2,4-triazine-3-carboxylic acid **4** in attempts to synthesis triazine-MESNa thioester **5**.

Instead, a tetrazine thioester was explored, adapting a literature protocol to synthesise the tetrazine carboxylic acid **6c** (**SCHEME 5**).[234] The tetrazine **6a** was synthesised from the nickel triflate-catalysed coupling of methoxyacetonitrile and phenylnitrile, following by oxidation of the dihydrotetrazine using sodium nitrate and 4M HCl to the methoxy-substituted tetrazine **6a** (**SCHEME 6A**). It is suggested that the nickel (II) catalyst can act as a Lewis acid, increasing nucleophilicity of the hydrazine, or the catalyst forms an amidrazone intermediate by binding to the nitrile and hydrazine (**SCHEME 6B**), though there is not conclusive evidence supporting this mechanism.[235] The methoxy group was demethylated by the addition of boron tribromide at -78 ºC, forming the tetrazine alcohol **6b**. Oxidation of tetrazine alcohol **6b** to tetrazine carboxylic acid **6c** was challenging, and several different oxidation conditions were explored. Chromium-based oxidation reagents such as PCC-Periodic Acid or Jones reagent resulted in the complexation of the tetrazine carboxylic acid **6c** – the carboxylic acid could not be easily dissociated from the complex. Instead, a non-metal-based approach was pursued, such as using TEMPO in Anelli's Oxidation. Ultimately, oxidation was achieved in a two-step process from Dess-Martin periodinane, to convert the alcohol to an intermediate aldehyde, and then Pinnick oxidation to the carboxylic acid **6c**, using sodium chlorite. The intermediate aldehyde is very sensitive towards any heating and degrades over hours. It is crucial to immediately purify the aldehyde through column chromatography after the reaction is completed, and quickly initiate the Pinnick oxidation once the aldehyde is isolated to maximise yields of **6c**.

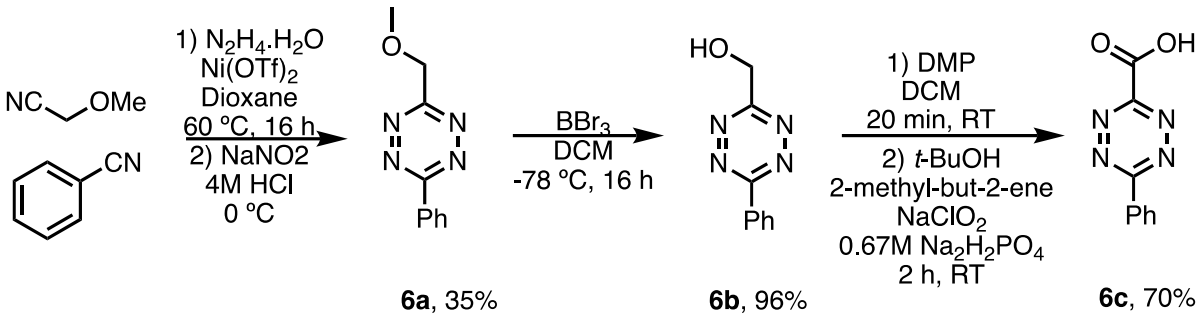


**SCHEME 5**. Synthesis of tetrazine carboxylic acid **6c**.

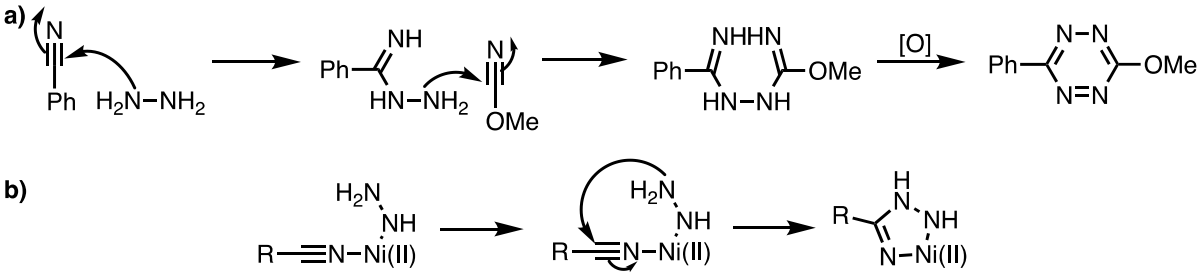


**SCHEME 6. A**) Mechanism of tetrazine synthesis from nitrile reagents and hydrazine. **B)** Suggested mechanism of amidrazone formation by the nickel catalyst.

Having successfully synthesised the tetrazine carboxylic acid **6c**, thioester synthesis was explored next. The EEDQ strategy, like in the triazine example, did not work. Instead, a multi-step one-pot synthesis was necessary (**SCHEME 7**).

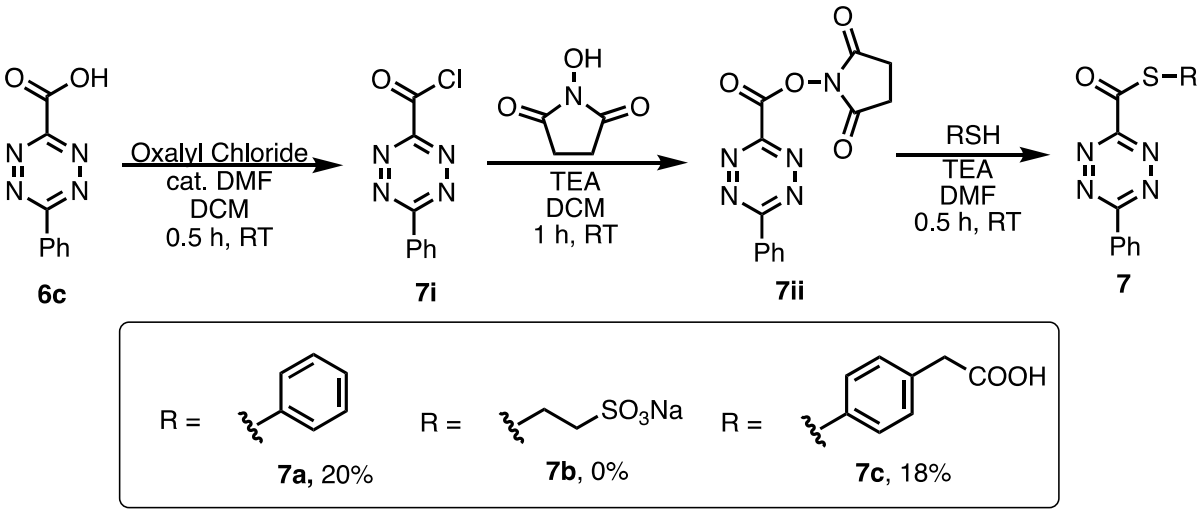


**SCHEME 7**. Synthesis of tetrazine thioesters **7a-7c**.

It was not possible to directly substitute the acyl chloride **7i** with a thiol, as this resulted in complex mixtures where the characteristic pink colour of tetrazines was lost, indicating reduction to the dihydrotetrazine. Similarly, it was not possible to synthesise

an NHS ester directly from the tetrazine carboxylic acid **6c**, due to the deactivated nature of the carboxylic acid. It was necessary to first convert the carboxylic acid **6c** to **7i** using thionyl chloride, and then quickly substitute the acyl chloride **7i** with *N*-hydroxysuccinimide to form the intermediate NHS ester **7ii**. The thiol was then added *in situ*, and it was possible to synthesise tetrazine thioesters **7a** and **7c** in low yields, with small quantities of tetrazine carboxylic acid **6c** (~20%) recovered. The reactivity and instability of the intermediates contributes towards this low yield, as **7i** and **7ii** are likely to degrade immediately upon formation. It was not possible to isolate tetrazine-MESNa thioester **7b** due to purification difficulties. The MESNa group is extremely polar, so column chromatography was attempted using DCM/MeOH. However, the tetrazine thioester esterifies to methyl ester tetrazine on the column in the presence of MeOH. An alternative alkyl thiol, methyl thioglycolate, was explored. However, this thiol caused reduction of the tetrazine ring to dihydrotetrazine upon concentration *in vacuo* (**SCHEME 8**).

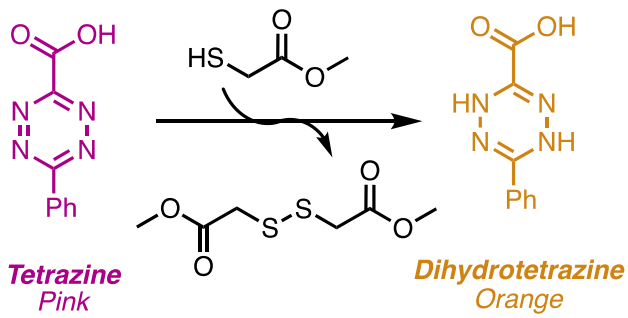


**SCHEME 8**. Reduction of tetrazine ring to dihydrotetrazine *via* methyl thioglycolate.

This reduction was not observed for the other thiols investigated in the developed synthetic route. The redox strength of thiols suggested for tetrazine thioester synthesis must be considered. Analogues of methyl thioglycolate have demonstrated good activity as disulfide bond reducing agents.[236] The aromatic thiols are likely poorer reducing agents and have less of a tendency to form disulfide bonds themselves during the redox process, so do not affect the tetrazine ring. Nonetheless, it was possible to synthesise two very interesting and novel tetrazine thioesters, **7a** and **7c**, for further exploration in bioconjugation studies.

## 2.2. Bioconjugation studies

Bioconjugation of these reagents was then explored on trastuzumab Fab, due to its suitability in CLT investigations (**FIG. 54**). Fab was prepared by the pepsin and papain digestion from Ontruzant, a Herceptin biosimilar (see section 6.2.1.). Fab has a single native disulfide bond, and this must be reduced to the free cysteine thiols prior to the addition of the thioester for transthioesterification. As previously discussed, there are proximal lysine residues (K221, K225) with distances of 6-8 Å to the cysteine residues. Increasing the pH of the reaction will enable deprotonation of the proximal lysine amine sidechains (pKa 10.5), which leads to their increased reactivity with the nearby acyl group. Upon acyl transfer to form the Fab CLT conjugate, forming a lysine-modified species, the disulfide bond spontaneously reforms.

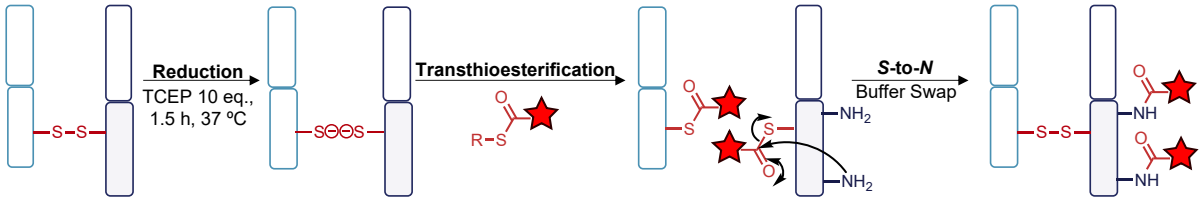


**FIGURE 54.** Example of the CLT protocol on trastuzumab Fab.

### 2.2.1. Pyridine thioester

#### 2.2.1.1. Transthioesterification

The pyridine-MESNa thioester **1** was explored for Fab bioconjugation (**SCHEME 9**) in control and reaction experiments.

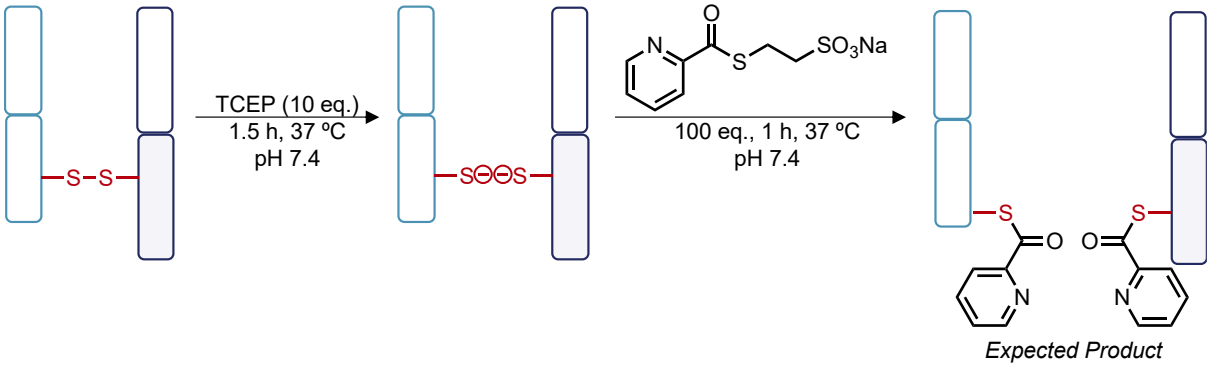


**SCHEME 9.** Bioconjugation conditions of pyridine-MESNa thioester **1** on reduced Fab. The conditions shown are the final optimised conditions utilised for the reagent.

Control experiments on non-reduced Fab (100 eq., 4 h, 22 ºC, pH 7.4), indicating that the pyridine-MESNa thioester **1** does not react unselectively with lysine residues (**FIG. 55A**). Upon reduction and addition to reduced Fab with 100 eq. of reagent, full

modification of the LC and HC cysteine residues was observed (**FIG. 55B**). Promisingly, this complete transthioesterification occurred within 1 h at 37 ºC, which is much faster than the previous generation of alkyl thioesters. Such rapid reactions indicate that the electron-withdrawing ring is increasing the reactivity of the thioester, as designed and desired. After removing the excess thioester, no change was observed when the pyridine thioester Fab conjugate was left at pH 7.4 over 24 h (**FIG. 55C**), indicating good stability against hydrolysis at this pH, but also indicating higher pH conditions are still needed for acyl transfer and CLT.

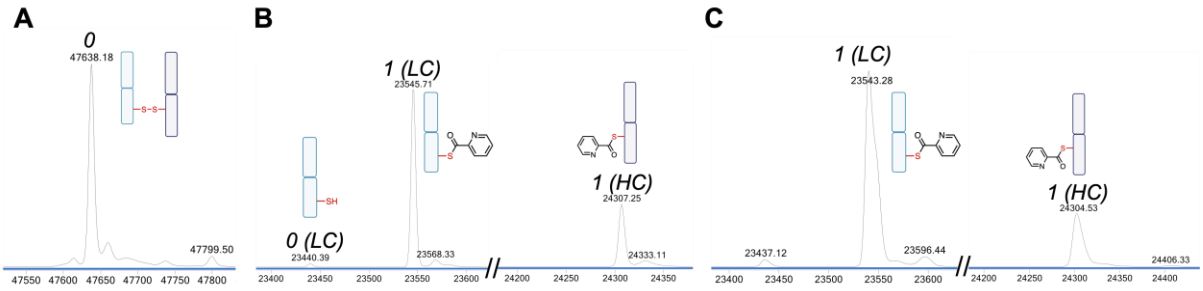


**FIGURE 55.** LCMS of pyridine-MESNa thioester **1** reactions on Fab. **A)** Control study on non-reduced Fab. **B)** Pyridine-MESNa thioester **1**, 100 eq., 1 h, 37 ºC, pH 7.4. **C**) Pyridine-MESNa thioester **1**, conjugate incubated for 24 h, 37 ºC, pH 7.4. Mass of native Fab = 47638 Da. Mass of native LC = 23440 Da. Mass of native HC = 24200 Da. Expected mass of addition = 106 Da.

### 2.2.1.2. CLT of pyridine thioester conjugate

After confirming successful and selective transthioesterification, CLT of the pyridine-MESNa thioester **1** was explored next (**SCHEME 10**). Despite having a more electron-deficient carbonyl, the pyridine-MESNa thioester **1** is still not reactive enough at pH 7.4, due to the low nucleophilicity of the proximal lysine. Ideally, both proximal lysine residues would be modified by the pyridine thioester conjugate in faster timeframes than the alkyl thioesters. Like the original CLT protocol, increasing pH remains key.

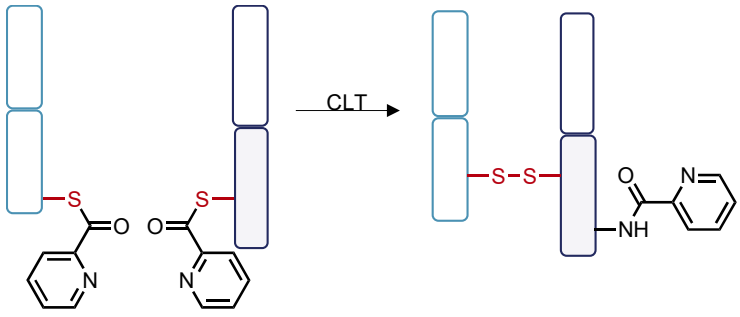


**SCHEME 10**. CLT of pyridine thioester Fab conjugate to the CLT amide conjugate.

pH 8.4 was selected for CLT conditions. Incubating the pyridine thioester Fab conjugate at 12 ºC for 24 h did not result in complete conversion. There were significant amounts of modified LC and modified HC leftover, indicating acyl transfer did not occur efficiently. It was necessary to increase the temperature to 22 ºC to see meaningful and complete acyl transfer (**FIG. 56A**). The major product of this acyl transfer condition is the single lysine-modified CLT conjugate (50%), whilst conversion to the double lysine-modified CLT conjugate (30%) was the second major product. There were also notable amounts of native Fab (20%) recovered, indicating some thioester hydrolysis had occurred. Hydrolysis of the pyridine thioester conjugate, to 2-pyridinecarboxylic acid, means there are fewer acyl groups conjugated on Fab available to transfer to the proximal lysine residues, and so incomplete conversion occurs. Further experiments indicated that the pyridine thioester conjugate undergoes complete acyl transfer in 6 h (**FIG. 56B**), though conversion to the desired double lysine-modified species remains low due to competing hydrolysis at the elevated pH. Timeframes of 4 h did not lead to complete conversion, and small amounts of modified LC and modified HC were leftover (**FIG. 56C**).

Hydrolysis was significantly competing with acyl transfer at pH 8.4, so pH 8.0 was explored next. The lower pH may provide a better balance between increased lysine nucleophilicity and reduced hydrolysis due to hydroxide ion attack. Whilst it was possible to increase the ratio of single modified-lysine conjugate to double modified-lysine conjugate, the acyl transfer is also much slower at pH 8.0. The reaction was not complete after 24 h, as some modified LC was leftover, compared to pH 8.4 where the acyl transfer is complete within 6 h (**FIG. 56D**). Higher temperatures would likely increase the rates of acyl transfer and hydrolysis to the same extent.

Overall, the pyridine-MESNa thioesters demonstrated much faster transthioesterification and acyl transfer than conventional thioesters, achieving complete CLT conjugate formation within 7 h from reduced Fab. These results confirm that introducing electron-withdrawing groups is effective in increasing the thioester reactivity, whilst also maintaining excellent selectivity for cysteine thiol sidechains. However, the acyl transfer reaction with the proximal lysines still does not overcome competing hydrolysis, with maximal conversion to double-modified lysine species limited to 30%. Nonetheless, the total amount of lysine-conjugated species, single or

double-modified, amounted to 80%, with a DAR of 1.1. For comparison, the alkyl thioesters achieve DARs of 1.5 in 72 h timeframes, thus the pyridine-MESNa thioester **1** demonstrates synthesis of slightly lower DAR conjugates but in far less time.

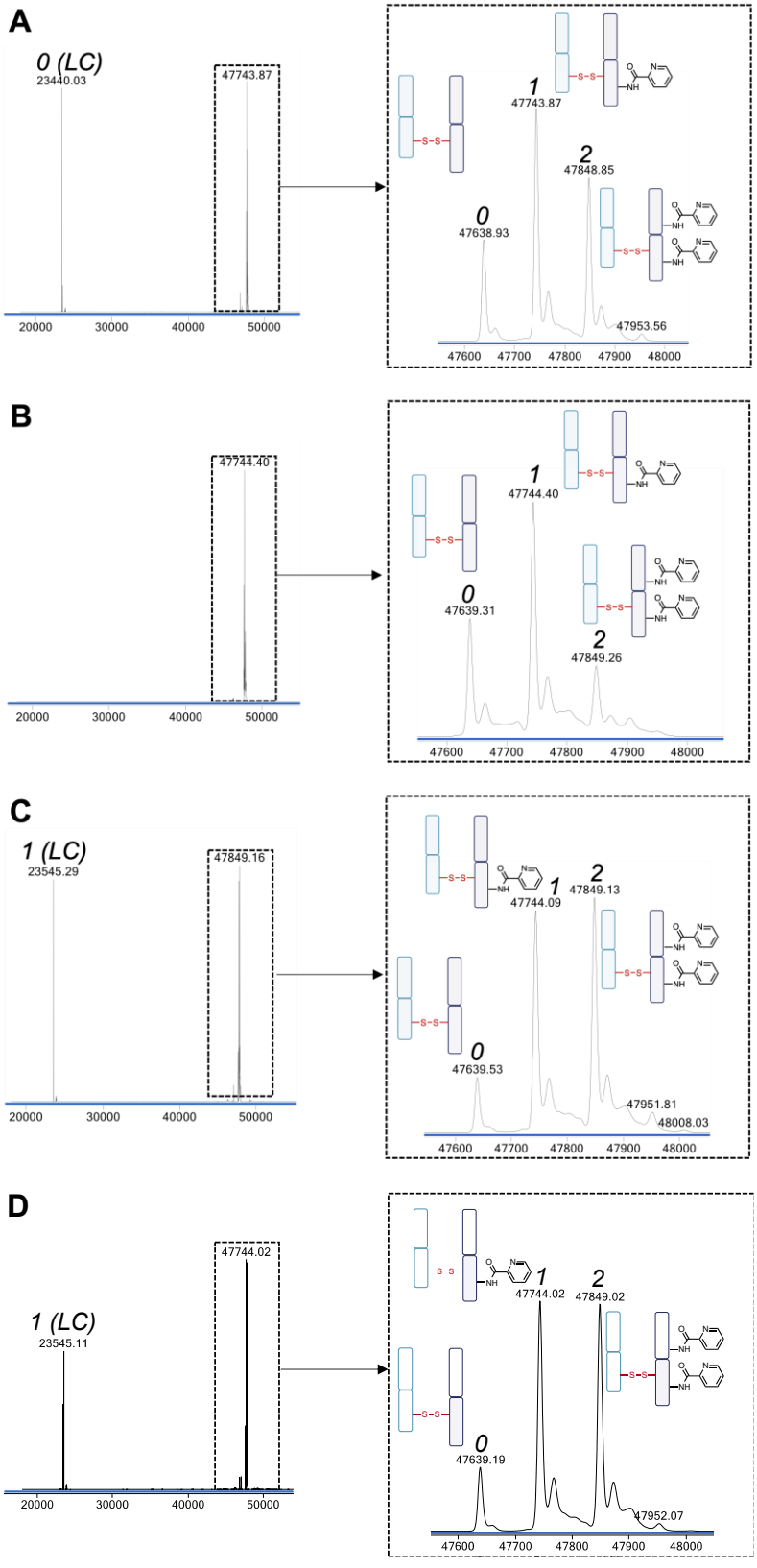

**FIGURE 56.** CLT of pyridine thioester conjugate. **A)** pH 8.4, 24 h, 22 ºC. **B)** pH 8.4, 6 h, 22 ºC. **C)** pH 8.4, 4 h, 22 ºC. **D)** pH 8.0, 24 h, 22 ºC. Mass of native Fab = 47638 Da. Mass of native LC = 23440 Da. Mass of modified LC = 23545 Da. Mass of native HC = 24200 Da. Expected mass of addition = 106 Da (2 additions = 212 Da).

### 2.2.2. Quinoline thioester

#### 2.2.2.1. Transthioesterification

The quinoline-MESNa thioester **2** features a quinoline ring with a similar electron-withdrawing effect to that of the pyridine-MESNa thioester. However, quinoline is more sterically hindered and more hydrophobic. This hydrophobicity may enable the quinoline thioester conjugate to fit within more hydrophobic pockets on the Fab protein surface, which could help reduce hydrolysis. However, this could also reduce the rate of acyl transfer due to increased steric bulk near the thioester site. This reagent was explored to further understand the impact of a bulkier acyl group on the rate of CLT.

Transthioesterification occurred under similar conditions to that of the pyridine-MESNa thioester **2** (**SCHEME 11**). Again, no modification was seen in control experiments (100 eq., 4 h, 22 ºC, pH 7.4) on non-reduced Fab (**FIG. 57A**). Conditions of 100 eq. of quinoline-MESNa thioester **2**, 1 h, 37 ºC, and pH 7.4 offered complete modification of the LC and HC (**FIG. 57B**). Thus, the transthioesterification step itself is not largely affected by the size and hydrophobicity of the quinoline ring. The electron-withdrawing inductive effect from the single nitrogen is responsible for the quinoline-MESNa thioester **2** showing similar reactivity to that of the previously explored pyridine-MESNa thioester **1**.

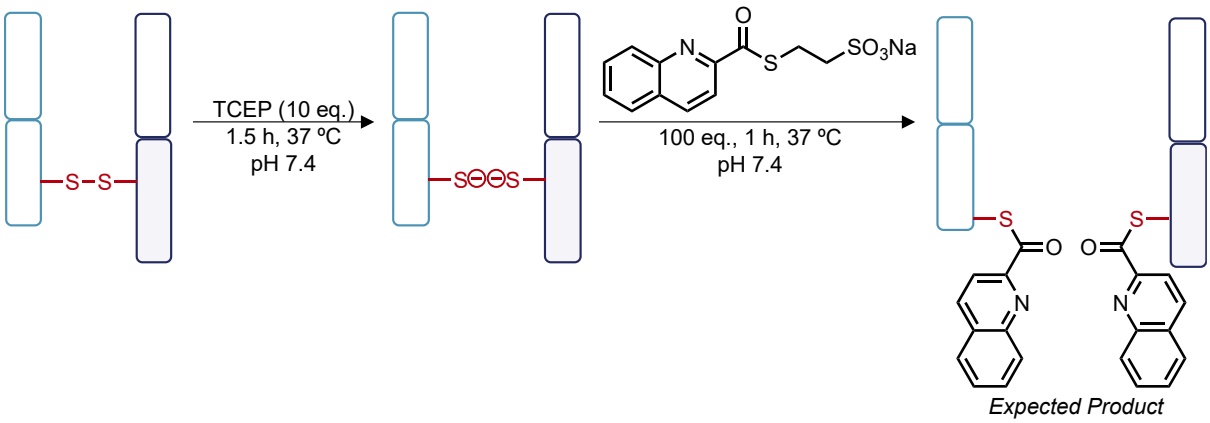


**SCHEME 11.** Bioconjugation conditions of quinoline-MESNa thioester **2** on reduced Fab. The conditions shown are the final optimised conditions utilised for the reagent.

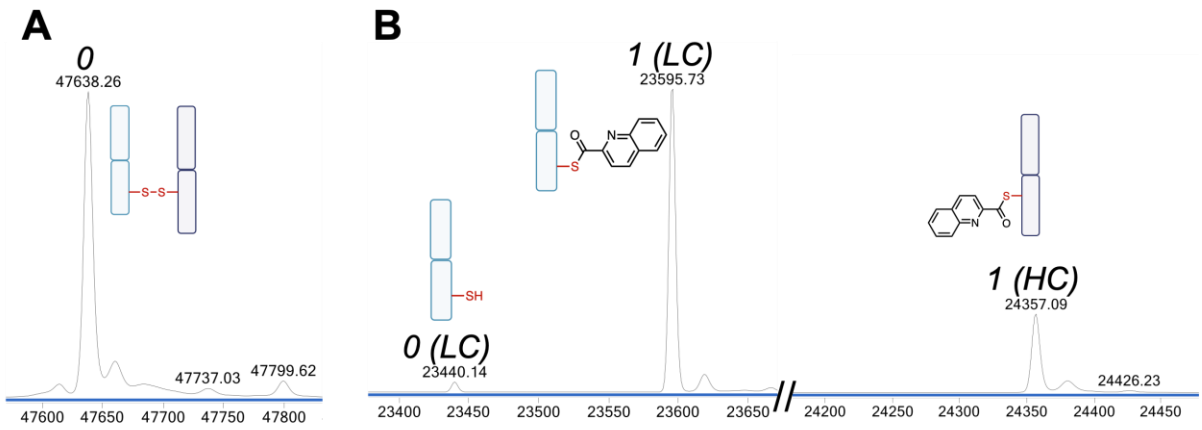


**FIGURE 57.** LCMS of quinoline-MESNa thioester **2** reactions on Fab. **A)** Control study on non-reduced Fab. **B)** Quinoline-MESNa thioester **2**, 100 eq., 1 h, 37 ºC, pH 7.4. Mass of native Fab = 47638 Da. Mass of native LC = 23440 Da. Mass of native HC = 24200 Da. Expected mass of addition = 156 Da.

### 2.2.2.2. CLT of quinoline thioester conjugate

CLT of the quinoline thioester conjugate was explored next (**SCHEME 12**).

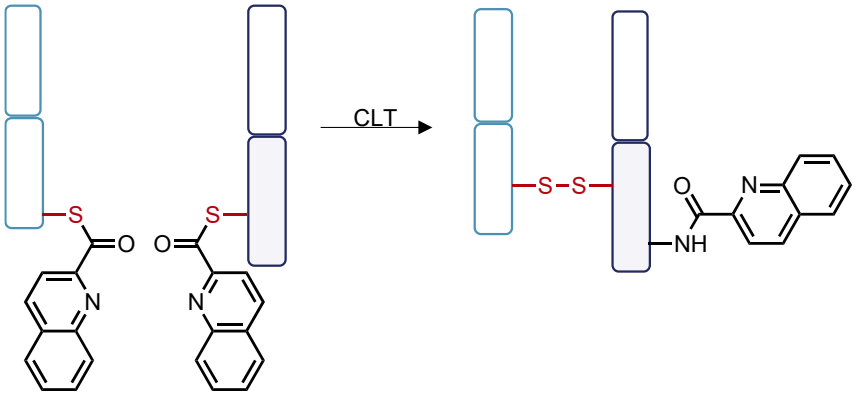


**SCHEME 12.** CLT of quinoline thioester conjugate.

However, unlike the pyridine thioester conjugate, the quinoline thioester conjugate did not yield any notable modification (**FIG. 58**) under the same CLT conditions. There is a negligible amount of single-lysine modification, whilst there are significant amounts of native LC leftover. This indicates that the quinoline thioester has hydrolysed, releasing quinoline-2-carboxylic acid, without reacting with the proximal amine groups and transferring to the proximal lysine residues.

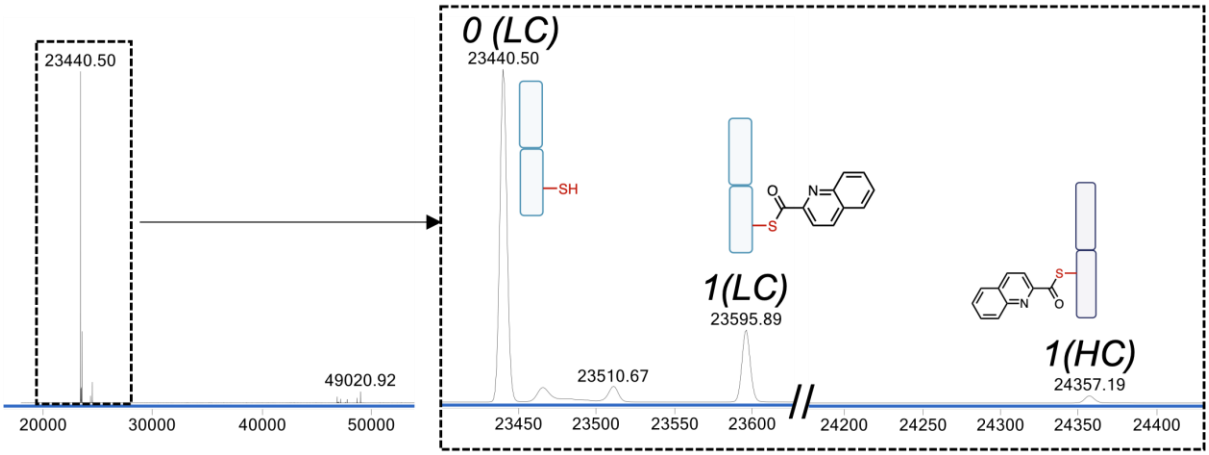


**FIGURE 58.** CLT of quinoline thioester conjugate under conditions of pH 8.4, 24 h, 22 ºC. Mass of native Fab = 47638 Da. Mass of native LC = 23440 Da. Mass of native HC = 24200 Da. Expected mass of addition = 156 Da.

Thus, the quinoline-MESNa thioester **2** was found to be wholly unsuitable for CLT purposes. Despite having the same inductive electron-withdrawing effect as pyridine, from a single nitrogen atom, the rate of transfer is several magnitudes lower. However, this reagent does give a better understanding of steric bulk considerations for CLT reagents. It is likely the hydrophobicity and steric hindrance around the thioester site decreased the availability of the carbonyl for nucleophilic attack by the proximal lysine residues, reducing the rate of acyl transfer. Additionally, the large size of the quinoline ring may result in an unfavourable ring conformation during the intermediate *S*-to-*N* acyl transfer step. Meanwhile, the hydroxide ions in aqueous conditions are free to continue to attack and hydrolyse the thioester over time.

### 2.2.3. Pyrimidine thioester

#### 2.2.3.1. Transthioesterification

The pyrimidine-MESNa thioester **3** has two nitrogen atoms neighbouring the thioester carbonyl, affording greater electron-withdrawal, further reducing the electron-density at the thioester site. Control experiments (100 eq., 4 h, 22 ºC, pH 7.4) were initially conducted at pH 7.4, in line with previous electron-deficient thioesters, however significant unselective modification was observed. The pyrimidine-MESNa thioester **3** is engaging with lysine residues at pH 7.4, leading to multiple lysine-modified species (**FIG. 59A**). Lowering pH would lower lysine reactivity, due to more protonation of the amine sidechain (pKa 10.5), so further control experiments were conducted at pH 6.0 (100 eq., 4 h, 22 ºC, pH 6.0). Promisingly, the amount of unselective modification

observed significantly decreased, with only a small amount of modification seen on native Fab (**FIG. 59B**).

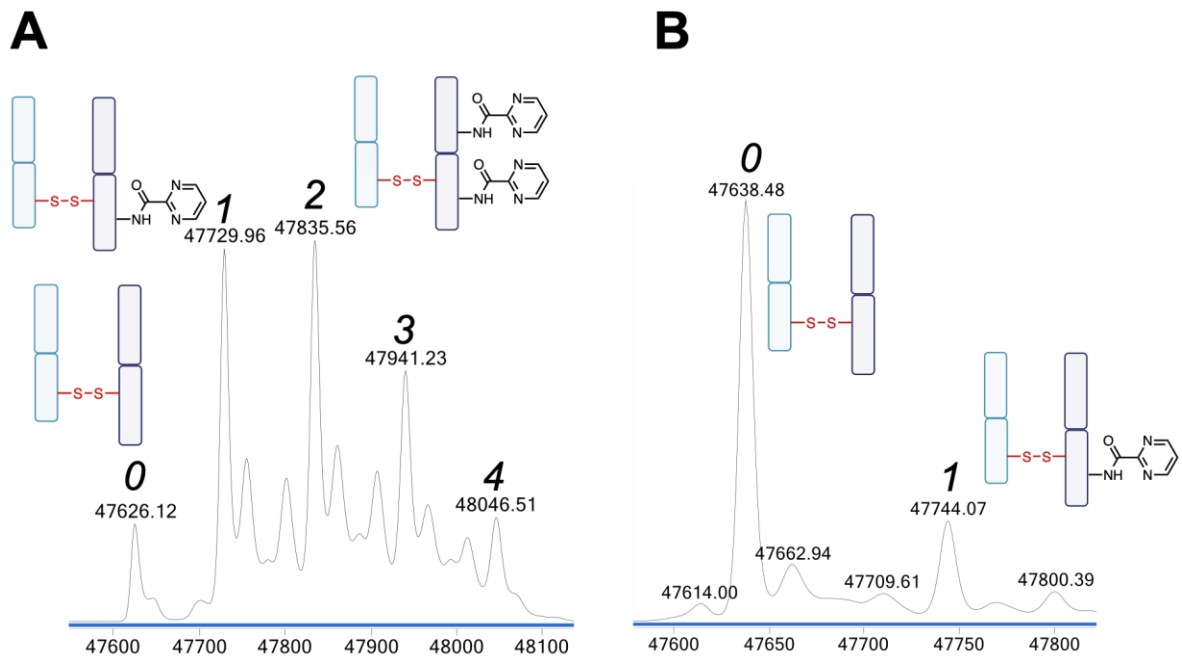


**FIGURE 59**. Bioconjugation of pyrimidine-MESNa thioester **3** on non-reduced, native Fab as control experiments. **A)** 100 eq., 4 h, 22 ºC, pH 7.4, **B)** 100 eq., 4 h, 22 ºC, pH 6.0. Mass of native Fab = 47624 Da (A) or 47638 (B). Mass of native LC = 23440 Da. Mass of native HC = 24200 Da. Expected mass of addition = 106 Da.

With pH 6.0 demonstrating good control of pyrimidine-MESNa thioester **3** addition, this was chosen for transthioesterification on reduced Fab (**SCHEME 13**).

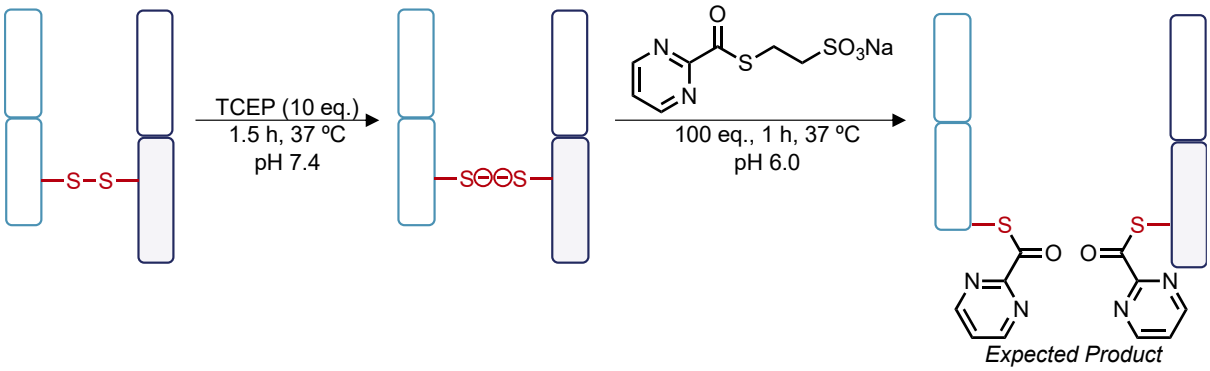


**SCHEME 13.** Bioconjugation conditions of pyrimidine-MESNa thioester **3** on Fab, in non-reduced Fab (control) and reduced Fab (reaction). The conditions shown are the final optimised conditions utilised for the reagent.

Incubation of pyrimidine-MESNa thioester **3** (100 eq., 1 h, 37 ºC, pH 6.0) on reduced Fab showed full modification of the LC and HC under optimised conditions (**FIG. 60**). This reagent is the first example of electron-deficient thioesters that react efficiently and rapidly with cysteine residues at lower pH. The reaction was complete within 1 h at 37 ºC, demonstrating rapid reactions with thiols even when they are more likely to be found in a protonated state, as the cysteine thiol pKa is 8.5.

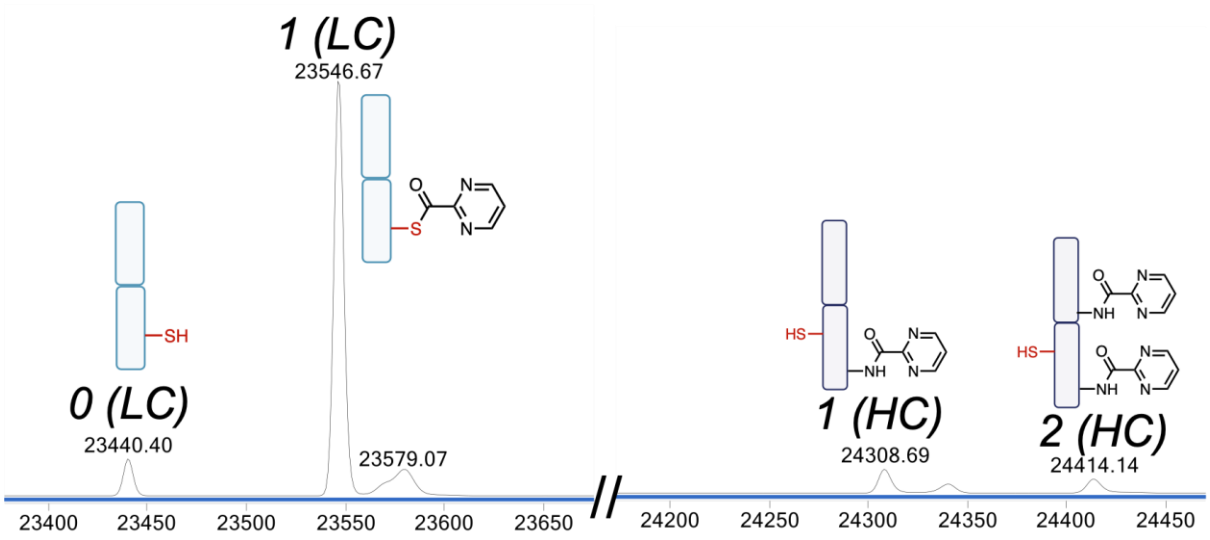


**FIGURE 60**. Transthioesterification of pyrimidine-MESNa thioester **3** under conditions of 100 eq., 1 h, 37 ºC, pH 6.0.

### 2.2.3.2. CLT of pyrimidine thioester conjugate

The CLT conjugate of the pyrimidine thioester is very similar to that of the pyridine thioester, though the addition of the extra nitrogen enables faster protein reactions at lower pH (**SCHEME 14**).

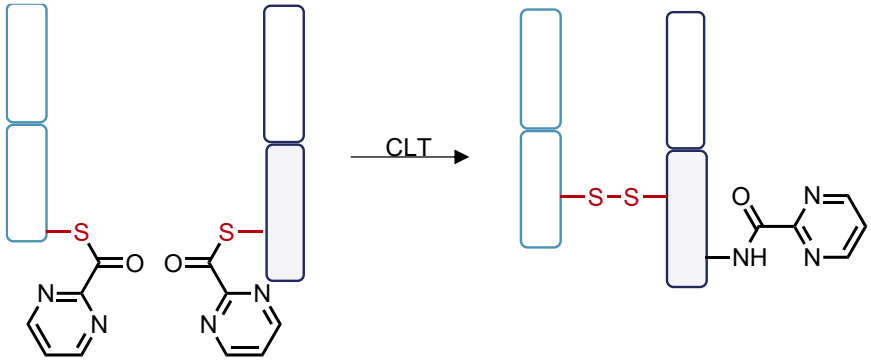


**SCHEME 14.** CLT of pyrimidine thioester conjugate.

Transthioesterification occurring at pH 6.0 provided complete modification of cysteine thiols, so it was reasoned that acyl transfer could occur at lower pH too. Acyl transfer at pH 6.5 indicated complete acyl transfer at 4 h, which is faster than the pyridine thioester, whilst occurring at lower pH (**FIG. 61A**). Like the pyridine thioester, the major product is the single lysine-modified species (50%), with double lysine-modified species the second major product (35%), and some native Fab reformed (15%). There is slightly more double lysine-modified conjugate with the pyrimidine thioester conjugate than the pyridine thioester conjugate. This could be due to two factors – 1) the lower pH results in fewer hydroxide ions attacking the intermediate pyrimidine thioester conjugate, and 2) the pyrimidine thioester conjugate is sufficiently reactive to engage in acyl transfer reactions faster than hydrolysis can occur. Despite the increased reactivity however, hydrolysis remains a substantial competing reaction.

Higher pH conditions were investigated too, to examine if they could enable rapid CLT at reaction rates that can outcompete hydrolysis. pH 8.4 at 22 ºC for 4 h led to significant hydrolysis of the thioester conjugate, and thus the major product was native Fab, with some single lysine-modified CLT conjugate (**FIG. 61B**). Similarly, pH 7.4 at 22 ºC gave completion in similar times to the other investigated conditions, but hydrolysis became more prominent, with it becoming responsible for the formation of more native Fab (35%) in comparison to pH 6.5 CLT studies (**FIG. 61C**).

Overall, the pyrimidine-MESNa thioester **3** enables transthioesterification to occur at similar times to that of pyridine-MESNa thioester **1** and quinoline-MESNa thioester **2**, though at lower pH, which indicates the rate of reaction would be faster at pH 7.4 Promisingly, it enables faster CLT than either single nitrogen-containing thioester. Within 5 h total reaction time from reduced Fab, it is possible to generate CLT conjugates, with the major species corresponding to a single lysine-modified conjugate. In comparison to the pyridine thioester conjugate, there is slightly more double modified-lysine species. In total, there is 85% lysine modified species, giving conjugates with a DAR of 1.2 – this is greater than the DAR of 1.1 from the pyridine thioester CLT conjugate, but less than the DAR of 1.5 from an alkyl thioester CLT conjugate, though the pyrimidine CLT conjugate forms much more rapidly in comparison. Uniquely, this pyrimidine-MESNa thioester **3** enables protein reactions to occur at far lower pH than seen in previous work involving thioesters on Fab. This is

especially useful during the acyl transfer step, as the lysine residues are even less nucleophilic at this pH, due to the higher pKa of the lysine amine sidechain and are even more likely to exist in their protonated form. This further highlights the effectiveness of introducing electron-withdrawing groups adjacent to the thioester carbonyl.

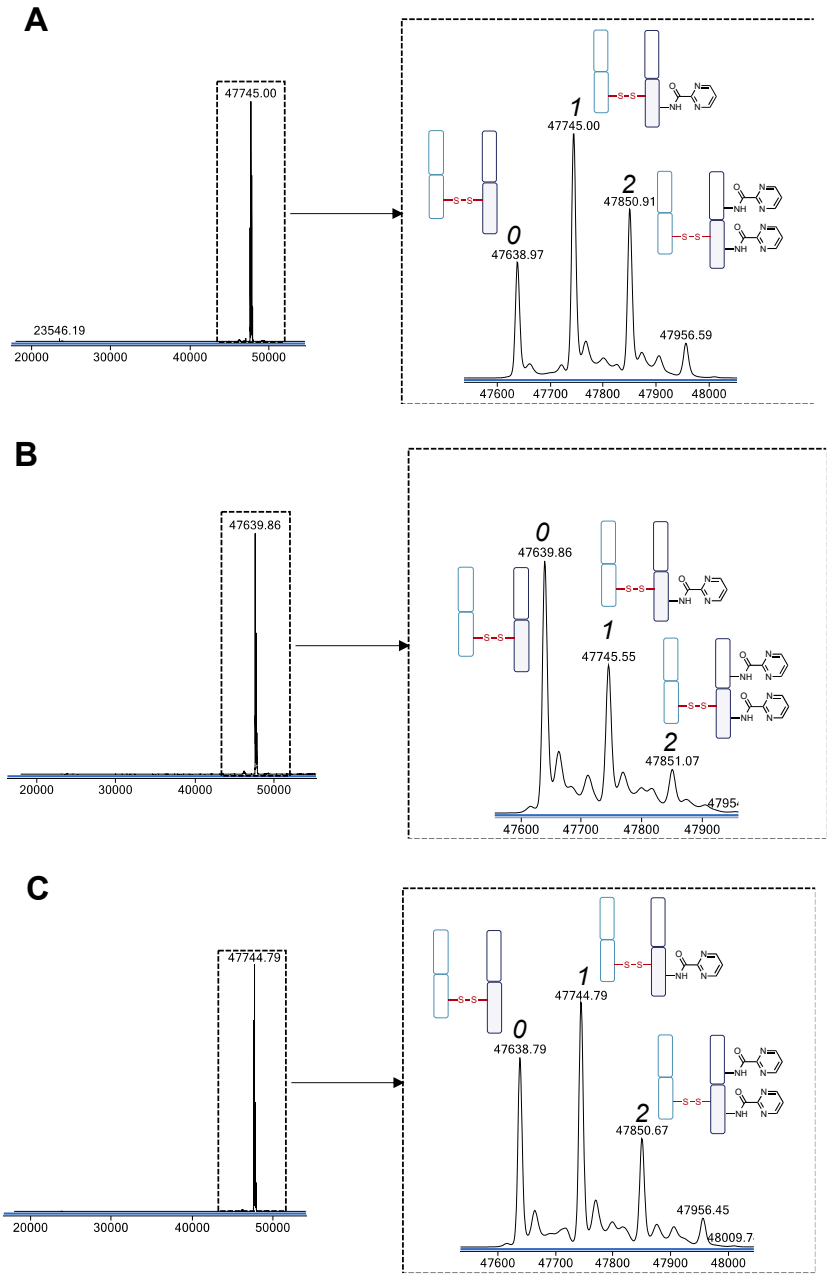


**FIGURE 61.** CLT of pyrimidine thioester conjugate. **A)** pH 6.5, 4 h, 22 ºC. **B)** pH 8.4, 4 h, 22 ºC. **C)** pH 7.4, 4 h, 22 ºC. Mass of native Fab = 47638 Da. Mass of native LC = 23440 Da. Mass of modified LC = 23545 Da. Mass of native HC = 24200 Da. Expected mass of addition = 107 Da (2 additions = 214 Da).

### 2.2.4. Tetrazine thioester

#### 2.2.4.1. Fab bioconjugation

The limited water solubility of tetrazine-thiophenol thioester **7a** meant that it was not explored for Fab bioconjugation, so tetrazine-MPAA thioester **7c** was the focus of this study. The pyrimidine thioester work provided a starting basis for tetrazine bioconjugation, as it indicated that very electron-deficient rings with strong electron-withdrawing group abilities demonstrate favourable reactivity at lower pH and react quickly too. pH 5.5 was chosen for transthioesterification of Fab with the tetrazine-MPAA thioester **7c** (**SCHEME 15**).

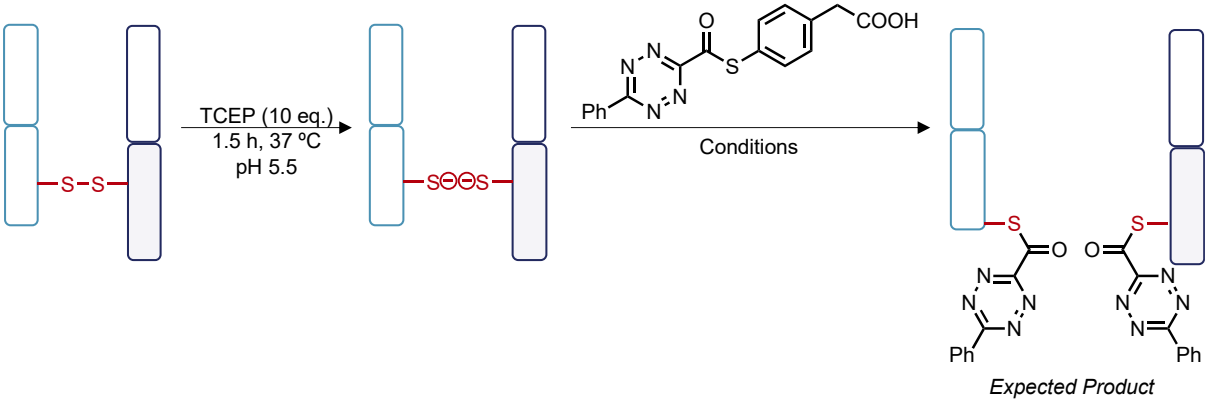


**SCHEME 15.** Tetrazine-MPAA thioester **7c** bioconjugation on Fab.

Control experiments (50 eq., 1 h, 22 ºC, pH 5.5) showed no unselective lysine modification (**FIG. 62A**). Bioconjugation on reduced Fab was investigated next. Experiments showed that complete LC and HC modification was observed in just 5 minutes at pH 5.5, indicating a rapid transthioesterification reaction with cysteine thiols that far outperforms other similar thioesters and the electron-deficient thioesters explored previously (**FIG. 62B**).

However, literature studies have demonstrated that tetrazines are susceptible towards TCEP and thiol-induced reduction.[237] To investigate whether this occurs in the tetrazine-MPAA thioester **7c**, it was added to Fab sequentially, with TCEP remaining in solution. In a separate experiment, TCEP was removed from the reaction and the tetrazine-MPAA thioester **7c** was added in the same conditions. From these studies, it would be possible to more accurately determine the identity and structure of the species conjugated onto the LC and HC cysteines. The tetrazine ring must retain its oxidised form to be compatible with iEDDA, and this electron-poor ring is also

important in maintaining a strong electron-withdrawing effect onto the thioester carbonyl, ensuring that subsequent CLT can occur rapidly too.

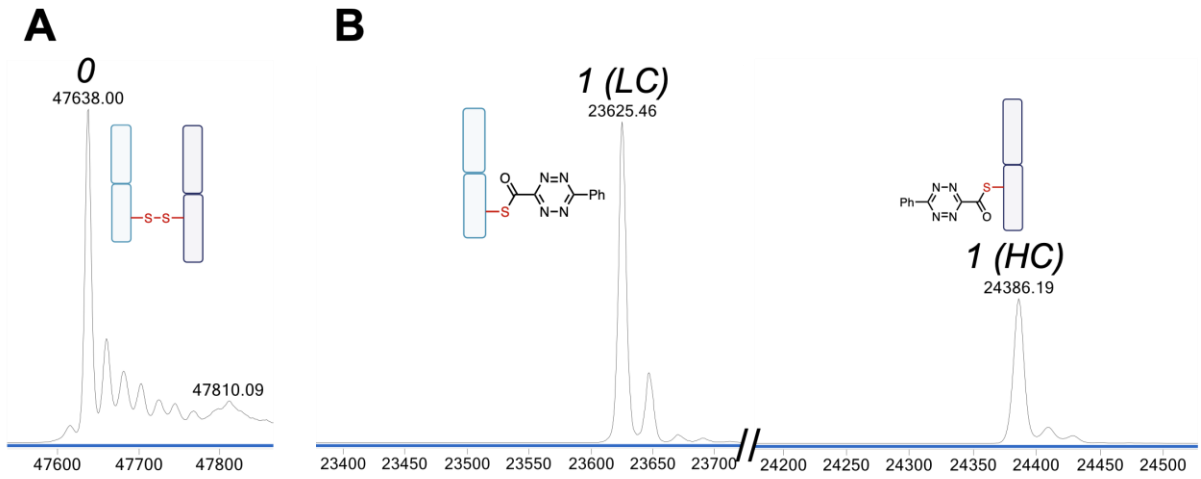


**FIGURE 62.** Bioconjugation of tetrazine-MPAA thioester **7c**. **A)** Control on non-reduced native Fab, 50 eq., 1 h, 22 ºC, pH 5.5. **B)** Reaction on reduced Fab, 50 eq., 5 min, 22 ºC, pH 5.5. Mass of native Fab = 47638 Da. Mass of native LC = 23439 Da. Mass of native HC = 24200 Da. Expected mass of addition = 185 Da. Smaller unlabelled peaks correspond to sodium adducts (M+Na, +23 Da).

The results suggest that TCEP triggers reduction of the tetrazine ring to dihydrotetrazine **8a** (**SCHEME 16**). When the reaction is incubated in the presence of TCEP, there is a gradual discolouration from pink, characteristic of the tetrazine ring, to yellow, characteristic of the dihydrotetrazine ring, over 0.5 h. As no dihydrotetrazine was observed during the synthesis of tetrazine-MPAA thioester **7c**, it is unlikely that MPAA, released during transthioesterification or during thioester hydrolysis, is responsible for this reduction. In the absence of TCEP, there are a mixture of two conjugate species on the LC and HC, with a mass difference of 10 Da (**FIG. 63A**). It is likely that the species with mass 23615 Da corresponds to the hydrolysed tetrazine ring **8b** (**SCHEME 16**), whilst the other species with mass 23625 Da corresponds to the desired tetrazine thioester conjugate. Over 0.5 h, there is gradual hydrolysis of the intact tetrazine ring to a hydrolysed ring species (**FIG. 63B**). Thus, there are two potential routes for deactivation of the tetrazine in the absence of TCEP – hydrolysis of the tetrazine ring itself to **8b**, or hydrolysis of the thioester, releasing the tetrazine carboxylic acid **6c**. In comparison, the suspected dihydrotetrazine conjugate formed from *in situ* TCEP reduction remains stable under similar timeframes (**FIG. 63C**).

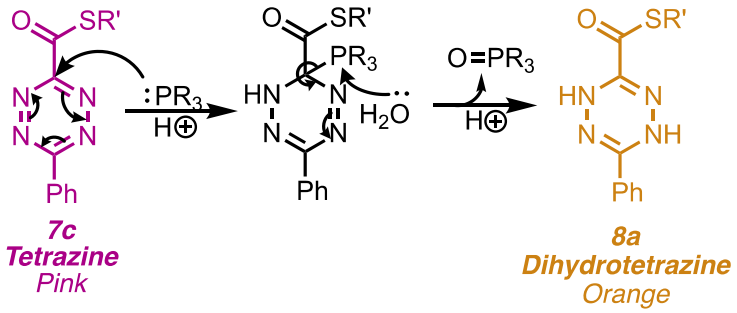


**SCHEME 16.** Proposed mechanism for TCEP reaction of tetrazine to generate dihydrotetrazine in aqueous conditions.

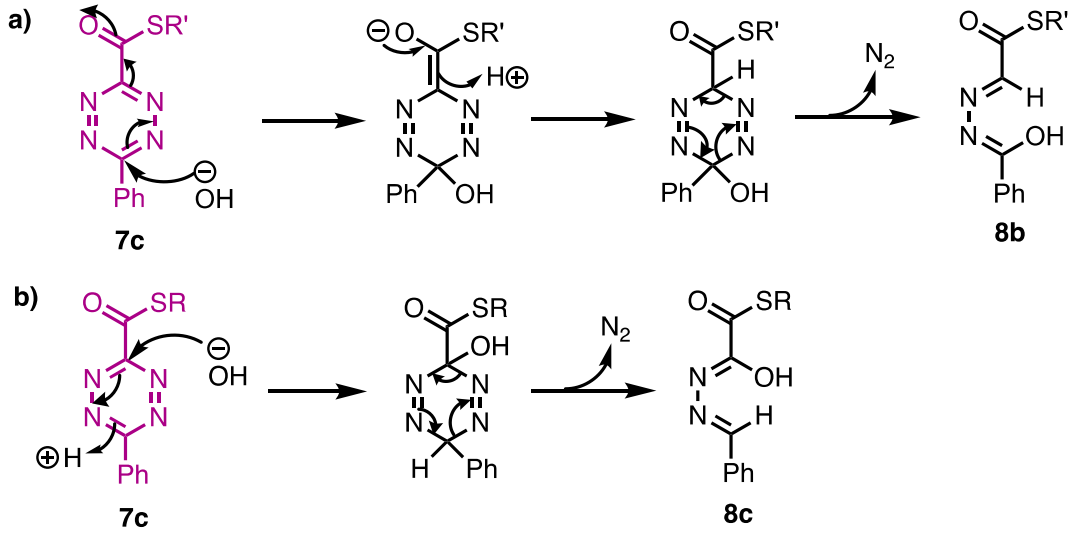


**SCHEME 17.** Proposed mechanism for tetrazine ring hydrolysis in water. **A)** 1,6-Michael addition reaction. **B)** Direct hydroxide ion attack

The tetrazine ring system features an extremely electron-deficient and electrophilic carbon atom as a result of the inductive electron-withdrawing effects from the nitrogen atoms and the adjacent carbonyl group. The nucleophilic phosphine atom of TCEP attacks this carbon atom, and elimination of TCEP enables dihydrotetrazine **8a** to form. The dihydrotetrazine is more thermodynamically stable as the ring system is less electron-deficient. Generation of **8a** effectively caps the thiols due to the stability of the conjugate, preventing further reactions with other thioester species in solution. Additionally, the ring itself could be hydrolysed through a 1,6-Michael addition reaction to give **8b,** or through direct attack of the hydroxide ion the electron-deficient carbon atom, as seen in the TCEP reaction, to give **8c.** The regioisomer **8b** is likely preferred as the carbon adjacent to the carbonyl group is likely more stable, as the introduced hydroxide group is further away, so there is less inductive electron-withdrawal.

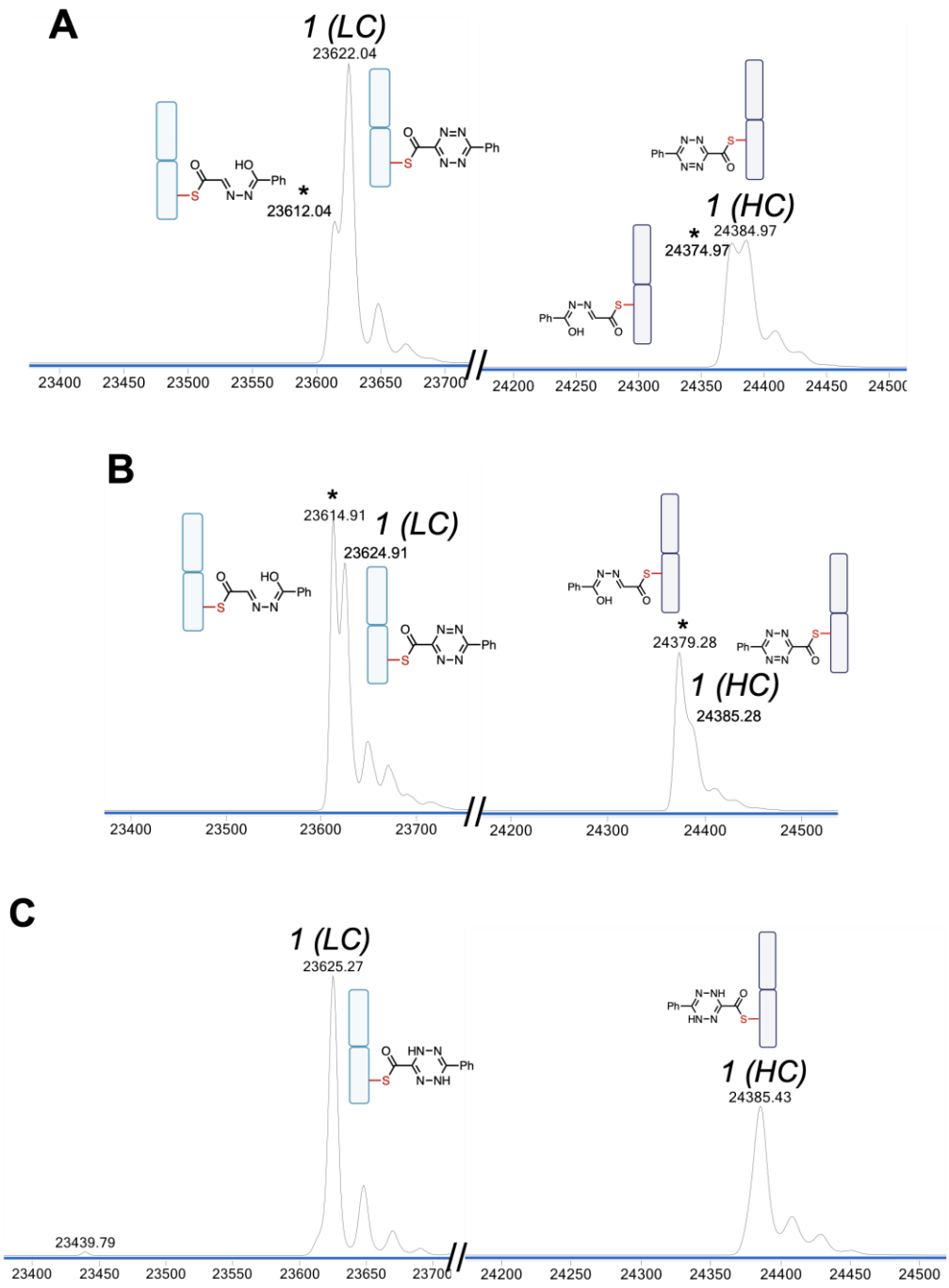


**FIGURE 63.** LCMS analysis of investigation of the stability of the conjugate seen upon addition of tetrazine-MPAA thioester **7c**. **A)** 5 minutes, 22 ºC, pH 5.5. **B)** 0.5 h, 22 ºC, pH 5.5. **C)** In the presence of TCEP, 0.5 h, pH 5.5, 22 ºC. Mass of native Fab = 47638 Da. Mass of native LC = 23439 Da. Mass of native HC = 24200 Da. Expected mass of addition = 185 Da. Smaller unlabelled peaks correspond to sodium adducts (M+Na, +23 Da). Peaks marked asterisk (*) indicate the suspected hydrolysed ring species **8b** (mass = 175 Da).

### 2.2.4.2. Exploring tetrazine reactivity

Identifying whether the dihydrotetrazine or tetrazine ring system is the dominant species in the presence of TCEP on conjugated Fab is difficult through LCMS analysis since both species have similar masses. However, only the tetrazine species can undergo iEDDA, and the tetrazine would also enable much faster CLT. As the dihydrotetrazine is not useful for iEDDA and does not provide meaningful electron-withdrawing effects, transthioesterification reactions were carried out in the absence of TCEP to minimise any dihydrotetrazine formation. pH 6.5, 4 h, and 22 ºC was selected as a starting point, as it proved effective for the CLT of pyrimidine thioester **3**, so could be suitable for tetrazine thioester conjugate CLT too (**SCHEME 18**).

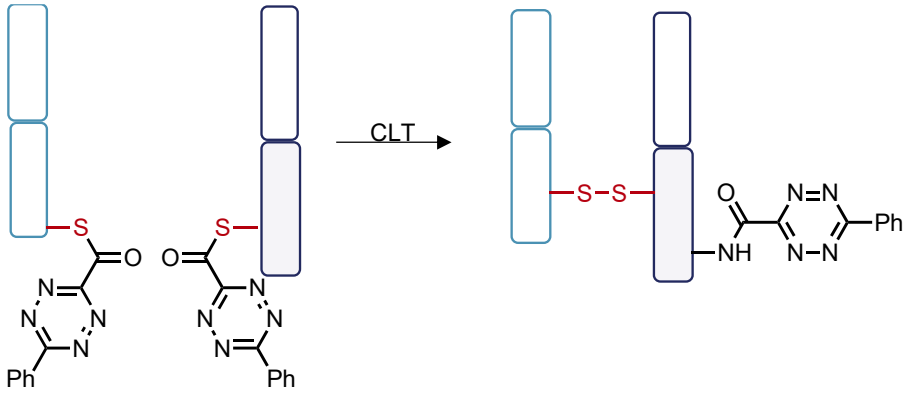


**SCHEME 18**. CLT of potential tetrazine thioester conjugate.

However, CLT was largely unsuccessful at pH 6.5 (**FIG. 64A**). The major product was native Fab, whilst there are small amounts of single modified-lysine species. It was apparent that there were significant amounts of hydrolysed tetrazine ring present on the LC, and some leftover tetrazine-related species too. The tetrazine thioester conjugate is likely hydrolysing rapidly – both at the thioester site, and on the tetrazine ring itself. Higher pH conditions (for example pH 7.4), in an attempt to outcompete hydrolysis and quickly form a more stable amide product, were also unsuccessful (**FIG. 64B**), returning mostly native Fab.

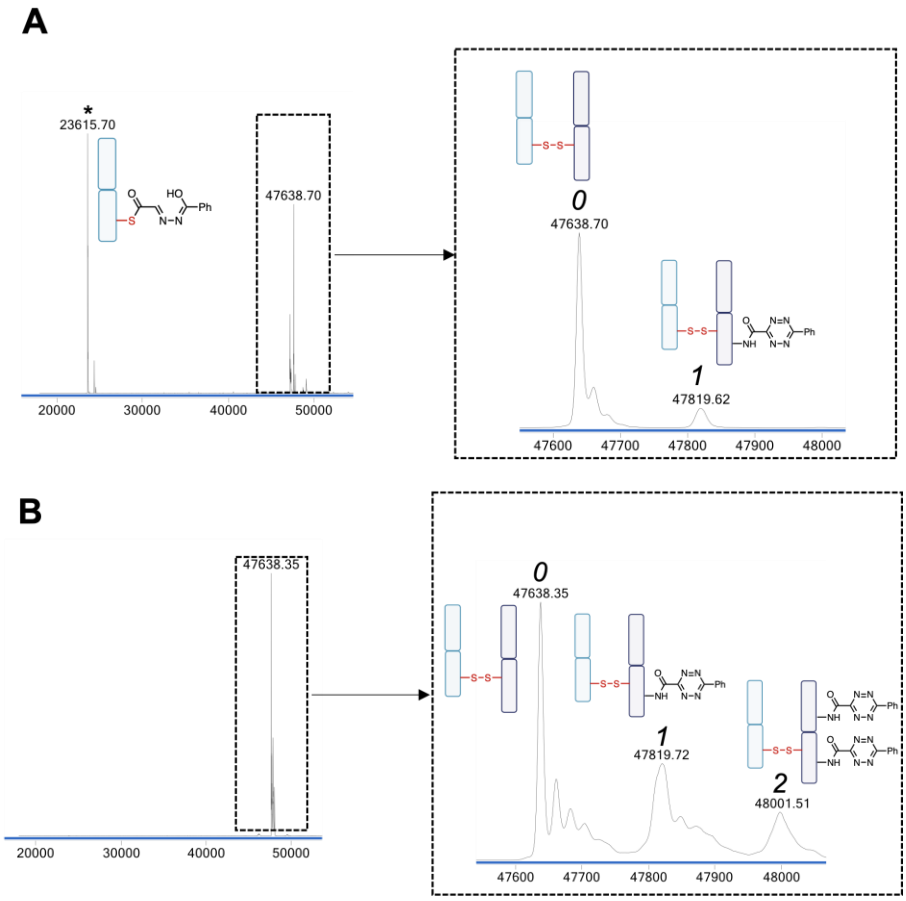


**FIGURE 64.** CLT of tetrazine thioester conjugate under different conditions. **A)** pH 6.5, 4 h, 22 ºC. **B)** pH 7.4, 4 h, 22 ºC. Mass of native Fab = 47638 Da. Mass of native LC = 23439 Da. Mass of native HC = 24200 Da. Expected mass of addition = 185 Da. Smaller unlabelled peaks correspond to sodium adducts (M+Na, +23 Da).\

It was considered that the resultant amide itself could be unstable. Amide bonds are also electron-withdrawing, though their electron-withdrawing strength is less than that of carboxylic acids. It is possible that the lysine-modified CLT conjugate forms quickly, but the tetrazine ring or amide bond of this conjugate are also hydrolysed immediately. To investigate whether this occurs, iEDDA was explored.

iEDDA between BCN and tetrazine forms a pyridazine compound in very quick timeframes, requiring less than 10 minutes. The reaction is also not pH dependent. The pyridazine is generally stable in aqueous conditions, as the resultant ring system is far less electron deficient. This ring system is somewhat analogous to the previously explored pyridine and pyrimidine ring systems, which have demonstrated sufficient levels of aqueous stability. Undergoing iEDDA with the Fab conjugate of the tetrazine-MPAA thioester **7c** transthioesterification step would form an intermediate pyridazine,

which could be explored for CLT (**SCHEME 19**). After the 5 min transthioesterification step at pH 5.5, excess tetrazine is removed and BCN is added.

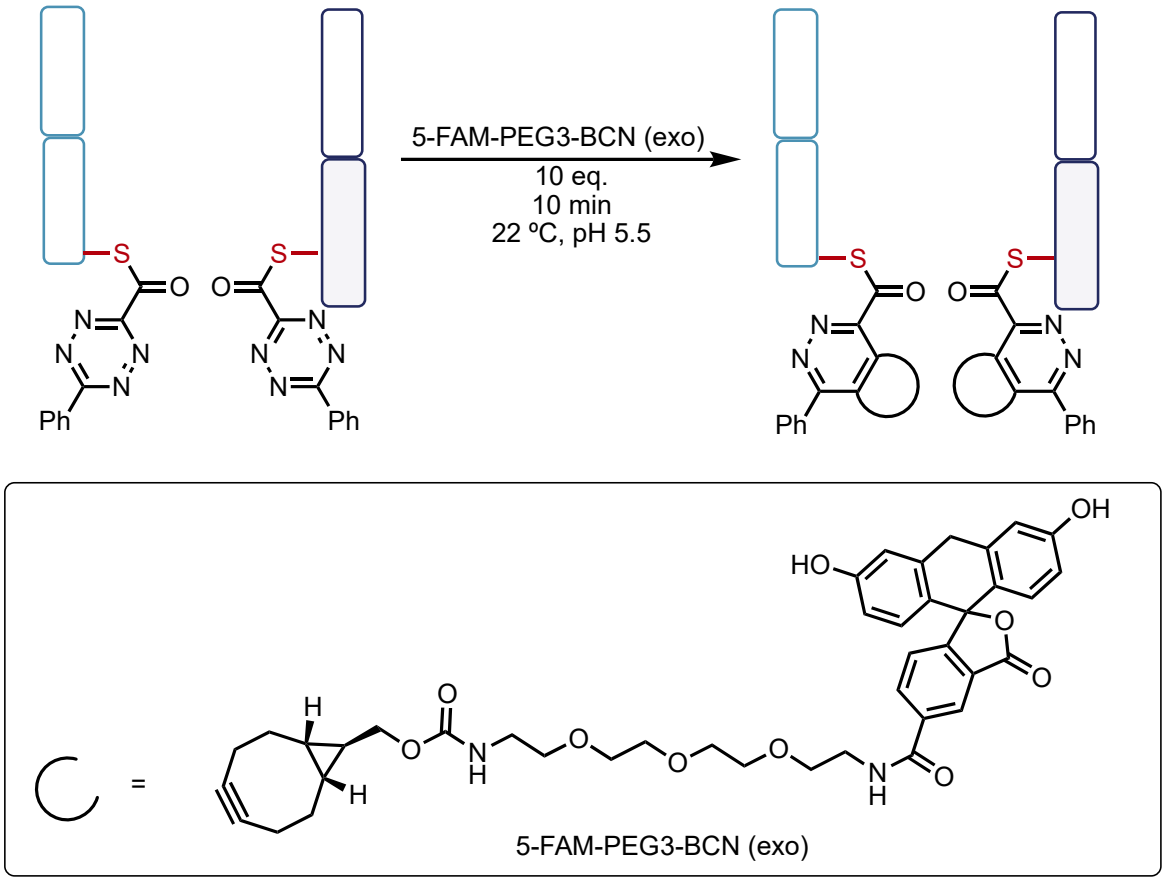


**SCHEME 19.** iEDDA of tetrazine thioester conjugate with a BCN compound.

However, iEDDA was completely unsuccessful on the Fab tetrazine thioester conjugate. No modification was observed, and instead the thioester hydrolysed off the cysteine residues (**FIG. 65A**). The large steric bulk of the incoming BCN dienophile may prevent CLT, as observed in the quinoline-MESNa thioester **2** studies. Transthioesterification was also attempted with 2.2 eq. of tetrazine-MPAA thioester **7c** for 1 min at pH 7.4, to observe whether it is possible to enable immediate transthioesterification and CLT and therefore minimise tetrazine degradation prior to iEDDA. Instead, only hydrolysis of the tetrazine ring on the LC and tetrazine thioester was observed (**FIG. 65B**). It was not possible to form the pyridazine ring structure as desired. This further exemplifies the immense reactivity of the tetrazine thioester, and its instability in aqueous conditions.

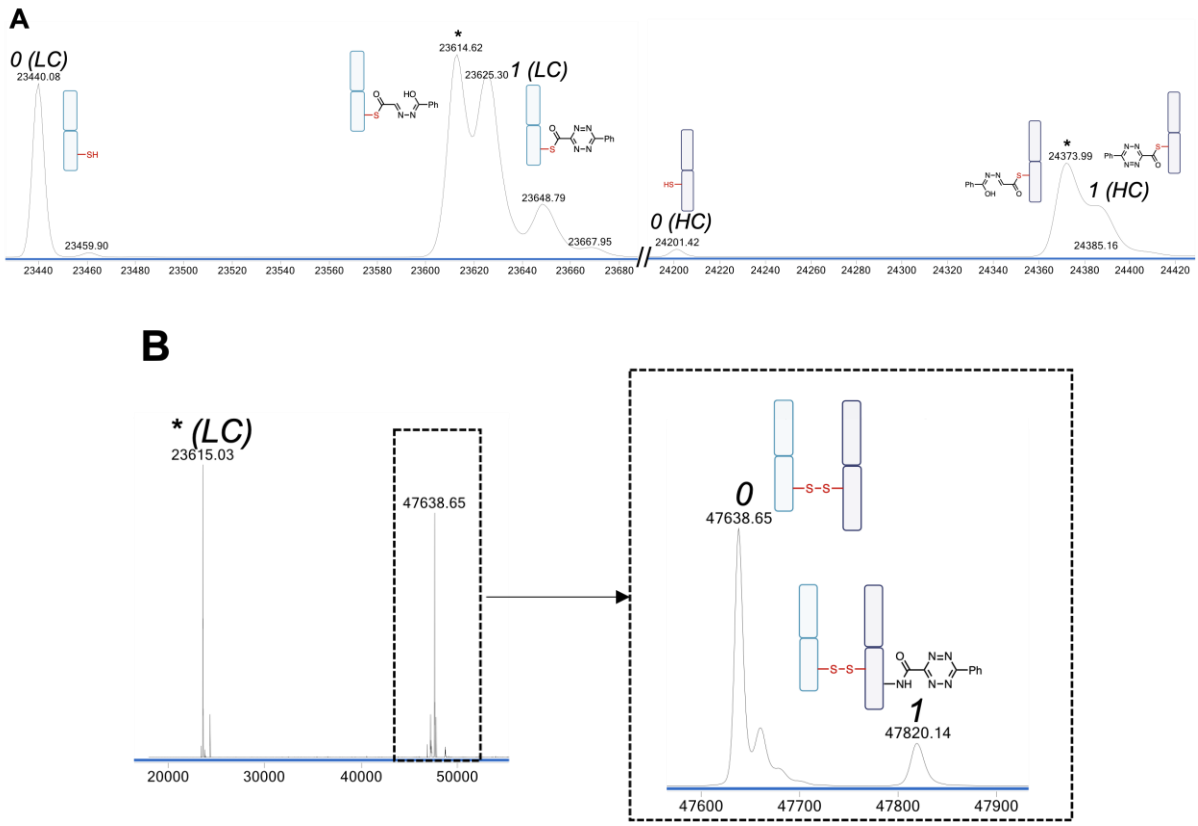


**FIGURE 65.** iEDDA attempts on tetrazine thioester conjugate. **A)** Transthioesterification at pH 5.5, 22 ºC, 5 min, followed by iEDDA with 5-FAM-PEG3-BCN (10 eq., 22 ºC, 10 min, pH 5.5). **B)** Transthioesterification at pH 7.4, 22 ºC, 1 min, followed by iEDDA with 5-FAM-PEG3-BCN (10 eq., 22 ºC, 10 min, pH 7.4). Mass of native Fab = 47638 Da. Mass of native LC = 23439 Da. Mass of native HC = 24200 Da. Expected mass of addition (tetrazine-MPAA thioester **7c**) = 185 Da. Expected mass of addition (5-FAM-PEG3-BCN) = 724 Da.

These experiments have indicated the difficulty in controlling the reactivity of the tetrazine-MPAA thioester for Fab modification. Whilst previous thioesters explored are limited mostly by thioester hydrolysis, the tetrazine thioester explored here has two points of susceptibility towards hydrolysis – the thioester itself, and the tetrazine ring. Whilst the tetrazine electron-withdrawing group results in a very electron-deficient thioester carbonyl that undergoes 5 min transthioesterification, this has further increased its susceptibility to hydrolysis. Meanwhile, the addition of a thioester carbonyl adjacent to the tetrazine ring has served to withdraw electrons away from the ring as well, making the ring more prone towards nucleophilic attack by hydroxide ions and TCEP. These two electronic features make it challenging to optimise the bioconjugation conditions to develop an effective Fab modification reagent.

#### 2.2.4.3. Stability investigations of tetrazine thioester

The tetrazine thioester demonstrates significant reactivity towards nucleophiles that limits its suitability for Fab bioconjugation. However, the reagent could nonetheless find appropriate use in other protein-related applications, such as on peptides for example. The electron-withdrawing effect of the carbonyl makes the tetrazine ring extremely electron-deficient, thus it could engage in iEDDA faster than typical commercially available tetrazines. It is important to understand the stability of the tetrazine thioester in aqueous conditions, which would help guide future development and applications. In particular, pH could play a major role in finding suitable conditions in which the tetrazine-MPAA thioester **7c** shows workable stability.

To achieve this, a series of stability investigations were conducted. The tetrazine-MPAA thioester **7c** was incubated in a variety of conditions, including 100% MeCN and 20:80 MeCN:buffer. The same concentration of tetrazine was used across all studies. LCMS-compatible volatile buffers with pH ranging between 5.0-8.0 were selected. The tetrazine-MPAA thioester **7c** was added to these solutions and stirred for 10 minutes, which is a relevant timeframe for peptide reactions with tetrazine compounds and subsequent functionalisation *via* iEDDA. The mixture was then immediately analysed by LCMS (**FIG. 66**).

In anhydrous MeCN, there is no degradation of tetrazine-MPAA thioester **7c** over 10 minutes. Similarly, pH 5.0 results indicate that the tetrazine-MPAA thioester **7c** is stable at this pH. Some degradation is observed at pH 6.0, and this corresponds to hydrolysis of the thioester and the release of MPAA. There are additional impurities present, some of which correspond to small amounts of hydrolysed tetrazine ring species **8b**. At pH 7.0 and pH 8.0, the tetrazine-MPAA thioester **7c** begins to degrade, with ES+ scans showing the presence of a new m/z ion with mass of 335 Da, with the retention time slightly lowered (3.74 min to 3.67 min). This likely corresponds to the gradual formation of the hydrolysed tetrazine ring species **8b**, which is more polar due to the additional hydroxyl group. There is also a new species eluting at 2.50 min, which corresponds to the tetrazine carboxylic acid species **6c**, indicating hydrolysis of the thioester is promoted by higher pH. These results indicate that as pH increases, the tetrazine-MPAA thioester **7c** becomes increasingly unstable and prone to degradation, and this was indeed reflected in the bioconjugation studies.

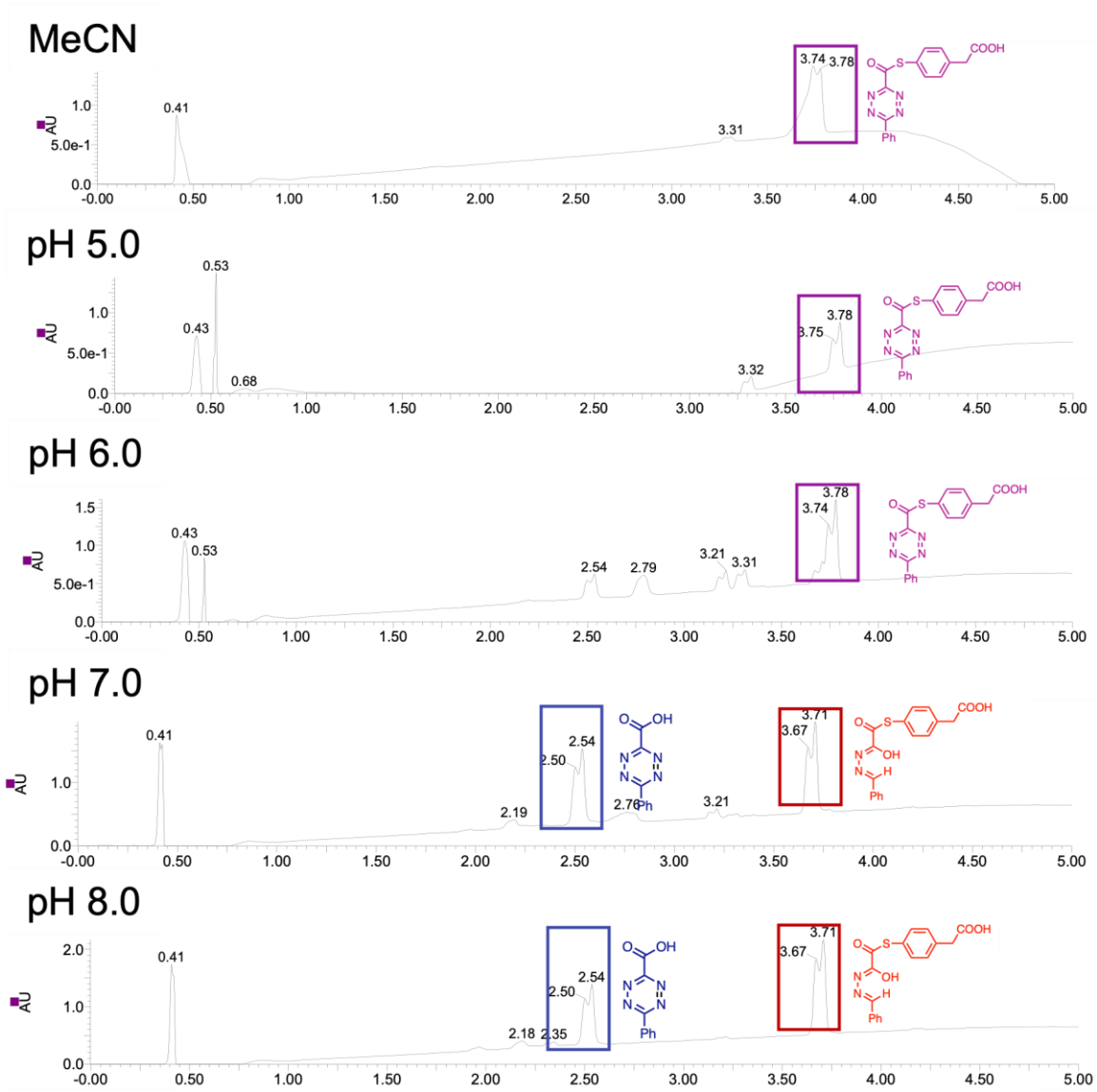


**FIGURE 66.** LCMS analysis of tetrazine-MPAA thioester **7c** in different buffer conditions. Pink compound = tetrazine-MPAA thioester **7c**. Blue compound = Tetrazine carboxylic acid **6c**. Red compound = tetrazine-MPAA hydrolysed ring species **8b**. See Appendix for ES+ scans of the highlighted peaks.

These results also demonstrate why the tetrazine-MPAA thioester **7c** was not compatible with CLT. Above pH 6.0, tetrazine hydrolysis occurs, but this pH is needed in Fab bioconjugation experiments to enable lysine reactivity. Additionally, complete hydrolysis occurs very rapidly, within 10 minutes, which makes finding a window for CLT very difficult, especially at lower pH where the lysine amines are protonated. However, the tetrazine-MPAA thioester **7c** shows good stability at pH 5.0, and this could provide an opportunity for *N*-terminal cysteine modification work.

### 2.2.4.4. Tetrazine thioester for *N*-terminal cysteine modification

The tetrazine thioester instability in aqueous conditions makes it unsuitable for the modification of Fab through CLT. However, the tetrazine-MPAA thioester **7c** could prove to be a very effective NCL reagent for the *N*-terminal modification of cysteine-containing peptides. Whilst CLT is limited by the acyl transfer step, due to the distance to the proximal lysine residues, NCL on cysteine is often limited by the initial transthioesterification where the intramolecular acyl transfer often occurs spontaneously and instantly. Thus, the tetrazine-MPAA thioester **7c** could overcome its aqueous stability issues by quickly forming an amide bond, minimising thioester hydrolysis, and then undergoing immediate iEDDA to form a more stable pyridazine structure, minimising tetrazine ring hydrolysis. To investigate this, experiments of tetrazine thioester reactions with *O*-Me-cysteine and BCN-amine were conducted as initial proof-of-concepts at pH 5.0, which showed the greatest tetrazine thioester stability (**SCHEME 20**).

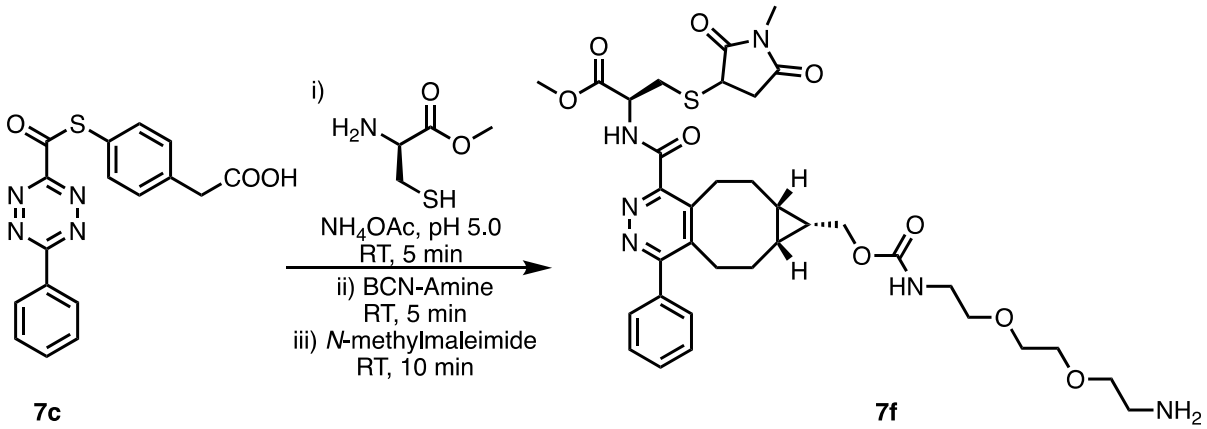


**SCHEME 20.** Reaction between tetrazine-MPAA thioester **7c** and *O*-Me-cysteine, followed by iEDDA with BCN-Amine and subsequent maleimide capping.

The tetrazine-MPAA thioester **7c** was added to an equivalent amount of cysteine at RT and stirred for 5 min, before BCN-amine (1.5 eq.), the dienophile for iEDDA, was added and the reaction mixed at RT for a further 5 min. A slight excess was used to account for potential oxidation of the BCN ring. Following this, *N*-methylmaleimide was added, to cap any free thiols and confirm that NCL successfully occurs, and the reaction shaken at RT for a further 10 min. LCMS analysis was then conducted of the resultant final species, pyridazine **7f** (**FIG. 67**). Structures and LCMS analysis of intermediate steps are shown in the Appendix (**FIG. S.95** – **FIG. S.97**).

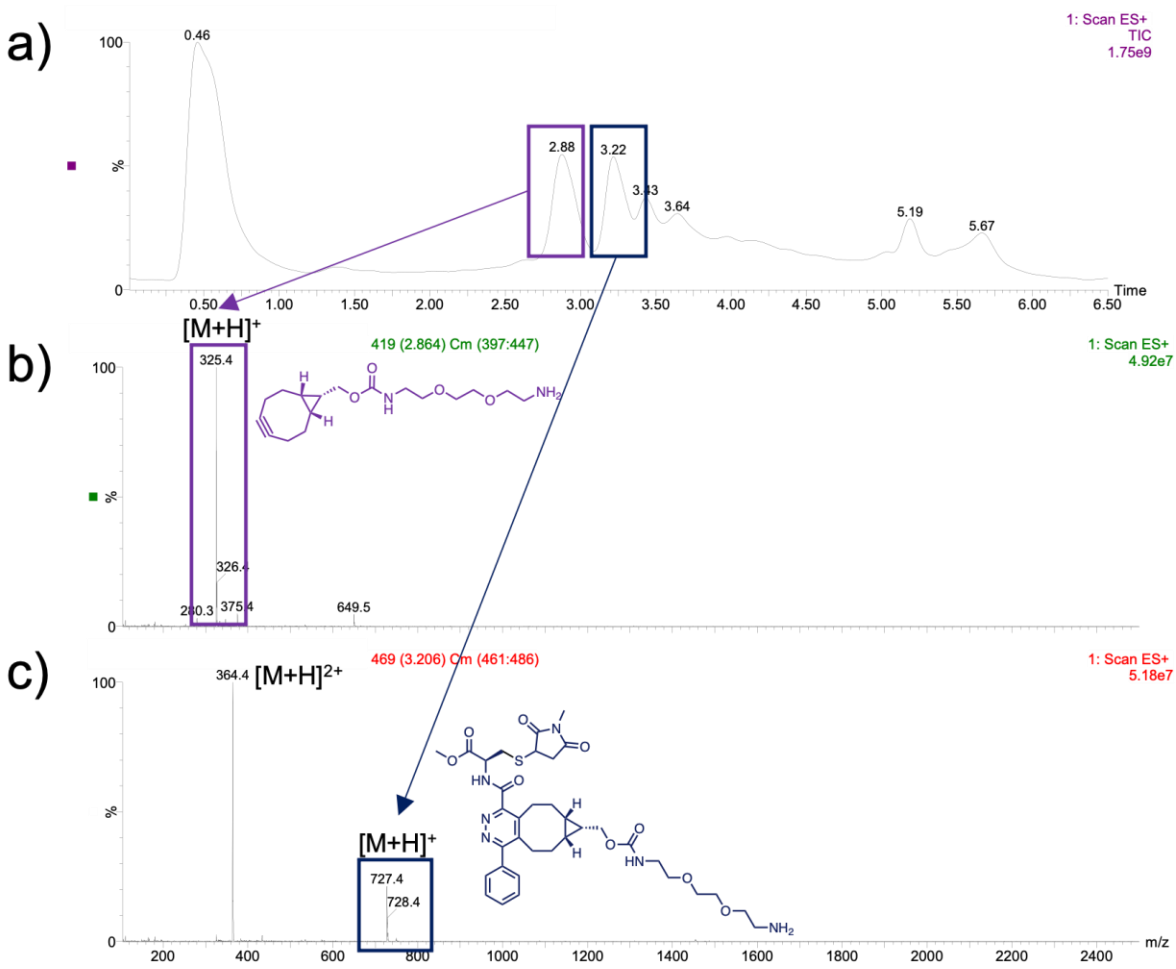


**FIGURE 67.** LCMS analysis of tetrazine-MPAA thioester **7c** reaction with *O*-Me-cysteine, BCN-amine, and *N*-methylmaleimide to synthesise **7f**. **A)** ES+ TIC. **B)** ES+ scan of peak at 2.88 min, determined to be BCN-amine (purple). **C)** ES+ scan of peak at 2.22 min, determined the desired clicked product **7f** (navy). See Appendix for full collected ES+ data for individual steps of the reaction.

It is possible to observe the complete cysteine transthioesterification and subsequent NCL (Appendix **FIG. S.95**). Promisingly, there is no hydrolysed ring species or leftover starting material. Amides are slightly weaker electron-withdrawing groups than acids and thioesters, NCL so could help stabilise the ring structure against hydrolysis before iEDDA. Following iEDDA with BCN-Amine, the major product from this reaction is the desired clicked compound **7e** (Appendix **FIG. S.96**), which forms a stable pyridazine ring. There is some leftover BCN-amine, which is expected since it was used in excess. Additionally, maleimide capping has successfully occurred, forming a succinimide linkage between the freed thiol and the maleimide ring, confirming NCL, to form the final *N*-terminal-modified cysteine **7f** (Appendix **FIG. S.97**).

Thus, the tetrazine thioester presented here enables a 10 minute protocol for the modification of *O*-Me-cysteine. The tetrazine thioester also features very good water solubility, an excellent leaving group for NCL in MPAA, and demonstrates rapid transthioesterification reactions, whilst having a clickable diene ring for iEDDA. This would be a very useful and effective method of functionalising peptides with fluorophores, drugs, or other interesting moieties within minutes. Overall, the reactivity of the tetrazine thioester and its potential for click reactions makes a very exciting reagent for NCL, and it demonstrates very exciting possibilities for rapid *N*-terminal cysteine peptide modifications. More work is needed to understand the yield of the reaction by isolating the final species obtained.

### 2.3. Overall summary and conclusion of electron-deficient thioesters

The results here demonstrate that electron-deficient thioesters enable faster transthioesterification and CLT because of an electron-withdrawing effect on the thioester – a greater electron-withdrawing effect by the introduction of additional neighbouring nitrogen atoms enables faster reactions with trastuzumab Fab than previously seen for CLT, with the greatest reactivity seen in a pyrimidine thioester, followed by a pyridine thioester. The pyrimidine reagent **2** demonstrates particularly useful results, obtaining complete modification and conjugates of DAR 1.2 within 6.5 h total reaction time, in comparison to the 3-days previously required by the alkyl thioesters. The reactivity of this reagent enables it to engage with amino acid residues at lower pH than previously explored, which could be useful in eliminating undesired side reactions with other nucleophilic amino acids. This enables a fast approach towards site-selectively modified Fab conjugates with stable amide bonds, which is of interest for the development of homogeneous ADCs. However, another aim for these electron-deficient thioesters was to overcome competing hydrolysis. This was not possible in these reagents, and instead they are more hydrolytically susceptible than the alkyl thioesters, even at lower pH, leading to lower DARs.

Additionally, whilst increased electron-deficiency results in increased reactivity, the tetrazine thioester has shown that a balance between reactivity and stability must be obtained. As a result of the tetrazine ring itself and the electron-withdrawing effect of the thioester carbonyl, the highly reactive tetrazine thioester demonstrates two hydrolysis pathways – at the thioester position, and on the ring itself. This limits its

suitability as a CLT reagent due its instability on the timescale required to achieve lysine transfer. However, the tetrazine thioester demonstrates exceptional reactivity for *N*-terminal cysteine modification, with reactions complete within minutes. Utilising the tetrazine thioester in this manner can overcome its aqueous stability issues, and with more investigations it is likely to prove one of the fastest available clickable NCL reagents in existing literature.

Therefore, overall, the pyrimidine thioester demonstrates the best results for CLT as it enables a much faster bioconjugation process at lower pH whilst demonstrating good levels of stability. Expansion of the utility of these reagents beyond CLT (i.e., for NCL) demonstrates the tetrazine thioester as an exceptionally promising reagent. These studies show there is merit in pursuing electron-deficient thioesters for both CLT and NCL for *N*-terminal cysteine modification.

### 2.4. Further work on electron-deficient thioesters

The pyridine thioester **1** and pyrimidine thioester **3** show good reactivity and quick bioconjugation. However, these compounds do not currently have any functionality. Ideally, a bioorthogonal handle would be inserted to enable bioorthogonal reactions through click chemistry. Examples could include alkynes, azides, and tetrazines (**SCHEME 20**). These groups could engage in CuAAC, SPAAC, or iEDDA respectively. The azide and tetrazine insertions may also act as *p*-substituted electron-withdrawing groups through the mesomeric effect.

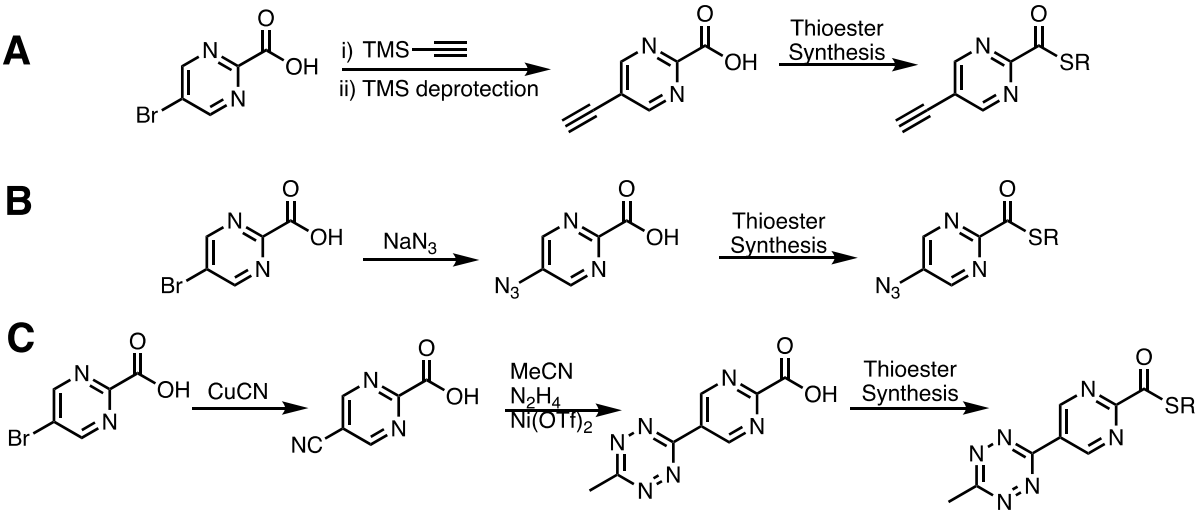


**SCHEME 21**. Proposed synthesis of functionalised pyrimidine thioester **3**. **A**) Insertion of alkyne. **B**) Insertion of azide. **C)** Insertion of tetrazine.

Additionally, charged nitrogen systems could be of interest. This could involve the established pyridine or pyrimidine systems – alkylation of the nitrogen atom would create a very electron-deficient ring system that would serve to strongly withdraw electrons from the thioester carbonyl, further increasing reactivity. This could provide a way of achieving similar electron-deficiency to that observed in the tetrazine thioester without having a ring system susceptible towards hydrolysis itself.

Attempts to synthesise the triazine thioester **5** were unsuccessful, potentially due to side-reactions with the added thiol – the alkene bond within the ring system is likely somewhat electrophilic as a result of the inductive electron-withdrawing effect of the neighbouring nitrogen atoms. To remedy this, an alternative synthesis could be used to replace the unsubstituted alkene. For example, introducing methyl groups by using dimethylglyoxal instead of glyoxal could prevent the formation of side-products resulting from addition to the alkene. Other substituted glyoxal compounds could be used to insert other functionalities onto the triazine ring, possibly enabling the synthesis of tri-functional reagents. A potential triazine thioester may prove to be an ideal balance of electron-deficiency for rapid protein reactions and good aqueous stability for CLT purposes.

Furthermore, the tetrazine thioester **7c** shows rapid reactivity, however its usefulness for CLT is limited by its aqueous instability. The attached phenyl ring could provide a way of improving hydrolytic stability of the tetrazine ring itself. The addition of electron-donating groups on the *p*-position of the phenyl ring would help stabilise the tetrazine ring against hydrolysis through the mesomeric effect, though this may also deactivate the tetrazine, making it a weaker electron-withdrawing group and reducing the rate of iEDDA. It would be necessary to investigate suitable electron-donating groups that could achieve a balance between improved stability and maximal reactivity.

Other substituents instead of phenyl groups could be used instead too (**FIG. 67**). Vinyl ethers have been shown to enable increased tetrazine iEDDA reactivity without behaving as electron-withdrawing groups.[238] Studies have shown that vinyl ether substituted tetrazines show markedly better stability than pyridine-substituted tetrazines. This increased reactivity is thought to be due to the O-N intramolecular repulsion, which could help balance the electron-withdrawing effect of the thioester carbonyl and improve aqueous stability.

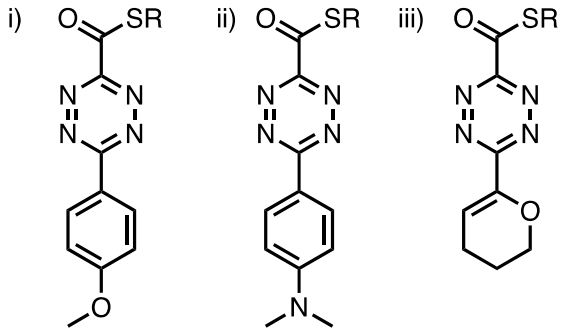


**FIGURE 68.** Examples of alternative tetrazine thioester designs. i) phenyl methoxy substituent ii) phenyl tri-substituted amine substituent iii) vinyl ether substituent.

Finally, the tetrazine-MPAA thioester **7c** shows limitations in CLT but shows remarkable proficiency as an *N*-terminal cysteine modification reagent, achieving such modification within 10 mins. Whilst *N*-terminal cysteine peptides are rare in nature, the *N*-terminus is often an ideal location for modification as it does not impact the folding of the protein structure, so it is a very interesting and well-studied strategy for protein modification.[239] In this work, only a simple *O*-Me-cysteine compound with a non-functionalised BCN-amine was utilised for initial investigations. However, the tetrazine thioester **7c** could be further applied for NCL in a variety of very interesting *N*-terminal cysteine peptides for therapeutic benefit.[240] The synthesis of *N*-terminal cysteine peptides and subsequent functionalisation *via* NCL using a tetrazine thioester could provide the rapid generation of large peptide libraries that differ in fluorophores, cytotoxic drugs, and any other functionality that can be incorporated onto BCN derivatives for iEDDA.

Thus, there is still much opportunity in terms of further optimising and improving the chemistry of the electron-deficient thioesters, especially for the tetrazine thioester where there is an array of potential modifications at the phenyl position to potentially make the tetrazine thioester a better CLT reagent. Nonetheless, there is also significant scope for the use of the tetrazine thioester in peptide modifications.

# 3. Investigation into the discovery of novel reagents for CLT

Thioesters are generally popular reagents for protein modification due to their high cysteine selectivity, however there are several other organosulfur reagents that have not been explored on protein systems and remain relatively less explored in literature. These include thiocarbonates, thiocarbamates, dithiocarbonates, and carbonimidodithioates. The C-S bond in these reagents differ in electronics, steric, and bond characteristics, and this will significantly impact the reactivity observed. As part of this chapter, convenient synthesis towards these reagents will be described, and their potential as protein modification will be explored, with a particular focus towards their capabilities as CLT reagents on trastuzumab Fab.

## 3.1. Thiocarbonates

Thiocarbonates have been explored for the construction of polymers,[241] as thiol protecting groups,[242] and have featured in pharmacologically relevant compounds.[243] They are less explored than their carbonate ester counterparts, with few studies on their possible use as protein modification reagents. In the thiocarbonate, the introduction of an oxygen atom nearby the carbonyl has implications on reactivity, compared to both thioesters and carbonate esters. Oxygen is electronegative, so has an inductive effect, withdrawing electrons away from the C=O carbon atom. In addition, the oxygen atom also has a lone pair that can delocalise into the system. To further understand thiocarbonate reactivity, the bond properties of carbonates are useful as comparisons.[244] In carbonates, the three oxygen atoms in a typical carbonate ester share partial double bond characteristics, bound by partial $\pi$-bonds, in a resonating structure. However, in thiocarbonates, the sulfur atom is larger than oxygen, and thus there is less overlap between the large sulfur 3p orbital and the smaller carbon 2p orbital, leading to minimal $\pi$-interactions and minimal C=S bond characteristics. This can be further understood from $^{13}$C NMR chemicals shifts – the thioester carbon has the highest chemical shift (~190 ppm), followed by a thiocarbonate (~170 ppm), and lastly carbonate (~150 ppm), reflecting decreasing deshielding of the central carbon atom. Thus, thiocarbonates are likely to be more stable than corresponding thioesters due to the presence of partial double bonds resulting from bond interactions with the introduced oxygen atom (**FIG. 69**).

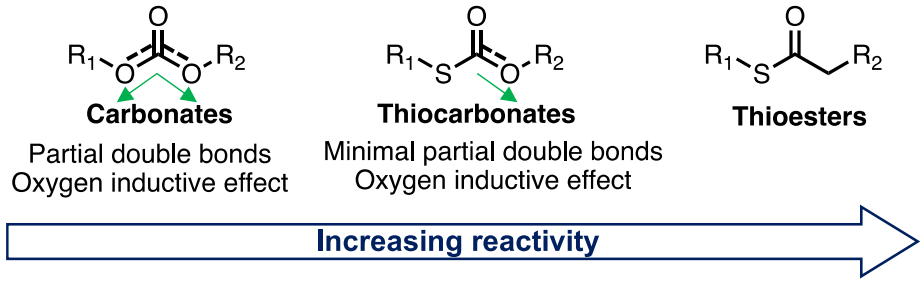


**FIGURE 69.** Structures and bond properties of carbonates, thiocarbonates, and thioesters, with their predicted order of reactivity.

Such stability could be beneficial for CLT, since thioesters commonly suffer from competing hydrolysis in aqueous conditions. Thiocarbonates could provide sufficient stability of the intermediate cysteine conjugate against hydrolysis, maximising acyl groups available for acyl transfer to nearby lysine. Additionally, the lysine-conjugated product would consist of a carbamate bond (**FIG. 70**), which themselves are very stable. Carbamates have also been used in ADCs within the design of self-immolative linkers.[245]

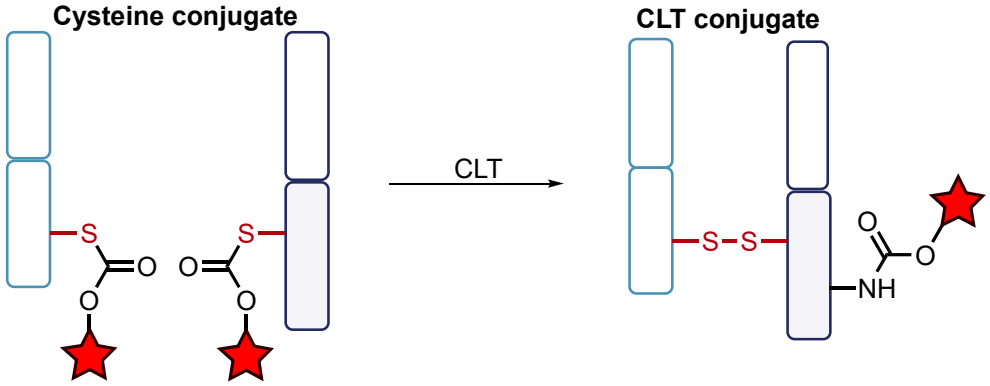


**FIGURE 70.** Cysteine and possible CLT conjugate from thiocarbonates.

### 3.1.1. Chemical synthesis

Organic chemistry strategies towards the synthesis of thiocarbonates sometimes involves the use of very toxic reagents, such as phosgene gas or triphosgene.[246] An alternative synthetic procedure that uses commercially available reagents in mild conditions is desirable. Thus, the use of *N*,*N*'-disuccinimidyl carbonate (DSC) was selected as a suitable starting material.

DSC consists of two activated NHS groups, which can be easily substituted with a variety of nucleophiles, such as thiols, alcohols, and amines (**SCHEME 22**). The

alcohol alkyne propyn-1-ol was selected for synthesis of the carbonate ester, with the alkyne providing possible late-stage functionalisation *via* click chemistry. For the synthesis of alkyl thiocarbonate **9** and aryl thiocarbonate **10**, addition of the alcohol occurred in a dropwise manner, to prevent double addition to both NHS esters. It was important to add the alcohol first, as otherwise the intermediate thiol-NHS carbonate ester is substituted by alcohol at the sulfur and oxygen positions, leading to mixtures of products. Following complete addition to synthesise the intermediate alkyne carbonate ester, the alkyl thiol MESNa (for thiocarbonate **9**) or the aryl thiol MPAA (for thiocarbonate **10**) were added, synthesising the thiocarbonates in good yields. Anhydrous conditions were important, as this minimised DSC hydrolysis and improved yields. Both thiols are commonly used in NCL and have good water solubility.

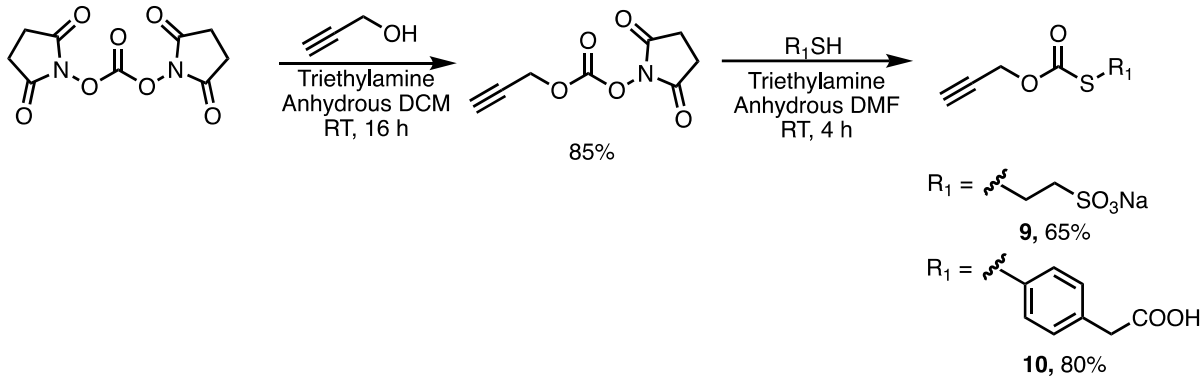


**SCHEME 22.** Synthetic route utilised for thiocarbonates **9** and **10**.

Following successful synthesis of both alkyl and aryl thiocarbonates, these reagents were then explored on Fab in bioconjugation studies. It is expected the alkyl thiocarbonate **9** would feature less reactivity than the aryl thiocarbonate **10**, as the latter has an aromatic, better leaving group in MPAA.

### 3.1.2. Bioconjugation of thiocarbonates on Fab

#### 3.1.2.1. Standard bioconjugation conditions

Control studies were conducted on non-reduced Fab. At pH 7.4, the control studies (100 eq., 4 h, 22 ºC, pH 7.4) showed no bioconjugation for either thiocarbonate (**FIG. 71A**). However, on reduced Fab (**SCHEME 23**), no reactivity was observed with either alkyl thiocarbonate **9** or aryl thiocarbonate **10**, under conditions of 100 eq., 4 h, 22 ºC, at pH 7.4 (**FIG. 71B** and **71C)**. Only native LC and HC were left over, suggesting no reactivity towards these thiocarbonates under the investigated conditions. Increasing temperature to 37 ºC had no effect on bioconjugation within the same timeframe.

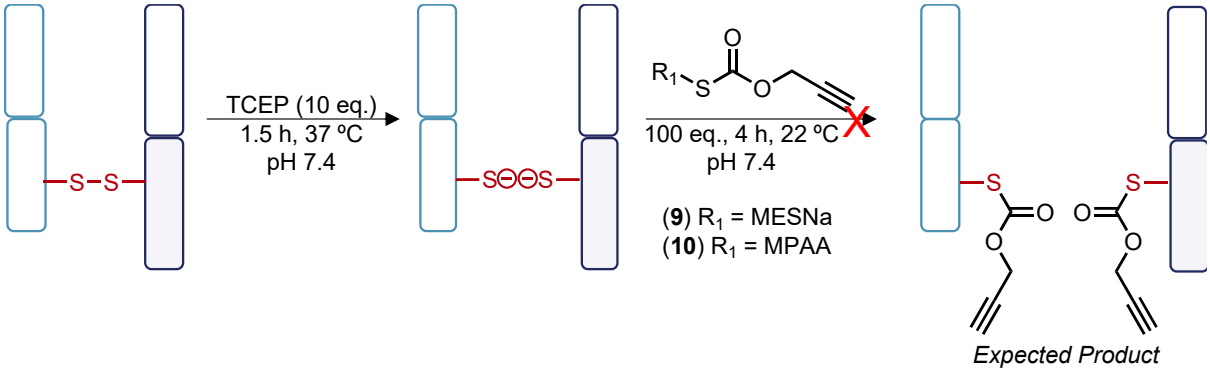


**SCHEME 23.** Initial bioconjugation conditions of thiocarbonate **9** and thiocarbonate **10** on reduced Fab at pH 7.4.

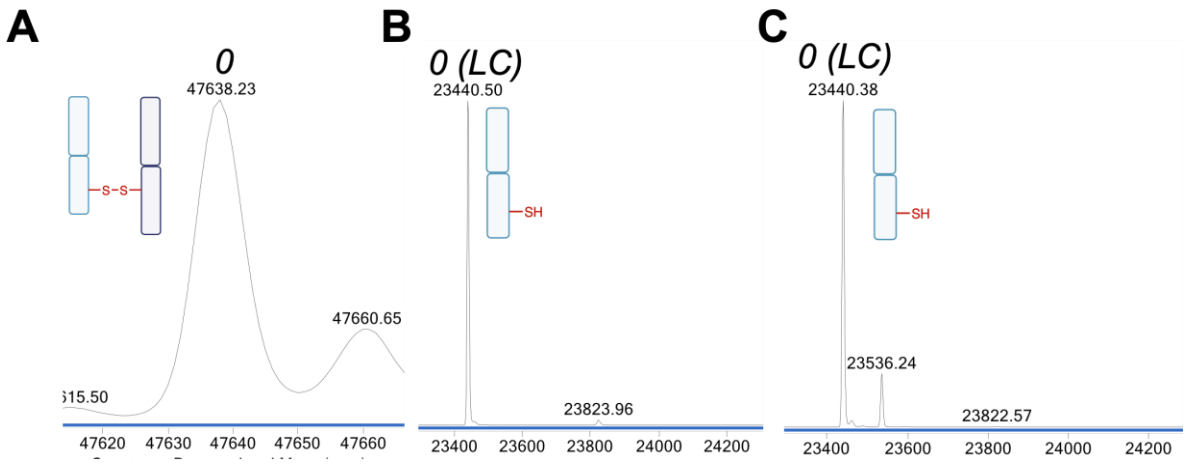


**FIGURE 71.** LCMS of thiocarbonate reactions at conditions of 100 eq., 4 h, 22 ºC, pH 7.4. **A)** Control study on non-reduced Fab. **B)** Alkyl thiocarbonate **9**. **C)** Aryl thiocarbonate **10**. Mass of native Fab = 47638 Da. Mass of native LC = 23440 Da. Mass of native HC = 24200 Da. Expected mass of addition = 83 Da.

### 3.1.2.2. Investigations of thiocarbonates at elevated pH

The cysteine thiol sidechains have a pKa of ~8.3 – increasing reaction pH would lead to a greater probability of deprotonation of the thiol sidechain, making the cysteine residues more nucleophilic. Thus, further studies on thiocarbonates were conducted at pH 8.4. The alkyl thiocarbonate **9** showed better selectivity for cysteine than the aryl thiocarbonate **10**, showing no modification of native Fab. Following this result, bioconjugation on reduced Fab was attempted, using 100 eq. of alkyl thiocarbonate **9** for 4 h, 22 ºC, at pH 8.4 (**FIG. 72A**). However, only native Fab was returned. This could result from the hydrolysis of the thiocarbonate at pH 8.4, before it can react with the cysteine residues, though this was not tested. Thiocarbonate hydrolysis releases free

thiol, which can oxidise themselves to form disulfides, which in turn catalyses cysteine oxidation. In the case of the aryl thiocarbonate **10**, significant unselective modification was observed on native Fab when using 100 eq. of reagent (**FIG 72B**). The several lysine residues on Fab likely form carbamates. The significant increase in reactivity of the aryl thiocarbonate **10** can be explained by the superior aryl leaving group in MPAA.

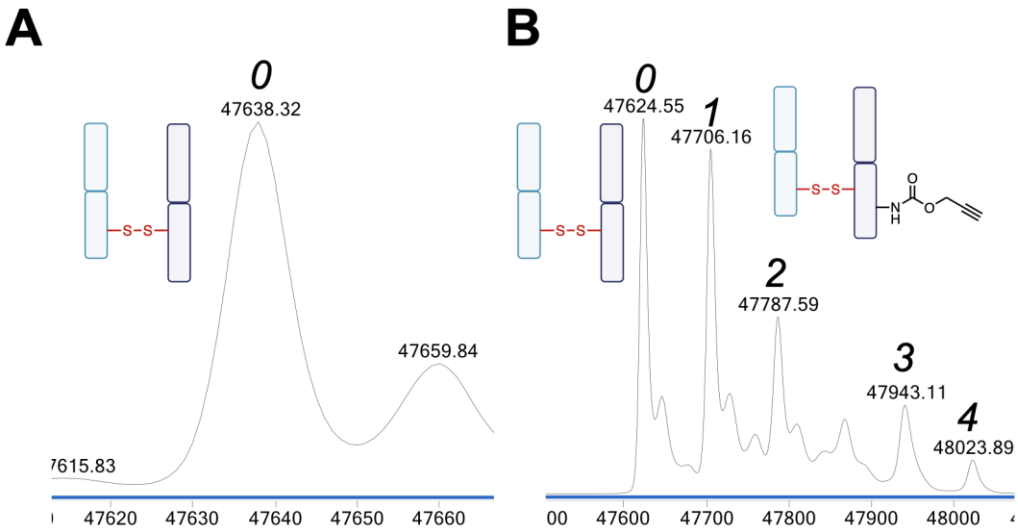


**FIGURE 72.** Bioconjugation of thiocarbonates on native Fab, with conditions of 100 eq., 4 h, 22 ºC, pH 8.4. **A)** Alkyl thiocarbonate **9**. **B)** Aryl thiocarbonate **10**. 0, 1, 2, 3, 4 refer to number of additions. Mass of native Fab = 47638 Da (A) or 47624 Da (B, due LCMS calibration shift). Mass of native LC = 23440 Da. Mass of native HC = 24200 Da. Expected mass of addition = 83 Da. Smaller unlabelled peaks correspond to sodium adducts (M+Na, +23 Da).

Lowering equivalents and time of bioconjugation did not overcome the respective issues of the alkyl or aryl thiocarbonates. For the alkyl thiocarbonate **9**, 10 eq. for 2 h at 22 ºC of reagent once again returned native Fab, with no cysteine bioconjugation observed. 10 eq. of aryl thiocarbonate **10** still resulted in some unselective modification (**FIG. 73A**), however this was significantly more controlled than seen when using 100 eq. of reagent. Thus, 10 eq. of aryl thiocarbonate **10** was applied to reduced Fab, to observe whether it is indeed possible to achieve greater control of modification (**FIG. 73B**). Native LC and HC are leftover. The results indicate some cysteine thiol selectivity, as there is not a statistical distribution of modifications as commonly seen in unselective lysine conjugation. Whilst not possible to eliminate all lysine conjugation, lowering equivalents can help favour cysteine thiol selectivity.

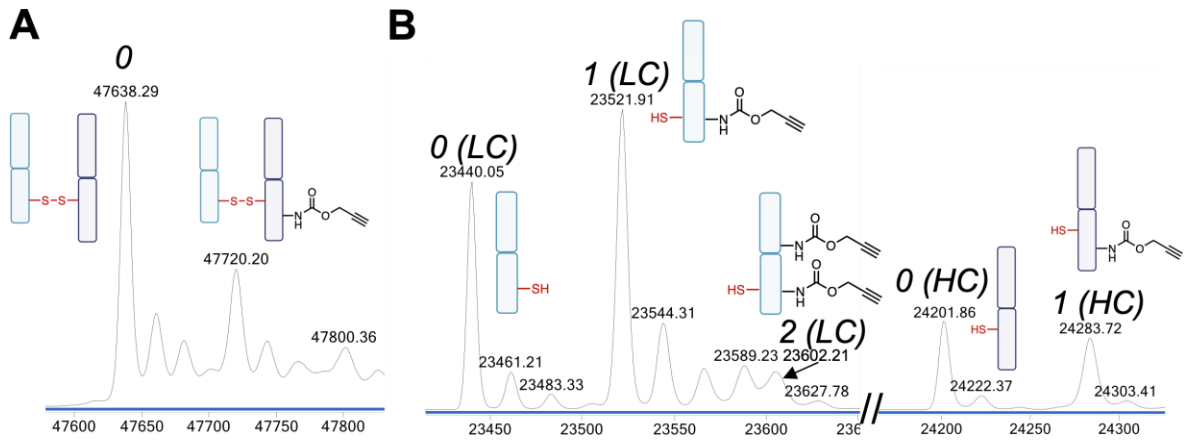


**FIGURE 73.** Aryl thiocarbonate **10** bioconjugation on Fab using conditions of 10 eq. 2 h, 22 ºC at pH 8.4. **A)** Control experiment on non-reduced Fab. **B)** LC and HC regions on reduced Fab. 0, 1 refers to number of additions. Mass of native Fab = 47638 Da. Mass of native LC = 23440 Da. Mass of native HC = 24200 Da. Expected mass of addition = 83 Da. Smaller unlabelled peaks correspond to sodium adducts (M+Na, +23 Da).

### 3.1.2.3. Summary and outlook of thiocarbonates

The reactivity of these reagents is currently determined by the thiol leaving group, and not the thiocarbonate as initially designed and desired. At pH 7.4, the reagents do not demonstrate significant reactivity. However, when pH is increased, the leaving group of the respective thiocarbonate significantly dictates reactivity. An alkyl leaving group results in the reformation of native Fab, leading to no cysteine bioconjugation. Using an aryl leaving group at lower equivalents and higher pH can somewhat favour cysteine bioconjugates, though some background lysine modification is still seen. However, they leave significant amounts of unmodified LC and unmodified HC. From these investigations, the thiocarbonates were determined to not be ideal as CLT reagents, as they cannot efficiently modify cysteine residues at pH 7.4, and higher pH conditions lead to incomplete cysteine bioconjugation.

Nonetheless, these experiments did demonstrate the potential of thiocarbonates for protein-related applications. The modular and mild synthetic route designed for thiocarbonates enables easy installation of functional groups of interest, such as click handles, PEG chains for aqueous solubility, and fluorophores. The thiocarbonates could be very useful for peptide modification, for example for carbamate formation at

lysine. Existing strategies involving carbamates for protein modification include targeting serine residues in enzyme active sites.[247,248]

### 3.2. Thiocarbamates

Thiocarbamates have also been explored here as potential novel reagents for CLT. Thiocarbamates feature prominently in biologically active molecules, such as pesticides and antiviral agents.[249,250] Similarly to the thiocarbonates, the thiocarbamates feature a heteroatom adjacent to the carbonyl group. The nitrogen atom features a lone pair, which can delocalise into the carbonyl electronic system (**FIG. 74**). This resonance contributes towards the stabilisation of thiocarbamates in a similar mechanism to that seen in typical amides, carbamates, and urea. Whilst the nitrogen is slightly electron-withdrawing, lone pair resonance and the partial double characteristics mean the central carbonyl carbon is more shielded than seen in thioesters or thiocarbonates, reflected in the $^{13}C$ NMR shift of a typical thiocarbamate (~165 ppm). In particular, compared to the thiocarbonates previously explored, these nitrogen-dependent factors suggest that the thiocarbamates should demonstrate greater stability, and indeed this is reflected in their widespread use as durable pesticides with long shelf-lives.[251] Thiocarbamates are likely less stable than analogous carbamates, as the latter has an oxygen atom with more efficient orbital overlap, leading to more electron resonance and hence more double bond character.

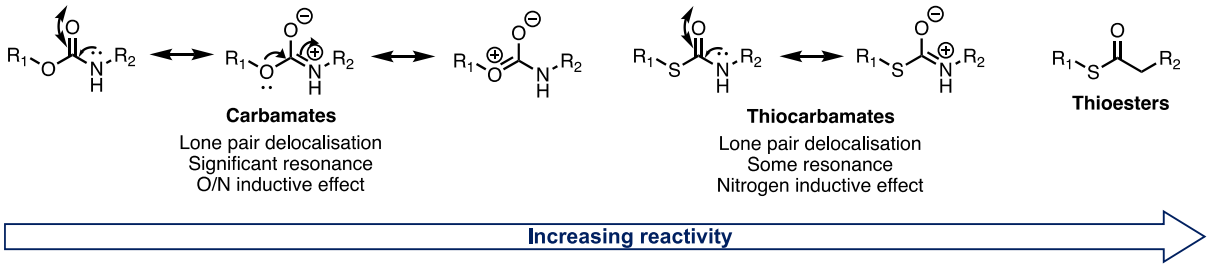


**FIGURE 74.** Structure and bond properties of carbamates, thiocarbamates, and the thioesters, with their predicted order of reactivity.

Additionally, the CLT product formed after the acyl transfer would be a lysine-modified urea conjugate (**FIG. 75**). Current other strategies to achieve urea formation on proteins are unselective, commonly utilising isocyanate reagents. Isocyanates suffer from several limitations, including promiscuous reactivity with nucleophilic protein residues such as terminal amino groups and arginine,[252] poor stability in aqueous conditions,[253] and long-term compound storage issues. Thiocarbamates were

designed with a view towards controlling reactivity, whilst enabling the formation of non-cleavable urea linkages on the proximal lysine residues.

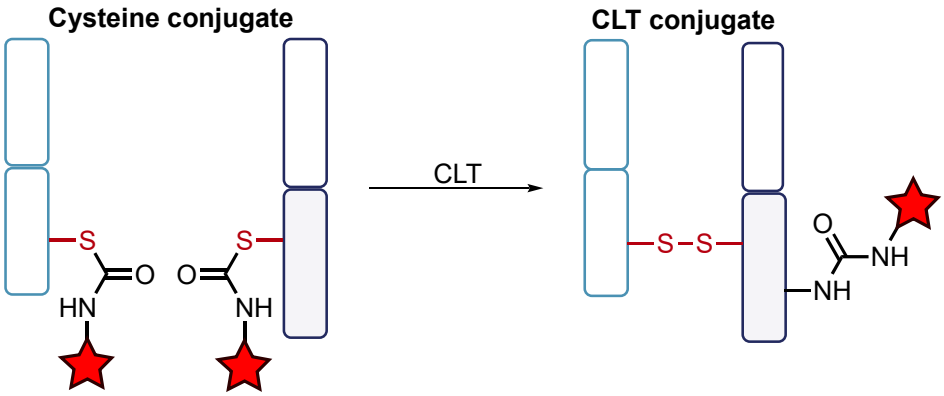


**FIGURE 75.** Cysteine and possible CLT conjugate from bioconjugation of thiocarbamates.

### 3.2.1. Chemical synthesis

Literature synthetic routes towards thiocarbamates include iodine-catalysed and electrochemical strategies.[254,255] Initial attempts to synthesise thiocarbamates utilised the same DSC protocol used for the synthesis of thiocarbonates – dropwise addition of the amine, followed by thiol addition. However, it was not possible to synthesise the intermediate propargylamine-NHS carbamate product, required for synthesis of the final thiocarbamate. Multiple conditions were attempted, including utilising different bases, base-free conditions, diluting the reaction, and heating the reaction vessel. In all cases, complex mixtures were observed *via* crude NMR of the sample, and on TLC. It is likely unexpected side-reactions occurred, preventing formation of the desired carbamate-NHS ester intermediate and instead forming side-products. This could involve amine addition to both activated esters, creating complex reaction mixtures.

A strategy using isocyanates was explored (**SCHEME 24**). There are no commercially available alkyne isocyanates available, so a simple isocyanate was used for initially exploring the synthesis and bioconjugation of thiocarbamates. Methyl thiocarbonate or thiophenol was added to phenyl isocyanate, and it was possible to synthesise the alkyl thiocarbamate **11** and aryl thiocarbamate **12** respectively in good yields.

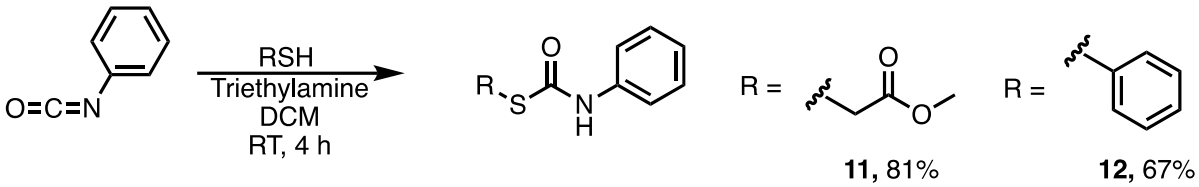


**SCHEME 24.** Synthesis of alkyl thiocarbamate (**11**) and aryl thiocarbamate (**12**).

### 3.2.2. Bioconjugation of thiocarbamates

#### 3.2.2.1. Standard bioconjugation conditions

Bioconjugation studies on Fab followed (**SCHEME 25**). Initial control studies with the alkyl thiocarbamate **11** on non-reduced Fab (20 eq., 4 h, 22 ºC, pH 7.4) indicated some lack of selectivity (**FIG. 76A**). Some addition was observed, likely on lysine residues, corresponding to formation of the urea conjugate. Nonetheless, this unselective addition was not significant. In reaction conditions, where Fab is reduced to open the disulfide bond, minimal modification of the LC and HC was observed, with most of the Fab chains left unmodified as its native form (**FIG. 76B**). Higher equivalents of 50 eq. alkyl thiocarbamate **11** showed even further unselective modification (**FIG. 76C**) and did not significantly improve conversion (**FIG. 76D**).

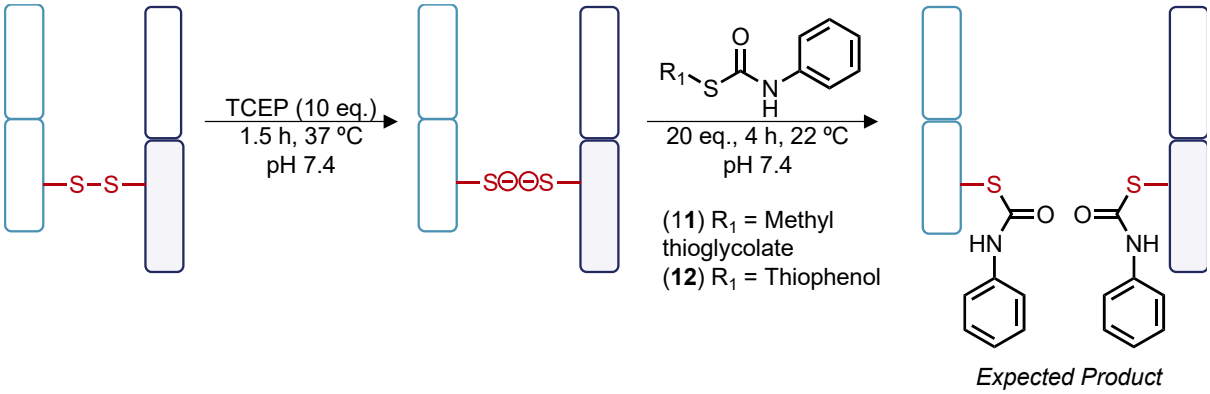


**SCHEME 25.** Initial bioconjugation conditions explored for alkyl thiocarbamate **11** and aryl thiocarbamate **12** on reduced Fab.

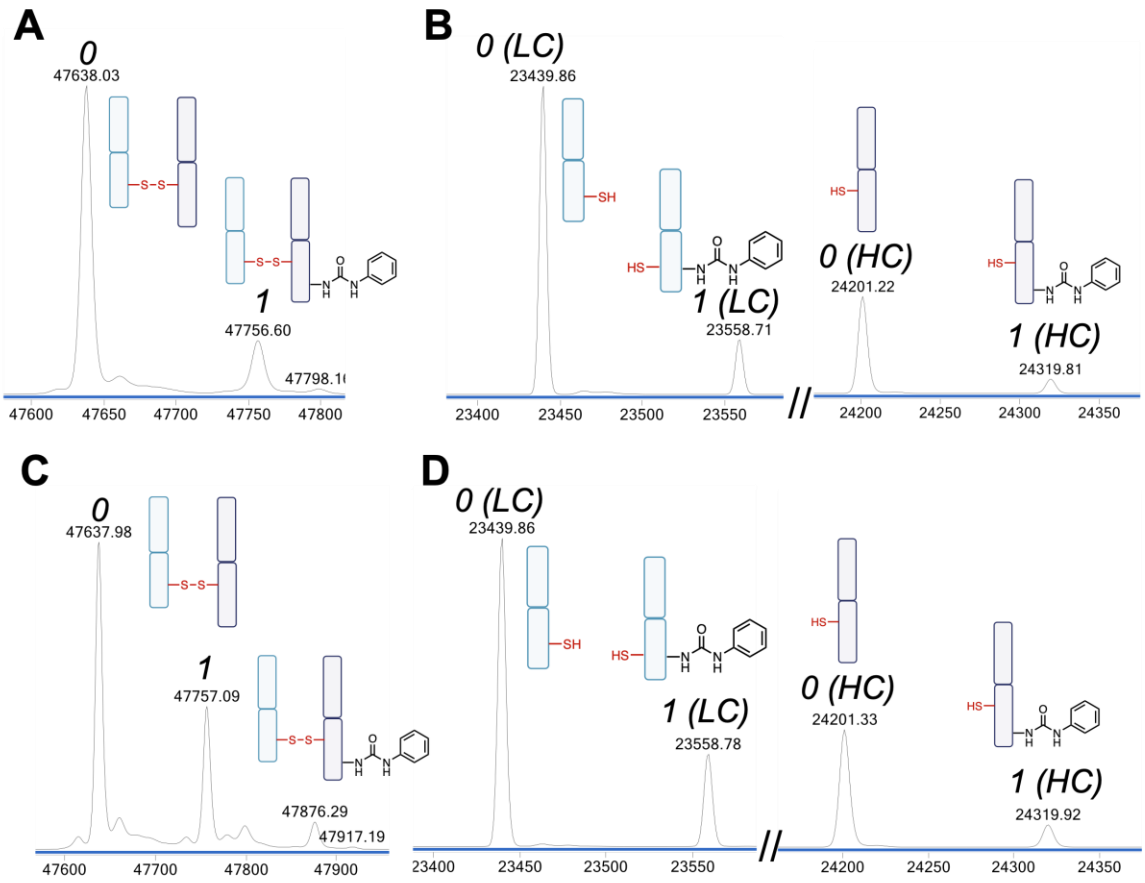


**FIGURE 76.** Bioconjugation of alkyl thiocarbamate **11** under varying equivalents, 4 h, 22 ºC, at pH 7.4. **A)** Control reaction on reduced Fab, using 20 eq. **B)** Reaction on reduced Fab, using 20 eq. **C)** Control reaction on reduced Fab, using 50 eq. **D)** Reaction on reduced Fab, using 50 eq. 0, 1 refer to number of additions. Mass of native Fab = 47638 Da. Mass of native LC = 23440 Da. Mass of native HC = 24200 Da. Expected mass of addition = 120 Da.

To confirm unselective addition is responsible for the observed LC and HC modifications, cysteine (100 eq., 1 h, 37 ºC, pH 7.4) was added (**FIG. 77**) – small molecule cysteine can cleave the thiol-conjugate through thiol-transfer but cannot cleave the urea that forms unselectively. It is clear from these results that most of the conjugation seen occurs on lysine residues on the LC and HC, instead of the cysteine residues as desired. Whilst higher equivalents could enable further LC and HC modification, they would also result in more unselective additions, thus these conditions were not explored further.

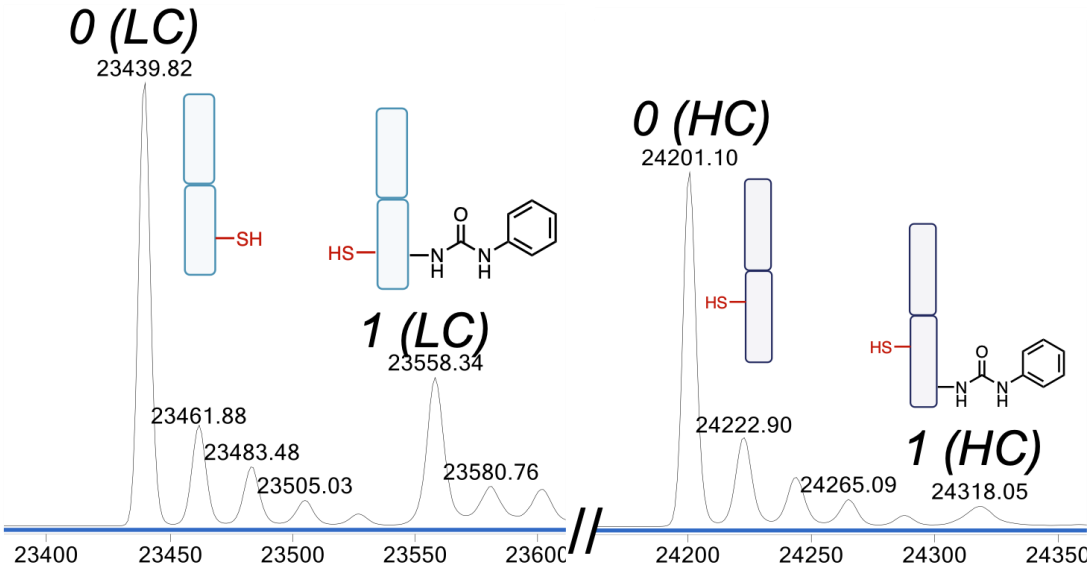


**FIGURE 77.** Addition of cysteine (100 eq., 4 h, 37 ºC, pH 7.4) to alkyl thiocarbamate conjugate. 0, 1 refer to number of additions. Mass of native Fab = 47638 Da. Mass of native LC = 23440 Da. Mass of native HC = 24200 Da. Expected mass of addition = 120 Da. Smaller unlabelled peaks correspond to sodium adducts (M+Na, +23 Da).

The aryl thiocarbamate **12** was next explored, firstly in control experiments. Due to the improved leaving group ability of thiophenol, it is expected the aryl thiocarbamate **12** should demonstrate greater reactivity, and hence could improve modification efficiency. However, unselective modification also becomes a more pronounced issue too. At 20 eq., there was significant modification of native Fab and a distribution of additions, corresponding to unselective lysine modification (**FIG. 78A**). There is very little native Fab leftover, even when using aryl thiocarbamate **12** for short timeframes (10 eq., 1 h, 22 ºC, pH 7.4) (**FIG. 78B**).

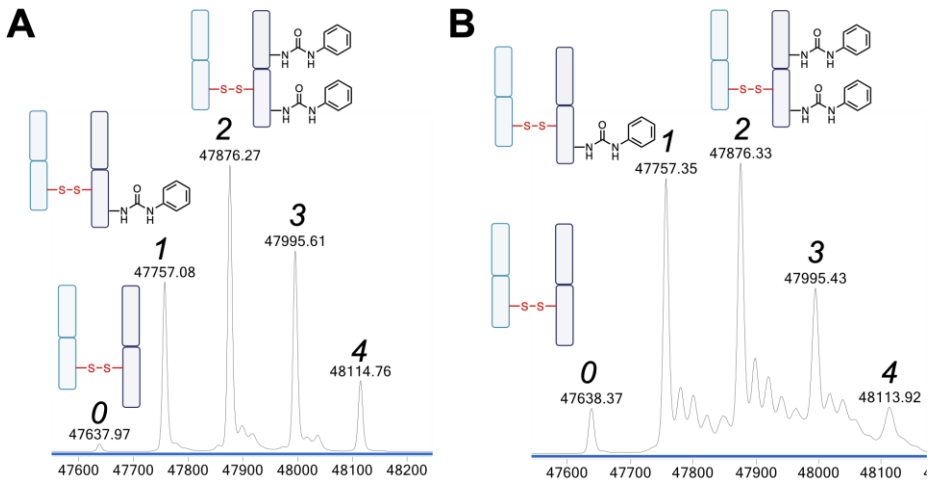

**FIGURE 78.** Control experiments of aryl thiocarbamate **12** on non-reduced, native Fab. **A)** 20 eq., 4 h, 22 ºC, pH 7.4. **B)** 10 eq., 1 h, pH 7.4, 22 ºC. 0, 1, 2, 3, 4 refer to number of additions. Mass of native Fab = 47638 Da. Mass of native LC = 23440 Da. Mass of native HC = 24200 Da. Expected mass of addition = 120 Da. Smaller unlabelled peaks correspond to sodium adducts (M+Na, +23 Da).

### 3.2.2.2. Lower pH investigations of thiocarbamates

Lowering pH to 6.0 did not completely prevent undesired unselective addition, despite the reduced reactivity of the lysine residues (**FIG. 79A**). Several modifications were seen on non-reduced Fab in control experiments, though to a lesser extent than the investigations at pH 7.4. Conjugation on reduced Fab confirmed similar findings – multiple additions were seen on the LC and HC (**FIG. 79B**). There is a statistical distribution of modifications, again indicating unselective lysine modification.

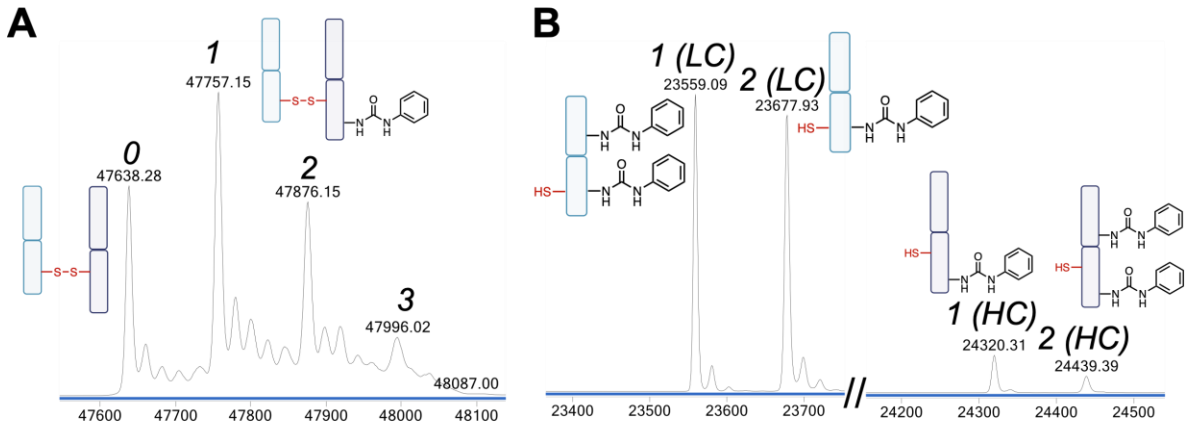


**FIGURE 79.** Bioconjugation of aryl thiocarbamate **12** on Fab, under the conditions of 10 eq., 2 h, 22 ºC, pH 6.0. **A)** Control reaction on non-reduced Fab. **B)** Reaction on reduced Fab. 0, 1, 2, 3 refer to number of additions. Mass of native Fab = 47638 Da. Mass of native LC = 23440 Da. Mass of native HC = 24200 Da. Expected mass of addition = 120 Da. Smaller unlabelled peaks correspond to sodium adducts (M+Na, +23 Da).

### 3.2.2.3. Thiocarbamate and isocyanate interconversion

Initial suggestions were that the thiocarbamates should demonstrate good stability and controlled reactivity due to the stabilisation effect of the nitrogen lone pair in the thiocarbamate group, but all bioconjugation results have contradicted this prediction, and have demonstrated an extremely reactive species. Thiocarbamates have a weaker C-S bond in their structure, resulting from poorer orbital overlap between the

larger sulfur 3s orbital and the smaller carbon 2s orbital. As a result, thiocarbamates may undergo spontaneous elimination to form isocyanates (**SCHEME 26**).

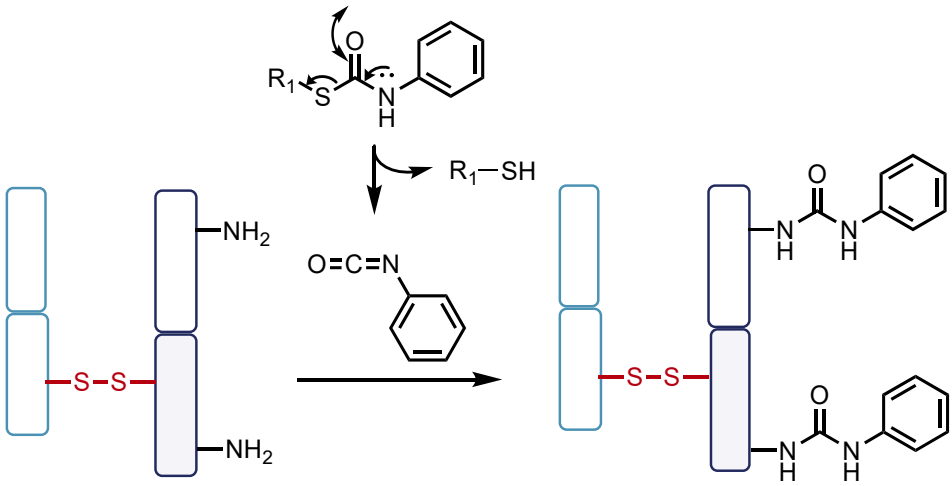


**SCHEME 26.** Isocyanate elimination from thiocarbamates, and the resultant reaction of phenylisocyanate with native Fab on lysine residues, forming urea conjugates.

The isocyanate readily reacts rapidly with amines, and thus it is likely this causes the unselective lysine modification seen. Given that the alkyl thiocarbamate **11** has an alkyl thiol leaving group and the aryl thiocarbamate **12** has an aryl thiol leaving group, this explains the difference in reactivity between the two on native Fab – the aryl thiocarbamate **12** more readily forms phenylisocyanate by losing its thiophenol. Additionally, this elimination is not pH dependent, as a highly reactive species was observed at pH 6.0, and this species reacted extensively with lysine residues. This reaction can be followed by TLC – the addition of either thiocarbamate to water and tracking the reaction over 4 h shows the almost immediate degradation of the starting thiocarbamates into a mixture of compounds corresponding to leftover starting material, phenylisocyanate, and the released thiol. The reaction does not proceed to completion, indicating that the thiocarbamate-isocyanate reaction pathway is reversible in the absence of amine.

### 3.2.3. Summary and outlook of thiocarbamates

The outcome of the thiocarbamate studies on Fab currently suggest they are not suitable for use as CLT reagents. The possibility of forming isocyanate in buffer is problematic, as these functional groups are highly lysine reactive, and thus unselective. Some studies have shown that alkylation of the carbamate nitrogen can reduce isocyanate formation,[256] however, attempts to alkylate the synthesised

thiocarbamate using sodium hydride and methyl iodide caused degradation of the thiocarbamate, due to the instability of thiol-reactive moiety towards strongly basic conditions. Further tuning of the thiocarbamates would be desirable to make them more useful as bioconjugation reagents. *N*-alkylation could offer a way of controlling isocyanate elimination and offer an opportunity to insert dual-functionality.

### 3.3. Dithiocarbonates

Dithiocarbonates have been proposed here as novel and alternative re-bridging reagents of disulfide bonds and subsequent transfer to lysine residues. Unlike other re-bridging reagents such as maleimides, PDs, or bis-sulfones, the dithiocarbonates introduce a bridge consisting of only one carbon atom. As this single carbon bridge is smaller and with a shorter bond distance more comparable to native disulfide bonds, this minimises disruption to the tertiary structure. There is potential for functionalisation through nucleophile addition and through CLT. Whilst some dithiocarbonates are commercially available, they have not been explored for protein modification, and are relatively unexplored in general.

Like the thioesters, the dithiocarbonates have C-S bonds which dictate their reactivity. They contain two C-S bonds near the carbonyl carbon; thus, both bonds can be easily substituted by nucleophiles such as other thiols or amines. Compared to other reagents such as bicarbonates, urea, and thioesters, dithiocarbonates should demonstrate the greatest reactivity due to the weaker C-S bond, resulting from the poorer orbital overlap between the carbon and sulfur atoms. The CLT product of dithiocarbonates would be a thiocarbamate, which could then be substituted by nucleophiles. This could provide another strategy to introduce functionality into the dithiocarbonate re-bridging protocol (**FIG. 80**).

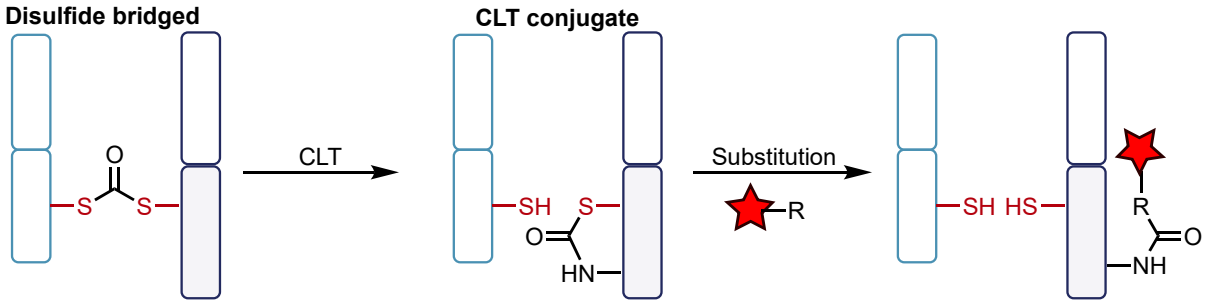


**FIGURE 80.** Cysteine and possible CLT conjugate from bioconjugation of dithiocarbonates, and their potential substitution with a functionalised nucleophile.

The thiocarbamate may also rearrange to generate the isocyanate, which would likely react with water to release carbon dioxide and remove the structure from Fab.

### 3.3.1. Chemical synthesis

The synthesis of the dithiocarbonates utilised the general DSC substitution protocol as explored previously (**SCHEME 27**). Triethylamine (TEA) and diisopropylethylamine (DIPEA) did not yield the desired product, however using *N*-methylmorpholine (NMM) and enabling NMM to react with DSC first, before addition of the thiol, enabled successful synthesis of the target alkyl dithiocarbonate **13** and aryl dithiocarbonate **14.** NMM (pKa 7.6) has a lower pKa than TEA (pKa 10.7, DMSO) and DIPEA (pKa 10.6, DMSO), so it is likely that NMM's ability to act as a nucleophilic catalyst is crucial for the synthesis of dithiocarbonates (**SCHEME 28**).

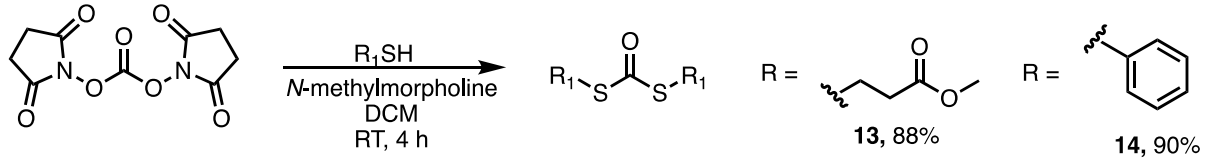


**SCHEME 27.** Synthesis of dithiocarbonates.

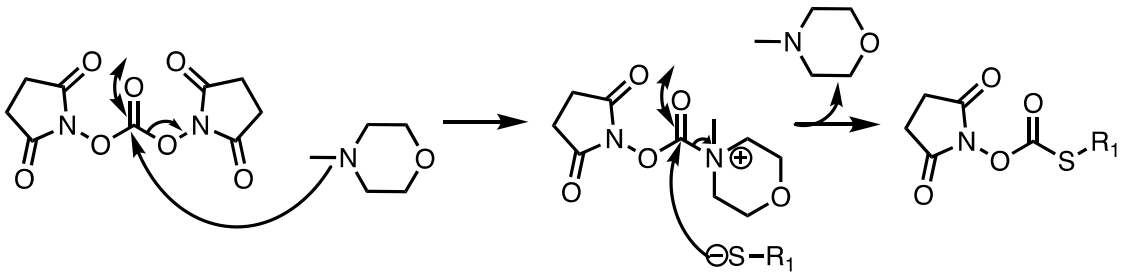

**SCHEME 28.** NMM nucleophilic catalyst mechanism for thiocarbonate synthesis.

### 3.3.2. Bioconjugation of dithiocarbonates

#### 3.3.2.1. Re-bridging Fab conditions

Bioconjugation of both alkyl and aryl dithiocarbonates was then pursued on Fab (**SCHEME 29**). Due to solubility issues of the aryl dithiocarbonate **14**, causing precipitation in aqueous solution, it was investigated at lower equivalents than the alkyl dithiocarbonate **13**. However, this did not significantly impact bioconjugation. Control experiments (20 eq., 4 h, 22 ºC, pH 7.4) confirmed no undesired side-reactivity with lysine residues occurred when either dithiocarbonate was added to native Fab.

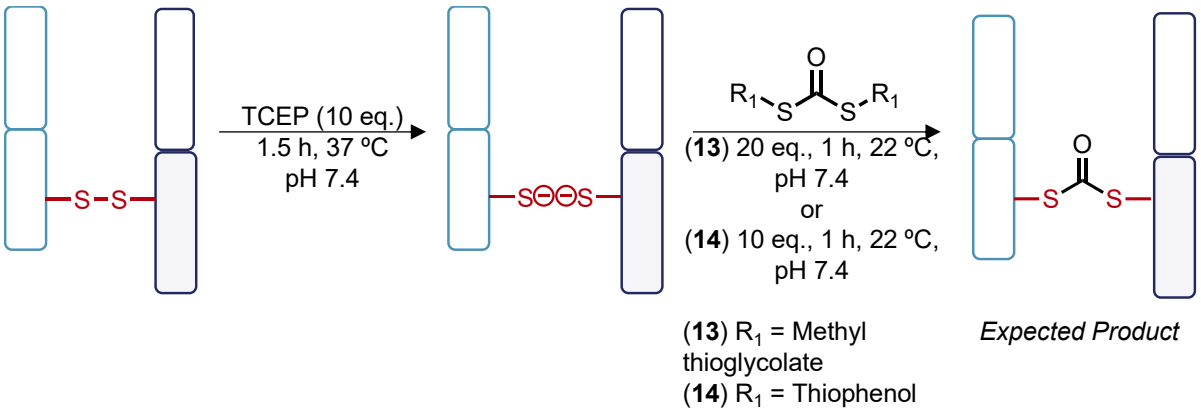


**SCHEME 29.** Bioconjugation conditions employed for alkyl dithiocarbonate **13** and aryl dithiocarbonate **14** on reduced Fab.

For both dithiocarbonates, complete conversion into a re-bridged Fab construct was observed within 1 h, confirmed *via* LCMS analysis (**FIG. 81A** and **FIG. 81B)** and SDS-PAGE analysis (**FIG. 82**). The SDS-PAGE of the aryl dithiocarbonate **6** shows small amounts of leftover LC and HC after 0.5 h, however these bands completely disappear after 1 h, giving 100% re-bridged species according to densitometry analysis. The addition of *N*-Boc-cysteine under mild conditions (100 eq., 4 h, 22 ºC, pH 7.4) did not cleave the dithiocarbonate. However, when the temperature of the reaction was increased to 37 ºC, it was possible to regenerate native Fab with a disulfide bond within 24 h at pH 7.4 (**FIG. S.49**). This confirms that the carbonyl re-bridging occurs between adjacent cysteine residues that normally compose the native disulfide bond.

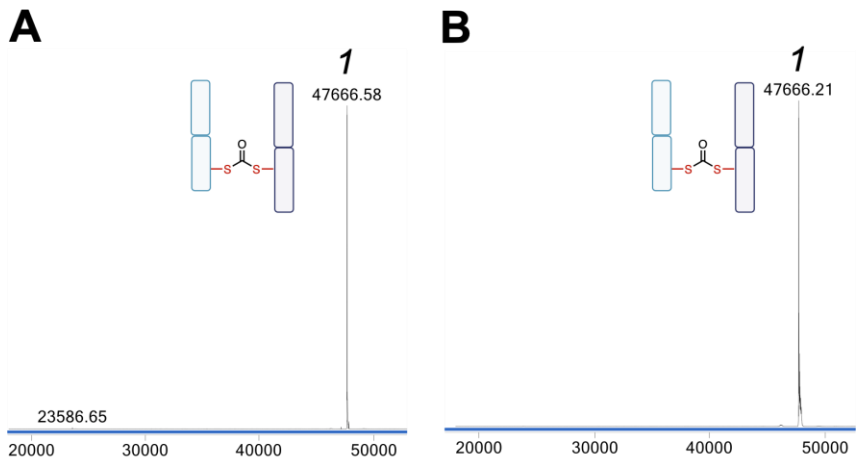


**FIGURE 81.** Dithiocarbonate re-bridging of Fab after 1 h. **A)** Alkyl thiocarbonate **13**, 20 eq., 1 h, 22 ºC, pH 7.4. **B)** Aryl thiocarbonate **14**, 10 eq., 10 h, 22 ºC, pH 7.4. 1 refers to number of additions. Mass of native Fab = 47638 Da. Expected mass of addition = 28 Da.

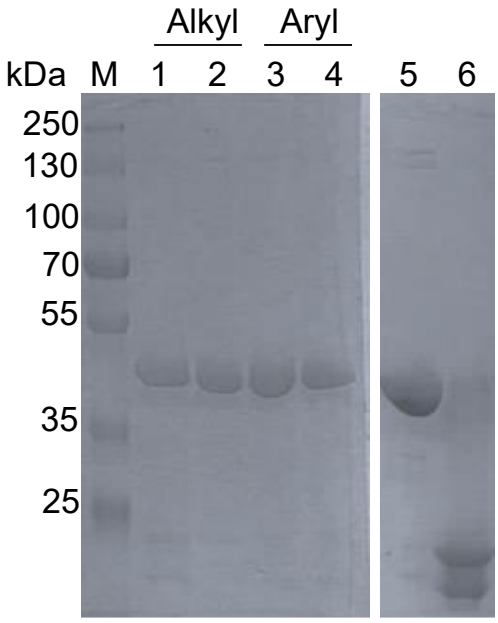


**FIGURE 82**. SDS-PAGE analysis of dithiocarbonate re-bridging. Lane M: Protein Ladder. Lane 1: 0.5 h, alkyl thiocarbonate **13**. Lane 2: 1.0 h, alkyl thiocarbonate **13**. Lane 3: 0.5 h, aryl thiocarbonate **14.** Lane 4: 1.0 h, aryl thiocarbonate **14.** Lane 5: Native Fab. Lane 6: Reduced Fab.

### 3.3.2.2. CLT of dithiocarbonate re-bridged conjugate

Having confirmed successful re-bridging of Fab using the dithiocarbonates, functionalisation of the bridge was investigated next. The target CLT conjugate, where a thiocarbamate forms between the conjugated cysteine and a nearby lysine, was not detected *via* LCMS analysis as no modified HC was seen, even after 24 h of incubation at 37 ºC, pH 8.4 (**FIG. 83**). Instead, leftover re-bridged conjugate, native Fab and native LC were the observed products. The dithiocarbonate likely suffers from hydrolysis in a similar manner to that of thioesters. Once one of the thioester-like moieties is hydrolysed, it undergoes decarboxylation to cleave itself from the protein.

In addition, there is a small amount of fragmented HC present. Prolonged incubation of antibodies at 37 ºC has shown to result in the cleavage of peptide bonds.[257] This is evident in the LCMS of the CLT attempt, where a peak with a mass of 23615 Da is present after 24 h incubation at 37 ºC, corresponding to a mass loss of 586 Da in the HC region. This does not occur in other Fab conjugates incubated for similar times at similar temperatures, thus the dithiocarbonate bridge likely has a role in enabling this fragmentation to occur more easily. However, the major product remains the

dithiocarbonate bridged species, indicating this re-bridging strategy offers a stable bridge against hydrolysis that can survive in elevated pH for many hours.

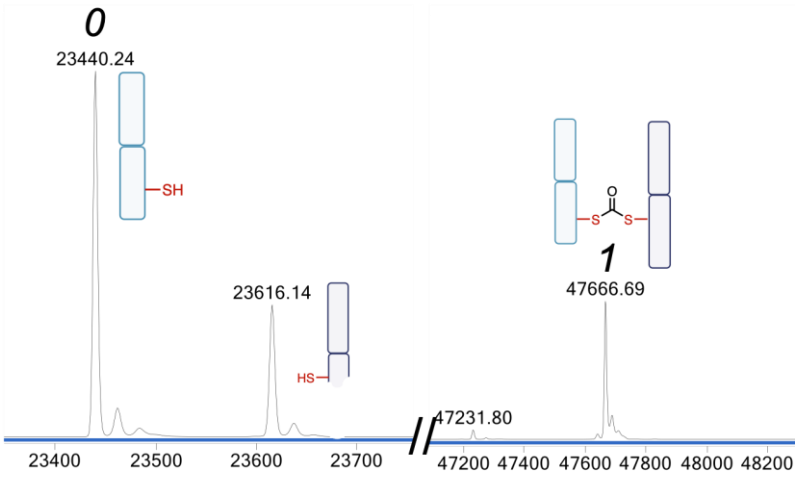


**FIGURE 83.** LCMS of dithiocarbonate CLT attempt, under conditions of pH 8.4, 37 ºC, 24 h. 0, 1 refer to number of additions. Mass of native Fab = 47638 Da. Expected mass of addition = 28. Smaller unlabelled peaks correspond to sodium adducts (M+Na, +23). Expected mass of addition = 28 Da. 23616 Da corresponds to fragmented HC.

### 3.3.3.3. Nucleophiles for functionalisation of dithiocarbonate conjugate

CLT would enable the formation of an intermediate conjugate reactive towards nucleophilic addition, and thus enable functionalisation to occur by substituting the remaining thioester bond with a nucleophile. Since CLT was not possible, direct addition of nucleophiles to the dithiocarbonate re-bridged species was explored instead, including alcohol, amine, and thiol nucleophiles of varying nucleophilicity and pKa (**FIG. 84**). Previous investigations demonstrated it was difficult to form thiocarbonates and thiocarbamates on Fab, so the addition of alcohol or amine nucleophiles to dithiocarbonates could provide an alternative route. Whilst previous studies show thiocarbamates spontaneously and reversibly form isocyanates, which react unselectively, a strategy to enable *in situ* generation of a single isocyanate species could be beneficial, especially if this isocyanate could be generated in a controlled manner at the disulfide bond region, nearby the targeted proximal lysine residues. Depending on the effectiveness of substitution, it is possible the bridge is completely removed and only native Fab is leftover, however this could be controlled by adjusting the strength of nucleophile or the conditions employed during this step.

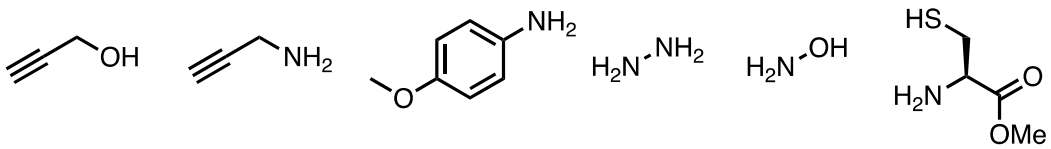

| Propargyl Alcohol | Propargyl Amine | *p*-Anisidine | Hydrazine | Hydroxyl -amine | Cysteine |
|---|---|---|---|---|---|
| pKa 13.6 | pKaH 7.9 | pKaH 5.3 | pKaH 8.0 | pKaH 6.0 | pKaH 8.6 |

**FIGURE 84.** Nucleophiles and their pKa or pKaH for substitution of dithiocarbonate bridge

The dithiocarbonate bridge demonstrated remarkable stability towards alcohol and amine addition. Even when 100 eq. of propargyl alcohol (**FIG. 85A**) or propargyl amine (**FIG. 85B**) were added for 24 h at 37 ºC, pH 7.4, there was no substitution of the dithiocarbonate bridge, and no substitution was observed. *p*-Anisidine was also explored – this amine contains an electron-donating amine on the aromatic ring and has a low pKa. Thus, in buffer conditions at pH 7.4, the amine is fully deprotonated and is an effective nucleophile. However, even 1000 eq. of *p*-anisidine for 24 h at 37 ºC did not cause any modification of the dithiocarbonate bridge (**FIG. 85C**), further demonstrating the stability of the short carbonyl bridge towards nucleophilic addition of alcohols and amines.

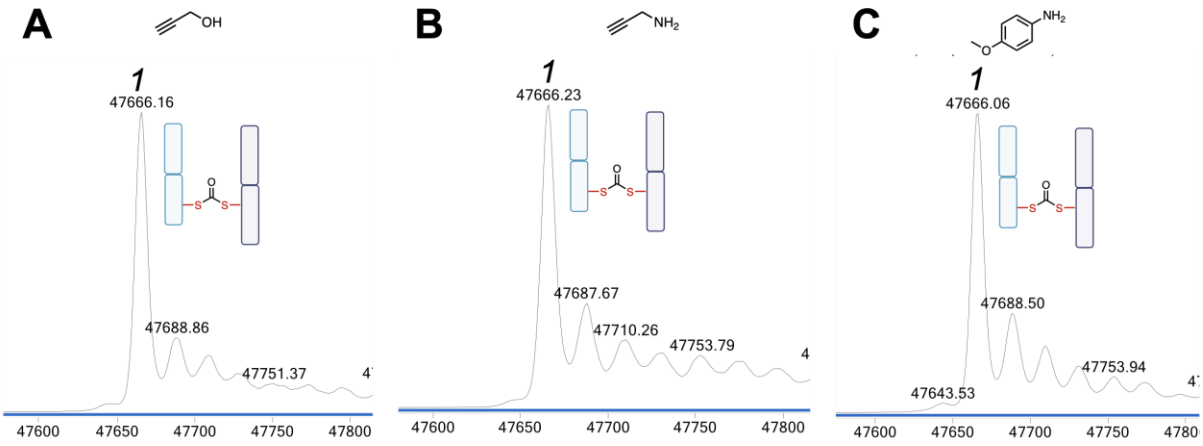


**FIGURE 85.** Dithiocarbonate bridge substitution with alcohol and amine nucleophiles. **A)** Propargyl alcohol, 100 eq., 37 ºC, 24 h, pH 7.4. **B)** Propargyl amine, 100 eq., 37 ºC, 24 h, pH 7.4. **C)** *p*-Anisidine, 1000 eq., 37 ºC, 24 h, pH 7.4. Mass of re-bridged Fab = 47666 Da. Expected mass of addition = 56 Da (propargyl alcohol), 55 Da (propargyl amine), 123 Da (*p*-anisidine). Smaller unlabelled peaks correspond to sodium adducts (M+Na, +23 Da).

Hydrazine and hydroxylamine nucleophiles were also explored. Both nucleophiles feature the $\alpha$-effect due to the neighbouring atom with a free lone pair, which enhances their nucleophilicity relative to typical alcohol or amine nucleophiles. There are several suggestions for explaining the $\alpha$-effect, including stabilisation of the transition state (TS) for example.[258] Computational studies indicate that hydrazine demonstrates greater reactivity than hydroxylamine, but both are interesting nucleophiles as they could potentially enable the insertion of a reactive handle.[259]

However, neither nucleophile provided a desirable result for functionalisation. Hydrazine addition under standard conditions (100 eq., 24 h, 37 ºC, pH 7.4) caused some cleavage of the dithiocarbonate bridge (**FIG. 86A**), whilst hydroxylamine under the same conditions caused bridge cleavage to a lesser extent (**FIG. 86B**). Whilst not ideal for functionalisation of the bridge, it does indicate a significant amount of stability against various nucleophilic groups, including even those with the $\alpha$-effect.

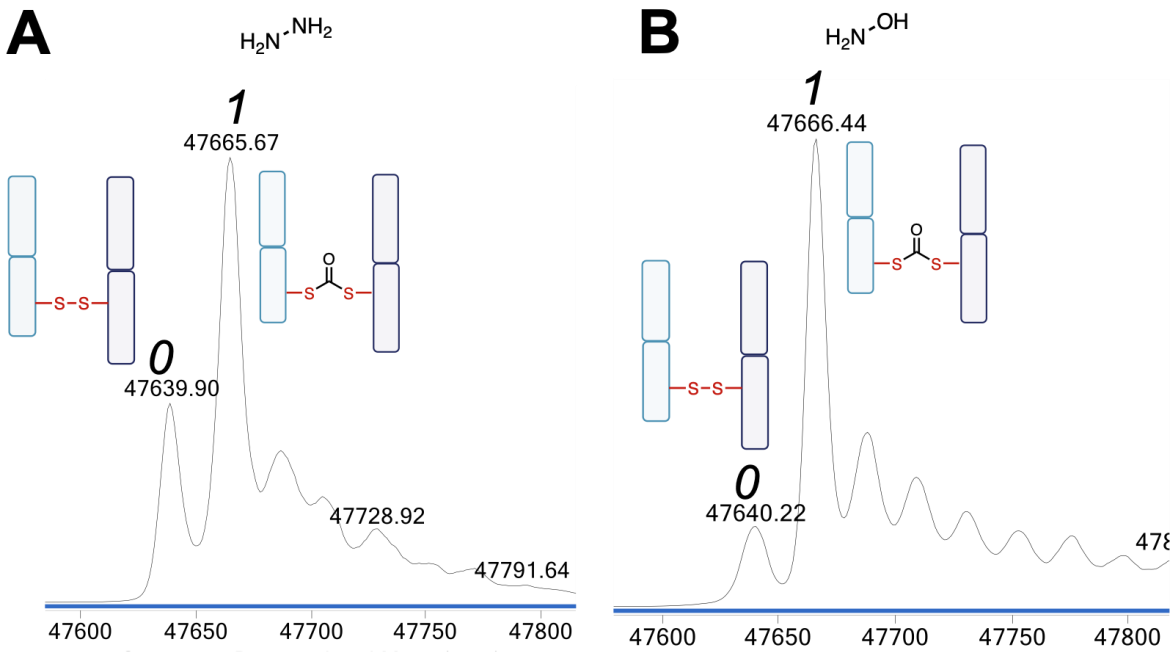


**FIGURE 86.** Dithiocarbonate bridge substitution with hydrazine and hydroxylamine nucleophiles. **A)** Hydrazine, 100 eq., 37 ºC, 24 h, pH 7.4. **B)** Hydroxylamine, 100 eq., 37 ºC, 24 h, pH 7.4. Mass of native Fab = 47638 Da. Mass of re-bridged Fab = 47666 Da. Expected mass of addition = 32 Da (hydrazine), 33 Da (hydroxylamine), 123 Da (*p*-anisidine). Smaller unlabelled peaks correspond to sodium adducts (M+Na, +23 Da).

Previous investigations showed that *N*-Boc-cysteine showed cleavage of the carbonyl bridge, as previously discussed, so *O*-Me-cysteine was next explored. *O*-Me-cysteine has two nucleophilic sites – the thiol sidechain, and the *N*-terminal amine. NCL should occur, first *via* thioesterification with the thiol, before an acyl transfer generates the amide product. If thiol reacts with both sides of the bridge faster than the amine reacts or NCL occurs, then bridge cleavage will be observed, as seen in *N*-Boc-cysteine studies (section 2.2.3.2.1.). Incubation for 4 h (100 eq., 22 ºC, pH 7.4) showed the formation of native Fab, in addition to a species where *O*-Me-cysteine was added onto the dithiocarbonate re-bridged conjugate. This species appears in the mass region corresponding to Fab, thus the structure could correspond to a few different structures (**FIG. 87**). It is likely transthioesterification between the cysteine thiol and the dithiocarbonate re-bridged conjugate occurs, breaking the bridge. Then, NCL occurs with the *N*-terminal amine substituting the dithiocarbonate to form a thiocarbamate. The thiocarbamate is then eliminated over time as an isocyanate. Potentially, this could be a strategy of introducing a single equivalent of isocyanate nearby the proximal lysines to form a urea conjugate, which could offer a point of functionalisation through the free thiol. However, incubation of the cysteine addition step for 24 h, 22 ºC, pH 7.4 results in the complete formation of native Fab, which indicates there is no urea conjugate. It is possible that the free isocyanate reacts with water to form a carbamic acid, and this can undergo decarboxylation to release carbon dioxide and free *O*-Me-cysteine.

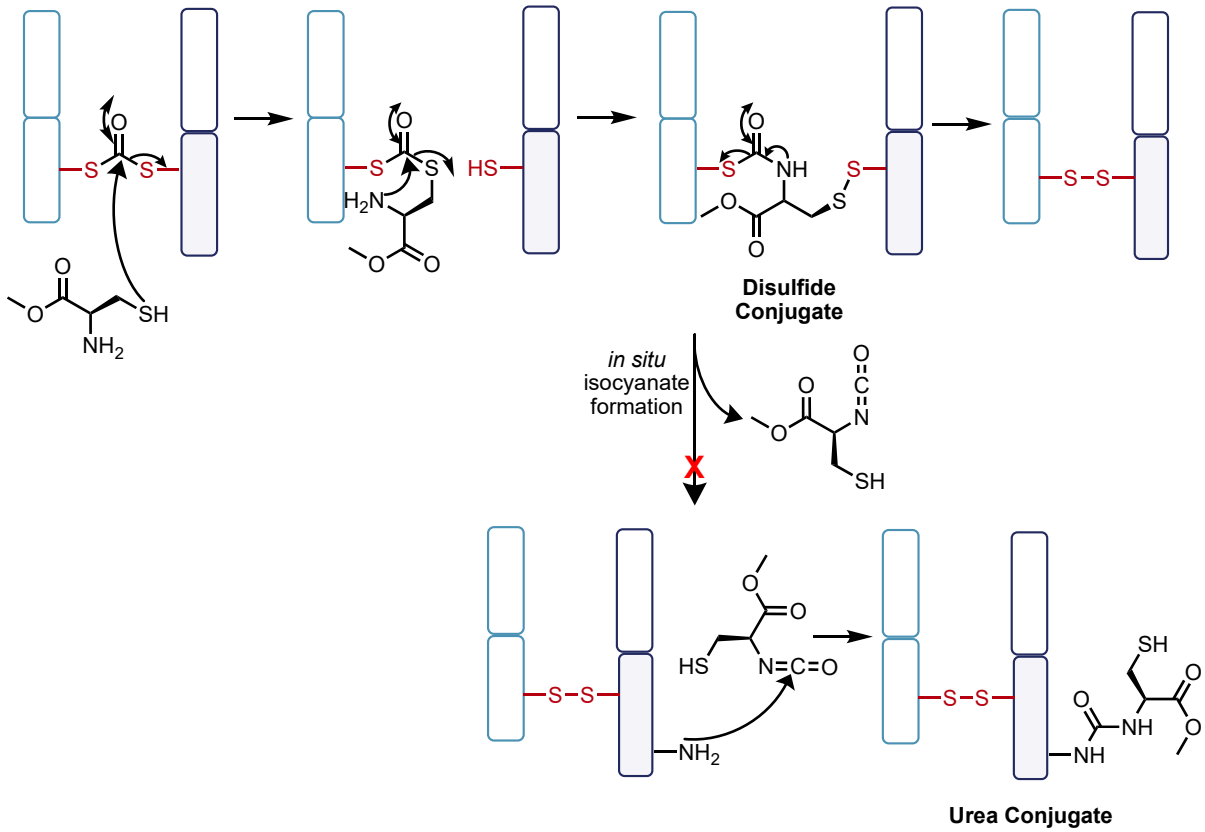


**FIGURE 87.** Possible route of *O*-Me-cysteine modification of Fab, including a disulfide conjugate or a urea conjugate through *in situ* isocyanate generation.

To further identify which species is the conjugate present after 4 h, a subsequent reaction was conducted. TCEP (10 eq., 1.5 h, 37 ºC, pH 7.4) was added, and then *N*-methylmaleimide (100 eq., 1 h, 22 ºC, pH 7.4) was added. After TCEP reduction, the species was cleaved off Fab, and maleimide capping was observed only on the native LC and HC (**FIG. 88**). Another reaction where maleimide was directly added to the species, without prior TCEP reduction, showed no modification – isocyanate formation should provide a free thiol, as shown in the urea conjugate. These results indicate that the intermediate species corresponded to the disulfide conjugate. Whilst the disulfide conjugate likely forms as an intermediate, spontaneous intramolecular rearrangement of the thiocarbamate to isocyanate, which happens over 24 h, removes the dithiocarbonate bridge. Thus, the addition of cysteine does not offer a route towards dithiocarbonate functionalisation, and instead primarily works to remove the bridged species and restore native Fab over time.

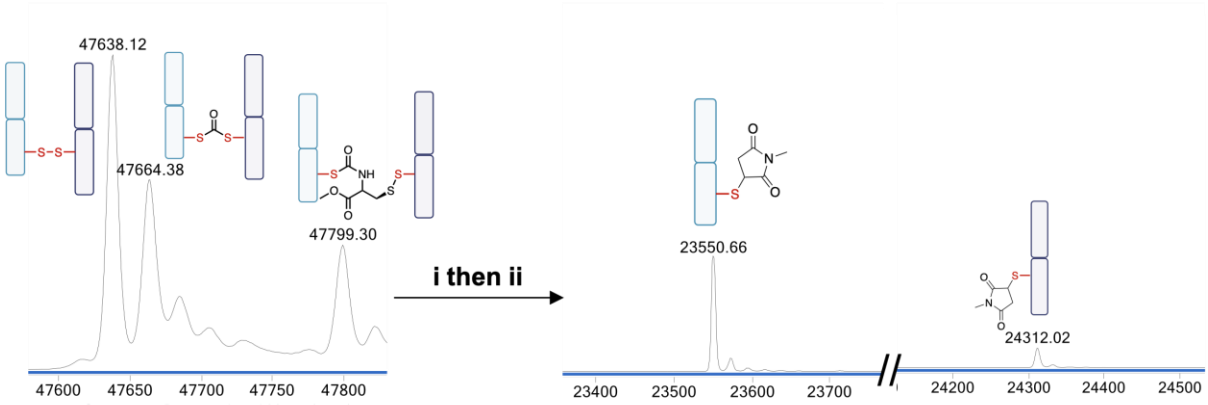


**FIGURE 88.** Determining the structure of the species resulting from *O*-Me-cysteine addition to the dithiocarbonate re-bridged Fab conjugate. i) TCEP, 10 eq., 1.5 h, 37 ºC, pH 7.4; ii) *N*-methylmaleimide, 50 eq., 0.5 h, 22 ºC, pH 7.4. Reduction of the disulfide conjugate followed by subsequent maleimide capping restores capped native LC and HC. Mass of native Fab = 47638 Da. Mass of re-bridged Fab = 47666 Da. Mass of native LC = 23439 Da. Mass of native HC = 24200 Da. Expected mass of addition = 131 Da (*O*-Me-cysteine), 111 Da (*N*-methylmaleimide). Smaller unlabelled peaks correspond to sodium adducts (M+Na, + 23 Da).

The dithiocarbonates do not show any susceptibility towards non-thiol nucleophiles, and this can be beneficial for site-selective re-bridging of cysteine residues in the presence of other nucleophilic amino acids. This does however limit their potential as versatile chemical biology reagents, due to their lack of functionality.

### 3.3.3.4. Stability investigations of dithiocarbonate conjugate

The dithiocarbonate re-bridged conjugate has shown remarkable stability against a variety of nucleophiles and is only cleaved after prolonged incubation with large excess of thiol-based nucleophiles such as cysteine. Whilst not functionalised here, the chemistry and stability of the dithiocarbonate is nonetheless of interest as it could potentially be applied as a bioconjugate linker outside of disulfide re-bridging.

To investigate aqueous stability, the dithiocarbonate re-bridged conjugate was synthesised, and excess dithiocarbonate reagent was removed. The resultant conjugate was then incubated at 22 ºC, pH 7.4 for 7 days (**FIG. 89**). There was no noticeable degradation in such conditions, indicating the dithiocarbonate re-bridged conjugate is stable in aqueous solutions for long-periods of time. Considering that

ADCs typically have a half-life of 3-5 days and mAbs have a half-life of 2-4 weeks, the dithiocarbonate conjugates demonstrate acceptable levels of aqueous stability.

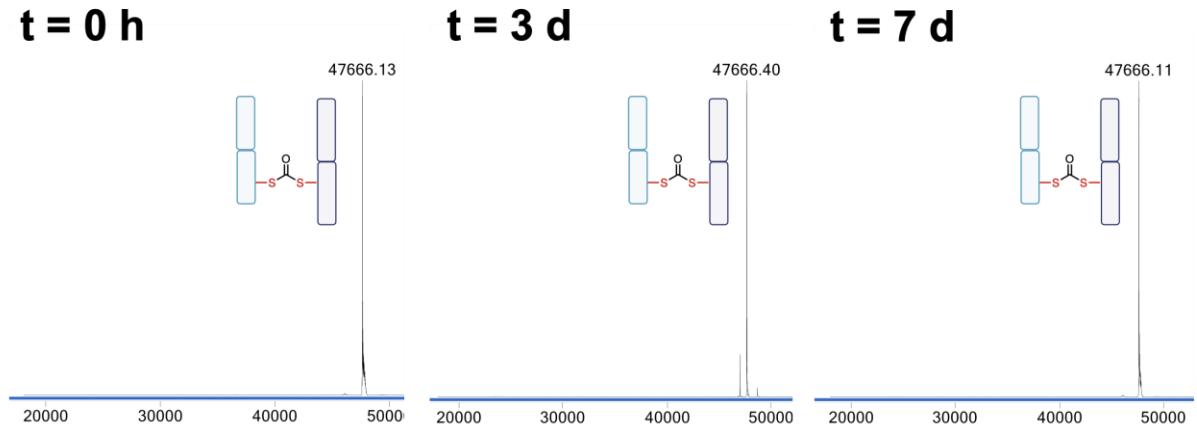


**FIGURE 89.** Aqueous stability of dithiocarbonate re-bridged conjugate over 7 days in pH 7.4 conditions at 22 ºC. Mass of native Fab = 47638 Da. Mass of dithiocarbonate re-bridged conjugate = 47666 Da.

In terms of application in ADCs, the endosomal and serum stability is more relevant. The endosome has high concentrations of GSH (5 mM) and a slightly more acidic pH (pH 6.5), while the blood serum has lower concentrations of GSH (5 $\mu$M) and physiological pH (pH 7.4). Buffers were prepared with GSH and pH mimicking that of endosomal or serum conditions respectively, and the dithiocarbonate conjugate was incubated in the respective buffer for 24 h at 37 ºC, with additional timepoints taken at 1 h, 2 h, 4 h (**FIG. 90**). Longer timeframes are not viable with this particular stability investigation, as it is likely that the GSH in solution gradually oxidises to form an unreactive disulfide over time. Promisingly, the dithiocarbonate conjugate demonstrated no degradation after 4 h incubation in either endosomal or serum conditions. Only after 24 h of incubation at 37 ºC was some degradation observed in both conditions. In serum conditions, where pH is 7.4, there is some fragmentation of the HC to a species with mass 23615 Da, seen in the previously discussed CLT conditions – elevated temperature and pH seems to drive this fragmentation process. Nonetheless, the amount is minimal in comparison to intact dithiocarbonate conjugate, and there is no native Fab. In endosomal conditions, where GSH concentration is higher, there is very slight deconjugation of the dithiocarbonate bridge, with a small amount of native Fab present. The higher concentration of GSH causes loss of the bridge due to transthioesterification between the GSH-thiol and the dithiocarbonate.

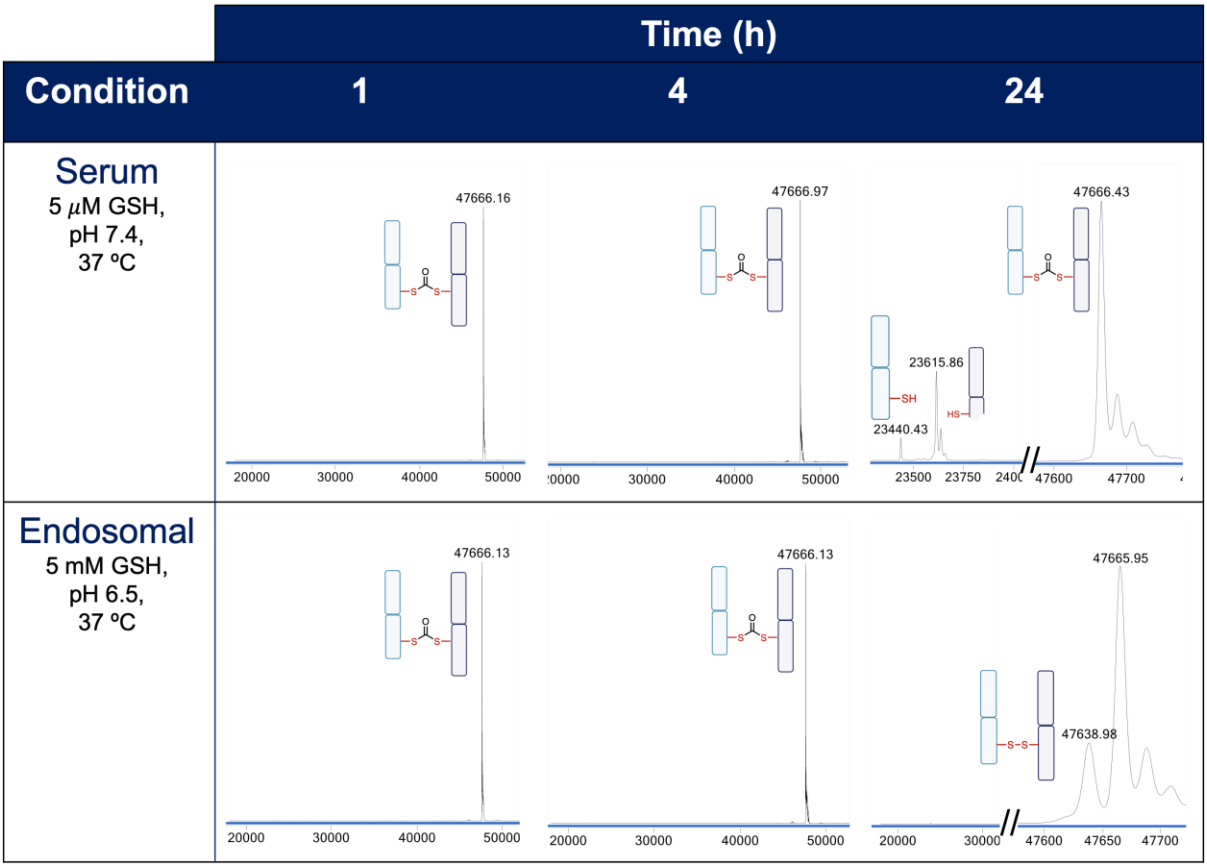


**FIGURE 90.** Serum (5 $\mu$M GSH, pH 7.4, 37 ºC) and endosomal (5 mM GSH, pH 6.5, 37 ºC) stability investigation of the dithiocarbonate conjugate. Mass of native Fab = 47638 Da. Mass of dithiocarbonate re-bridged conjugate = 47666 Da.

Thus, the dithiocarbonate conjugate show remarkable stability in biologically relevant conditions, which gives them promise as linkers.

### 3.3.3.5. Full antibody re-bridging with dithiocarbonates

A common problem when working with mAbs is their tendency to form mixed disulfides that result in the formation of half-antibodies, and these mixed species can impact the stability and functionality of mAb-based conjugates. Additionally, half-antibody formation and half-antibody exchanges have been shown to reduce the efficacy of mAbs and ADCs in tumour models.[159] Whilst mutations have been suggested to prevent half-antibody formation to maintain efficacy, this is an expensive, time-consuming, and technically challenging process.

Whilst not functionalised, these dithiocarbonate reagents were then explored out of interest on trastuzumab for disulfide re-bridging (**SCHEME 30**).

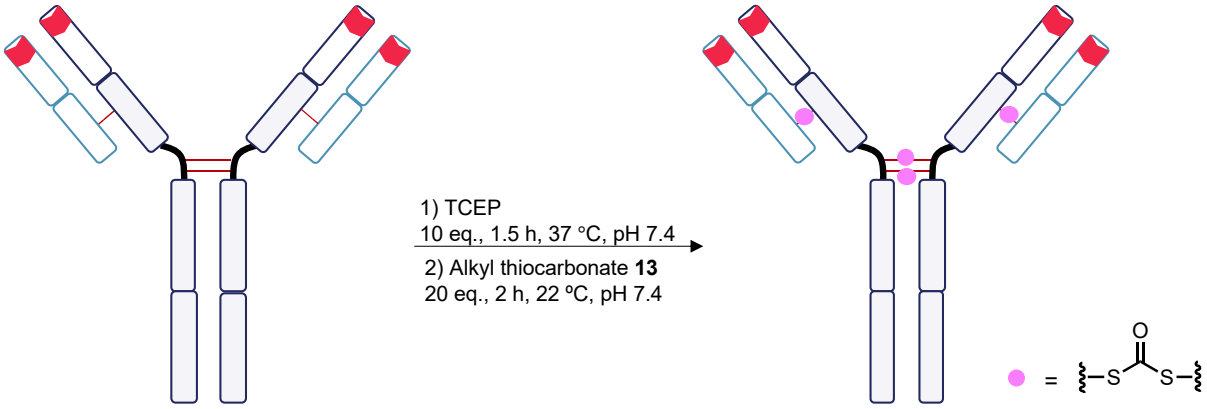


**SCHEME 30**. Alkyl dithiocarbonate **13** re-bridging of trastuzumab.

Following reduction of trastuzumab's disulfide bonds, the alkyl dithiocarbonate **13** was added *in situ*. After 2 h, the LCMS (**FIG. 91**) and SDS-PAGE (**FIG. 92**) analysis was conducted. Both results demonstrate the formation of half-antibody formation. LCMS is not quantitative, as smaller protein species ionise more effectively and subsequently appear larger. The SDS-PAGE indicates the major product of this reaction is the correctly re-bridged full mAb species – the band corresponding to mAb mass (70%) is more intense than the half-antibody band *via* densitometry analysis (30%).

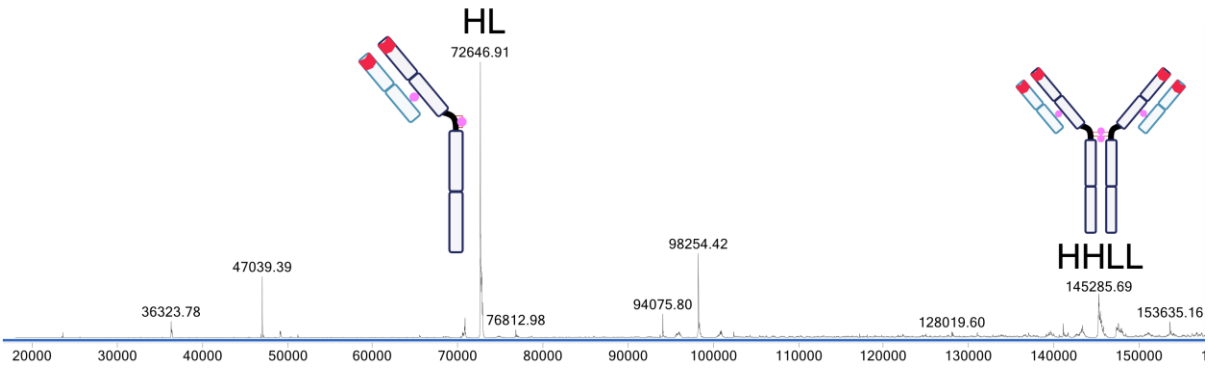


**FIGURE 91.** LCMS of dithiocarbonate re-bridging reaction on trastuzumab. Native HL (half-antibody) = 72594 Da. Native HHLL (full antibody) = 145167 Da. Expected mass of addition = 112 Da (4 disulfides x 28 Da per dithiocarbonate bridge).

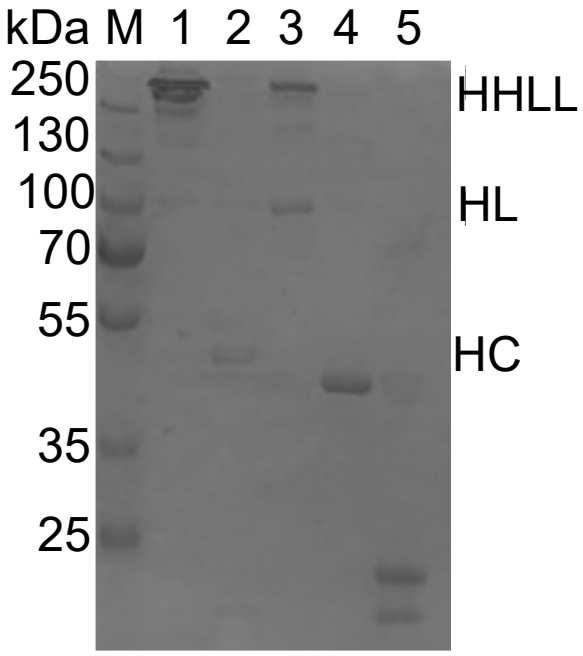


**FIGURE 92.** SDS-PAGE analysis of alkyl dithiocarbonate **13** re-bridging of trastuzumab. Lane M: protein ladder, Lane 1: trastuzumab, Lane 2: reduced trastuzumab, Lane 3: Dithiocarbonate re-bridged conjugate, Lane 4: trastuzumab Fab, Lane 5: reduced trastuzumab Fab.

### 3.3.4. Summary and outlook of dithiocarbonates

The dithiocarbonates enable a clean and efficient re-bridging strategy of Fab, inserting a carbonyl bridge of only one carbon atom, which is smaller than other re-bridging reagents available in literature. Full antibody re-bridging favours formation of the correctly re-bridged species, though a significant amount of half-antibody forms. The dithiocarbonate conjugates demonstrate excellent aqueous, serum-mimicking, and endosomal-mimicking stability at 22 ºC. Only when temperature is elevated to 37 ºC does some degradation occur over 24 h, but the dithiocarbonate remains the major species. However, it is currently not possible to functionalise these reagents, which limits their use as protein modification reagents, as CLT does not occur under typical conditions, and they are not prone towards substitution by non-thiol nucleophiles.

Nonetheless, the dithiocarbonates present a unique, short re-bridging strategy of proteins that very closely mimic the structural properties of native disulfides that retain high stability. Their stability could enable them to become useful and stable bioconjugate linkers outside of disulfide bridging, for example as non-cleavable linkers, or generally to join two thiol-containing moieties such as peptides.

### 3.4. Carbonimidodithioates

The small size and good re-bridging properties of dithiocarbonates has shown them to be effective reagents, but their lack of functionalisation point limits their applicability for chemical biology applications. Carbonimidodithioates have been proposed to overcome this limitation – they have a nitrogen imine functional group (C=NR), which offers an insertion site for functional properties, such as click handles for example. Like the dithiocarbonates, there are two C-S bonds that can be substituted by nucleophiles, particularly relevant for cysteine thioesterification reactions. Their typical use in literature often involves the substitution of one of the C-S bonds with nucleophiles, such as amines for example, and they are more commonly used as intermediates towards carbonates or carbamates.[260] They have not been very widely used or explored in recent years, and they have not been utilised in chemical biology applications either.

To understand and predict the chemistry and reactivity of carbonimidodithioates, imines are useful analogous compounds. Compared to carbonyls, imines have a smaller dipole moment, resulting from the lower electronegativity of nitrogen compared to oxygen. As a result, imines are less prone towards nucleophilic substitution, as the attached carbon is more electron-rich. These considerations suggest that the carbonimidodithioates will demonstrate slower reactivity than their dithiocarbonate counterparts when utilised as re-bridging reagents. Despite the potential lower reactivity, the small length of bridge and functional potential makes carbonimidodithioates intriguing reagents for bioconjugation purposes. In CLT conditions, thioamidines could potentially be generated, which would represent a novel functional group of interesting properties for antibody modification (**FIG. 93**).

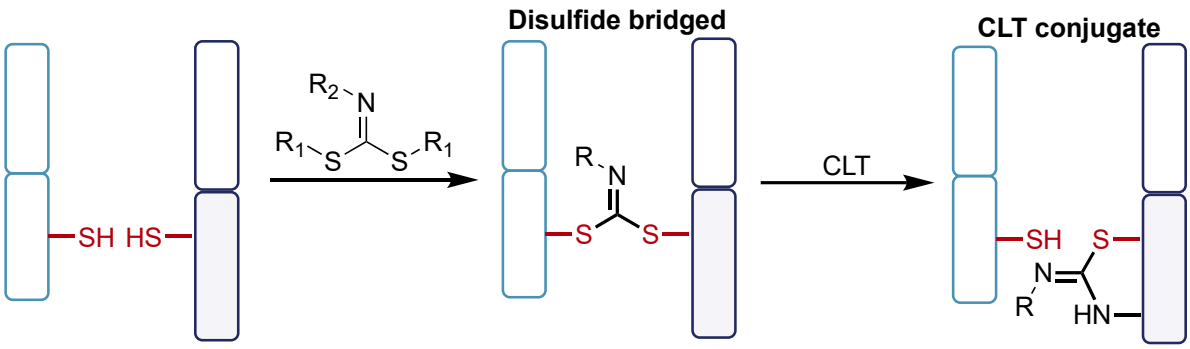


**FIGURE 93.** Cysteine and CLT conjugate from the application of carbonimidodithioates.

### 3.4.1. Chemical synthesis

Organic synthesis of the carbonimidodithioates followed literature protocols, using carbon disulfide as the starting material. Propargylamine was added, which contains a linear alkyne for potential click chemistry. The intermediate of this amine addition is a carbamodithioic acid, and this can be alkylated using an excess of methyl iodide to synthesise the final carbonimidodithioate **15** in good yields (61%) (**SCHEME 31**). Only an alkyl derivative, with methanethiol as the leaving group, was synthesised. Attempts to substitute the methanethiol leaving group with a better aryl thiol leaving group such as thiophenol have been attempted in literature but have not shown much success, so this was not pursued. Nonetheless, the carbonimidodithioate **7** provides a suitable starting reagent to explore the carbonimidodithioates as Fab re-bridging reagents.

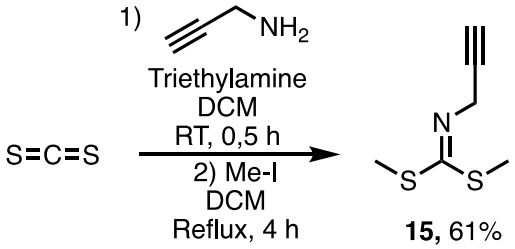


**SCHEME 31.** Synthesis of carbonimidodithioate **7** *via* carbon disulfide.

### 3.4.2. Bioconjugation studies

#### 3.4.2.1. Re-bridging Fab conditions

Control experiments confirmed no unselective modification, and reactions on reduced Fab followed (**SCHEME 32**). Initial investigations utilised the dithiocarbonate re-bridging conditions, using 20 eq. of carbonimidodithioate **7** for 1-2 h at 22 ºC, pH 7.4.

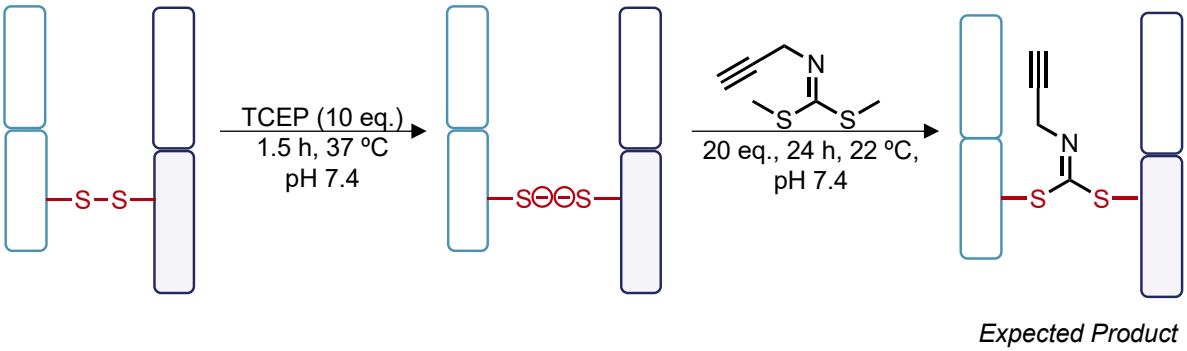


**SCHEME 32**. Bioconjugation of carbonimidodithioate on reduced Fab.

However, no modification was observed under these conditions. Instead, conditions of 20 eq., 24 h, 22 ºC, pH 7.4 were needed to fully re-bridge Fab with the

carbonimidodithioate (**FIG. 94**). This indicates that the carbonimidodithioates show reduced reactivity in comparison to the dithiocarbonates, as a result of their more electron-rich carbon electrophile, and the poorer leaving groups in methanethiol.

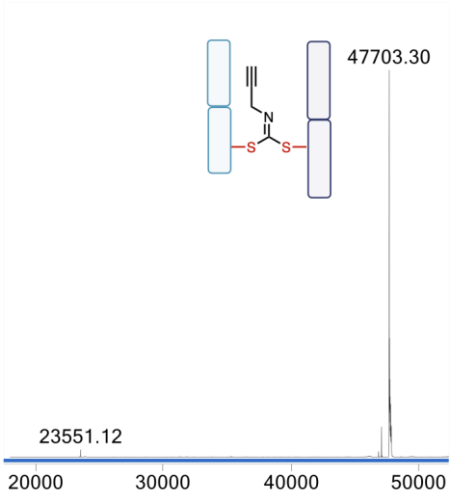


**FIGURE 94.** LCMS of carbonimidodithioate **15** re-bridging on Fab, using conditions of 20 eq., 24 h, 22 ºC, pH 7.4. Mass of native Fab = 47638 Da. Mass of carbonimidodithioate re-bridged conjugate = 47703 Da. Expected mass of addition = 65 Da. Smaller unlabelled peaks correspond to sodium adducts (M+Na, +23 Da).

In an attempt to increase the rate of reactivity and enable faster formation of the carbonimidodithioate re-bridged conjugate, 100 eq. of carbonimidodithioate **15** were used at 37 ºC. More available reagent should mean more electrophiles for reactions with the cysteine thiols, and higher temperatures increase the rate of reaction. The reaction was monitored every 1 h for 6 h by SDS-PAGE, however no complete re-bridging was observed. Instead, the major product according to SDS-PAGE (**FIG. 95**) and LCMS analysis (**FIG. 96**) appeared to be the mono-substituted species, instead of the desired re-bridged species. SDS-PAGE shows the presence of re-bridged Fab, modified LC and modified HC at 100 equivalents (Lanes 3-7). This is also seen at 20 eq. (Lane 8), which could be due to protein cleavage under denaturing conditions, as LCMS indicates almost complete conversion. According to LCMS analysis, maximum conversion to the fully re-bridged species was observed after 4 h, but this decreased over time during the 5 h and 6 h timepoints. In LCMS analysis, there was no native Fab, native LC, or native HC, indicating that hydrolysis was a competing reaction, and it is instead likely that larger equivalents causes trapping of the free cysteine thiols.

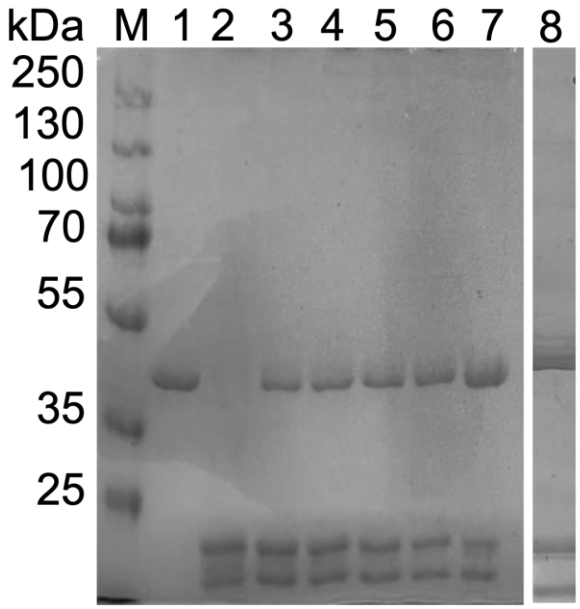


**FIGURE 95.** SDS-PAGE analysis of carbonimidodithioate **15** re-bridging of Fab. Lanes 3-7: 100 eq., 37 ºC. Lane 8: 20 eq., 22 ºC. Lane M: protein ladder, Lane 1: Fab, Lane 2: reduced Fab, Lane 3: 1 h, Lane 4: 2 h, Lane 5: 4 h, Lane 6: 5 h, Lane 7: 6 h, Lane 8: 24 h.

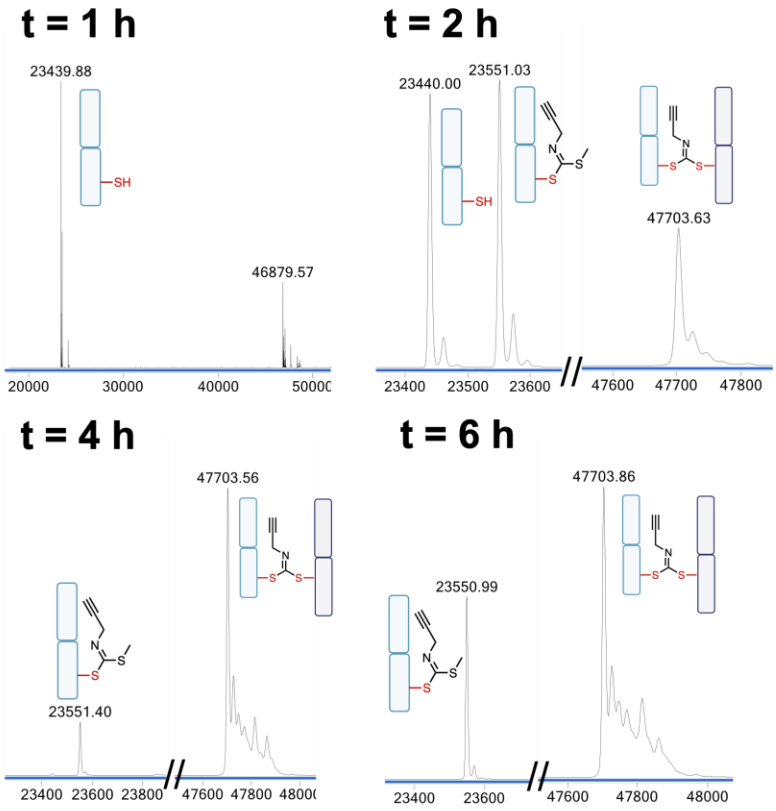


**FIGURE 96.** LCMS analysis of carbonimidodithioate **15** re-bridging over time using conditions of 100 eq., 37 ºC, pH 7.4.

At lower equivalents, there is less carbonimidodithioate, and di-substitution to for the desired re-bridged species occurs preferentially. At higher equivalents, re-bridging is not the major product, and there is more mono-substituted species. When a large excess of carbonimidodithioate **15** is applied, there is a higher concentration of carbonimidodithioate species, which results in greater trapping of the cysteine thiols to cause mono-substitution instead of di-substitution for re-bridging. Additionally, at higher equivalents it is possible that some reversibility occurs due to the larger release of methanethiol (MeSH) (**SCHEME 33**) – there is more mono-substituted conjugate after 6 h in comparison to the earlier 4 h timepoint when 100 eq. of carbonimidodithioate **15** is used.

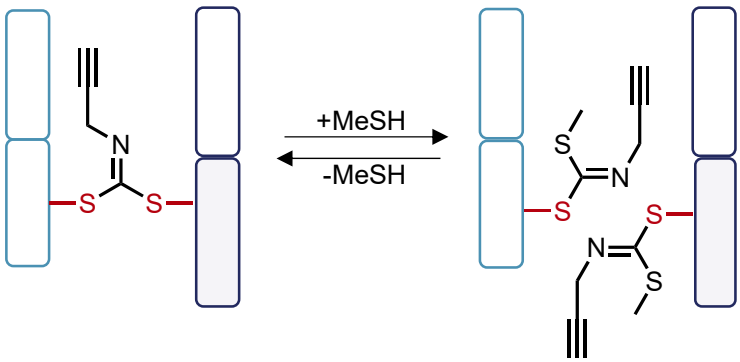


**SCHEME 33.** Reversibility of carbonimidodithioate re-bridging in the presence of methanethiol (MeSH), which enables switching between the re-bridged conjugate and the mono-modified conjugate.

Thus, the carbonimidodithioate **15** enables re-bridging or mono-modification depending on the conditions employed during the conjugation step. Higher equivalents favour mono-modification and is reversible, whilst lower equivalents lead to a slower conjugation but enables complete re-bridging.

### 3.4.2.2. CLT of carbonimidodithioate conjugate

CLT of the carbonimidodithioate re-bridged conjugate was investigated next. The carbonimidodithioate re-bridged conjugate was incubated in pH 8.4 conditions for 24 h at 37 ºC (**FIG. 97A**). However, the re-bridged conjugate remained intact under these conditions. The mono-substituted conjugate was also investigated under similar conditions (pH 8.4, 6 h, 37 ºC), but no CLT was observed (**FIG. 97B**) – only modified LC was observed, whilst the proximal lysines are located on the HC.

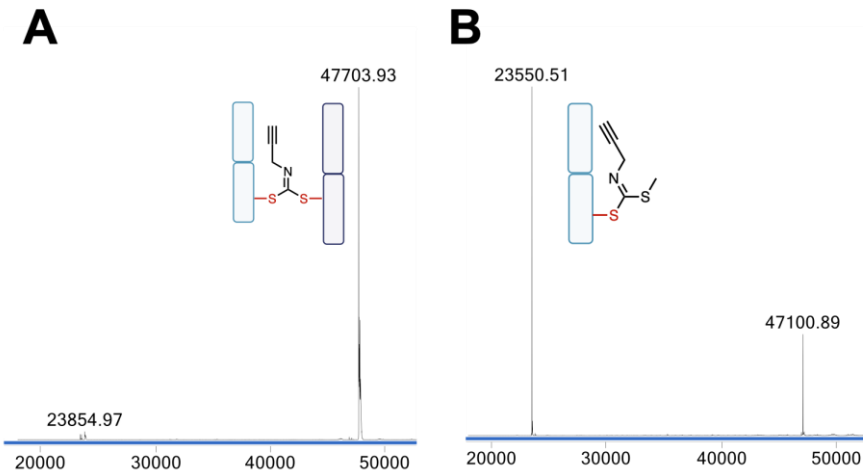


**FIGURE 97.** Carbonimidodithioate Fab conjugate CLT. **A)** Re-bridged carbonimidodithioate, pH 8.4, 24 h, 37 ºC. **B)** Mono-substituted carbonimidodithioate, pH 8.4, 6 h, 37 ºC. Mass of native Fab = 47638 Da. Mass of re-bridged carbonimidodithioate = 47704 Da. 41000 Da is deconvolution artefact.

Whilst neither carbonimidodithioate conjugate demonstrates meaningful CLT activity, this experiment does represent an indication of their general hydrolytic stability – even at pH 8.4 at 37 ºC for 24 h, no noticeable hydrolysis to native Fab is observed. To further probe the reactivity of this group towards amines, *p*-anisidine (1000 eq., 1-24 h, 37 ºC, pH 7.4) was added (**FIG. 98**). As previously mentioned, *p*-anisidine is an interesting amine nucleophile due to its low pKa, high nucleophilicity in physiological conditions, and as a model for further functionalisation.

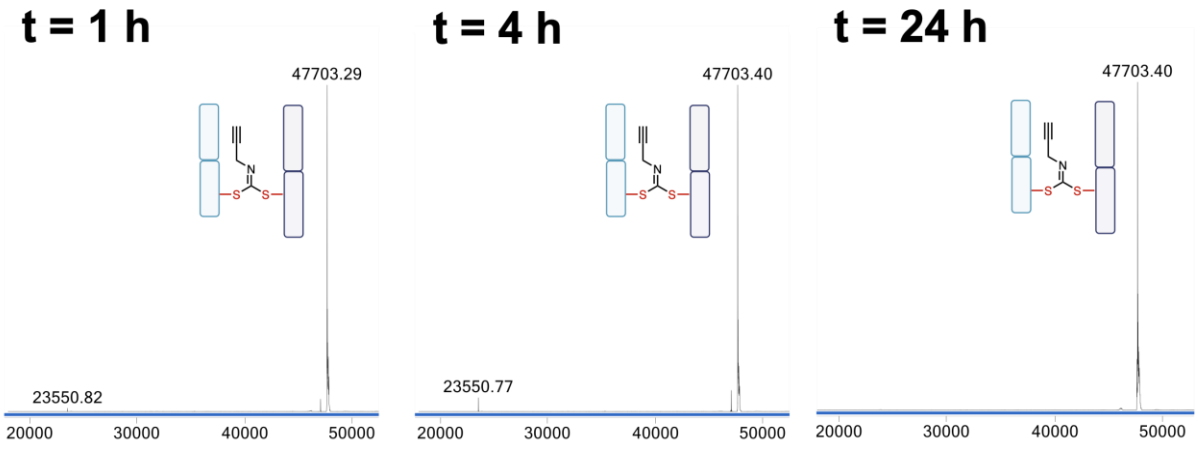


**FIGURE 98.** *p*-anisidine addition to carbonimidodithioate re-bridged conjugate over time. Mass of native Fab = 47638 Da. Mass of carbonimidodithioate conjugate – 47704 Da. Smaller unlabelled peaks correspond to sodium adducts (M+Na, +23 Da).

No reactivity was observed. Over time, there is some loss of the re-bridged species due to minimal hydrolysis, but the major product remains the correctly re-bridged conjugate. This result further confirms that the carbonimidodithioate does not demonstrate meaningful amine reactivity, which would explain why no CLT was observed. Whilst not useful for CLT and lysine modification, this does mean the carbonimidodithioate shows very high thiol selectivity over other nucleophiles.

### 3.4.2.3. Stability investigations of carbonimidodithioate conjugate

Like the dithiocarbonates, understanding the stability of the carbonimidodithioate conjugates is important to determine their usefulness in protein applications. They demonstrate very good aqueous stability, with no degradation of the conjugate seen over 7 days of incubation in pH 7.4 conditions (**FIG. 99**).

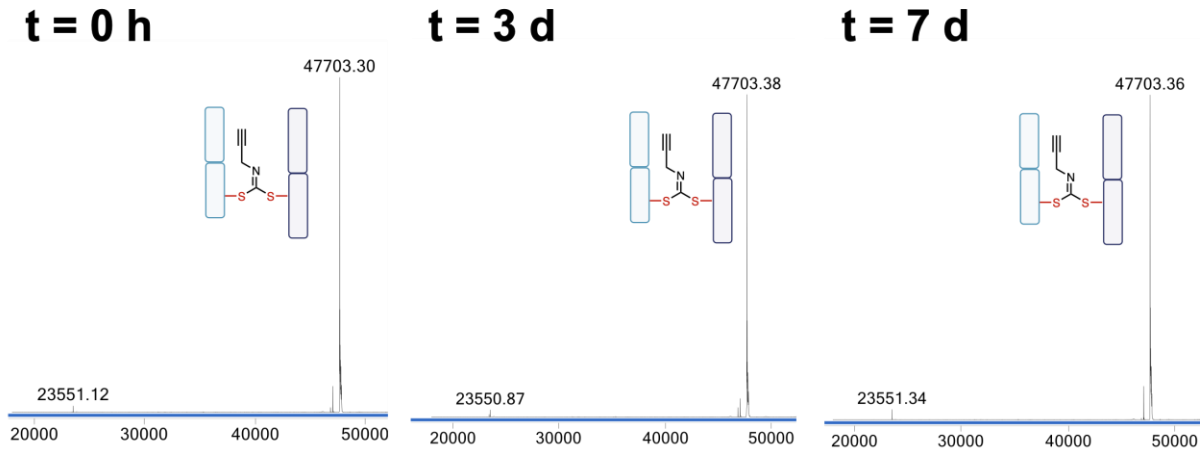


**FIGURE 99.** Aqueous stability of carbonimidodithioate re-bridged conjugate over 7 days, in pH 7.4 conditions at 22 ºC. Mass of native Fab = 47638 Da. Mass of carbonimidodithioate conjugate = 47704 Da.

Serum and endosomal stability were also investigated (**FIG. 100**). Promisingly, in both sets of conditions, minimal loss of re-bridged species was observed. The most significant loss was seen after 24 h incubation in endosomal conditions, where the concentration of GSH, a competing thiol, is higher, however the major product remains the correctly re-bridged species. Overall, these results demonstrate the carbonimidodithioate reagents and their subsequent conjugates are remarkably stable against a wide variety of conditions that are relevant for use in ADCs.

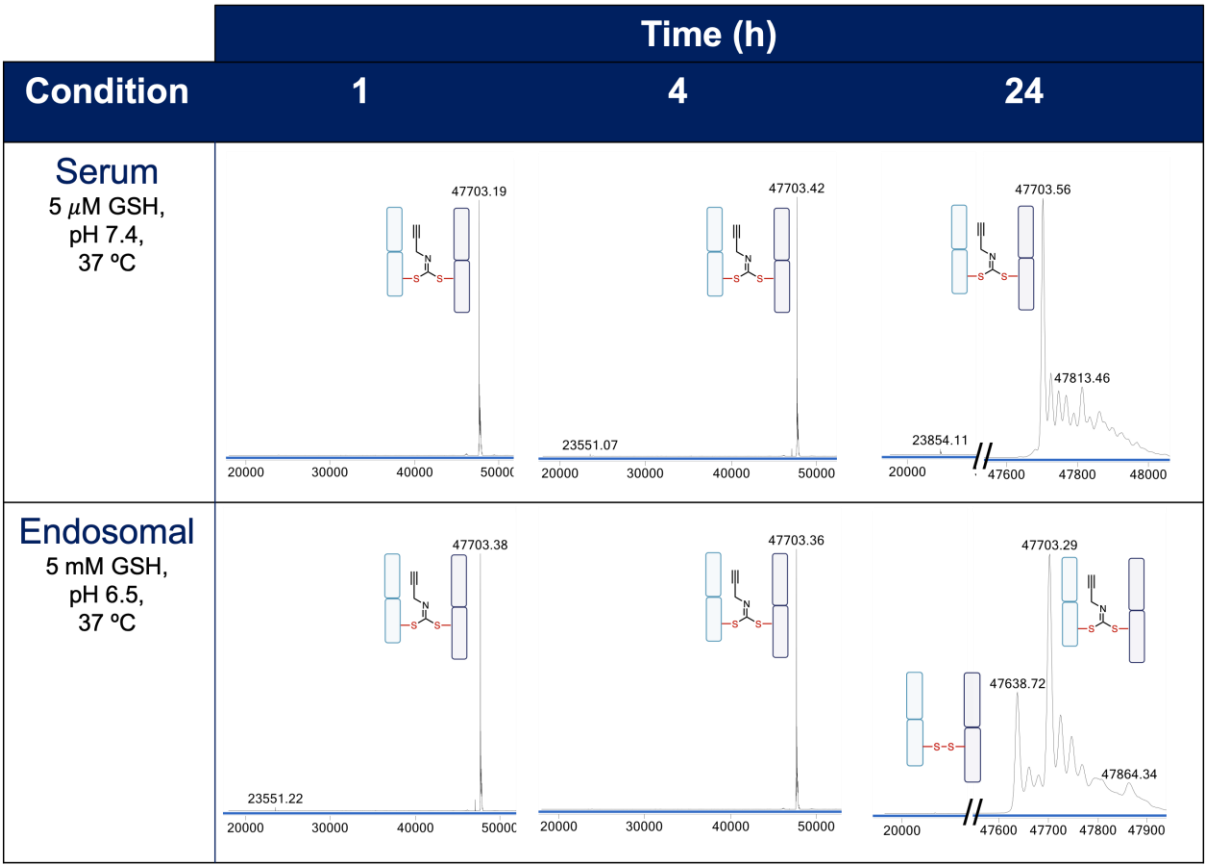


**FIGURE 100.** Serum (5 $\mu$M GSH, pH 7.4 37 ºC) and endosomal (5 mM GSH, pH 6.5, 37 ºC) stability investigation of the carbonimidodithioate conjugate.

### 3.4.2.4. Full antibody re-bridging with carbonimidodithioates

With their conjugation and stability confirmed on Fab, it was next relevant to explore the carbonimidodithioate **15** on full trastuzumab (**SCHEME 34**).

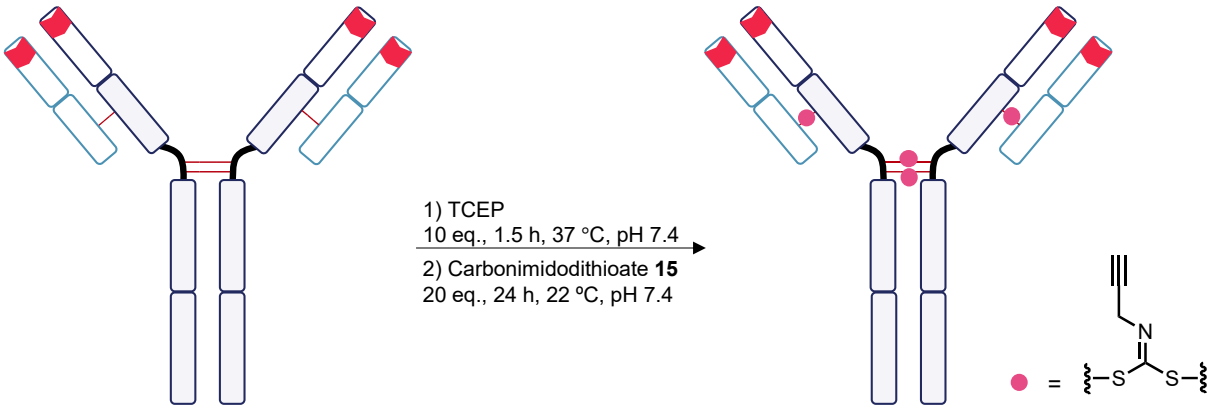


**SCHEME 34.** Carbonimidodithioate **15** bioconjugation on trastuzumab.

Carbonimidodithioate **15** returns mostly half-antibody, and this is reflected in both SDS-PAGE (**FIG. 101**) and LCMS analysis (**FIG. 102**). The SDS-PAGE band

corresponding to half-antibody (50%) is far more intense than the full antibody band (25%) *via* densitometry, whilst LCMS analysis shows very small amounts of full antibody too. Also, there is a significant quantity of full HC (25%), which has not undergone re-bridging with the reagent. It is necessary develop carbonimidodithioates that have better leaving groups to enable full re-bridging. Ideally, the thiol released would self-quench, so it does not trigger reversibility.

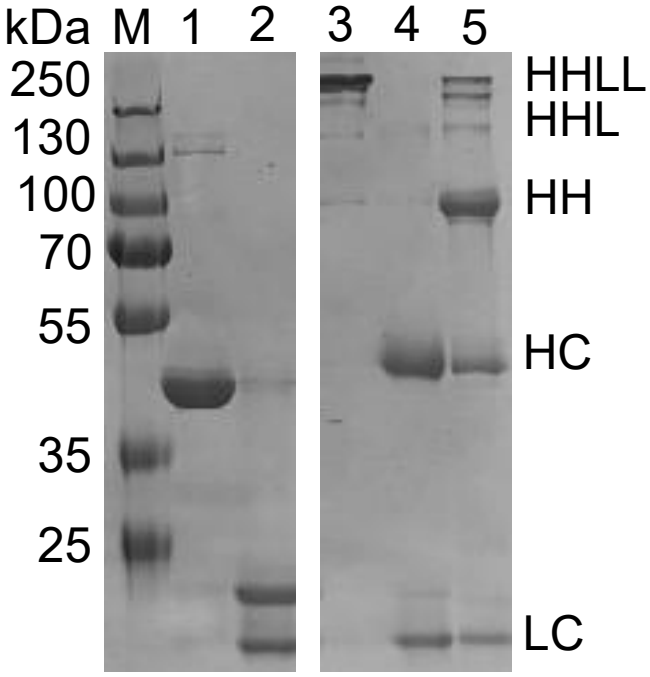


**FIGURE 101.** SDS-PAGE analysis of carbonimidodithioate **15** re-bridging of trastuzumab. M: protein ladder, 1: trastuzumab Fab, 2: reduced trastuzumab Fab, 3: trastuzumab, 4: reduced trastuzumab, 5: carbonimidodithioate re-bridged conjugate.

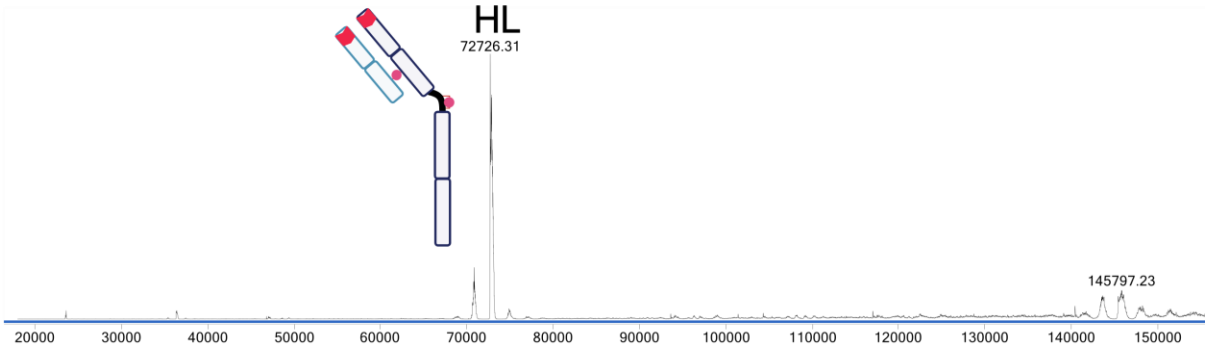


**FIGURE 102.** LCMS of carbonimidodithioate **15** re-bridging on trastuzumab. Native HHLL (full antibody) = 145167 Da Native HL (half-antibody) = 72594 Da. Expected mass of addition = 264 Da (4 disulfides x 66 Da per carbonimidodithioate bridge).

### 3.4.3. Summary and outlook of carbonimidodithioates

The carbonimidodithioates show remarkable potential as novel bioconjugation reagents. Like the dithiocarbonates, they form very efficient, short re-bridging conjugates with very good stability against relevant conditions. Additionally, the introduction of a nitrogen atom enables direct functionalisation – a click handle was introduced here, but this could seemingly be any other amine that has a biologically useful handle, such as a fluorophore for example. The stability of these compounds is significant, but it does mean they are quite slow to react with cysteine thiols, with the cleanest re-bridging seen at low equivalents and 24 h. Future iterations of carbonimidodithioates could incorporate different thiol leaving groups, such as MESNa or MPAA, and this will improve the rate of thioesterification.

## 3.5. Overall summary and conclusion

Investigations into novel functional groups for CLT have shown the difficulty in replicating the ideal reactivity profile of thioesters – nature itself has utilised thioesters for acyl transfer reactions in the Krebs cycle, using acetoacetyl coenzyme A.[261] Convenient synthetic routes were developed towards each functional group, and this could provide simple routes for future investigation of these reagents.

The thiocarbonates demonstrated good stability at pH 7.4, however this resulted in a lack of reactivity even when conditions attempted to increase the rate of reaction, by increasing temperature and equivalents of reagent. Higher pH showed some thiol-preference by the aryl thiocarbonate **10**, but it is difficult to achieve complete modification of LC and HC whilst preventing uncontrolled lysine reactions. The stability of the thiocarbonates at pH 7.4 could be beneficial for other protein-related applications, particularly on smaller peptides where there are fewer lysine residues available for modification. The thiocarbamates did not react as expected, and instead reacted *via* the *in situ* formation of isocyanates, which react promiscuously with lysine residues. Again, the thiol leaving group determined the reactivity of the reagent more than the thiocarbamate functional group itself, with greater isocyanate formation seen in the aryl thiocarbamate **12** corresponding to undesirable and unselective lysine modification, even at lower pH.

The re-bridging reagents demonstrated more usefulness as general protein modification reagents, though their ability to engage in CLT was lacking. The

dithiocarbonates demonstrate quick and efficient re-bridging of Fab at relatively low equivalents. More importantly, they demonstrate very good stability in all biologically relevant conditions, including in aqueous, serum-mimicking, and endosomal-mimicking conditions. Their lack of functionality is a disadvantage, and disappointingly it was not possible to introduce functionality through various attempts. However, the carbonimidodithioates are particularly interesting, as they demonstrate very good stability against a variety of conditions whilst possessing a site of functionality. This functionality could feasibly be used to introduce fluorophores or cytotoxic reagents.

Exploring these reagents has not provided the desired outcome in terms of improving and finding new routes towards CLT, however it has provided a much better understanding of tolerable and useful functional groups for bioconjugation purposes more generally. Additionally, their use as Fab and full antibody modification reagents has been explored, and some show promise as general chemical biology reagents, such as the carbonimidodithioates.

### 3.6. Further work on novel reagents for CLT

The current reagents proposed have limitations, and these could be overcome by improving the reagent design. For example, the thiocarbonates show limited reactivity at pH 7.4 – introducing electron-withdrawing substituents at the carbonate position could assist in creating a more reactive compound at pH 7.4. For example, instead of propargyl alcohol, a fluoroalcohol could be used instead as a proof-of-concept to further understand whether there is scope for thiocarbonate improvements.

The thiocarbamates show very limited use as a protein modification reagent due to the spontaneous elimination of isocyanates and could not be explored further. However, alkylating the nitrogen has been shown to somewhat prevent this reversible thiocarbamate-isocyanate elimination process. Additionally, this alkylation could be useful to introduce a further point of functionalisation. As mentioned earlier, initial attempts to achieve this on the synthesised thiocarbamates were unsuccessful due to thioester degradation, however using a trityl thioester could be beneficial – the trityl group is very stable against a wide range of conditions, particularly in the presence of strong base. So, a trityl thiocarbamate could be synthesised first, which is then alkylated at the *N*-position, before deprotecting the thioacid and lastly alkylating the thioacid to form the desired thiocarbamate (**SCHEME 35**).

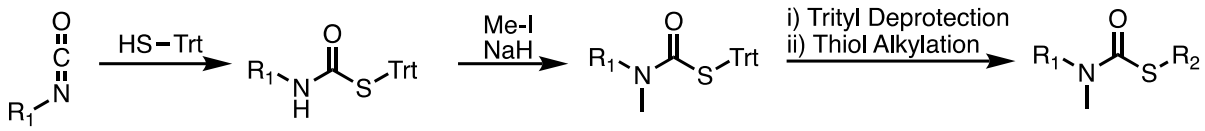


**SCHEME 35.** Proposed route for the synthesis of *N*-alkylated thiocarbamates.

The carbonimidodithioates show excellent re-bridging properties and have a useful site of modification on the nitrogen. Their reactivity properties could be optimised further by improving the thiol leaving group. It would be necessary to utilise a different route towards these carbonimidodithioate compounds to synthesise derivatives with improved thiol leaving groups (**SCHEME 36**).[262] This would enable faster reactions on Fab. In terms of improving the reactivity of the reagent for CLT, it may be necessary to modify the amine utilised during synthesis. An amine with an electron-withdrawing group may increase the reactivity of the carbonimidodithioate carbon towards other nucleophiles such as the proximal lysine residues. A combination of tuning the thiol leaving group and the properties of the amine handle could be used to control its reactivity once attached onto the cysteine residues and could help promote CLT.

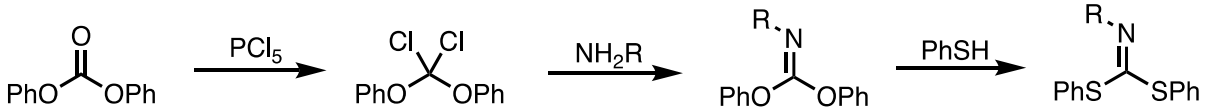


**SCHEME 36.** Proposed route for the synthesis of thiophenol-substituted carbonimidodithioates, starting from commercially available diphenyl carbonate.

Additionally, there are other functional groups that could be of interest, such thioimidates or dithioesters. Dithioesters have been shown to form thioimidates on *N*-terminal cysteine through the elimination of hydrogen sulfide.[263] On Fab, this could occur through the action of the proximal lysine residues, forming cyclic thioimidates. Several attempts were made in this project towards synthesising dithioesters from known literature protocols including Lawesson's reagent for the conversion of carboxylic acids, and the substitution of amine-activated thioamides with thiols (not shown), but none thus far provided any desired dithioester. Instead, an approach using carbon disulfide and Grignard reagent is suggested (**SCHEME 37**).[264]

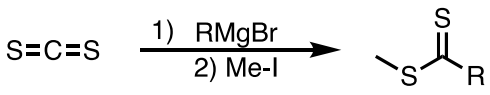


**SCHEME 37.** Proposed route for the synthesis of a methyl dithioester.

# 4. Dual-reactive thioesters

Thioesters offer exquisite selectivity for cysteine residues, compared to other electrophiles. However, they have shortcomings in their own stability against aqueous conditions. This selectivity could be utilised to introduce secondary reactive handles at the site of conjugation. This chapter explores early work investigating a design of dual-reactive thioesters that utilise the selectivity of thioesters to enable directed reactivity with proximal lysine residues on trastuzumab Fab.

## 4.1. Aldehyde-Thioester

Aldehydes react reversibly with amines, in the presence of an acid catalyst, to form imines. The application of a reducing agent, such as sodium cyanoborohydride, reduces the imine to a stable amine. The formation of such amine-linked conjugates is highly desirable, due to the stability of the amine bond. However, achieving this in a site-selective manner using aldehydes is difficult due to the reversibility of imine formation. Over time, the imine forms and hydrolyses repeatedly, modifying multiple lysine residues, at different conjugation sites. Iminoboronates have demonstrated the potential of aldehyde-mediated protein modification within reasonable timeframes, however these reagents react reversibly and unselectively with all lysine residue.[265]

A dual-reactive thioester with an aldehyde handle could introduce the aldehyde close to the proximal lysine residues to enable their site-selective modification. This would represent one of the first examples of achieving site-selective amine formation on Fab and would provide another strategy towards achieving homogeneous ADCs. Additionally, the potential for CLT still exists. (**SCHEME 38**).

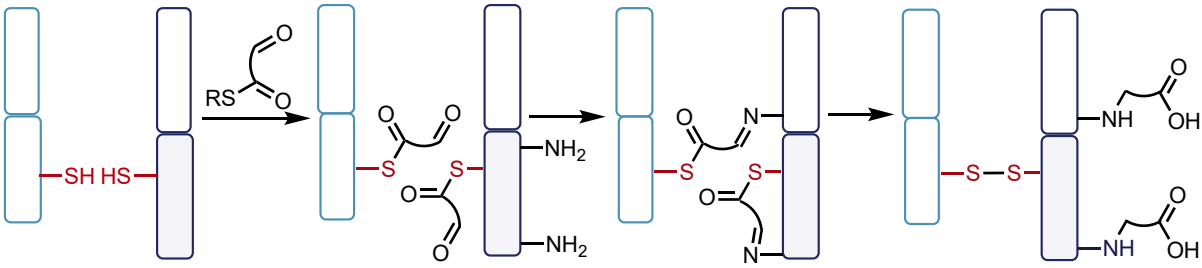


**SCHEME 38.** Possible lysine modification mechanisms for an aldehyde-thioester.

Proximity between the aldehyde and thioester groups could enable intramolecular rearrangements on the protein, which would generate stable amide conjugates (**SCHEME 39**). Thus, a *o*-substituted aldehyde-thioester is highly desirable.

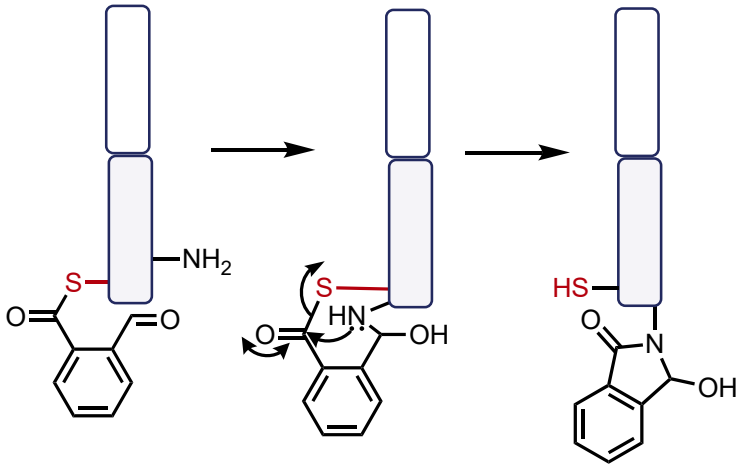


**SCHEME 39.** Intramolecular rearrangement from a *o*-substituted aldehyde-thioester.

### 4.1.1. Chemical synthesis

The synthesis of *p*-aldehyde thioester **16** occurred in straightforward conditions (**SCHEME 39**). EDC coupling to the starting carboxylic acid generated an activated intermediate, which is subsequently substituted by thiophenol to return the target compound **16** in very good yields. The aldehyde substituted at the *para*- position likely has some electron-withdrawing effect on the thioester, which could help reactivity.

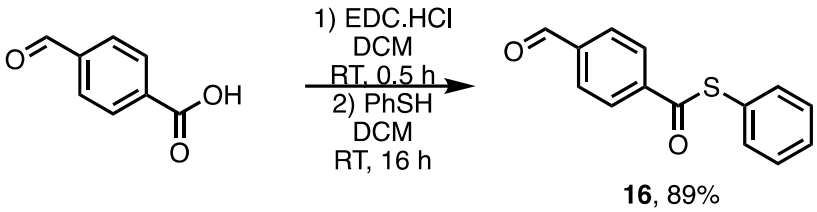


**16**, 89%

**SCHEME 40.** Synthesis of *p*-aldehyde thioester **16**.

Synthesis of the target *o*-aldehyde thioester **17** was not successful (**SCHEME 41**). Attempts to use coupling conditions for the conversion of commercially available 2-carboxybenzaldehyde were unsuccessful.

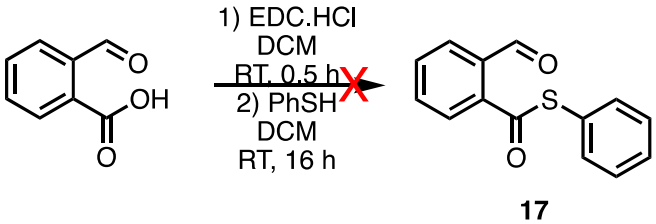


**17**

**SCHEME 41.** Attempted synthesis of *o*-aldehyde thioester **17** from 2-carboxybenzaldehyde.

Other synthetic attempts included starting from 2-bromobenzaldehyde (**SCHEME 42**). The aldehyde in the starting material was protected by the addition of ethylene glycol, forming the acetal **18**. The aryl bromide was then subjected to Bouveault aldehyde synthesis with *n*-BuLi, to form the Grignard reagent, and DMF was added to form the target aldehyde **19** in good yields.

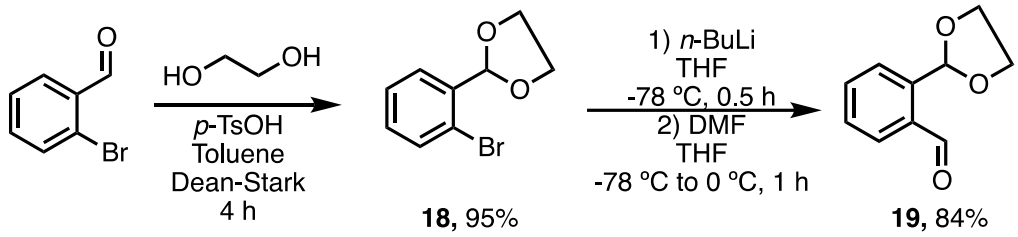


**SCHEME 42**. Bouveault aldehyde synthesis of **19** from 2-bromobenzaldehyde.

Direct conversion of the aldehyde to the thioester was then attempted *via* several literature strategies (**TABLE 2**). These strategies often convert the aldehyde directly into the thioester through radical-based mechanisms (entries 1-3) or attempt to activate the aldehyde as an intermediate hydrazine (entry 4).

**TABLE 2.** Literature strategies to convert **19** into the desired thioester.

| Ref | Reagents (equivalents) | Solvent | T (ºC) | Time (h) | Yield (%) |
|---|---|---|---|---|---|
| [266] | TEAB (0.1 eq.), $K_2S_2O_8$ (0.1 eq.), PhSH (1.0 eq.) | DCE | 90 | 40 | 0 |
| [267] | DMP (6 eq.), $NaN_3$ (6.5 eq.), PhSH (1.0 eq.) | DCM | RT | 16 | 0 |
| [268] | $FeBr_2$ (0.05 eq.), *t*-BHP (0.5 eq.), PhSH (1.0 eq.), | $H_2O$ | 110 | 16 | 0 |
| [269] | DIAD (1.2 eq.), $Cs_2CO_3$ (1.0 eq.), PhSH (1.1 eq.) | DMF | RT | 16 | 0 |

However, none of the strategies yielded any product. In most cases, complex mixtures were observed by TLC and crude NMR. This could be due to the hydrogen located in the acetal ring – a radical generated at that position is relatively stable due to the

tertiary carbon position. This radical species could then react with other generated radicals, which leads to multiple compounds being formed. Attempting to convert **19** from an aldehyde into a carboxylic acid *via* Pinnick oxidation led to acetal deprotection due to acidic conditions needed during reaction work-up, and due to the adjacent carboxylic acid group. So, 2-carboxybenzaldehyde and its tautomer formed instead.

Whilst it was not possible to synthesise the desired *o*-substituted aldehyde-thioester **17**, the synthesis of *p*-substituted aldehyde-thioester **16** was possible, and this was pursued in Fab bioconjugation studies.

### 4.1.2. Bioconjugation studies

#### 4.1.2.1. Transthioesterification

Bioconjugation studies were conducted on reduced and non-reduced Fab for control and transthioesterification reactions respectively (**SCHEME 43**). Due to poor aqueous solubility, only 20 eq. of aldehyde-thioester **16** was used.

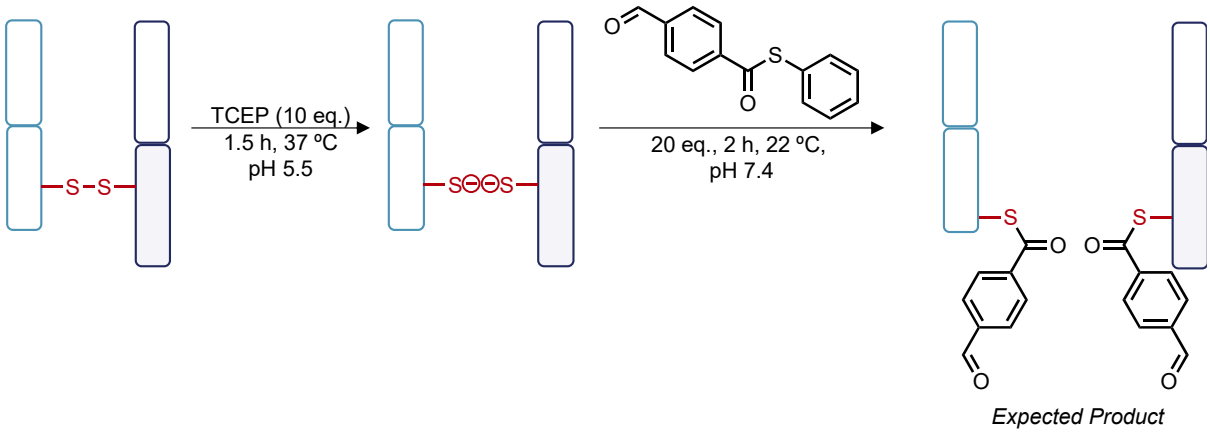


**SCHEME 43.** Bioconjugation conditions of aldehyde-thioester **16** on reduced Fab. The conditions shown are the final optimised conditions utilised for the reagent.

Promisingly, the control study showed minimal unselective lysine modification (**FIG. 103A**). It is possible that imines form transiently on lysine residues, however this formation generally prefers lower pH conditions. The addition of the aldehyde-thioester **16** on reduced Fab underwent complete transthioesterification in 2 h, as a result of the improved thiophenol leaving group and the electron-withdrawing effect from the *p*-aldehyde (**FIG. 103B**)**.** With the transthioesterification conditions established, the next stage of the investigation concerned imine formation and subsequent reduction to form an amine-linked conjugate.

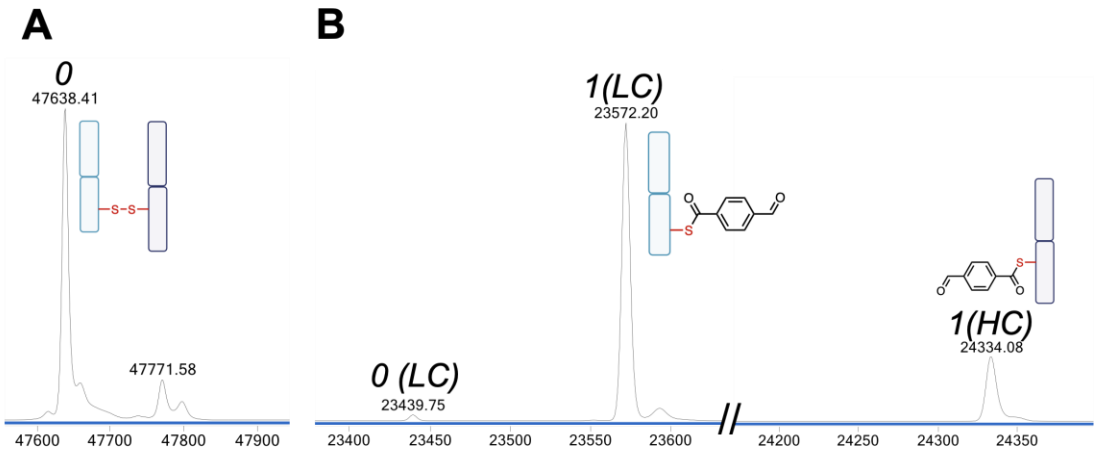


**FIGURE 103.** LCMS analysis of aldehyde-thioester **16** bioconjugation on Fab. **A)** Control on native Fab, 20 eq., 4 h, 22 ºC. **B)** Reaction on reduced Fab, 20 eq., 2 h, 22 ºC. Mass of native Fab = 47638 Da. Mass of native LC = 23439 Da. Mass of native HC = 24200 Da. Expected mass of addition = 133 Da.

### 4.1.2.2. Formation of amine-linked conjugate

To promote imine formation, the excess aldehyde-thioester **16** was removed from the reaction mixture, and the aldehyde-thioester Fab conjugate was buffer swapped to pH 5.0. Imine formation occurs more readily at lower pH, and pH 5.0 was seen as an ideal pH for imine formation and reduction, whilst preventing Fab denaturation. After incubation for 4 h at 22 ºC in pH 5.0, sodium cyanoborohydride (100 eq., 1 h 37 ºC, pH 5.0) was added. LCMS analysis suggests the loss of an oxygen, with peaks seen corresponding to the addition of a species with the mass 118 Da (**FIG. 104**). This indicates that imine formation was observed and successful reduction to the amine occurred, as no leftover aldehyde-thioester species was seen during LCMS analysis.

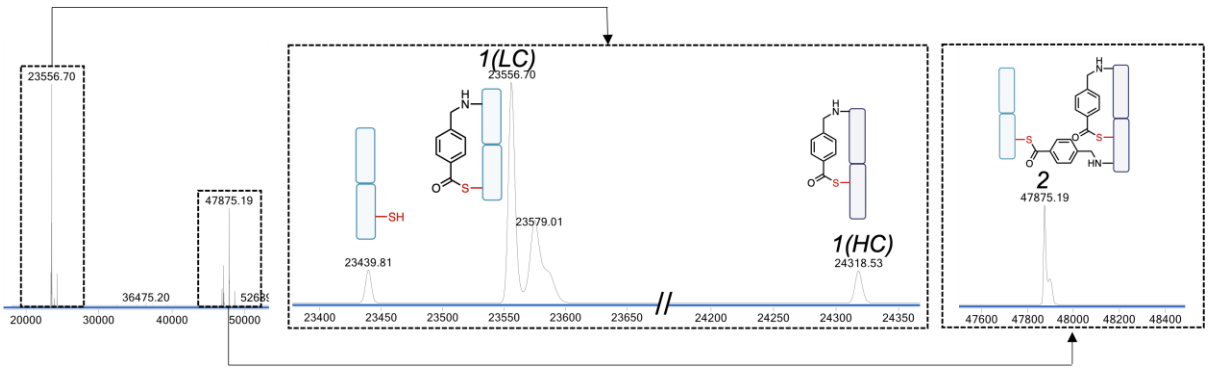


**FIGURE 104.** LCMS analysis of Fab conjugate resulting from the reduction of the thioester-aldehyde conjugate following imine formation. Mass of native Fab = 47638

Da. Mass of native LC = 23439 Da. Mass of native HC = 24200 Da. Expected mass of addition = 118 Da. Smaller unlabelled peaks correspond to sodium adducts (M+Na, +23 Da).

Due to differences in ionisation of differently sized protein conjugates, the cross-linked species may appear to be a minor product, but it is important to note that LCMS is not quantitative. To further confirm whether the observed conjugate was amine-linked, *O*-Me-cysteine was added (100 eq., 2 h, 22 ºC, pH 7.4) (**FIG. 105**). Amine conjugates are stable towards thiol addition, whilst thioesters undergo transthioesterification with cysteine – any imine conjugate would be removed due to loss of lysine proximity.

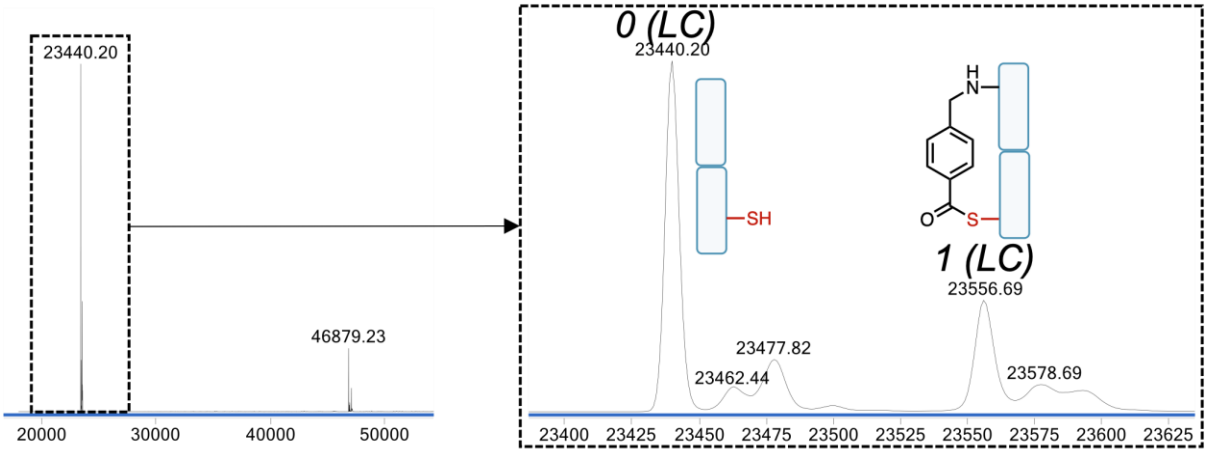


**FIGURE 105.** LCMS analysis of conjugate after the addition of *O*-Me-cysteine. Mass of native Fab = 47638 Da. Mass of native LC = 23439 Da. Mass of native HC = 24200 Da. Expected mass of addition = 118 Da. 46879 Da species corresponds to LC-LC and is a deconvolution artefact.

The results are somewhat inconclusive as the HC conjugate cannot be seen in the LCMS analysis. Smaller proteins ionise more effectively on LCMS, and dominate the signal, meaning only the native LC and LC conjugate can be observed here. The proximal HC lysine residues are expected to be more reactive from the understanding gained during CLT studies, thus it is expected that the amine conjugate forms on the HC preferentially. It would be expected for the added cysteine to displace the thioester from the cysteine thiol of Fab and undergo NCL to form an amide conjugate with an expected addition of 267 Da (**SCHEME 44**). The freed thiol may also form a disulfide bond with the HC cysteine thiol, preventing re-oxidation to the native disulfide bond. It is also possible that thioester hydrolysis occurs. Thus, there may be several species

on the HC, all corresponding to an amine-linked product. Due to multiple modified HC conjugates, their ionisation is poor, and the peak intensity is further diluted, making them even more difficult to detect *via* LCMS. There is also more native LC, resulting from the loss of the cross-linked conjugate as the thioester-modified cysteine on the LC will undergo transthioesterification and subsequent NCL. The leftover modified LC likely corresponds to minimal unselective modification on the LC lysine residues.

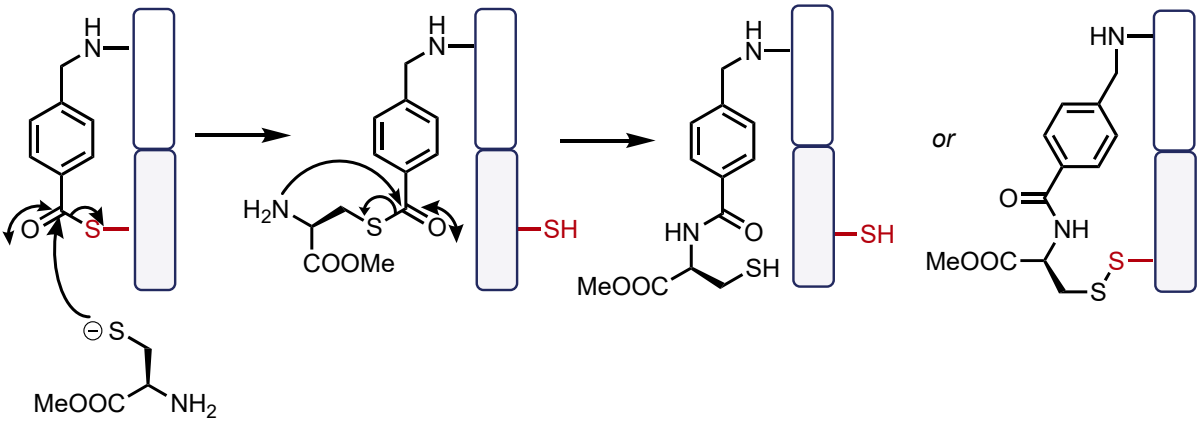


**SCHEME 44.** *O*-Me-cysteine transthioesterification and NCL on the modified HC amine-linked species.

To more accurately identify the structure of the resultant conjugates, it is necessary to properly investigate and identify the HC species – this could be achieved by the addition of Ellman's reagent to re-oxidise the cysteine thiols and reform the native disulfide bond. The species observable by LCMS would be a Fab conjugate, and it would be possible to determine the number of successful amine linkages formed to understand the success of the aldehyde-thioester strategy more thoroughly.

### 4.2. Summary and outlook of dual-reactive thioesters

This work provides insights into the potential of a thioester-aldehyde as a new strategy of modifying lysine residues in a controlled manner. Aldehydes are not hydrolytically susceptible, and this could be key in maximising lysine modification. In the designed aldehyde-thioester, the thiophenol leaving group and mesomeric electron-withdrawing effect from the *p*-aldehyde enable 2 h transthioesterification. Imine formation conditions and subsequent sodium borohydride reduction suggest a 5 h total reaction time is required for full conversion to the amine-linked conjugate. However, current LCMS analysis is inconclusive, due to the poor ionisation properties of the HC conjugates, making them difficult to observe. Nonetheless, these early studies suggest

utilising thioester selectivity for cysteine residues and inserting a secondary reactive group could prove to be an advantageous method for site-selective and controlled modification of lysine residues, which may serve to provide an alternative method to affinity-guided techniques which require the costly synthesis, design, and optimisation of affinity peptides.

### 4.3. Further work on dual-reactive thioesters

It is worth investigating aldehyde reagents that demonstrate better reactivity for protein modification. Iminoboronates have been shown to demonstrate stable imine formation at rates more suitable for chemical biology applications.[270] Synthesising an aldehyde with a substituted boronic acid could enable improved and stable imine formation, which could help ensure complete modification of the lysine residues. These iminoboronates also could demonstrate suitable stability as Fab modification reagents themselves. Other intriguing strategies include the phospha-Mannich reactions with alkylphosphites.[185] These involve the addition of functionalised alkylphosphite nucleophiles to the intermediate, reversible imine, which then forms stable and irreversible aminophosphite conjugates. Whilst these strategies are useful for non-specific lysine modification, combining their chemical properties with the cysteine selectivity of thioesters could offer a way of achieving more controlled and site-selective lysine modification on antibody fragments.

Additionally, other reactive functional groups could be combined with thioesters. One intriguing example is a disulfide-thioester. It is extremely challenging to synthesise disulfide-thioesters due to the competition between the disulfide and the activated carboxylic acid for the added thiol. It is also necessary to ensure the thioester moiety reacts before the disulfide, otherwise the reduced Fab disulfide bridge would simply re-oxidise. However, a disulfide-thioester could prove very interesting – through CLT, it may be possible to introduce a free thiol, which could serve as a further functionalisation site by the addition of thiol-selective and reactive reagents such as maleimides or thioesters (**SCHEME 45**). This would provide a small molecule-based alternative to antibody engineering for the insertion of reactive nucleophilic groups.

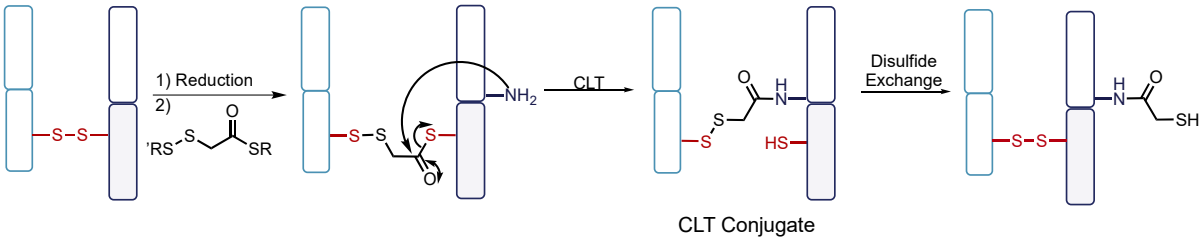


**SCHEME 45.** Potential conjugation strategy of a disulfide-thioester.

A diazotransfer-thioester could also be of interest (**SCHEME 46**). Work in literature has shown the success of this method for the conversion of primary amines to azides in various proteins, relying on a proximity-induced modification of specific lysine residues.[271] The thioesters could provide a very good platform for the diazotisation of the proximal lysine residues on Fab, due to their high levels of selectivity for the cysteine residues. The insertion of azides would enable further functionalisation through CuAAC or SPAAC. This could provide a way of modifying proximal lysine residues in a site-selective manner without succumbing to the hydrolytic instability of conventional thioesters at elevated pH. However, this strategy is not traceless, unlike CLT, leaving behind the deactivated diazotransfer-thioester which would need to be removed to reform the disulfide bond, increasing experimental complexity and time.

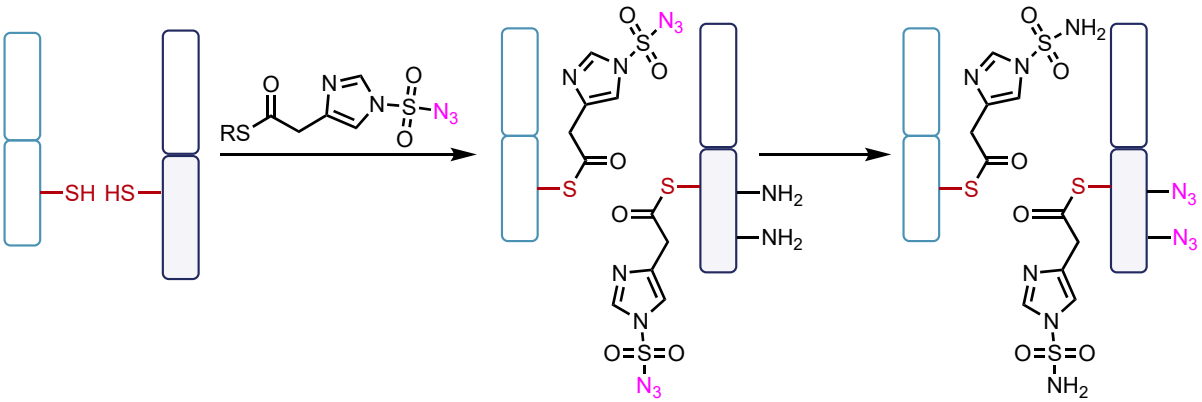

**SCHEME 46.** Potential conjugation strategy for a diazotransfer-thioester.

Thus, there is much scope for the development of dual-reactive thioesters, and it may be possible to improve upon existing proximity-driven modification reagents by the introduction of cysteine-selective thioesters into their designs.

# 5. Conclusion

The CLT protocol has enabled a strategy towards the synthesis of more homogeneous and site-selectively modified antibody conjugates. This thesis has sought to investigate chemistry compatible with CLT and probe the limits of chemical reactivity and reagent designs that are suitable for the modification of antibody fragments.

The work here on electron-deficient thioesters has demonstrated their suitability as faster CLT thioester reagents. The introduction of electron-withdrawing groups near the thioester carbonyl resulted in faster reactions at pH 6.0. The pyrimidine thioester demonstrated the best performance as a CLT reagent, with DARs of 1.2 achievable within 6.5 h of total reaction time. However, competing hydrolysis is elevated in these more reactive reagents, leading to lower DARs than alkyl thioesters. Investigations on tetrazine thioesters have also helped understand the limit of electron-deficiency – introducing very electron-poor rings significantly reduces the aqueous stability of compounds, and they become incompatible with the timescales needed for CLT. Nonetheless, work here has shown that the tetrazine thioester can enable rapid NCL and subsequent iEDDA on small molecule cysteine, achieving modification within minutes, and such reagents may be more suitable for *N*-terminal cysteine modification.

Other studies here have investigated alternative carbonyls with thiol leaving groups for Fab modification, including thiocarbonates, thiocarbamates, dithiocarbonates, and carbonimidodithioates. These reagents show limited success as CLT reagents themselves, as it is difficult to achieve a balance between controlled cysteine selectivity whilst preventing promiscuous reactivity with other amino acid residues – the thioesters have proved superior in that regard. Nonetheless, the carbonimidodithioates are promising, demonstrating clean and stable re-bridging of Fab whilst offering a site of functionalisation. There is still much scope for optimisation of these compounds, and they may prove to be valuable chemical biology reagents.

Finally, this work has explored the initial potential of dual-reactive thioesters. An aldehyde-thioester enables the formation of amine conjugates within reasonable timeframes, though there is still work to be done in optimising characterisation. This work has also shown the versatility of thioesters as a result of their cysteine selectivity, as they enable proximity-directed modifications through simple reagent designs.

# 6. Experimental

## 6.1. Synthesis General Remarks

All commercially available materials were purchased from Merck, Fluorochem, or ThermoFischer and used without any further purification. All organic syntheses were carried out at atmospheric pressure, under argon. Room temperature (RT) is defined as 20-22 ºC. The *in vacuo* concentration of solvents occurred at 40 ºC. Thin layer chromatography was used to monitor reaction progress, using Merck KGaA silica gel 60 $F_{254}$ TLC plates, which were visualised with a UVLS-26 EL series UV lamp at 254 nm or 365 nm. Potassium permanganate, bromocresol green, ninhydrin, and iodine were used as stains where appropriate. Flash chromatography was carried out using a Biotage Isolera One 3.0, using Gracesolv normal phase columns. Dry loading occurred by adsorbing the crude material onto Geduran SI 60 silica gel (40-63 µM).

$^{1}$H NMR and $^{13}$C NMR analysis was conducted on a Bruker Avance Neo 700 with a 5 mm helium-cooled broadband cryoprobe or a Bruker Avance III 600 equipped with a DCH cryoprobe. $^{1}$H NMR experiments were carried out at 700 MHz or 600 MHz. $^{13}$C NMR experiments were carried out at 176 MHz or 151 MHz. All NMR experiments were conducted at room temperature, unless defined otherwise. All NMR analysis was carried out in the deuterated solvent system mentioned. Chemical shifts are reported in parts per million (ppm) and coupling constants (*J*) in hertz (Hz). Multiplicity of signals are defined as follows: singlet (s), doublet (d), triplet (t), quartet (q), pentet (p), hextet (h), multiplet (m), or a combination of these. COSY, HMBC, and HSQC were used to assist in assignment. Infrared spectra were collected on a Bruker ALPHA FTIR spectrometer with frequencies reported in reciprocal centimetres ($cm^{-1}$). Melting points on solid compounds were collected on Gallenkemp digital melting point apparatus 5A 6797 and are uncorrected. High-resolution mass spectra of small molecules were acquired with electrospray ionisation (ES/ES+/ES-) modes and were collected at the Department of Chemistry, University College London at one of the following instruments: Finnigan MAT 900 XP double focusing hybrid (EBqQ) mass spectrometer, Thermo Scientific Orbitrap Q Exactive Plus mass spectrometer, Thermo Scientific TRACE 1310 GC-LCMS connected to Thermo Scientific ISQ single quadrupole mass spectrometer, or Waters LCT Premier XE QTOF mass spectrometer. Small molecule studies were collected on a Waters Aquity UPLC

system, connected to a Waters Acquity Single Quadrapole Detector (SQD). 7.5 μL of sample was submitted into an Accucore Vanquish C18) column at 50 ºC with a flow rate of 0.3 mL/min. Gradient elution of mobile phase A (water with 0.1% formic acid) and mobile phase B (acetonitrile with 0.1% formic acid) was used as per Table S.1.

**TABLE S.1.** LCMS gradient for small molecule LCMS analysis on Waters Aquity UPLC.

| Time (min) | Mobile phase A (water + 0.1% formic acid) (%) | Mobile phase B (acetonitrile + 0.1% formic acid) (%) |
|---|---|---|
| 0.00 | 99 | 1 |
| 1.00 | 60 | 40 |
| 3.00 | 40 | 60 |
| 4.00 | 30 | 70 |
| 5.00 | 30 | 70 |
| 5.50 | 40 | 60 |
| 6.00 | 99 | 1 |

### 6.1.1. Synthesis and characterisation of compounds

**General procedure for the synthesis of electron-deficient thioesters**

Carboxylic acid (1 eq.) and EEDQ (2.2 eq) were dissolved in DMF (0.4M). The resultant solution was stirred at RT for 0.5 h. Sodium 2-mercaptoethanesulfonate (1 eq.) was added, and the reaction mixture was stirred heated at 80 ºC for 16 h. The solution was cooled to RT and iodine (1 eq.) was added, the resultant solution was stirred at RT for 0.5 h. The solvent was removed *in vacuo* and the residue was purified by column chromatography (gradient elution from DCM to 20% MeOH in DCM) to afford the target thioesters.

**Sodium 2-(picolinoylthio)ethane-1-sulfonate (1)**

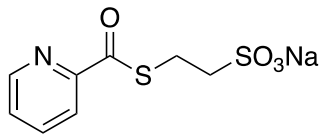

Orange solid (166 mg, 0.62 mmol, 31%); mp >250 ºC (decomposition); $^{1}$H NMR (700 MHz, DMSO-d$_6$) $\delta_H$ 8.70 (ddd, 1H, *J* = 4.7, 1.7, 0.9 Hz, Ar***H***). 8.03 (td, 1H, *J* = 7.7, 1.7 Hz, Ar***H***), 7.92 (dt, 1H, *J* = 7.8, 1.1 Hz, Ar***H***), 7.70 (ddd, 1H, *J* = 7.6, 4.7, 1.2 Hz, Ar***H***), 3.18 – 3.14 (m, 2H, C***H***$_2$SO$_3$), 2.67 – 2.64 (m, 2H, C***H***$_2$S); ); $^{13}$C NMR (176 MHz, DMSO-d$_6$) $\delta_C$ 194.4 (***C***=O), 152.8 (Ar***C***), 150.3 (Ar***C***), 138.9 (Ar***C***), 129.5 (Ar***C***), 121.4 (Ar***C***), 52.1 (***C***H$_2$S), 24.6 (S***C***H$_2$C); IR (solid) $\nu_{max}$ / cm$^{-1}$ 1674 (C=O), 1583 (COS), 1417 (C-C); HRMS (ES+) calcd for [C$_8$H$_{10}$NO$_4$S$_2$]$^+$ [M+H]$^+$ 248.0046, Observed: 248.0046.

**Sodium 2-((quinoline-2-carbonyl)thio)ethane-1-sulfonate (2)**

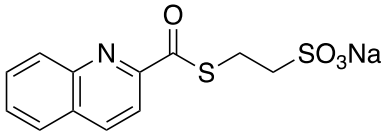

Orange solid (146 mg, 0.46 mmol, 46%); mp >250 ºC (decomposition); $^{1}$H NMR (700 MHz, MeOD) $\delta_H$ 8.46 (d, 1H, *J* = 8.5 Hz, Ar***H***), 8.17 (dd, 1H, *J* = 8.5, 1.1 Hz, Ar***H***), 8.04 (d, 1H, *J* = 8.5 Hz, Ar***H***), 8.00 (dt, 1H, *J* = 6.8, 0.7 Hz, Ar***H***), 7.85 (ddd, 1H, *J* = 8.4, 6.9, 1.5 Hz, Ar***H***), 7.71 (ddd, 1H, *J* = 8.1, 6.8, 1.2 Hz, Ar***H***), 3.43 – 3.41 (m, 2H, C***H***$_2$SO$_3$), 3.14 – 3.12 (m, 2H, C***H***$_2$S); $^{13}$C NMR (176 MHz, MeOD) $\delta_C$ 194.7 (***C***=O), 152.6 (Ar***C***), 148.2 (Ar***C***), 138.9 (Ar***C***), 131.6 (Ar***C***), 131.6 (Ar***C***), 130.9 (Ar***C***), 129.9 (Ar***C***), 129.0 (Ar***C***), 117.7 (Ar***C***), 52.1 (***C***H$_2$S), 24.7 (***C***H$_2$C); IR (solid) $\nu_{max}$ / cm$^{-1}$ 1647 (C=O), 1568 (COS), 1410 (C-C), HRMS (ES+) calcd for [C$_{12}$H$_{12}$NO$_4$S$_2$]$^+$ 298.0202, Observed: 298.0202.

**Sodium 2-((pyrimidine-2-carbonyl)thio)ethane-1-sulfonate (3)**

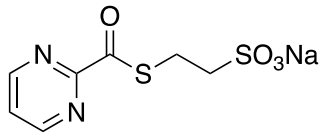

Yellow solid (146 mg, 0.54 mmol, 27%); mp >250 ºC (decomposition); $^{1}$H NMR (700 MHz, DMSO-d$_6$) $\delta_H$ 9.01 (d, 2H, *J* = 4.8 Hz, Ar***H***), 7.77 (t, 1H, *J* = 4.8 Hz, Ar***H***), 3.21 –

3.17 (m, 2H, C***H***$_2$SO$_3$), 2.69 – 2.66 (m, 2H, C***H***$_2$S); $^{13}$C NMR (176 MHz, DMSO-d$_6$) $\delta_C$ 190.7 (***C***=O), 158.2 (Ar***C***), 124.5 (Ar***C***), 50.5 (***C***H$_2$S), 24.8 (***C***H$_2$C); IR (solid) $\nu_{max}$ / cm$^{-1}$ 1676 (C=O), 1568 (COS), 1409 (C=C); HRMS (ES+) calcd for $[C_7H_9N_2O_4S_2]^+$ $[M+H]^+$ 248.9998, Observed: 248.9998.

**Ethyl thiooxamate**[233]

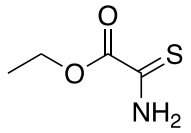


Ethyl oxamate (1.17 g, 10.0 mmol) and Lawesson's reagent (2.02 g, 5.00 mmol) were added to anhydrous THF (20 mL). The resultant yellow solution was stirred at reflux for 2 h. After completion, the solution was cooled to RT, concentrated *in vacuo*, and the yellow-orange residue was purified by column chromatography (gradient elution from cyclohexane to 30% EtOAc in cyclohexane) to give the light-yellow solid ethyl thiooxoamate (1.18 g, 8.88 mmol, 88%).

mp 61-64 ºC (lit: 62-66 ºC)[272]; $^1$H NMR (600 MHz, DMSO-d$_6$) $\delta_H$ 10.3 (s, 1H, N***H***), 10.0 (s, 1H, N***H***), 4.2 (q, 2H, *J* = 7.1 Hz, C***H$_2$***), 1.25 (t, 3H, *J* = 7.1 Hz, C***H$_3$***); $^{13}$C NMR (151 MHz, DMSO-d$_6$) $\delta_C$ 190.6 (***C***=S), 162.5 (***C***=O), 61.1 (***C***H$_2$), 13.8 (***C***H$_3$); IR (solid) $\nu_{max}$ / cm$^{-1}$ 1701 (C=O), 1101 (C=S), 1053 (C-O); HRMS (ES+) calcd for $[C_4H_7NO_2S]^+$ $[M+H]^+$ 134.0918, Observed: 134.0917.

**Ethyl oxalamidrazonate**[233]

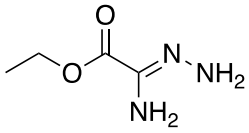


Ethyl thiooxamate (800 mg, 6.00 mmol) was dissolved in EtOH (10 mL) and stirred at RT for 5 min. 1M hydrazine in THF (6 mL, 6.00 mmol) was added dropwise over 0.5 h. The resultant orange solution was stirred at RT for 3 h. After completion, the solution was cooled to RT and the solvent was removed by *in vacuo* concentration. The resultant yellow-orange residue was purified by recrystallation from DCM:Et$_2$O (30 mL, 1:4) to give ethyl oxalamidrazonate as a yellow-orange solid (323 mg, 2.46 mmol, 41%.

mp 98-100 ºC (lit: 92-94 ºC)[273]; $^{1}$H NMR (600 MHz, DMSO-$d_6$) $\delta_H$ 5.36 (s, 2H, N***H₂***), 4.12 ppm (q, 2H, *J* = 7.0 Hz, C***H₂***), 1.21 (t, 3H, *J* = 6.0 Hz); $^{13}$C NMR (151 MHz, DMSO-$d_6$) $\delta_C$ 162.4 (***C***=O), 135.4 (***C***=N), 61.5 (***C***$H_2$), 14.3 (***C***$H_3$); IR (solid) $\nu_{max}$ / cm$^{-1}$ 1699 (C=O), 1670 (C=N), 1151 (C-O); HRMS (ES+) calcd for $[C_4H_9N_3O_2]^+$ 132.1350, Observed: 132.1350.

**Ethyl-1,2,4-triazine-3-carboxylate**[233]

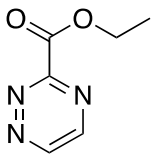

Ethyl oxalamidrazonate (262 mg, 2.00 mmol) was dissolved in THF (10 mL) and cooled to -78 ºC. AcOH (0.23 mL, 0.04 mmol) was added with 40% glyoxal in water (0.25 mL, 2.20 mmol) in THF (10 mL) and the orange solution was stirred at -78 ºC for 10 min. After 10 min, the solution was warmed to RT and stirred for 16 h. After completion, the solvent was removed *in vacuo* and the yellow-orange residue was purified by column chromatography (gradient elution from cyclohexane to 30% EtOAc in cyclohexane) to give the yellow solid ethyl-1,2,4-triazine-3-carboxylate (205 mg, 1.34 mmol, 67%).

mp 75-77 ºC (lit: 73-74 ºC)[274]; $^{1}$H NMR (600 MHz, DMSO-$d_6$) $\delta_H$ 9.62 (d, 1H, NC***H***), 9.04 (d, 1H, C***H***), 4.45 (q, 2H, *J* = 7.3 Hz, C***H₂***), 1.36 (t, 3H, *J* = 6.9 Hz); $^{13}$C NMR (151 MHz, DMSO-$d_6$) $\delta_C$ 162.2 (***C***=O), 156.8 (***C***COO), 151.6 (***C***H), 150.7 (***C***H), 62.4 (C***H₂***), 14.0 (***C***$H_3$); IR (solid) $\nu_{max}$ / cm$^{-1}$ 3002 (C-H), 2990 (C-H), 1789 (C=O), 1376 (N=N), 1201 (C-O); HRMS (ES+) calcd for $[C_6H_8N_3O_2]^+$ $[M+H]^+$ 154.0607, Observed: 154.0611.

**1,2,4-triazine-3-carboxylic acid (4)**[233]

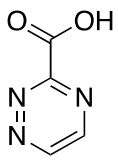

Ethyl-1,2,4-triazine-3-carboxylate (150 mg, 1.20 mmol) was dissolved in EtOH (2.5 mL). KOH (1.20 mmol) in EtOH (2.5 mL) was added at RT. The reaction mixture was

stirred for 0.5 h at RT. The solution was concentrated *in vacuo*, and 1M HCl (1.2 mL) was added to the resultant brown solid. After 10 min, the solution was extracted with EtOAc (3 x 10 mL) and dried with $Na_2SO_4$. The solution was filtered and concentrated *in vacuo* to yield the brown solid 1,2-4-triazine-3-carboxylic acid (108 mg, 0.86 mmol, 72%).

mp 81-82 ºC; $^1$H NMR (600 MHz, DMSO) $\delta_H$ 9.60 (s, 1H, NC***H***), 9.04 (s, 1H, C***H***); $^{13}$C NMR (151 MHz, DMSO) $\delta_C$ 163.8 (***C***=O), 157.6 (***C***COO), 151.4 (***C***H), 150.7 (***C***H); IR (solid) $\nu_{max}$ / cm$^{-1}$ 3026 (OH), 2993 (C-H), 1732 (C=O), 1319 (N=N), 1186 (C-O); HRMS (ES+) calcd for $[C_4H_6N_3O_3]^+$ $[M+H+H_2O]^+$ 144.0401, Observed: 144.0404.

**3-(methoxymethyl)-6-phenyl-1,2,4,5-tetrazine (6a)**

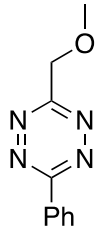


Methoxyacetonitrile (1.56 mL, 21.0 mmol), phenyl nitrile (0.721 mL, 7.0 mmol) and $Ni(OTf)_2$ (1.25 g, 3.5 mmol) added to 64% hydrazine hydrate (4.50 mL, 35 mmol). The purple-red solution was stirred at 60 ºC for 16 h. The resultant dark red solution was cooled to RT and diluted with $dH_2O$ (10 mL). The reaction mixture was poured into a solution of sodium nitrate (2.42 g, 35.0 mmol) in $dH_2O$ (10 mL) at 0 ºC. The mixture was acidified with 4M HCl (~30 mL) until the effervescence stopped. Extraction then occurred with EtOAc (5 x 30 mL) and DCM (1 x 30 mL). The organic layers were combined, dried ($MgSO_4$), and concentrated *in vacuo* to give a purple oil, which was purified by column chromatography (gradient elution from cyclohexane to 10% EtOAc in cyclohexane), affording 3-(methoxymethyl)-6-phenyl-1,2,4,5-tetrazine as a pink solid (497 mg, 2.45 mmol, 35%).

mp 57-59 ºC (lit: 59-60 ºC)[275]; $^1$H NMR (600 MHz, $CDCl_3$) $\delta_H$ 8.62 (d, 2H, *J* = 6.8 Hz, Ar***H***), 7.66 – 7.63 (m, 2H, Ar***H***), 7.62 – 7.59 (m, 3H, Ar***H***), 5.10 (s, 2H, C***H₂***), 3.64 (s, 3H, C***H₃***); $^{13}$C NMR (151 MHz, $CDCl_3$) $\delta_C$ 166.3 (Ar***C***), 165.2 (Ar***C***), 133.1 (Ar***C***), 131.7 (2 × Ar***C***), 129.5 (2 × Ar***C***), 128.5 (Ar***C***), 72.3 (***C***$H_2O$), 59.8 ($CH_3$); IR (solid) $\nu_{max}$ / cm-

[1] 3049 (C-H), 1421 (N=N), 1112 (C-O); HRMS (ES+) calcd for $[C_{10}H_{11}ON_4]^+$ $[M+H]^+$ 203.0929, Observed: 203.0927.

**(6-phenyl-1,2,4,5-tetrazin-3-yl)methanol (6b)**

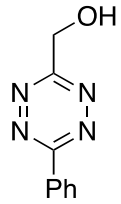


3-(methoxymethyl)-6-phenyl-1,2,4,5-tetrazine (310 mg, 1.50 mmol) was dissolved in DCM (10 mL) and cooled to -78 ºC. 1M $BBr_3$ in DCM (7.5 mL, 7.50 mmol) was added dropwise over 10 min at -78 ºC. The reaction was left to warm to RT over 16 h. The resultant orange solution was cooled to 0 ºC, and MeOH (20 mL) was added slowly followed by $dH_2O$ (20 mL). The purple-red solution was extracted with DCM (4 x 20 mL) and EtOAc (1 x 20 mL). The organic layers were combined and dried ($Na_2SO_4$). The solution was filtered, and the solvent was removed *in vacuo*. The resultant purple residue was purified by column chromatography (gradient elution from cyclohexane to 30% EtOAc in cyclohexane) to obtain (6-phenyl-1,2,4,5-tetrazin-3-yl)methanol as a red solid (271 mg, 1.44 mmol, 96%).

mp 104-105 ºC (lit: 92-95 ºC)[275]; $^1$H NMR (600 MHz, $CDCl_3$) $\delta_H$ 8.62 (d, 2H, *J* = 7.3 Hz, Ar***H***), 7.68 – 7.65 (m, 2H, Ar***H***), 7.63 – 7.60 (m, 3H, Ar***H***), 5.33 (s, 2H, C***H₂***), 3.06 (t, 1H, O***H***); $^{13}$C NMR (151 MHz, $CDCl_3$) $\delta_C$ 167.4 (Ar***C***), 165.6 (Ar***C***), 133.2 (Ar***C***), 131.6 (2 × Ar***C***), 129.5 (2 × Ar***C***), 128.4 (Ar***C***), 62.9 (***C***$H_2O$); IR (solid) $\nu_{max}$ / cm$^{-1}$ 3282 (O-H), 2931 (C-H), 1596 (C=O), 1346 (N=N), 1051 (C-O); HRMS (ES+) calcd for $[C_9H_9ON_4]^+$ $[M+H]^+$ 189.0771, Observed: 189.0768.

**6-phenyl-1,2,4,5-tetrazine-3-carboxylic acid (6c)**

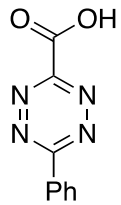

(6-phenyl-1,2,4,5-tetrazin-3-yl)methanol (150 mg, 0.80 mmol) and DMP (520 mg, 1.20 mmol) were dissolved in DCM (10 mL), and stirred at RT for 0.5 h. Flash column chromatography was used to isolate 6-phenyl-1,2,4,5-tetrazine-3-carbaldehyde (gradient elution from DCM to 30% EtOAc in DCM). To crude 6-phenyl-1,2,4,5-tetrazine-3-carbaldehyde (149 mg, 0.80 mmol) was added *t*-BuOH (6 mL) and 2-methyl-but-2-ene (1.0 mL). $NaClO_2$ (164 mg, 1.60 mmol) in 0.67M $NaH_2PO_4$ (1.40 mL) was added, and the reaction was stirred at 30 ºC for 2 h. 1M HCl (20 mL) was added, and the solution was extracted with EtOAc (3 x 20 mL) and dried ($Na_2SO_4$). The solution was filtered and concentrated *in vacuo* to obtain a crude red-pink solid. Column chromatography followed (gradient elution from DCM to 20% MeOH in DCM) to isolate 6-phenyl-1,2,4,5-tetrazine-3-carboxylic acid as a pink solid (113 mg, 0.56 mmol, 70%).

mp 202-203 ºC; $^{1}$H NMR (600 MHz, MeOD) $\delta_H$ 8.61 (d, 2H, *J* = 7.4 Hz, Ar***H***), 7.69 – 7.67 (m, 2H, Ar***H***), 7.64 – 7.63 (m, 3H, Ar***H***); $^{13}$C NMR (151 MHz, MeOH) $\delta_C$ 166.4 (***C***OOH), 162.2 (Ar***C***), 160.1 (Ar***C***), 134.2 (Ar***C***), 133.4 (2 × Ar***C***), 130.8 (2 × Ar***C***), 129.5 (Ar***C***); IR (solid) $\nu_{max}$ / cm$^{-1}$ 3344 (O-H), 3027 (C-H), 1651 (C=O), 1436 (C-O), 1281 (N=N); HRMS (ES+) calcd for [$C_9H_5O_2N_4$] 201.0418, Observed: 201.0412.

**_S_-phenyl 6-phenyl-1,2,4,5-tetrazine-3-carbothioate (7a)**

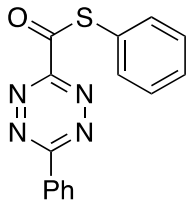


6-phenyl-1,2,4,5-tetrazine-3-carboxylic acid (20.0 mg, 0.10 mmol) was dissolved in DCM (2.5 mL). 2M oxalyl chloride in DCM (0.10 mL, 0.20 mmol) with DMF (10 µL) was added, and the mixture was stirred at RT for 0.5 h. The purple-red solution was concentrated *in vacuo* to obtain a purple-red residue. The residue was dissolved in DCM (2 mL), and NHS (23.0 mg, 0.20 mmol) in DCM (1 mL) with TEA (14 µL, 0.10 mmol) were added. The reaction was stirred at RT for 1 h. Thiophenol (9 µL, 0.10 mmol) in DMF (0.20 mL) was added, and the reaction was stirred for at RT for 1 h. The solution was concentrated *in vacuo*, and the residue was purified by column chromatography (gradient elution cyclohexane to 5% EtOAc in cyclohexane) to afford

*S*-phenyl 6-phenyl-1,2,4,5-tetrazine-3-carbothioate as a red solid (5.88 mg, 0.02 mmol, 20%).

mp >250 ºC; $^{1}$H NMR (600 MHz, $CDCl_3$) 8.74 (d, 2H, Ar***H***), 7.73 – 7.71 (m, 2H, Ar***H***), 7.66 – 7.64 (m, 3H, Ar***H***), 7.61 – 7.59 (m, 2H, Ar***H***), 7.53 – 7.52 (m, 3H, Ar***H***); $^{13}$C NMR (151 MHz, $CD_3CN$) $\delta_C$ 185.8 (***C***OS), 164.1 (Ar***C***), 159.9 (Ar***C***), 138.0 (Ar***C***), 137.3 (2 × Ar***C***), 134.9 (Ar***C***), 132.2 (2 × Ar***C***), 131.3 (2 × Ar***C***), 129.7 (2 × Ar***C***), 129.6 (Ar***C***), 129.3 (Ar***C***); IR (solid) $\nu_{max}$ / cm$^{-1}$ 2993 (C-H), 1732 (C=O), 1381 (COS), 1319 (N=N); HRLCMS (ES+) calcd for $[C_{15}H_{11}ON_3S]$ $[M+H]^+$ 294.0575, Observed: 294.0581.

**2-(4-((6-phenyl-1,2,4,5-tetrazine-3-carbonyl)thio)phenyl)acetic acid (7c)**

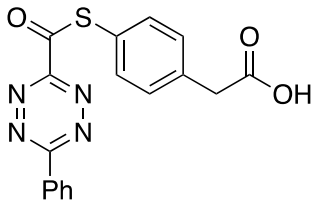


6-phenyl-1,2,4,5-tetrazine-3-carboxylic acid (20.0 mg, 0.10 mmol) was dissolved in DCM (2.5 mL). 2M oxalyl chloride in DCM (0.10 mL, 0.20 mmol) with DMF (10 µL) was added, and the mixture was stirred at RT for 0.5 h. The purple-red solution was concentrated *in vacuo* to obtain a purple-red residue. The residue was dissolved in DCM (2 mL), and NHS (23.0 mg, 0.20 mmol) in DCM (1 mL) and TEA (14 µL, 0.10 mmol) was added. The reaction was stirred at RT for 1 h. 4-mercaptophenyl acetic acid (16.8 mg, 0.10 mmol) in DMF (0.20 mL) was added, and the reaction was stirred for at RT for 1 h. The solution was concentrated *in vacuo*, and the residue was purified by column chromatography (gradient elution DCM to 100% EtOAc) to afford 2-(4-((6-phenyl-1,2,4,5-tetrazine-3-carbonyl)thio)phenyl)acetic acid as a pink solid (6.37 mg, 0.018 mmol, 18%).

mp >250 ºC; $^{1}$H NMR (600 MHz, $CD_3CN$) 8.67 (d, 2H, *J* = 6 Hz, Ar***H***), 7.80 – 7.77 (m, 2H, Ar***H***), 7.73 – 7.71 (m, 2H, Ar***H***), 7.58 (d, 2H, *J* = 7.8 Hz), 7.48 (d, 2H, *J* = 7.8 Hz); $^{13}$C NMR (151 MHz, $CD_3CN$) $\delta_C$ 187.6 (***C***OS), 172.7 (***C***OOH), 166.5 (Ar***C***), 160.0 (Ar***C***), 138.4 (Ar***C***), 136.0 (2 × Ar***C***), 135.0 (2 × Ar***C***), 132.3 (Ar***C***), 131.9 (2 × Ar***C***), 130.7 (2 × Ar***C***), 129.9 (Ar***C***), 125.5 (Ar***C***), 40.6 (***C***H$_2$); IR (solid) $\nu_{max}$ / cm$^{-1}$ 3100 (br, O-H), 3056 (C-H), 1568 (COS), 1456 (N=N); HRMS (ES+) calcd for $[C_{17}H_{13}O_3N_4S]^+$ [M+H]+ 353.0703, Observed: 353.0699.

**Prop-2-yn-1-yl (2,5-dioxopyrrolidin-1-yl) carbonate**

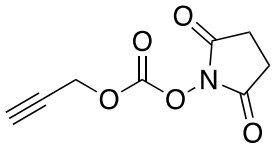

Disuccinimidyl carbonate (1.02 g, 4.00 mmol) and *N*-methylmorpholine (0.44 mL, 4.00 mmol) were dissolved in MeCN (25 mL). Propargyl alcohol (0.12 mL, 2.00 mmol) in MeCN (10 mL) was added dropwise over 4 h at RT. The light-yellow solution stirred over 16 h. The yellow solution was concentrated *in vacuo* and the white residue purified by column chromatography (gradient elution from hexane to 50 % EtOAc in hexane) to afford the target compound as a white solid (336 mg, 1.70 mmol, 85%).

mp 101-102 ºC (lit: 107 ºC)[276]; $^{1}$H NMR (600 MHz, $CDCl_3$) $\delta_H$ 4.89 (d, 2H, *J* = 2.5 Hz, OC***H***$_2$), 2.65 (t, 1H, *J* = 2.5, 0.6 Hz, ***H***C≡C), 2.17 (s, 4H, C***H***$_2$); $^{13}$C NMR (151 MHz, $CDCl_3$) $\delta_C$ 168.5 (O(***C***O)O), 151.4 (***C***=O), 77.9, ($H_2$***C***≡C), 58.3 (H***C***≡$CH_2$), 25.6 (***C***$H_2$); IR (solid) $\nu_{max}$ / cm$^{-1}$ 3260 (C-H), 1728 (C=O); HRMS (ES+) calcd for $[C_8H_8NO_5]^+$ $[M+H]^+$ 198.0397, Observed: 198.0397.

**General procedure for the synthesis of thiocarbonates**

Prop-2-yn-1-yl (2,5-dioxopyrrolidin-1-yl) carbonate (1 eq.) was dissolved in DMF (0.5M). Sodium 2-mercaptoethanesulfonate (1 eq.) in DMF (0.25M) was added, in addition to TEA (1 eq). The resultant colourless solution was stirred at RT for 4 h. The solution was concentrated *in vacuo*, and the residue purified by column chromatography (gradient elution from DCM to 10% MeOH in DCM), affording the target thiocarbonates.

**Sodium 2-(((prop-2-yn-1-yloxy)carbonyl)thio)ethane-1-sulfonate (9)**

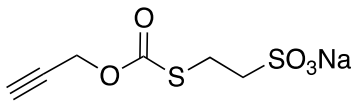

White solid (79.9 mg, 0.325 mmol, 65%); mp 170-171 ºC; $^{1}$H NMR (600 MHz, MeOD) $\delta_H$ 4.83 (d, 2H, *J* = 2.5 Hz, OC***H***$_2$), 3.26 – 3.23 (m, 2H, ***H***$_2$$CSO_3Na$), 3.13 – 3.09 (m, 2H, C***H***$_2$S), 3.01 (t, 1H, *J* = 2.5 Hz, ***H***C≡C). $^{13}$C NMR (151 MHz, MeOD) $\delta_C$ 171.3 (***C***=O), 78.1 (***C***≡CH, 77.1 (H***C***≡$CH_2$), 55.3 (O***C***$H_2$), 52.5 (***C***$H_2SO_3Na$), 27.1 (***C***$H_2$S),

IR (solid) $\nu_{max}$ / $cm^{-1}$ 1708 3289 (C-H), (C=O), 1643 (COS); HRMS (ES+) calcd for $[C_6H_7O_5S_2Na]^+$ $[M+H]^+$ 246.2268, Observed: 246.2267.

**2-(4-(((prop-2-yn-1-yloxy)carbonyl)thio)phenyl)acetic acid (10)**

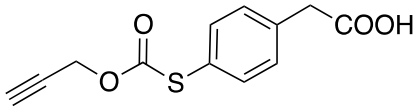


White solid (100 mg, 0.40 mmol, 80%); mp 132-133 ºC; $^1$H NMR (600 MHz, MeOD) $\delta_H$ 7.51 – 7.47 (m, 2H, Ar***H***), 7.40 – 7.34 (m, 2H Ar***H***), 4.82 (d, 2H, *J* = 2.5 Hz, OC***H***$_2$), 3.66 (s, 2H, C***H***$_2$COOH), 3.03 (t, 1H, *J* = 2.5 Hz, ***H***C≡C); $^{13}$C NMR (151 MHz, MeOD) $\delta_C$ 174.9 (***C***OOH), 170.4 (***C***OS), 138.3 (Ar***C***), 136.0 (2 × Ar***C***), 131.47 (2 × Ar***C***), 126.93 (Ar***C***), 77.98 (***C***≡CH), 77.34 (H***C***≡C), 55.66 (***C***H$_2$O), 41.53 ***C***H$_2$COOH); IR (solid) $\nu_{max}$ / $cm^{-1}$ 3287 (C-H), 2918 (COOH), 1701 (C=O), 1698 (COS); HRMS (ES+) calcd for $[C_{12}H_{11}O_4S]^+$ $[M+H]^+$ 251.0373, Observed: 251.0373.

**General procedure for synthesis of thiocarbamates**

Thiol (1.1 eq.) and TEA (1.1 eq.) was added to a solution of phenyl isocyanate (1 eq.) in DMC (0.4M). The reaction was stirred at RT for 4 h. The solvent was removed *in vacuo* and the residue was purified by column chromatography (gradient elution from cyclohexane to EtOAc in cyclohexane) to afford the target thiocarbamates.

**Methyl 2-((phenylcarbamoyl)thio)acetate (11)**

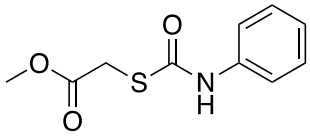


Yellow oil (366 mg. 1.62 mmol, 81%); $^1$H NMR (700 MHz, $CDCl_3$) $\delta_H$ 7.40 (d, 2H, *J* = 9.5 Hz, Ar***H***), 7.28 (t, 2H, *J* = 8.14 Hz, Ar***H***), 7.10 (t, 1H, *J* = 7.5 Hz), 3.78 (s, 2H, C***H***$_2$), 3.75 (s, 3H, C***H***$_3$); $^{13}$C NMR (171 MHz, $CDCl_3$) $\delta_C$ 170.3 (***C***OO), 164.3 (***C***OS), 129.7 (Ar***C***), 125.5 (2 × Ar***C***), 127.4 (Ar***C***), 124.8 (2 × Ar***C***), 53.2 (***C***H$_2$), 32.7 (***C***H$_3$); ); IR (oil) $\nu_{max}$ / $cm^{-1}$ 3039 (N-H), 1658 (C=O), 1597 (COS), 1212 (C-O); HRMS (ES+) calcd for $C_{10}H_{12}NO_3S]^+$ $[M+H]^+$ 226.532, Observed: 226.0531.

***S*-phenyl phenylcarbamothioate (12)**

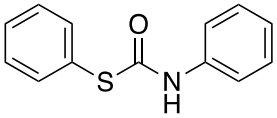

White solid (310 mg. 1.34 mmol, 67%); mp 113-115 ºC (lit: 110-112 ºC)[277]; $^{1}$H NMR (700 MHz, $CDCl_3$) $\delta_H$ 7.52 – 7.51 (m, 2H, Ar***H***), 7.48 – 7.7 (m, 2H, Ar***H***), 7.44 – 7.43 (m, 3H, Ar***H***), 7.30 (t, 2H, *J* = 7.3 Hz, Ar***H***), 7.06 (t, 1H, *J* = 6.7 Hz, Ar***H***); $^{13}$C NMR (171 MHz, $CDCl_3$) $\delta_C$ 162.9 (***C***OS), 138.9 (Ar***C***), 135.4 (Ar***C***), 129.2 (2 × Ar***C***), 129.1 (2 × Ar***C***), 129.0 (2 × Ar***C***), 128.8 (2 × Ar***C***), 123.6 (Ar***C***), 119.0 (Ar***C***); IR (oil) $\nu_{max}$ / cm$^{-1}$ 3307 (N-H), 1734 (C=O), 1597 (COS), 1145 (C-S); HRMS (ES+) calcd for $[C_{13}H_{12}NOS]^+$ $[M+H]^+$ 230.0634, Observed: 230.0630.

**General procedure for the synthesis of dithiocarbonates**

Disuccinimidyl carbonate (1 eq.) and *N*-methylmorpholine (1 eq. l) was dissolved in DCM (0.15M). Thiol (2.2 eq.) was added, and solution stirred at RT for 16 h. The solution was concentrated *in vacuo*, and EtOAc (20 mL) was added. The precipitate was filtered, and the light-yellow filtrate was concentrated *in vacuo*. The light-yellow residue was purified by column chromatography (gradient elution from hexane to EtOAc in hexane), affording the target dithiocarbonates.

**Diethyl 2,2'-(carbonylbis(sulfanediyl))diacetate (13)**

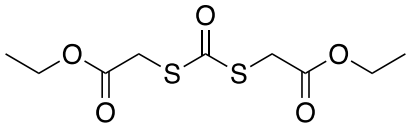

Colourless oil (125 mg, 0.468 mmol, 78 %); $^{1}$H NMR (700 MHz, $CDCl_3$) $\delta_H$ 4.18 (q, 4H, *J* = 7.3, C***H₂***), 3.86 (s, 4H, C***H₂***S), 1.26 (t, 6H, *J* = 7.1, C***H₃***); $^{13}$C NMR (176 MHz, $CD_3OD$) $\delta_C$ 188.8 (***C***OS), 170.0 (2 × ***C***OO), 63.3 (2 × ***C***$H_2O$), 33.3 (2 × ***C***$H_2S$), 14.6 (2 × ***C***$H_3$); IR (oil) $\nu_{max}$ / cm$^{-1}$ 1767 (C=O), 1724 (COS); HRMS (ES+) calcd for 266.3260, Observed: 266.3258.

***S*,*S*-diphenyl carbonodithioate (14)**

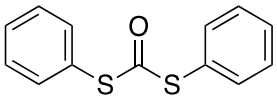

Colourless oil (126 mg, 0.510 mmol, 85 %); $^{1}$H NMR (700 MHz, $CD_3OD$) $\delta_H$ 7.51-7.41 (m, 10H, Ar***H***), $^{13}$C NMR (176 MHz, $CDCl_3$) $\delta_C$ 189.1 (***C***OS), 136.4 (2 × Ar***C***), 131.4 (Ar***C***), 130.6 (2 × Ar***C***), 128.4 (Ar***C***); IR (oil) $\nu_{max}$ / cm$^{-1}$ 3057 (C=C), 1724 (COS); HRMS (ES+) calcd for 247.0246, Observed: 247.0246.

**Dimethyl prop-2-yn-1-ylcarbonimidodithioate (15)**

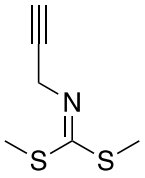


Carbon disulfide (60.0 µL, 1.00 mmol), propargylamine (63.0 µL, 1.00 mmol), and TEA (140 µL, 1.00 mmol) were added to DCM (5 mL) and stirred at RT for 0.5 h. Methyl iodide (75 µL, 1.20 mmol) was added, and the reaction mixture was stirred at reflux for 4 h. The mixture was cooled to RT, and methyl iodide (75 µL, 1.20 mmol) and TEA (140 µL, 1.00 mmol) were added again. The reaction was stirred until completion. After 2 h, the reaction was cooled to RT and dilute with DCM (10 mL). The solution was washed with d$H_2O$ (2 x 10 mL) and brine (10 mL) and then dried ($Na_2SO_4$). The mixture was filtered, and the solution was concentrated *in vacuo*. The yellow oil was purified by column chromatography (gradient elution from cyclohexane to 10% EtOAc in cyclohexane) to afford the brown-yellow oil dimethyl prop-2-yn-1-ylcarbonimidodithioate (97.0 mg, 0.61 mmol, 61%).

$^{1}$H NMR (700 MHz, $CDCl_3$) $\delta_H$ 4.24 (d, 2H, *J* = 2.6 Hz, C***H₂***), 2.57 (s, 3H, C***H₃***), 2.42 (s, 3H, C***H₃***), 2.27 (t, 1H, *J* = 2.6 Hz, C***H***); $^{13}$C NMR (176 MHz, $CDCl_3$) $\delta_C$ 152.2 (***C***=N), 81.4 (***C***$H_2$), 71.0 (***C***H), 15.1 (***C***$H_3$), 15.0 (***C***$H_3$); IR (oil) $\nu_{max}$ / cm$^{-1}$ 3288 (C≡C) 1670 (C=N), 674 (C-S), HRMS (ES+) calcd for $[C_6H_{10}NS_2]^+$ $[M+H]^+$ 160.0910, Observed: 160.0910.

***S*-phenyl 4-formylbenzothioate (16)**

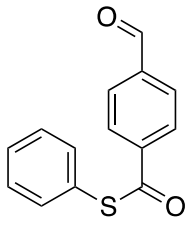

4-formylbenzoic acid (0.300 g, 2.00 mmol) and EDC.HCl (422 mg, 2.20 mmol) were dissolved in DCM (10 mL). The mixture was stirred at RT for 0.5. Thiophenol (0.26 mL, 2.20 mmol) was added, and the reaction was stirred until completion. After 16 h, the reaction was extracted with EtOAc (3 x 15 mL), washed with $dH_2O$ (3 x 15 mL), and brine (1 x 15 mL). The organic layers were combined and dried ($MgSO_4$), filtered, and concentrated *in vacuo*. The resultant white residue was purified by column chromatography (gradient elution from cyclohexane to 3% EtOAc in cyclohexane) to afford the white solid *S*-phenyl 4-formylbenzothioate (431 mg, 1.78 mmol, 89%).

mp 115-116 ºC; $^1$H NMR (700 MHz, $CDCl_3$) $\delta_H$ 10.1 (s, 1H, C***H***O), 8.18 (d, 2H, *J* = 7 Hz, Ar***H***), 8.00 (d, 2H, *J* = 6.7 Hz, Ar***H***), 7.53 – 7.52 (m, 2H, Ar***H***), 7.49 – 7.48 (m, 3H, Ar***H***); $^{13}$C NMR (176 MHz, $CDCl_3$) $\delta_C$ 191.7 (***C***HO), 189.7 (***C***OS), 141.2 (Ar***C***), 139.6 (Ar***C***), 135.1 (2 × Ar***C***), 130.1 (2 × Ar***C***), 130.0 (2 × Ar***C***), 129.6 (2 × Ar***C***), 128.6 (Ar***C***), 126.8 (Ar***C***); IR (solid) $\nu_{max}$ / cm$^{-1}$ 3319 (C-H), 2740 (C-H), 1691 (C=O), 1664 (C=O), 1193 (COS); HRMS (ES+) calcd for [$C_{14}H_{11}O_2S$] [M+H]+ 243.0474, Observed: 243.0474.

**2-(2-bromophenyl)-1,3-dioxolane (18)**[278]

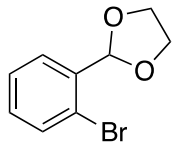


2-bromobenzaldehyde (0.584 mL, 5.00 mmol) was added to toluene (20 mL). Ethylene glycol (0.419 mL, 7.50 mmol) and *p*-TsOH.$H_2O$ (95.0 mg, 0.50 mmol) were added. The reaction mixture was heated to reflux under Dean-Stark apparatus for 16 h. The mixture was quenched with $dH_2O$ (20 mL) and extracted with EtOAc (3 x 30 mL). The organic layers were combined and dried ($Na_2SO_4$), and then concentrated *in vacuo*. The resultant oil was purified by column chromatography (gradient elution from cyclohexane to 5% EtOAc in cyclohexane) to afford 2-(2-bromophenyl)-1,3-dioxolane as a colourless oil (1.08 g, 4.75 mmol, 95%).

$^1$H NMR (700 MHz, $CDCl_3$) $\delta_H$ 7.63 (dd, 1H, *J* = 8.0 Hz, 1.0 Hz, Ar***H***), 7.57 (dd, 1H, *J* = 6.9 Hz, 2.0 Hz, Ar***H***), 7.43 – 7.41 (m, 1H), 7.33 (td, 1H, *J* = 6.1 Hz, 2.0 Hz, Ar***H***), 5.94 (s, 1H, C***H***), 4.09 – 3.97 (m, 4H, C***H₂***); $^{13}$C NMR (176 MHz, $CDCl_3$) $\delta_C$ 136.6 (Ar***C***), 132.9 (Ar***C***), 131.0 (Ar***C***), 128.3 (Ar***C***), 127.8 (Ar***C***), 122.3 (Ar***C***), 101.8 (***C***H), 65.1

(***C***$H_2$); IR (oil) $\nu_{max}$ / $cm^{-1}$ 2961 (C-H), 1254 (C-O), 1111 (C-H); HRLCMS (ES+) calcd for $[C_9H_9O_2Br]^+$ $[M+H]^+$ 228.9859, Observed: 228.9858.

**2-(1,3-dioxolan-2-yl)benzaldehyde (19)**[279]

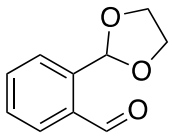

2-(2-bromophenyl)-1,3-dioxolane (1.15 g, 5.00 mmol) was dissolved in THF (30 mL) and cooled to -78 ºC. 2.5M *n*-BuLi in hexanes (3 mL, 7.50 mmol) was added dropwise over 5 min, and then stirred for a further 25 min. DMF (0.80 mL, 10.0 mmol) was then added dropwise at -78 ºC), and then the light-yellow mixture was warmed to 0 ºC. The reaction mixture was stirred at 0 ºC for 1 h, and then quenched with saturated $NH_4Cl$ (5 mL) and $dH_2O$ (5 mL). The mixture was extracted with EtOAc (4 x 20 mL), and the organic layers were combined and washed with brine (30 mL). The organic layer was dried ($Na_2SO_4$), filtered, and concentrated *in vacuo*. The residue was purified by column chromatography (gradient elution from cyclohexane to 10% EtOAc in cyclohexane) to afford 2-(1,3-dioxolan-2-yl)benzaldehyde as a colourless oil (753 mg, 4.20 mmol, 84%).

$^1$H NMR (700 MHz, $CDCl_3$) $\delta_H$ (s, 1H, C***H***O), 7.88 (d, 1H, *J* = 7.0 Hz, Ar***H***), 7.70 (d, 1H, *J* = 7.70 Hz, Ar***H***), 7.60 (p, 1H, *J* = 6.8 Hz, 4.0 Hz, Ar***H***), 6.36 (s, 1H, C***H***), 4.09 – 4.00 (m, 4H, C***H₂***); $^{13}$C NMR (176 MHz, $CDCl_3$) $\delta_C$ 192.2 (***C***HO), 139.3 (Ar***C***), 134.3 (Ar***C***), 133.8 (Ar***C***), 129.6 (Ar***C***), 128.7 (Ar***C***), 127.1 (Ar***C***), 100.7 (Ar***C***), 65.0 (Ar***C***); IR (oil) $\nu_{max}$ / $cm^{-1}$ 2949 (C-H), 2887 (C-H), 1691 (C=O), 1064 (C-O), 937 (C-H); HRMS (ES+) calcd for $[C_{10}H_{11}O_3]$+ [M+H]+ 179.0703, Observed: 179.0701.

**Tetrazine aqueous stability investigation**

To a solution of tetrazine thioester **7c** in MeCN (1 mM) was added the appropriate volume to buffers to create a 20% MeCN in buffer solution. The mixture was stirred for 10 min at RT, and then immediately analysed *via* LCMS. pH 5.0 = 100 mM ammonium acetate. pH 6.0 = 100 mM ammonium acetate. pH 7.0 = 100 mM ammonium bicarbonate. pH 8.0 = 100 mM ammonium acetate.

**Tetrazine thioester 7c *N*-terminal cysteine modification**

To a solution of tetrazine thioester 7c in ammonium acetate, pH 5.0 (1 mM) was added *O*-Me-cysteine.HCl in 50 mM ammonium acetate, pH 5.0 (1 mM, 1 eq.). The reaction mixture was shaken for 5 min at RT. BCN-amine in ammonium acetate, pH 5.0 (1 mM, 1.5 eq.) was added, and the reaction mixture was shaken for a further 5 min at RT. *N*-methylmaleimide in MeCN (1 mM, 1 eq.) was added, and the reaction mixture was shaken for 10 min at RT. The reaction mixture was directly analysed by Waters LCMS in ES+ mode.

## 6.2. Bioconjugation General Remarks

General reagents and solvents were purchased from commercial sources and used as supplied. All bioconjugation reactions were conducted in Eppendorf safe-lock tubes (1.5 mL or 2.0 mL) at atmospheric pressure, stated time and temperature. All experiments were carried out on Eppendorf Thermomixer at specified rpm. Centrifugation was carried out with a 5410 R centrifuge at manufacturer recommended rpm. Protein concentrations were determined using a NanoDrop 2000C in A280 mode, using molar extinction coefficients, $\varepsilon$, as follows: 68590 $M^{-1}cm^{-1}$ (trastuzumab Fab) or 215380 $M^{-1}cm^{-1}$ (trastuzumab).[280]

Working stocks of compounds were prepared in ultrapure, dry DMF stored at -20 ºC. TCEP.HCl was obtained from VWR and stored at 4 ºC. Buffer exchanges and the removal of excess small molecules was facilitated by using Sartorius VivaSpin 500 with a molecular weight cut-off of 10 kDa and used as per manufacturer's instructions (multiple washes with 5 x volume of solution into desired solvent). Following VivaSpin, the concentration of the Fab conjugate is re-calculated before the addition of small molecule compounds. All buffers were prepared with LCMS grade water and filter-sterilised before use. Conjugation buffer was made with 40 mM phosphates, 20 mM NaCl, 6 mM EDTA at pH 7.4 (unless specified, within pH 6.0-pH 7.4 range). BBS buffer was made with 80 mM boric acid, 20 mM NaCl at pH 8.0-8.4 (specified per experiment). Citrate phosphate buffer was made with 50 mM sodium phosphate dibasic, 50 mM citric acid, 6 mM EDTA at pH 5.0-6.0 (specified per experiment). Ammonium acetate buffer was 50 mM ammonium acetate at specified pH. For CLT, the same buffer recipes were followed, but without EDTA addition. The pH of buffers was adjusted using a Jenway 3510 pH meter.

For protein analysis, liquid chromatography mass spectrometry (LCMS) was performed at the Department of Chemistry, UCL, on an Agilent 1100/1200 LC system, with a 6510A QTOF mass spectrometer or a 6530A QTOF mass spectrometer. Samples for LCMS analysis were prepared in LCMS grade water using ZebaSpin (7 kDa) as per manufacturer's instructions. All Fab LCMS samples were prepared at 5 μM. For trastuzumab, LCMS samples were prepared at 6.5 μM, and the antibody was deglycosylated with 1 μL PNGase (NEB) for 16 h at 37 ºC prior to LCMS submission. Sodium adducts are commonly found as [M+23] in some of the obtained LCMS data.

2 µL of sample was injected through a 100 µL loop into the Agilent PLRPS 1000 Å column (150 mm x 2.1 mm, 8 µM particle size) at 60 ºC. Proteins were separated by gradient elution of mobile phase A (water with 0.1% formic acid) and mobile phase B (acetonitrile with 0.1% formic acid) as per the gradient(s) specified in Table S.2 (Agilent 6530) and Table S.3 (Agilent 6510). The flow rate was 0.8 mL/min (Agilent 6530) or 0.3 mL/min (Agilent 6510), and the 6530/6510 QTOF was prepared in positive mode. Other LCMS parameters include: VCap = 3500 V, gas temperature = 350 ºC, dry gas flow rate = 10 L/min, nebuliser = 30 psi, fragmentor = 380 V, skimmer = 65 V, acquisition rate = 0.5 spectra/s. Data was acquired with a LCMS scan within the *m/z* range 700-7000. Deconvolution of raw LCMS data to zero charge mass spectra was carried out using the maximum entropy deconvolution algorithm within the Agilent MassHunter software (v B.07.00). The number of compound additions is shown on the LCMS (0, 1, 2, 3... etc). For labelling of protein conjugates: LC refers to light chain, HC refers to heavy chain, HHLL refers to full antibody, and HL refers to half antibody. Deconvolution artefacts include species with masses corresponding to LC-LC (2xLC) or HC-HC (2xHC). Due to ionisation differences between smaller and larger proteins and subsequent ion detection, the HC cannot be observed in some of the obtained LCMS data.

**TABLE S.2.** LCMS gradient for protein LCMS analysis on Agilent 6530.

| Time (min) | Mobile phase A (water + 0.1% formic acid) (%) | Mobile phase B (acetonitrile + 0.1% formic acid) (%) |
|---|---|---|
| 0.00 | 80 | 20 |
| 1.00 | 80 | 20 |
| 6.50 | 40 | 60 |
| 7.50 | 40 | 60 |
| 7.60 | 80 | 20 |
| 8.50 | 80 | 20 |

**TABLE S.3.** LCMS gradient for protein LCMS analysis on Agilent 6510.

| Time (min) | Mobile phase A (water + 0.1% formic acid) (%) | Mobile phase B (acetonitrile + 0.1% formic acid) (%) |
|---|---|---|
| 0.0 | 85 | 15 |
| 2.0 | 85 | 15 |
| 3.0 | 68 | 32 |
| 4.0 | 68 | 32 |
| 14.0 | 65 | 35 |
| 18.0 | 5 | 95 |
| 20.0 | 5 | 95 |
| 22.0 | 85 | 15 |
| 25.0 | 85 | 15 |

For monitoring of re-bridging experiments, 12% SDS-PAGE with a 6% stacking gel was used. The components are shown in Table S.4. Samples were prepared with a 1:1 ratio of 3 µg of conjugate and 2 x SDS non-reducing loading dye (composition of 5 x loading dye: 1.6 mL of 10% (w/v) SDS, 8 mL glycerol, 4 mL distilled water, 1 mL 0.5 M Tris buffer pH 6.8, 25 mg bromophenol blue). Samples were heated at 80 ºC for 5 min before loading, loading 6 µL per lane. ThermoScientific Page Ruler Plus Pre-Stained Protein Ladder (4 µL) was used as a reference ladder for mass comparison. The gel was run at a constant voltage of 200 V for 60 min in 1X SDS running buffer (composition of 10X SDS running buffer: 30 g of Tris base, 144 g of glycine, 10 g of SDS in 1 L distilled water, adjusted to pH 8.3). Gels were stained using Coomassie blue stain (composition of stain: 10% ammonium sulfate (100 g), 0.1% Coomassie G-250 (500 mg), 3% phosphoric acid (30 mL), ethanol (200 mL), and distilled water (670 mL). Gels were destained with water and left shaking at 300 rpm overnight before analysis. Densitometry analysis of SDS-PAGE gels was conducted using the GelAnalyser V19.1 software.

**TABLE S.4.** Components of a 12% SDS-PAGE gel. Quantities presented can be used to prepare 4 gels.

| **Components** | **12% Separating** | **6% Stacking** |
|---|---|---|
| Distilled water | 8.0 mL | 5.3 mL |
| Acrylamide | 9.6 mL | 2.0 mL |
| 1.5M Tris pH 8.8 | 6.0 mL | / |
| 0.5M Tris pH 6.8 | / | 2.5 mL |
| 10% SDS | 240 µL | 100 µL |
| 10% APS | 240 µL | 100 µL |
| TEMED | 24 µL | 10 µL |

### 6.2.1. Bioconjugation and characterisation

**General procedure for the preparation of trastuzumab (Herceptin™) Fab fragment**[281]

Ontruzant (supplied by UCLH) (0.50 mL, 44.0 μM, 6.41 mg/mL) was buffer exchanged into NaOAc buffer (20 mM NaOAc, pH 3.1) *via* ultrafiltration (Amicon Ultra-4 Centrifugal Filter units with 10 kDa MWCO). Immobilized pepsin (0.15 mL) was also washed with NaOAc buffer (20 mM NaOAc, pH 3.1), using a Pierce™ centrifuge column. Trastuzumab (0.50 mL) was then added to the pepsin and the mixture was incubated at 37 ºC for 5 h, under constant agitation (1,100 rpm). The resin was then removed from the digest using a Pierce™ centrifuge column and washed with digest buffer (3 × 0.4 mL, 50 mM phosphate, 150 mM NaCl, 1 mM EDTA, pH 6.8). The digest was combined with the washes and the volume was adjusted to 0.5 mL, collected $F(ab')_2$. Next, immobilized papain (0.65 mL) was activated with 10 mM DTT in digest buffer (50 mM phosphate, 150 mM NaCl, 1 mM EDTA, pH 6.8). This was incubated at 37 ºC for 1.5 h under constant agitation (1,100 rpm). The resin was washed with digest buffer (4 × 0.4 mL, 50 mM phosphate, 150 mM NaCl, 1 mM EDTA, pH 6.8) without DTT, using a Pierce™ centrifuge column. $F(ab')_2$ (0.5 mL) was added to the washed papain and the mixture incubated at 37 ºC for 20 h under constant agitation (1,100 rpm). The resin was separated and washed with conjugation buffer (4 × 0.4 mL, 40 mM phosphate, 20 mM NaCl, 6 mM EDTA, pH 7.4). The digest was combined with the washes and the buffer was exchanged completely for conjugation buffer *via* ultrafiltration (10 kDa MWCO). The concentration was determined by UV/Vis absorbance and adjusted to 150 μM. Mass of native Fab = 47638 Da (or 47624), mass of native Fab LC = 23439, mass of Fab native HC = 24200.

**General Fab conjugation procedure with small molecules**

To Fab (20.0 μL, 0.0030 μmol, 150 μM, 7.15 mg/mL) in conjugation buffer, TCEP (0.20 μL, 0.030 μmol, 150 mM in $dH_2O$, 10 eq.) was added. After mixing for 1.5 h at 37 ºC, 300 rpm, the target reagents were added and incubated at the specified time and conditions. The excess reagent was removed *via* ultrafiltration (10 kDa MWCO). The sample was purified by ZebaSpin and submitted for LCMS analysis.

**General cysteine-to-lysine transfer procedure**

The thioester conjugate (prepared *via* General Fab conjugation procedure with small

molecules) is washed *via* ultrafiltration (10 kDa) into the specified buffer and pH. The concentration of the conjugate is calculated. The conjugate is diluted to 20 μM and incubated at the specified conditions. The sample was purified by ZebaSpin and submitted for LCMS analysis.

## Trastuzumab Fab

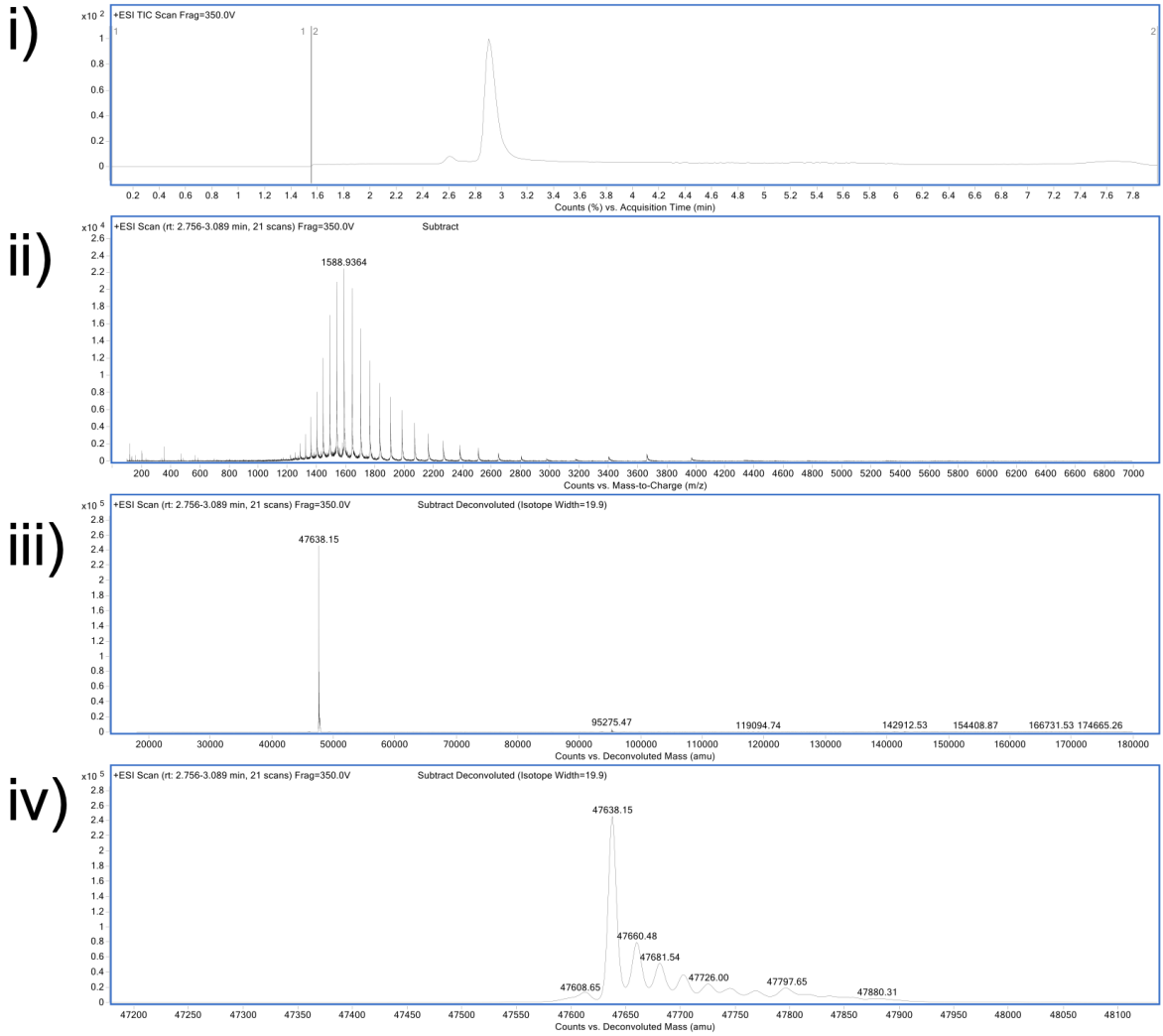


**FIGURE S.1.** LCMS of trastuzumab Fab. i) TIC. ii) non-deconvoluted ion series. iii) full range of deconvoluted ion series. iv) zoomed in of deconvoluted ion series. Expected mass of native Fab: 47638 Da. Observed mass: 47638 Da.

**Reduced Trastuzumab Fab**

To Fab (20.0 μL, 0.0030 μmol, 150 μM, 7.15 mg/mL) in conjugation buffer, TCEP (0.20 μL, 0.030 μmol, 150 mM in $dH_2O$, 10 eq.) was added. After mixing for 1.5 h at 37 ºC, 300 rpm. The excess reagent was removed *via* ultrafiltration (10 kDa MWCO), and the sample was submitted for LCMS analysis after ZebaSpin purification.

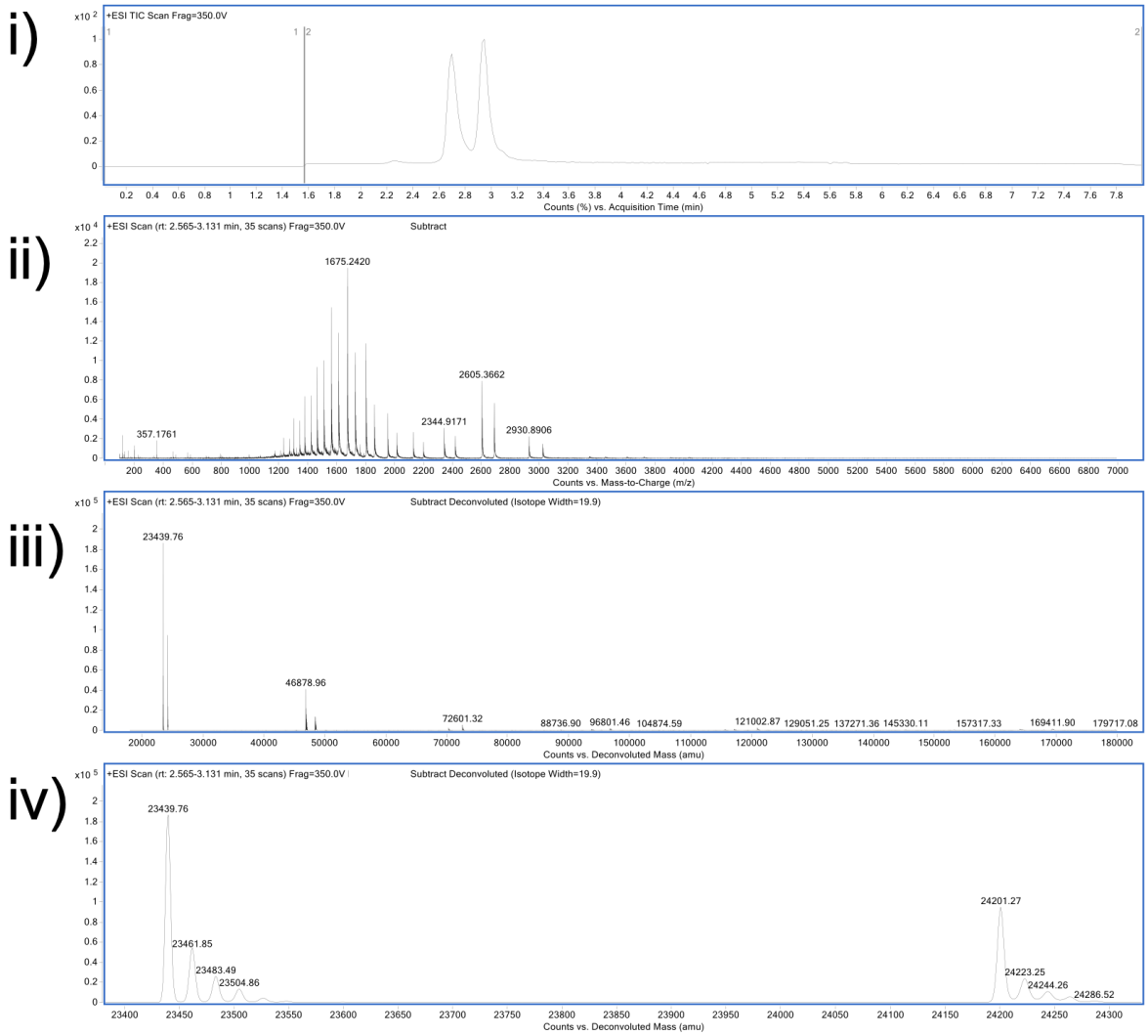


**FIGURE S.2.** LCMS of reduced trastuzumab Fab. i) TIC. ii) non-deconvoluted ion series. iii) full range of deconvoluted ion series. iv) zoomed in of deconvoluted ion series. Expected mass of native chains: LC 23439 Da, HC 24200 Da. Observed mass: LC 23439 Da, HC 24200 Da. Masses at 46878 Da and 48400 Da correspond to LC-LC and HC-HC respectively and result from deconvolution artefacts.

## Trastuzumab

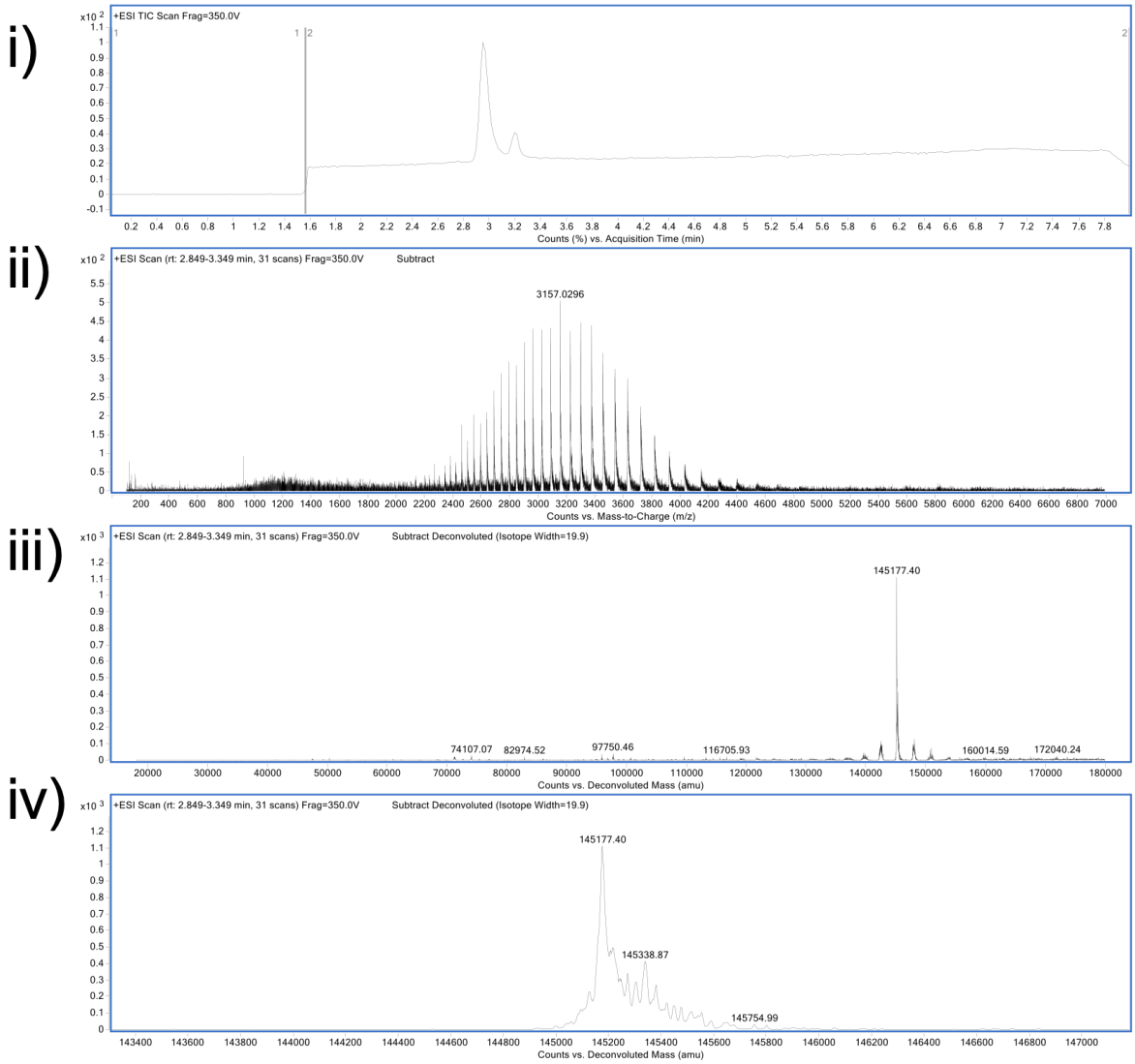


**FIGURE S.3.** LCMS of trastuzumab. i) TIC. ii) non-deconvoluted ion series. iii) full range of deconvoluted ion series. iv) zoomed in of deconvoluted ion series. Expected mass of native trastuzumab: 145177. Observed mass:145177 Da.

**Reduced Trastuzumab**

To trastuzumab (60.0 μL, 0.0013 μmol, 22 μM, 3.83 mg/mL) in conjugation buffer was added TCEP (0.88 μL, 0.013 μmol, 15.0 mM in $dH_2O$, 10 eq.). The excess reagent was removed *via* ultrafiltration (10 kDa MWCO) into ammonium acetate (pH 6.9) and purified by ZebaSpin for LCMS analysis. PNGase (1.0 μL) was added, and the sample was incubated for 16 h at 37 ºC prior to LCMS analysis.

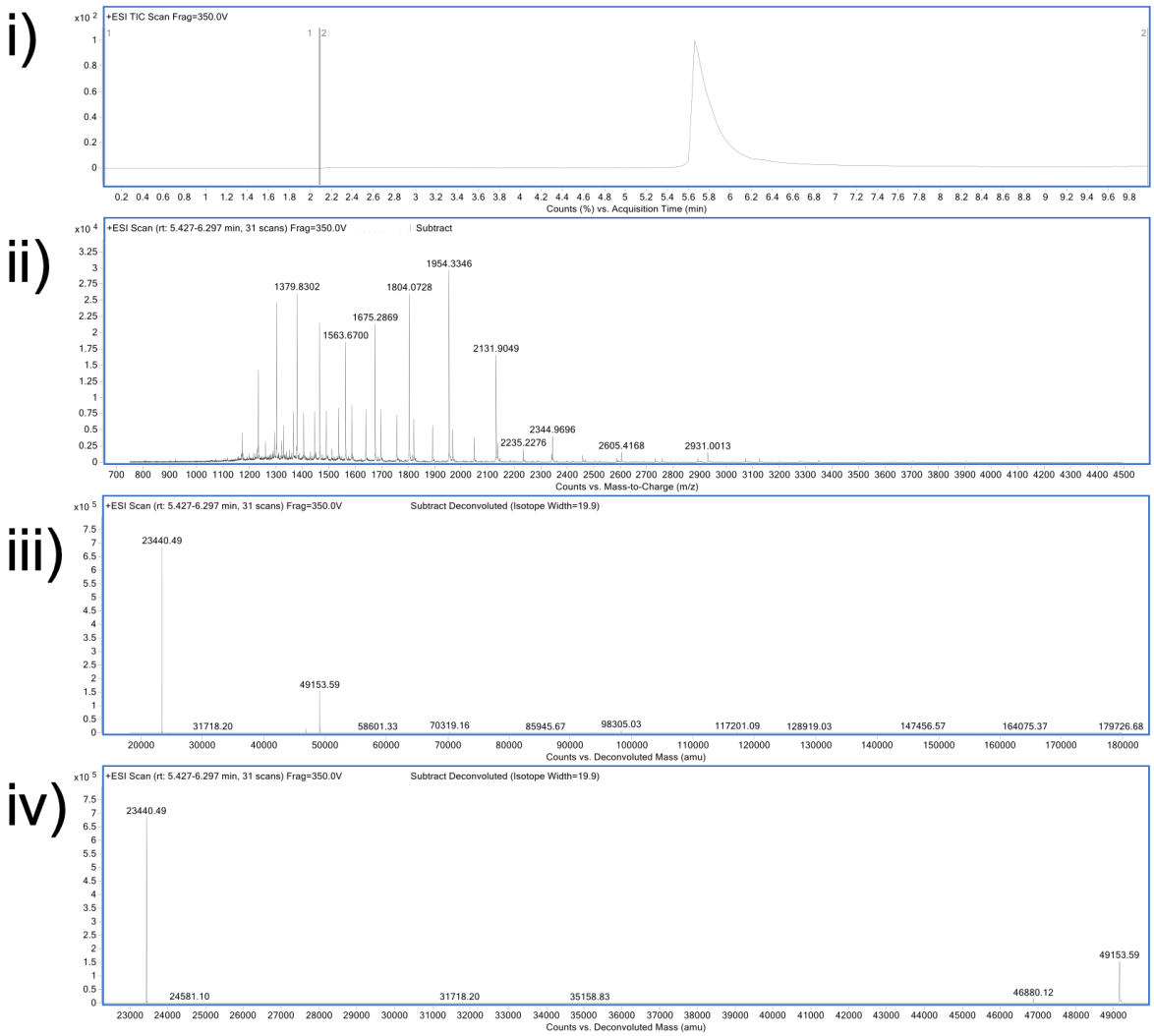


**FIGURE S.4.** LCMS of reduced trastuzumab. i) TIC. ii) non-deconvoluted ion series. iii) full range of deconvoluted ion series. iv) zoomed in of deconvoluted ion series. Expected mass of reduced trastuzumab: LC 23439 Da, HL 49153 Da. Observed mass: LC 23440 Da, HL 49153 Da.

**Pyridine thioester 1 conjugation on non-reduced Fab (control)**

To Fab (20.0 μL, 0.0030 μmol, 150 μM, 7.15 mg/mL) in conjugation buffer, pyridine thioester **1** (2.00 μL, 0.300 μmol, 150 mM in DMF, 100 eq.) was added. The sample was incubated for 4 h at 22 ºC, 300 rpm. The excess reagent was removed *via* ultrafiltration (10 kDa MWCO) into LCMS water, and the sample was purified by ZebaSpin for LCMS analysis.

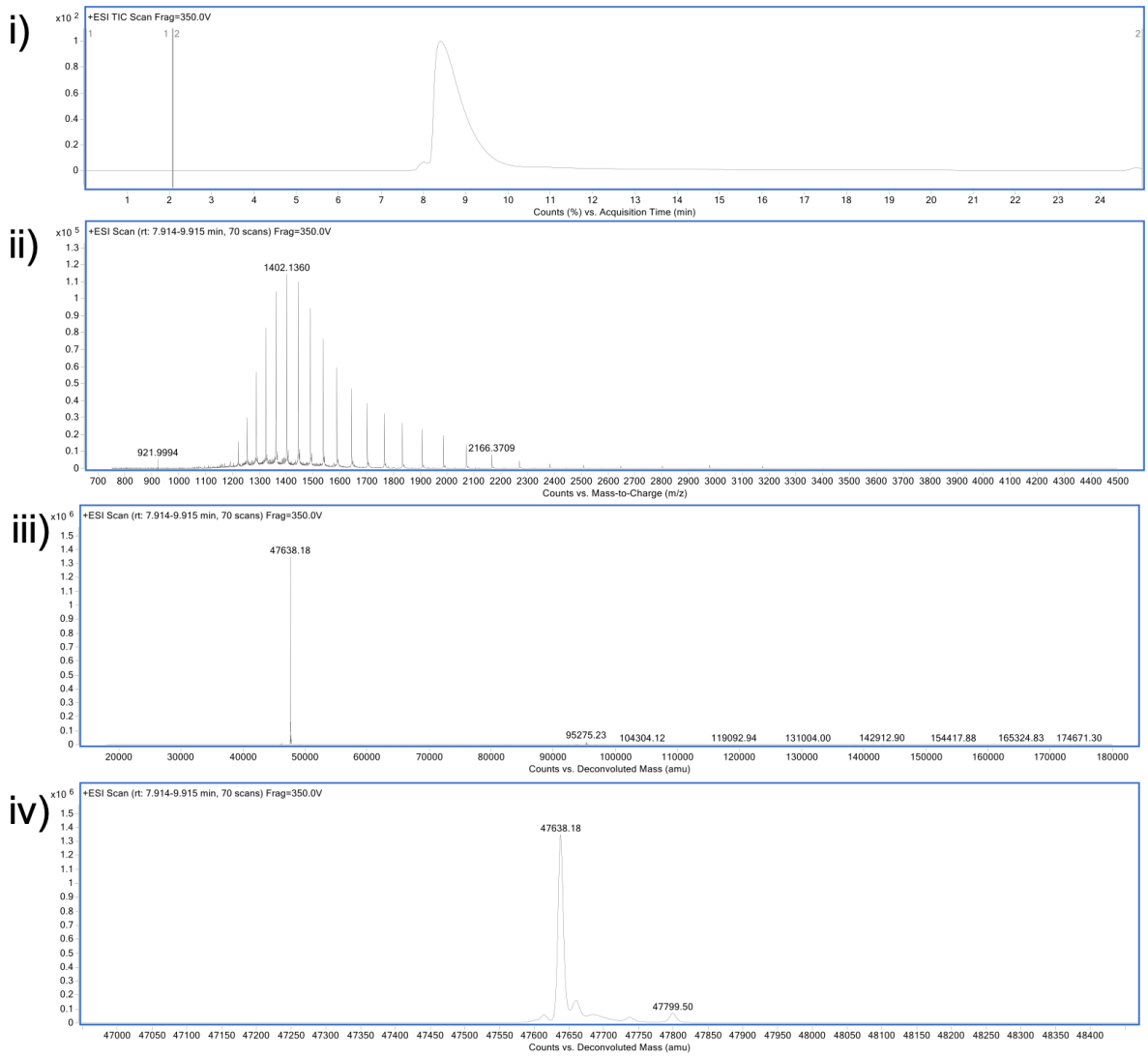


**FIGURE S.5.** LCMS analysis of pyridine thioester **1** control on native Fab. i) TIC. ii) non-convoluted ion series. iii) full range of deconvoluted ion series. iv) zoomed in of deconvoluted ion series. Expected mass of native Fab: 47638 Da. Observed: 47638 Da.

**Pyridine thioester 1 conjugation on reduced Fab (reaction)**

To Fab (20.0 μL, 0.0030 μmol, 150 μM, 7.15 mg/mL) in conjugation buffer, TCEP (0.20 μL, 0.030 μmol, 150 mM in $dH_2O$, 10 eq.) was added. After mixing for 1.5 h at 37 ºC, 300 rpm, pyridine thioester **1** (2.00 μL, 0.300 μmol, 150 mM in DMF, 100 eq.) was added and the reaction mixture was further incubated for 1 h at 37 ºC, 300 rpm. The excess reagent was removed *via* ultrafiltration (10 kDa MWCO) into LCMS water, and the sample was purified by ZebaSpin for LCMS analysis.

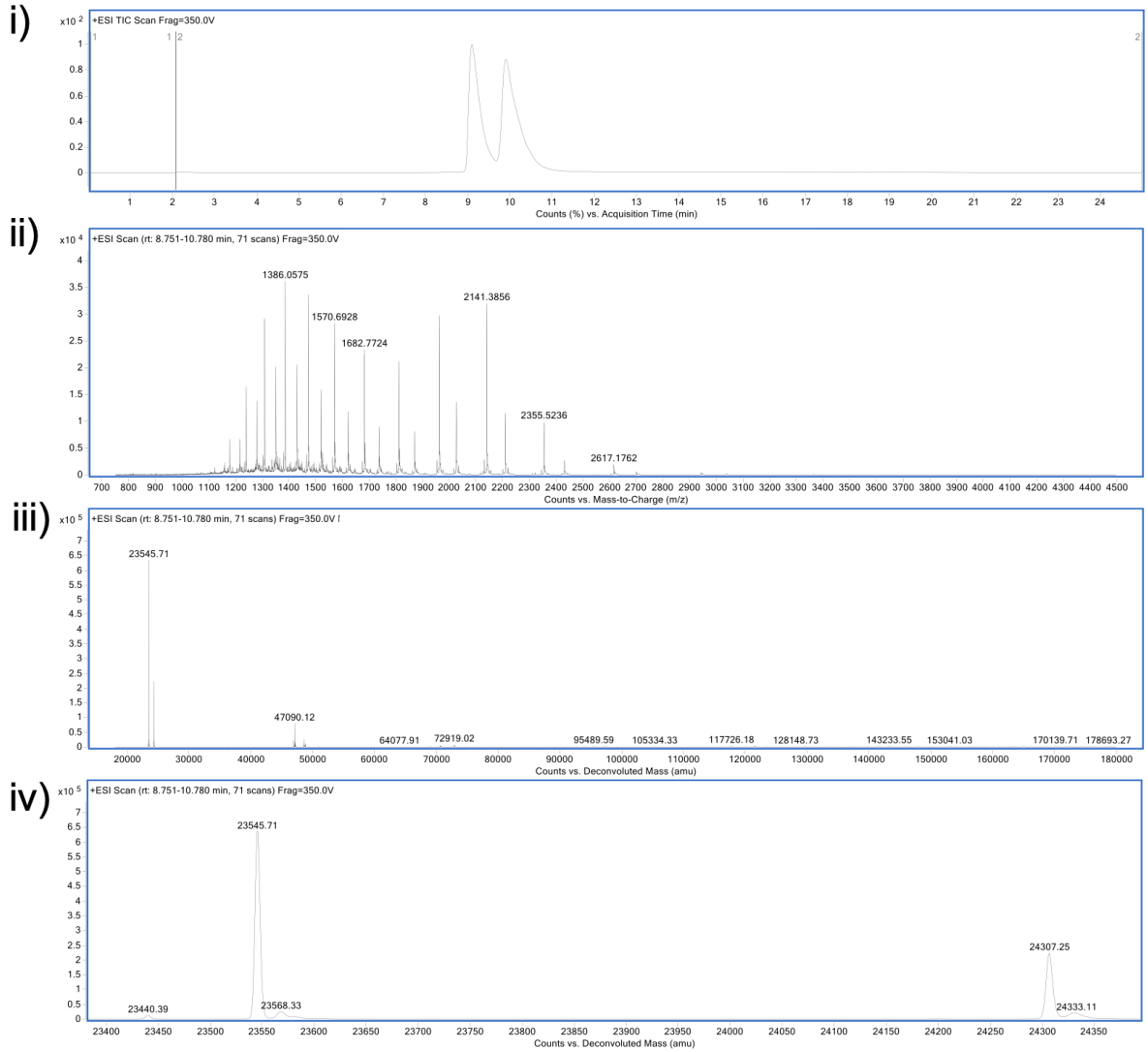


**FIGURE S.6.** LCMS analysis of pyridine thioester **1** reaction on reduced Fab. i) TIC. ii) non-convoluted ion series. iii) full range of deconvoluted ion series. iv) zoomed in of deconvoluted ion series. Expected mass of pyridine thioester conjugate: LC 23545 Da, HC 24306 Da. Observed: modified LC 23545 Da, modified HC 24307 Da. Mass of pyridine thioester **1** addition: 106 Da.

**Pyridine thioester 1 conjugation on reduced Fab (reaction), 24 h**

To Fab (20.0 μL, 0.0030 μmol, 150 μM, 7.15 mg/mL) in conjugation buffer, TCEP (0.20 μL, 0.030 μmol, 150 mM in $dH_2O$, 10 eq.) was added. After mixing for 1.5 h at 37 ºC, 300 rpm, pyridine thioester **1** (2.00 μL, 0.300 μmol, 150 mM in DMF, 100 eq.) was added and the reaction mixture was further incubated for 1 h at 37 ºC, 300 rpm. The excess reagent was removed *via* ultrafiltration into conjugation buffer, and incubated for a further 24 h at 37 ºC, 300 rpm. The sample was purified by ZebaSpin for LCMS analysis.

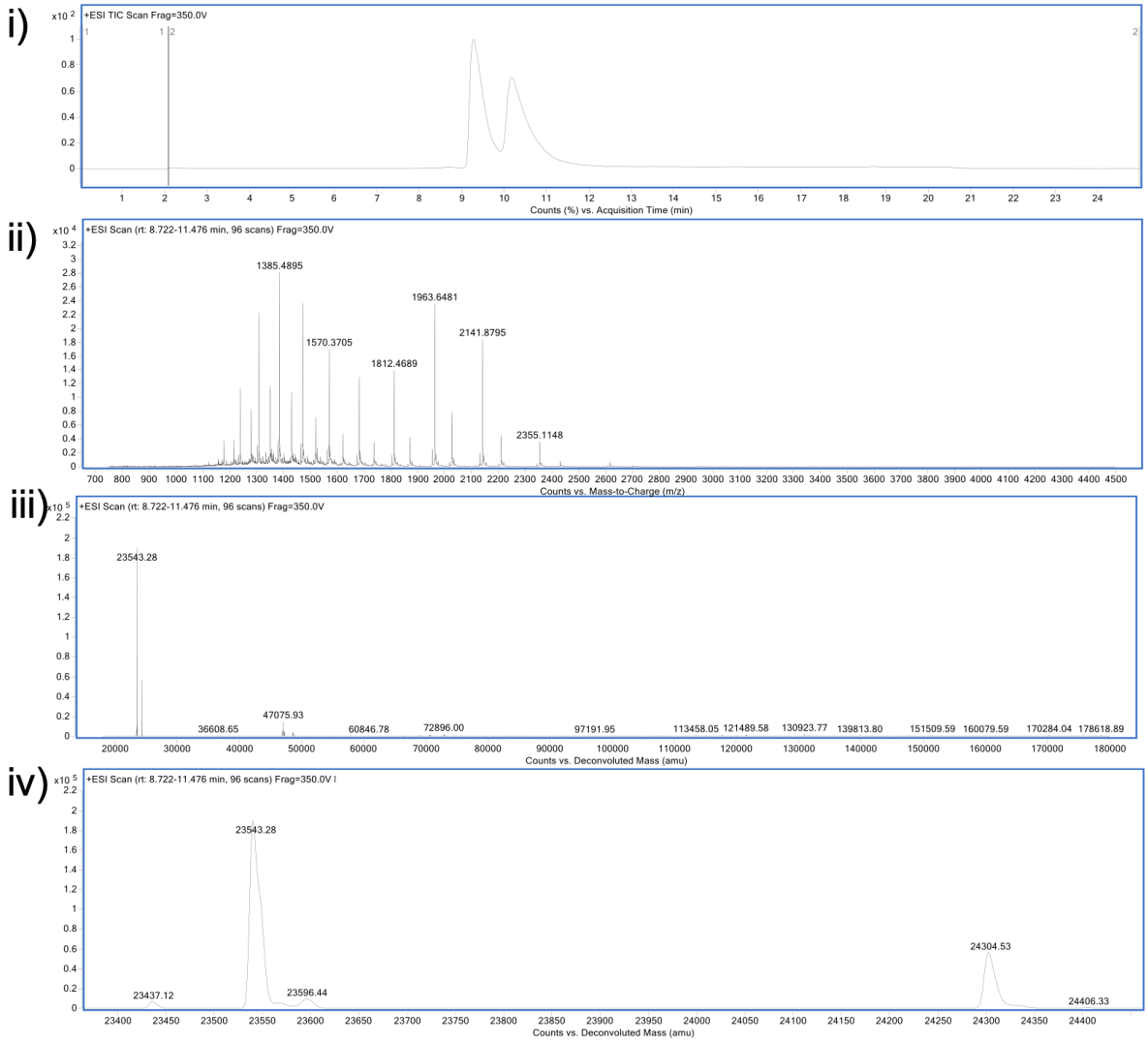


**FIGURE S.7.** LCMS analysis of pyridine thioester **1** reaction on reduced Fab. i) TIC. ii) non-convoluted ion series. iii) full range of deconvoluted ion series. iv) zoomed in of deconvoluted ion series. Expected mass of pyridine thioester conjugate: LC 23545 Da, HC 24306 Da. Observed: modified LC 23543 Da, modified HC 24304 Da. Mass of thioester addition: 106 Da.

**Pyridine thioester conjugate CLT at pH 8.4**

Prepared pyridine thioester conjugate (40 μL, 150 μM) was washed *via* ultrafiltration (10 kDa MWCO) into BBS pH 8.4 (5 x 80 μL). The concentration of the pyridine thioester conjugate calculated. The conjugate was diluted to 20 μM with BBS pH 8.4 and further incubated at pH 8.4 for 24 h at 22 ºC, 300 rpm. The sample was purified by ZebaSpin for LCMS analysis.

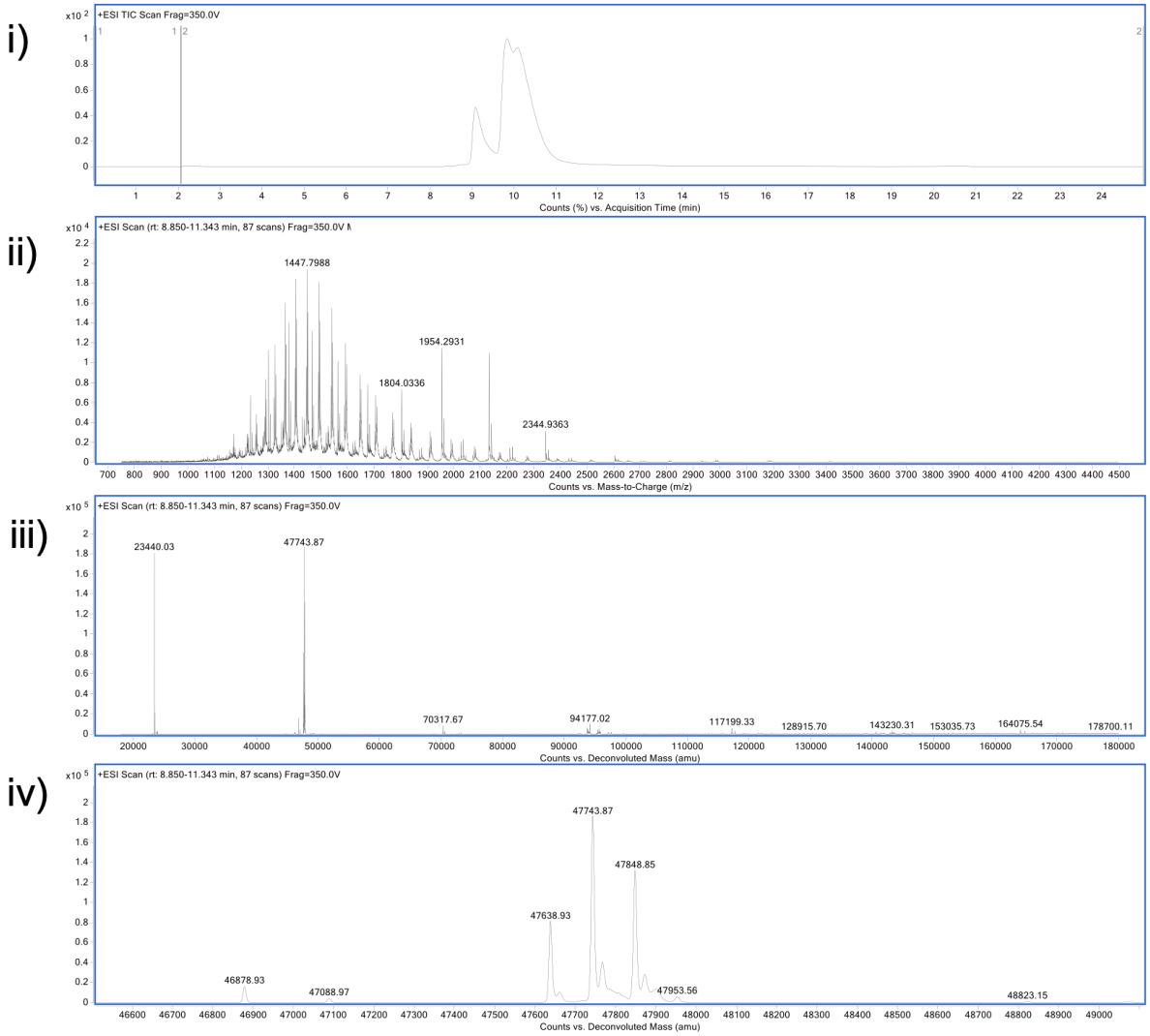


**FIGURE S.8.** LCMS analysis of pyridine CLT conjugate. i) TIC. ii) non-convoluted ion series. iii) full range of deconvoluted ion series. iv) zoomed in of deconvoluted ion series. Expected mass of pyridine CLT conjugate: 47638 Da (native, 0 additions), 47744 Da (1 addition), 47850 Da (2 additions). Observed: 47638 Da, 47744 Da, 47849 Da.

**Pyridine thioester conjugate CLT at pH 8.4, 6 h**

Prepared pyridine thioester conjugate (40 μL, 150 μM) was washed *via* ultrafiltration (10 kDa MWCO) into BBS pH 8.4 (5 x 80 μL). The concentration of the pyridine thioester conjugate was calculated. The conjugate was diluted to 20 μM with BBS pH 8.4 and further incubated at pH 8.4 for 6 h at 22 ºC, 300 rpm. The sample was purified by ZebaSpin for LCMS analysis.

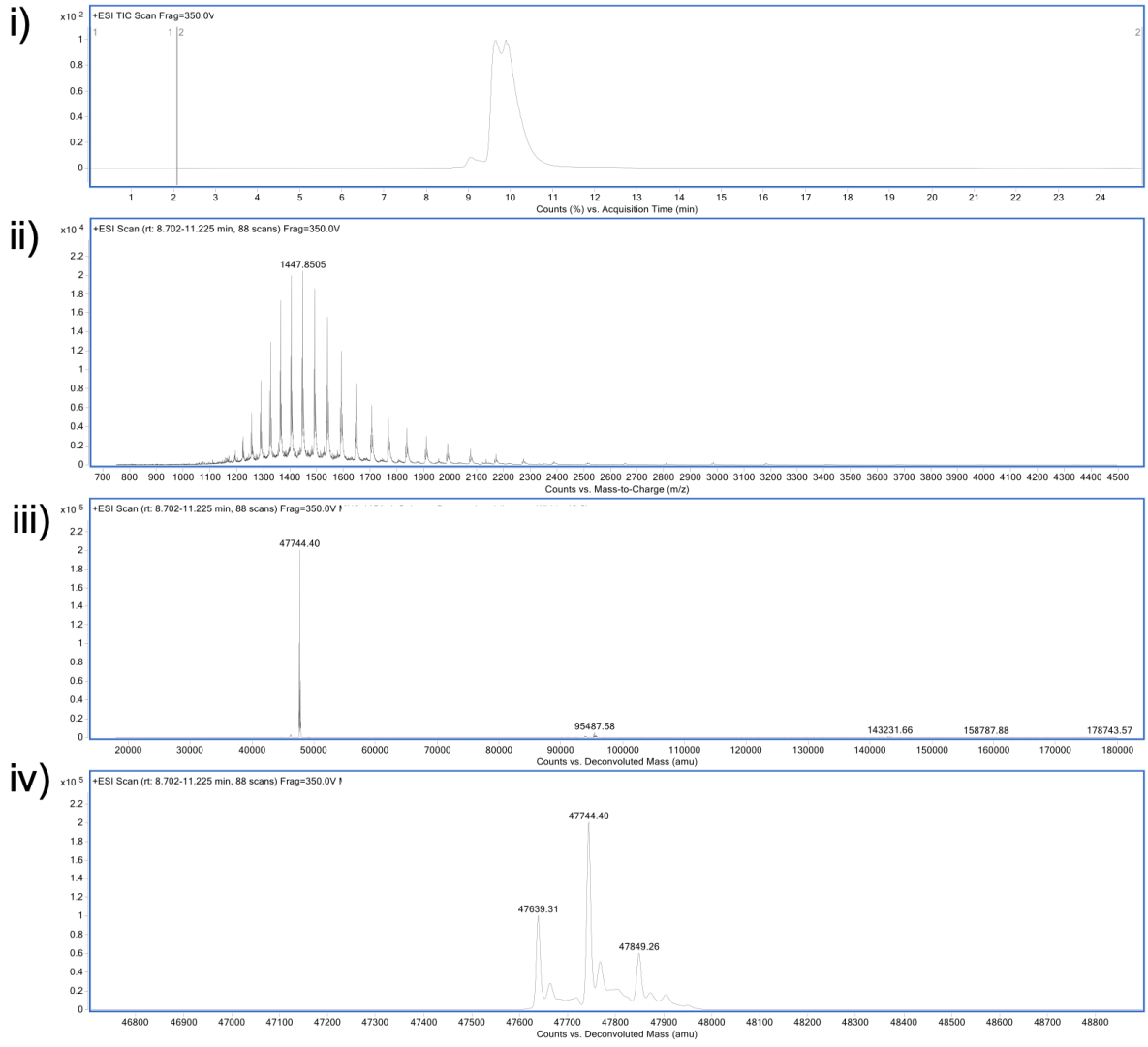


**FIGURE S.9.** LCMS analysis of pyridine CLT conjugate. i) TIC. ii) non-convoluted ion series. iii) full range of deconvoluted ion series. iv) zoomed in of deconvoluted ion series. Expected mass of pyridine CLT conjugate: 47638 Da (native, 0 additions), 47744 Da (1 addition), 47850 Da (2 additions). Observed: 47638 Da, 47744 Da, 47849 Da.

**Pyridine thioester conjugate CLT at pH 8.4, 4 h**

Prepared pyridine thioester conjugate (40 μL, 150 μM) was washed *via* ultrafiltration (10 kDa MWCO) into BBS pH 8.4 (5 x 80 μL). The concentration of the pyridine thioester conjugate was calculated. The conjugate was diluted to 20 μM with BBS pH 8.4 and further incubated at pH 8.4 for 4 h at 22 ºC, 300 rpm. The sample was purified by ZebaSpin for LCMS analysis.

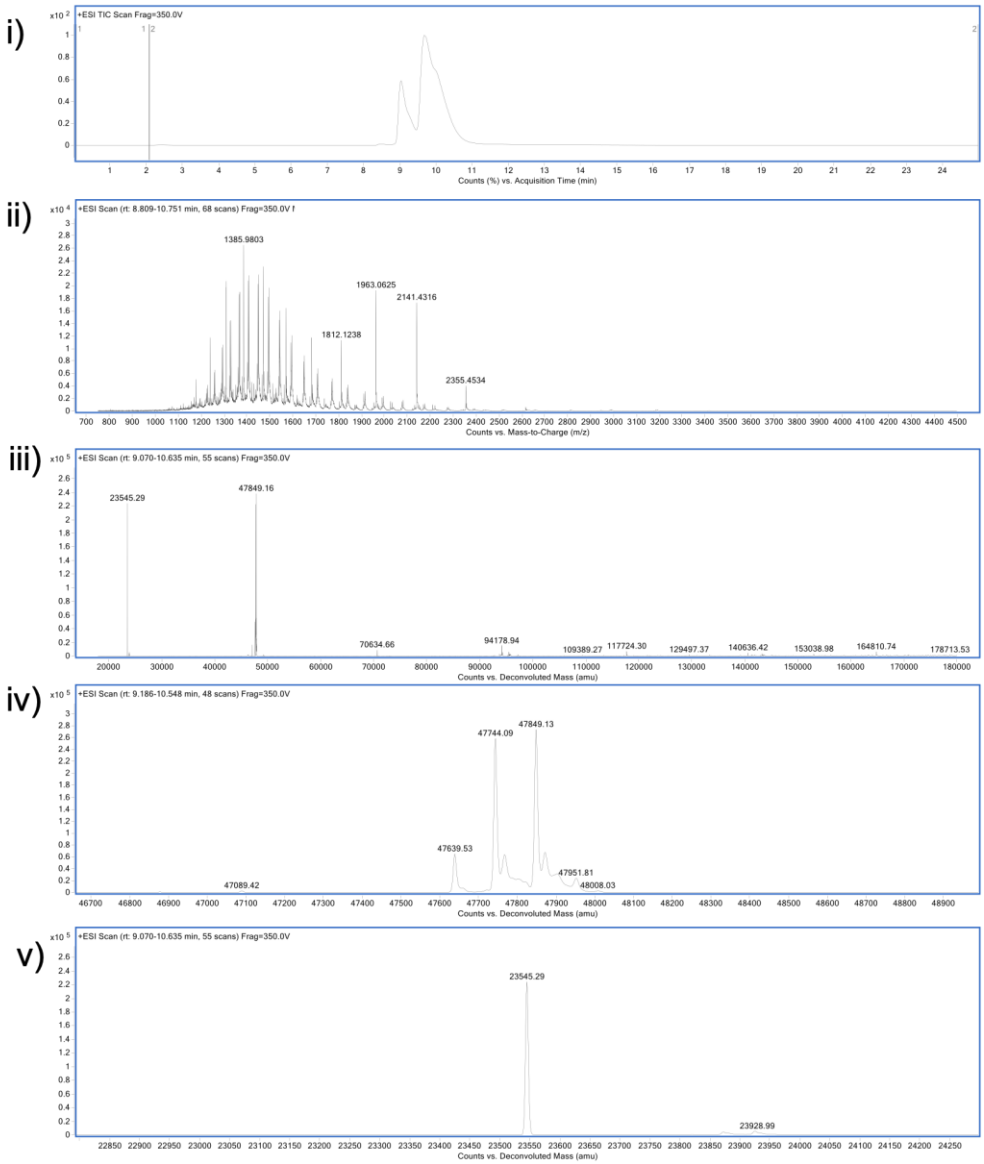


**FIGURE S.10.** LCMS analysis of pyridine CLT conjugate. i) TIC. ii) non-convoluted ion series. iii) full range of deconvoluted ion series. iv) and v) zoomed in of deconvoluted ion series. Expected mass of pyridine CLT conjugate: 47638 Da (native, 0 additions), 47744 Da (1 addition), 47850 Da (2 additions). Observed: 47639 Da, 47744 Da, 47849 Da, modified LC 23545 Da.

**Pyridine thioester conjugate CLT at pH 8.0, 24 h**

Prepared pyridine thioester conjugate (40 μL, 150 μM) was washed *via* ultrafiltration (10 kDa MWCO) into BBS pH 8.0 (5 x 80 μL). The concentration of the pyridine thioester conjugate was calculated. The conjugate was diluted to 20 μM with BBS pH 8.4 and further incubated at pH 8.0 for 24 h at 22 ºC, 300 rpm. The sample was purified by ZebaSpin for LCMS analysis.

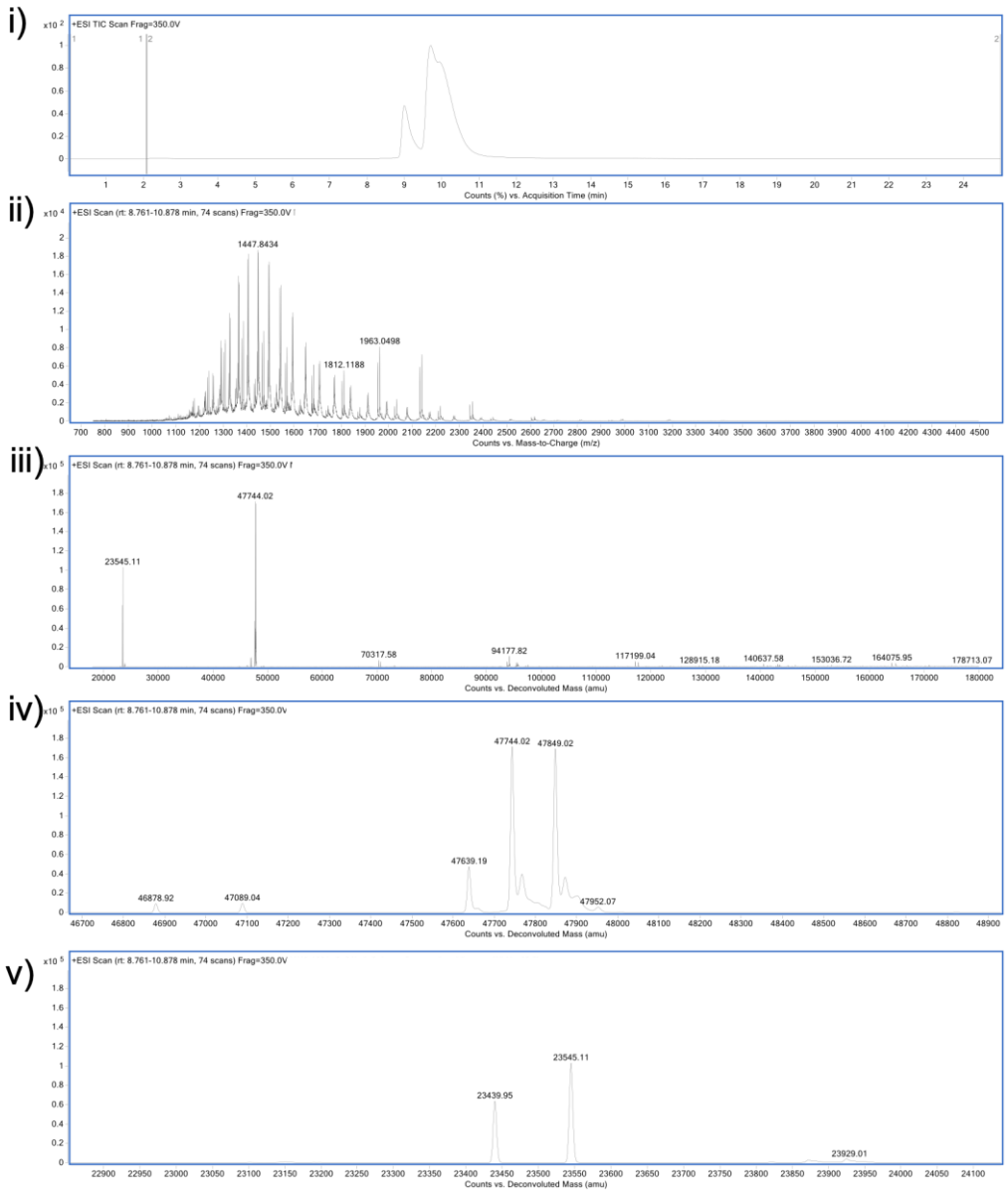


**FIGURE S.11.** LCMS analysis of pyridine CLT conjugate. i) TIC. ii) non-convoluted ion series. iii) full range of deconvoluted ion series. iv) zoomed in of deconvoluted ion series. Expected mass of pyridine CLT conjugate: 47638 Da (native, 0 additions), 47744 Da (1 addition), 47850 Da (2 additions). Observed: 47638 Da, 47744 Da, 47849 Da, LC 23439, modified LC 23545 Da.

**Quinoline thioester 2 conjugation on non-reduced Fab (control)**

To Fab (20.0 μL, 0.0030 μmol, 150 μM, 7.15 mg/mL) in conjugation buffer quinoline thioester **2** (2.00 μL, 0.300 μmol, 150 mM in DMF, 100 eq.) was added. The sample was incubated for 4 h at 22 ºC, 300 rpm. The excess reagent was removed *via* ultrafiltration (10 kDa MWCO) into LCMS water, and the sample was purified by ZebaSpin for LCMS analysis.

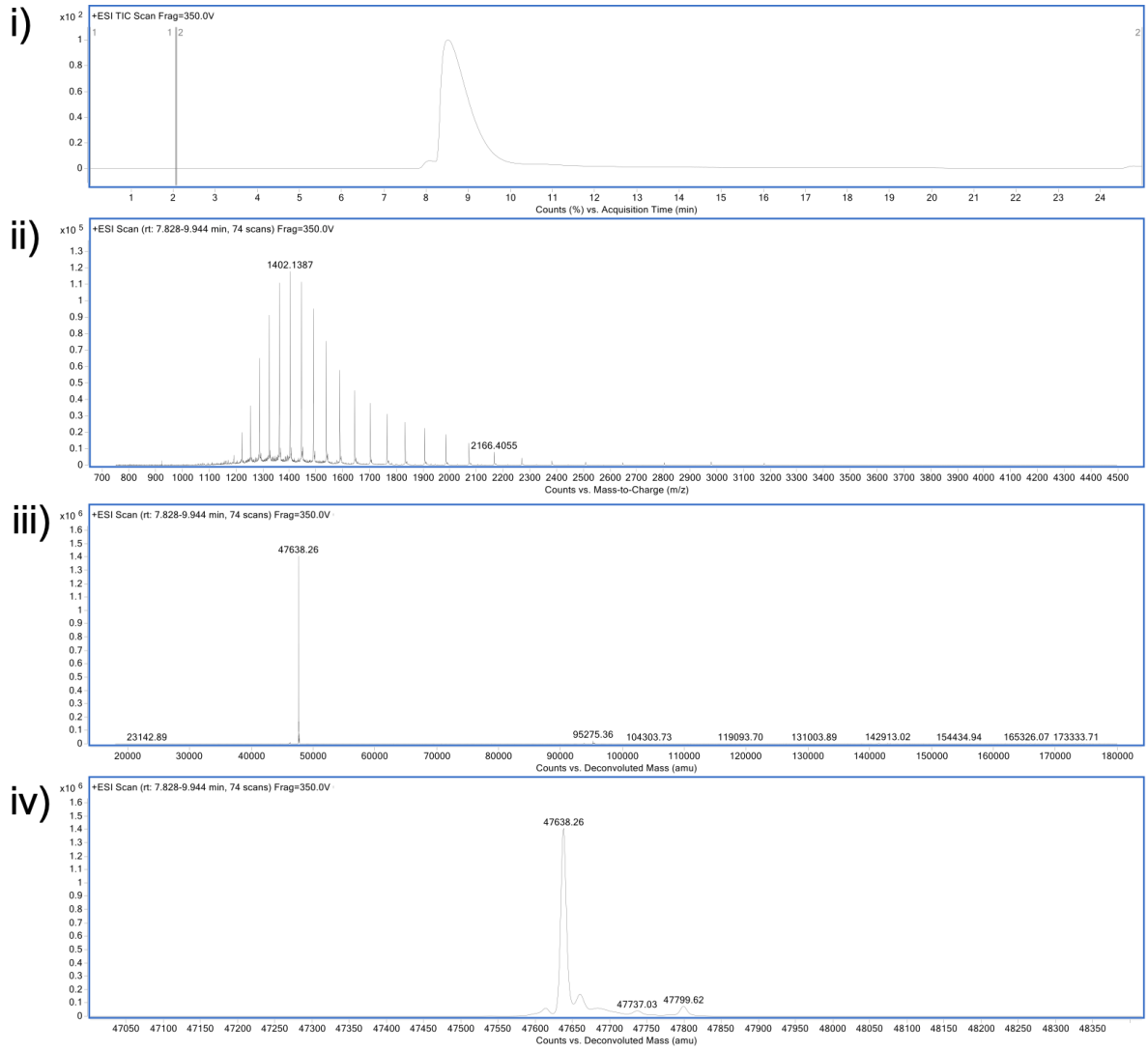


**FIGURE S.12.** LCMS analysis of quinoline thioester **2** control on native Fab. i) TIC. ii) non-convoluted ion series. iii) full range of deconvoluted ion series. iv) zoomed in of deconvoluted ion series. Expected mass of native Fab: 47638 Da. Observed: 47368 Da.

**Quinoline thioester 2 conjugation on reduced Fab (reaction)**

To Fab (20.0 μL, 0.0030 μmol, 150 μM, 7.15 mg/mL) in conjugation buffer, TCEP (0.20 μL, 0.030 μmol, 150 mM in $dH_2O$, 10 eq.) was added. After mixing for 1.5 h at 37 ºC, 300 rpm, quinoline thioester **2** (2.00 μL, 0.300 μmol, 150 mM in DMF, 100 eq.) was added and the reaction mixture was further incubated for 1 h at 37 ºC, 300 rpm. The excess reagent was removed *via* ultrafiltration (10 kDa MWCO) into LCMS water, and the sample was purified by ZebaSpin for LCMS analysis.

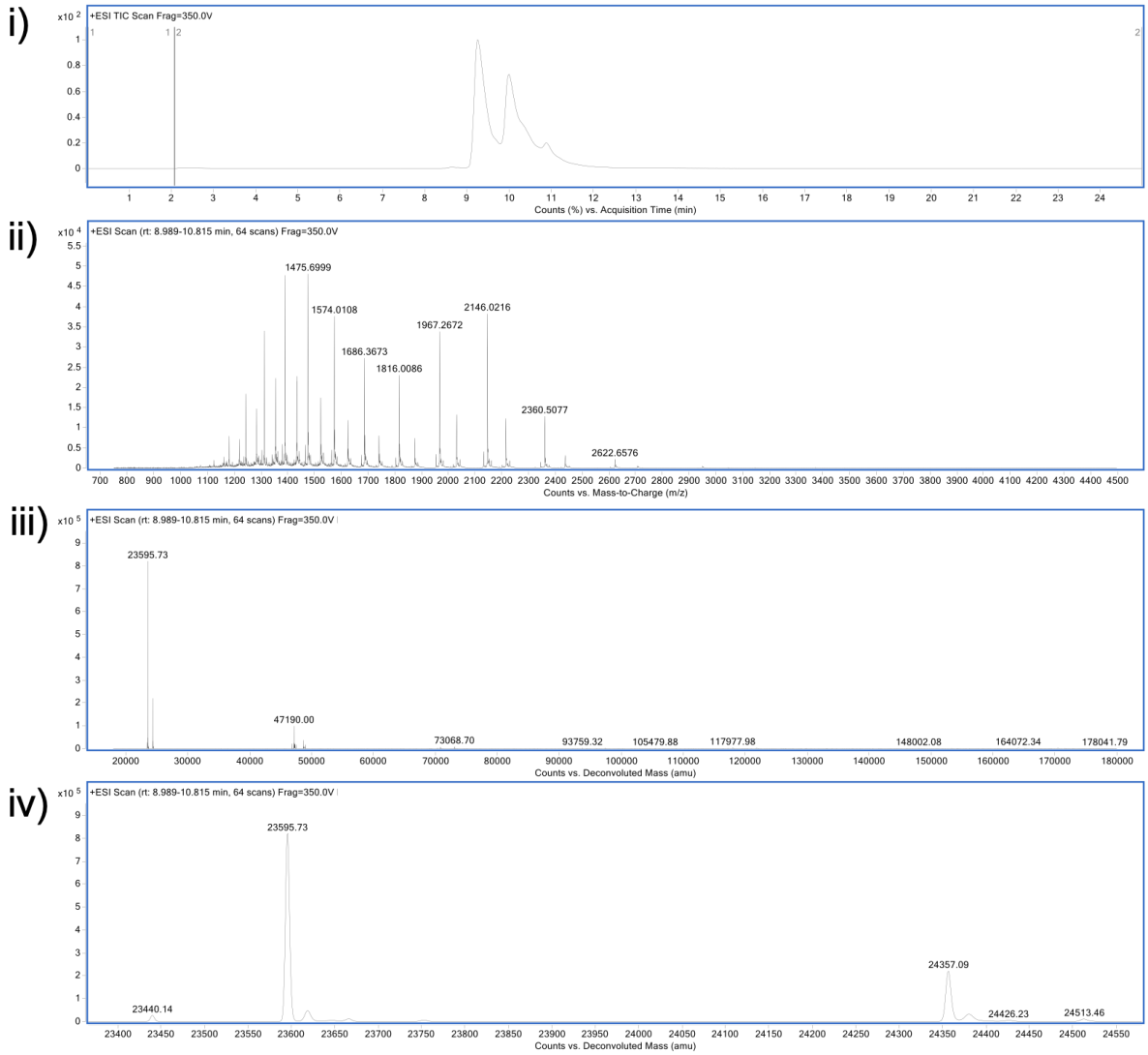


**FIGURE S.13.** LCMS analysis of quinoline thioester **2** reaction on reduced Fab. i) TIC. ii) non-convoluted ion series. iii) full range of deconvoluted ion series. iv) zoomed in of deconvoluted ion series. Expected mass of quinoline thioester conjugate: LC 23595 Da, HC 24356 Da. Observed: modified LC 23595 Da, HC modified 24357 Da. Mass of quinoline thioester **2** addition: 156 Da.

**Quinoline thioester conjugate CLT at pH 8.4**

Prepared quinoline thioester conjugate (40 μL, 150 μM) was washed *via* ultrafiltration (10 kDa MWCO) into BBS pH 8.4 (5 x 80 μL). The concentration of the quinoline thioester conjugate was calculated. The conjugate was diluted to 20 μM with BBS pH 8.4 and further incubated at pH 8.4 for 24 h at 22 ºC, 300 rpm. The sample was purified by ZebaSpin for LCMS analysis.

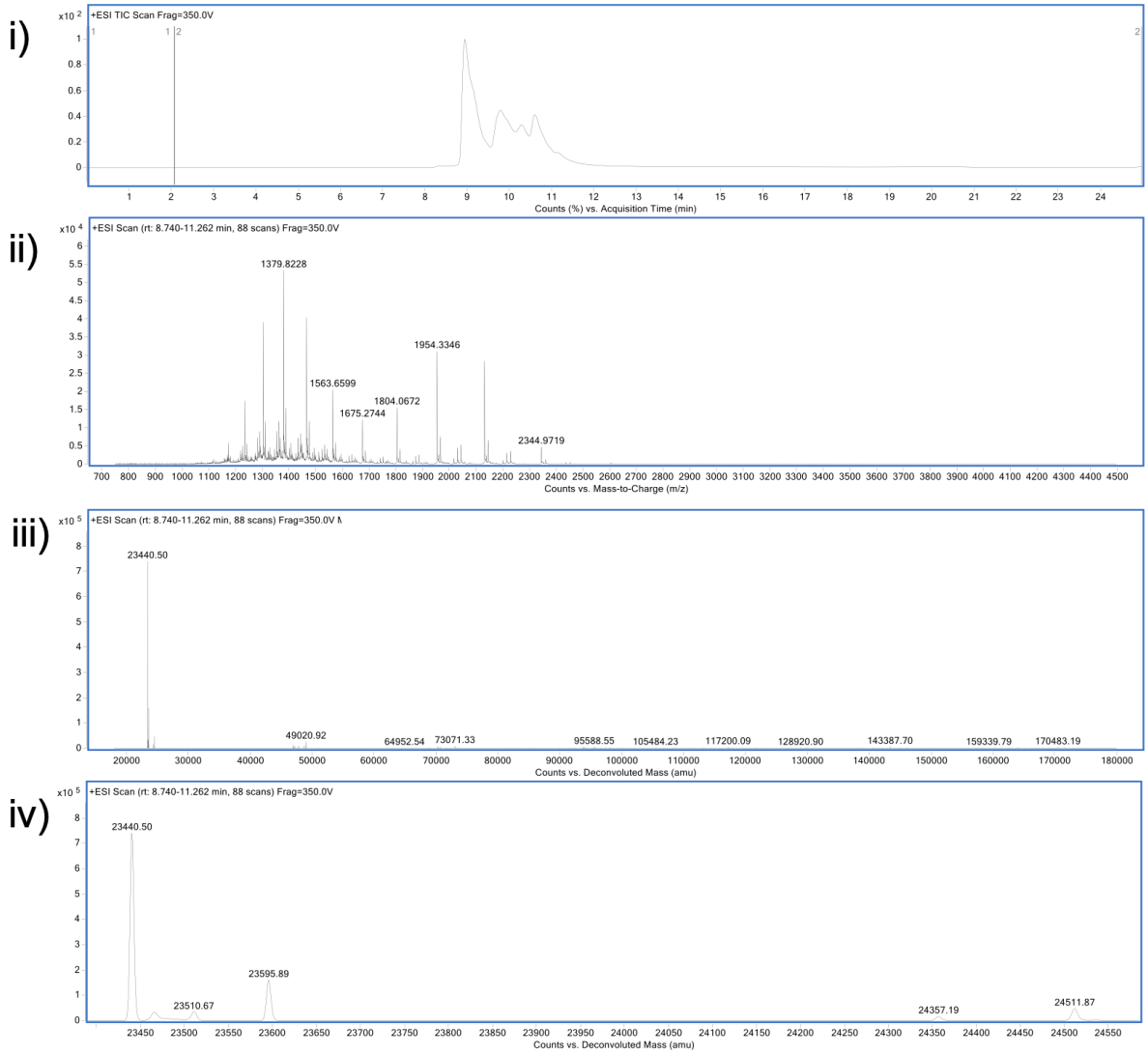


**FIGURE S.14.** LCMS analysis of quinoline CLT conjugate. i) TIC. ii) non-convoluted ion series. iii) full range of deconvoluted ion series. iv) zoomed in of deconvoluted ion series. Expected mass of quinoline CLT conjugate: 47638 Da (native, 0), 47794 Da (1 addition), 47950 Da (2 additions). Observed: LC 23440 Da, modified LC 23595 Da, modified HC 24357 Da, modified HC 24511 Da.

**Pyrimidine thioester 3 conjugation on non-reduced Fab (control), pH 7.4**

To Fab (20.0 μL, 0.0030 μmol, 150 μM, 7.15 mg/mL) in conjugation buffer, pyrimidine thioester **3** (2.00 μL, 0.300 μmol, 150 mM in DMF, 100 eq.) was added. The sample was incubated for 4 h at 22 ºC, 300 rpm. The excess reagent was removed *via* ultrafiltration (10 kDa MWCO) into LCMS water, and the sample was purified by ZebaSpin for LCMS analysis.

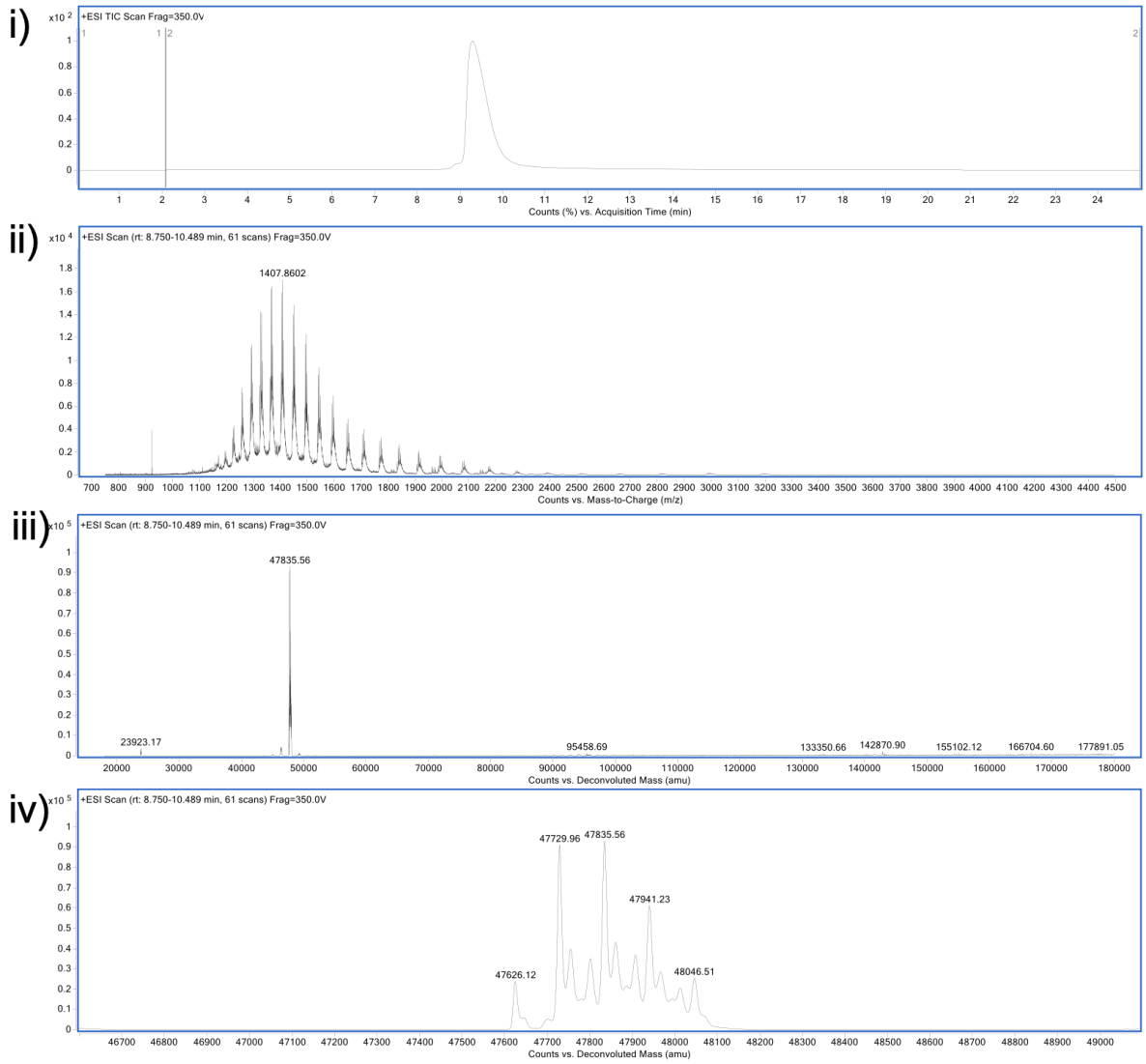


**FIGURE S.15.** LCMS analysis of pyrimidine thioester **3** control on native Fab. i) TIC. ii) non-convoluted ion series. iii) full range of deconvoluted ion series. iv) zoomed in of deconvoluted ion series. Expected mass of native Fab: 47626 Da. Observed: 47626 Da (0 additions), 47729 Da (1 addition), 47835 Da (2 additions), 47941 Da (3 additions), 48046 Da (4 additions). Mass of pyrimidine thioester **3** addition: 107 Da.

**Pyrimidine thioester 3 conjugation on non-reduced Fab (control), pH 6.0**

To Fab (20.0 μL, 0.0030 μmol, 150 μM, 7.15 mg/mL) in conjugation buffer at pH 6.0, pyrimidine thioester **3** (2.00 μL, 0.300 μmol, 150 mM in DMF, 100 eq.) was added. The sample was incubated for 4 h at 22 ºC, 300 rpm. The excess reagent was removed *via* ultrafiltration (10 kDa MWCO) into LCMS water, and the sample was purified by ZebaSpin for LCMS analysis.

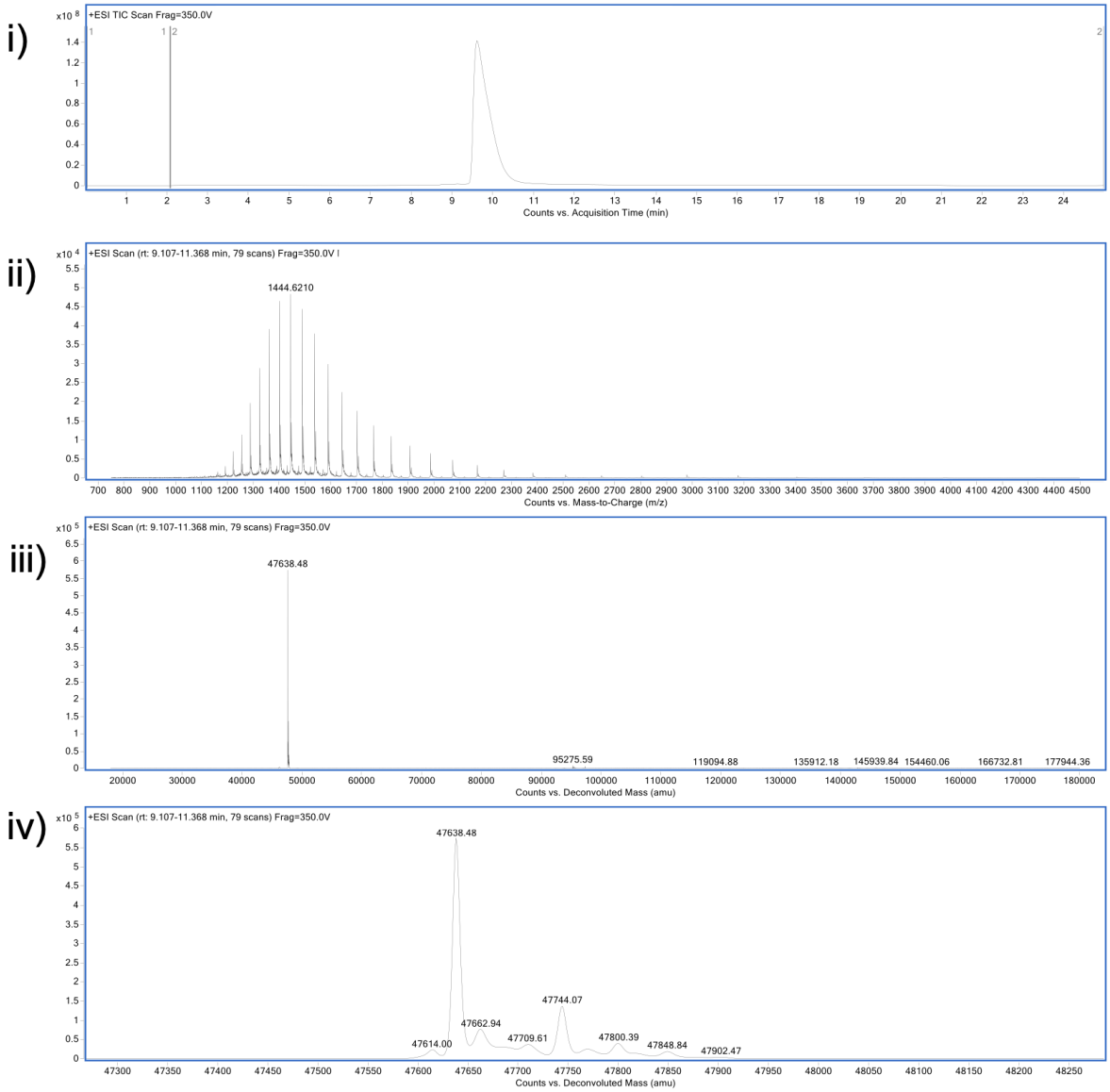


**FIGURE S.16.** LCMS analysis of pyrimidine thioester **3** control on native Fab at pH 6.0. i) TIC. ii) non-convoluted ion series. iii) full range of deconvoluted ion series. iv) zoomed in of deconvoluted ion series. Expected mass of native Fab: 47638 Da. Observed: 47638 (0 additions), 47744 (1 addition).

**Pyrimidine thioester 3 conjugation on reduced Fab (reaction)**

To Fab (20.0 μL, 0.0030 μmol, 150 μM, 7.15 mg/mL) in conjugation buffer at pH 6.0, TCEP (0.20 μL, 0.030 μmol, 150 mM in $dH_2O$, 10 eq.) was added. After mixing for 1.5 h at 37 ºC, 300 rpm, pyrimidine thioester **3** (2.00 μL, 0.300 μmol, 150 mM in DMF, 100 eq.) was added and the reaction mixture was incubated for 1 h at 37 ºC, 300 rpm. The excess reagent was removed *via* ultrafiltration (10 kDa MWCO) into LCMS water, and the sample was purified by ZebaSpin for LCMS analysis.

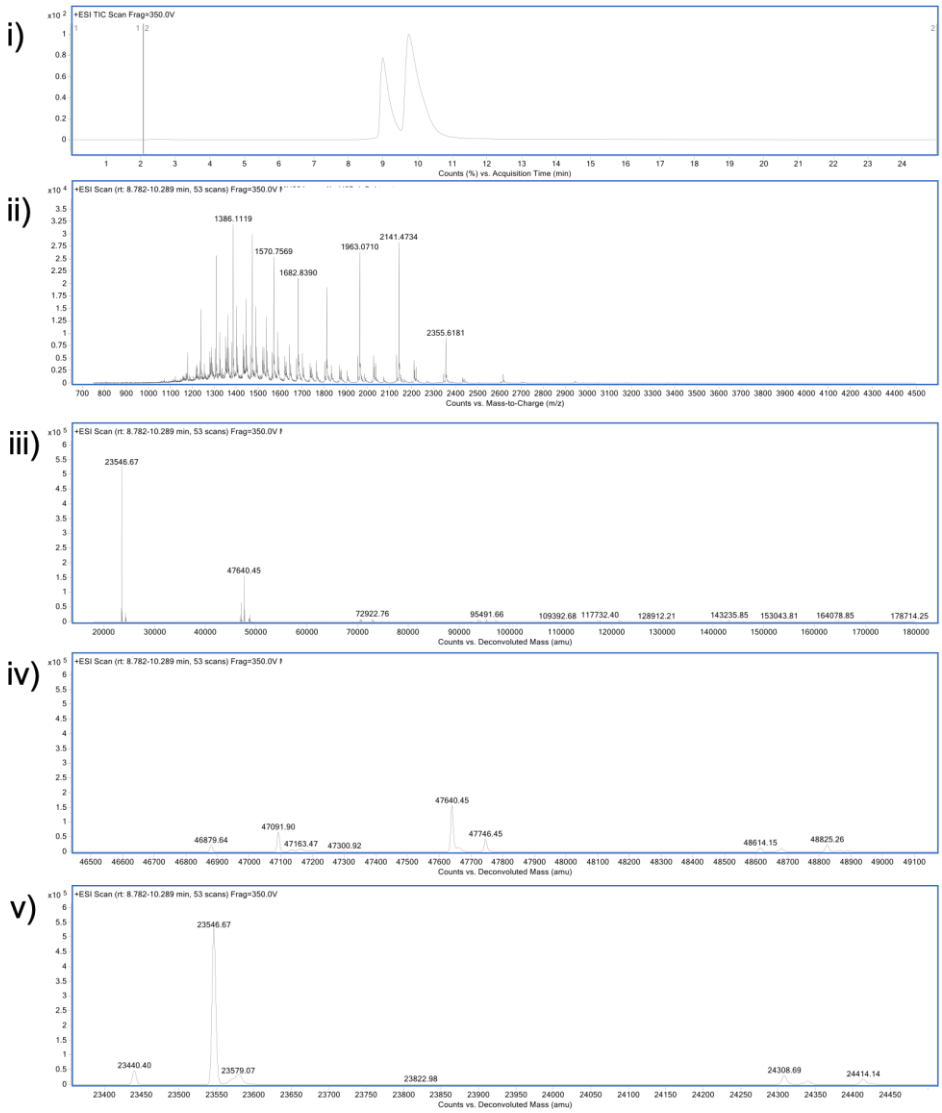


**FIGURE S.17.** LCMS analysis of pyrimidine thioester **3** reaction on reduced Fab at pH 6.0. i) TIC. ii) non-convoluted ion series. iii) full range of deconvoluted ion series. iv) and v) zoomed in of deconvoluted ion series. Expected mass of pyrimidine thioester conjugate: LC 23546 Da, HC 24307 Da. Observed: modified LC 23546 Da, modified HC 24308 Da, modified HC 24414 Da, native Fab 47640 Da (incomplete reduction at pH 6.0). Mass of pyrimidine thioester **3** addition: 107 Da.

**Pyrimidine thioester conjugate CLT at pH 6.5**

Prepared pyrimidine thioester conjugate (40 μL, 150 μM) was washed *via* ultrafiltration (10 kDa MWCO) into conjugation buffer at pH 6.5 (5 x 80 μL). The concentration of the pyrimidine thioester conjugate calculated. The conjugate was diluted to 20 μM with conjugation buffer pH 6.4 (260 μL) and further incubated at pH 6.5 for 4 h at 22 ºC, 300 rpm. The sample was purified by ZebaSpin for LCMS analysis.

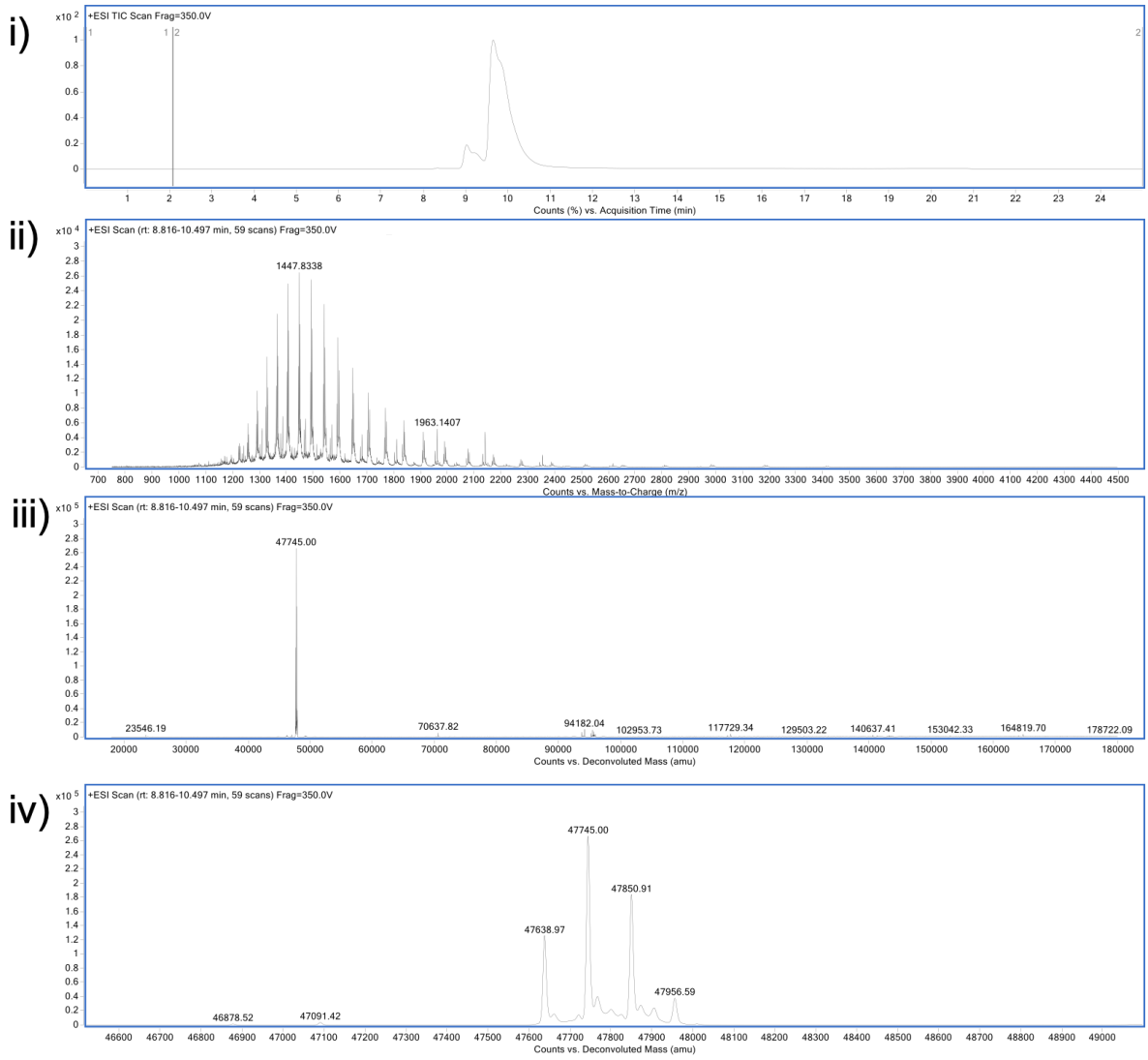


**FIGURE S.18.** LCMS analysis of pyrimidine CLT conjugate. i) TIC. ii) non-convoluted ion series. iii) full range of deconvoluted ion series. iv) zoomed in of deconvoluted ion series. Expected mass of pyrimidine CLT conjugate: 47638 Da (native, 0), 47745 Da (1 addition), 47851 Da (2 additions). Observed: 47638 Da, 47745 Da, 47850 Da, 47956 Da.

**Pyrimidine thioester conjugate CLT at pH 8.4**

Prepared pyrimidine thioester conjugate (40 μL, 150 μM) was washed *via* ultrafiltration 10 kDa MWCO) into BBS pH 8.4 (5 x 80 μL). The concentration of the pyrimidine thioester conjugate was calculated. The conjugate was diluted to 20 μM with BBS pH 8.4 (260 μL) and further incubated at pH 8.4 for 4 h at 22 ºC, 300 rpm. The sample was purified by ZebaSpin for LCMS analysis.

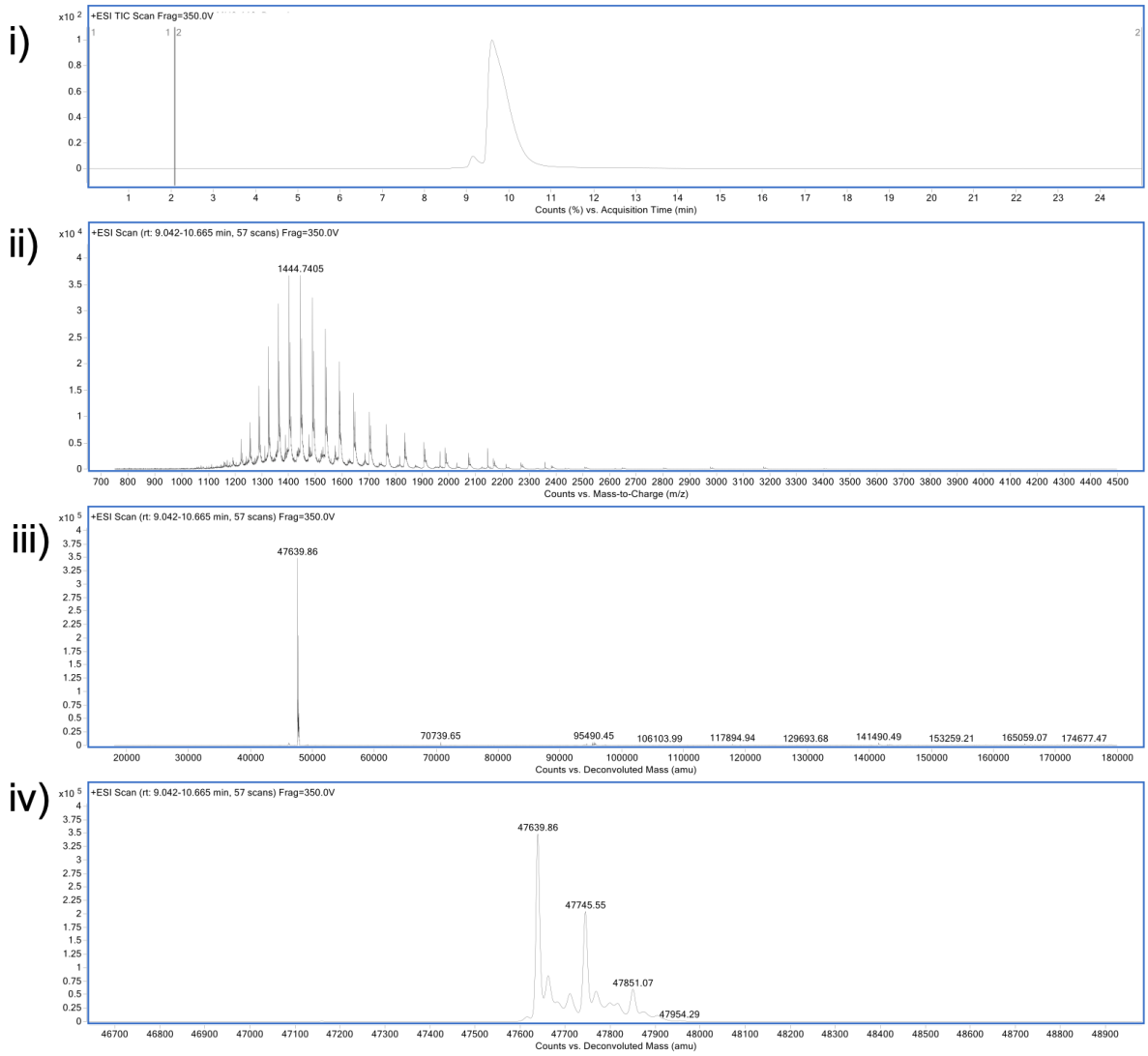


**FIGURE S.19.** LCMS analysis of pyrimidine CLT conjugate. i) TIC. ii) non-convoluted ion series. iii) full range of deconvoluted ion series. iv) zoomed in of deconvoluted ion series. Expected mass of pyrimidine CLT conjugate: 47638 Da (native, 0 additions), 47745 Da (1 addition), 47851 Da (2 additions). Observed: 47639 Da, 47745 Da, 47851 Da.

**Pyrimidine thioester conjugate CLT at pH 7.4**

Prepared pyrimidine thioester conjugate (40 μL, 150 μM) was washed *via* ultrafiltration 10 kDa MWCO) into conjugation buffer (5 x 80 μL). The concentration of the pyrimidine thioester conjugate was calculated. The conjugate was diluted to 20 μM with conjugation buffer and further incubated at pH 7.4 for 4 h at 22 ºC, 300 rpm. The sample was purified by ZebaSpin for LCMS analysis.

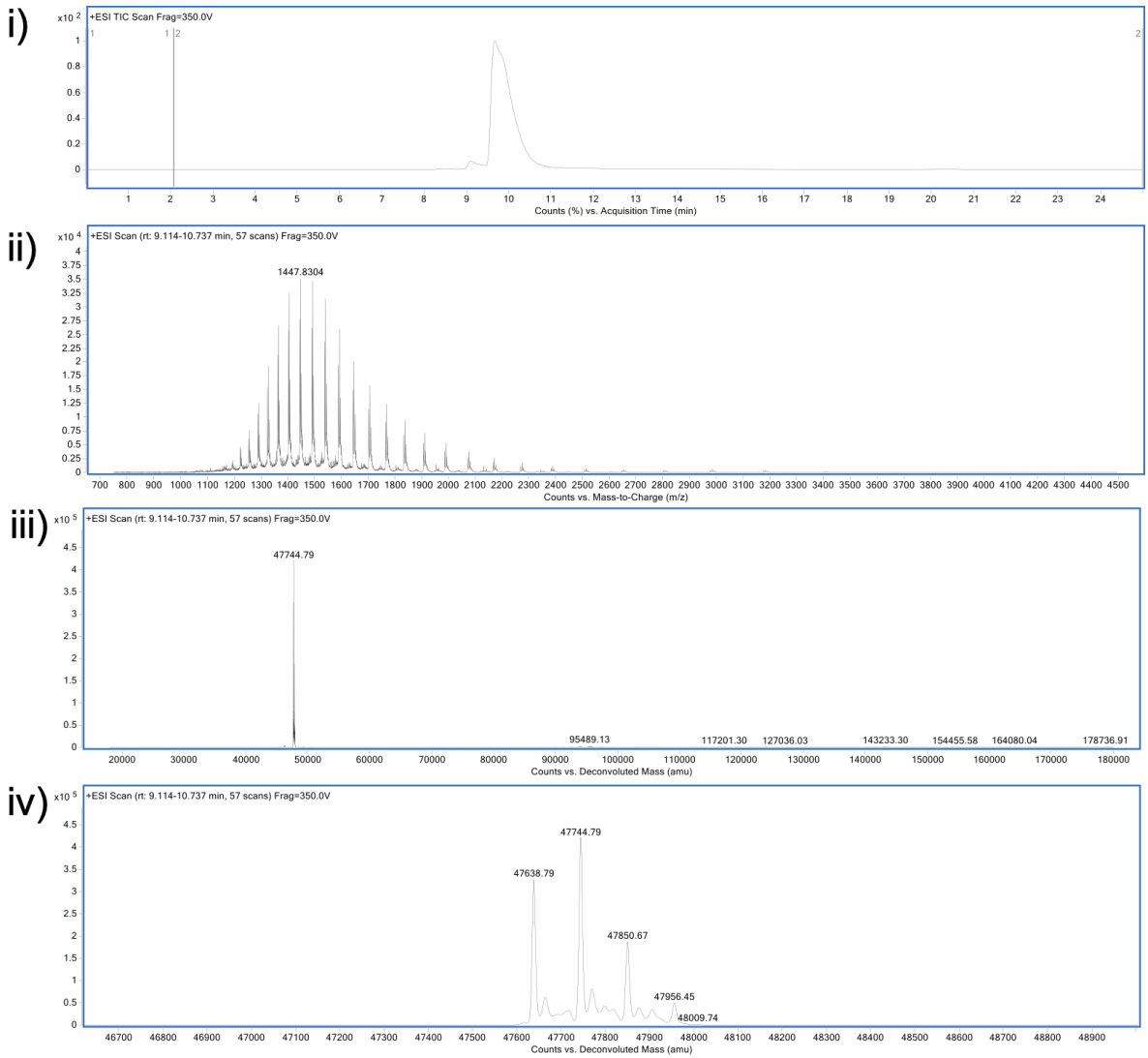


**FIGURE S.20.** LCMS analysis of pyrimidine CLT conjugate. i) TIC. ii) non-convoluted ion series. iii) full range of deconvoluted ion series. iv) zoomed in of deconvoluted ion series. Expected mass of pyridine thioester conjugate: 47638 Da (native, 0), 47744 Da (1 addition), 47850 Da (2 additions). Observed: 47638 Da, 47744 Da, 47850 Da, 47956 Da.

**Tetrazine thioester 7c conjugation on non-reduced Fab (control)**

To Fab (20.0 μL, 0.0030 μmol, 150 μM, 7.15 mg/mL) in citrate buffer at pH 5.0 was added tetrazine thioester **7c** (1.00 μL, 0.150 μmol, 150 mM in DMF, 50 eq.). The sample was incubated for 5 min at 22 ºC, 300 rpm. The excess reagent was removed *via* ultrafiltration (10 kDa MWCO) into LCMS water, and the sample was purified by ZebaSpin for LCMS analysis.

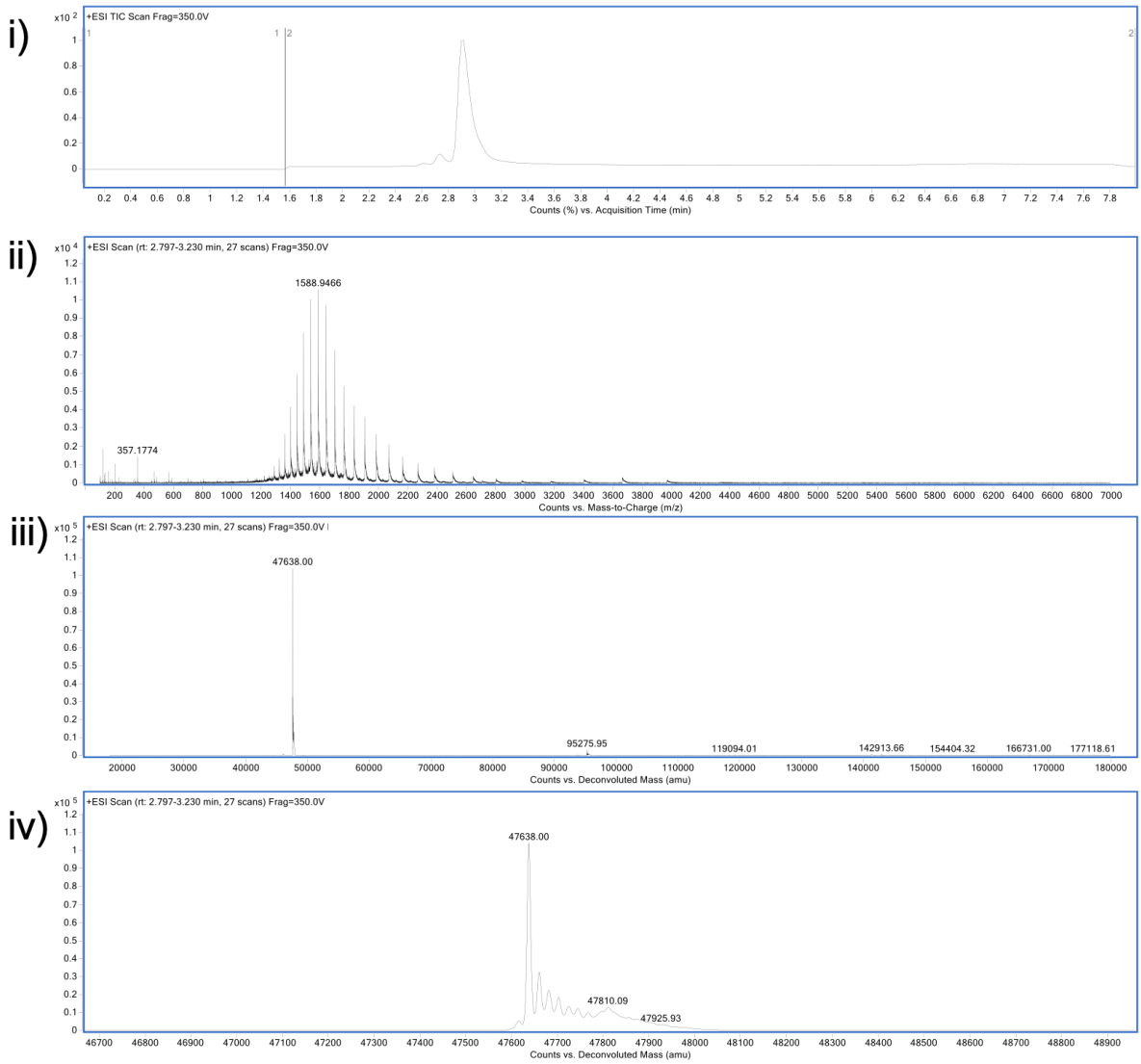


**FIGURE S.21.** LCMS analysis of tetrazine thioester **7c** control on native Fab at pH 5.5. i) TIC. ii) non-convoluted ion series. iii) full range of deconvoluted ion series. Iv) zoomed in of deconvoluted ion series. Expected mass of native Fab: 47638 Da. Observed: 47368 Da.

**Tetrazine thioester 7c conjugation on reduced Fab (reaction)**

To Fab (20.0 μL, 0.0030 μmol, 150 μM, 7.15 mg/mL) in citrate buffer at pH 5.5 was added TCEP (0.20 μL, 0.030 μmol, 150 mM in $dH_2O$, 10 eq.). After mixing for 1.5 h at 37 ºC, 300 rpm, tetrazine thioester **7c** (1.00 μL, 0.150 μmol, 150 mM in DMF, 50 eq.) was added and the reaction mixture was incubated for 5 min at 22 ºC, 300 rpm. The excess reagent was removed *via* ultrafiltration (10 kDa MWCO) into LCMS water, and the sample was purified by ZebaSpin for LCMS analysis.

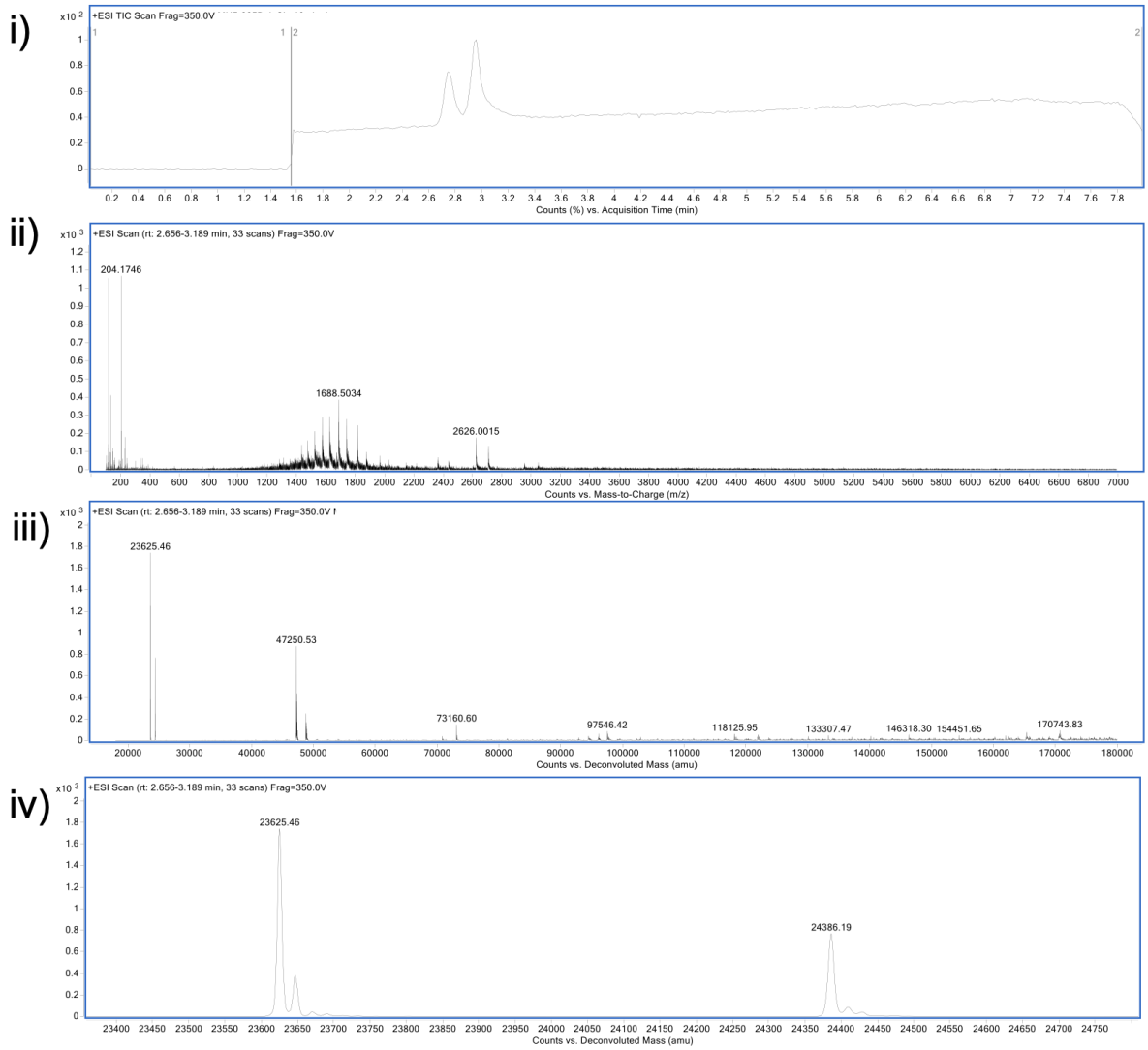


**FIGURE S.22.** LCMS analysis of tetrazine thioester **7c** reaction on reduced Fab at pH 5.5. i) TIC. ii) non-convoluted ion series. iii) full range of deconvoluted ion series. iv) zoomed in of deconvoluted ion series. Expected mass of tetrazine thioester conjugate: LC 23625 Da, HC 24385 Da. Observed: modified LC 23625 Da, modified HC 24386 Da. Mass of tetrazine thioester **7c** addition: 185 Da.

**Tetrazine thioester 7c conjugation on reduced Fab without TCEP, 5 min reaction**

To Fab (20.0 μL, 0.0030 μmol, 150 μM, 7.15 mg/mL) in conjugation buffer was added TCEP (0.20 μL, 0.030 μmol, 150 mM in $dH_2O$, 10 eq.). After mixing for 1.5 h at 37 ºC, 300 rpm, TCEP was removed by ultrafiltration (10 kDa MWCO) with citrate buffer at pH 5.5 (5 x 40 μL). The concentration of reduced Fab was calculated. Tetrazine thioester **7c** (150 mM in DMF, 50 eq.) was added and the reaction mixture was further incubated for 5 min at 22 ºC, 300 rpm. The excess reagent was removed *via* ultrafiltration (10 kDa MWCO) into LCMS water, and the sample was purified by ZebaSpin for LCMS analysis.

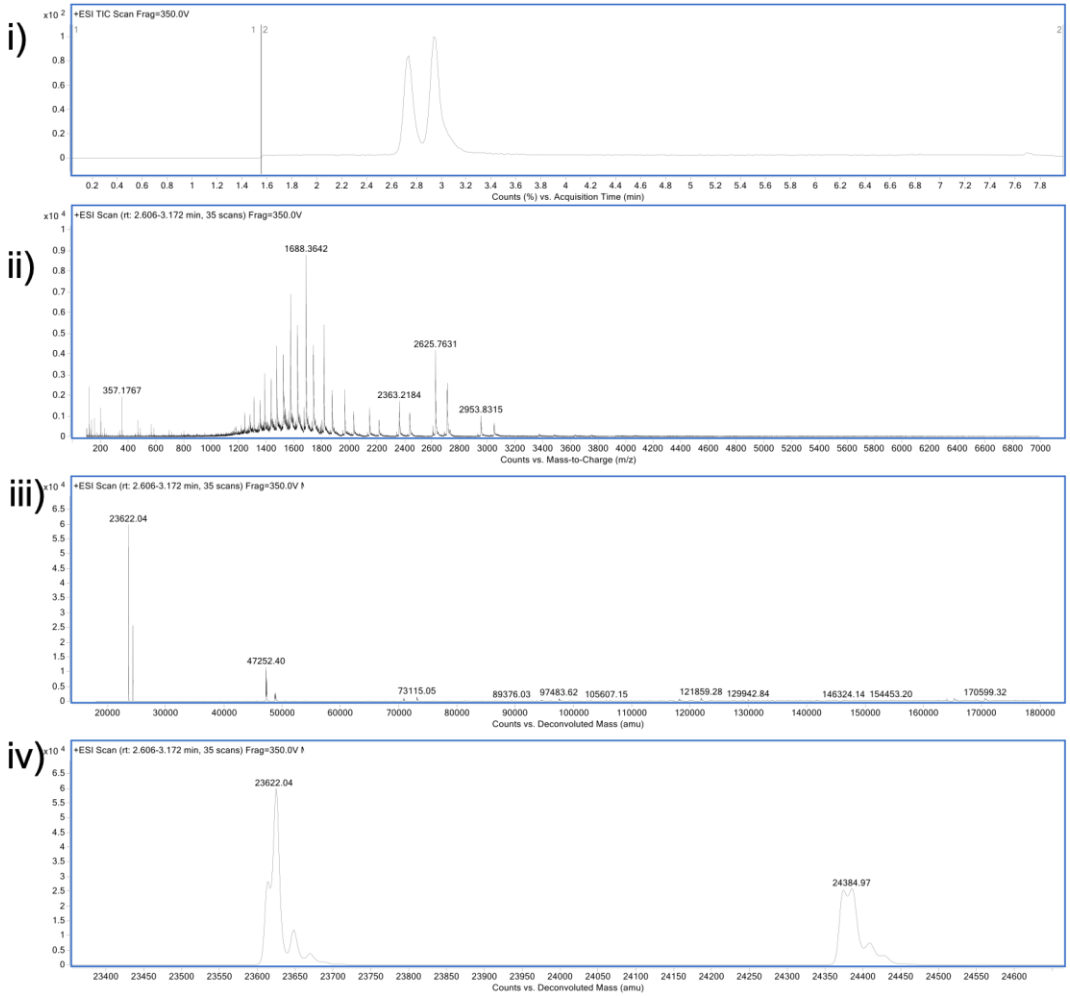


**FIGURE S.23.** LCMS analysis of tetrazine thioester **7c** reaction on reduced Fab, without TCEP. i) TIC. ii) non-convoluted ion series. iii) full range of deconvoluted ion series. iv) zoomed in of deconvoluted ion series. Expected mass of tetrazine thioester conjugate: LC 23625 Da, HC 24385 Da. Observed: modified LC 23612 Da, modified LC 23622 Da, modified HC 24374 Da, modified 24384 Da. Mass of tetrazine thioester **7c** addition: 185 Da.

**Tetrazine thioester 7c conjugation on reduced Fab without TCEP, 0.5 h reaction**

To Fab (20.0 μL, 0.0030 μmol, 150 μM, 7.15 mg/mL) in conjugation buffer was added TCEP (0.20 μL, 0.030 μmol, 150 mM in $dH_2O$, 10 eq.). After mixing for 1.5 h at 37 ºC, 300 rpm, TCEP was removed by ultrafiltration (10 kDa MWCO) with citrate buffer at pH 5.5 (5 x 40 μL). The concentration of reduced Fab was calculated. Tetrazine thioester **7c** (150 mM in DMF, 50 eq.) was added and the reaction mixture was further incubated for 0.5 h at 22 ºC, 300 rpm. The excess reagent was removed *via* ultrafiltration (10 kDa MWCO) into LCMS water, and the sample was purified by ZebaSpin for LCMS analysis.

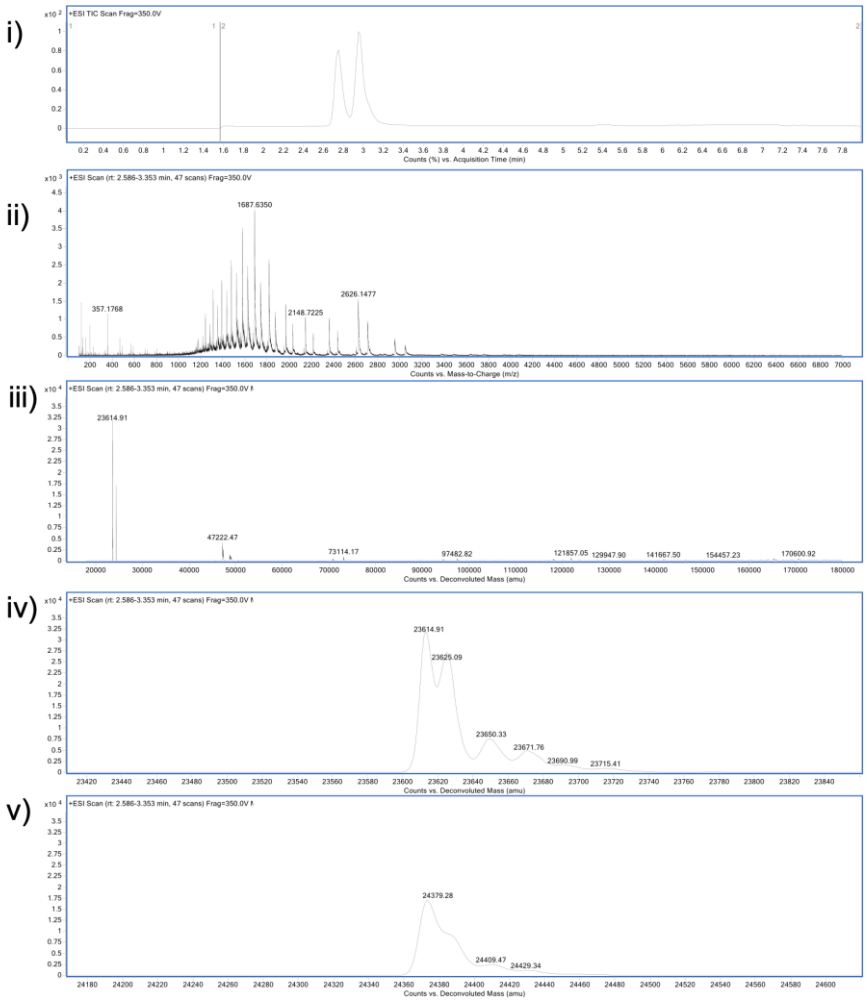


**FIGURE S.24.** LCMS analysis of tetrazine thioester **7c** reaction on reduced Fab, without TCEP for 0.5 h. i) TIC. ii) non-convoluted ion series. iii) full range of deconvoluted ion series. iv) and v) zoomed in of deconvoluted ion series. Expected mass of tetrazine thioester conjugate: LC 23625 Da, HC 24385 Da. Observed: modified LC 23614 Da, modified LC 23625 Da, modified HC 24379 Da, modified 24384 Da. Mass of tetrazine thioester **7c** addition: 185 Da.

**Tetrazine thioester 7c conjugation on reduced Fab with TCEP, 0.5 h**

To Fab (20.0 μL, 0.0030 μmol, 150 μM, 7.15 mg/mL) in citrate buffer at pH 5.5 was added TCEP (0.20 μL, 0.030 μmol, 150 mM in $dH_2O$, 10 eq.). After mixing for 1.5 h at 37 ºC, 300 rpm tetrazine thioester **7c** (1.00 μL, 0.150 μmol, 150 mM in DMF, 50 eq.) was added and the reaction mixture was incubated for 0.5 h at 22 ºC, 300 rpm. The excess reagent was removed *via* ultrafiltration (10 kDa MWCO) into LCMS water, and the sample was purified by ZebaSpin for LCMS analysis.

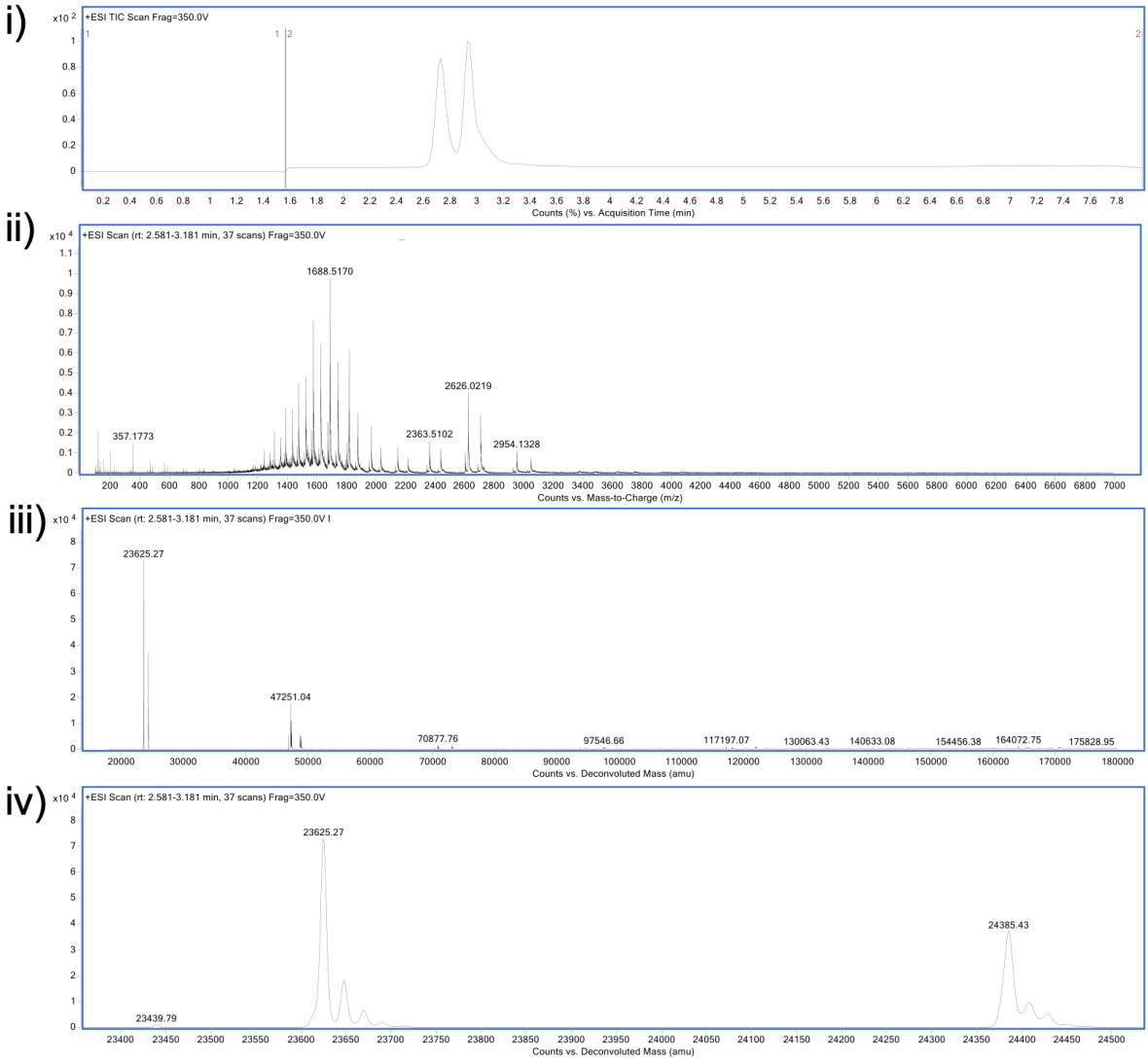


**FIGURE S.25.** LCMS analysis of tetrazine thioester **7c** reaction on reduced Fab, with TCEP for 0.5 h. i) TIC. ii) non-convoluted ion series iii) full range of deconvoluted ion series iv) zoomed in of deconvoluted ion series. Expected mass of tetrazine thioester conjugate: LC 23625 Da, HC 24385 Da. Observed: modified LC 23625 Da, modified HC 24385 Da. Mass of tetrazine thioester **7c** addition: 185 Da.

**Tetrazine thioester conjugate CLT at pH 6.5**

Prepared tetrazine thioester conjugate (40 μL, 150 μM) was washed *via* ultrafiltration 10 kDa MWCO) into conjugation buffer at pH 6.5 (5 x 80 μL). The concentration of the tetrazine thioester conjugate was calculated. The conjugate was diluted to 20 μM with conjugation buffer pH 6.5 and further incubated at pH 6.5 for 4 h at 22 ºC, 300 rpm. The sample was purified by ZebaSpin for LCMS analysis.

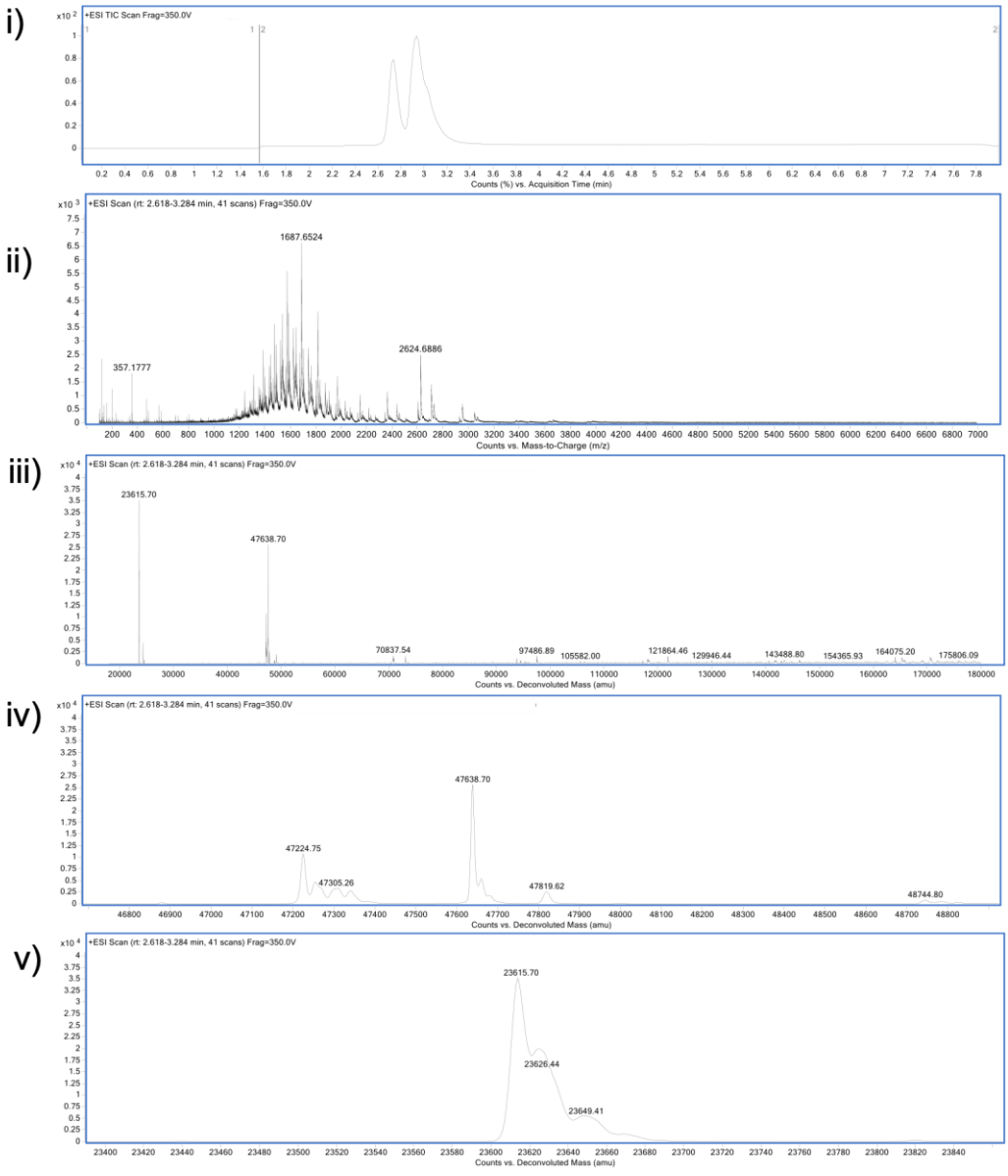


**FIGURE S.26.** LCMS analysis of tetrazine CLT conjugate. i) TIC. ii) non-convoluted ion series. iii) full range of deconvoluted ion series. iv) and v) zoomed in of deconvoluted ion series. Expected mass of tetrazine CLT conjugate: 47638 Da (native, 0), 47823 Da (1 addition), 48008 Da (2 additions). Observed: 47638 Da, 47819 Da, modified LC 23615 Da, modified LC 23626 Da.

**Tetrazine thioester conjugate CLT at pH 7.4**

Prepared tetrazine thioester conjugate (40 μL, 150 μM) was washed *via* ultrafiltration 10 kDa MWCO) into conjugation buffer (5 x 80 μL). The concentration of the tetrazine thioester conjugate was calculated. The conjugate was diluted to 20 μM with conjugation buffer and further incubated at pH 7.4 for 4 h at 22 ºC, 300 rpm. The sample was purified by ZebaSpin for LCMS analysis.

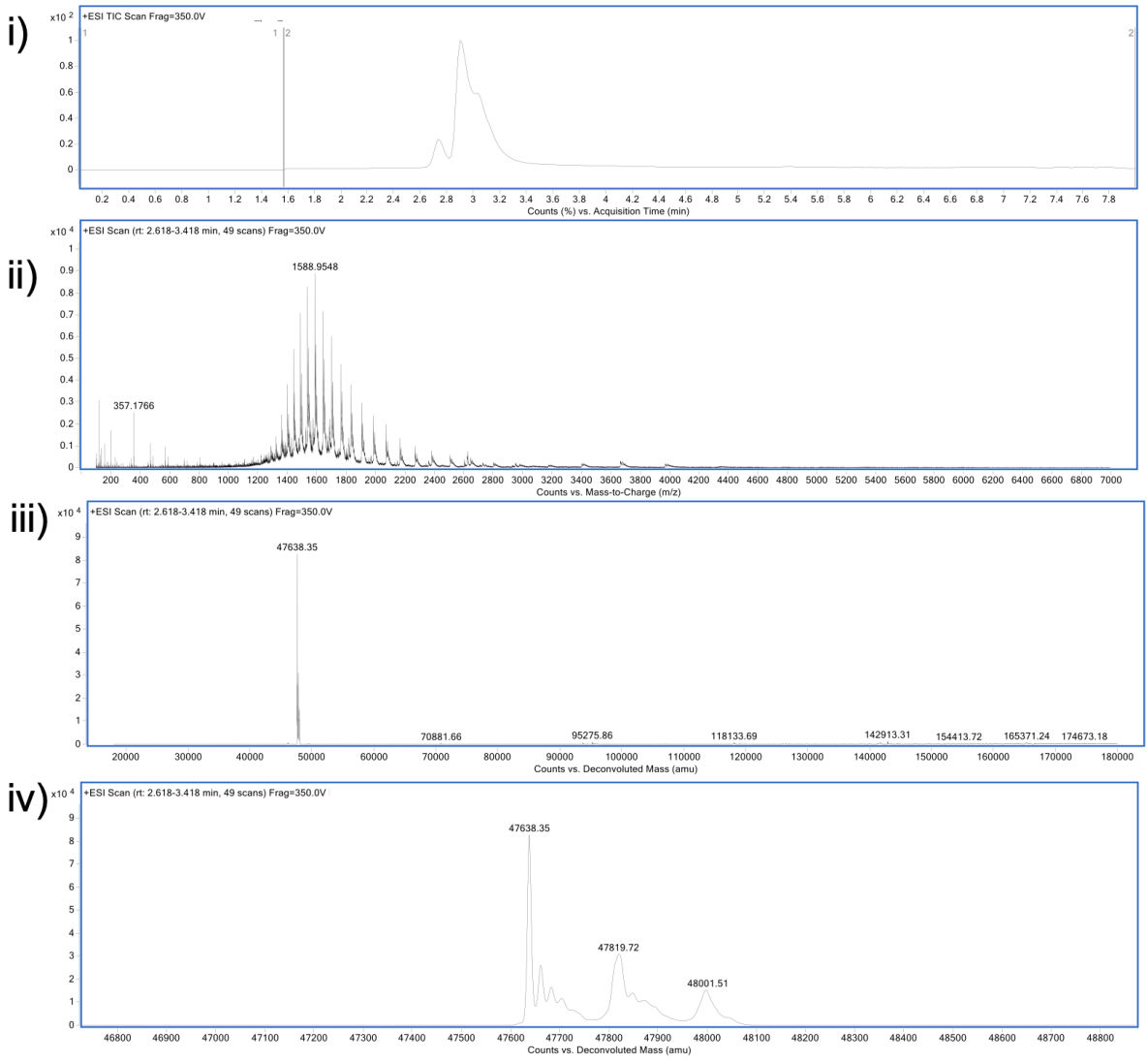


**FIGURE S.27.** LCMS analysis of tetrazine CLT conjugate. i) TIC. ii) non-convoluted ion series. iii) full range of deconvoluted ion series. iv) and v) zoomed in of deconvoluted ion series. Expected mass of tetrazine CLT conjugate: 47638 Da (native, 0), 47823 Da (1 addition), 48008 Da (2 additions). Observed: 47638 Da, 47819 Da, 48001 Da.

**Tetrazine thioester conjugate iEDDA with FAM-PEG3-BCN at pH 5.5**

To Fab (20.0 μL, 0.0030 μmol, 150 μM, 7.15 mg/mL) in conjugation buffer was added TCEP (0.20 μL, 0.030 μmol, 150 mM in $dH_2O$, 10 eq.). After mixing for 1.5 h at 37 ºC, TCEP was removed by ultrafiltration (10 kDa MWCO) with citrate buffer at pH 5.5 (5 x 40 μL). The concentration of reduced Fab was calculated. Tetrazine thioester **7c** (150 mM in DMF, 50 eq.) was added and the reaction mixture was incubated for 5 min at 22 ºC, 300 rpm. Prepared tetrazine thioester conjugate (50 μL, 100 μM) was washed *via* ultrafiltration 10 kDa MWCO) into conjugation buffer at pH 5.5 (1 x 100 μL). The concentration of the tetrazine thioester conjugate was calculated. FAM-PEG3-BCN (20 mM in DMSO, 10 eq.) was added, and the reaction further incubated for 10 min at 22 ºC, 300 rpm. The sample was purified by ZebaSpin for LCMS analysis.

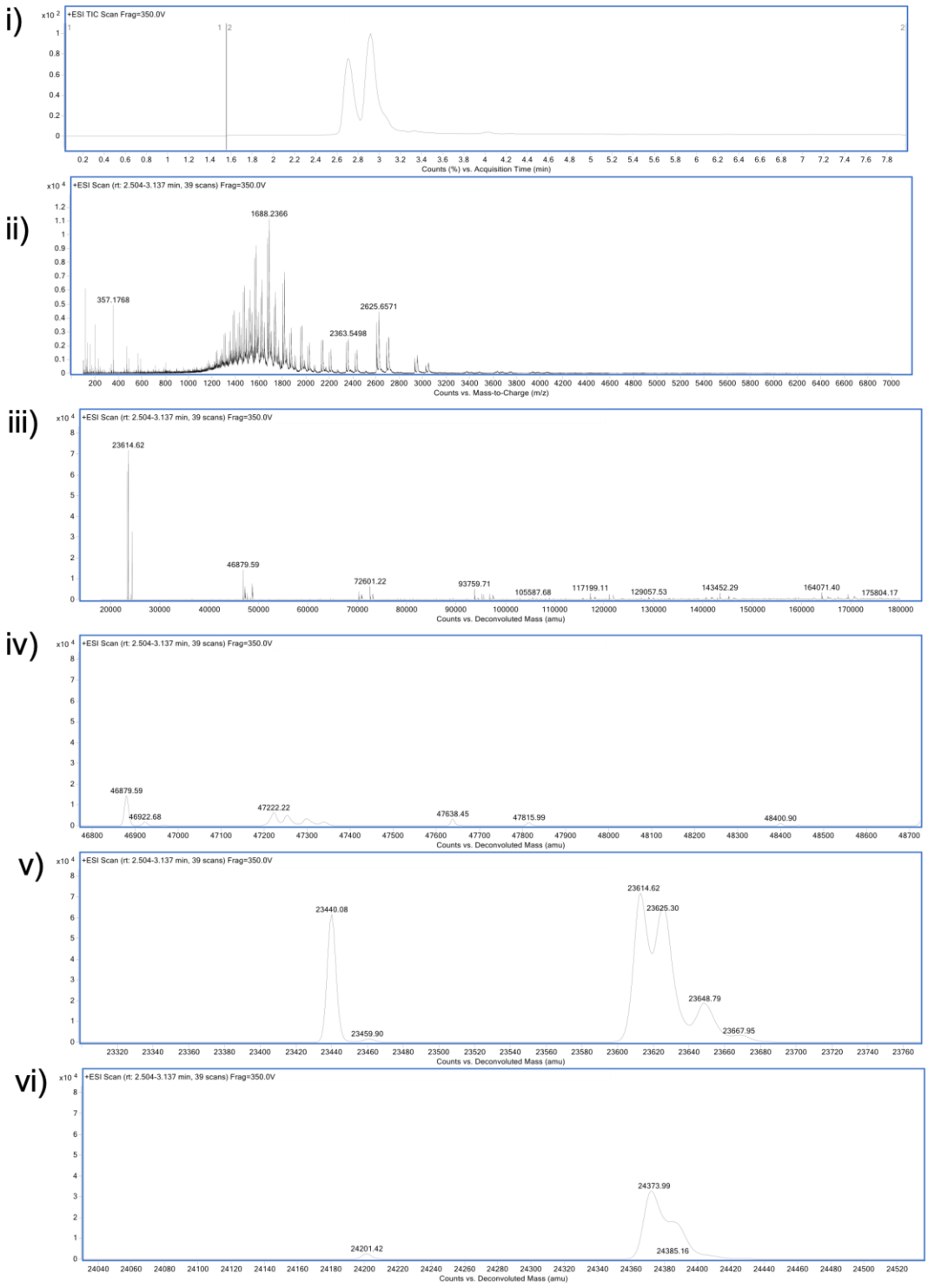


**FIGURE S.28.** LCMS analysis of tetrazine thioester conjugate followed by iEDDA with FAM-PEG3-BCN. i) TIC. ii) non-convoluted ion series. iii) full range of deconvoluted ion series. iv), v), and vi) zoomed in of deconvoluted ion series. Expected mass of tetrazine-iEDDA conjugate: 47638 Da (native, 0), 48521 Da (1 addition), 49404 Da (2 addition) Observed: LC 23440 Da, modified LC 23614 Da, modified LC 23625 Da, HC modified 24373 Da, HC modified 24383 Da.

**Tetrazine thioester conjugate iEDDA with FAM-PEG3-BCN at pH 7.4**

To Fab (20.0 μL, 0.0030 μmol, 150 μM, 7.15 mg/mL) in conjugation buffer was added TCEP (0.200 μL, 0.030 μmol, 150 mM in $dH_2O$, 10 eq.). After mixing for 1.5 h at 37 ºC, 300 rpm, TCEP was removed by ultrafiltration (10 kDa MWCO) with conjugation buffer at pH 7.4 (5 x 40 μL). The concentration of reduced Fab was calculated. Tetrazine thioester **7c** (150 mM in DMF, 50 eq.) was added and the reaction mixture was incubated for 1 min at 22 ºC, 300 rpm. Prepared tetrazine thioester conjugate (50 μL, 100 μM) was washed *via* ultrafiltration 10 kDa MWCO) into conjugation buffer at pH 7.4 (1 x 100 μL). The concentration of the tetrazine thioester conjugate was calculated. FAM-PEG3-BCN (20 mM in DMSO, 10 eq.) was added, and the reaction further incubated for 10 min at 22 ºC, 300 rpm. The sample was submitted for LCMS analysis by preparation.

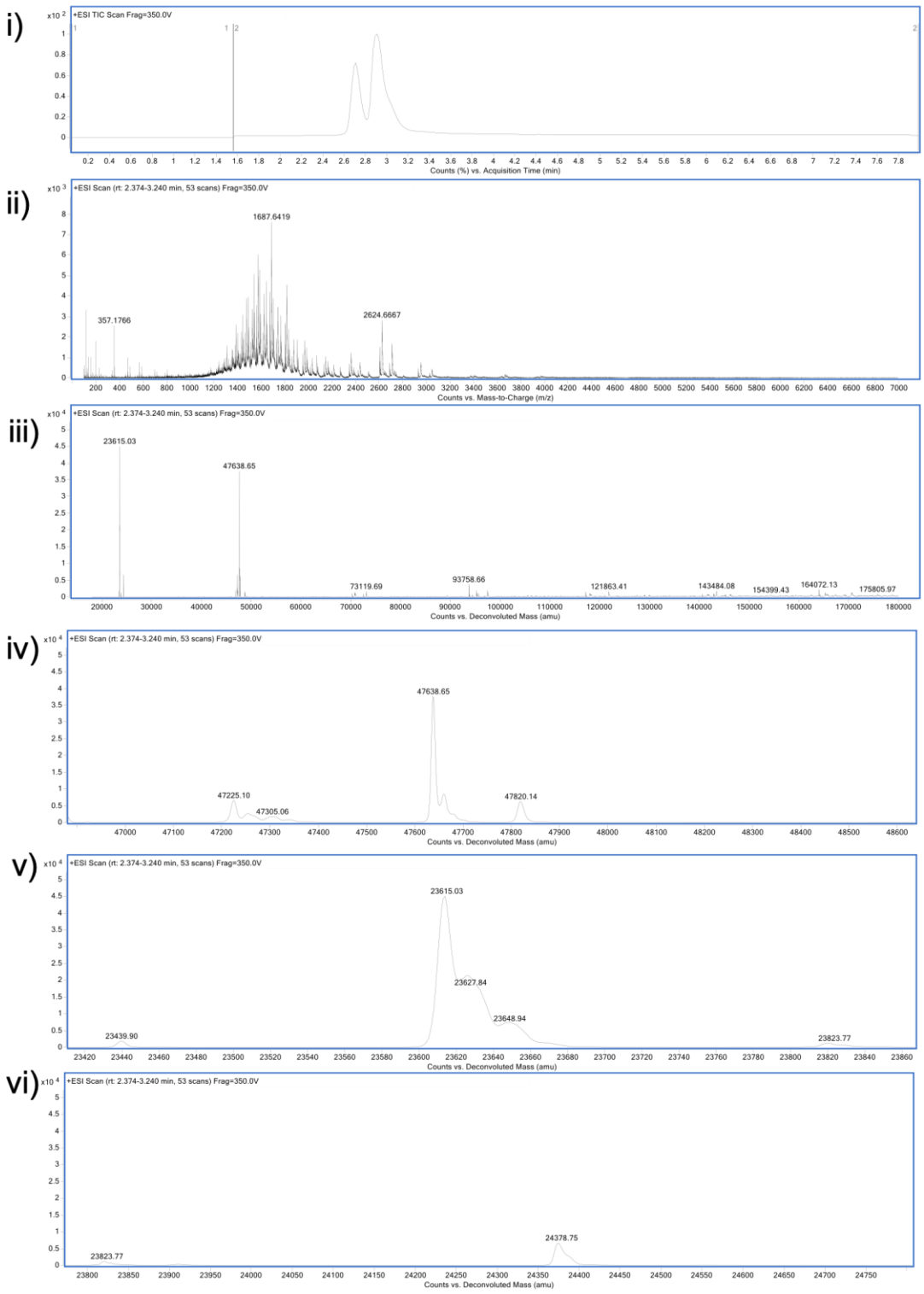


**FIGURE S.29.** LCMS analysis of tetrazine thioester conjugate followed by iEDDA with FAM-PEG3-BCN at pH 7.4. i) TIC. ii) non-convoluted ion series. iii) full range of deconvoluted ion series. iv), v), and vi) zoomed in of deconvoluted ion series. Expected mass of tetrazine-iEDDA conjugate: 47638 Da (native, 0), 48521 Da (1 addition), 49404 Da (2 addition) Observed: 47638 Da, LC 23440 Da, modified LC 23615 Da, modified LC 23627 Da, modified HC 24378 Da.

**Alkyl thiocarbonate 9 conjugation on non-reduced Fab (control)**

To Fab (20.0 μL, 0.0030 μmol, 150 μM, 7.15 mg/mL) in conjugation buffer was added alkyl thiocarbonate **9** (2.00 μL, 0.300 μmol, 150 mM in DMF, 100 eq.). The sample was incubated for 4 h at 22 ºC, 300 rpm. The excess reagent was removed *via* ultrafiltration (10 kDa MWCO) into LCMS water, and the sample was purified by ZebaSpin for LCMS analysis.

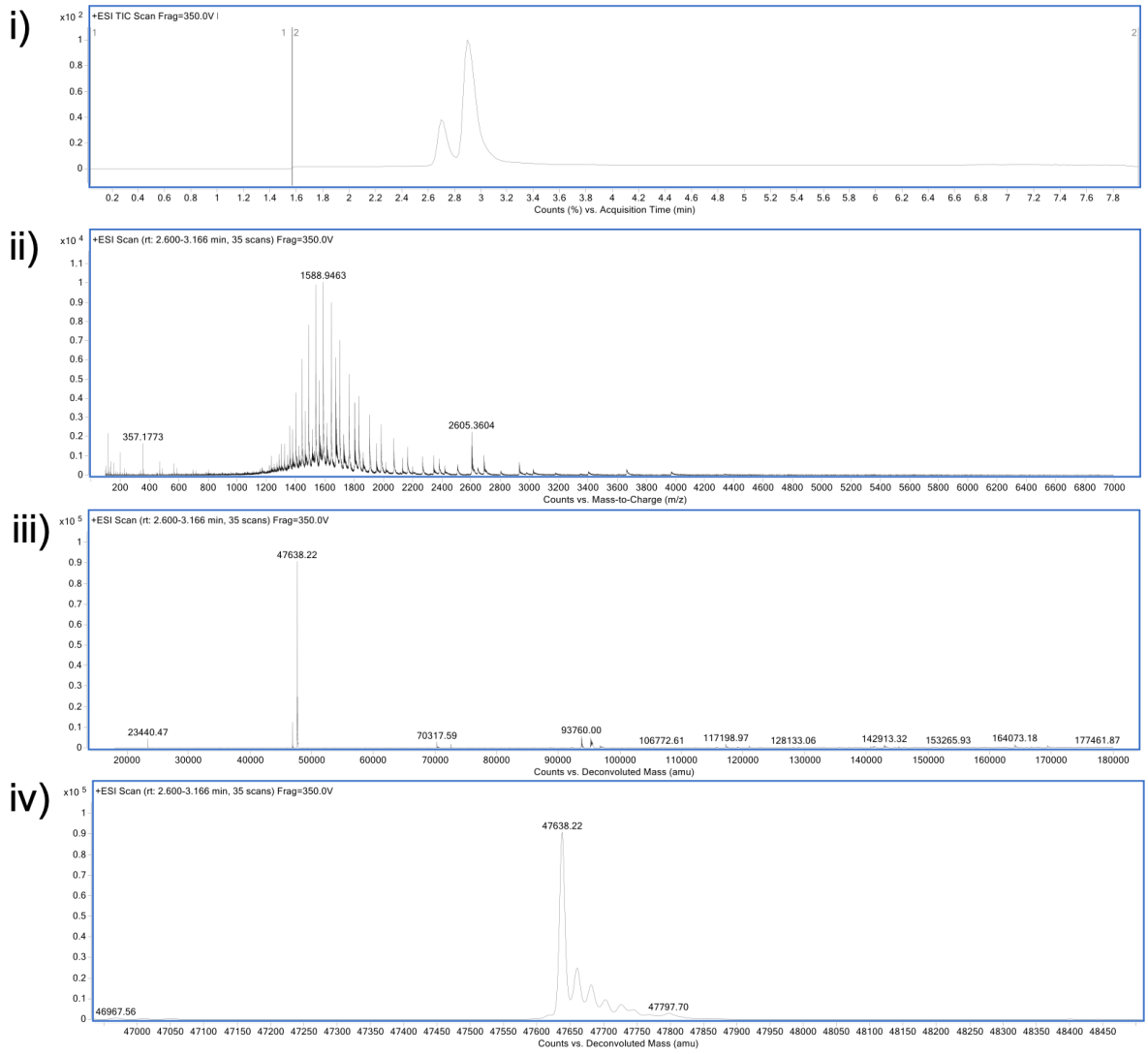


**FIGURE S.30.** LCMS analysis of alkyl thiocarbonate **9** control on native Fab. i) TIC. ii) non-convoluted ion series. iii) full range of deconvoluted ion series. iv) zoomed in of deconvoluted ion series. Expected mass of native Fab: 47638 Da. Observed: 47368 Da.

**Alkyl thiocarbonate 9 conjugation on reduced Fab (reaction)**

To Fab (20.0 μL, 0.0030 μmol, 150 μM, 7.15 mg/mL) in conjugation buffer was added TCEP (0.20 μL, 0.030 μmol, 150 mM in $dH_2O$, 10 eq.). After mixing for 1.5 h at 37 ºC, 300 rpm, alkyl thiocarbonate **9** (2.00 μL, 0.300 μmol, 150 mM in DMF, 100 eq.) was added and the reaction mixture was incubated for 4h at 22 ºC, 300 rpm. The excess reagent was removed *via* ultrafiltration (10 kDa MWCO) into LCMS water, and the sample was purified by ZebaSpin for LCMS analysis.

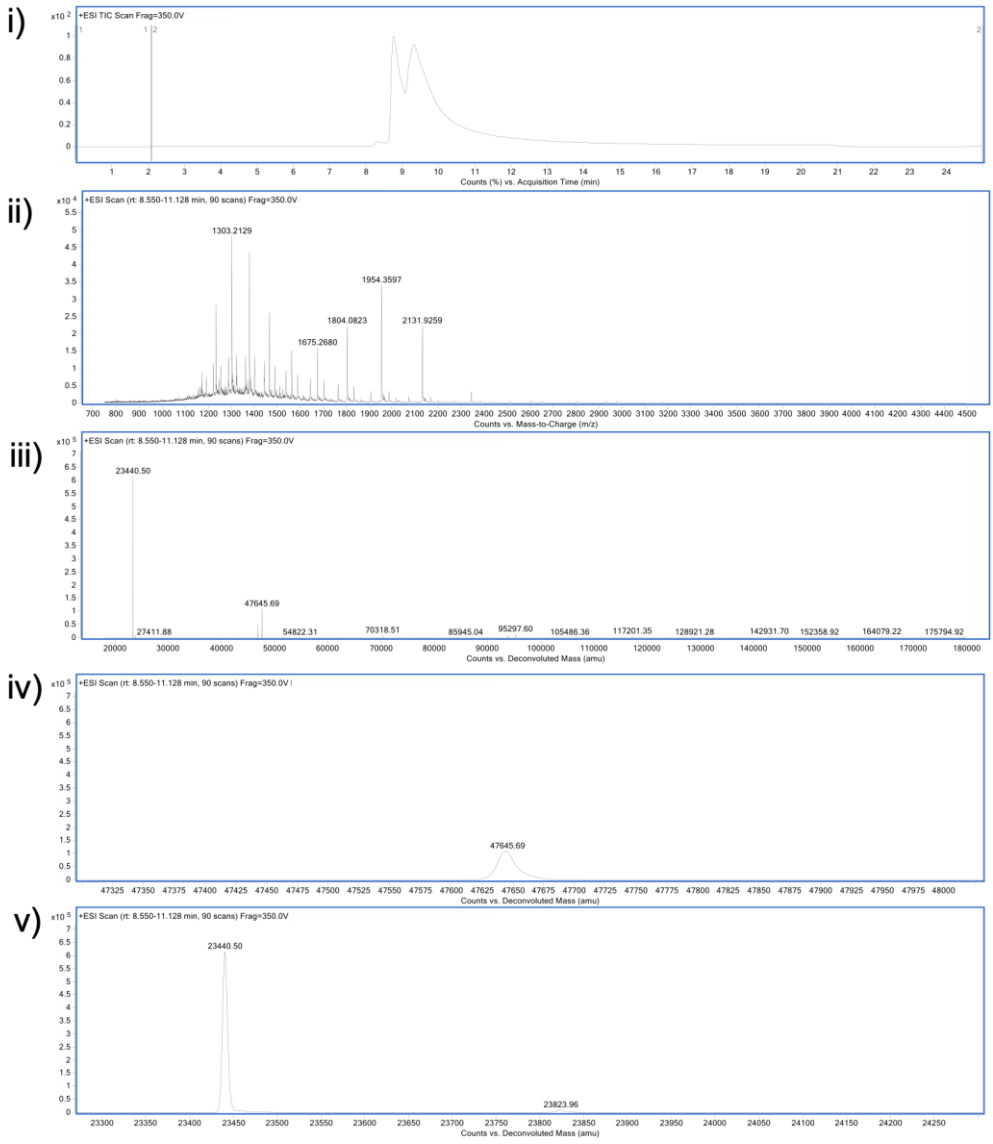


**FIGURE S.31.** LCMS analysis of alkyl thiocarbonate **9** reaction on reduced Fab. i) TIC. ii) non-convoluted ion series. iii) full range of deconvoluted ion series. iv) and v) zoomed in of deconvoluted ion series. Expected mass of thiocarbonate conjugate: LC 23523 Da, HC 24284 Da. Observed: LC 23439 Da. Mass of alkyl thiocarbonate **9** addition: 84 Da.

**Aryl thiocarbonate 10 conjugation on non-reduced Fab (control)**

To Fab (20.0 μL, 0.0030 μmol, 150 μM, 7.15 mg/mL) in conjugation buffer was added aryl thiocarbonate **10** (2.00 μL, 0.300 μmol, 150 mM in DMF, 100 eq.). The sample was incubated for 4 h at 22 ºC, 300 rpm. The excess reagent was removed *via* ultrafiltration (10 kDa MWCO) into LCMS water, and the sample was purified by ZebaSpin for LCMS analysis.

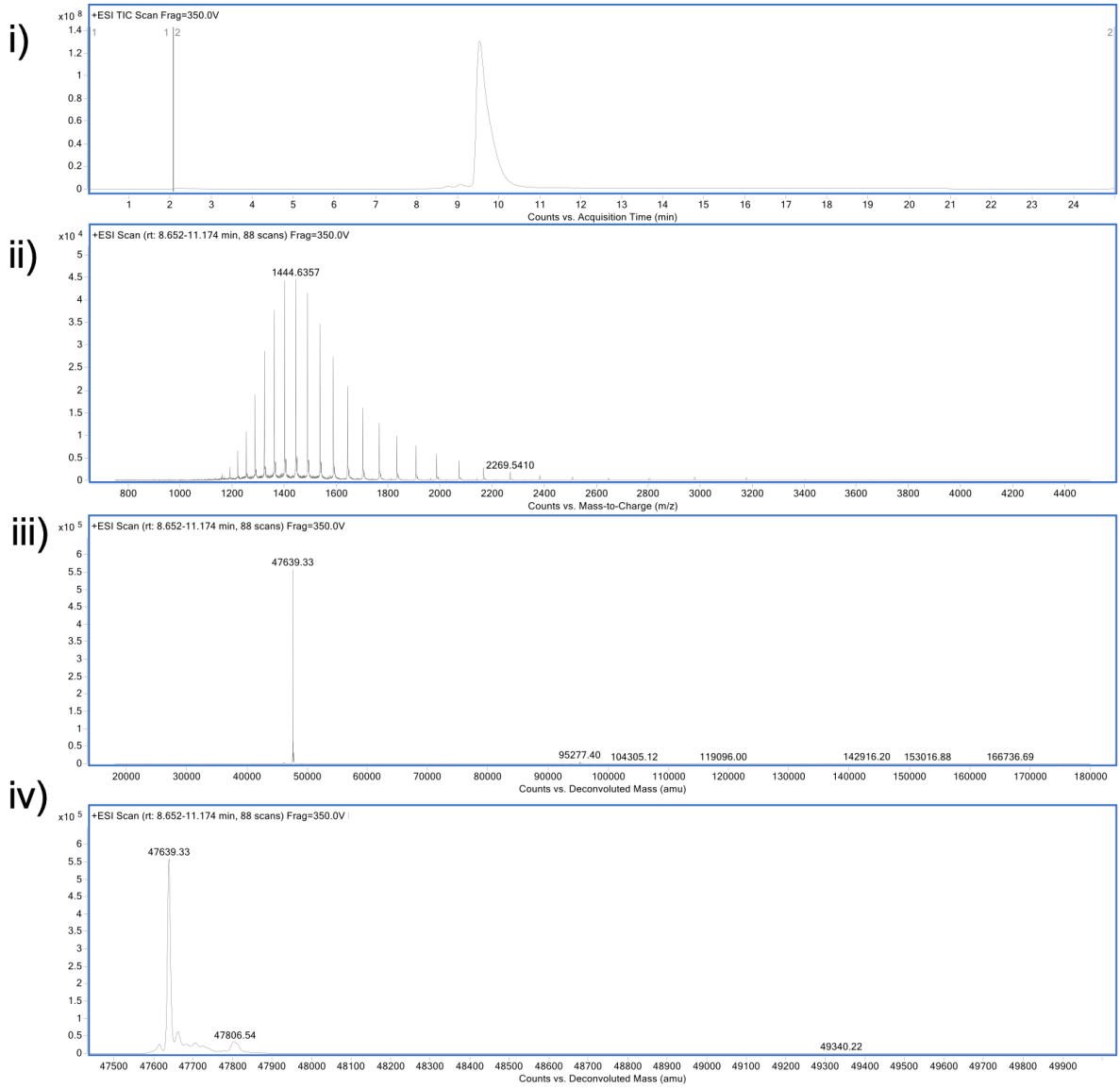


**FIGURE S.32.** LCMS analysis of aryl thiocarbonate **10** control on native Fab. i) TIC. ii) non-convoluted ion series. iii) full range of deconvoluted ion series. iv) zoomed in of deconvoluted ion series. Expected mass of native Fab: 47638 Da. Observed: 47369 Da.

**Aryl thiocarbonate 10 conjugation on reduced Fab (reaction)**

To Fab (20.0 μL, 0.0030 μmol, 150 μM, 7.15 mg/mL) in conjugation buffer was added TCEP (0.20 μL, 0.030 μmol, 150 mM in $dH_2O$, 10 eq.). After mixing for 1.5 h at 37 ºC, 300 rpm, aryl thiocarbonate **10** (2.00 μL, 0.300 μmol, 150 mM in DMF, 100 eq.) was added and the reaction mixture was incubated for 4 h at 22 ºC, 300 rpm. The excess reagent was removed *via* ultrafiltration (10 kDa MWCO) into LCMS water, and the sample was purified by ZebaSpin for LCMS analysis.

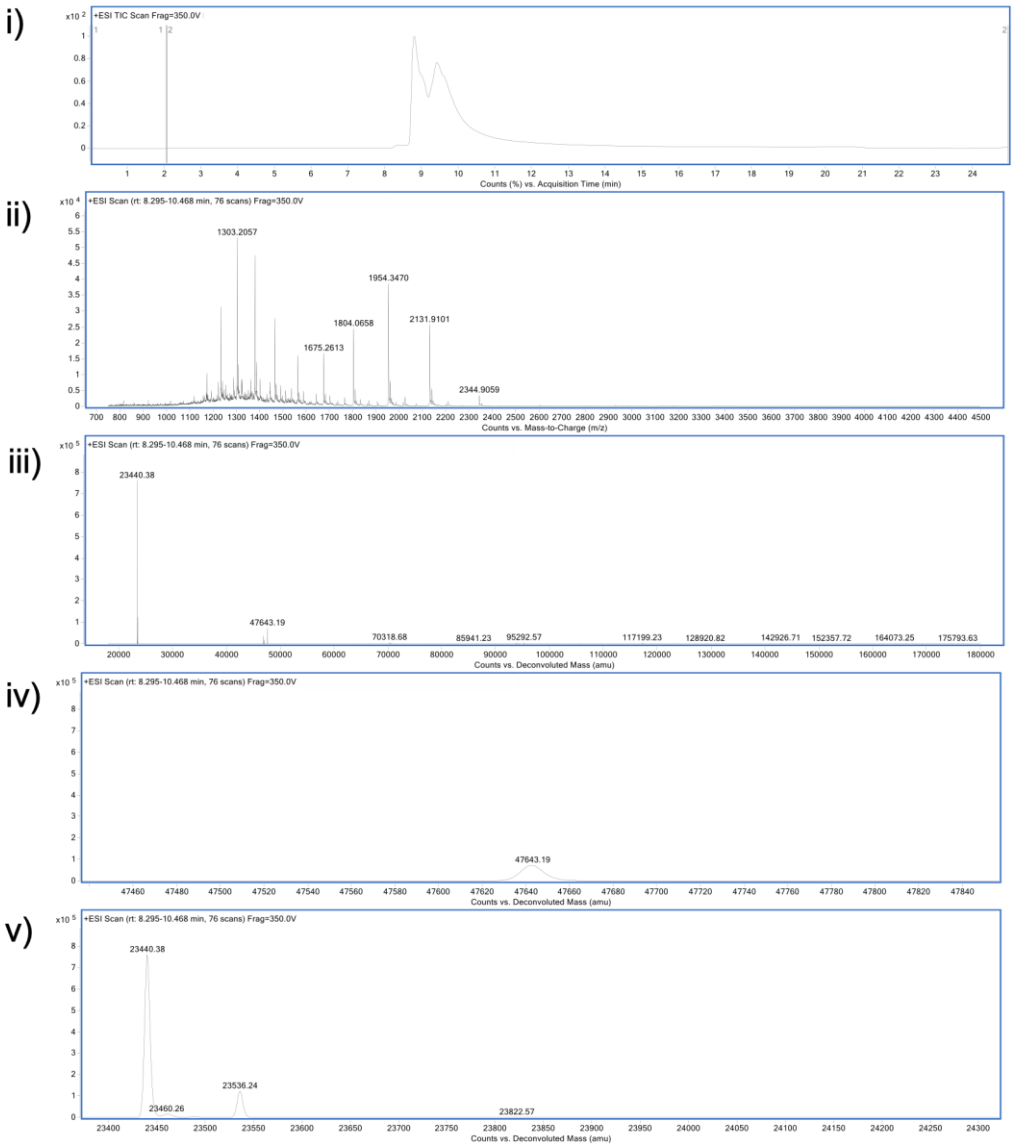


**FIGURE S.33.** LCMS analysis of aryl thiocarbonate **10** reaction on reduced Fab. i) TIC. ii) non-convoluted ion series. iii) full range of deconvoluted ion series. iv) and v) zoomed in of deconvoluted ion series. Expected mass of thiocarbonate conjugate: LC 23523 Da, HC 24284 Da. Observed: LC 23440 Da, modified LC 23536 Da. Mass of aryl thiocarbonate **10** addition: 84 Da.

**Alkyl thiocarbonate 9 conjugation on non-reduced Fab at pH 8.4 (control)**

To Fab (20.0 μL, 0.0030 μmol, 150 μM, 7.15 mg/mL) in BBS at pH 8.4 was added alkyl thiocarbonate **9** (2.00 μL, 0.300 μmol, 150 mM in DMF, 100 eq.). The sample was incubated for 4 h at 22 ºC, 300 rpm. The excess reagent was removed *via* ultrafiltration (10 kDa MWCO) into LCMS water, and the sample was purified by ZebaSpin for LCMS analysis.

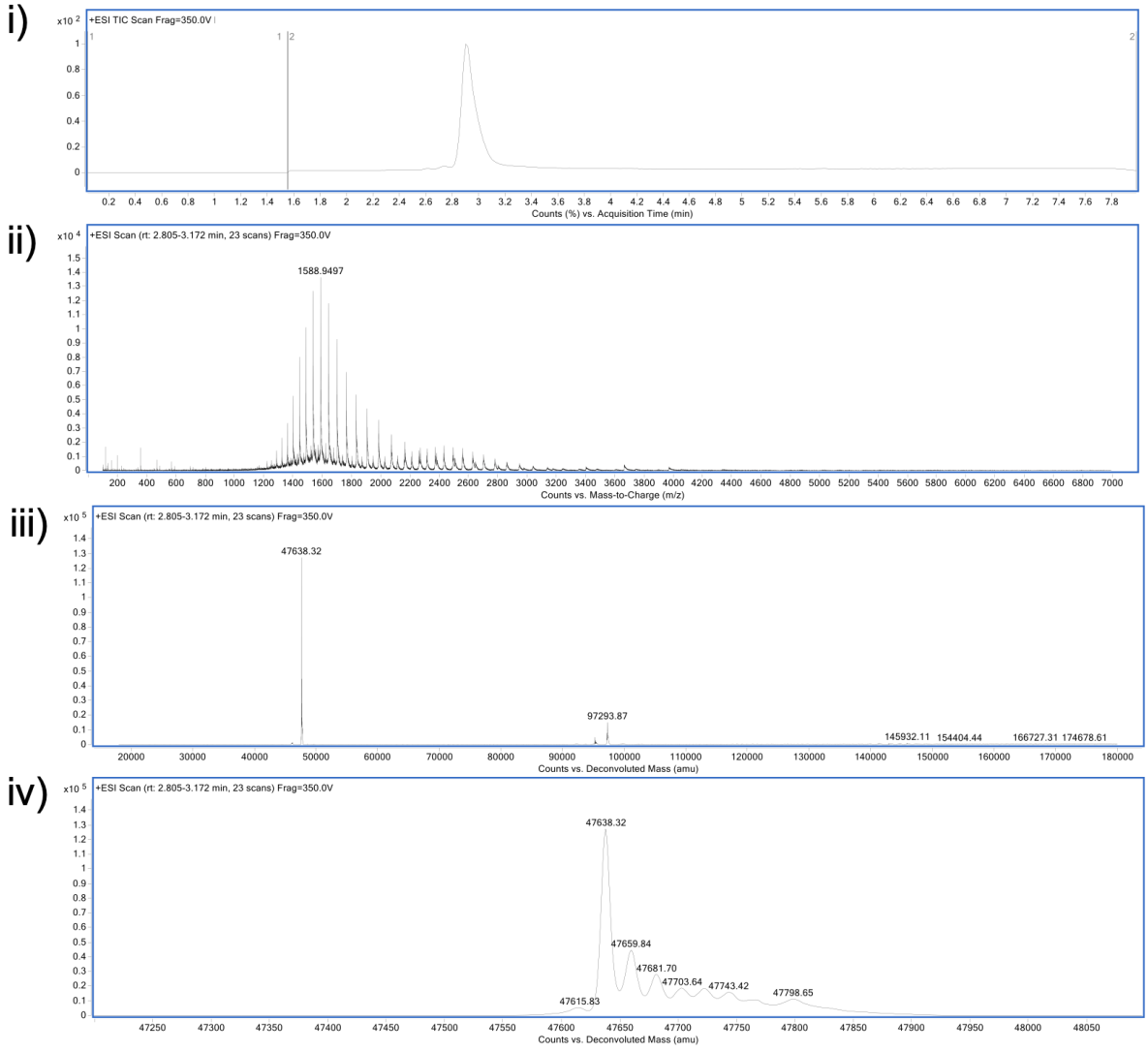


**FIGURE S.34.** LCMS analysis of alkyl thiocarbonate **9** control on native Fab at pH 8.4. i) TIC. ii) non-convoluted ion series. iii) full range of deconvoluted ion series. iv) zoomed in of deconvoluted ion series. Expected mass of native Fab: 47638 Da. Observed: 47368 Da.

**Aryl thiocarbonate 10 conjugation on non-reduced Fab at pH 8.4 (control)**

To Fab (20.0 μL, 0.0030 μmol, 150 μM, 7.15 mg/mL) in BBS at pH 8.4 was added aryl thiocarbonate **10** (2.00 μL, 0.300 μmol, 150 mM in DMF, 100 eq.). The sample was incubated for 4 h at 22 ºC, 300 rpm. The excess reagent was removed *via* ultrafiltration (10 kDa MWCO) into LCMS water, and the sample was purified by ZebaSpin for LCMS analysis.

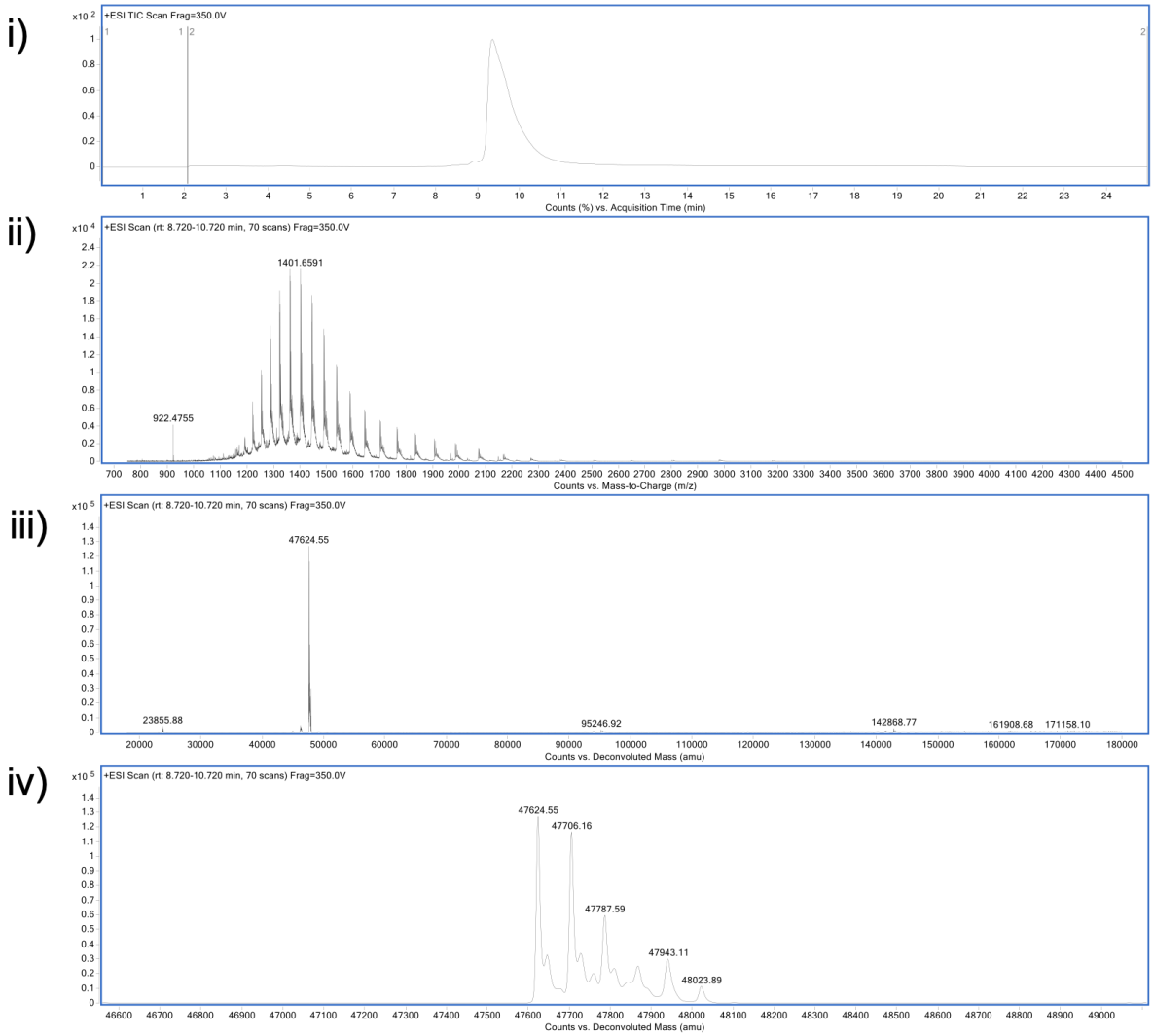


**FIGURE S.35.** LCMS analysis of aryl thiocarbonate **10** control on native Fab at pH 8.4. i) TIC. ii) non-convoluted ion series. iii) full range of deconvoluted ion series. iv) zoomed in of deconvoluted ion series. Expected mass of native Fab: 47638 Da. Observed: 47624 (native, 0 additions), 47706 (1 addition), 47787 (2 additions), 47869 (3 additions), 47943 (4 additions).

**Aryl thiocarbonate 10 conjugation on non-reduced Fab with 10 eq. at pH 8.4 (control)**

To Fab (20.0 μL, 0.0030 μmol, 150 μM, 7.15 mg/mL) in BBS at pH 8.4 was added aryl thiocarbonate **10** (0.20 μL, 0.030 μmol, 150 mM in DMF, 10 eq.). The sample was incubated for 2 h at 22 ºC, 300 rpm. The excess reagent was removed *via* ultrafiltration (10 kDa MWCO) into LCMS water, and the sample was purified by ZebaSpin for LCMS analysis.

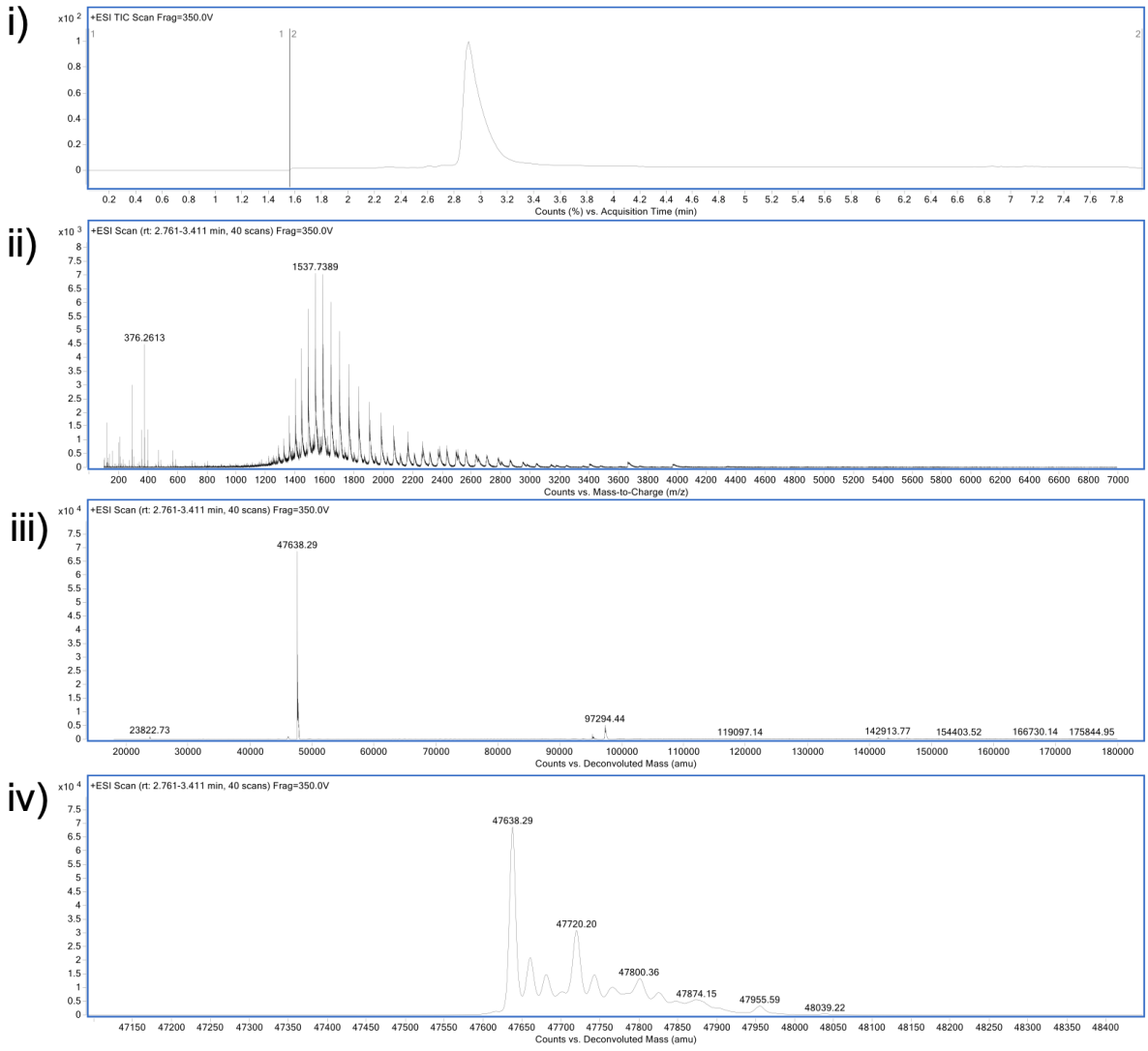


**FIGURE S.36.** LCMS analysis of aryl thiocarbonate **10** control on native Fab at pH 8.4 with 10 eq. reagent. i) TIC. ii) non-convoluted ion series. iii) full range of deconvoluted ion series. iv) zoomed in of deconvoluted ion series. Expected mass of native Fab: 47638 Da. Observed: 47638 (native, 0 additions), 47720 (1 addition).

**Aryl thiocarbonate 10 conjugation on reduced Fab with 10 eq. at pH 8.4 (reaction)**

To Fab (20.0 μL, 0.0030 μmol, 150 μM, 7.15 mg/mL) in BBS at pH 8.4 was added TCEP (0.20 μL, 0.030 μmol, 150 mM in $dH_2O$, 10 eq.). After mixing for 1.5 h at 37 ºC, 300 rpm, aryl thiocarbonate **10** (0.20 μL, 0.030 μmol, 150 mM in DMF, 10 eq.) was added and the reaction mixture was incubated for 2 h at 22 ºC, 300 rpm. The excess reagent was removed *via* ultrafiltration (10 kDa MWCO) into LCMS water, and the sample was purified by ZebaSpin for LCMS analysis.

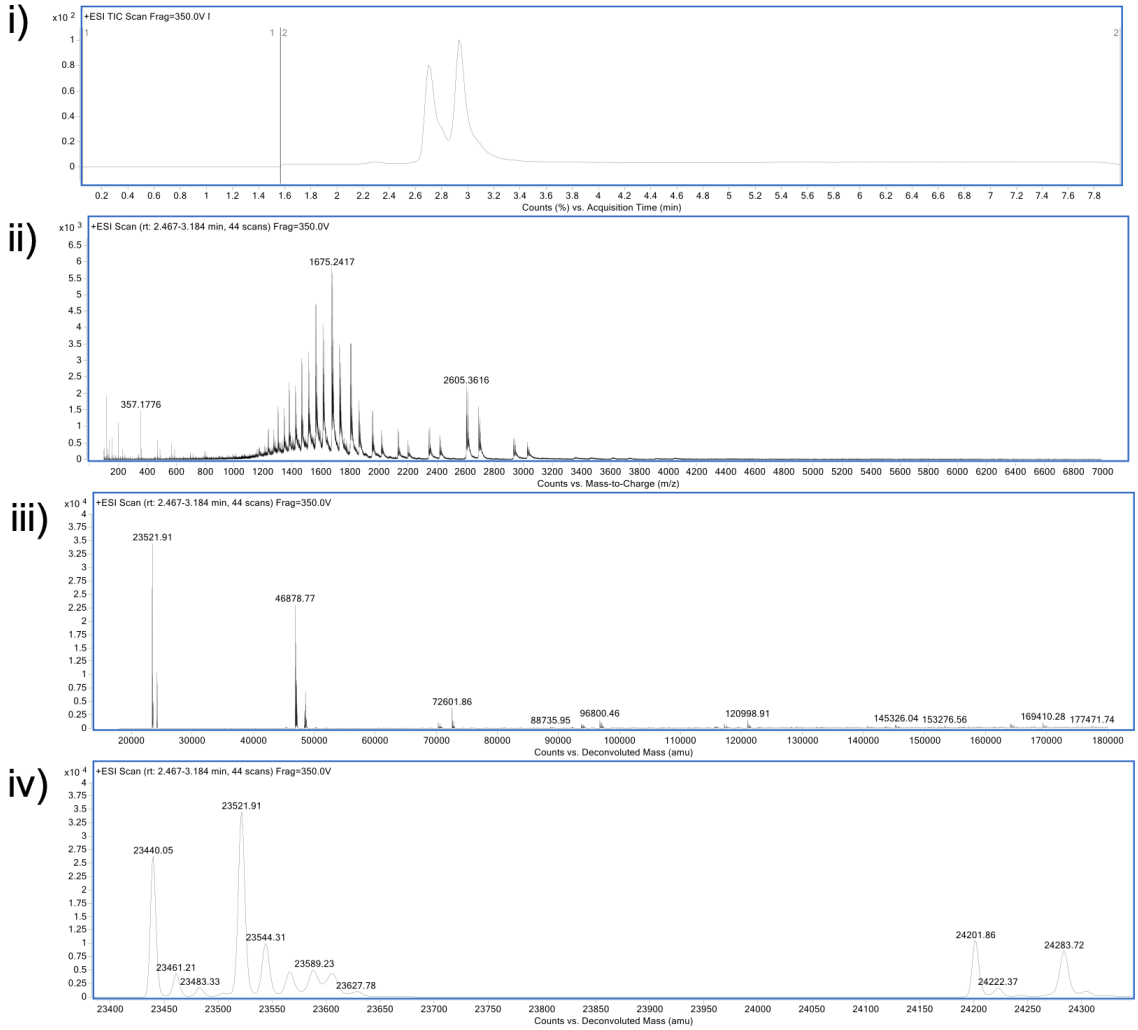


**FIGURE S.37.** LCMS analysis of aryl thiocarbonate **10** reaction on reduced Fab at pH 8.4 with 10 eq. of reagent. i) TIC. ii) non-convoluted ion series. iii) full range of deconvoluted ion series. iv) zoomed in of deconvoluted ion series. Expected mass of thiocarbonate conjugate: LC 23523 Da, HC 24284 Da. Observed: LC 23440 Da, modified LC 23521 Da (1 addition), LC modified 23605 Da (2 additions), HC 24201 Da, modified HC 24283 (1 addition). Mass of aryl thiocarbonate **10** addition: 84 Da.

**Alkyl thiocarbamate 11 conjugation on non-reduced Fab (control) with 20 eq.**

To Fab (20.0 μL, 0.0030 μmol, 150 μM, 7.15 mg/mL) in conjugation buffer was added alkyl thiocarbamate **11** (0.40 μL, 0.060 μmol, 150 mM in DMF, 20 eq.). The sample was incubated for 4 h at 22 ºC, 300 rpm. The excess reagent was removed *via* ultrafiltration (10 kDa MWCO) into LCMS water, and the sample was purified by ZebaSpin for LCMS analysis.

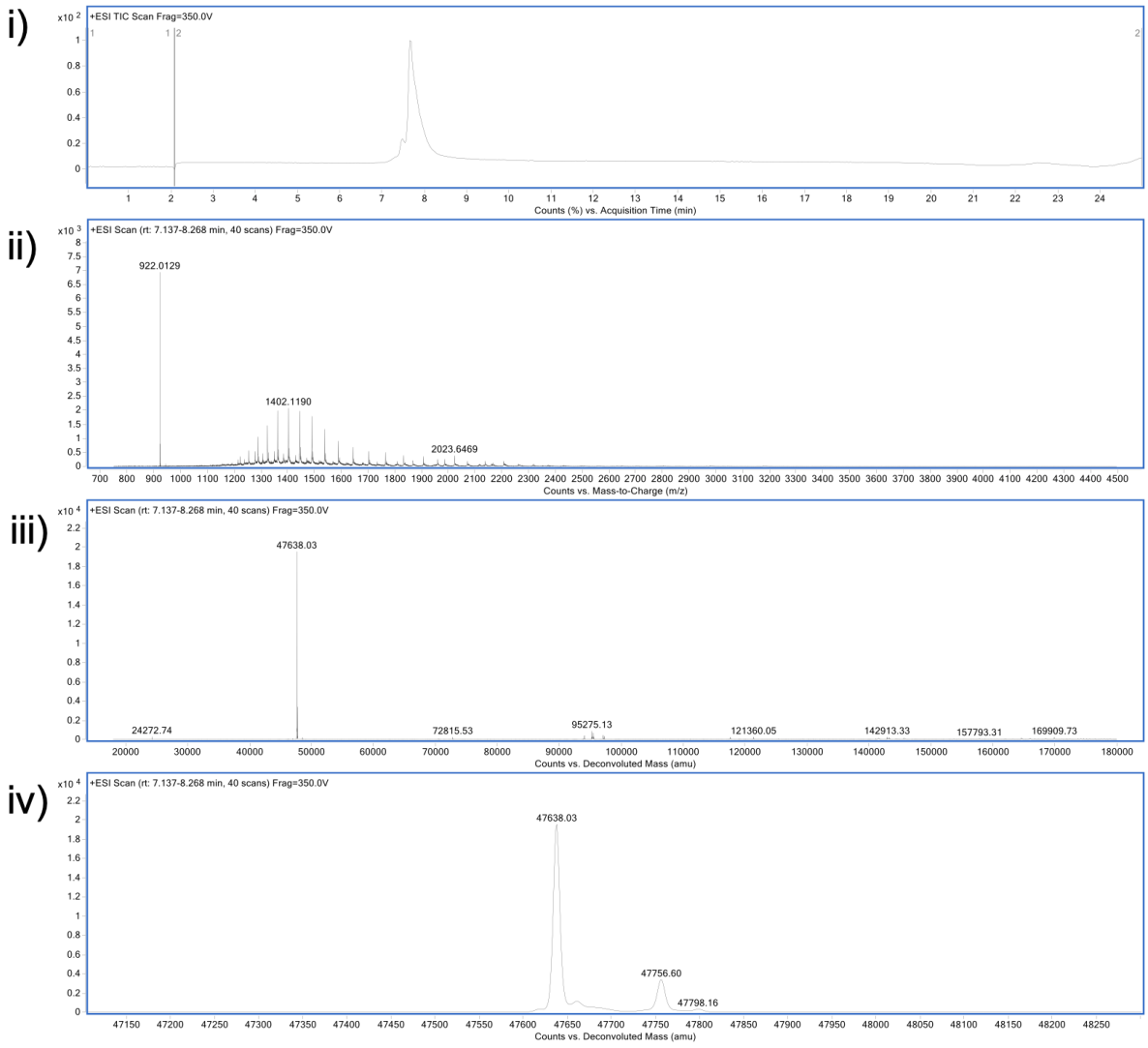


**FIGURE S.38.** LCMS analysis of alkyl thiocarbamate **11** control on native Fab. i) TIC. ii) non-convoluted ion series. iii) full range of deconvoluted ion series. iv) zoomed in of deconvoluted ion series. Expected mass of native Fab: 47638 Da. Observed: 47368 Da, 47756 Da (1 addition).

**Alkyl thiocarbamate 11 conjugation on reduced Fab (reaction) with 20 eq.**

To Fab (20.0 μL, 0.0030 μmol, 150 μM, 7.15 mg/mL) in conjugation buffer was added TCEP (0.20 μL, 0.030 μmol, 150 mM in $dH_2O$, 10 eq.). After mixing for 1.5 h at 37 ºC, 300 rpm, alkyl thiocarbamate **11** (0.40 μL, 0.060 μmol, 150 mM in DMF, 20 eq.) was added and the reaction mixture was incubated for 4 h at 22 ºC, 300 rpm. The excess reagent was removed *via* ultrafiltration (10 kDa MWCO) into LCMS water, and the sample was purified by ZebaSpin for LCMS analysis.

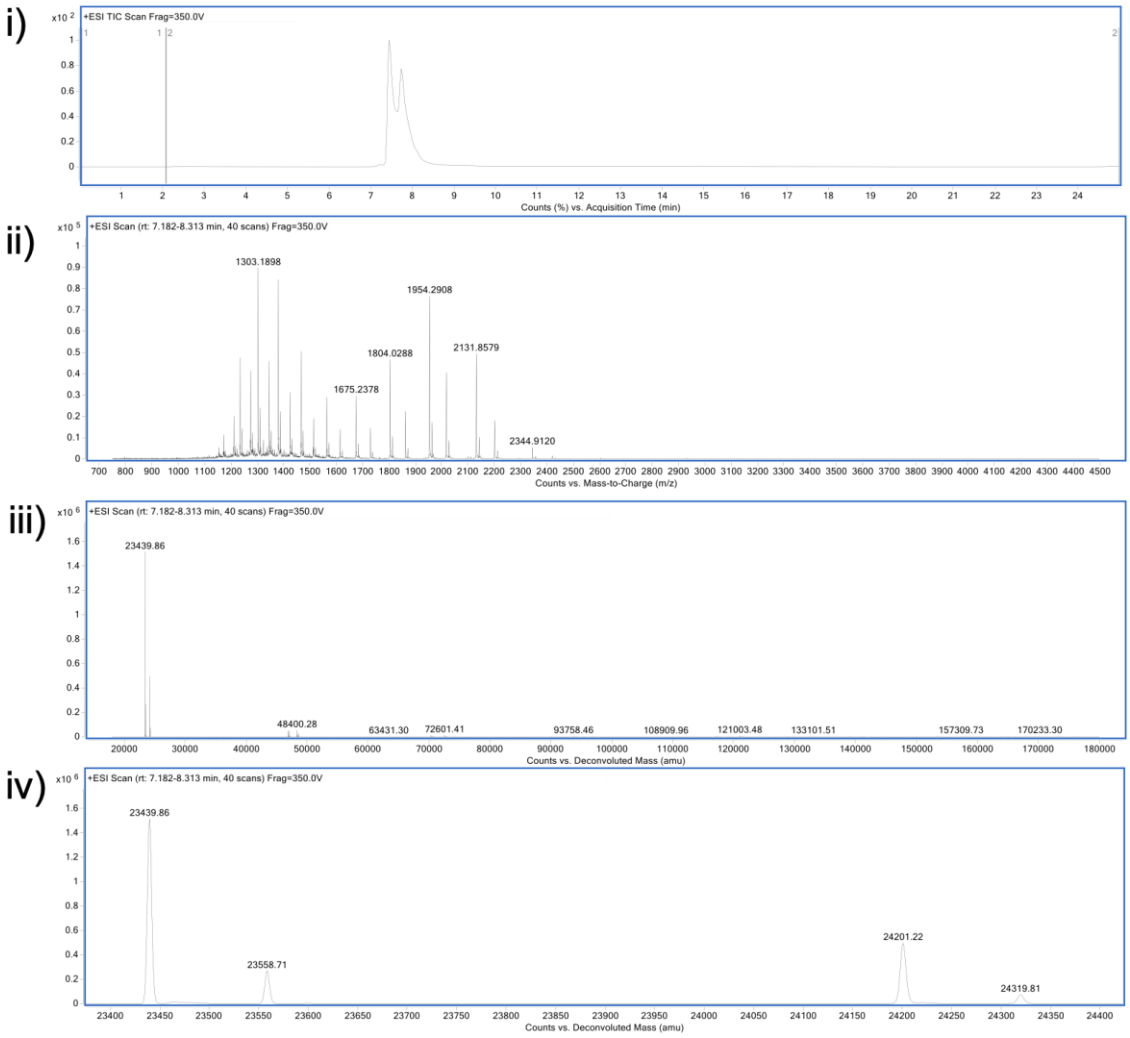


**FIGURE S.39.** LCMS analysis of alkyl thiocarbamate **11** reaction on reduced Fab. i) TIC. ii) non-convoluted ion series. iii) full range of deconvoluted ion series. iv) zoomed in of deconvoluted ion series. Expected mass of thiocarbamate conjugate: LC 23559 Da, HC 24320 Da. Observed: LC 23439 Da, modified 23558 Da (1 addition), HC 24201 Da, modified HC 24319 Da (1 addition). Mass of alkyl thiocarbamate **11** addition: 120.

**Alkyl thiocarbamate 11 conjugation on non-reduced Fab (control) with 50 eq.**

To Fab (20.0 μL, 0.0030 μmol, 150 μM, 7.15 mg/mL) in conjugation buffer was added alkyl thiocarbamate **11** (1.00 μL, 0.150 μmol, 150 mM in DMF, 50 eq.). The sample was incubated for 4 h at 22 ºC, 300 rpm. The excess reagent was removed *via* ultrafiltration (10 kDa MWCO) into LCMS water, and the sample was purified by ZebaSpin for LCMS analysis.

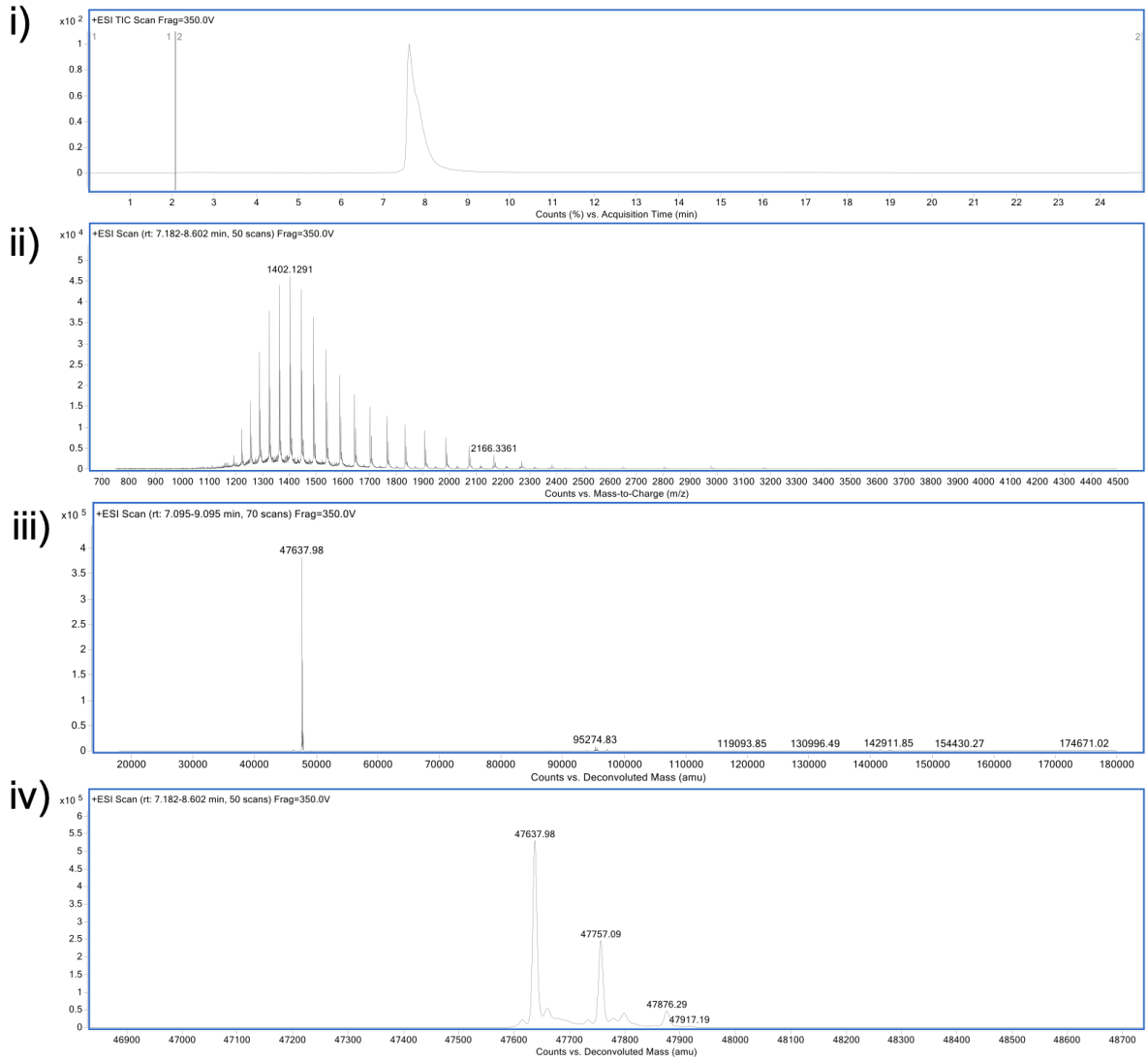


**FIGURE S.40.** LCMS analysis of alkyl thiocarbamate **11** control on native Fab with 50 eq. of reagent. i) TIC. ii) non-convoluted ion series. iii) full range of deconvoluted ion series. iv) zoomed in of deconvoluted ion series. Expected mass of native Fab: 47638 Da. Observed: 47367 Da, 47757 Da (1 addition).

**Alkyl thiocarbamate 11 conjugation on reduced Fab (reaction) with 50 eq.**

To Fab (20.0 μL, 0.0030 μmol, 150 μM, 7.15 mg/mL) in conjugation buffer was added TCEP (0.20 μL, 0.030 μmol, 150 mM in $dH_2O$, 10 eq.). After mixing for 1.5 h at 37 ºC, 300 rpm, alkyl thiocarbamate **11** (1.00 μL, 0.150 μmol, 150 mM in DMF, 50 eq.) was added and the reaction mixture was incubated for 4 h at 22 ºC, 300 rpm. The excess reagent was removed *via* ultrafiltration (10 kDa MWCO) into LCMS water, and the sample was purified by ZebaSpin for LCMS analysis.

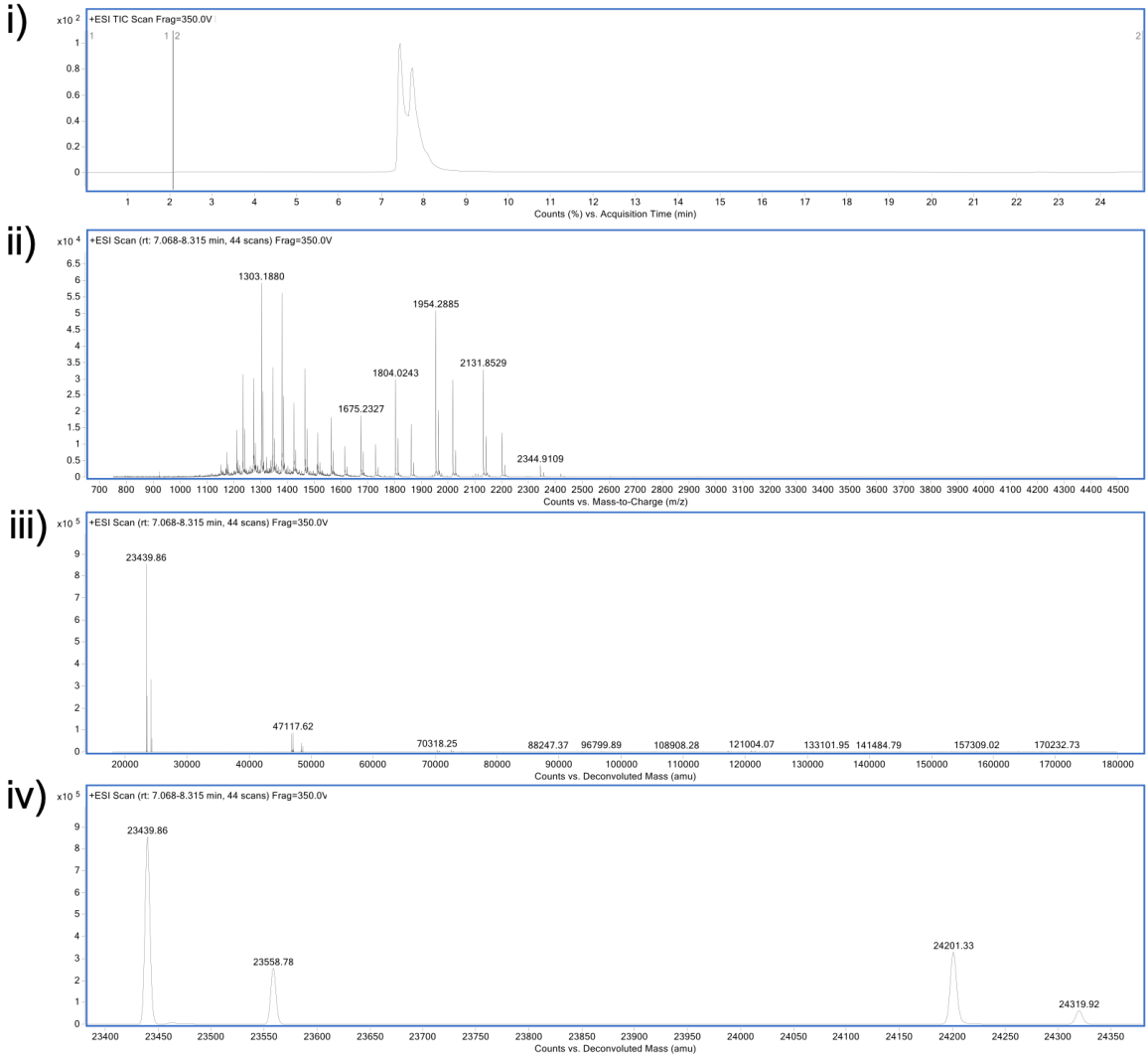


**FIGURE S.41.** LCMS analysis of alkyl thiocarbamate **11** reaction on reduced Fab. i) TIC. ii) non-convoluted ion series. iii) full range of deconvoluted ion series. iv) zoomed in of deconvoluted ion series. Expected mass of thiocarbamate conjugate: LC 23559 Da, HC 24320 Da. Observed: LC 24349 Da, modified 23558 Da (1 addition), HC 24200 Da, modified HC 24319 Da (1 addition). Mass of alkyl thiocarbamate **11** addition: 120 Da.

### *N*-Boc-cysteine addition to carbamate conjugate

Prepared carbamate conjugate (40 μL, 150 μM) was washed *via* ultrafiltration 10 kDa MWCO) into conjugation buffer (5 x 80 μL). The concentration of the carbamate conjugate was calculated. *N*-Boc-cysteine (150 mM in $dH_2O$, 100 eq.) was added, and the reaction mixture was further incubated for 4 at 37 ºC, 300 rpm. The excess reagent was removed *via* ultrafiltration (10 kDa MWCO) into LCMS water, and the sample was purified by ZebaSpin for LCMS analysis.

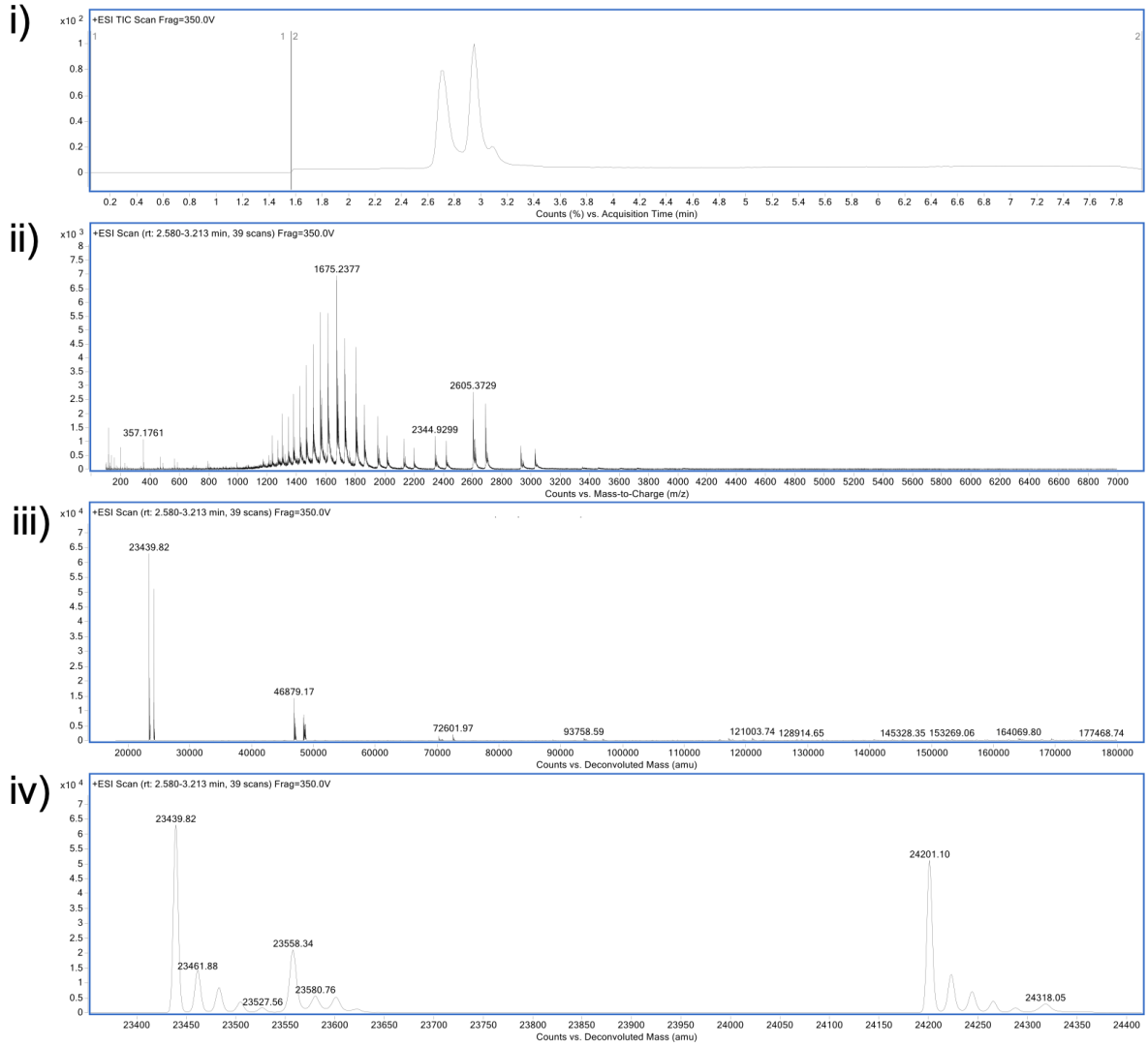


**FIGURE S.42.** LCMS analysis of cysteine addition to carbamate conjugate. i) TIC. ii) non-convoluted ion series. iii) full range of deconvoluted ion series. iv) zoomed in of deconvoluted ion series. Expected mass of thiocarbamate conjugate: LC 23559 Da, HC 24320 Da. Observed: LC 24349 Da, modified LC 23558 Da (1 addition), HC 24201 Da, modified HC 24318 Da (1 addition). Mass of alkyl thiocarbamate **11** addition: 120 Da.

**Aryl thiocarbamate 12 conjugation on non-reduced Fab (control) with 20 eq.**

To Fab (20.0 μL, 0.0030 μmol, 150 μM, 7.15 mg/mL) in conjugation buffer was added aryl thiocarbamate **12** (0.40 μL, 0.060 μmol, 150 mM in DMF, 20 eq.). The sample was incubated for 4 h at 22 ºC, 300 rpm. The excess reagent was removed *via* ultrafiltration (10 kDa MWCO) into LCMS water, and the sample was purified by ZebaSpin for LCMS analysis.

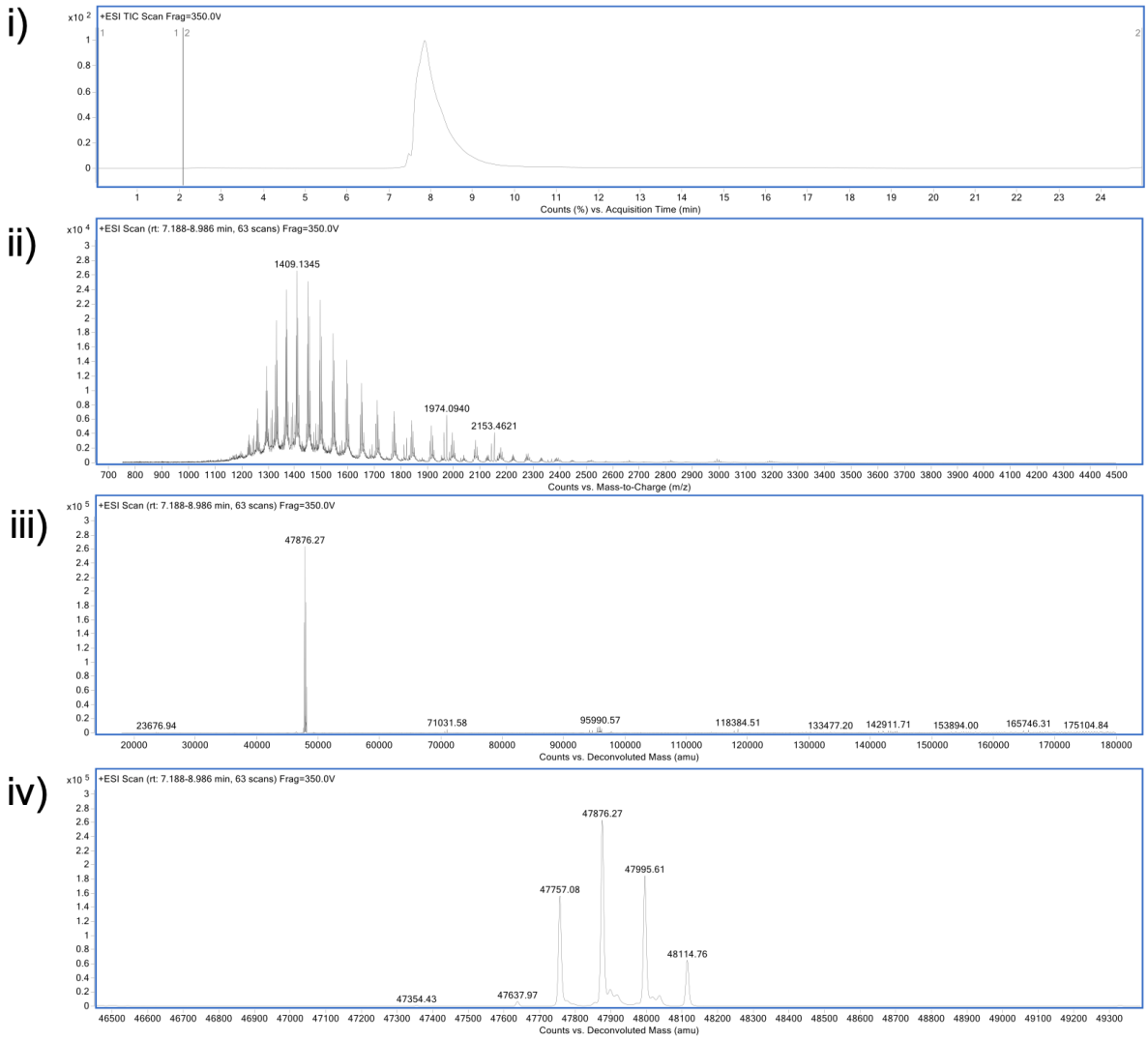


**FIGURE S.43.** LCMS analysis of aryl thiocarbamate **12** control on native Fab. i) TIC. ii) non-convoluted ion series. iii) full range of deconvoluted ion series. iv) zoomed in of deconvoluted ion series. Expected mass of native Fab: 47638 Da. Observed: 47367 Da, 47757 Da (1 addition), 47876 (2 additions), 47995 (3 additions), 48114 (4 additions). Mass of aryl thiocarbamate **12** addition = 120 Da.

**Aryl thiocarbamate 12 conjugation on reduced Fab (control) with 10 eq.**

To Fab (20.0 μL, 0.0030 μmol, 150 μM, 7.15 mg/mL) in conjugation buffer was added aryl thiocarbamate **12** (0.20 μL, 0.030 μmol, 150 mM in DMF, 10 eq.). The sample was incubated for 1 h at 22 ºC, 300 rpm. The excess reagent was removed *via* ultrafiltration (10 kDa MWCO) into LCMS water, and the sample was purified by ZebaSpin for LCMS analysis.

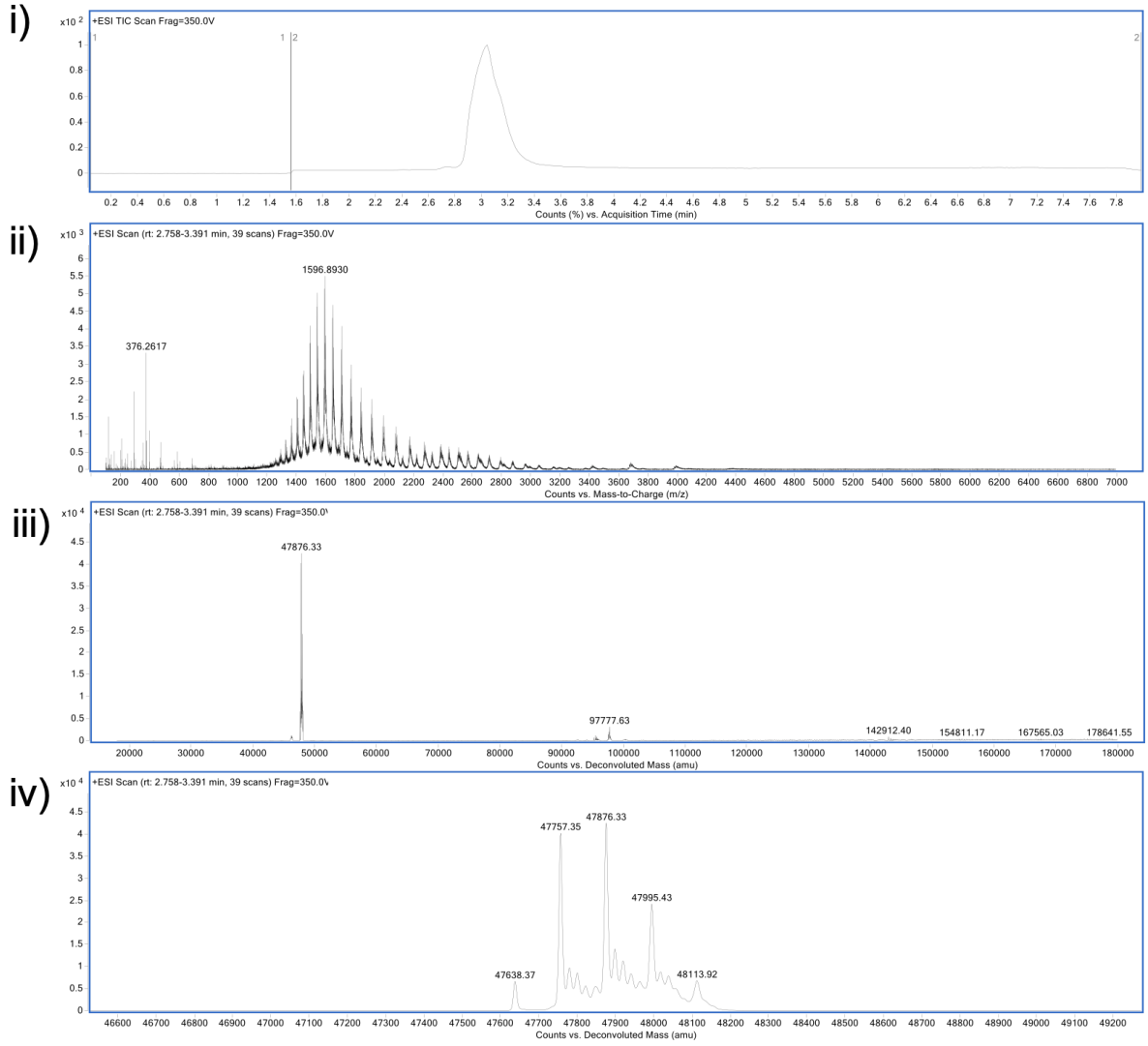


**FIGURE S.44.** LCMS analysis of aryl thiocarbamate **12** control on native Fab using 10 eq. of reagent. i) TIC. ii) non-convoluted ion series. iii) full range of deconvoluted ion series. iv) zoomed in of deconvoluted ion series. Expected mass of native Fab: 47638 Da. Observed: 47368 Da, 47757 Da (1 addition), 47876 (2 additions), 47995 (3 additions), 48113 (4 additions). Mass of aryl thiocarbamate **12** addition = 120 Da.

**Aryl thiocarbamate 12 conjugation on non-reduced Fab (control) at pH 6.0**

To Fab (20.0 μL, 0.0030 μmol, 150 μM, 7.15 mg/mL) in conjugation buffer at pH 6.0 was added aryl thiocarbamate **12** (0.20 μL, 0.030 μmol, 150 mM in DMF, 10 eq.). The sample was incubated for 2 h at 22 ºC, 300 rpm. The excess reagent was removed *via* ultrafiltration (10 kDa MWCO) into LCMS water, and the sample was purified by ZebaSpin for LCMS analysis.

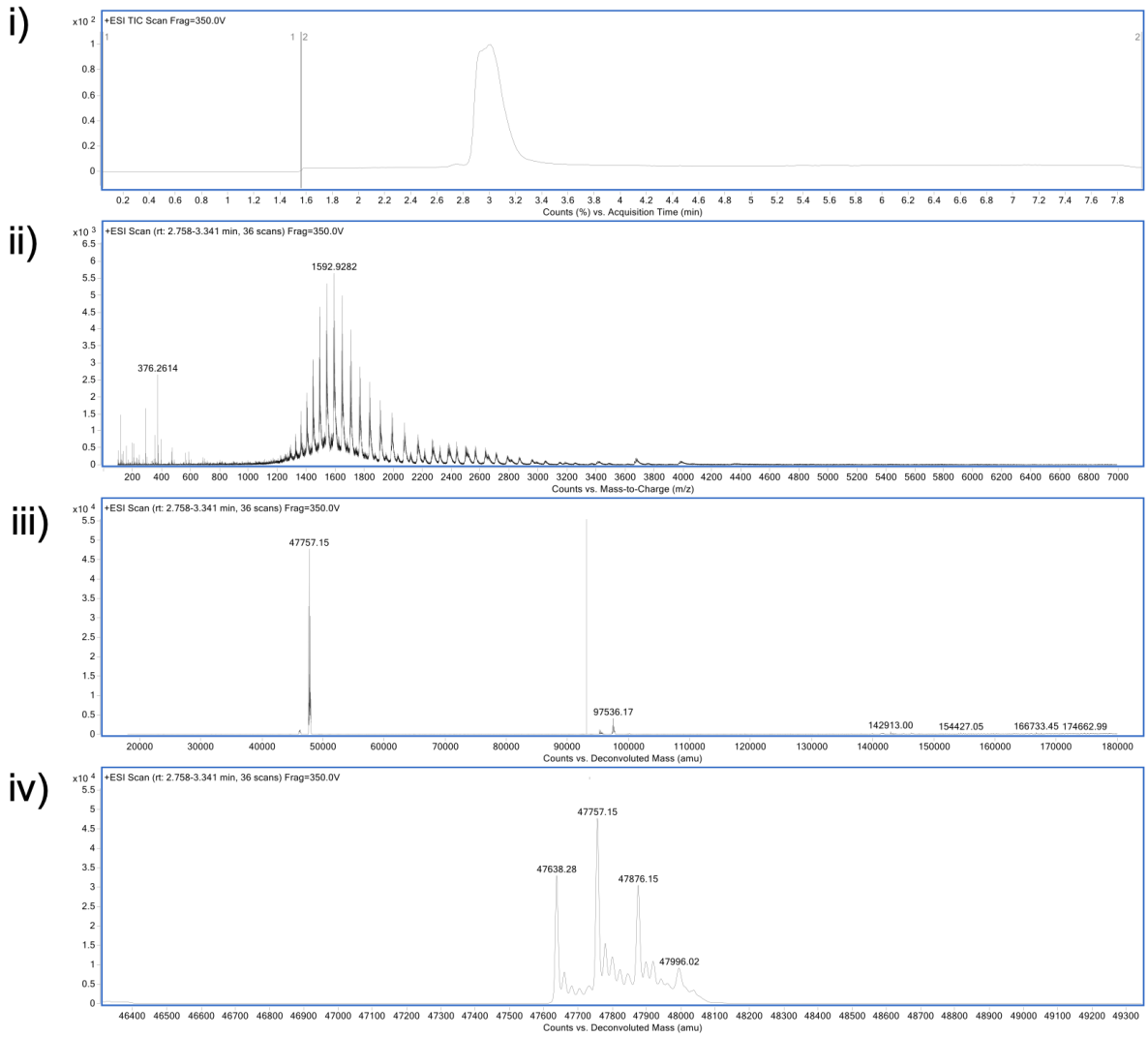


**FIGURE S.45.** LCMS analysis of aryl thiocarbamate **12** control on native Fab using at pH 6.0. i) TIC. ii) non-convoluted ion series. iii) full range of deconvoluted ion series. iv) zoomed in of deconvoluted ion series. Expected mass of native Fab: 47638 Da. Observed: 47368 Da, 47757 Da (1 addition), 47876 (2 additions), 47996 (3 additions). Mass of aryl thiocarbamate **12** addition = 120 Da.

**Aryl thiocarbamate 12 conjugation on reduced Fab (reaction) at pH 6.0**

To Fab (20.0 μL, 0.0030 μmol, 150 μM, 7.15 mg/mL) in conjugation buffer at pH 6.0 was added TCEP (0.20 μL, 0.030 μmol, 150 mM in $dH_2O$, 10 eq.). After mixing for 1.5 h at 37 ºC, 300 rpm, aryl thiocarbamate **12** (0.20 μL, 0.030 μmol, 150 mM in DMF, 10 eq.) was added and the reaction mixture was incubated for 2 h at 22 ºC, 300 rpm. The excess reagent was removed *via* ultrafiltration (10 kDa MWCO) into LCMS water, and the sample was purified by ZebaSpin for LCMS analysis.

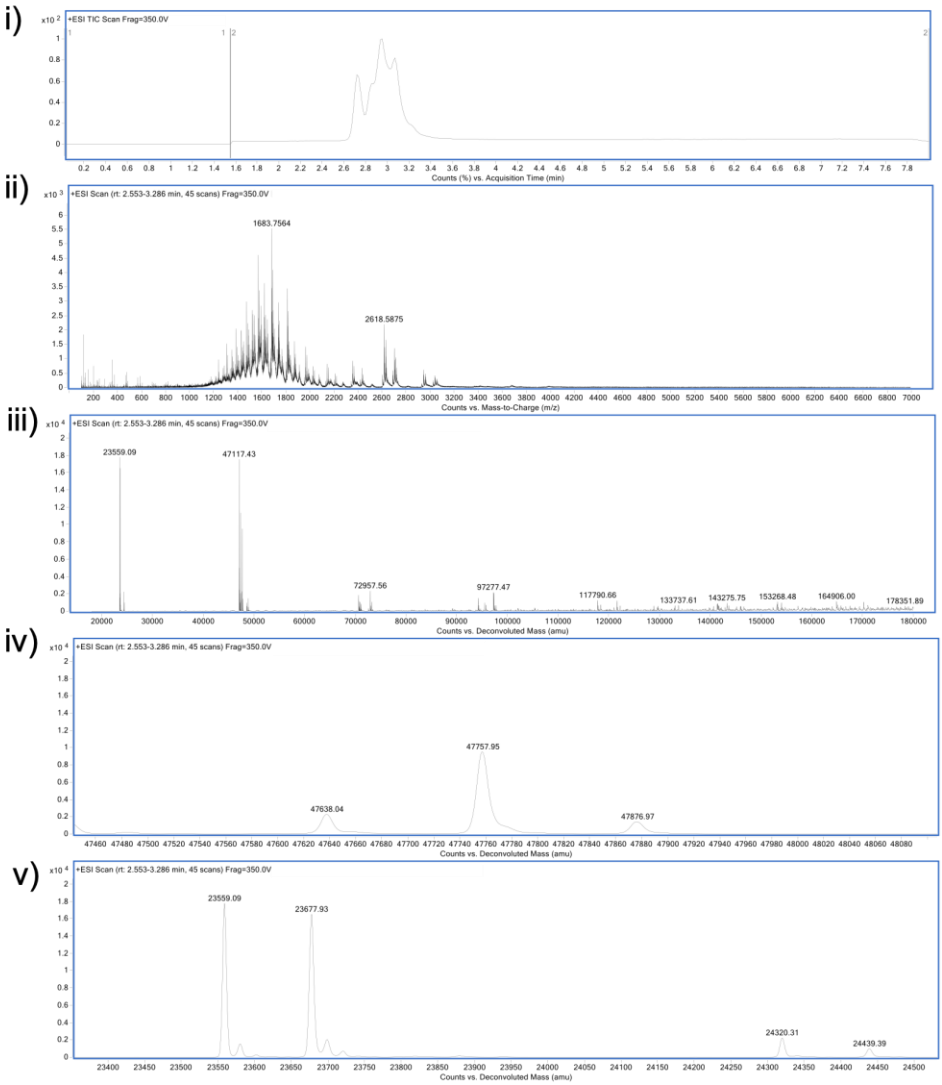


**FIGURE S.46.** LCMS analysis of aryl thiocarbamate **12** control reaction on Fab at pH 6.0. i) TIC. ii) non-convoluted ion series. iii) full range of deconvoluted ion series. iv) and v) zoomed in of deconvoluted ion series. Expected mass of native Fab: 47638 Da. Observed: 47368 Da, 47757 Da (1 addition), 47876 (2 additions), , modified LC 23559 (1 addition), modified LC 23677 (1 addition), modified HC 24320 (1 addition), modified HC 24439 (2 additions). Mass of aryl thiocarbamate **12** addition = 120 Da.

**Alkyl dithiocarbonate 13 re-bridging of Fab**

To Fab (20.0 μL, 0.0030 μmol, 150 μM, 7.15 mg/mL) in conjugation buffer was added TCEP (2.00 μL, 0.030 μmol, 150 mM in $dH_2O$, 10 eq.). After mixing for 1.5 h at 37 ºC, 300 rpm, alkyl dithiocarbonate **13** (0.40 μL, 0.060 μmol, 150 mM in DMF, 20 eq.) was added and the reaction mixture was incubated for 1 h at 22 ºC, 300 rpm. The excess reagent was removed *via* ultrafiltration (10 kDa MWCO) into LCMS water, and the sample was purified by ZebaSpin for LCMS analysis.

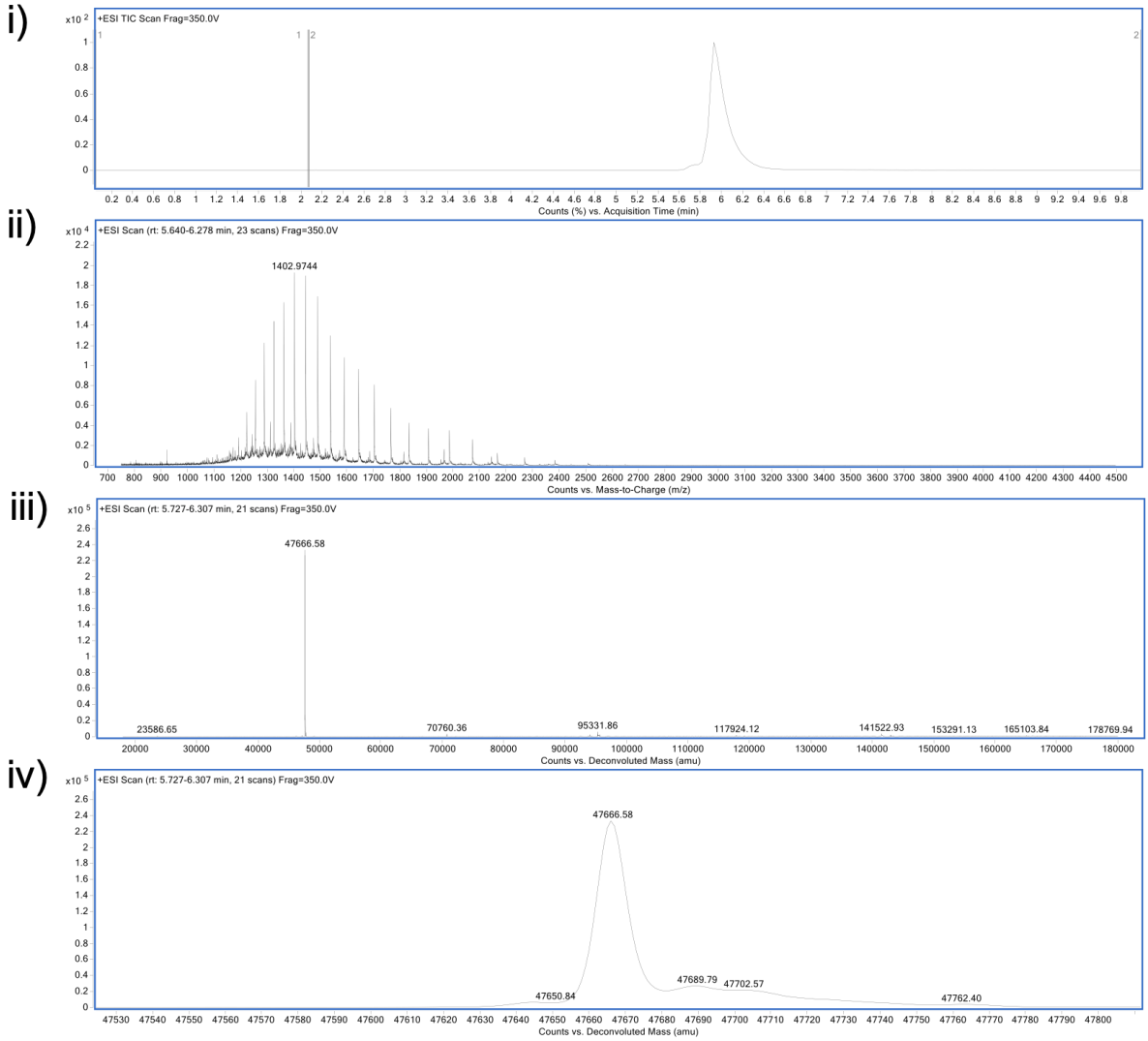


**FIGURE S.47.** LCMS analysis of alkyl dithiocarbonate **13** reaction on reduced Fab. i) TIC. ii) non-convoluted ion series. iii) full range of deconvoluted ion series. iv) zoomed in of deconvoluted ion series. Expected mass of dithiocarbonate conjugate: 47666 Da. Observed: 47666 Da. Mass of dithiocarbonate addition: 28 Da

**Aryl dithiocarbonate 14 re-bridging of Fab**

To Fab (20.0 μL, 0.0030 μmol, 150 μM, 7.15 mg/mL) in conjugation buffer was added TCEP (0.20 μL, 0.030 μmol, 150 mM in $dH_2O$, 10 eq.). After mixing for 1.5 h at 37 ºC, 300 rpm, alkyl dithiocarbonate **14** (0.20 μL, 0.030 μmol, 150 mM in DMF, 10 eq.) was added and the reaction mixture was incubated for 1 h at 22 ºC, 300 rpm. The excess reagent was removed *via* ultrafiltration (10 kDa MWCO) into LCMS water, and the sample was purified by ZebaSpin for LCMS analysis.

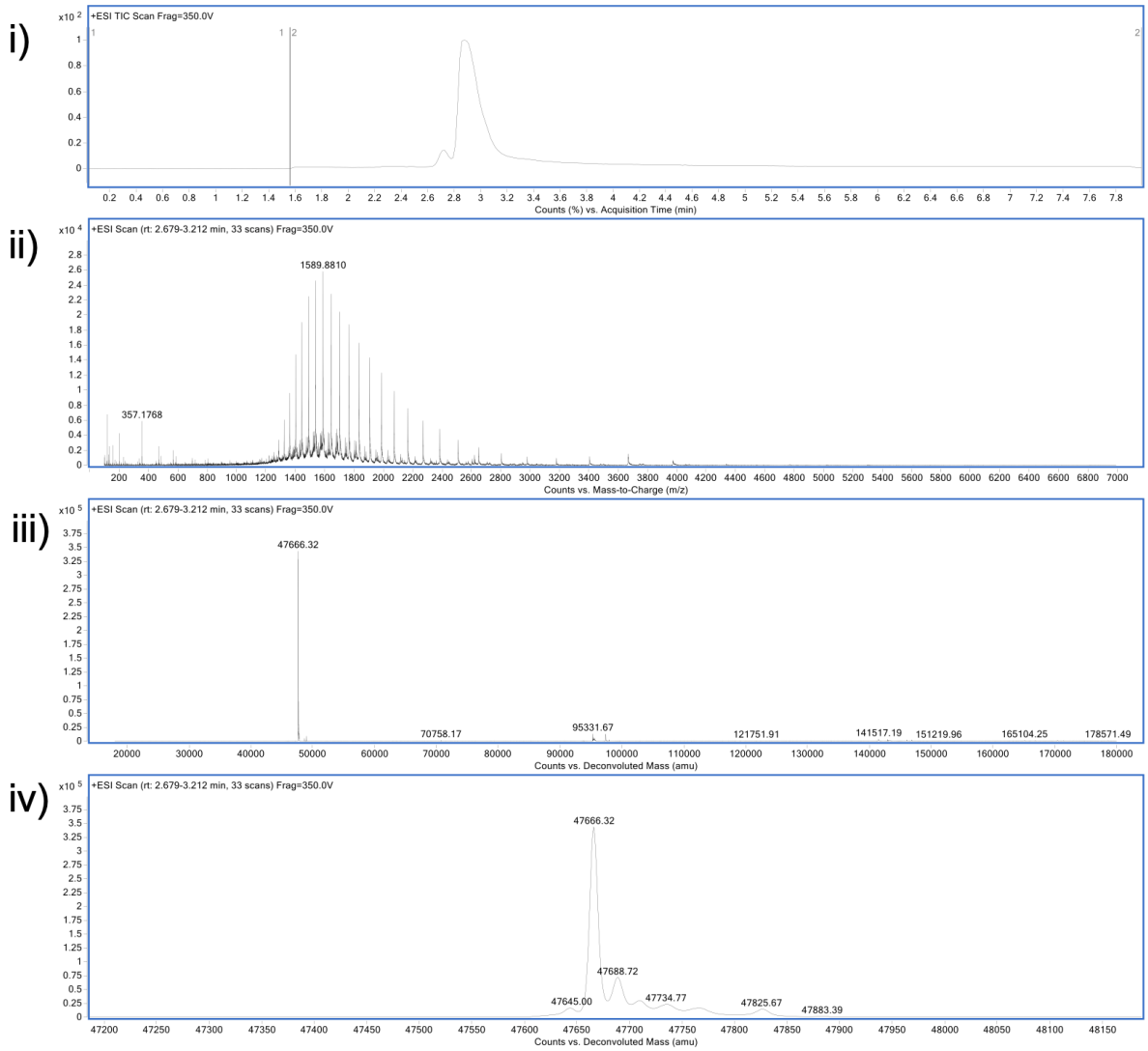


**FIGURE S.48.** LCMS analysis of aryl dithiocarbonate **14** reaction on reduced Fab. i) TIC. ii) non-convoluted ion series. iii) full range of deconvoluted ion series. iv) zoomed in of deconvoluted ion series. Expected mass of dithiocarbonate conjugate: 47666 Da. Observed: 47666 Da. Mass of dithiocarbonate addition: 28

**Dithiocarbonate re-bridged conjugate with cysteine addition**

Prepared dithiocarbonate re-bridged conjugate (40 µL, 150 µM) was washed *via* ultrafiltration (10 kDa MWCO) into conjugation buffer (5 x 80 µL). The concentration of the dithiocarbonate re-bridged conjugate was calculated. *N*Boc-cysteine (150 mM in $dH_2O$, 100 eq.) was added and the reaction mixture was further incubated for 24 h at 37 ºC, 300 rpm. The excess reagent was removed *via* ultrafiltration (10 kDa MWCO) into LCMS water, and the sample was purified by ZebaSpin for LCMS analysis.

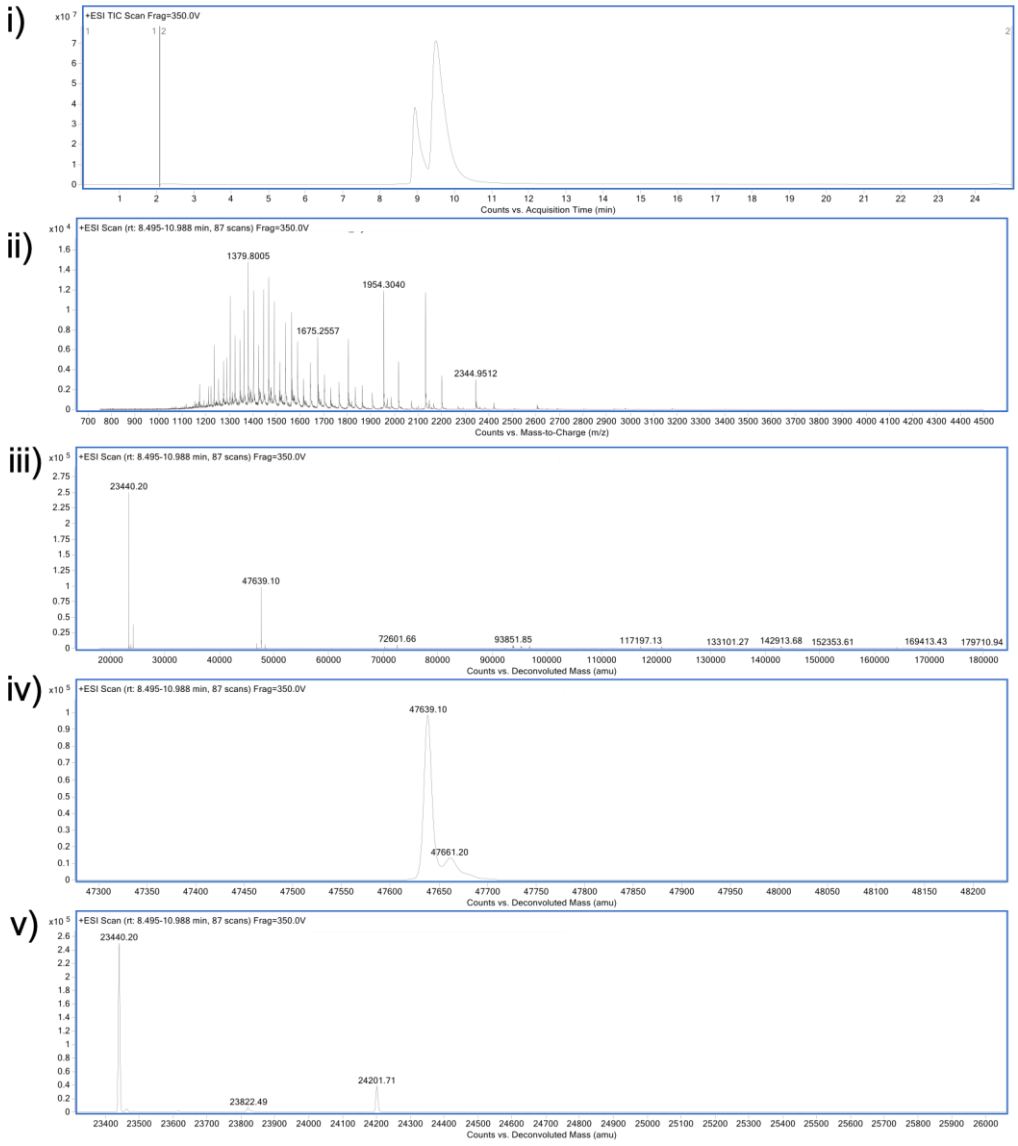


**FIGURE S.49.** LCMS analysis of cysteine addition to dithiocarbonate re-bridged conjugate. i) TIC. ii) non-convoluted ion series. iii) full range of deconvoluted ion series. iv) and v) zoomed in of deconvoluted ion series. Expected mass of native Fab: 47638 Da, native LC 24400 Da, native HC 24200 Da. Observed: 47369 Da, LC 24400 Da, HC 24201 Da.

**Dithiocarbonate re-bridged conjugate CLT**

Prepared dithiocarbonate re-bridged conjugate (40 μL, 150 μM) was washed *via* ultrafiltration 10 kDa MWCO) into BBS pH 8.4 (5 x 80 μL). The concentration of the dithiocarbamate re-bridged conjugate was calculated. The conjugate was diluted to 20 μM with BBS pH 8.4 and further incubated at pH 8.4 for 24 h at 22 ºC, 300 rpm. The sample was purified by ZebaSpin for LCMS analysis.

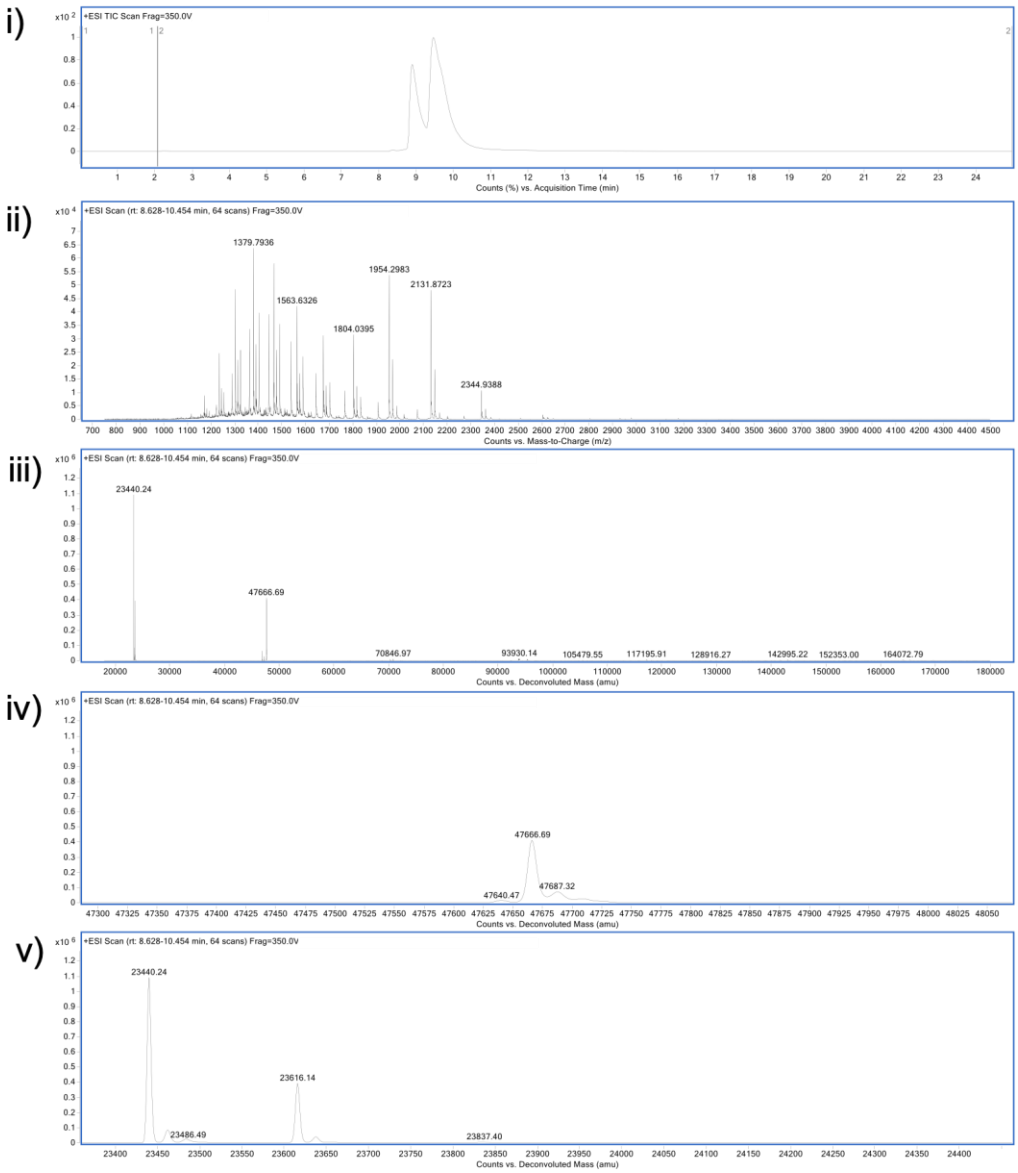


**FIGURE S.50.** LCMS analysis of dithiocarbonate re-bridged conjugate. i) TIC. ii) non-convoluted ion series. iii) full range of deconvoluted ion series. iv) and v) zoomed in of deconvoluted ion series. Expected mass of dithiocarbonate conjugate: 47666 Da, HC 24228 Da. Observed: LC 23440 Da, fragmented HC 23616 Da, 47666 Da.

**Dithiocarbonate re-bridged conjugate substitution with propargyl alcohol**

Prepared dithiocarbonate re-bridged conjugate (40 μL, 150 μM) was washed *via* ultrafiltration (10 kDa MWCO) into conjugation buffer (5 x 80 μL). The concentration of the dithiocarbonate re-bridged conjugate was calculated. Propargyl alcohol (150 mM in DMF, 100 eq.) was added, and the reaction mixture was further incubated for 24 h at 37 ºC, 300 rpm. The excess reagent was removed *via* ultrafiltration (10 kDa MWCO) into LCMS water, and the sample was purified by ZebaSpin for LCMS analysis.

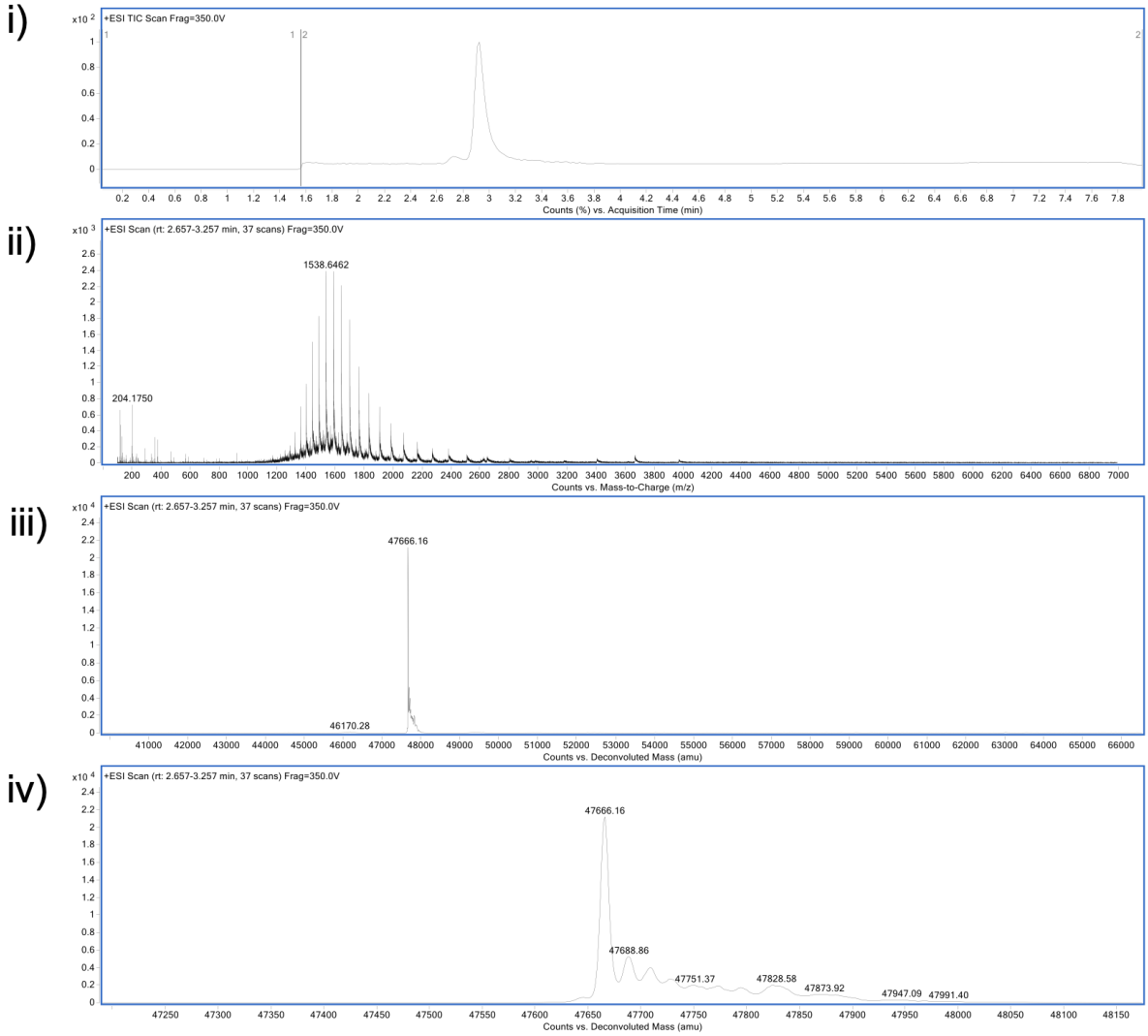


**FIGURE S.51.** LCMS analysis of propargyl alcohol addition to dithiocarbonate re-bridged conjugate. i) TIC. ii) non-convoluted ion series. iii) full range of deconvoluted ion series. iv) and v) zoomed in of deconvoluted ion series. Mass of dithiocarbonate re-bridged conjugate: 47666 Da. Observed: 47666 Da. Expected mass of propargyl alcohol addition: 56 Da.

**Dithiocarbonate re-bridged conjugate substitution with propargylamine**

Prepared dithiocarbonate re-bridged conjugate (40 μL, 150 μM) was washed *via* ultrafiltration (10 kDa MWCO) into conjugation buffer (5 x 80 μL). The concentration of the dithiocarbonate re-bridged conjugate was calculated. Propargylamine (150 mM in DMF, 100 eq.) was added, and the reaction mixture was further incubated for 24 h at 37 ºC, 300 rpm. The excess reagent was removed *via* ultrafiltration (10 kDa MWCO) into LCMS water, and the sample was purified by ZebaSpin for LCMS analysis.

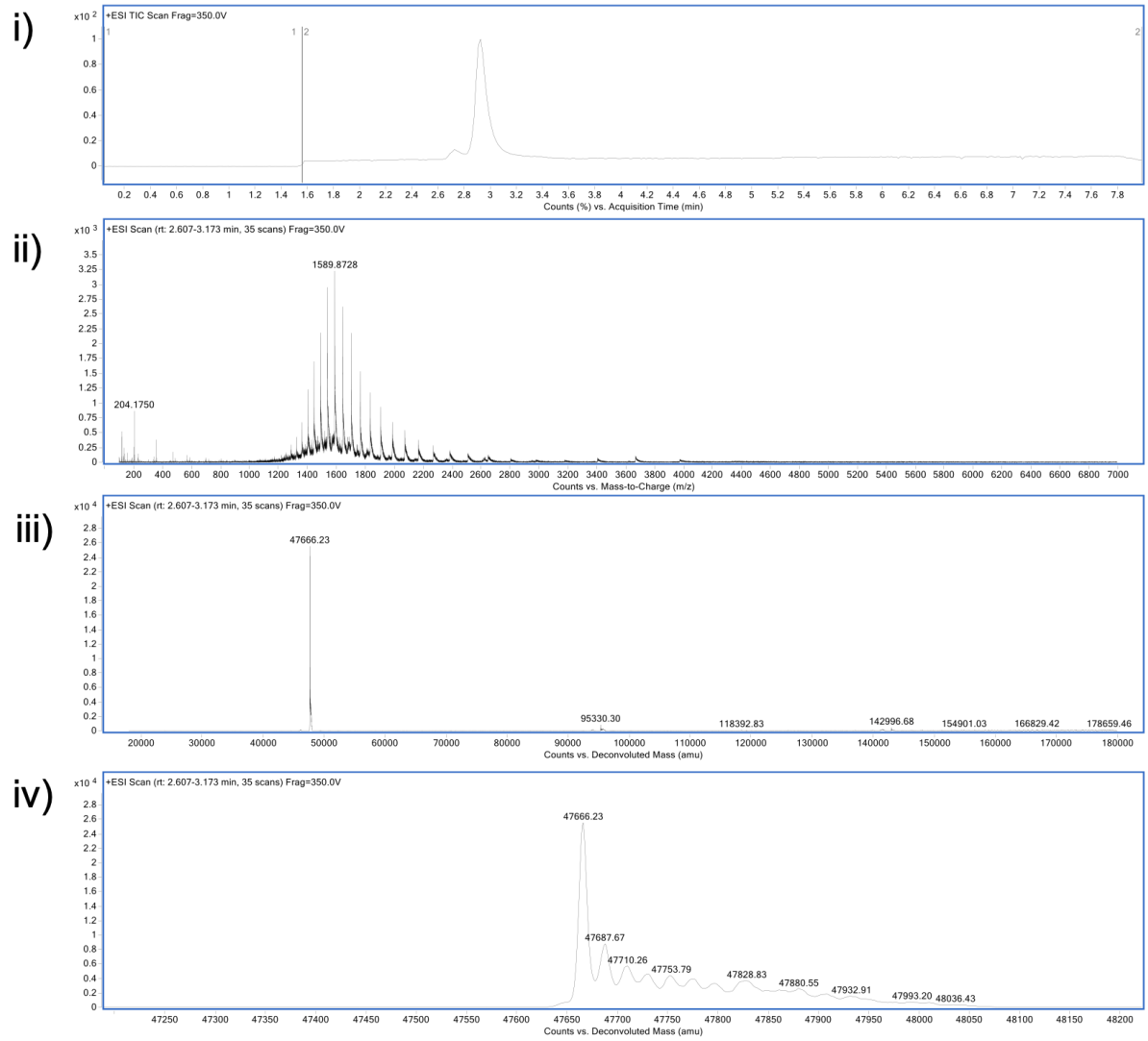


**FIGURE S.52.** LCMS analysis of propargylamine addition to dithiocarbonate re-bridged conjugate. i) TIC. ii) non-convoluted ion series. iii) full range of deconvoluted ion series. iv) and v) zoomed in of deconvoluted ion series. Mass of dithiocarbonate re-bridged conjugate: 47666 Da. Observed: 47666 Da. Expected mass of propargyl alcohol addition: 55 Da.

**Dithiocarbonate re-bridged conjugate substitution with *p*-anisidine**

Prepared dithiocarbonate re-bridged conjugate (40 µL, 150 µM) was washed *via* ultrafiltration (10 kDa MWCO) into conjugation buffer (5 x 80 µL). The concentration of the dithiocarbonate re-bridged conjugate was calculated. *p*-anisidine (150 mM in DMF, 100 eq.) was added, and the reaction mixture was further incubated for 24 h at 37 ºC, 300 rpm. The excess reagent was removed *via* ultrafiltration (10 kDa MWCO) into LCMS water, and the sample was purified by ZebaSpin for LCMS analysis.

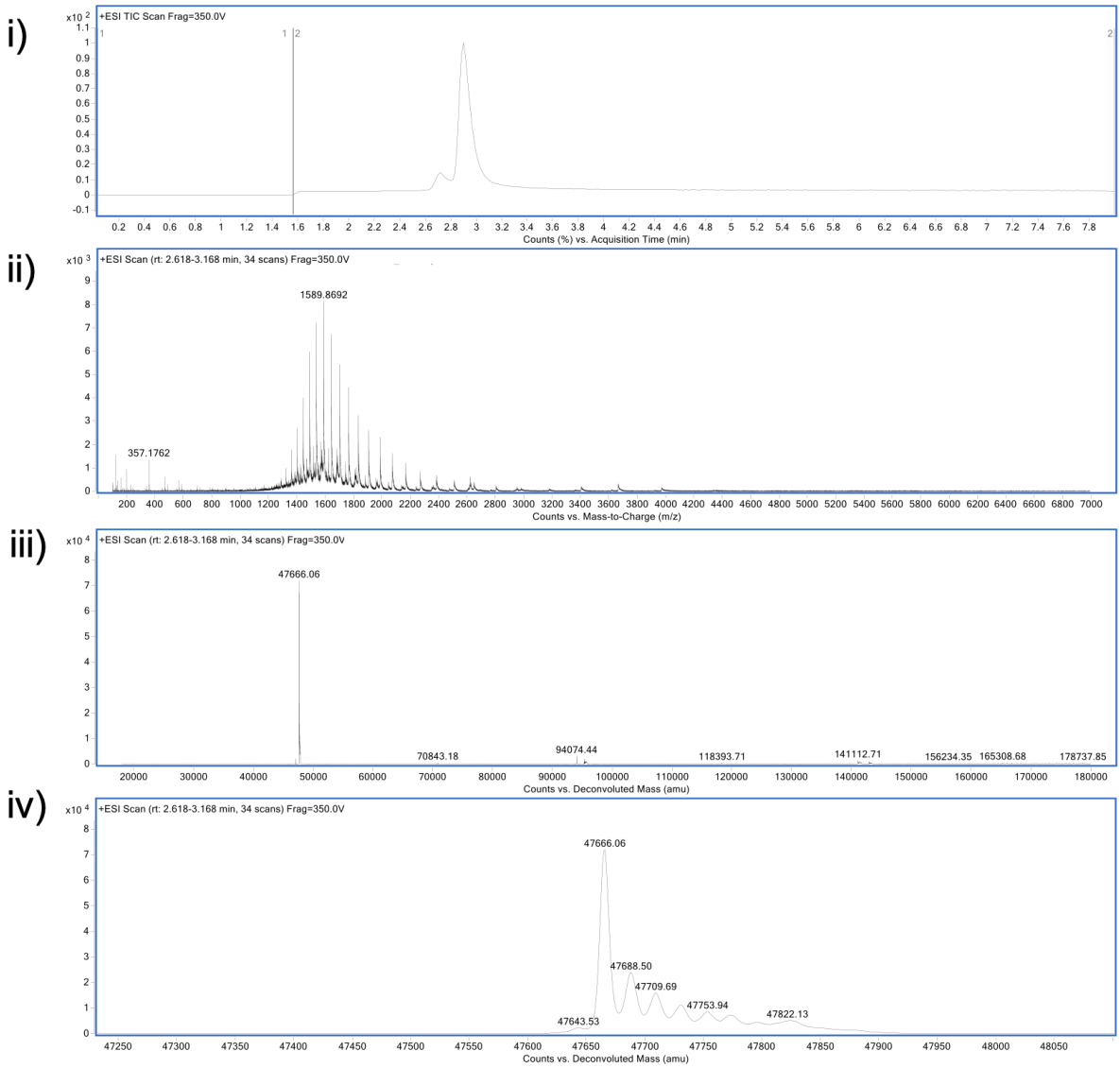


**FIGURE S.53.** LCMS analysis of *p*-anisidine addition to dithiocarbonate re-bridged conjugate. i) TIC. ii) non-convoluted ion series. iii) full range of deconvoluted ion series. iv) and v) zoomed in of deconvoluted ion series. Mass of dithiocarbonate re-bridged conjugate: 47666 Da. Observed: 47666 Da. Expected mass of *p*-anisidine addition: 123 Da.

**Dithiocarbonate re-bridged conjugate substitution with hydrazine**

Prepared dithiocarbonate re-bridged conjugate (40 μL, 150 μM) was washed *via* ultrafiltration (10 kDa MWCO) into conjugation buffer (5 x 80 μL). The concentration of the dithiocarbonate re-bridged conjugate was calculated. Hydrazine hydrate (150 mM in DMF, 100 eq.) was added, and the reaction mixture was further incubated for 24 h at 37 ºC, 300 rpm. The excess reagent was removed *via* ultrafiltration (10 kDa MWCO) into LCMS water, and the sample was purified by ZebaSpin for LCMS analysis.

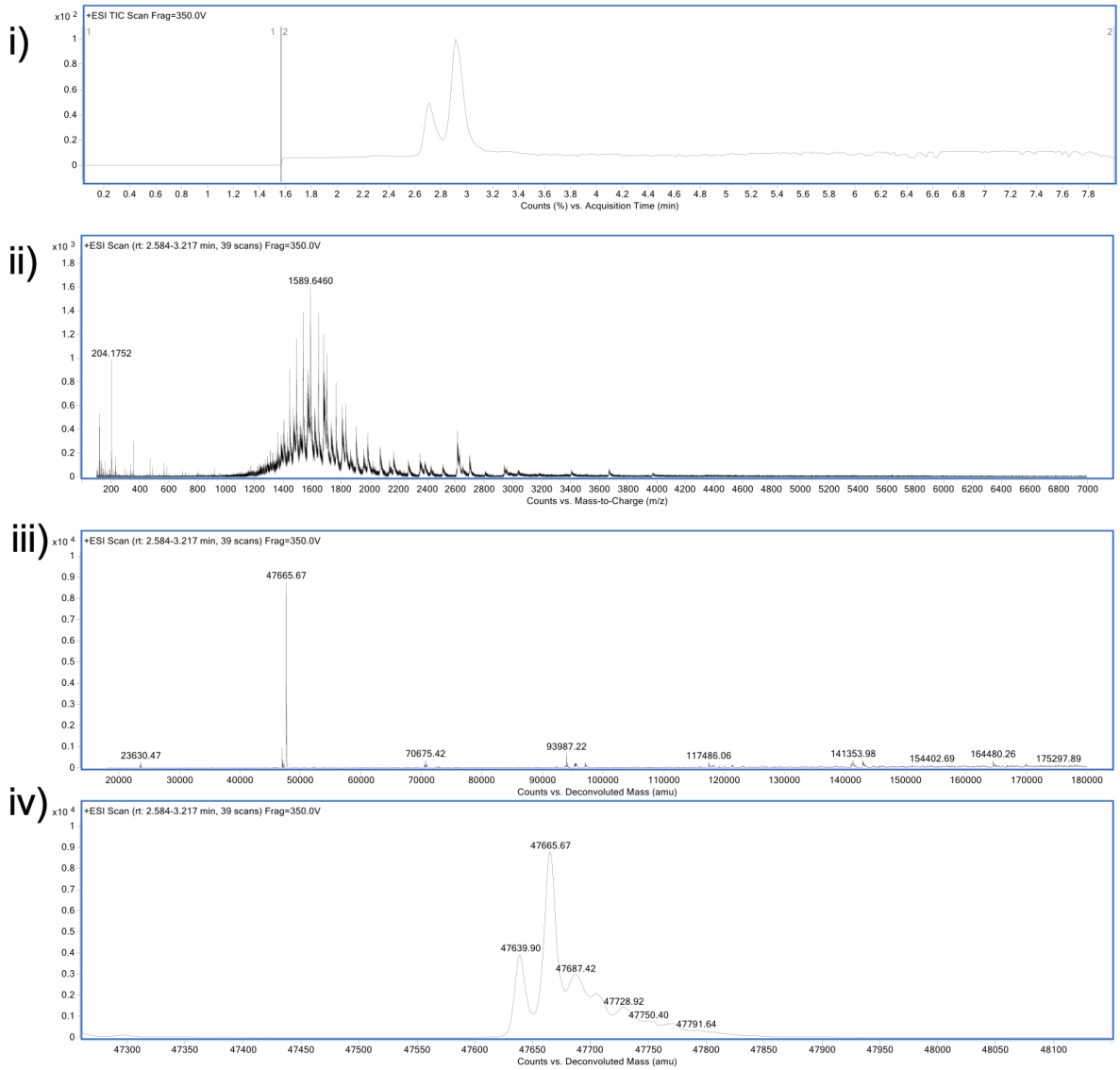


**FIGURE S.54.** LCMS analysis of hydrazine addition to dithiocarbonate re-bridged conjugate. i) TIC. ii) non-convoluted ion series. iii) full range of deconvoluted ion series. iv) and v) zoomed in of deconvoluted ion series. Mass of dithiocarbonate re-bridged conjugate: 47666 Da. Observed: 47666 Da, 47639 Da. Expected mass of hydrazine addition: 32 Da.

**Dithiocarbonate re-bridged conjugate substitution with hydroxylamine**

Prepared dithiocarbonate re-bridged conjugate (40 μL, 150 μM) was washed *via* ultrafiltration (10 kDa MWCO) into conjugation buffer (5 x 80 μL). The concentration of the dithiocarbonate re-bridged conjugate was calculated. Hydroxylamine (150 mM in DMF, 100 eq.) was added, and the reaction mixture was further incubated for 24 h at 37 ºC, 300 rpm. The excess reagent was removed *via* ultrafiltration (10 kDa MWCO) into LCMS water, and the sample was purified by ZebaSpin for LCMS analysis.

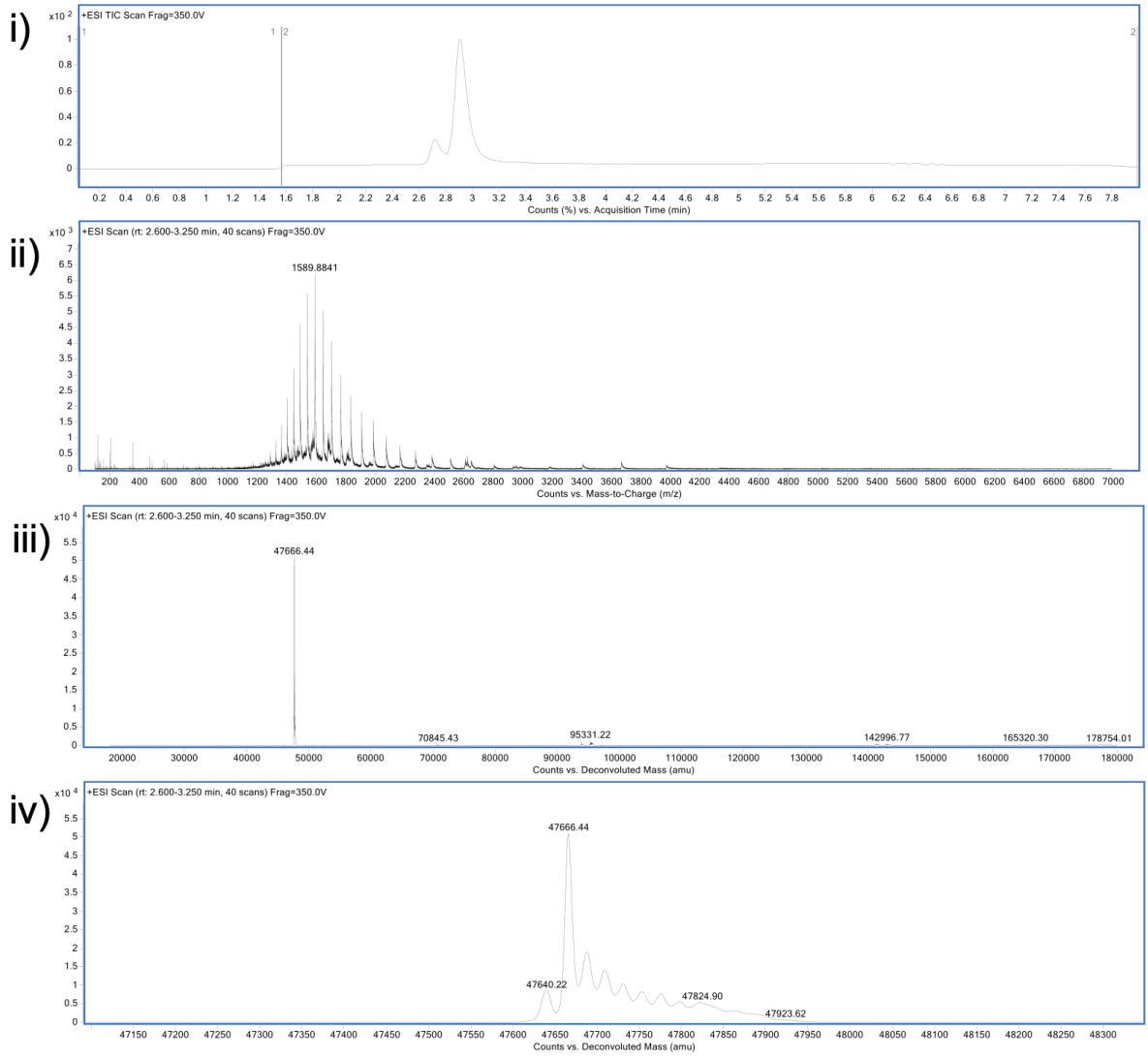


**FIGURE S.55.** LCMS analysis of hydroxylamine addition to dithiocarbonate re-bridged conjugate. i) TIC. ii) non-convoluted ion series. iii) full range of deconvoluted ion series. iv) and v) zoomed in of deconvoluted ion series. Mass of dithiocarbonate re-bridged conjugate: 47666 Da. Observed: 47666 Da, 47640 Da. Expected mass of hydroxylamine addition: 33 Da.

**Dithiocarbonate re-bridged conjugate substitution with *O*-Me-cysteine, 4 h**

Prepared dithiocarbonate re-bridged conjugate (40 µL, 150 µM) was washed *via* ultrafiltration (10 kDa MWCO) into conjugation buffer (5 x 80 µL). The concentration of the dithiocarbonate re-bridged conjugate was calculated. *O*-Me-cysteine (150 mM in $dH_2O$, 100 eq.) was added, and the reaction mixture was further incubated for 4 h at 37 ºC, 300 rpm. The excess reagent was removed *via* ultrafiltration (10 kDa MWCO) into LCMS water, and the sample was purified by ZebaSpin for LCMS analysis.

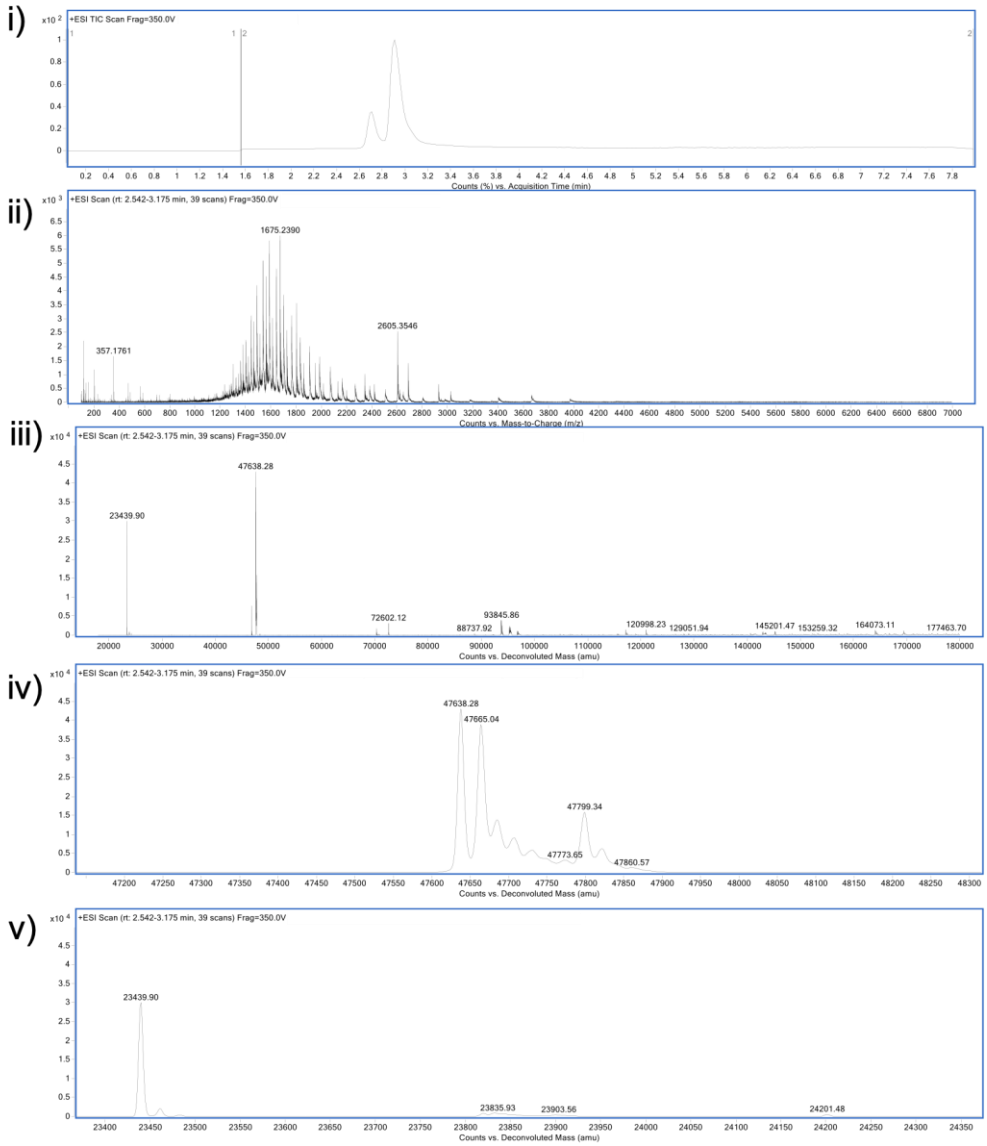


**FIGURE S.56.** LCMS analysis of 4 h OMe-cysteine addition to dithiocarbonate re-bridged conjugate. i) TIC. ii) non-convoluted ion series. iii) full range of deconvoluted ion series. iv) and v) zoomed in of deconvoluted ion series. Mass of dithiocarbonate re-bridged conjugate: 47666 Da. Observed: 47638 Da, 47665 Da, 47799 Da, LC 23439. Expected mass of OMe-cysteine addition: 136 Da.

**Dithiocarbonate and OMe-cysteine conjugate, TCEP and maleimide addition**

Prepared OMe-cysteine-dithiocarbonate re-bridged conjugate (40 μL, 150 μM) was washed *via* ultrafiltration (10 kDa MWCO) into conjugation buffer (5 x 80 μL). The concentration of the dithiocarbonate re-bridged conjugate was calculated. TCEP (150 mM in $dH_2O$, 10 eq.) was added, and the reaction mixture was further incubated for 1 h at 37 ºC, 300 rpm. Then, *N*-methylmaleimide (2.00 μL, 0.300 μmol, 150 mM in DMF, 50 eq.) was added, and the reaction incubated for a further 1 h at 37 ºC, 300 rpm. The excess reagent was removed *via* ultrafiltration (10 kDa MWCO) into LCMS water, and the sample was purified by ZebaSpin for LCMS analysis.

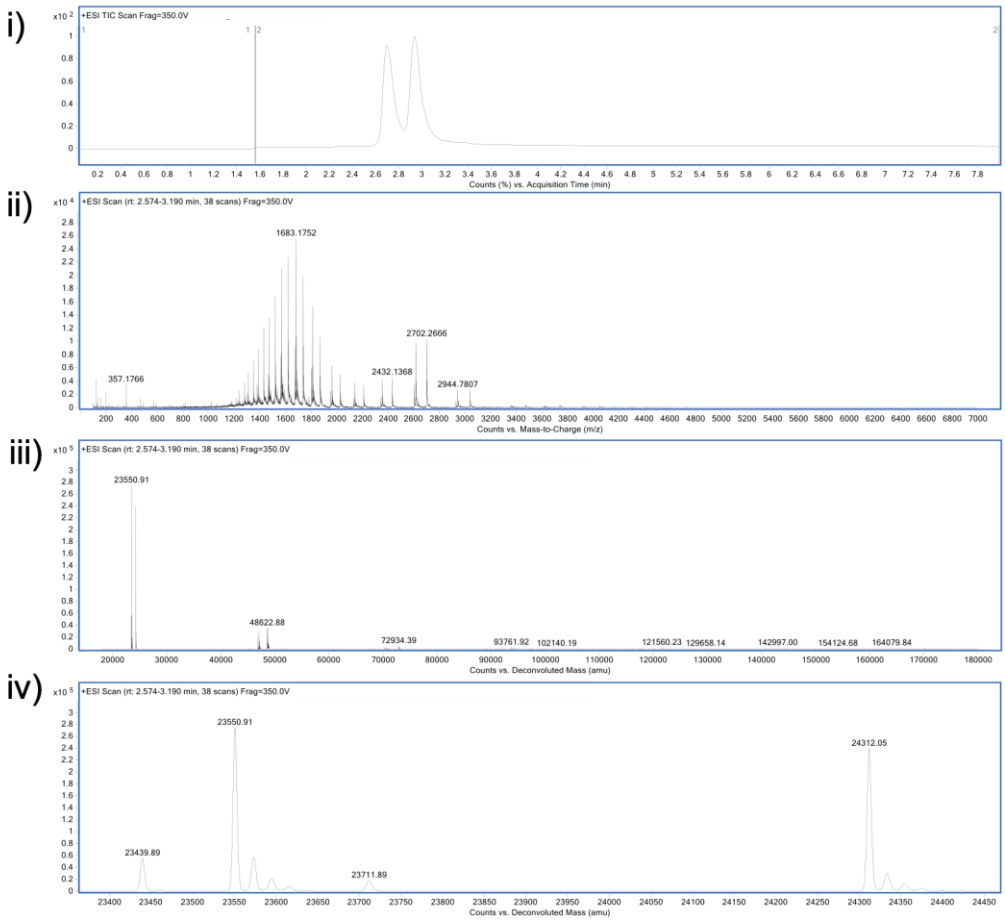


**FIGURE S.57.** LCMS analysis of TCEP and *N*-methylmaleimide addition to OMe-cysteine-dithiocarbonate re-bridged conjugate. i) TIC. ii) non-convoluted ion series. iii) full range of deconvoluted ion series. iv) and v) zoomed in of deconvoluted ion series. Mass of dithiocarbonate re-bridged conjugate: 47666 Da. Expected mass of maleimide-capped LC: 23550. Expected mass of maleimide-capped HC: 24211. Observed: LC 23439 Da, modified LC 23550, modified HC 24312. Expected mass of *N*-methylmaleimide addition: 111 Da.

**Dithiocarbonate re-bridged conjugate aqueous stability (3 days)**

Prepared dithiocarbonate re-bridged conjugate (40 μL, 150 μM) was washed *via* ultrafiltration 10 kDa MWCO) into LCMS water. The concentration of the conjugate was determined, and adjusted to 100 μM. The conjugate was incubated at 22 ºC for 3 days, 300 rpm. The sample was purified by ZebaSpin for LCMS analysis.

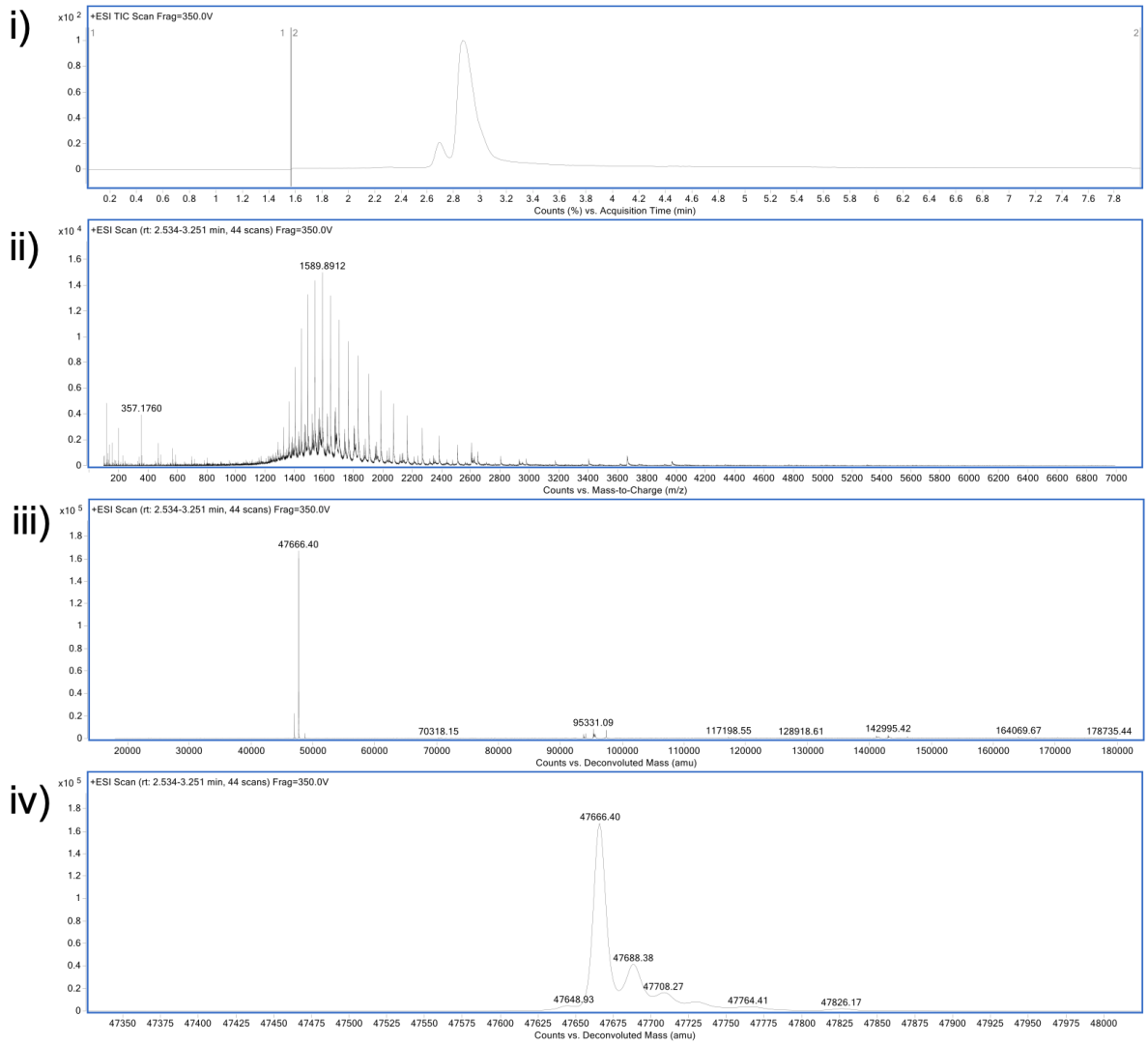


**FIGURE S.58.** LCMS analysis of 3-day aqueous stability of dithiocarbonate re-bridged conjugate. i) TIC. ii) non-convoluted ion series. iii) full range of deconvoluted ion series. iv) zoomed in of deconvoluted ion series. Expected mass of dithiocarbonate re-bridged conjugate: 47666 Da. Observed: 47666 Da.

**Dithiocarbonate re-bridged conjugate aqueous stability (7 days)**

Prepared dithiocarbonate re-bridged conjugate (40 μL, 150 μM) was washed *via* ultrafiltration 10 kDa MWCO) into LCMS water. The concentration of the conjugate was determined, and adjusted to 100 μM. The conjugate was incubated at 22 ºC for 7 days, 300 rpm. The sample was purified by ZebaSpin for LCMS analysis.

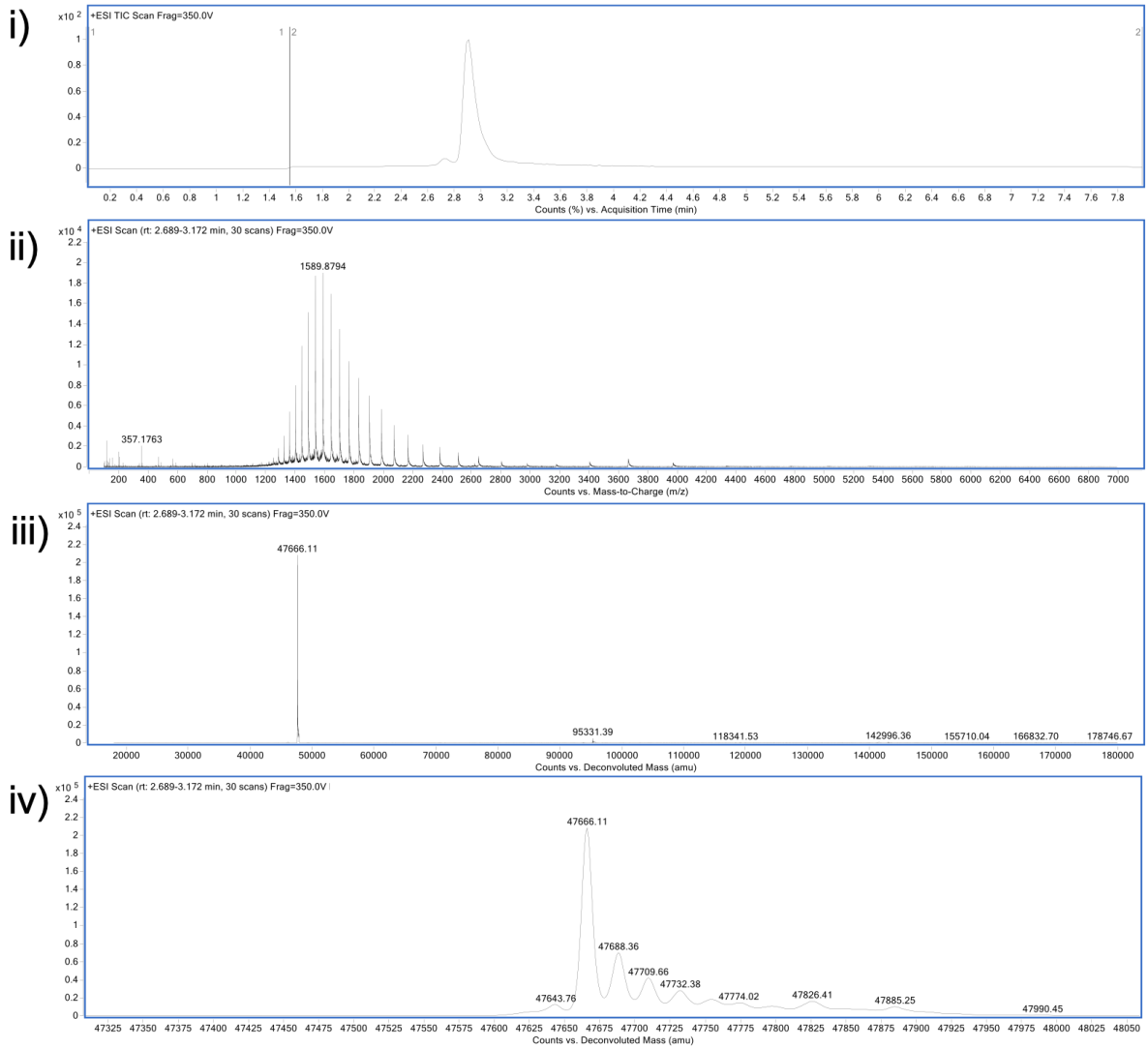


**FIGURE S.59.** LCMS analysis of 7-day aqueous stability of dithiocarbonate re-bridged conjugate. i) TIC. ii) non-convoluted ion series. iii) full range of deconvoluted ion series. iv) zoomed in of deconvoluted ion series. Expected mass of dithiocarbonate re-bridged conjugate: 47666 Da. Observed: 47666 Da.

**Dithiocarbonate re-bridged conjugate serum-mimicking stability (1 h)**

Prepared dithiocarbonate re-bridged conjugate (40 μL, 150 μM) was washed *via* ultrafiltration 10 kDa MWCO) into LCMS water. The concentration of the dithiocarbonate re-bridged conjugate was calculated. The conjugate was diluted to 7 μM by the addition of serum-mimicking solution (glutathione, 100 μM stock, conjugation buffer at pH 7.4). The reaction mixture was further incubated at 37 ºC, 300 rpm over time. Time points were taken at 1 h, 4 h, and 24 h. The sample(s) were prepared by ZebaSpin for LCMS analysis.

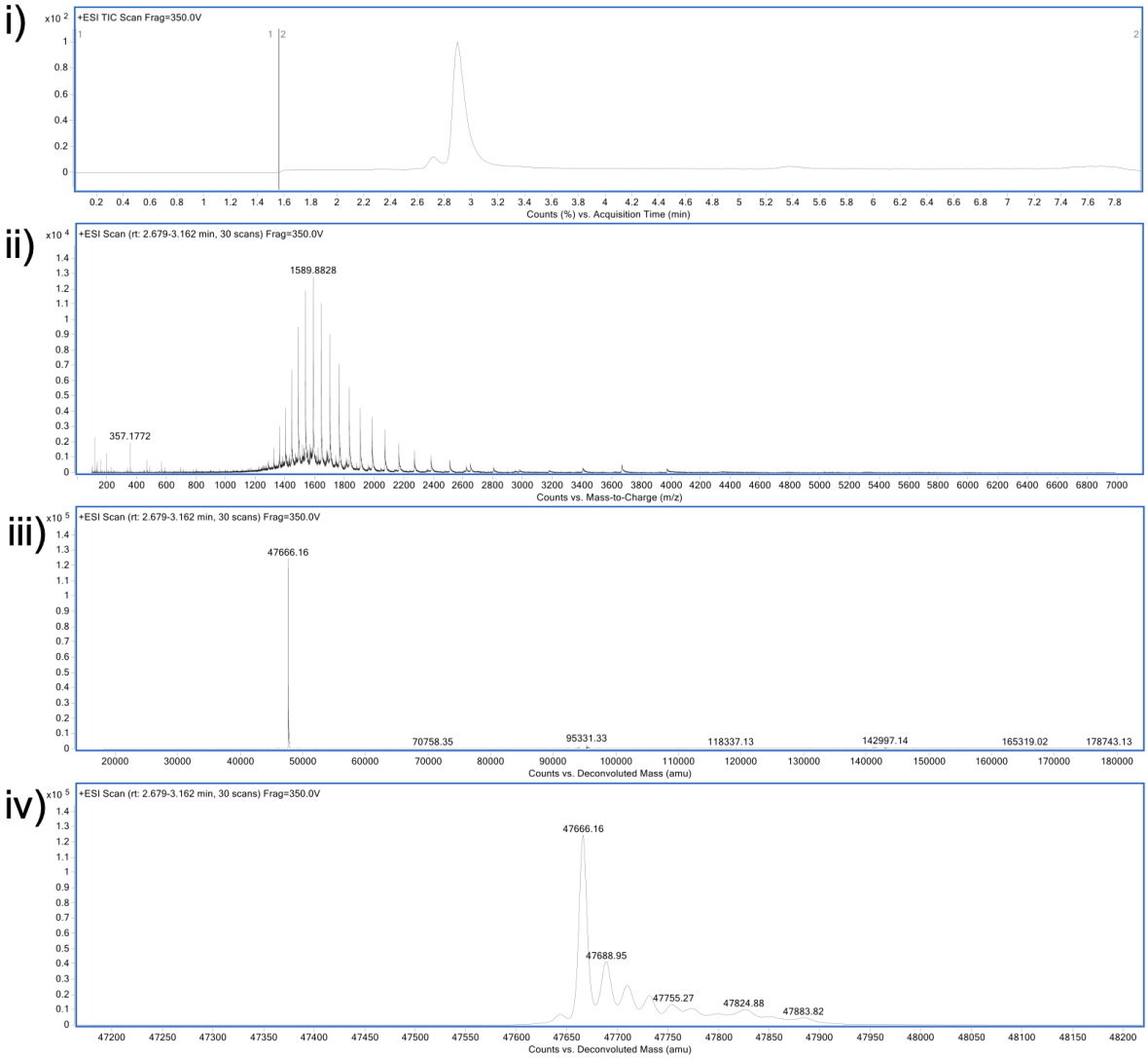


**FIGURE S.60.** LCMS analysis of 1 h serum stability of dithiocarbonate re-bridged conjugate. i) TIC. ii) non-convoluted ion series. iii) full range of deconvoluted ion series. iv) zoomed in of deconvoluted ion series. Expected mass of dithiocarbonate re-bridged conjugate: 47666 Da. Observed: 47666 Da.

**Dithiocarbonate re-bridged conjugate serum-mimicking stability (4 h)**

Timepoint taken after 4 h incubation of dithiocarbonate re-bridged conjugate in serum-mimicking conditions. See 1 h timepoint for method.

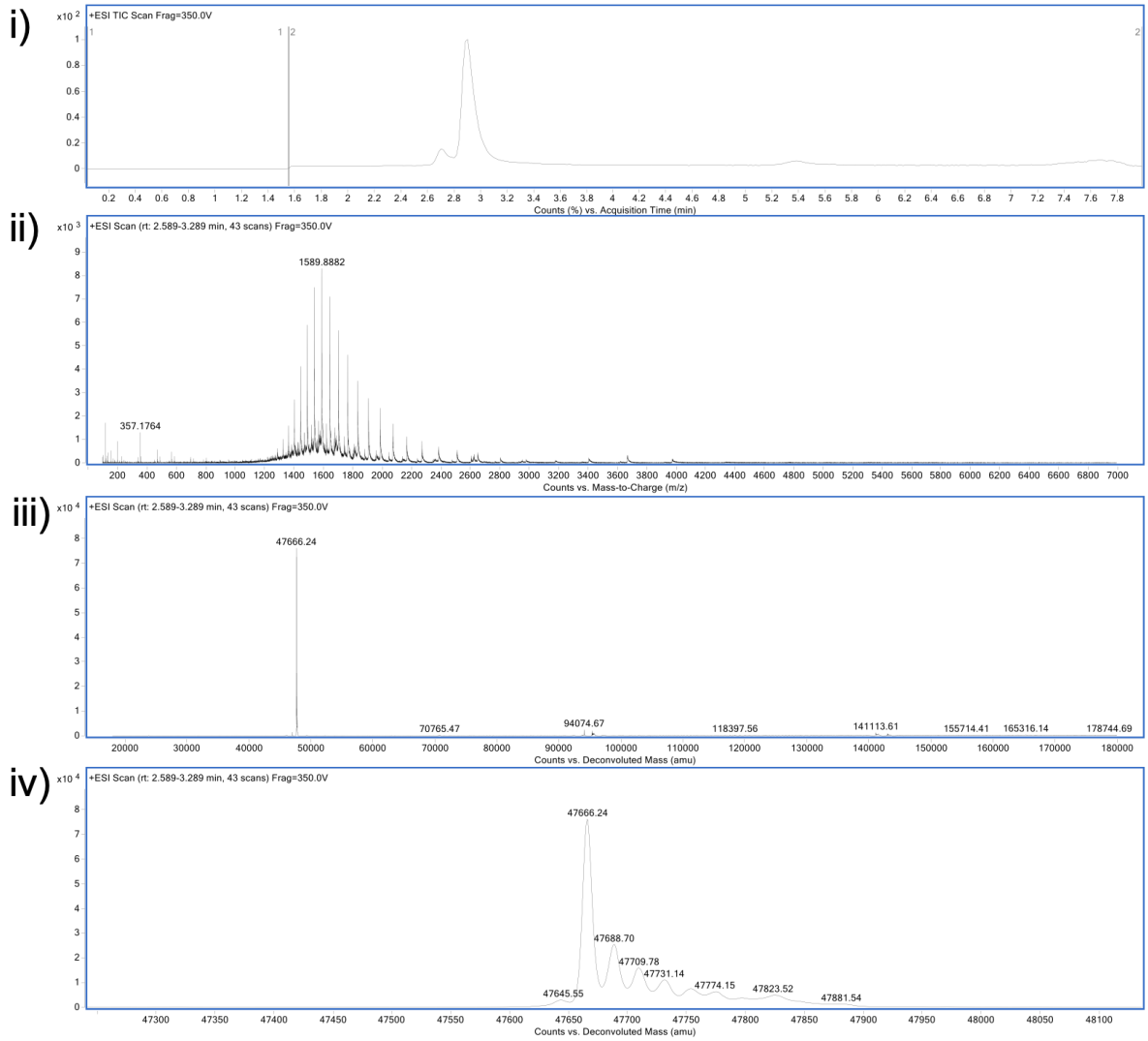


**FIGURE S.61.** LCMS analysis of 4 h serum stability of dithiocarbonate re-bridged conjugate. i) TIC. ii) non-convoluted ion series. iii) full range of deconvoluted ion series. iv) zoomed in of deconvoluted ion series. Expected mass of dithiocarbonate re-bridged conjugate: 47666 Da. Observed: 47666 Da.

**Dithiocarbonate re-bridged conjugate serum-mimicking stability (24 h)**

Timepoint taken after 24 h incubation of dithiocarbonate re-bridged conjugate in serum-mimicking conditions. See 1 h timepoint for method.

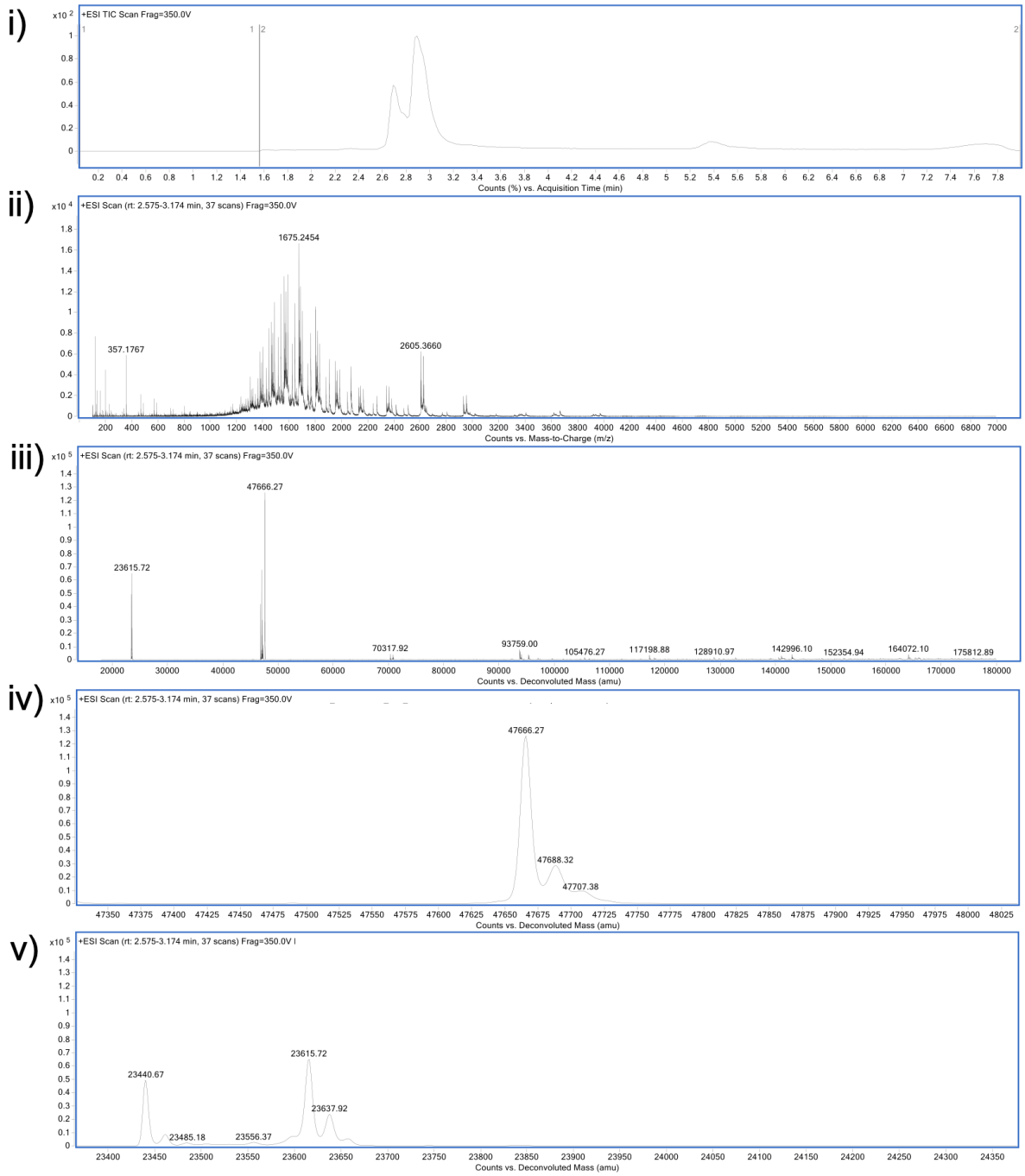


**FIGURE S.62.** LCMS analysis of 4 h serum stability of dithiocarbonate re-bridged conjugate. i) TIC. ii) non-convoluted ion series. iii) full range of deconvoluted ion series. iv) zoomed in of deconvoluted ion series. Expected mass of dithiocarbonate re-bridged conjugate: 47666 Da. Observed: 47666 Da, LC 23440, fragmented HC 23615.

**Dithiocarbonate re-bridged conjugate endosomal-mimicking stability (1 h)**

Prepared dithiocarbonate re-bridged conjugate (40 μL, 150 μM) was washed *via* ultrafiltration 10 kDa MWCO) into LCMS water. The concentration of the dithiocarbonate re-bridged conjugate was calculated. The conjugate was diluted to 7 μM by the addition of early endosomal-mimicking solution (glutathione, 100 mM, conjugation buffer at pH 6.5). The reaction mixture was further incubated at 37 ºC, 300 rpm over time. Time points were taken at 1 h, 4 h, and 24 h. The sample(s) were prepared by ZebaSpin for LCMS analysis.

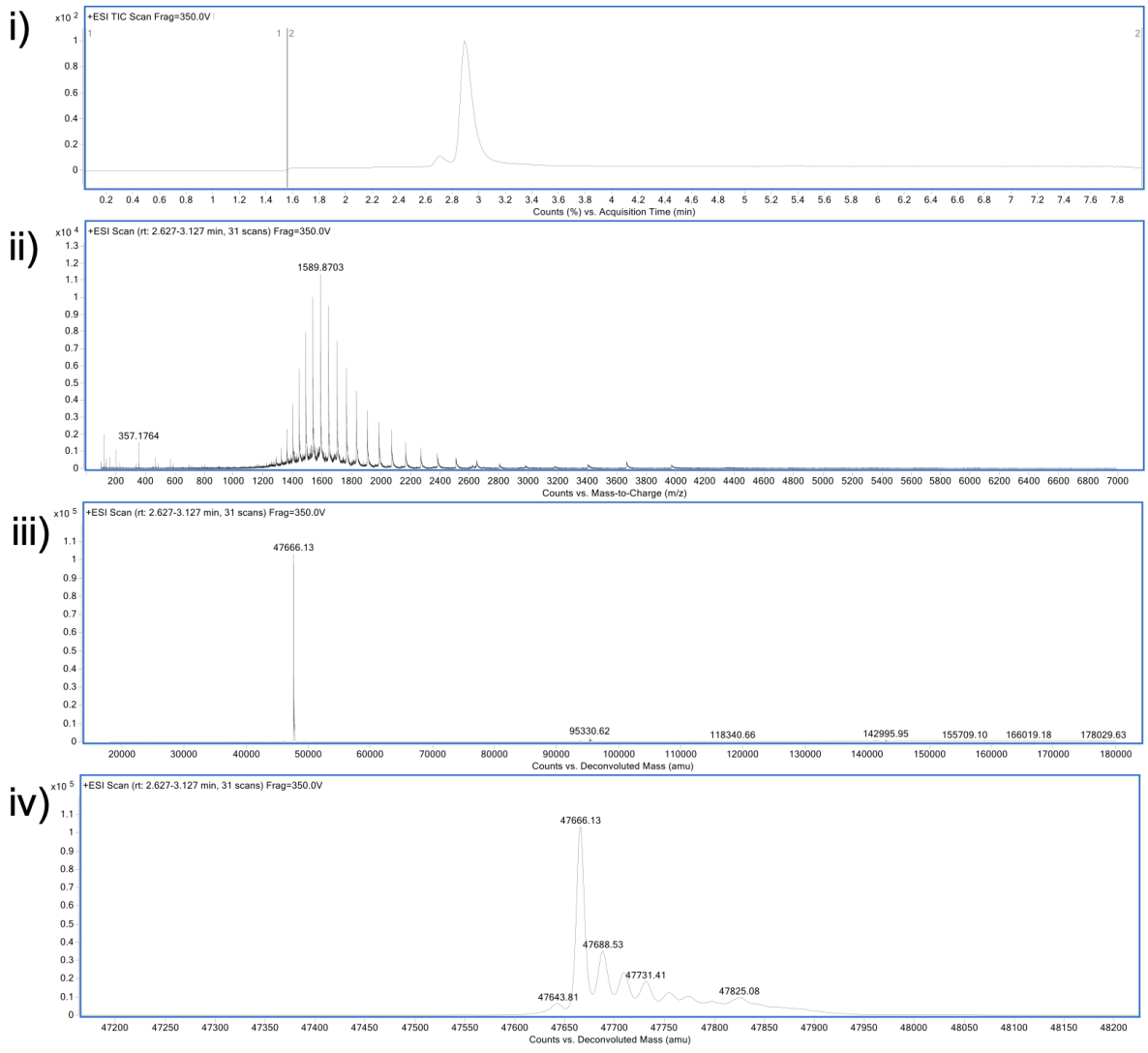


**FIGURE S.63.** LCMS analysis of 1 h early endosomal stability of dithiocarbonate re-bridged conjugate. i) TIC. ii) non-convoluted ion series. iii) full range of deconvoluted ion series. iv) zoomed in of deconvoluted ion series. Expected mass of dithiocarbonate re-bridged conjugate: 47666 Da. Observed: 47666 Da.

**Dithiocarbonate re-bridged conjugate endosomal-mimicking stability (4 h)**

Timepoint taken after 4 h incubation in early endosomal-mimicking conditions. See 1 h timepoint for method.

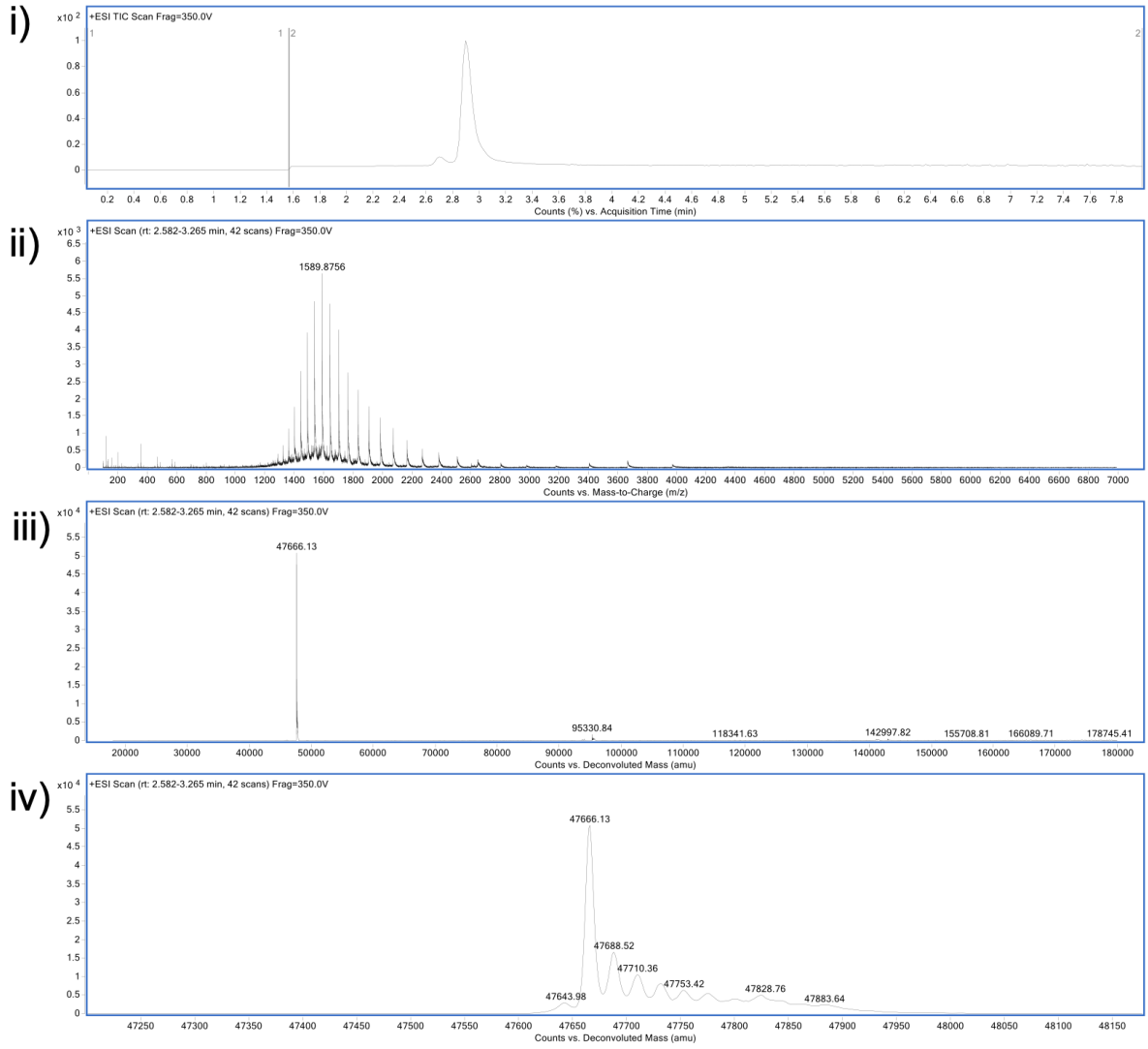


**FIGURE S.64.** LCMS analysis of 4 h endosomal stability of dithiocarbonate re-bridged conjugate. i) TIC. ii) non-convoluted ion series. iii) full range of deconvoluted ion series. iv) zoomed in of deconvoluted ion series. Expected mass of dithiocarbonate re-bridged conjugate: 47666 Da. Observed: 47666 Da.

**Dithiocarbonate re-bridged conjugate endosomal-mimicking stability (24 h)**

Timepoint taken after 24 h incubation in early endosomal-mimicking conditions. See 1 h timepoint for method.

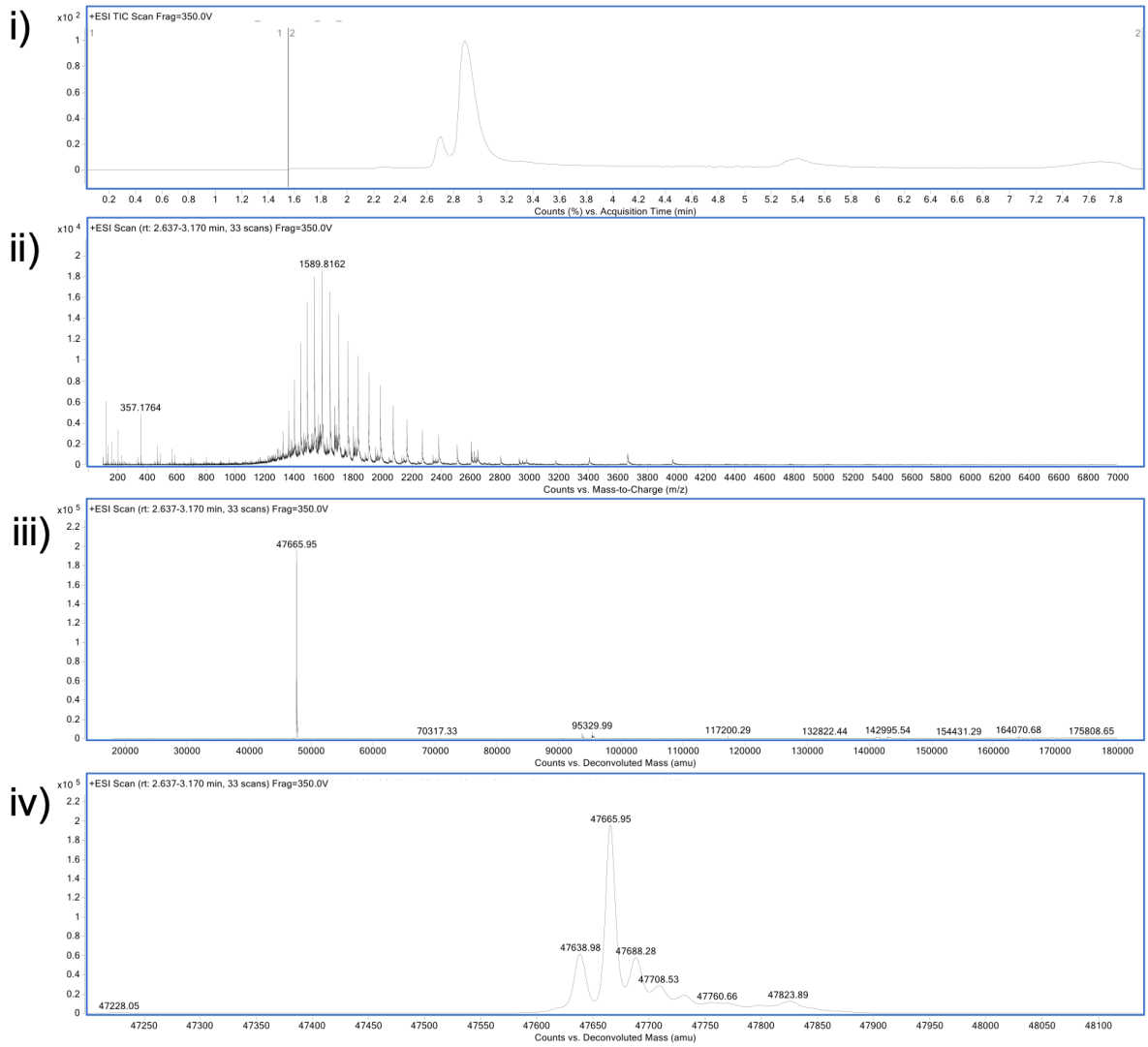


**FIGURE S.65.** LCMS analysis of 24 h early endosomal stability of dithiocarbonate re-bridged conjugate. i) TIC. ii) non-convoluted ion series. iii) full range of deconvoluted ion series. iv) zoomed in of deconvoluted ion series. Expected mass of dithiocarbonate re-bridged conjugate: 47666 Da. Observed: 47666 Da, 47638 Da.

**Alkyl dithiocarbonate 13 re-bridging of trastuzumab**

To trastuzumab (60.0 μL, 0.0013 μmol, 22 μM, 3.83 mg/mL) in conjugation buffer was added TCEP (0.88 μL, 0.013 μmol, 15.0 mM in $dH_2O$, 10 eq.). After mixing for 1.5 h at 37 ºC, 300 rpm, alkyl dithiocarbonate **13** (0.18 μL, 0.013 μmol, 150 mM in DMF, 20 eq.) was added and the reaction mixture was incubated for 1 h at 22 ºC, 300 rpm. The excess reagent was removed *via* ultrafiltration (10 kDa MWCO) into ammonium acetate (pH 6.9) and purified by ZebaSpin for LCMS analysis. PNGase (1.0 μL) was added, and the sample was incubated for 16 h at 37 ºC prior to LCMS analysis.

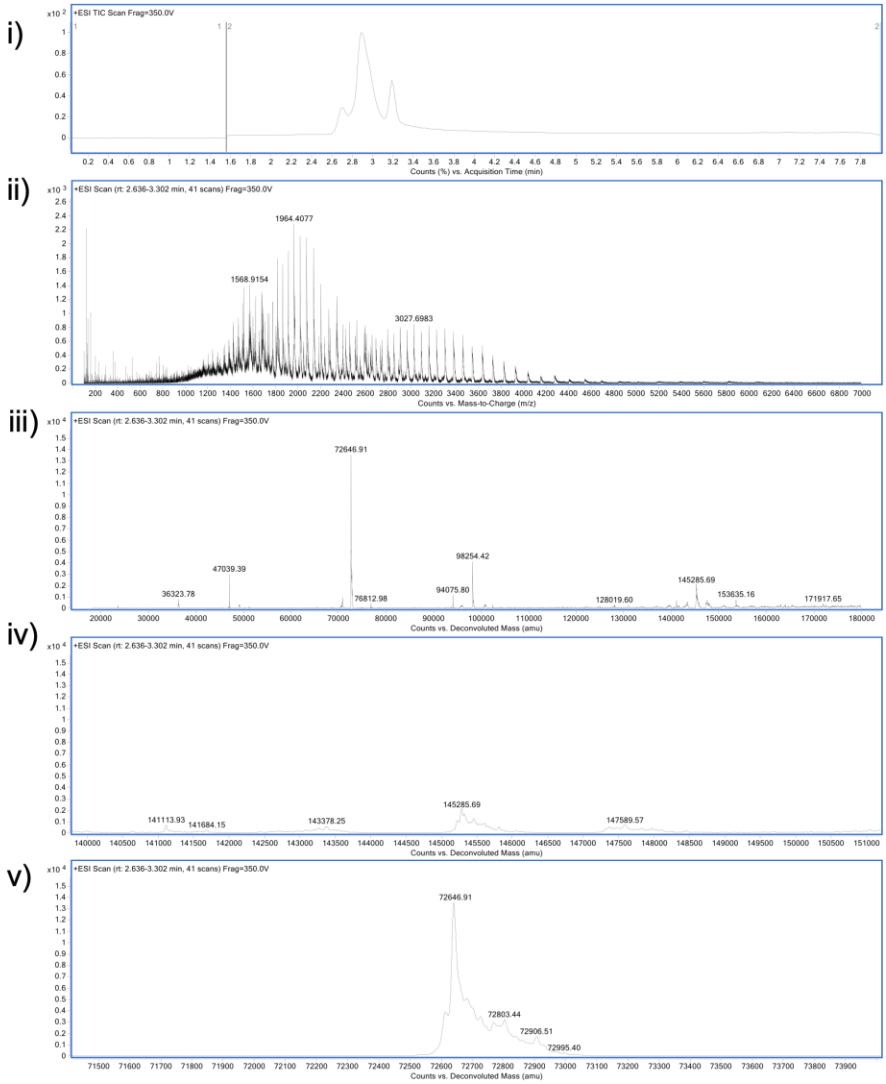


**FIGURE S.66.** Alkyl dithiocarbonate **13** re-bridging of trastuzumab. i) TIC. ii) non-convoluted ion series. iii) full range of deconvoluted ion series. iv) and v) zoomed in of deconvoluted ion series. Expected mass of dithiocarbonate re-bridged conjugate: HHLL 145298 Da, HL 72650. Observed: modified HHLL 145285 Da, modified HL 72646 Da.

**Carbonimidodithioate 15 re-bridging of Fab with 20 eq.**

To Fab (20.0 μL, 0.0030 μmol, 150 μM, 7.15 mg/mL) in conjugation buffer was added TCEP (0.20 μL, 0.030 μmol, 150 mM in $dH_2O$, 10 eq.). After mixing for 1.5 h at 37 ºC, 300 rpm, carbonimidodithioate **15** (0.40 μL, 0.060 μmol, 150 mM in DMF, 20 eq.) was added and the reaction mixture was incubated for 24 h at 22 ºC, 300 rpm. The excess reagent was removed *via* ultrafiltration (10 kDa MWCO) into LCMS water, and the sample was purified by ZebaSpin for LCMS analysis.

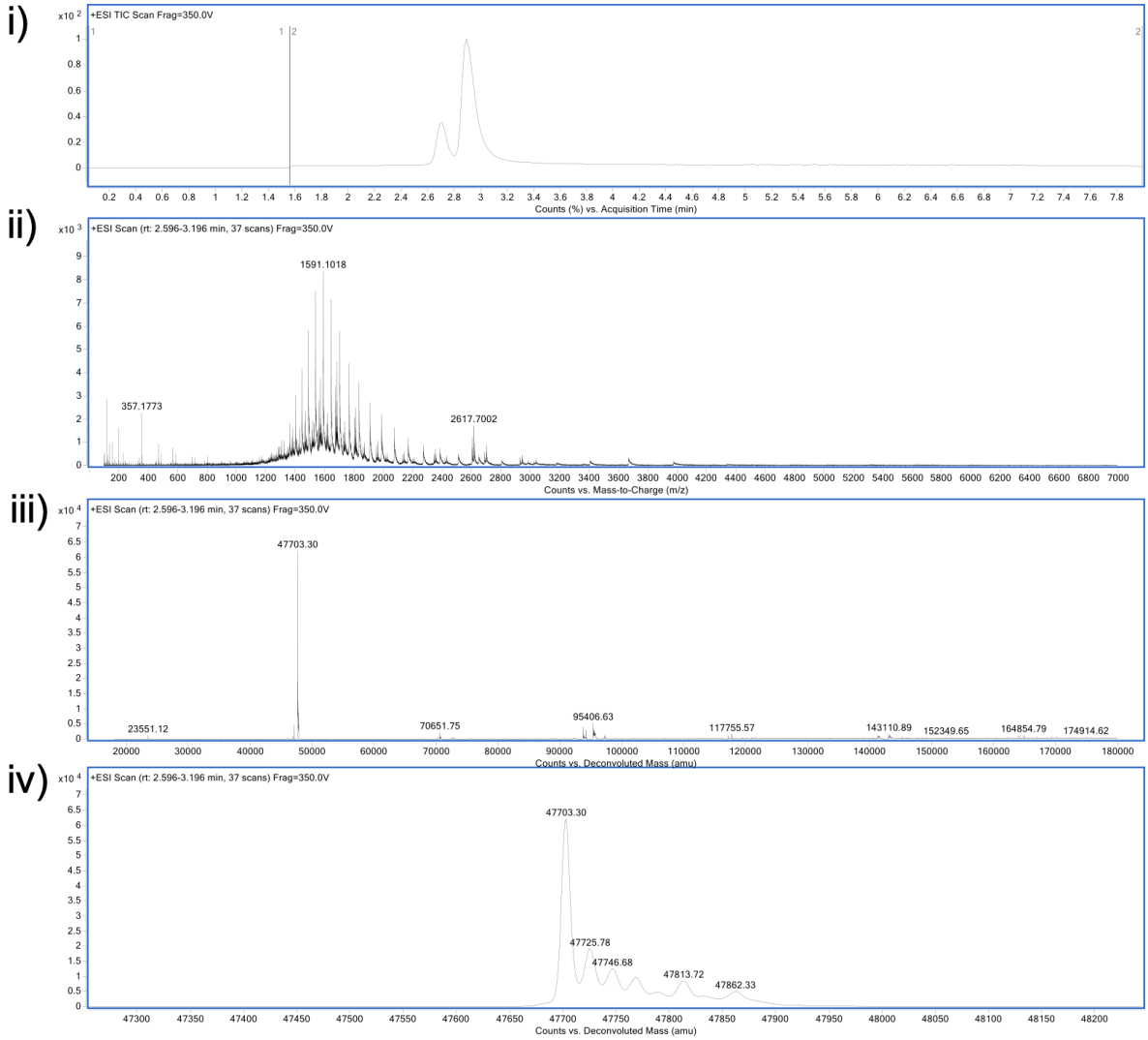


**FIGURE S.67.** Carbonimidodithioate **15** re-bridging of Fab. i) TIC. ii) non-convoluted ion series. iii) full range of deconvoluted ion series. iv) zoomed in of deconvoluted ion series. Expected mass of carbonimidodithioate re-bridged conjugate: 47703 Da. Observed: mass: 47703 Da. Mass of carbonimidodithioate **15** addition: 65 Da.

**Carbonimidodithioate 15 re-bridging of Fab with 100 eq., 1 h**

To Fab (20.0 μL, 0.0030 μmol, 150 μM, 7.15 mg/mL) in conjugation buffer was added TCEP (0.20 μL, 0.030 μmol, 150 mM in $dH_2O$, 10 eq.). After mixing for 1.5 h at 37 ºC, 300 rpm, carbonimidodithioate **15** (2.00 μL, 0.300 μmol, 150 mM in DMF, 100 eq.) was added and the reaction mixture was incubated over time at 22 ºC, 300 rpm. Timepoints were taken at 1 h, 2 h, 4 h, and 6 h. The excess reagent was removed *via* ultrafiltration (10 kDa MWCO) into LCMS water, and the sample was purified by ZebaSpin for LCMS analysis.

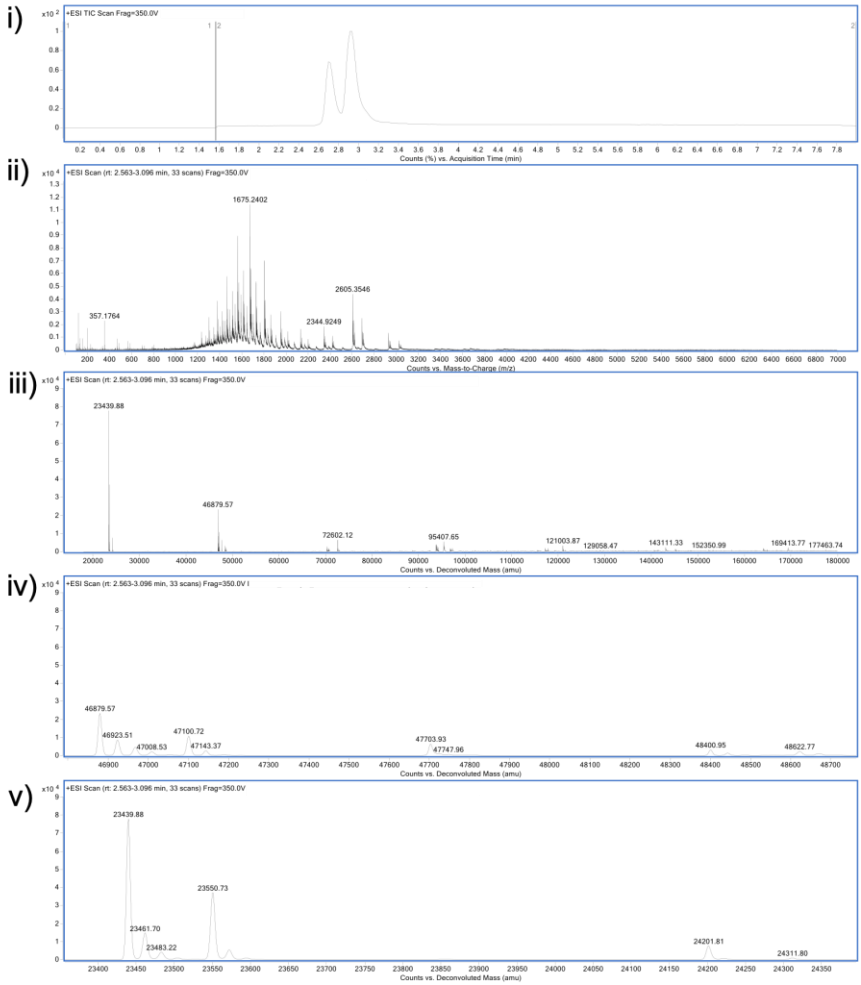


**FIGURE S.68.** Carbonimidodithioate **15** re-bridging of Fab with 100 eq. of reagent, after 1 h. i) TIC. ii) non-convoluted ion series. iii) full range of deconvoluted ion series. iv) and v) zoomed in of deconvoluted ion series. Expected mass of carbonimidodithioate re-bridged conjugate: 47703 Da. Observed: mass: LC 23439 Da, modified LC 23550 Da, HC 24201 Da, modified HC 24311 Da. Mass of mono-substituted carbonimidodithioate **15** addition: 112 Da. Mass of re-bridging carbonimidodithioate **15** addition: 65 Da.

**Carbonimidodithioate 15 re-bridging of Fab with 100 eq., 2 h**

Timepoint taken after 2 h incubation of reduced Fab with 100 eq. of carbonimidodithioate **15**. See 1 h timepoint for method.

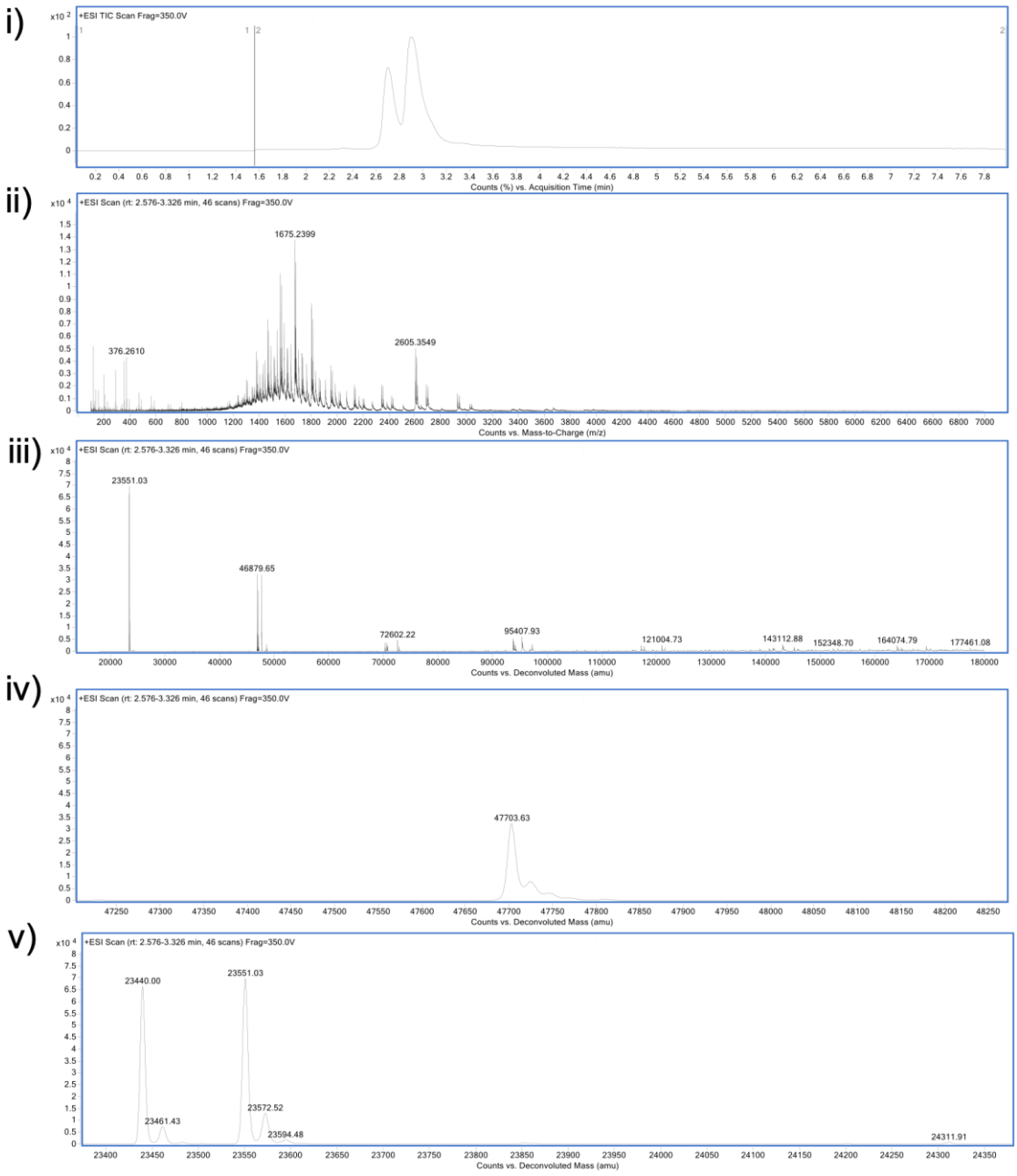


**FIGURE S.69.** Carbonimidodithioate **15** re-bridging of Fab with 100 eq. of reagent, after 2 h. i) TIC. ii) non-convoluted ion series. iii) full range of deconvoluted ion series. iv) and v) zoomed in of deconvoluted ion series. Expected mass of carbonimidodithioate re-bridged conjugate: 47703 Da. Observed: mass: 47703 Da, LC 23440 Da, modified LC 23551 Da, modified HC 24311 Da. Mass of mono-substituted carbonimidodithioate **15** addition: 112 Da. Mass of re-bridging carbonimidodithioate **15** addition: 65 Da.

**Carbonimidodithioate 15 re-bridging of Fab with 100 eq., 4 h**

Timepoint taken after 4 h incubation of reduced Fab with 100 eq. of carbonimidodithioate **15**. See 1 h timepoint for method.

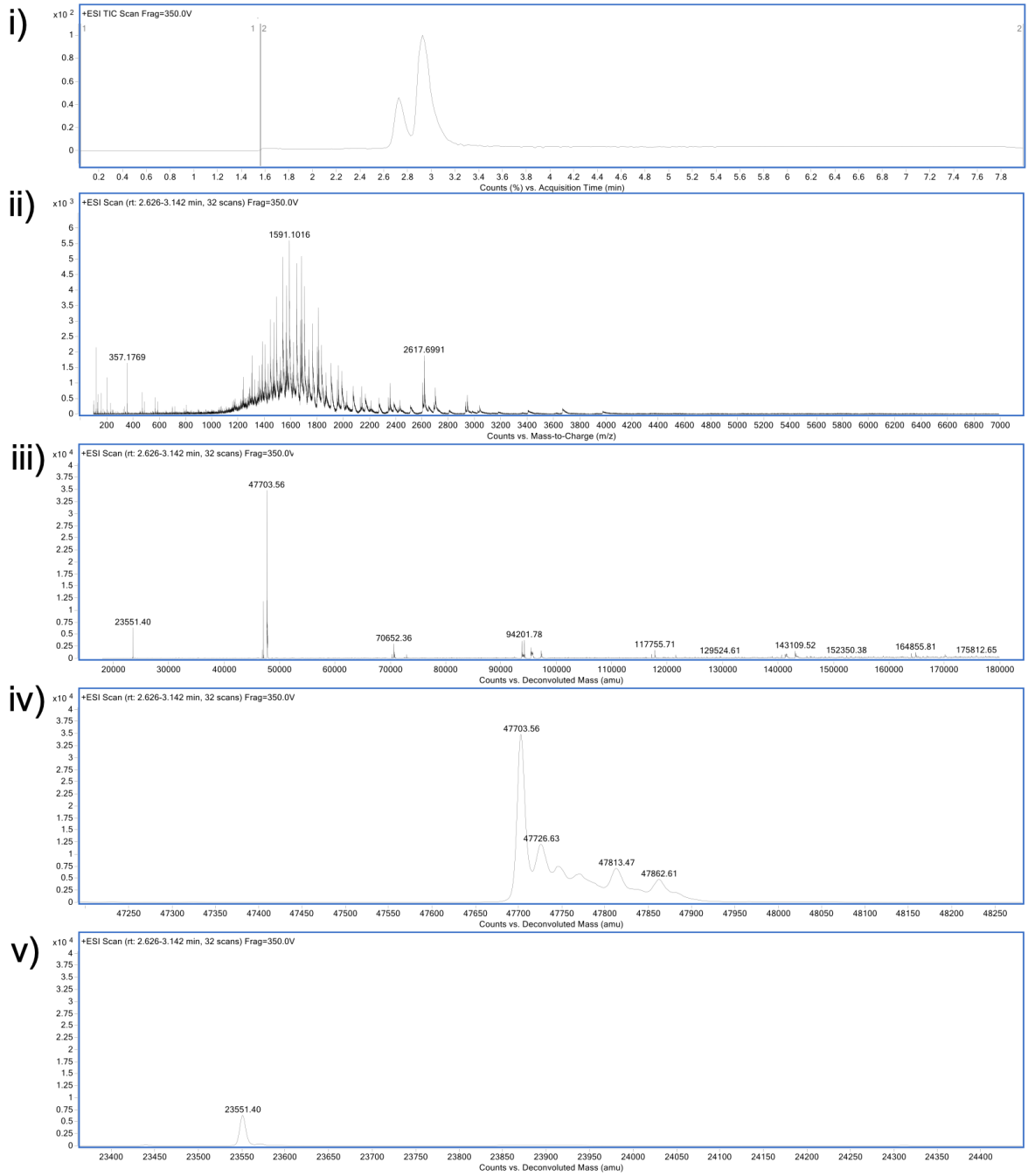


**FIGURE S.70.** Carbonimidodithioate **15** re-bridging of Fab with 100 eq. of reagent, after 4 h. i) TIC. ii) non-convoluted ion series. iii) full range of deconvoluted ion series. iv) and v) zoomed in of deconvoluted ion series. Expected mass of carbonimidodithioate re-bridged conjugate: 47703 Da. Observed: mass: 47703 Da, modified LC 23551 Da. Mass of mono-substituted carbonimidodithioate **15** addition: 112 Da. Mass of re-bridging carbonimidodithioate **15** addition: 65 Da.

**Carbonimidodithioate 15 re-bridging of Fab with 100 eq., 6 h**

Timepoint taken after 6 h incubation of reduced Fab with 100 eq. of carbonimidodithioate **15**. See 1 h timepoint for method.

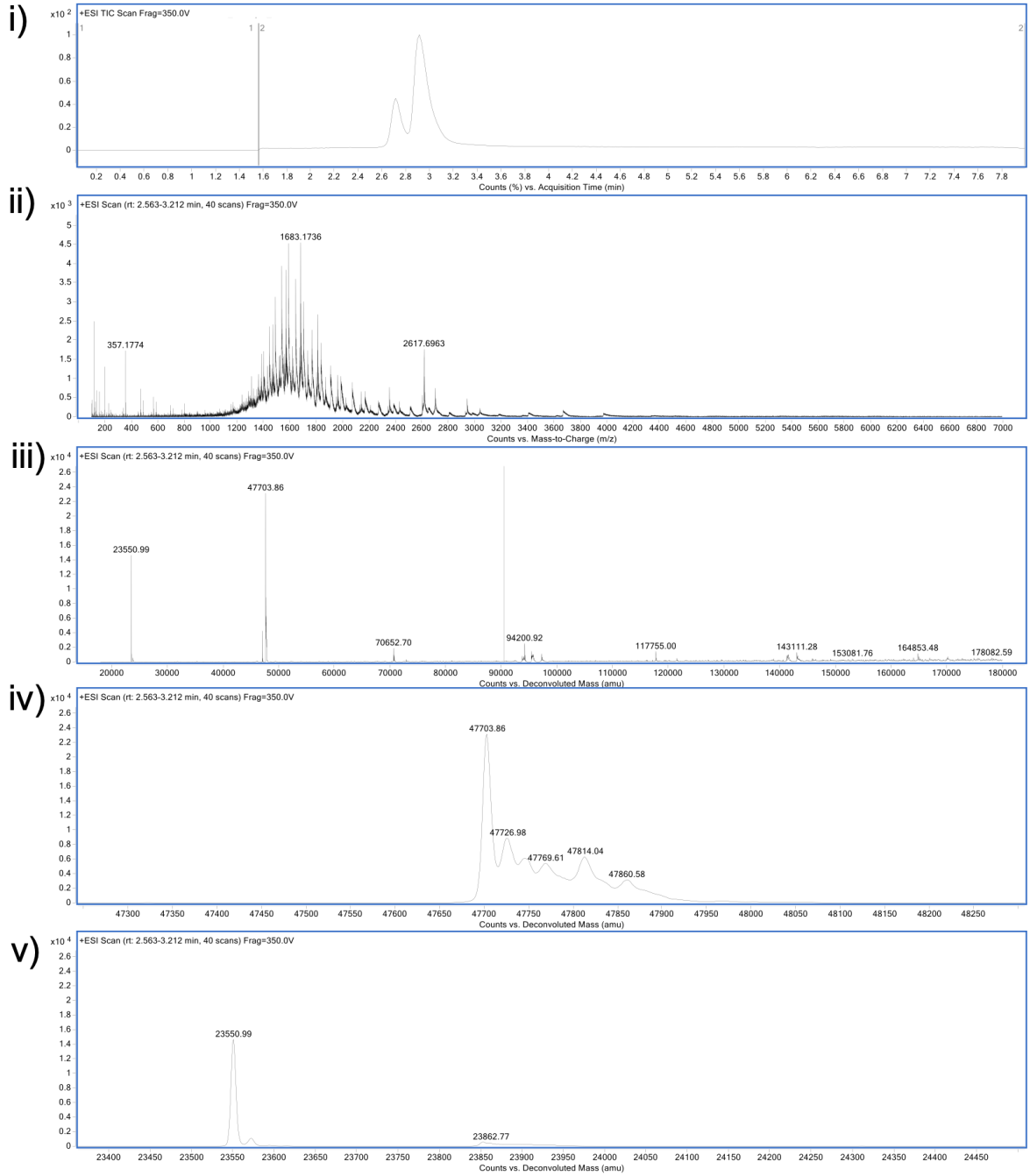


**FIGURE S.71.** Carbonimidodithioate **15** re-bridging of Fab with 100 eq. of reagent, after 4 h. i) TIC. ii) non-convoluted ion series. iii) full range of deconvoluted ion series. iv) and v) zoomed in of deconvoluted ion series. Expected mass of carbonimidodithioate re-bridged conjugate: 47703 Da. Observed: mass: 47703 Da, modified LC 23551 Da. Mass of mono-substituted carbonimidodithioate **15** addition: 112 Da. Mass of re-bridging carbonimidodithioate **15** addition: 65 Da.

**Carbonimidodithioate re-bridged conjugate CLT**

Prepared carbonimidodithioate re-bridged conjugate (40 μL, 150 μM) was washed *via* ultrafiltration 10 kDa MWCO) into BBS pH 8.4 (5 x 80 μL). The concentration of the carbonimidodithioate re-bridged conjugate was calculated. The conjugate was diluted to 20 μM with BBS pH 8.4 and further incubated at pH 8.4 for 24 h at 22 ºC, 300 rpm The sample was purified by ZebaSpin for LCMS analysis.

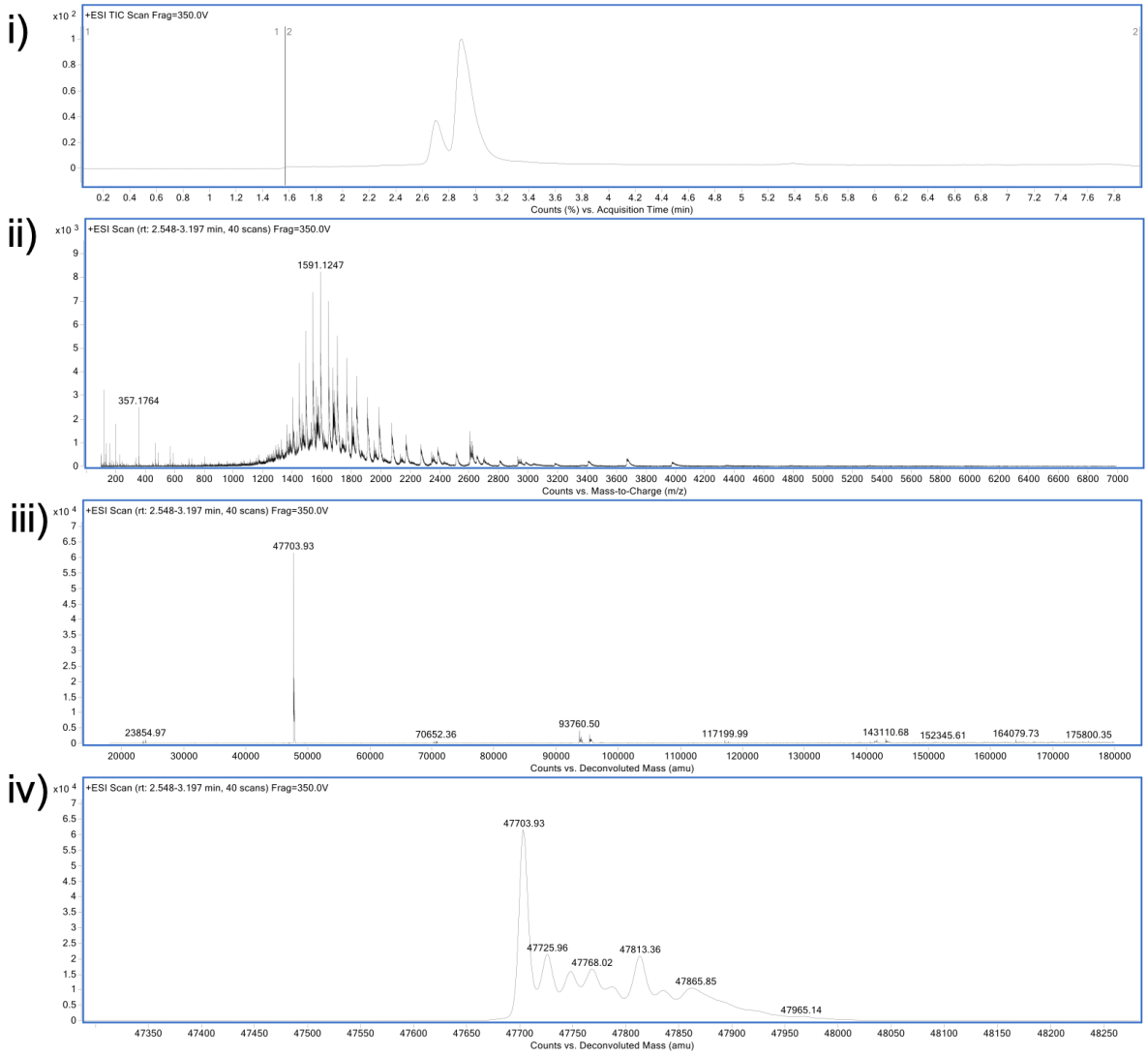


**FIGURE S.72.** LCMS analysis of carbonimidodithioate re-bridged conjugate. i) TIC. ii) non-convoluted ion series. iii) full range of deconvoluted ion series. iv) zoomed in of deconvoluted ion series. Expected mass of carbonimidodithioate conjugate: 47703 Da. Observed: 47703 Da.

**Carbonimidodithioate mono-substituted conjugate CLT**

Prepared carbonimidodithioate mono-substituted conjugate (40 μL, 150 μM) was washed *via* ultrafiltration 10 kDa MWCO) into BBS pH 8.4 (5 x 80 μL). The concentration of the carbonimidodithioate mono-substituted conjugate was calculated. The conjugate was diluted to 20 μM with BBS pH 8.4 and further incubated at pH 8.4 for 24 h at 22 ºC, 300 rpm. The sample was purified by ZebaSpin for LCMS analysis.

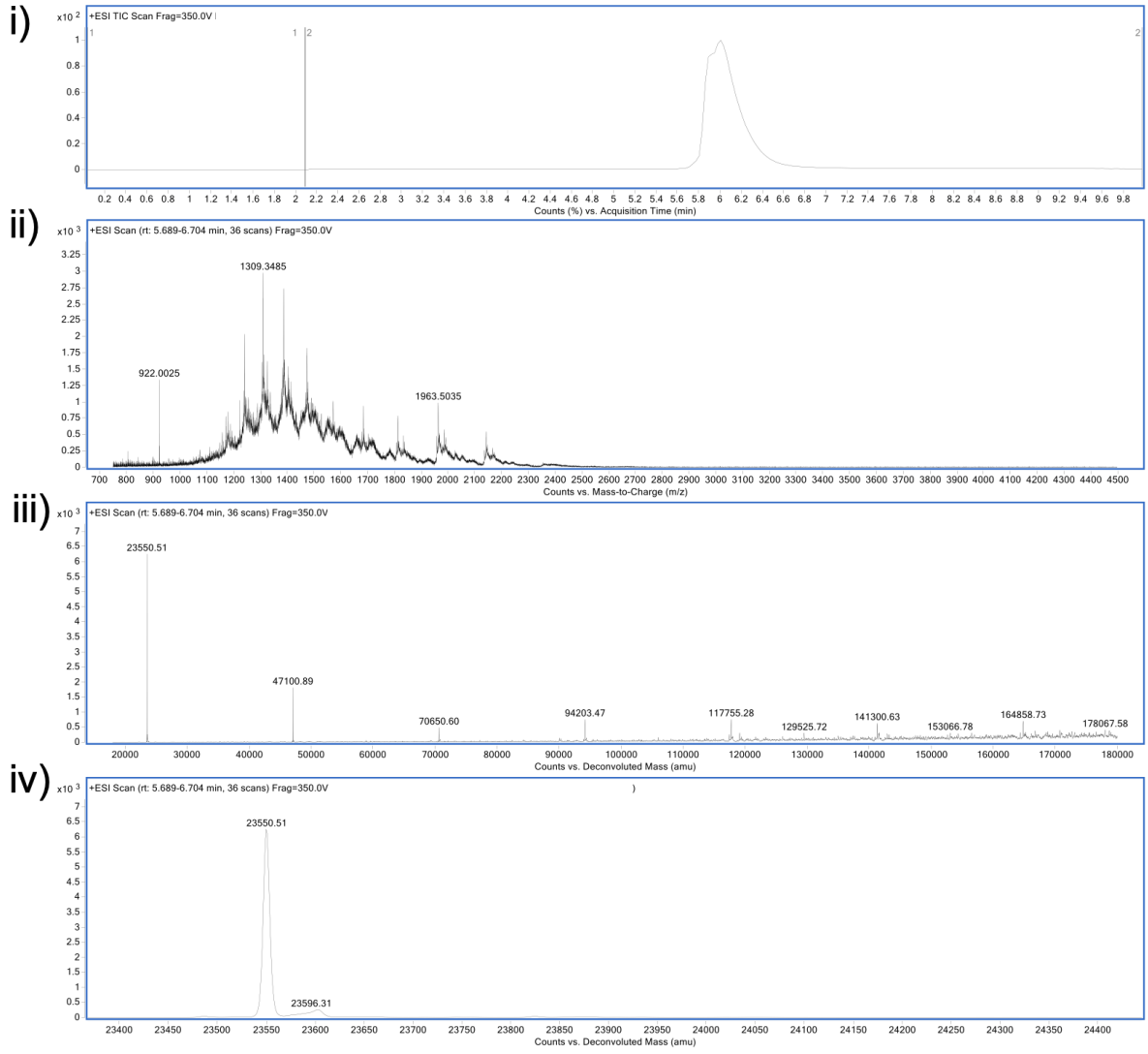


**FIGURE S.73.** LCMS analysis of mono-substituted conjugate. i) TIC. ii) non-convoluted ion series. iii) full range of deconvoluted ion series. iv) zoomed in of deconvoluted ion series. Expected mass of mono-substituted carbonimidodithioate conjugate: 23550 Da. Observed: 23550 Da.

**Carbonimidodithioate re-bridged conjugate substitution with *p*-anisidine, 1 h**

Prepared carbonimidodithioate re-bridged conjugate (40 μL, 150 μM) was washed *via* ultrafiltration (10 kDa MWCO) into conjugation buffer (5 x 80 μL). The concentration of the carbonimidodithioate re-bridged conjugate was calculated. *p*-anisidine (150 mM in DMF, 100 eq.) was added and the reaction mixture was further incubated over time at 37 ºC, 300 rpm. Timepoints were taken at 1 h, 4 h, and 24 h. The excess reagent was removed *via* ultrafiltration (10 kDa MWCO) into LCMS water, and the sample was purified by ZebaSpin for LCMS analysis.

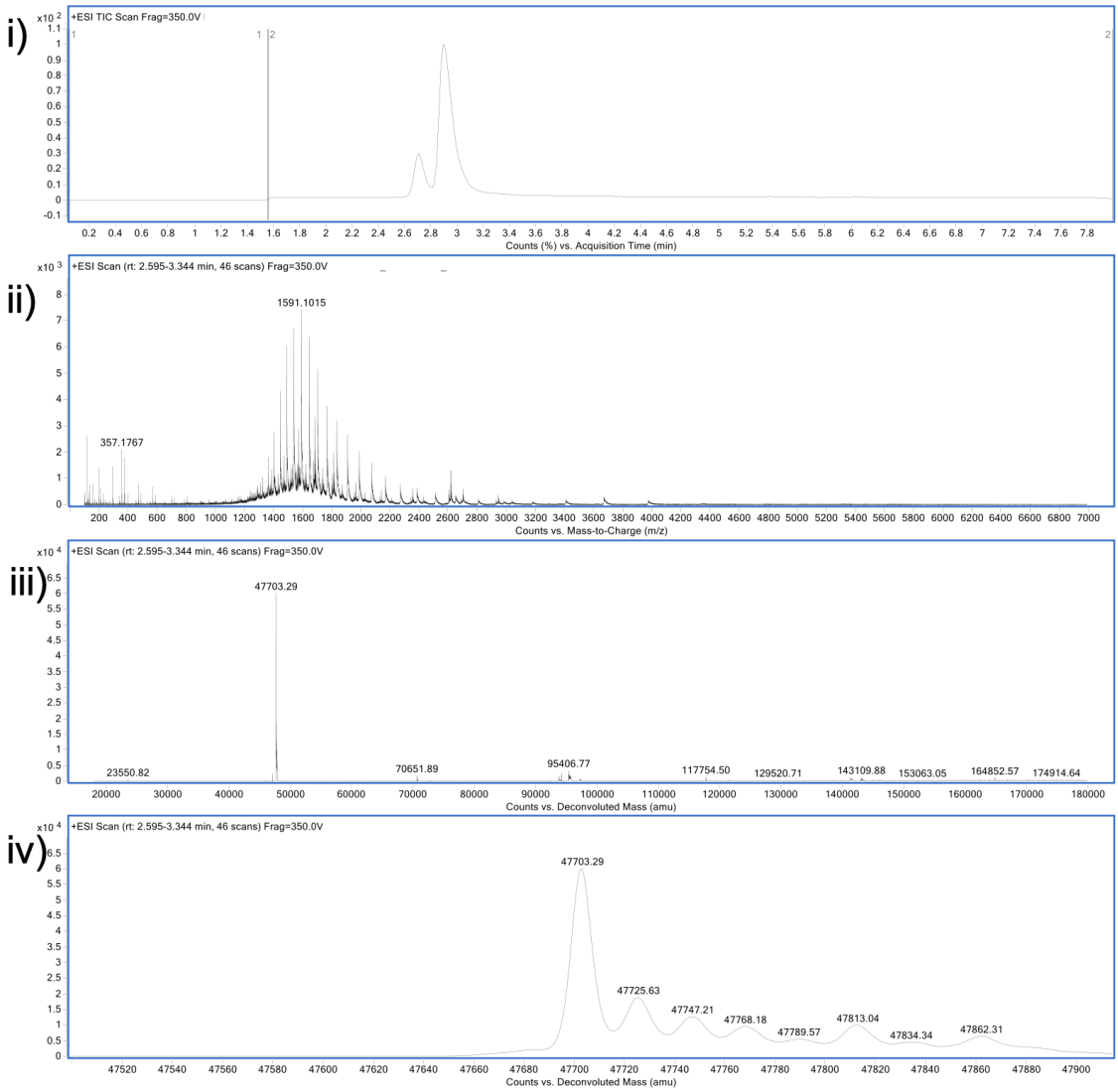


**FIGURE S.74.** LCMS analysis of 1 h *p*-anisidine addition to carbonimidodithioate re-bridged conjugate. i) TIC. ii) non-convoluted ion series. iii) full range of deconvoluted ion series. iv) and v) zoomed in of deconvoluted ion series. Mass of dithiocarbonate re-bridged conjugate: 47703 Da. Observed: 47703 Da. Expected mass of *p*-anisidine addition: 123 Da.

**Carbonimidodithioate re-bridged conjugate substitution with *p*-anisidine, 4 h**

Timepoint taken after 4 h incubation with *p*-anisidine addition to carbonimidodithioate re-bridged conjugate. See 1 h timepoint for method.

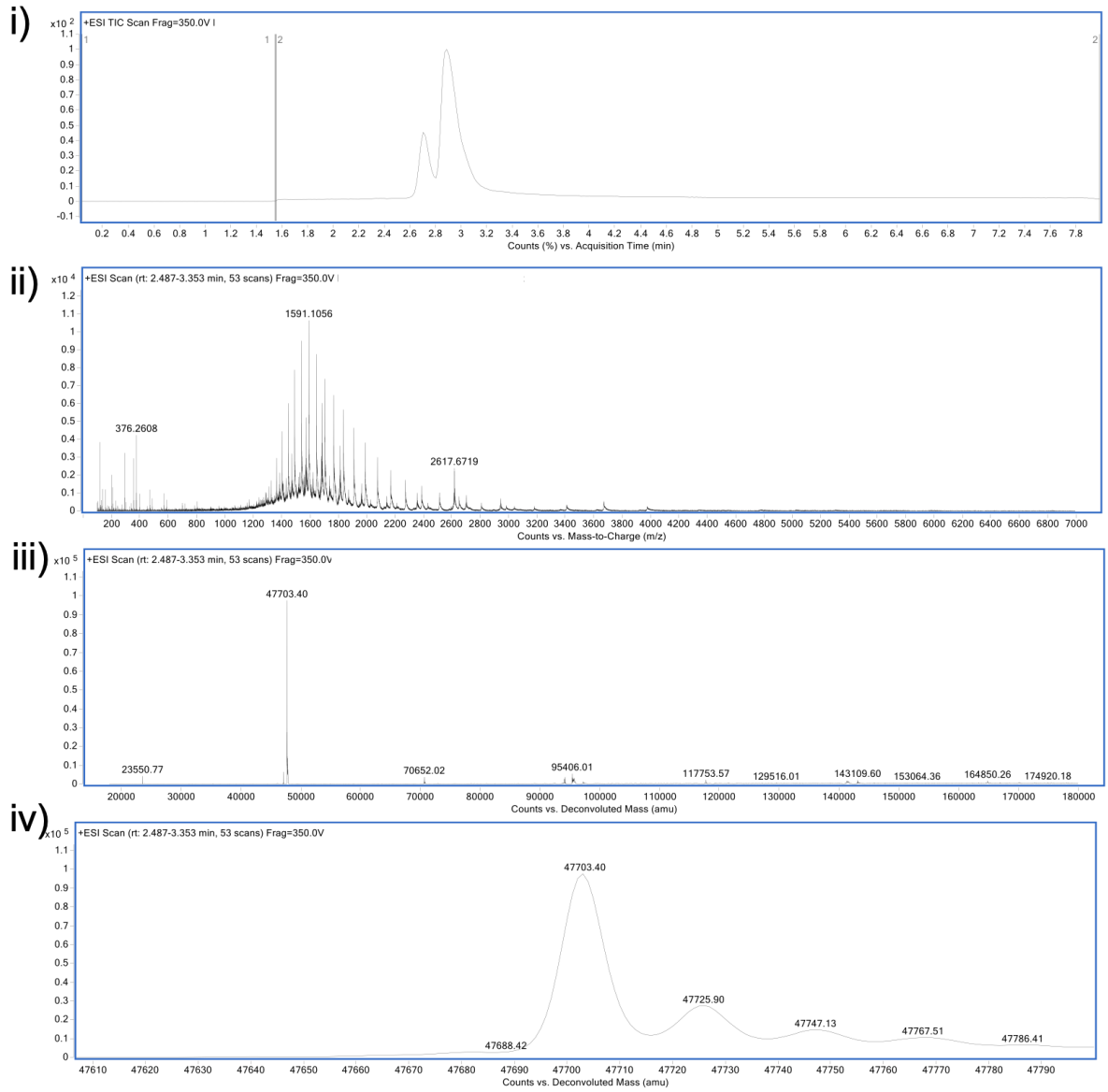


**FIGURE S.75.** LCMS analysis of 4 h *p*-anisidine addition to carbonimidodithioate re-bridged conjugate. i) TIC. ii) non-convoluted ion series. iii) full range of deconvoluted ion series. iv) and v) zoomed in of deconvoluted ion series. Mass of dithiocarbonate re-bridged conjugate: 47703 Da. Observed: 47703 Da. Expected mass of *p*-anisidine addition: 123 Da.

**Carbonimidodithioate re-bridged conjugate substitution with *p*-anisidine, 24 h**

Timepoint taken after 4 h incubation with *p*-anisidine addition to carbonimidodithioate re-bridged conjugate. See 1 h timepoint for method.

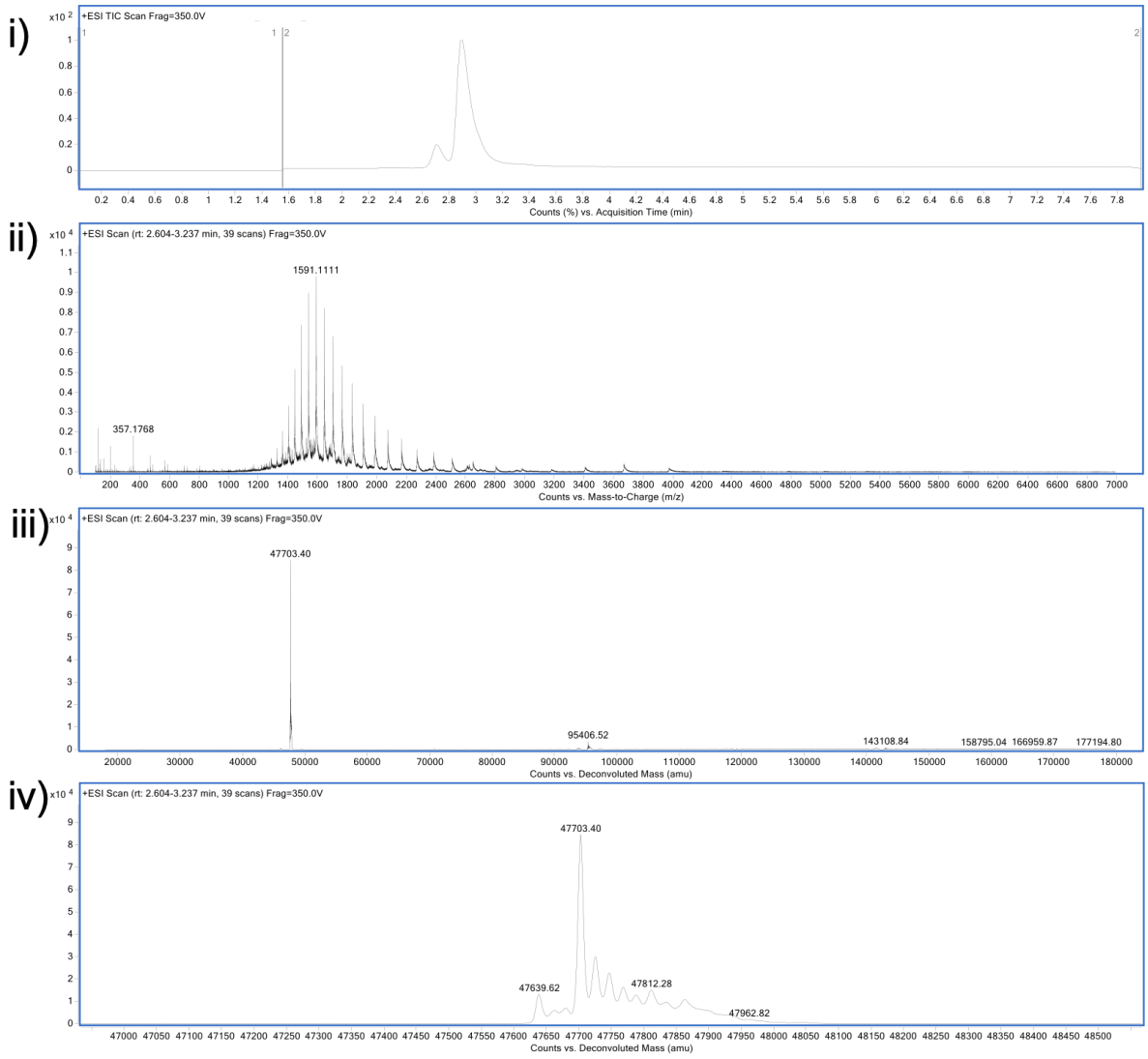


**FIGURE S.76.** LCMS analysis of 24 h *p*-anisidine addition to carbonimidodithioate re-bridged conjugate. i) TIC. ii) non-convoluted ion series. iii) full range of deconvoluted ion series. iv) and v) zoomed in of deconvoluted ion series. Mass of dithiocarbonate re-bridged conjugate: 47703 Da. Observed: 477703 Da, 47639 Da. Expected mass of *p*-anisidine addition: 123 Da.

**Carbonimidodithioate re-bridged conjugate aqueous stability (3 days)**

Prepared carbonimidodithioate re-bridged conjugate (40 μL, 150 μM) was washed *via* ultrafiltration 10 kDa MWCO) into LCMS water. The concentration of the carbonimidodithioate re-bridged conjugate was calculated, and adjusted to 100 μM. The conjugate was incubated at 22 ºC for 3 days, 300 rpm. The sample was purified by ZebaSpin for LCMS analysis.

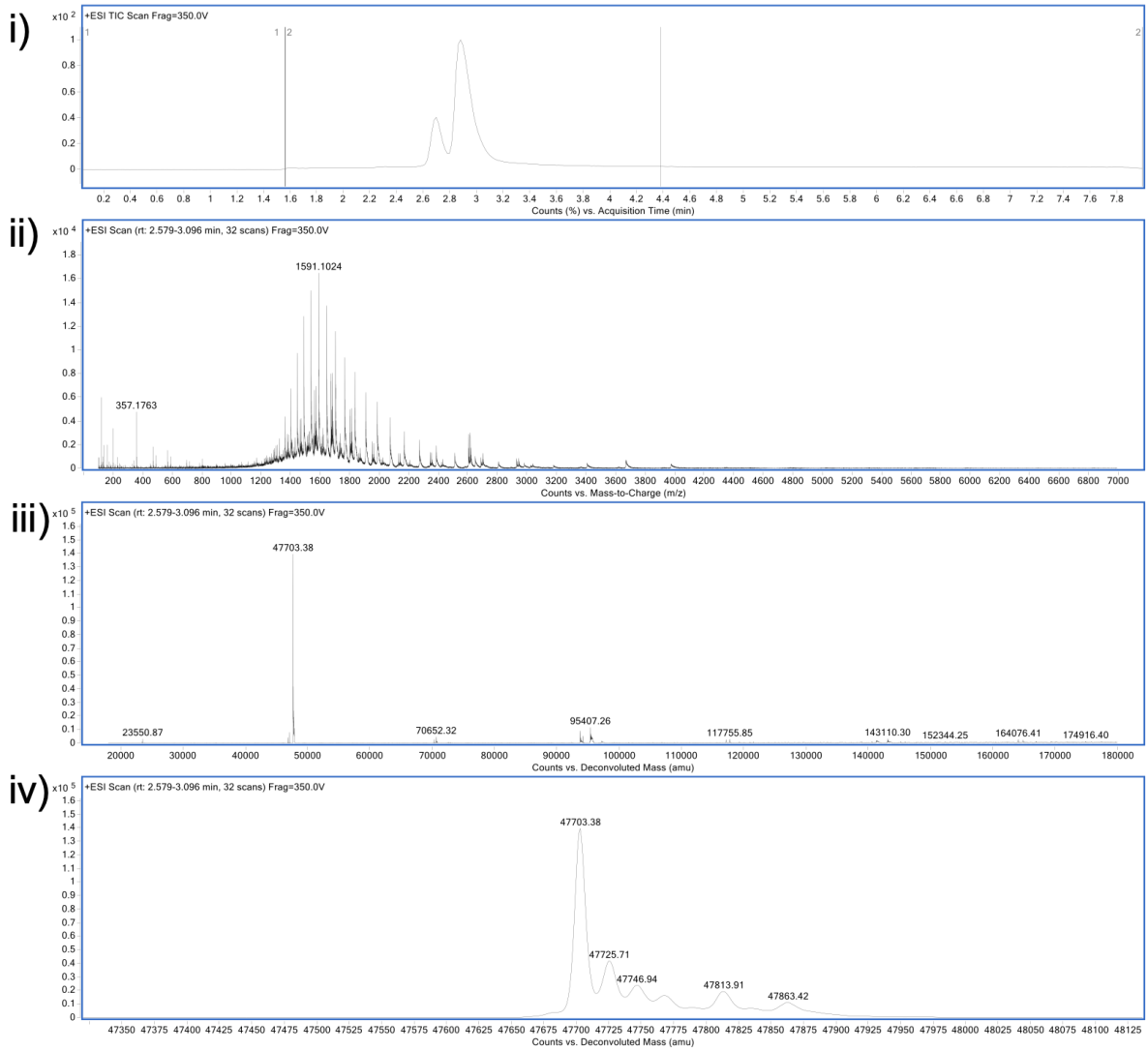


**FIGURE S.77.** LCMS analysis of 3-day aqueous stability of carbonimidodithioate re-bridged conjugate. i) TIC. ii) non-convoluted ion series. iii) full range of deconvoluted ion series. iv) zoomed in of deconvoluted ion series. Expected mass of dithiocarbonate re-bridged conjugate: 47703 Da. Observed: 47703 Da.

**Carbonimidodithioate re-bridged conjugate aqueous stability (7 days)**

Prepared carbonimidodithioate re-bridged conjugate (40 μL, 150 μM) was washed *via* ultrafiltration 10 kDa MWCO) into LCMS water. The concentration of the carbonimidodithioate re-bridged conjugate was calculated, and adjusted to 100 μM. The conjugated was incubated at 22 ºC for 7 days, 300 rpm. The sample was purified by ZebaSpin for LCMS analysis.

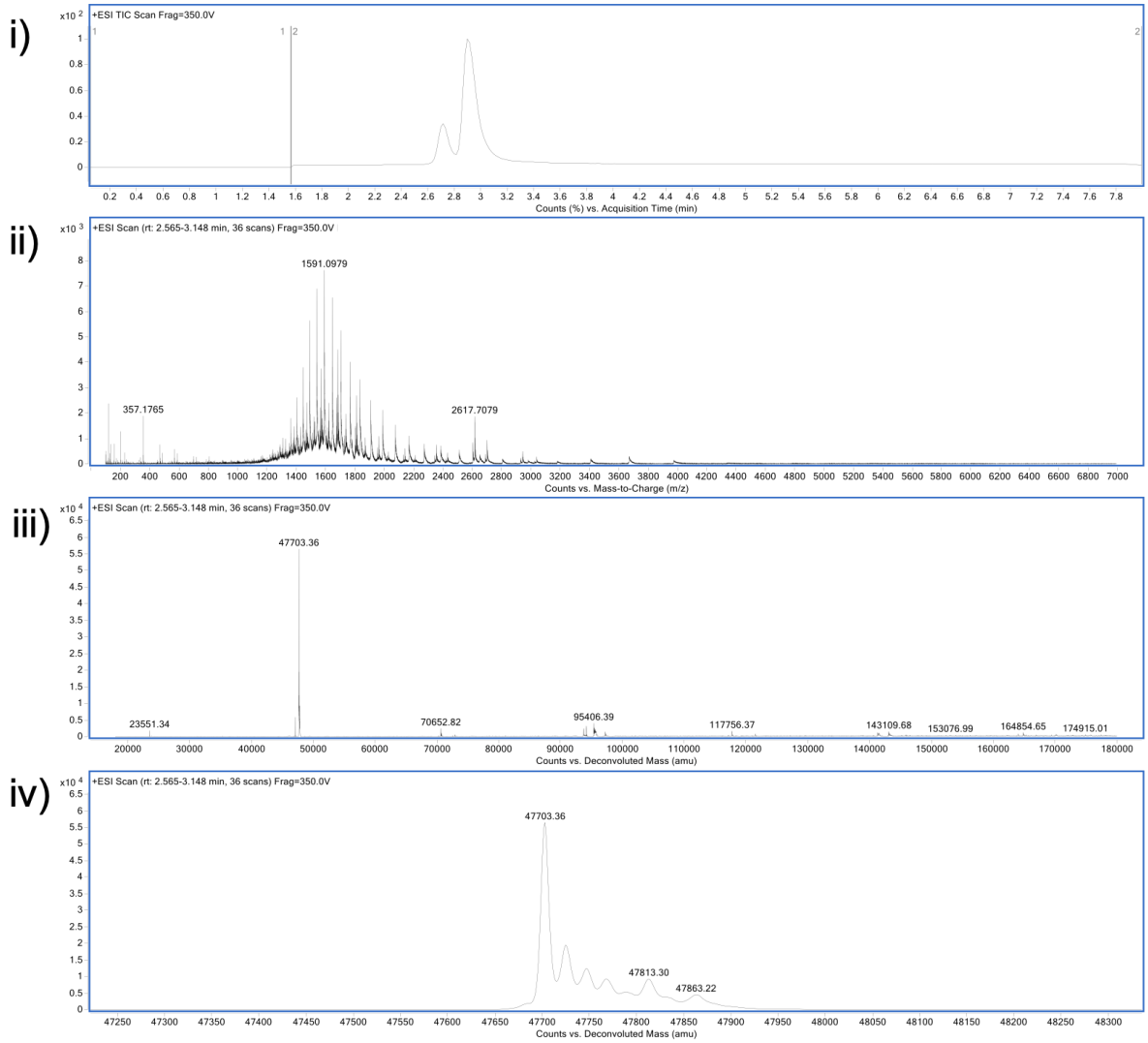


**FIGURE S.78.** LCMS analysis of 7-day aqueous stability of carbonimidodithioate re-bridged conjugate. i) TIC. ii) non-convoluted ion series. iii) full range of deconvoluted ion series. iv) zoomed in of deconvoluted ion series. Expected mass of dithiocarbonate re-bridged conjugate: 47703 Da. Observed: 47703 Da.

**Carbonimidodithioate re-bridged conjugate serum stability (1 h)**

Prepared carbonimidodithioate re-bridged conjugate (40 μL, 150 μM) was washed *via* ultrafiltration 10 kDa MWCO) into LCMS water. The concentration of the carbonimidodithioate re-bridged conjugate was calculated. The conjugate was diluted to 7 μM by the addition of serum-mimicking solution (glutathione, 100 μM stock, conjugation buffer at pH 7.4). The reaction mixture was further incubated at 37 ºC, 300 rpm over time. Time points were taken at 1 h, 4 h, and 24 h. The sample(s) were prepared by ZebaSpin for LCMS analysis.

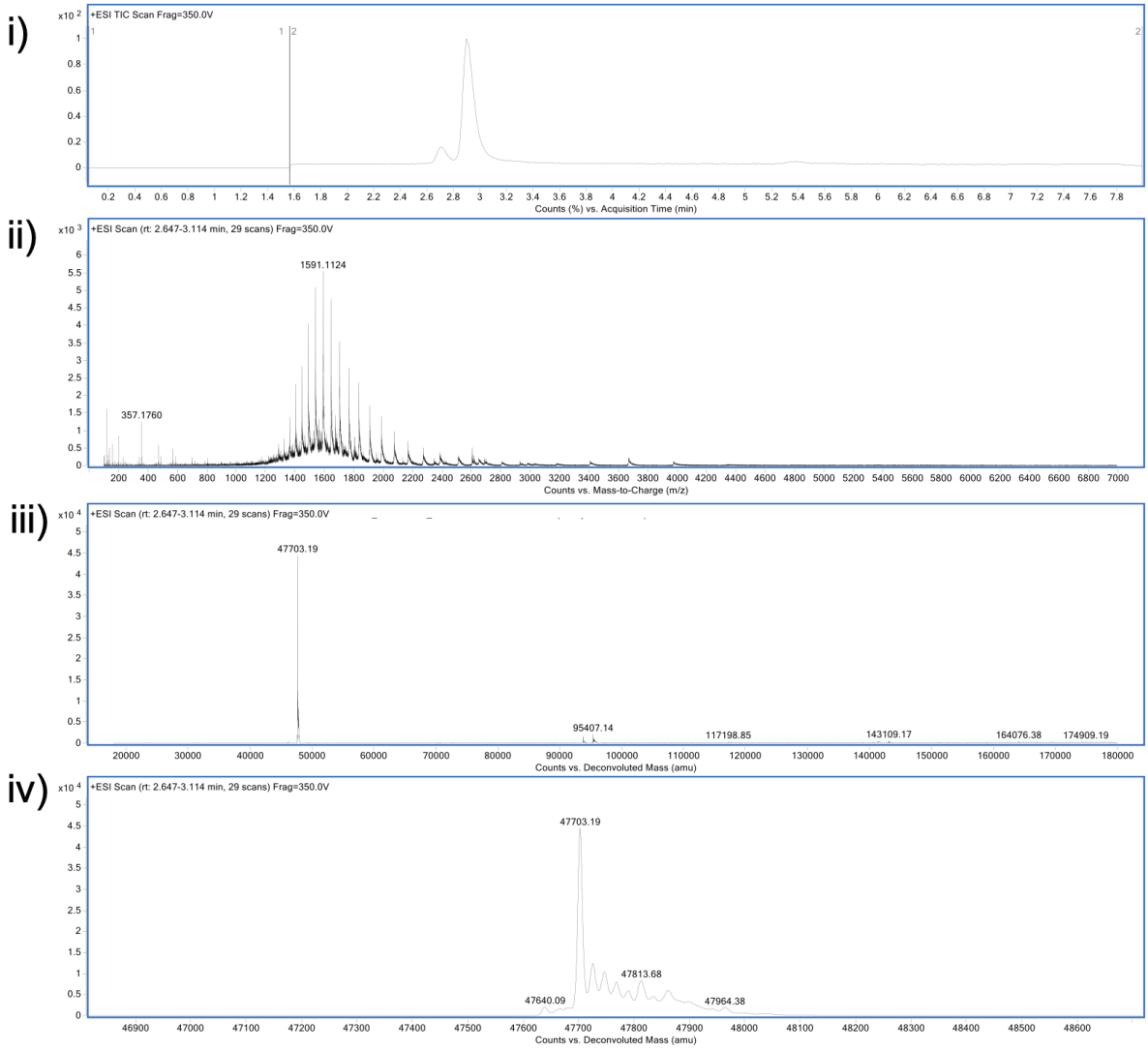


**FIGURE S.79.** LCMS analysis of 1 h serum stability of dithiocarbonate re-bridged conjugate. i) TIC. ii) non-convoluted ion series. iii) full range of deconvoluted ion series. iv) zoomed in of deconvoluted ion series. Expected mass of dithiocarbonate re-bridged conjugate: 47703 Da. Observed: 47703 Da.

**Carbonimidodithioate re-bridged conjugate serum stability (4 h)**

Timepoint taken after 4 h incubation of carbonimidodithioate re-bridged conjugate in serum-mimicking conditions. See 1 h timepoint for method.

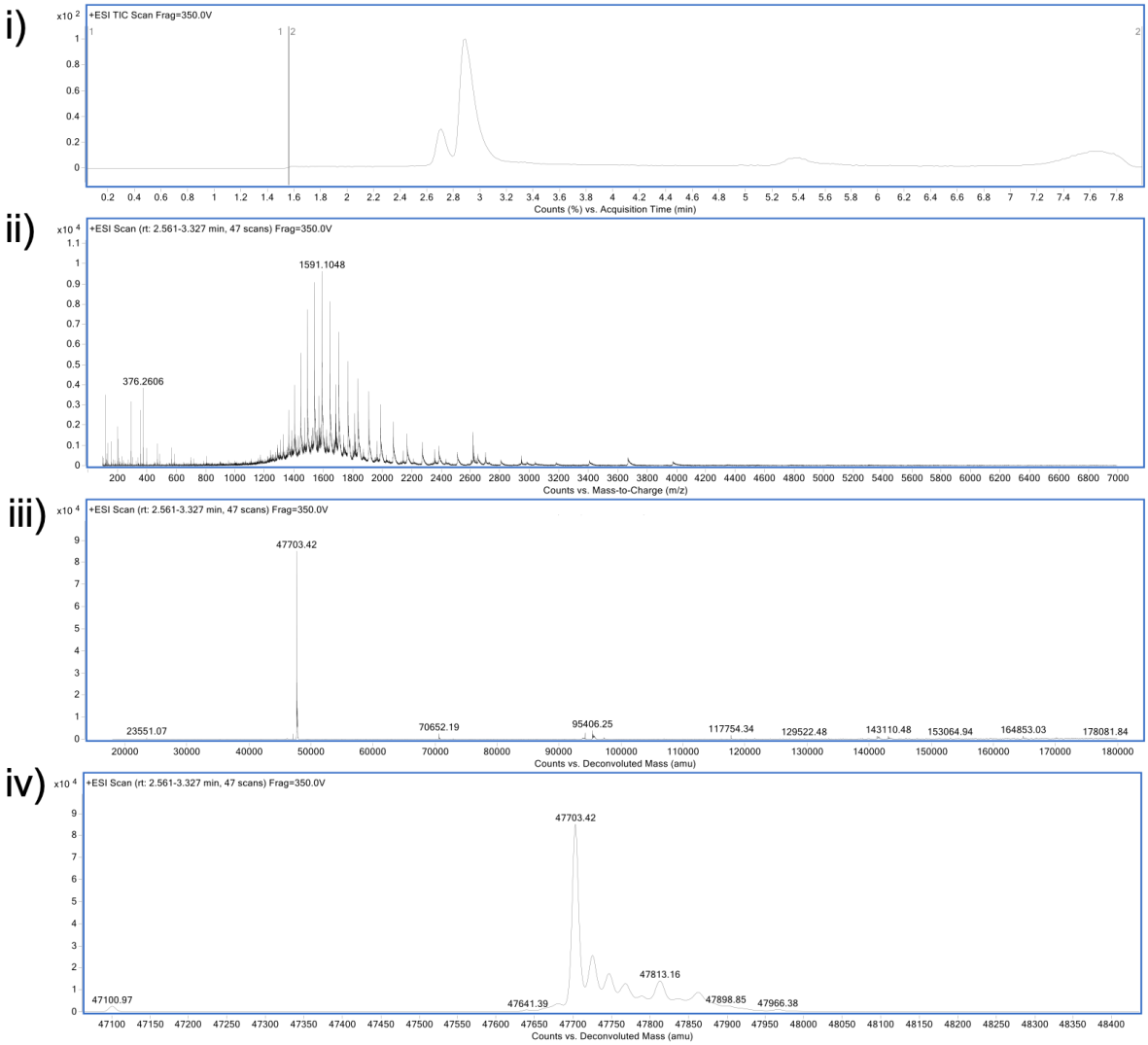


**FIGURE S.80.** LCMS analysis of 4 h serum stability of dithiocarbonate re-bridged conjugate. i) TIC. ii) non-convoluted ion series. iii) full range of deconvoluted ion series. iv) zoomed in of deconvoluted ion series. Expected mass of dithiocarbonate re-bridged conjugate: 47703 Da. Observed: 47703 Da.

**Carbonimidodithioate re-bridged conjugate serum stability (24 h)**

Timepoint taken after 24 h incubation of carbonimidodithioate re-bridged conjugate in serum-mimicking conditions. See 1 h timepoint for method.

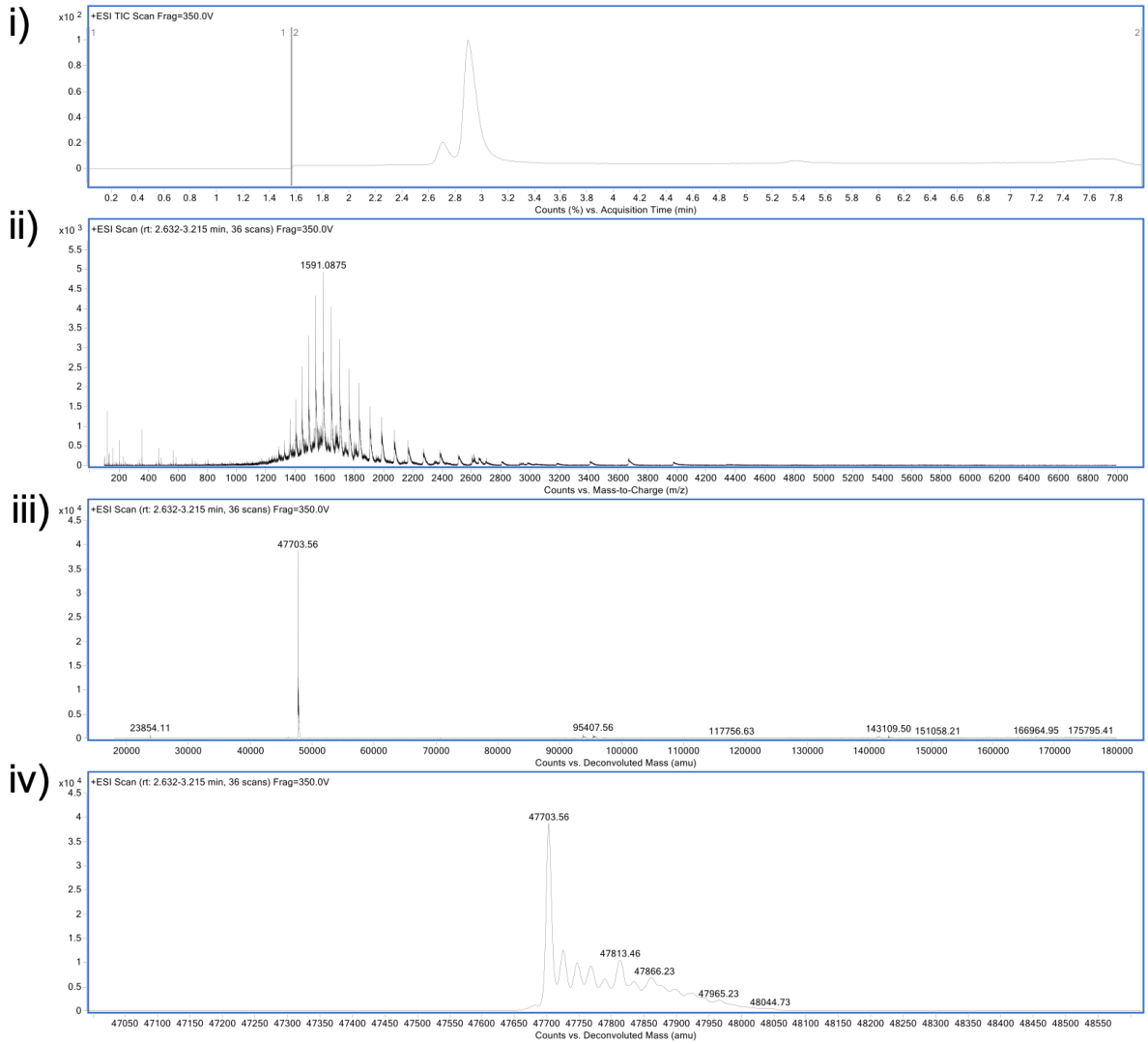


**FIGURE S.81.** LCMS analysis of 24 h serum stability of dithiocarbonate re-bridged conjugate. i) TIC. ii) non-convoluted ion series. iii) full range of deconvoluted ion series. iv) zoomed in of deconvoluted ion series. Expected mass of dithiocarbonate re-bridged conjugate: 47703 Da. Observed: 47703 Da.

**Carbonimidodithioate re-bridged conjugate early endosomal stability (1 h)**

Prepared carbonimidodithioate re-bridged conjugate (40 μL, 150 μM) was washed *via* ultrafiltration 10 kDa MWCO) into LCMS water. The concentration of the carbonimidodithioate re-bridged conjugate was calculated. The conjugate was diluted to 7 μM by the addition of early endosomal-mimicking solution (glutathione, 100 mM stock, conjugation buffer at pH 6.5). The reaction mixture was further incubated at 37 ºC, 300 rpm over time. Time points were taken at 1 h, 4 h, and 24 h. The sample(s) were prepared by ZebaSpin for LCMS analysis.

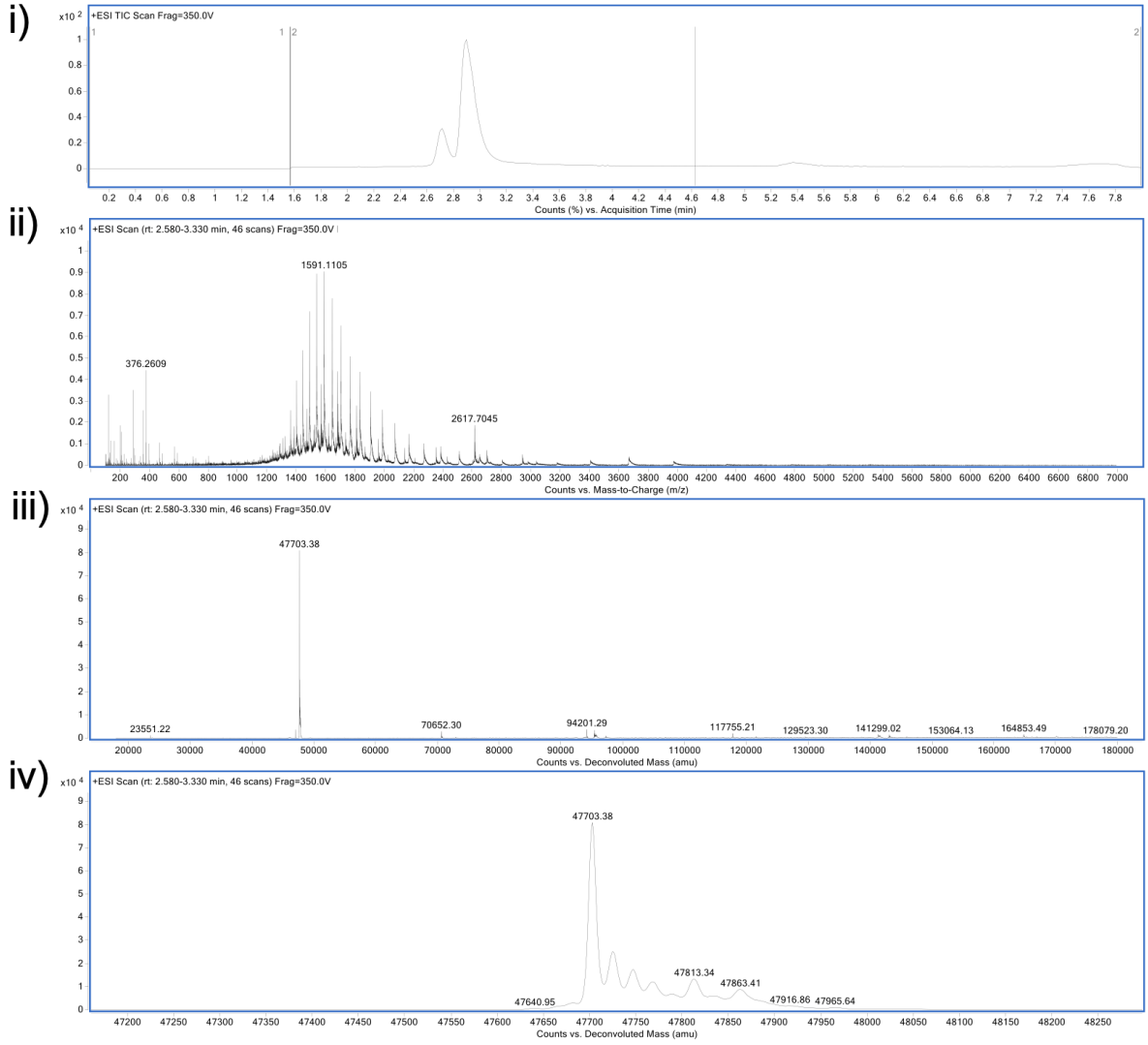


**FIGURE S.82.** LCMS analysis of 1 h early endosomal stability of dithiocarbonate re-bridged conjugate. i) TIC. ii) non-convoluted ion series. iii) full range of deconvoluted ion series. iv) zoomed in of deconvoluted ion series. Expected mass of dithiocarbonate re-bridged conjugate: 47703 Da. Observed: 47703 Da.

**Carbonimidodithioate re-bridged conjugate endosomal stability (4 h)**

Timepoint taken after 4 h incubation of carbonimidodithioate re-bridged conjugate in early endosomal-mimicking conditions. See 1 h timepoint for method.

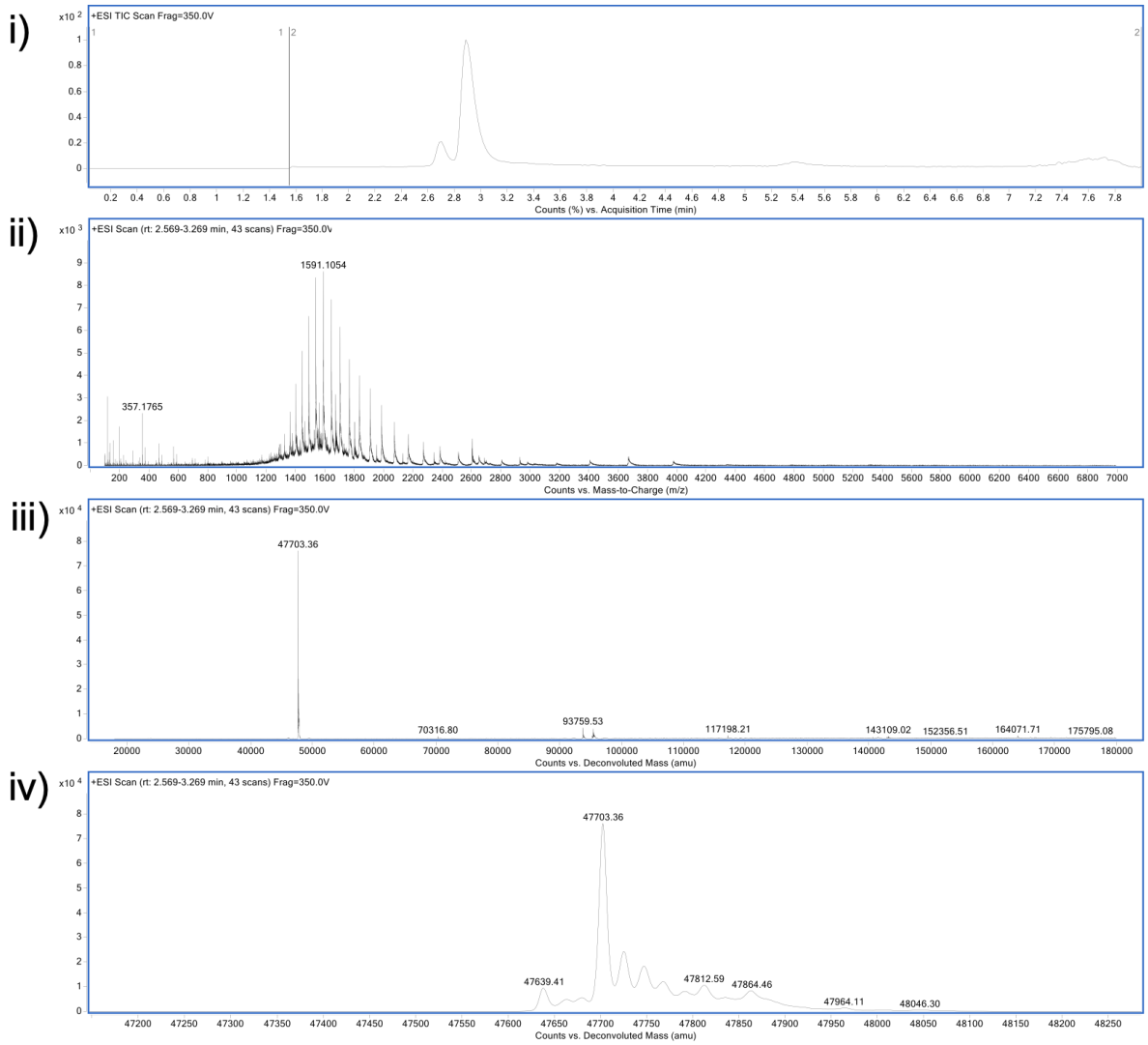


**FIGURE S.83.** LCMS analysis of 4 h endosomal stability of dithiocarbonate re-bridged conjugate. i) TIC. ii) non-convoluted ion series. iii) full range of deconvoluted ion series. iv) zoomed in of deconvoluted ion series. Expected mass of dithiocarbonate re-bridged conjugate: 47703 Da. Observed: 47703 Da, 47639 Da.

**Carbonimidodithioate re-bridged conjugate endosomal stability (24 h)**

Timepoint taken after 24 h incubation of carbonimidodithioate re-bridged conjugate in early endosomal-mimicking conditions. See 1 h timepoint for method.

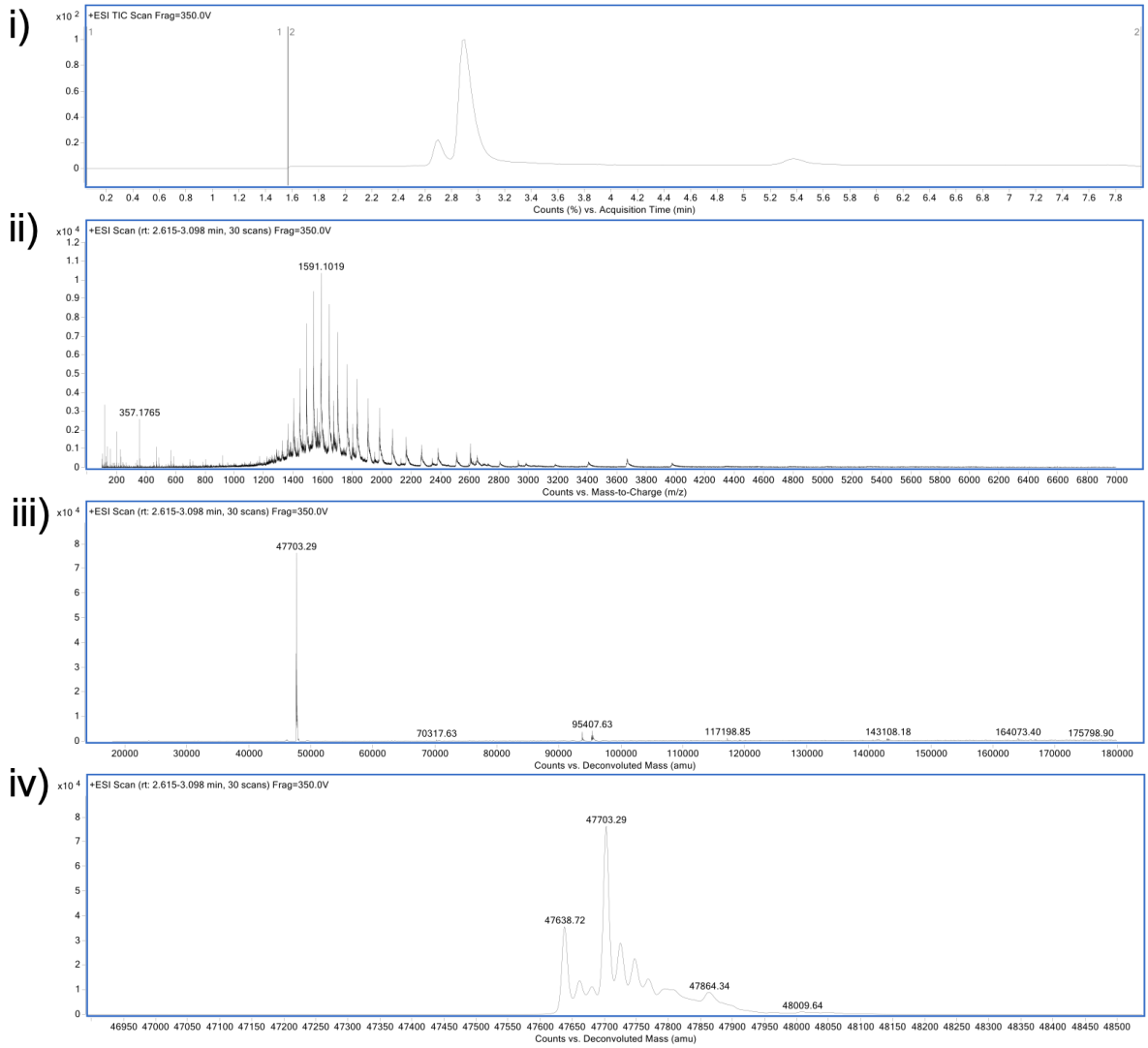


**FIGURE S.84.** LCMS analysis of 24 h early endosomal stability of dithiocarbonate re-bridged conjugate. i) TIC. ii) non-convoluted ion series. iii) full range of deconvoluted ion series. iv) zoomed in of deconvoluted ion series. Expected mass of dithiocarbonate re-bridged conjugate: 47703 Da. Observed: 47703 Da, 47638 Da.

**Carbonimidodithioate re-bridging of trastuzumab**

To trastuzumab (60.0 μL, 0.0013 μmol, 22 μM, 3.83 mg/mL) in conjugation buffer was added TCEP (0.88 μL, 0.013 μmol, 15.0 mM in $dH_2O$, 10 eq.). After mixing for 1.5 h at 37 ºC, 300 rpm, carbonimidodithioate **15** (0.18 μL, 0.013 μmol, 150 mM in DMF, 20 eq.) was added and the reaction mixture was incubated for 24 h at 22 ºC, 300 rpm. The excess reagent was removed *via* ultrafiltration (10 kDa MWCO) into ammonium acetate (pH 5.0) and prepared by ZebaSpin for LCMS analysis. PNGase (1.0 μL) was added, and the sample was incubated for 16 h at 37 ºC prior to LCMS analysis.

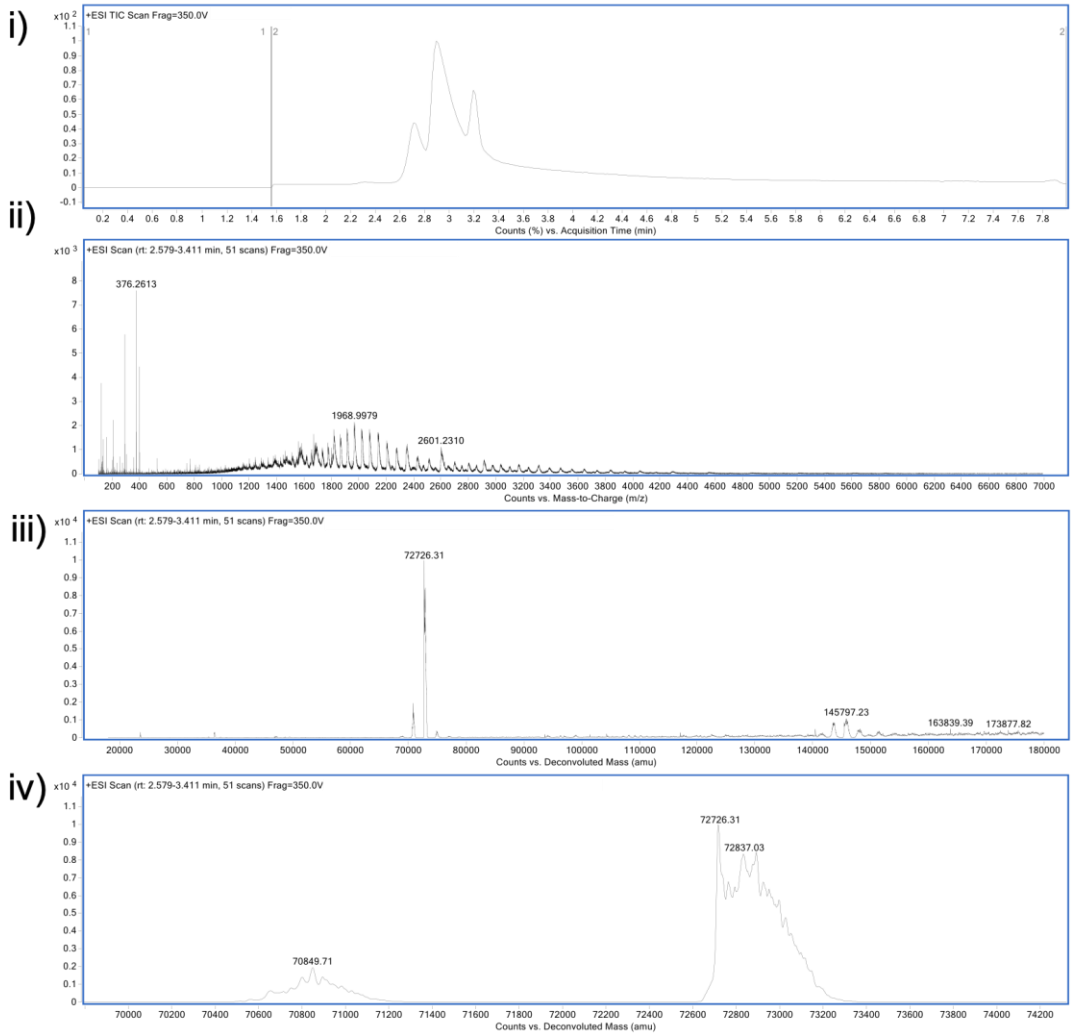


**FIGURE S.85.** Carbonimidodithioate **15** re-bridging of trastuzumab. i) TIC. ii) non-convoluted ion series. iii) full range of deconvoluted ion series. iv) zoomed in of deconvoluted ion series. Expected mass of dithiocarbonate re-bridged conjugate: HHLL 145446 Da (4 additions), HL 72724 Da (2 additions). Observed: re-bridged modified HL 72726 Da (2 re-bridging additions), modified HL 72837 Da modified HHLL 145797 Da.

**Aldehyde-thioester 16 conjugation on non-reduced Fab (control)**

To Fab (20.0 μL, 0.0030 μmol, 150 μM, 7.15 mg/mL) in conjugation buffer was added aldehyde-thioester (0.40 μL, 0.060 μmol, 150 mM in DMF, 20 eq.). The sample was incubated for 4 h at 22 ºC, 300 rpm. The excess reagent was removed *via* ultrafiltration (10 kDa MWCO) into LCMS water, and the sample was purified by ZebaSpin for LCMS analysis.

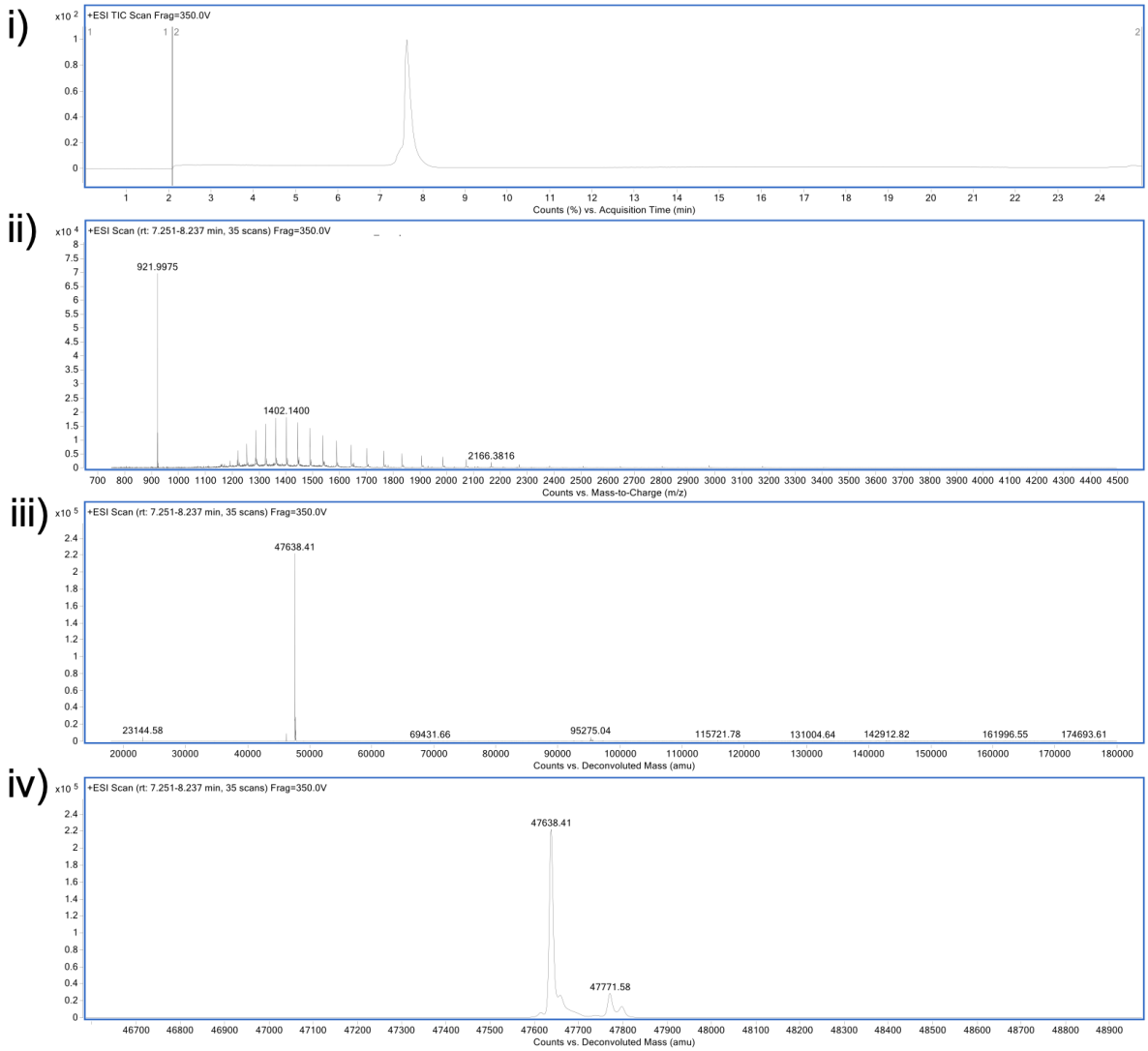


**FIGURE S.86.** LCMS analysis of aldehyde-thioester **16** control on native Fab. i) TIC. ii) non-convoluted ion series. iii) full range of deconvoluted ion series. iv) zoomed in of deconvoluted ion series. Expected mass of native Fab: 47638 Da. Observed: 47368 Da.

**Aldehyde-thioester 16 conjugation on reduced Fab (reaction)**

To Fab (20.0 μL, 0.0030 μmol, 150 μM, 7.15 mg/mL) in conjugation buffer was added TCEP (0.20 μL, 0.030 μmol, 150 mM in $dH_2O$, 10 eq.). After mixing for 1.5 h at 37 ºC, 300 rpm, aldehyde-thioester **16** (0.40 μL, 0.060 μmol, 150 mM in DMF, 20 eq.) was added and the reaction mixture was incubated for 2 h at 37 ºC, 300 rpm. The excess reagent was removed *via* ultrafiltration (10 kDa MWCO) into LCMS water, and the sample was purified by ZebaSpin for LCMS analysis.

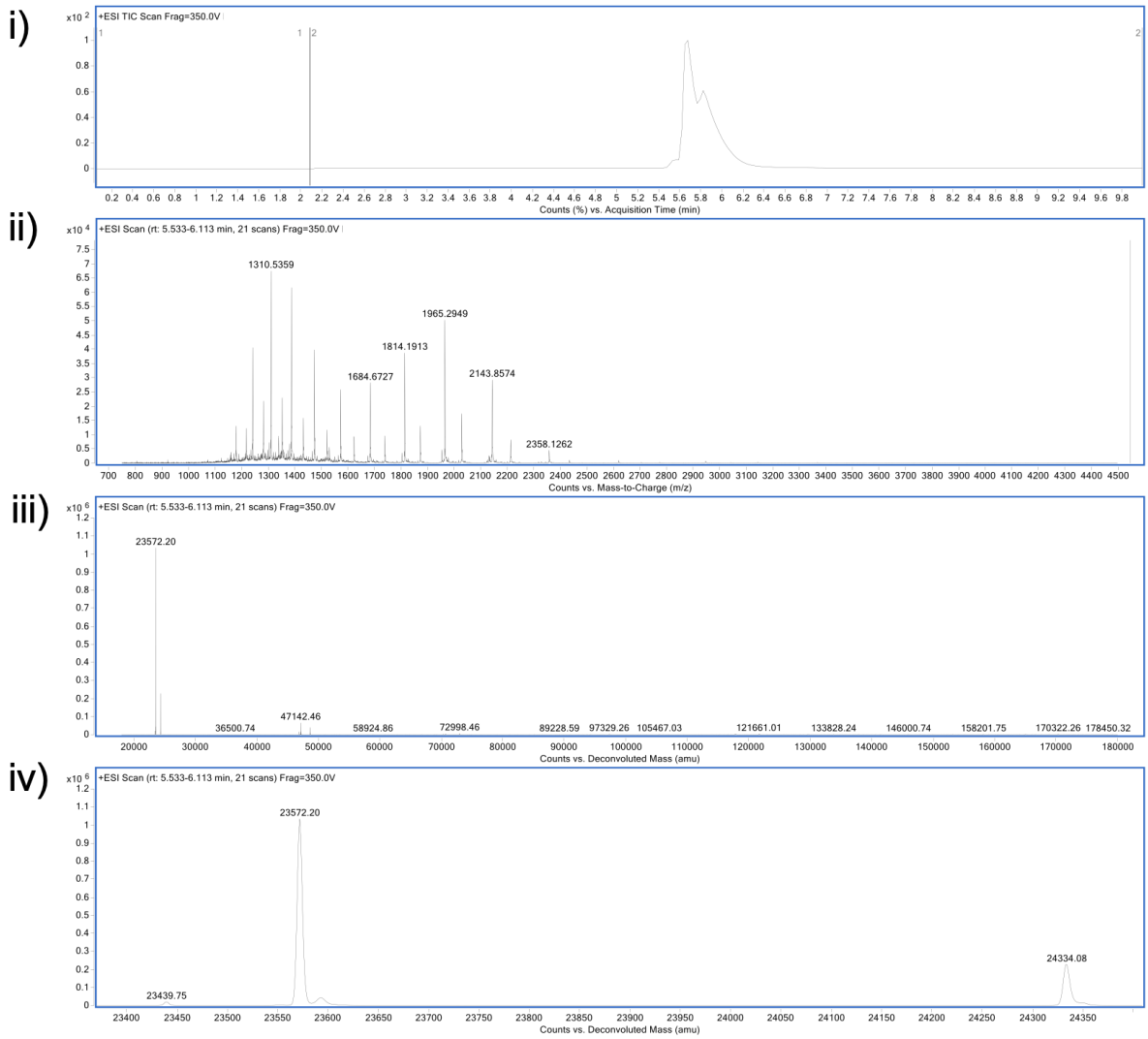


**FIGURE S.87.** LCMS analysis of aldehyde-thioester **16** reaction on reduced Fab. i) TIC. ii) non-convoluted ion series. iii) full range of deconvoluted ion series. iv) zoomed in of deconvoluted ion series. Expected mass of aldehyde-thioester conjugate: LC 23572 Da, HC 24333 Da. Observed: modified LC 23572 Da, modified HC 24334 Da. Mass of aldehyde-thioester **16** addition: 133 Da.

**Reduction of aldehyde-thioester conjugate**

Prepared aldehyde-thioester conjugate (40 μL, 150 μM) was washed *via* ultrafiltration 10 kDa MWCO) into citrate buffer at pH 5.0 (5 x 80 μL). The concentration of the aldehyde-thioester conjugate was calculated. Sodium cyanoborohydride (150 mM in citrate buffer at pH 5.0, 100 eq.) was added and the reaction was further incubated for 1 h at 37 ºC, 300 rpm. The sample was purified by ZebaSpin for LCMS analysis.

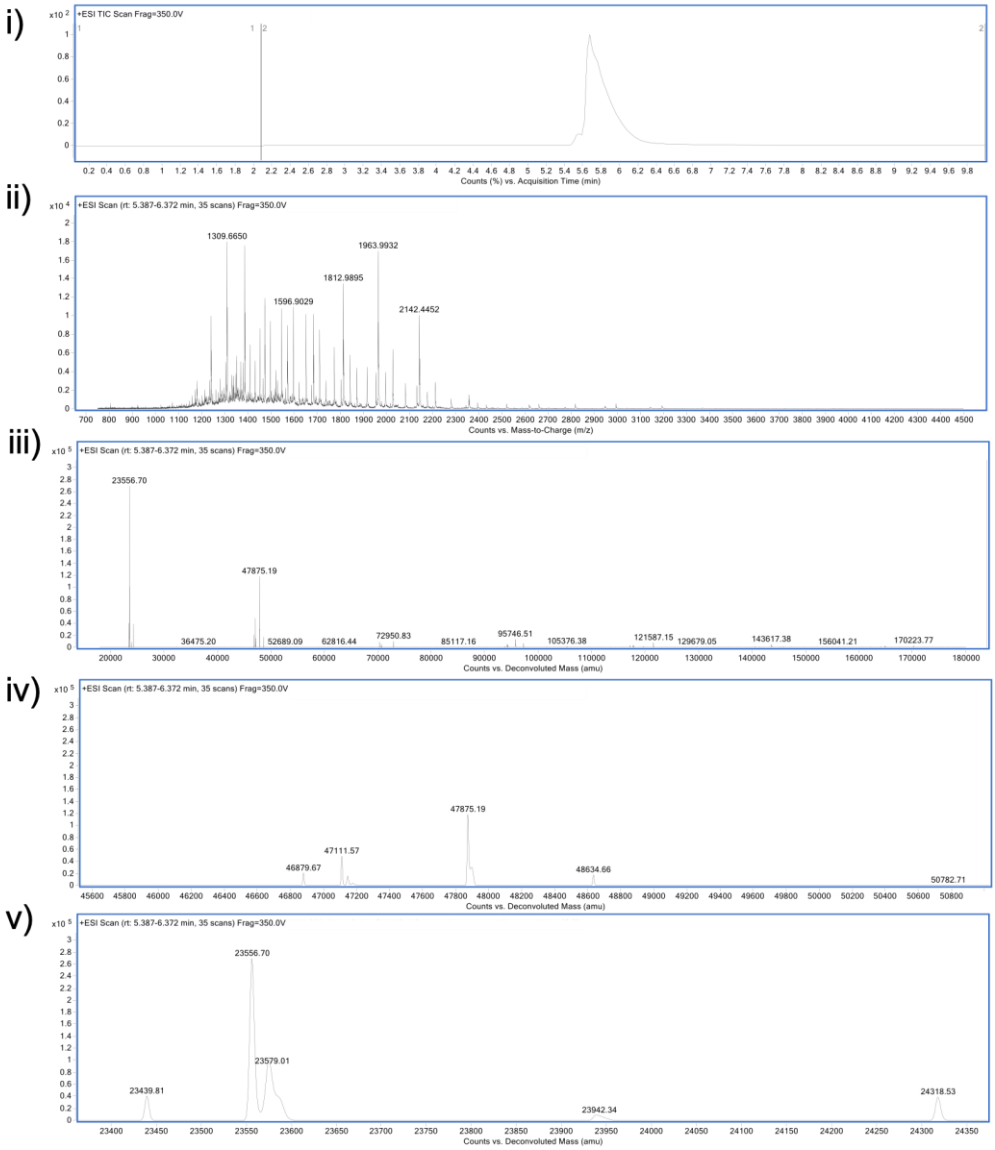


**FIGURE S.88.** LCMS analysis of aldehyde-thioester conjugate reduction with sodium cyanoborohydride. i) TIC. ii) non-convoluted ion series. iii) full range of deconvoluted ion series. iv) zoomed in of deconvoluted ion series. Expected mass of reduced aldehyde-thioester conjugate: LC 23557 Da, HC 24318 Da. Observed: modified LC 23556 Da, sodium adduct LC 23579 Da, modified HC 24318 Da, re-bridged 47875 Da.

**Cysteine addition to reduced aldehyde-thioester conjugate**

Prepared reduced aldehyde-thioester conjugate (40 µL, 150 µM) was washed *via* ultrafiltration 10 kDa MWCO) into conjugation buffer at pH 7.4 (5 x 80 µL). The concentration of the aldehyde-thioester conjugate was calculated. *N*-Boc-cysteine (150 mM in $dH_2O$, 100 eq.) was added, and the reaction was further incubated for 2 h at 37 ºC, 300 rpm. The sample was purified by ZebaSpin for LCMS analysis.

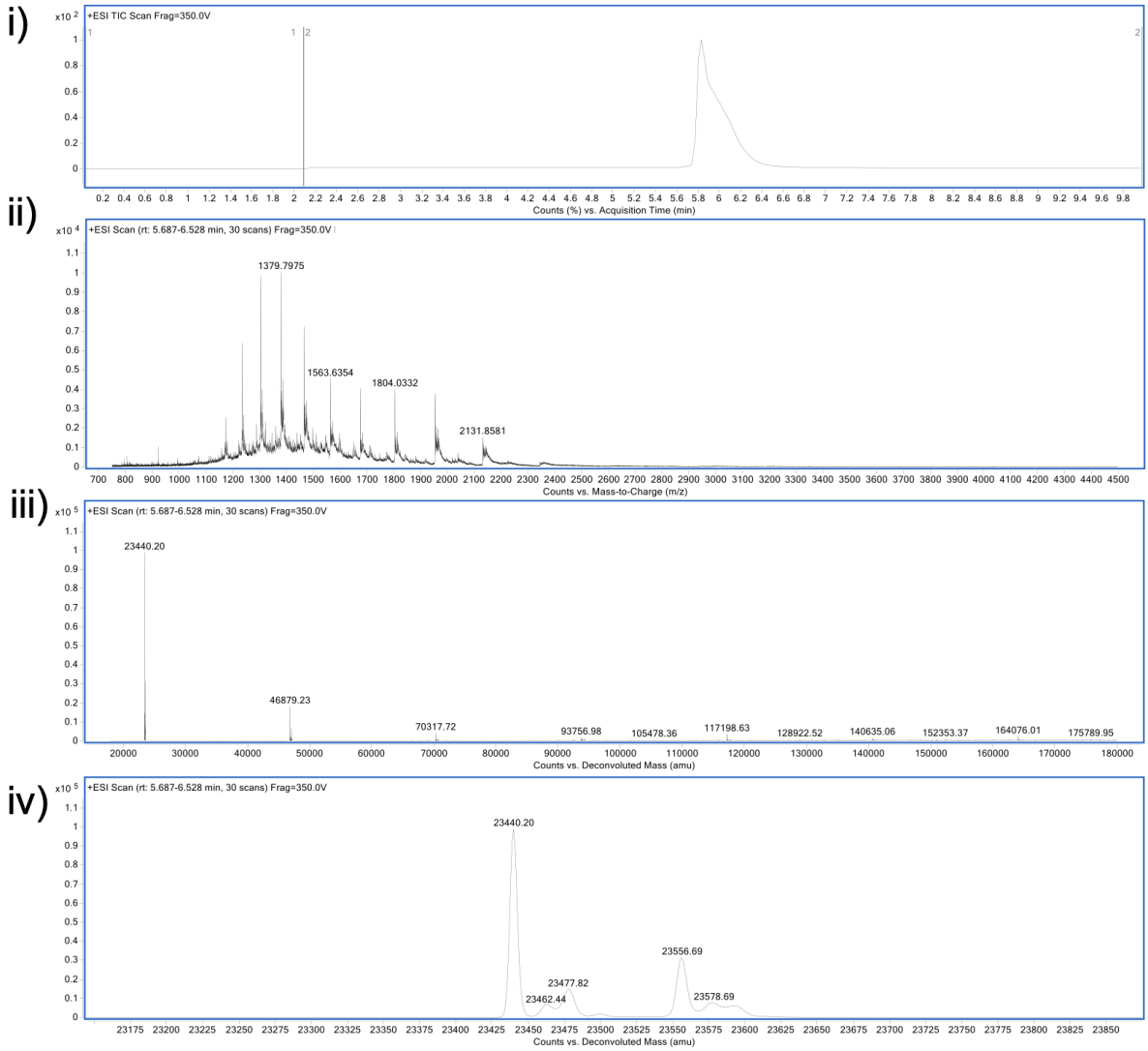


**FIGURE S.89.** LCMS analysis of cysteine addition reduced aldehyde-thioester conjugate. i) TIC. ii) non-convoluted ion series. iii) full range of deconvoluted ion series. iv) zoomed in of deconvoluted ion series. Expected mass of reduced aldehyde-thioester conjugate: LC 23556 Da, HC 24318 Da. Observed: LC 23440, modified LC 23556 Da, sodium adduct LC 23578 Da.

# 7. References


1 International Human Genome Sequencing Consortium, *Nature*, 2004, **431**, 931–945.

2 S. Ramazi and J. Zahiri, *Database*, 2021, **2021**, 1–20.

3 H. Xu, Y. Wang, S. Lin, W. Deng, D. Peng, Q. Cui and Y. Xue, *Genomics, Proteomics Bioinforma.*, 2018, **16**, 244–251.

4 N. Stephanopoulos and M. B. Francis, *Nat. Chem. Biol.*, 2011, **7**, 876–884.

5 C. D. Spicer and B. G. Davis, *Nat. Commun.*, 2014, 5.

6 K. Strebhardt and A. Ullrich, *Nat. Rev. Cancer*, 2008, 8, 473–480.

7 P. Polakis, *Pharmacol. Rev.*, 2016, **68**, 3–19.

8 P. J. Burke, J. Z. Hamilton, S. C. Jeffrey, J. H. Hunter, S. O. Doronina, N. M. Okeley, J. B. Miyamoto, M. E. Anderson, I. J. Stone, M. L. Ulrich, J. K. Simmons, E. E. McKinney, P. D. Senter and R. P. Lyon, *Mol. Cancer Ther.*, 2017, **16**, 116–123.

9 T. Satomaa, H. Pynnönen, A. Vilkman, T. Kotiranta, V. Pitkänen, A. Heiskanen, B. Herpers, L. Price, J. Helin and J. Saarinen, *Antibodies*, 2018, **7**, 15.

10 C. M. Yamazaki, A. Yamaguchi, Y. Anami, W. Xiong, Y. Otani, J. Lee, N. T. Ueno, N. Zhang, Z. An and K. Tsuchikama, *Nat. Commun.*, 2021, **12**, 3528.

11 Y. V. Kovtun, C. A. Audette, Y. Ye, H. Xie, M. F. Ruberti, S. J. Phinney, B. A. Leece, T. Chittenden, W. A. Blättler and V. S. Goldmacher, *Cancer Res.*, 2006, **66**, 3214–3221.

12 K. J. Norsworthy, C.-W. Ko, J. E. Lee, J. Liu, C. S. John, D. Przepiorka, A. T. Farrell and R. Pazdur, *Oncologist*, 2018, **23**, 1103–1108.

13 N. C. Richardson, Y. L. Kasamon, H. Chen, R. A. de Claro, J. Ye, G. M. Blumenthal, A. T. Farrell and R. Pazdur, *Oncologist*, 2019, **24**, e180–e187.

14 G. von Minckwitz, C.-S. Huang, M. S. Mano, S. Loibl, E. P. Mamounas, M. Untch, N. Wolmark, P. Rastogi, A. Schneeweiss, A. Redondo, H. H. Fischer, W. Jacot, A. K. Conlin, C. Arce-Salinas, I. L. Wapnir, C. Jackisch, M. P. DiGiovanna, P. A. Fasching, J. P. Crown, P. Wülfing, Z. Shao, E. Rota Caremoli, H. Wu, L. H. Lam, D. Tesarowski, M. Smitt, H. Douthwaite, S. M. Singel and C. E. Geyer, *N. Engl. J. Med.*, 2019, **380**, 617–628.

15 I. R. Yurkiewicz, L. Muffly and M. Liedtke, *Drug Des. Devel. Ther.*, 2018, **12**,

2293–2300.
16 E. D. Deeks, *Drugs*, 2019, **79**, 1467–1475.
17 T. Powles, J. E. Rosenberg, G. P. Sonpavde, Y. Loriot, I. Durán, J.-L. Lee, N. Matsubara, C. Vulsteke, D. Castellano, C. Wu, M. Campbell, M. Matsangou and D. P. Petrylak, *N. Engl. J. Med.*, 2021, **384**, 1125–1135.
18 P. Narayan, C. L. Osgood, H. Singh, H. J. Chiu, T. K. Ricks, E. C. Y. Chow, J. Qiu, P. Song, J. Yu, F. Namuswe, M. Guiterrez-Lugo, S. Hou, W. F. Pierce, K. B. Goldberg, S. Tang, L. Amiri-Kordestani, M. R. Theoret, R. Pazdur and J. A. Beaver, *Clin. Cancer Res.*, 2021, **27**, 4478–4485.
19 Y. Y. Syed, *Drugs*, 2020, **80**, 1019–1025.
20 K. Tzogani, K. Penttilä, J. Lähteenvuo, T. Lapveteläinen, L. Lopez Anglada, C. Prieto, B. Garcia-Ochoa, H. Enzmann, C. Gisselbrecht, J. Delgado and F. Pignatti, *Oncologist*, 2021, **26**, 70–76.
21 B. Xu, *Eur. J. Clin. Pharmacol.*, 2022, **78**, 707–719.
22 E. S. Kim and Z. T. Al-Salama, *Drugs Ther. Perspect.*, 2022, **38**, 382–388.
23 W. Hoffman, F. G. Lakkis and G. Chalasani, *Clin. J. Am. Soc. Nephrol.*, 2016, **11**, 137–154.
24 D. N. Forthal, in *Antibodies for Infectious Diseases*, ASM Press, Washington, DC, USA, 2015, pp. 23–48.
25 A. K. E. Palm and C. Henry, *Front. Immunol.*, 2019, **10**, 1787.
26 G. Vidarsson, G. Dekkers and T. Rispens, *Front. Immunol.*, 2014, **5**, 1–17.
27 H. W. Schroeder and L. Cavacini, *J. Allergy Clin. Immunol.*, 2010, **125**, S41–S52.
28 G. Köhler and C. Milstein, *Nature*, 1975, **256**, 495–497.
29 M. A. Hooks, C. S. Wade and W. J. Millikan, *Pharmacother. J. Hum. Pharmacol. Drug Ther.*, 1991, **11**, 26–37.
30 J. J. Tjandra, L. Ramadi and I. F. C. McKenzie, *Immunol. Cell Biol.*, 1990, **68**, 367–376.
31 R. Barderas and E. Benito-Peña, *Anal. Bioanal. Chem.*, 2019, **411**, 2475–2479.
32 R. M. Lu, Y. C. Hwang, I. J. Liu, C. C. Lee, H. Z. Tsai, H. J. Li and H. C. Wu, *J. Biomed. Sci.*, 2020, **27**, 1–30.
33 K. T. Xenaki, S. Oliveira and P. M. P. van Bergen en Henegouwen, *Front. Immunol.*, 2017, **8**, 1-6.

34 T. Yokota, D. E. Milenic, M. Whitlow and J. Schlom, *Cancer Res.*, 1992, **52**, 3402–3408.
35 P. Holliger and P. J. Hudson, *Nat. Biotechnol.*, 2005, **23**, 1126–1136.
36 R. V. Kholodenko, D. V. Kalinovsky, I. I. Doronin, E. D. Ponomarev and I. V. Kholodenko, *Curr. Med. Chem.*, 2019, **26**, 396–426.
37 A. Frenzel, M. Hust and T. Schirrmann, *Front. Immunol.*, 2013, **4**, 1–20.
38 A. L. Nelson, *MAbs*, 2010, **2**, 77–83.
39 M. P. Kelly, F. T. Lee, K. Tahtis, B. E. Power, F. E. Smyth, M. W. Brechbiel, P. J. Hudson and A. M. Scott, *Cancer Biother. Radiopharm.*, 2008, **23**, 411–423.
40 L. Testa, W. J. Van Gaal, R. Bhindi, G. G. L. Biondi-Zoccai, A. Abbate, P. Agostoni, I. Porto, F. Andreotti, F. Crea and A. P. Banning, *J. Thorac. Cardiovasc. Surg.*, 2008, **136**, 884–893.
41 R. J. Kreitman and I. Pastan, *Clin. Cancer Res.*, 2011, **17**, 6398–6405.
42 A. Bates and C. A. Power, *Antibodies*, 2019, **8**, 28.
43 A. P. Chapman, P. Antoniw, M. Spitali, S. West, S. Stephens and D. J. King, *Nat. Biotechnol.*, 1999, **17**, 780–783.
44 E. Davé, R. Adams, O. Zaccheo, B. Carrington, J. E. Compson, S. Dugdale, M. Airey, S. Malcolm, H. Hailu, G. Wild, A. Turner, J. Heads, K. Sarkar, A. Ventom, D. Marshall, M. Jairaj, T. Kopotsha, L. Christodoulou, M. Zamacona, A. D. Lawson, S. Heywood and D. P. Humphreys, *MAbs*, 2016, **8**, 1319–1335.
45 M. Hutt, A. Färber-Schwarz, F. Unverdorben, F. Richter and R. E. Kontermann, *J. Biol. Chem.*, 2012, **287**, 4462–4469.
46 R. E. Kontermann, *BioDrugs*, 2009, **23**, 93–109.
47 L. Ducry and B. Stump, *Bioconjug. Chem.*, 2010, 21, 5–13.
48 J. D. Bargh, A. Isidro-Llobet, J. S. Parker and D. R. Spring, *Chem. Soc. Rev.*, 2019, 48, 4361–4374.
49 R. A. Firestone, D. Willner, S. J. Hofstead, H. D. King, T. Kaneko, G. R. Braslawsky, R. S. Greenfield, P. A. Trail, S. J. Lasch, A. J. Henderson, A. M. Casazza, I. Hellström and K. E. Hellström, *J. Control. Release*, 1996, **39**, 251–259.
50 V. H. J. Van Der Velden, *Blood*, 2000, **96**, 3197–3204.
51 C. Selby, PharmD, BCOP, L. R. Yacko, PharmD, BCPS and A. E. Glode, PharmD, BCOP, *J. Adv. Pract. Oncol.*, 2019, **10**, 68–82.
52 S. O. Doronina, B. E. Toki, M. Y. Torgov, B. A. Mendelsohn, C. G. Cerveny, D.

F. Chace, R. L. DeBlanc, R. P. Gearing, T. D. Bovee, C. B. Siegall, J. A. Francisco, A. F. Wahl, D. L. Meyer and P. D. Senter, *Nat. Biotechnol.*, 2003, **21**, 778–784.

53 P. Kovaříková, Z. Mrkvičková and J. Klimeš, *J. Pharm. Biomed. Anal.*, 2008, **47**, 360–370.

54 A. Bardia, I. A. Mayer, L. T. Vahdat, S. M. Tolaney, S. J. Isakoff, J. R. Diamond, J. O'Shaughnessy, R. L. Moroose, A. D. Santin, V. G. Abramson, N. C. Shah, H. S. Rugo, D. M. Goldenberg, A. M. Sweidan, R. Iannone, S. Washkowitz, R. M. Sharkey, W. A. Wegener and K. Kalinsky, *N. Engl. J. Med.*, 2019, **380**, 741–751.

55 D. V. Santi, L. Cabel and F.-C. Bidard, *Ann. Transl. Med.*, 2021, **9**, 1113–1113.

56 D. M. Goldenberg and R. M. Sharkey, *Expert Opin. Biol. Ther.*, 2020, **20**, 871–885.

57 J. E. Gray, R. S. Heist, A. N. Starodub, D. R. Camidge, E. A. Kio, G. A. Masters, W. T. Purcell, M. J. Guarino, J. Misleh, C. J. Schneider, B. J. Schneider, A. Ocean, T. Johnson, L. Gandhi, K. Kalinsky, R. Scheff, W. A. Messersmith, S. V. Govindan, P. P. Maliakal, B. Mudenda, W. A. Wegener, R. M. Sharkey and D. M. Goldenberg, *Clin. Cancer Res.*, 2017, **23**, 5711–5719.

58 M. C. Finniss, K. S. Chu, C. J. Bowerman, J. C. Luft, Z. A. Haroon and J. M. DeSimone, *Med. Chem. Commun.*, 2014, **5**, 1355–1358.

59 T. Rady, L. Turelli, M. Nothisen, E. Tobaldi, S. Erb, F. Thoreau, O. Hernandez-Alba, S. Cianferani, F. Daubeuf, A. Wagner and G. Chaubet, *Bioconjug. Chem.*, 2022, **33**, 1860–1866.

60 S. Sugio, A. Kashima, S. Mochizuki, M. Noda and K. Kobayashi, *Protein Eng.*, 1999, **12**, 439–446.

61 M. P. Gamcsik, M. S. Kasibhatla, S. D. Teeter and O. M. Colvin, *Biomarkers*, 2012, **17**, 671–691.

62 E. Lee and D. H. Lee, *BMB Rep.*, 2017, **50**, 401–410.

63 B. A. Kellogg, L. Garrett, Y. Kovtun, K. C. Lai, B. Leece, M. Miller, G. Payne, R. Steeves, K. R. Whiteman, W. Widdison, H. Xie, R. Singh, R. V. J. Chari, J. M. Lambert and R. J. Lutz, *Bioconjug. Chem.*, 2011, **22**, 717–727.

64 J. I. Geller, J. G. Pressey, M. A. Smith, R. A. Kudgus, M. Cajaiba, J. M. Reid, D. Hall, D. A. Barkauskas, S. D. Voss, S. Y. Cho, S. L. Berg, J. S. Dome, E. Fox and B. J. Weigel, *Cancer*, 2020, **126**, 5303–5310.

65 Q. Wang, J. Guan, J. Wan and Z. Li, *RSC Adv.*, 2020, **10**, 24397–24409.

66 C. S. Gondi and J. S. Rao, *Expert Opin. Ther. Targets*, 2013, **17**, 281–291.

67 G. M. Dubowchik and R. A. Firestone, *Bioorg. Med. Chem. Lett.*, 1998, **8**, 3341–3346.

68 M. Dorywalska, P. Strop, J. A. Melton-Witt, A. Hasa-Moreno, S. E. Farias, M. Galindo Casas, K. Delaria, V. Lui, K. Poulsen, C. Loo, S. Krimm, G. Bolton, L. Moine, R. Dushin, T.-T. Tran, S.-H. Liu, M. Rickert, D. Foletti, D. L. Shelton, J. Pons and A. Rajpal, *Bioconjug. Chem.*, 2015, **26**, 650–659.

69 M. Dorywalska, R. Dushin, L. Moine, S. E. Farias, D. Zhou, T. Navaratnam, V. Lui, A. Hasa-Moreno, M. G. Casas, T.-T. Tran, K. Delaria, S.-H. Liu, D. Foletti, C. J. O'Donnell, J. Pons, D. L. Shelton, A. Rajpal and P. Strop, *Mol. Cancer Ther.*, 2016, **15**, 958–970.

70 A. Dal Corso, S. Cazzamalli, R. Gébleux, M. Mattarella and D. Neri, *Bioconjug. Chem.*, 2017, **28**, 1826–1833.

71 T. Nakada, T. Masuda, H. Naito, M. Yoshida, S. Ashida, K. Morita, H. Miyazaki, Y. Kasuya, Y. Ogitani, J. Yamaguchi, Y. Abe and T. Honda, *Bioorg. Med. Chem. Lett.*, 2016, **26**, 1542–1545.

72 J. D. Bargh, S. J. Walsh, A. Isidro-Llobet, S. Omarjee, J. S. Carroll and D. R. Spring, *Chem. Sci.*, 2020, **11**, 2375–2380.

73 Z. Su, D. Xiao, F. Xie, L. Liu, Y. Wang, S. Fan, X. Zhou and S. Li, *Acta Pharm. Sin. B*, 2021, **11**, 3889–3907.

74 X. Wang, Y. Liu, X. Fan, J. Wang, W. S. C. Ngai, H. Zhang, J. Li, G. Zhang, J. Lin and P. R. Chen, *J. Am. Chem. Soc.*, 2019, **141**, 17133–17141.

75 R. R. Nani, A. P. Gorka, T. Nagaya, H. Kobayashi and M. J. Schnermann, *Angew. Chemie Int. Ed.*, 2015, **54**, 13635–13638.

76 B. Spangler, T. Kline, J. Hanson, X. Li, S. Zhou, J. A. Wells, A. K. Sato and A. R. Renslo, *Mol. Pharm.*, 2018, **15**, 2054–2059.

77 E. Oflazoglu, I. J. Stone, K. Gordon, C. G. Wood, E. A. Repasky, I. S. Grewal, C.-L. Law and H.-P. Gerber, *Clin. Cancer Res.*, 2008, **14**, 6171–6180.

78 A. G. Poison, J. Calemine-Fenaux, P. Chan, W. Chang, E. Christensen, S. Clark, F. J. De Sauvage, D. Eaton, K. Elkins, J. Michael Elliott, G. Frantz, R. N. Fuji, A. Gray, K. Harden, G. S. Ingle, N. M. Kljavin, H. Koeppen, C. Nelson, S. Prabhu, H. Raab, S. Ross, J. P. Stephan, S. J. Scales, S. D. Spencer, R. Vandlen, B. Wranik, S. F. Yu, B. Zheng and A. Ebens, *Cancer Res.*, 2009, **69**,

2358–2364.

79 G. Curigliano, V. Bagnardi, M. Ghioni, J. Louahed, V. Brichard, F. F. Lehmann, A. Marra, D. Trapani, C. Criscitiello and G. Viale, *The Breast*, 2020, **49**, 202–209.

80 L. Chen, L. Wang, H. Shion, C. Yu, Y. Q. Yu, L. Zhu, M. Li, W. Chen and K. Gao, *MAbs*, 2016, **8**, 1210–1223.

81 S. Lonial, H. C. Lee, A. Badros, S. Trudel, A. K. Nooka, A. Chari, A. O. Abdallah, N. Callander, N. Lendvai, D. Sborov, A. Suvannasankha, K. Weisel, L. Karlin, E. Libby, B. Arnulf, T. Facon, C. Hulin, K. M. Kortüm, P. Rodríguez-Otero, S. Z. Usmani, P. Hari, R. Baz, H. Quach, P. Moreau, P. M. Voorhees, I. Gupta, A. Hoos, E. Zhi, J. Baron, T. Piontek, E. Lewis, R. C. Jewell, E. J. Dettman, R. Popat, S. D. Esposti, J. Opalinska, P. Richardson and A. D. Cohen, *Lancet Oncol.*, 2020, **21**, 207–221.

82 R. V. J. Chari, *Acc. Chem. Res.*, 2008, **41**, 98–107.

83 R. L. Bai, G. R. Pettit and E. Hamel, *J. Biol. Chem.*, 1990, **265**, 17141–17149.

84 J. C. Mirsalis, J. Schindler-Horvat, J. R. Hill, J. E. Tomaszewski, S. J. Donohue and C. A. Tyson, *Cancer Chemother. Pharmacol.*, 1999, **44**, 395–402.

85 A. Maderna and C. A. Leverett, *Mol. Pharm.*, 2015, **12**, 1798–1812.

86 Y.-J. Wang, Y.-Y. Li, X.-Y. Liu, X.-L. Lu, X. Cao and B.-H. Jiao, *Mar. Drugs*, 2017, **15**, 18.

87 C. Chalouni and S. Doll, *J. Exp. Clin. Cancer Res.*, 2018, **37**, 20.

88 A. B. Waight, K. Bargsten, S. Doronina, M. O. Steinmetz, D. Sussman and A. E. Prota, *PLoS One*, 2016, **11**, e0160890.

89 M. P. Johansson, H. Maaheimo and F. S. Ekholm, *Sci. Rep.*, 2017, **7**, 15920.

90 P. Liu-Kreyche, H. Shen, A. M. Marino, R. A. Iyer, W. G. Humphreys and Y. Lai, *Front. Pharmacol.*, 2019, **10**, 1–9.

91 H. K. Erickson, W. C. Widdison, M. F. Mayo, K. Whiteman, C. Audette, S. D. Wilhelm and R. Singh, *Bioconjug. Chem.*, 2010, **21**, 84–92.

92 M. Lopus, E. Oroudjev, L. Wilson, S. Wilhelm, W. Widdison, R. Chari and M. A. Jordan, *Mol. Cancer Ther.*, 2010, **9**, 2689–2699.

93 M. Barok, H. Joensuu and J. Isola, *Breast Cancer Res.*, 2014, **16**, 209.

94 G. D. Leonard, T. Fojo and S. E. Bates, *Oncologist*, 2003, **8**, 411–424.

95 Y. V. Kovtun, C. A. Audette, M. F. Mayo, G. E. Jones, H. Doherty, E. K. Maloney, H. K. Erickson, X. Sun, S. Wilhelm, O. Ab, K. C. Lai, W. C. Widdison,

B. Kellogg, H. Johnson, J. Pinkas, R. J. Lutz, R. Singh, V. S. Goldmacher and R. V. J. Chari, *Cancer Res.*, 2010, **70**, 2528–2537.

96 J. B. Biggins, K. C. Onwueme and J. S. Thorson, *Science*, 2003, **301**, 1537–1541.

97 N. Zein, A. Sinha, W. McGahren and G. Ellestad, *Science*, 1988, **240**, 1198–1201.

98 M. L. Linenberger, T. Hong, D. Flowers, E. L. Sievers, T. A. Gooley, J. M. Bennett, M. S. Berger, L. H. Leopold, F. R. Appelbaum and I. D. Bernstein, *Blood*, 2001, **98**, 988–994.

99 W. Leimgruber, V. Stefanović, F. Schenker, A. Karr and J. Berger, *J. Am. Chem. Soc.*, 1965, **87**, 5791–5793.

100 K. M. Rahman, C. H. James and D. E. Thurston, *Nucleic Acids Res.*, 2011, **39**, 5800–5812.

101 J. A. Hartley, *Expert Opin. Investig. Drugs*, 2011, **20**, 733–744.

102 F. Zammarchi, S. Corbett, L. Adams, P. C. Tyrer, K. Kiakos, N. Janghra, T. Marafioti, C. E. Britten, C. E. G. Havenith, S. Chivers, F. D'Hooge, D. G. Williams, A. Tiberghien, P. W. Howard, J. A. Hartley and P. H. van Berkel, *Blood*, 2018, **131**, 1094–1105.

103 J. A. Hartley, M. J. Flynn, J. P. Bingham, S. Corbett, H. Reinert, A. Tiberghien, L. A. Masterson, D. Antonow, L. Adams, S. Chowdhury, D. G. Williams, S. Mao, J. Harper, C. E. G. Havenith, F. Zammarchi, S. Chivers, P. H. van Berkel and P. W. Howard, *Sci. Rep.*, 2018, **8**, 10479.

104 P. H. Clingen, *Nucleic Acids Res.*, 2005, **33**, 3283–3291.

105 L. Galluzzi, L. Senovilla, I. Vitale, J. Michels, I. Martins, O. Kepp, M. Castedo and G. Kroemer, *Oncogene*, 2012, **31**, 1869–1883.

106 J. A. Hartley, *Expert Opin. Biol. Ther.*, 2021, **21**, 931–943.

107 M. Hamadani, G. P. Collins, P. F. Caimi, F. Samaniego, A. Spira, A. Davies, J. Radford, T. Menne, A. Karnad, J. M. Zain, P. Fields, K. Havenith, H. G. Cruz, S. He, J. Boni, J. Feingold, J. Wuerthner and S. Horwitz, *Lancet Haematol.*, 2021, **8**, e433–e445.

108 J. Cummings and J. F. Smyth, *Ann. Oncol.*, 1993, **4**, 533–543.

109 N. Takegawa, Y. Nonagase, K. Yonesaka, K. Sakai, O. Maenishi, Y. Ogitani, T. Tamura, K. Nishio, K. Nakagawa and J. Tsurutani, *Int. J. Cancer*, 2017, **141**, 1682–1689.

110 R. Mullangi, P. Ahlawat and N. R. Srinivas, *Biomed. Chromatogr.*, 2010, **24**, 104–123.

111 D. M. Goldenberg, T. M. Cardillo, S. V. Govindan, E. A. Rossi and R. M. Sharkey, *Oncotarget*, 2020, **11**, 942–942.

112 X. Sun, J. F. Ponte, N. C. Yoder, R. Laleau, J. Coccia, L. Lanieri, Q. Qiu, R. Wu, E. Hong, M. Bogalhas, L. Wang, L. Dong, Y. Setiady, E. K. Maloney, O. Ab, X. Zhang, J. Pinkas, T. A. Keating, R. Chari, H. K. Erickson and J. M. Lambert, *Bioconjug. Chem.*, 2017, **28**, 1371–1381.

113 S. L. Ho and A. H. J. Wang, *J. Taiwan Inst. Chem. Eng.*, 2009, **40**, 123–129.

114 E. Friedmann, *BBA - Biochim. Biophys. Acta*, 1952, **9**, 65–75.

115 B. H. Northrop, S. H. Frayne and U. Choudhary, *Polym. Chem.*, 2015, **6**, 3415–3430.

116 T. Müller and D. Winter, *Mol. Cell. Proteomics*, 2017, **16**, 1173–1187.

117 S. C. Alley, D. R. Benjamin, S. C. Jeffrey, N. M. Okeley, D. L. Meyer, R. J. Sanderson and P. D. Senter, *Bioconjug. Chem.*, 2008, **19**, 759–765.

118 N. W. C. J. Van De Donk and E. Dhimolea, *MAbs*, 2012, **4**, 458–465.

119 R. P. Lyon, J. R. Setter, T. D. Bovee, S. O. Doronina, J. H. Hunter, M. E. Anderson, C. L. Balasubramanian, S. M. Duniho, C. I. Leiske, F. Li and P. D. Senter, *Nat. Biotechnol.*, 2014, **32**, 1059–1062.

120 S. D. Fontaine, R. Reid, L. Robinson, G. W. Ashley and D. V. Santi, *Bioconjug. Chem.*, 2015, **26**, 145–152.

121 L. M. Tedaldi, M. E. B. Smith, R. I. Nathani and J. R. Baker, *Chem. Commun.*, 2009, 6583–6585.

122 M. E. B. Smith, F. F. Schumacher, C. P. Ryan, L. M. Tedaldi, D. Papaioannou, G. Waksman, S. Caddick and J. R. Baker, *J. Am. Chem. Soc.*, 2010, **132**, 1960–1965.

123 P. Moody, M. E. B. Smith, C. P. Ryan, V. Chudasama, J. R. Baker, J. Molloy and S. Caddick, *ChemBioChem*, 2012, **13**, 39–41.

124 N. Forte, M. Livanos, E. Miranda, M. Morais, X. Yang, V. S. Rajkumar, K. A. Chester, V. Chudasama and J. R. Baker, *Bioconjug. Chem.*, 2018, **29**, 486–492.

125 B. Bernardim, M. J. Matos, X. Ferhati, I. Compañón, A. Guerreiro, P. Akkapeddi, A. C. B. Burtoloso, G. Jiménez-Osés, F. Corzana and G. J. L. Bernardes, *Nat. Protoc.*, 2019, **14**, 86–99.

126 R. P. Lyon, T. D. Bovee, S. O. Doronina, P. J. Burke, J. H. Hunter, H. D. Neff-Laford, M. Jonas, M. E. Anderson, J. R. Setter and P. D. Senter, *Nat. Biotechnol.*, 2015, **33**, 733–735.

127 S. Kolodych, O. Koniev, Z. Baatarkhuu, J. Y. Bonnefoy, F. Debaene, S. Cianférani, A. Van Dorsselaer and A. Wagner, *Bioconjug. Chem.*, 2015, **26**, 197–200.

128 R. Tessier, R. K. Nandi, B. G. Dwyer, D. Abegg, C. Sornay, J. Ceballos, S. Erb, S. Cianférani, A. Wagner, G. Chaubet, A. Adibekian and J. Waser, *Angew. Chemie*, 2020, **132**, 11054–11063.

129 E. V. Vinogradova, C. Zhang, A. M. Spokoyny, B. L. Pentelute and S. L. Buchwald, *Nature*, 2015, **526**, 687–691.

130 M. Kasper, A. Stengl, P. Ochtrop, M. Gerlach, T. Stoschek, D. Schumacher, J. Helma, M. Penkert, E. Krause, H. Leonhardt and C. P. R. Hackenberger, *Angew. Chemie Int. Ed.*, 2019, **58**, 11631–11636.

131 A. Abbas, B. Xing and T.-P. Loh, *Angew. Chemie Int. Ed.*, 2014, **53**, 7491–7494.

132 K. Tokunaga, M. Sato, K. Kuwata, C. Miura, H. Fuchida, N. Matsunaga, S. Koyanagi, S. Ohdo, N. Shindo and A. Ojida, *J. Am. Chem. Soc.*, 2020, **142**, 18522–18531.

133 G. J. L. Bernardes, G. Casi, S. Trüssel, I. Hartmann, K. Schwager, J. Scheuermann and D. Neri, *Angew. Chemie Int. Ed.*, 2012, **51**, 941–944.

134 H. F. Motiwala, Y.-H. Kuo, B. L. Stinger, B. A. Palfey and B. R. Martin, *J. Am. Chem. Soc.*, 2020, **142**, 1801–1810.

135 T. H. Schneider, M. Rieger, K. Ansorg, A. N. Sobolev, T. Schirmeister, B. Engels and S. Grabowsky, *New J. Chem.*, 2015, **39**, 5841–5853.

136 R. B. Del Rosario, R. L. Wahl, S. J. Brocchini, R. G. Lawton and R. H. Smith, *Bioconjug. Chem.*, 1990, **1**, 51–59.

137 G. Badescu, P. Bryant, M. Bird, K. Henseleit, J. Swierkosz, V. Parekh, R. Tommasi, E. Pawlisz, K. Jurlewicz, M. Farys, N. Camper, X. Sheng, M. Fisher, R. Grygorash, A. Kyle, A. Abhilash, M. Frigerio, J. Edwards and A. Godwin, *Bioconjug. Chem.*, 2014, **25**, 1124–1136.

138 M. Pabst, W. McDowell, A. Manin, A. Kyle, N. Camper, E. De Juan, V. Parekh, F. Rudge, H. Makwana, T. Kantner, H. Parekh, A. Michelet, X. B. Sheng, G. Popa, C. Tucker, F. Khayrzad, D. Pollard, K. Kozakowska, R. Resende, A.

Jenkins, F. Simoes, D. Morris, P. Williams, G. Badescu, M. P. Baker, M. Bird, M. Frigerio and A. Godwin, *J. Control. Release*, 2017, **253**, 160–164.

139 F. F. Schumacher, J. P. M. Nunes, A. Maruani, V. Chudasama, M. E. B. Smith, K. A. Chester, J. R. Baker and S. Caddick, *Org. Biomol. Chem.*, 2014, **12**, 7261–7269.

140 C. R. Behrens, E. H. Ha, L. L. Chinn, S. Bowers, G. Probst, M. Fitch-Bruhns, J. Monteon, A. Valdiosera, A. Bermudez, S. Liao-Chan, T. Wong, J. Melnick, J. W. Theunissen, M. R. Flory, D. Houser, K. Venstrom, Z. Levashova, P. Sauer, T. S. Migone, E. H. Van Der Horst, R. L. Halcomb and D. Y. Jackson, *Mol. Pharm.*, 2015, **12**, 3986–3998.

141 J. P. M. Nunes, M. Morais, V. Vassileva, E. Robinson, V. S. Rajkumar, M. E. B. Smith, R. B. Pedley, S. Caddick, J. R. Baker and V. Chudasama, *Chem. Commun.*, 2015, **51**, 10624–10627.

142 M. Morais, J. P. M. Nunes, K. Karu, N. Forte, I. Benni, M. E. B. Smith, S. Caddick, V. Chudasama and J. R. Baker, *Org. Biomol. Chem.*, 2017, **15**, 2947–2952.

143 C. R. Behrens, E. H. Ha, L. L. Chinn, S. Bowers, G. Probst, M. Fitch-Bruhns, J. Monteon, A. Valdiosera, A. Bermudez, S. Liao-Chan, T. Wong, J. Melnick, J. Theunissen, M. R. Flory, D. Houser, K. Venstrom, Z. Levashova, P. Sauer, T. Migone, E. H. van der Horst, R. L. Halcomb and D. Y. Jackson, *Mol. Pharm.*, 2015, **12**, 3986–3998.

144 A. Maruani, M. E. B. Smith, E. Miranda, K. A. Chester, V. Chudasama and S. Caddick, *Nat. Commun.*, 2015, **6**, 2–10.

145 E. Robinson, J. P. M. Nunes, V. Vassileva, A. Maruani, J. C. F. Nogueira, M. E. B. Smith, R. B. Pedley, S. Caddick, J. R. Baker and V. Chudasama, *RSC Adv.*, 2017, **7**, 9073–9077.

146 S. Shao, M. H. Tsai, J. Lu, T. Yu, J. Jin, D. Xiao, H. Jiang, M. Han, M. Wang and J. Wang, *Bioorganic Med. Chem. Lett.*, 2018, **28**, 1363–1370.

147 M. T. W. Lee, A. Maruani, J. R. Baker, S. Caddick and V. Chudasama, *Chem. Sci.*, 2016, **7**, 799–802.

148 B. Shi, M. Wu, Z. Li, Z. Xie, X. Wei, J. Fan, Y. Xu, D. Ding, S. H. Akash, S. Chen and S. Cao, *Cancer Med.*, 2019, **8**, 1793–1805.

149 P. L. Stern and R. Harrop, *Cancer Immunol. Immunother.*, 2017, **66**, 415–426.

150 R. Huang, Y. Sheng, D. Wei, J. Yu, H. Chen and B. Jiang, *Eur. J. Med. Chem.*,

2020, **190**, 112080.

151 S. J. Walsh, S. Omarjee, W. R. J. D. Galloway, T. T. L. Kwan, H. F. Sore, J. S. Parker, M. Hyvönen, J. S. Carroll and D. R. Spring, *Chem. Sci.*, 2019, **10**, 694–700.

152 S. J. Walsh, S. Omarjee, F. M. Dannheim, D. L. Couturier, D. Bexheti, L. Mendil, G. Cronshaw, T. Fewster, C. Gregg, C. Brodie, J. L. Miller, R. Houghton, J. S. Carroll and D. R. Spring, *Chem. Commun.*, 2022, **58**, 1962–1965.

153 N. Gupta, J. Kancharla, S. Kaushik, A. Ansari, S. Hossain, R. Goyal, M. Pandey, J. Sivaccumar, S. Hussain, A. Sarkar, A. Sengupta, S. K. Mandal, M. Roy and S. Sengupta, *Chem. Sci.*, 2017, **8**, 2387–2395.

154 A. Chrzastek, I. A. Thanasi, J. A. Irving, V. Chudasama and J. R. Baker, *Chem. Sci.*, 2022, **13**, 11533-11539.

155 O. Koniev, I. Dovgan, B. Renoux, A. Ehkirch, J. Eberova, S. Cianférani, S. Kolodych, S. Papot and A. Wagner, *Medchemcomm*, 2018, **9**, 827–830.

156 N. Griebenow, A. M. Dilmaç, S. Greven and S. Bräse, *Bioconjug. Chem.*, 2016, **27**, 911–917.

157 Y. Chen, W. Yang, J. Wu, W. Sun, T. P. Loh and Y. Jiang, *Org. Lett.*, 2020, **22**, 2038–2043.

158 L. P. Y. Liu-Shin, A. Fung, A. Malhotra and G. Ratnaswamy, *MAbs*, 2018, **10**, 1190–1199.

159 P. Herbener, K. Schönfeld, M. König, M. Germer, J. M. Przyborski, K. Bernöster and J. Schüttrumpf, *PLoS One*, 2018, **13**, 1–22.

160 P. M. S. D. Cal, J. B. Vicente, E. Pires, A. V. Coelho, L. F. Veiros, C. Cordeiro and P. M. P. Gois, *J. Am. Chem. Soc.*, 2012, **134**, 10299–10305.

161 L. Hao, Q. Zhou, Y. Piao, Z. Zhou, J. Tang and Y. Shen, *J. Control. Release*, 2021, **330**, 362–371.

162 A. Narayanan and L. H. Jones, *Chem. Sci.*, 2015, **6**, 2650–2659.

163 T. Nakamura, Y. Kawai, N. Kitamoto, T. Osawa and Y. Kato, *Chem. Res. Toxicol.*, 2009, **22**, 536–542.

164 S. Diethelm, M. A. Schafroth and E. M. Carreira, *Org. Lett.*, 2014, **16**, 3908–3911.

165 N. Jentoft and D. G. Dearborn, *J. Biol. Chem.*, 1979, **254**, 4359–4365.

166 V. Gautier, A. J. Boumeester, P. Lössl and A. J. R. Heck, *Proteomics*, 2015,

**15**, 2756–2765.

167 X. Hu, E. Bortell, F. W. Kotch, A. Xu, B. Arve and S. Freese, *Org. Process Res. Dev.*, 2017, **21**, 601–610.

168 G. W. Anderson, F. M. Callahan and J. E. Zimmerman, *J. Am. Chem. Soc.*, 1967, **89**, 178–178.

169 N. Joubert, A. Beck, C. Dumontet and C. Denevault-Sabourin, *Pharmaceuticals*, 2020, **13**, 245.

170 M. T. Kim, Y. Chen, J. Marhoul and F. Jacobson, *Bioconjug. Chem.*, 2014, **25**, 1223–1232.

171 L. Wang, G. Amphlett, W. A. Blättler, J. M. Lambert and W. Zhang, *Protein Sci.*, 2005, **14**, 2436–2446.

172 S. Mädler, C. Bich, D. Touboul and R. Zenobi, *J. Mass Spectrom.*, 2009, **44**, 694–706.

173 S. Kishimoto, Y. Nakashimada, R. Yokota, T. Hatanaka, M. Adachi and Y. Ito, *Bioconjug. Chem.*, 2019, **30**, 698–702.

174 K. Yamada, N. Shikida, K. Shimbo, Y. Ito, Z. Khedri, Y. Matsuda and B. A. Mendelsohn, *Angew. Chemie Int. Ed.*, 2019, **58**, 5592–5597.

175 C. Yu, J. Tang, A. Loredo, Y. Chen, S. Y. Jung, A. Jain, A. Gordon and H. Xiao, *Bioconjug. Chem.*, 2018, **29**, 3522–3526.

176 M. W. Handlogten, T. Kiziltepe, D. T. Moustakas and B. Bilgiçer, *Chem. Biol.*, 2011, **18**, 1179–1188.

177 N. J. Alves, M. M. Champion, J. F. Stefanick, M. W. Handlogten, D. T. Moustakas, Y. Shi, B. F. Shaw, R. M. Navari, T. Kiziltepe and B. Bilgicer, *Biomaterials*, 2013, **34**, 5700–5710.

178 D. Lac, C. Feng, G. Bhardwaj, H. Le, J. Tran, L. Xing, G. Fung, R. Liu, H. Cheng and K. S. Lam, *Bioconjug. Chem.*, 2016, **27**, 159–169.

179 G. H. Pham, W. Ou, B. Bursulaya, M. DiDonato, A. Herath, Y. Jin, X. Hao, J. Loren, G. Spraggon, A. Brock, T. Uno, B. H. Geierstanger and S. E. Cellitti, *ChemBioChem*, 2018, **19**, 799–804.

180 C. Rader, J. M. Turner, A. Heine, D. Shabat, S. C. Sinha, I. A. Wilson, R. A. Lerner and C. F. Barbas, *J. Mol. Biol.*, 2003, **332**, 889–899.

181 A. R. Nanna, X. Li, E. Walseng, L. Pedzisa, R. S. Goydel, D. Hymel, T. R. Burke, W. R. Roush and C. Rader, *Nat. Commun.*, 2017, **8**, 1112.

182 D. Hwang, K. Tsuji, H. Park, T. R. Burke and C. Rader, *Bioconjug. Chem.*,

2019, **30**, 2889–2896.

183 M. J. Matos, B. L. Oliveira, N. Martínez-Sáez, A. Guerreiro, P. M. S. D. Cal, J. Bertoldo, M. Maneiro, E. Perkins, J. Howard, M. J. Deery, J. M. Chalker, F. Corzana, G. Jiménez-Osés and G. J. L. Bernardes, *J. Am. Chem. Soc.*, 2018, **140**, 4004–4017.

184 R. J. Spears and M. A. Fascione, *Org. Biomol. Chem.*, 2016, **14**, 7622–7638.

185 M. Chilamari, N. Kalra, S. Shukla and V. Rai, *Chem. Commun.*, 2018, **54**, 7302–7305.

186 K. J. Hamblett, P. D. Senter, D. F. Chace, M. M. C. Sun, J. Lenox, C. G. Cerveny, K. M. Kissler, S. X. Bernhardt, A. K. Kopcha, R. F. Zabinski, D. L. Meyer and J. A. Francisco, *Clin. Cancer Res.*, 2004, **10**, 7063–7070.

187 M. Haque, N. Forte and J. R. Baker, *Chem. Commun.*, 2021, **57**, 10689–10702.

188 S. Koide and S. S. Sidhu, *ACS Chem. Biol.*, 2009, **4**, 325–334.

189 J. Gavrilyuk, H. Ban, M. Nagano, W. Hakamata and C. F. Barbas, *Bioconjug. Chem.*, 2012, **23**, 2321–2328.

190 J. Gavrilyuk, H. Ban, H. Uehara, S. J. Sirk, K. Saye-Francisco, A. Cuevas, E. Zablowsky, A. Oza, M. S. Seaman, D. R. Burton and C. F. Barbas, *J. Virol.*, 2013, **87**, 4985–4993.

191 I. Dovgan, S. Erb, S. Hessmann, S. Ursuegui, C. Michel, C. Muller, G. Chaubet, S. Cianférani and A. Wagner, *Org. Biomol. Chem.*, 2018, **16**, 1305–1311.

192 J. Janin, *Nature*, 1979, **277**, 491–492.

193 K. Peciak, E. Laurine, R. Tommasi, J. Choi and S. Brocchini, *Chem. Sci.*, 2019, **10**, 427–439.

194 S. R. Adusumalli, D. G. Rawale, U. Singh, P. Tripathi, R. Paul, N. Kalra, R. K. Mishra, S. Shukla and V. Rai, *J. Am. Chem. Soc.*, 2018, **140**, 15114–15123.

195 J. J. Hu, P. Y. He and Y. M. Li, *J. Pept. Sci.*, 2021, **27**, e3286

196 K. J. Malawska, S. Takano, K. Oisaki, H. Yanagisawa, M. Kikkawa, T. Tsukuda and M. Kanai, *ChemRxiv*, 2022, DOI:10.26434/chemrxiv-2022-993zl.

197 Y. Seki, T. Ishiyama, D. Sasaki, J. Abe, Y. Sohma, K. Oisaki and M. Kanai, *J. Am. Chem. Soc.*, 2016, **138**, 10798–10801.

198 B. Q. Shen, K. Xu, L. Liu, H. Raab, S. Bhakta, M. Kenrick, K. L. Parsons-Reponte, J. Tien, S. F. Yu, E. Mai, D. Li, J. Tibbitts, J. Baudys, O. M. Saad, S.

J. Scales, P. J. McDonald, P. E. Hass, C. Eigenbrot, T. Nguyen, W. A. Solis, R. N. Fuji, K. M. Flagella, D. Patel, S. D. Spencer, L. A. Khawli, A. Ebens, W. L. Wong, R. Vandlen, S. Kaur, M. X. Sliwkowski, R. H. Scheller, P. Polakis and J. R. Junutula, *Nat. Biotechnol.*, 2012, **30**, 184–189.

199 H. Liu and K. May, *MAbs*, 2012, 4, 17–23.

200 J. R. Junutula, H. Raab, S. Clark, S. Bhakta, D. D. Leipold, S. Weir, Y. Chen, M. Simpson, S. P. Tsai, M. S. Dennis, Y. Lu, Y. G. Meng, C. Ng, J. Yang, C. C. Lee, E. Duenas, J. Gorrell, V. Katta, A. Kim, K. McDorman, K. Flagella, R. Venook, S. Ross, S. D. Spencer, W. Lee Wong, H. B. Lowman, R. Vandlen, M. X. Sliwkowski, R. H. Scheller, P. Polakis and W. Mallet, *Nat. Biotechnol.*, 2008, **26**, 925–932.

201 J. R. Junutula, K. M. Flagella, R. A. Graham, K. L. Parsons, E. Ha, H. Raab, S. Bhakta, T. Nguyen, D. L. Dugger, G. Li, E. Mai, G. D. L. Phillips, H. Hiraragi, R. N. Fuji, J. Tibbitts, R. Vandlen, S. D. Spencer, R. H. Scheller, P. Polakis and M. X. Sliwkowski, *Clin. Cancer Res.*, 2010, **16**, 4769–4778.

202 J. D. Sadowsky, T. H. Pillow, J. Chen, F. Fan, C. He, Y. Wang, G. Yan, H. Yao, Z. Xu, S. Martin, D. Zhang, P. Chu, J. Dela Cruz-Chuh, A. O'Donohue, G. Li, G. Del Rosario, J. He, L. Liu, C. Ng, D. Su, G. D. Lewis Phillips, K. R. Kozak, S. F. Yu, K. Xu, D. Leipold and J. Wai, *Bioconjug. Chem.*, 2017, **28**, 2086–2098.

203 J. P. M. Nunes, V. Vassileva, E. Robinson, M. Morais, M. E. B. Smith, R. B. Pedley, S. Caddick, J. R. Baker and V. Chudasama, *RSC Adv.*, 2017, **7**, 24828–24832.

204 C. Zhou, S. Lehar, J. Gutierrez, C. M. Rosenberger, N. Ljumanovic, J. Dinoso, N. Koppada, K. Hong, A. Baruch, M. Carrasco-Triguero, O. Saad, S. Mariathasan and A. V. Kamath, *MAbs*, 2016, **8**, 1612–1619.

205 M. Peck, G. S. M. E. R. R. D. Nicholas Lewin-Koh, A. V. Kamath, D. S. D. M. C.-T. O. S. A. C. Lisa Teufel, M. Leonardelli and J. A. Tavela, *Antimicrob. Agents Chemother.*, 2019, **63**, 1–12.

206 S. Lin, X. Yang, S. Jia, A. M. Weeks, M. Hornsby, P. S. Lee, R. V. Nichiporuk, A. T. Iavarone, J. A. Wells, F. D. Toste and C. J. Chang, *Science*, 2017, **355**, 597–602.

207 J. Y. Axup, K. M. Bajjuri, M. Ritland, B. M. Hutchins, C. H. Kim, S. A. Kazane, R. Halder, J. S. Forsyth, A. F. Santidrian, K. Stafin, Y. Lu, H. Tran, A. J. Seller,

S. L. Biroc, A. Szydlik, J. K. Pinkstaff, F. Tian, S. C. Sinha, B. Felding-Habermann, V. V. Smider and P. G. Schultz, *Proc. Natl. Acad. Sci. U. S. A.*, 2012, **109**, 16101–16106.

208 D. Jackson, J. Atkinson, C. I. Guevara, C. Zhang, V. Kery, S. J. Moon, C. Virata, P. Yang, C. Lowe, J. Pinkstaff, H. Cho, N. Knudsen, A. Manibusan, F. Tian, Y. Sun, Y. Lu, A. Sellers, X. C. Jia, I. Joseph, B. Anand, K. Morrison, D. S. Pereira and D. Stover, *PLoS One*, 2014, **9**, e83865.

209 E. S. Zimmerman, T. H. Heibeck, A. Gill, X. Li, C. J. Murray, M. R. Madlansacay, C. Tran, N. T. Uter, G. Yin, P. J. Rivers, A. Y. Yam, W. D. Wang, A. R. Steiner, S. U. Bajad, K. Penta, W. Yang, T. J. Hallam, C. D. Thanos and A. K. Sato, *Bioconjug. Chem.*, 2014, **25**, 351–361.

210 M. P. Vanbrunt, K. Shanebeck, Z. Caldwell, J. Johnson, P. Thompson, T. Martin, H. Dong, G. Li, H. Xu, F. D'Hooge, L. Masterson, P. Bariola, A. Tiberghien, E. Ezeadi, D. G. Williams, J. A. Hartley, P. W. Howard, K. H. Grabstein, M. A. Bowen and M. Marelli, *Bioconjug. Chem.*, 2015, **26**, 2249–2260.

211 D. L. Hatfield and V. N. Gladyshev, *Mol. Cell. Biol.*, 2002, **22**, 3565–3576.

212 T. Hofer, J. D. Thomas, T. R. Burke and C. Rader, *Proc. Natl. Acad. Sci.*, 2008, **105**, 12451–12456.

213 X. Li, C. G. Nelson, R. R. Nair, L. Hazlehurst, T. Moroni, P. Martinez-Acedo, A. R. Nanna, D. Hymel, T. R. Burke and C. Rader, *Cell Chem. Biol.*, 2017, **24**, 433-442.e6.

214 P. Agarwal, J. Van Der Weijden, E. M. Sletten, D. Rabuka and C. R. Bertozzi, *Proc. Natl. Acad. Sci. U. S. A.*, 2013, **110**, 46–51.

215 J. Liu, R. M. Barfield and D. Rabuka, in *Bioconjugation: Methods and Protocols*, eds. S. Massa and N. Devoogdt, Springer New York, New York, NY, 2019, pp. 131–147.

216 P. M. Drake, A. Carlson, J. M. McFarland, S. Bañas, R. M. Barfield, W. Zmolek, Y. C. Kim, B. C. B. Huang, R. Kudirka and D. Rabuka, *Mol. Cancer Ther.*, 2018, **17**, 161–168.

217 T. R. and D. I. Corp., Study of TRPH-222 in Patients With Relapsed and/or Refractory B-Cell Lymphoma.

218 H. Schneider, L. Deweid, O. Avrutina and H. Kolmar, *Anal. Biochem.*, 2020, 595, 113615.

219 S. Beck, J. Schultze, H.-J. Räder, R. Holm, M. Schinnerer, M. Barz, K. Koynov and R. Zentel, *Polymers (Basel).*, 2018, **10**, 141.

220 J. J. Bruins, J. A. M. Damen, M. A. Wijdeven, L. P. W. M. Lelieveldt, F. L. Van Delft and B. Albada, *Bioconjug. Chem.*, 2021, **32**, 2167–2172.

221 P. Dawson, T. Muir, I. Clark-Lewis and S. Kent, *Science*, 1994, **266**, 776–779.

222 S. B. H. Kent, *Chem. Soc. Rev.*, 2009, **38**, 338–351.

223 S. Kent, *Bioorg. Med. Chem.*, 2017, **25**, 4926–4937.

224 S. S. Kulkarni, J. Sayers, B. Premdjee and R. J. Payne, *Nat. Rev. Chem.*, 2018, **2**, 0122.

225 E. C. B. Johnson and S. B. H. Kent, *J. Am. Chem. Soc.*, 2006, **128**, 6640–6646.

226 C. Haase and O. Seitz, *European J. Org. Chem.*, 2009, 2096–2101.

227 A. Brik, S. Ficht, Y. Y. Yang, C. S. Bennett and C. H. Wong, *J. Am. Chem. Soc.*, 2006, **128**, 15026–15033.

228 K. Ha, M. Chahar, J. C. M. Monbaliu, E. Todadze, F. K. Hansen, A. A. Oliferenko, C. E. Ocampo, D. Leino, A. Lillicotch, C. V. Stevens and A. R. Katritzky, *J. Org. Chem.*, 2012, **77**, 2637–2648.

229 A. R. Katritzky, N. E. Abo-Dya, S. R. Tala and Z. K. Abdel-Samii, *Org. Biomol. Chem.*, 2010, **8**, 2316–2319.

230 T. M. Hackeng, J. H. Griffin and P. E. Dawson, *Proc. Natl. Acad. Sci. U. S. A.*, 1999, **96**, 10068–10073.

231 N. Forte, I. Benni, K. Karu, V. Chudasama and J. R. Baker, *Chem. Sci.*, 2019, **10**, 10919–10924.

232 B. L. Oliveira, Z. Guo and G. J. L. Bernardes, *Chem. Soc. Rev.*, 2017, **46**, 4895–4950.

233 K. Peewasan and H.-A. Wagenknecht, *ChemBioChem*, 2017, **18**, 1473–1476.

234 Y. Zheng, X. Ji, B. Yu, K. Ji, D. Gallo, E. Csizmadia, M. Zhu, M. R. Choudhury, L. K. C. De La Cruz, V. Chittavong, Z. Pan, Z. Yuan, L. E. Otterbein and B. Wang, *Nat. Chem.*, 2018, **10**, 787–794.

235 J. Yang, M. R. Karver, W. Li, S. Sahu and N. K. Devaraj, *Angew. Chemie - Int. Ed.*, 2012, **51**, 5222–5225.

236 S. Ogawa, K. Fujii, K. Kaneyama and K. Arai, *Sen'i Gakkaishi*, 2008, **64**, 137–144.

237 B. J. Umlauf, K. A. Mix, V. A. Grosskopf, R. T. Raines and E. V. Shusta,

*Bioconjug. Chem.*, 2018, **29**, 1605–1613.

238 D. Svatunek, M. Wilkovitsch, L. Hartmann, K. N. Houk and H. Mikula, *J. Am. Chem. Soc.*, 2022, **144**, 8171–8177.

239 C. B. Rosen and M. B. Francis, *Nat. Chem. Biol.*, 2017, **13**, 697–705.

240 L. Wang, N. Wang, W. Zhang, X. Cheng, Z. Yan, G. Shao, X. Wang, R. Wang and C. Fu, *Signal Transduct. Target. Ther.*, 2022, **7**, 48

241 T. Habets, F. Siragusa, A. J. Müller, Q. Grossman, D. Ruffoni, B. Grignard and C. Detrembleur, *Polym. Chem.*, 2022, **13**, 3076–3090.

242 M. Le Neindre, B. Magny and R. Nicolaÿ, *Polym. Chem.*, 2013, **4**, 5577–5584.

243 E. Dyer and H. S. Bender, *J. Med. Chem.*, 1964, **7**, 10–14.

244 D. Stueber, D. Patterson, C. L. Mayne, A. M. Orendt, D. M. Grant and R. W. Parry, *Inorg. Chem.*, 2001, **40**, 1902–1911.

245 R. V. Kolakowski, K. T. Haelsig, K. K. Emmerton, C. I. Leiske, J. B. Miyamoto, J. H. Cochran, R. P. Lyon, P. D. Senter and S. C. Jeffrey, *Angew. Chemie - Int. Ed.*, 2016, **55**, 7948–7951.

246 B. Movassagh and M. Soleiman-Beigi, *Synth. Commun.*, 2010, **40**, 3467–3471.

247 T. A. Shaw, M. H. Powdrill, A. R. Sherratt, K. Garland, B.-J. Li, A. M. Beauchemin and J. P. Pezacki, *RSC Med. Chem.*, 2021, **12**, 797–803.

248 A. B. Cognetta, M. J. Niphakis, H. C. Lee, M. L. Martini, J. J. Hulce and B. F. Cravatt, *Chem. Biol.*, 2015, **22**, 928–937.

249 Y. S. Chen, I. Schuphan and J. E. Casida, *J. Agric. Food Chem.*, 1979, **27**, 709–712.

250 A. Goel, S. J. Mazur, R. J. Fattah, T. L. Hartman, J. A. Turpin, M. Huang, W. G. Rice, E. Appella and J. K. Inman, *Bioorg. Med. Chem. Lett.*, 2002, **12**, 767–770.

251 A. Muñoz, E. Borrás, M. Ródenas, T. Vera and H. A. Pedersen, *Environ. Sci. Technol.*, 2018, **52**, 9136–9144.

252 J. M. Hettick, T. B. Ruwona and P. D. Siegel, *J. Am. Soc. Mass Spectrom.*, 2009, **20**, 1567–1575.

253 M. S. Rolph, A. L. J. Markowska, C. N. Warriner and R. K. O'Reilly, *Polym. Chem.*, 2016, **7**, 7351–7364.

254 P. Bao, L. Wang, H. Yue, Y. Shao, J. Wen, D. Yang, X. Zhao, H. Wang and W. Wei, *J. Org. Chem.*, 2019, **84**, 2976–2983.

255 B. K. Malviya, V. P. Verma and S. Sharma, *Org. Biomol. Chem.*, 2021, **19**, 9491–9500.

256 C. M. Levinn, J. L. Mancuso, R. E. Lutz, H. M. Smith, C. H. Hendon and M. D. Pluth, *J. Org. Chem.*, 2021, **86**, 5443–5451.

257 J. Vlasak and R. Ionescu, *MAbs*, 2011, **3**, 253–263.

258 T. Hansen, P. Vermeeren, F. M. Bickelhaupt and T. A. Hamlin, *Angew. Chemie - Int. Ed.*, 2021, **60**, 20840–20848.

259 P. R. Campodónico, R. A. Tapia and C. Suárez-Rozas, *Front. Chem.*, 2022, **9**, 1–9.

260 M. Anbazhagan, T. Indrasena Reddy and S. Rajappa, *J. Chem. Soc. Perkin Trans. 1*, 1997, 1623–1628.

261 N. A. McGrath and R. T. Raines, *Acc. Chem. Res.*, 2011, **44**, 752–761.

262 R. Lee Webb, D. S. Eggleston, C. S. Labaw, J. J. Lewis and K. Wert, *J. Heterocycl. Chem.*, 1987, **24**, 275–278.

263 M. M. Cerda, T. D. Newton, Y. Zhao, B. K. Collins, C. H. Hendon and M. D. Pluth, *Chem. Sci.*, 2019, **10**, 1773–1779.

264 P. Beslin and Y. Vallee, *Tetrahedron*, 1985, **41**, 2691–2705.

265 J. P. M. António, H. Faustino and P. M. P. Gois, *Org. Biomol. Chem.*, 2021, **19**, 6221–6226.

266 X. Zhu, Y. Shi, H. Mao, Y. Cheng and C. Zhu, *Adv. Synth. Catal.*, 2013, **355**, 3558–3562.

267 S. B. Bandgar, B. P. Bandgar, B. L. Korbad and S. S. Sawant, *Tetrahedron Lett.*, 2007, **48**, 1287–1290.

268 Y.-T. Huang, S.-Y. Lu, C.-L. Yi and C.-F. Lee, *J. Org. Chem.*, 2014, **79**, 4561–4568.

269 A. Maruani, M. T. W. Lee, G. Watkins, A. R. Akhbar, H. Baggs, A. Shamsabadi, D. A. Richards and V. Chudasama, *RSC Adv.*, 2016, **6**, 3372–3376.

270 A. J. van der Zouwen, A. Jeucken, R. Steneker, K. F. Hohmann, J. Lohse, D. J. Slotboom and M. D. Witte, *Chem. - A Eur. J.*, 2021, **27**, 3292–3296.

271 J. Lohse, L. J. Y. M. Swier, R. C. Oudshoorn, G. Médard, B. Kuster, D. J. Slotboom and M. D. Witte, *Bioconjug. Chem.*, 2017, **28**, 913–917.

272 I. Pendrak, S. Barney, R. Wittrock, D. M. Lambert and W. D. Kingsbury, *J. Org. Chem.*, 1994, **59**, 2623–2625.

273 A. M. Palmer, B. Grobbel, C. Brehm, P. J. Zimmermann, W. Buhr, M. P. Feth, H. C. Holst and W. A. Simon, *Bioorganic Med. Chem.*, 2007, **15**, 7647–7660.

274 W. W. Paudler and J. M. Barton, *J. Org. Chem.*, 1966, **31**, 1720–1722.

275 S. A. Lang, B. D. Johnson and E. Cohen, *J. Heterocycl. Chem.*, 1975, **12**, 1143–1153.

276 R. Ramesh, S. Rajasekaran, R. Gupta and S. Chandrasekaran, *Org. Lett.*, 2006, **8**, 1933–1936.

277 H. K. Oh, *Bull. Korean Chem. Soc.*, 2012, **33**, 2427–2430.

278 C. Che, S. Li, Z. Yu, F. Li, S. Xin, L. Zhou, S. Lin and Z. Yang, *ACS Comb. Sci.*, 2013, **15**, 202–207.

279 B. Ravindra, B. G. Das and P. Ghorai, *Org. Lett.*, 2014, **16**, 5580–5583.

280 F. Bryden, A. Maruani, H. Savoie, V. Chudasama, M. E. B. Smith, S. Caddick and R. W. Boyle, *Bioconjug. Chem.*, 2014, **25**, 611–617.

281 M. T. W. Lee, A. Maruani, J. R. Baker, S. Caddick and V. Chudasama, *Chem. Sci.*, 2016, **7**, 799–802.

# 8. Appendix

## LCMS of tetrazine thioester aqueous stability

Expected mass of tetrazine-MPAA thioester 7c = 352 Da

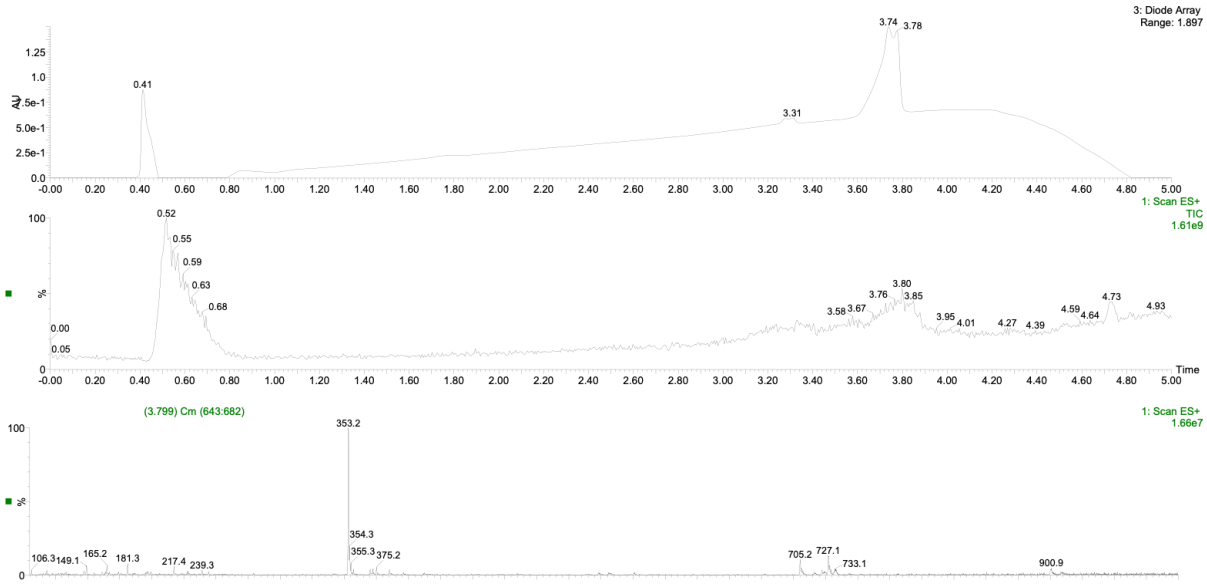


**FIGURE S.90.** Diode array and ES+ scans of tetrazine thioester **7c** in MeCN. ES+ scan of peak at 3.80 min is shown.

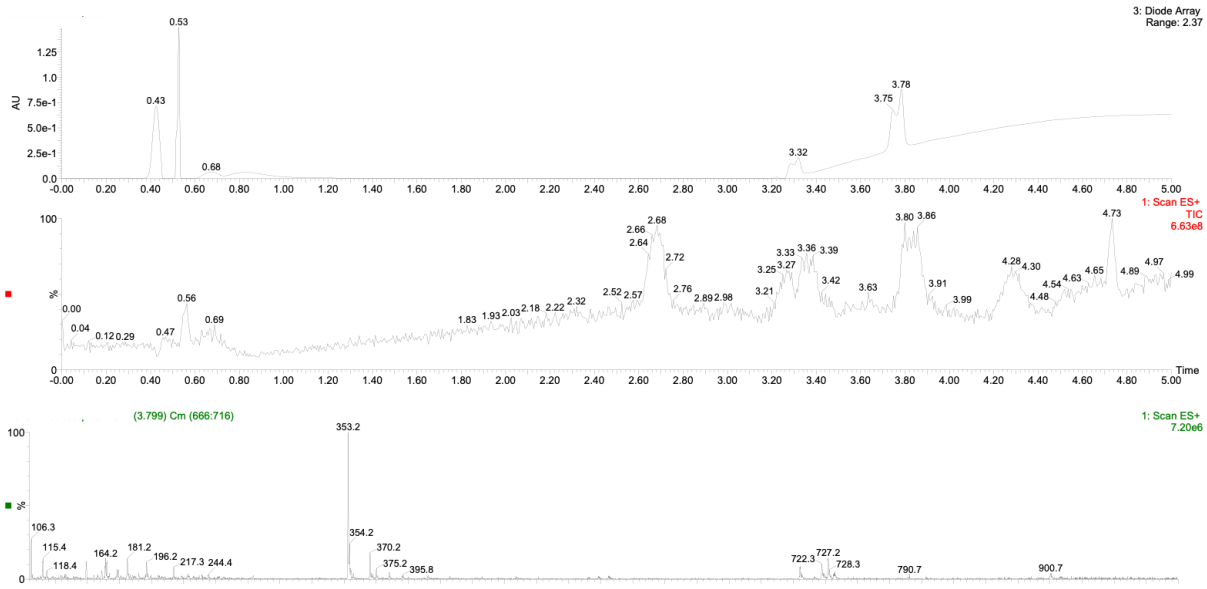


**FIGURE S.91.** Diode array and ES+ scans of tetrazine thioester **7c** in pH 5.0. ES+ scan of peak at 3.80 min is shown.

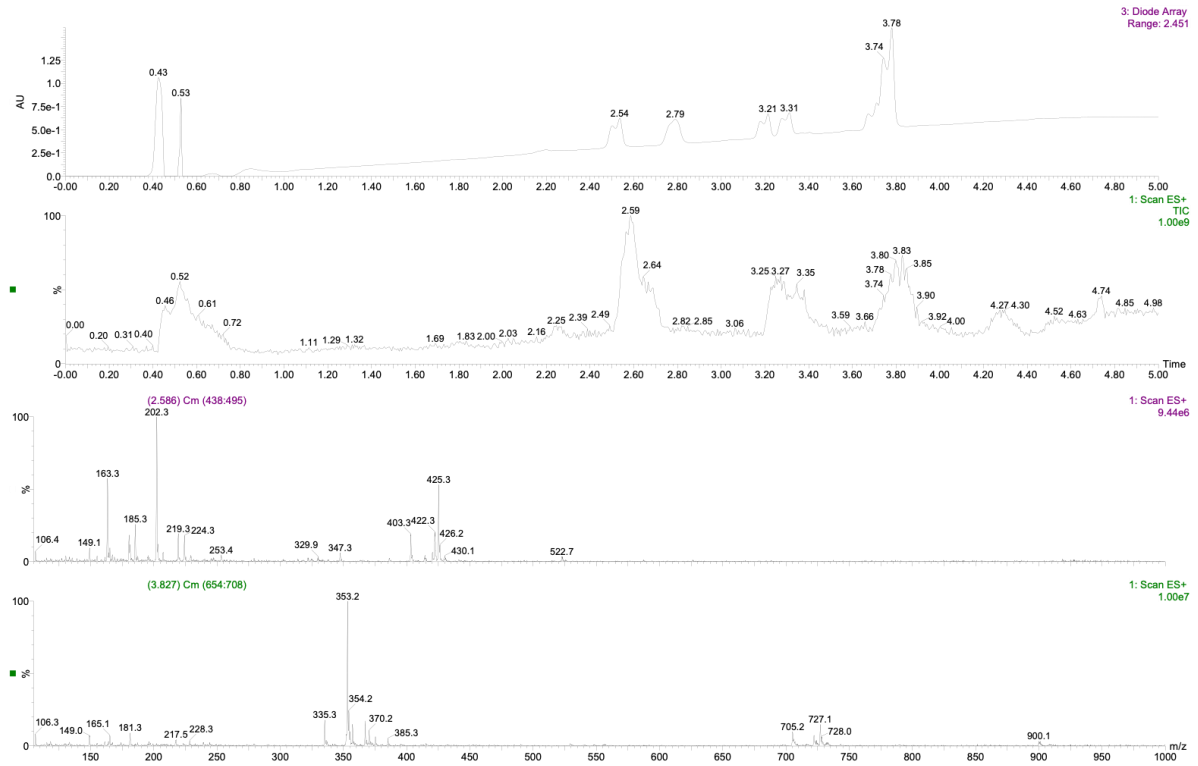


**FIGURE S.92.** Diode array and ES+ scans of tetrazine thioester **7c** in pH 6.0. ES+ scan of peak at 2.58 min (top) and 3.83 min (bottom) are shown.

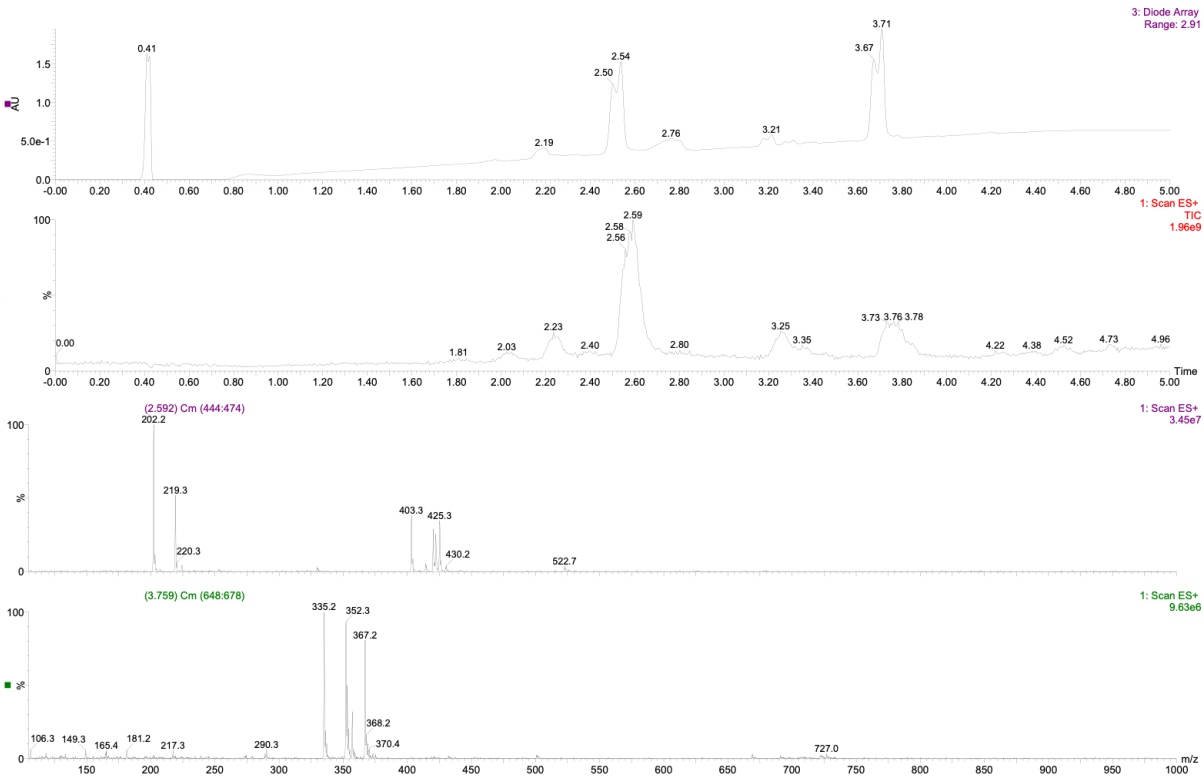


**FIGURE S.93.** Diode array and ES+ scans of tetrazine thioester **7c** in pH 7.0 buffer. ES+ scan of peaks at 2.59 min and 3.76 min is shown.

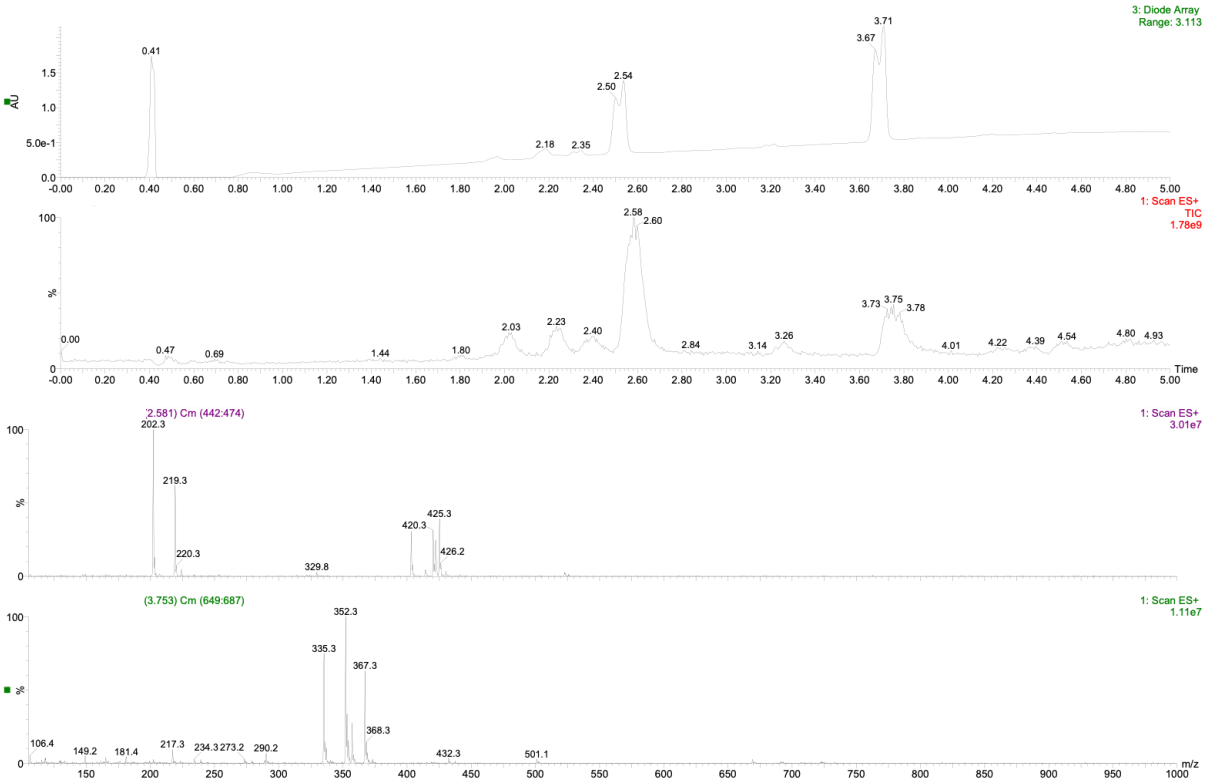


**FIGURE S.94.** Diode array and ES+ scans of tetrazine thioester **7c** in pH 7.0 buffer. ES+ scan of peaks at 2.59 min and 3.76 min is shown.

## LCMS of tetrazine thioester *N*-terminal cysteine modification

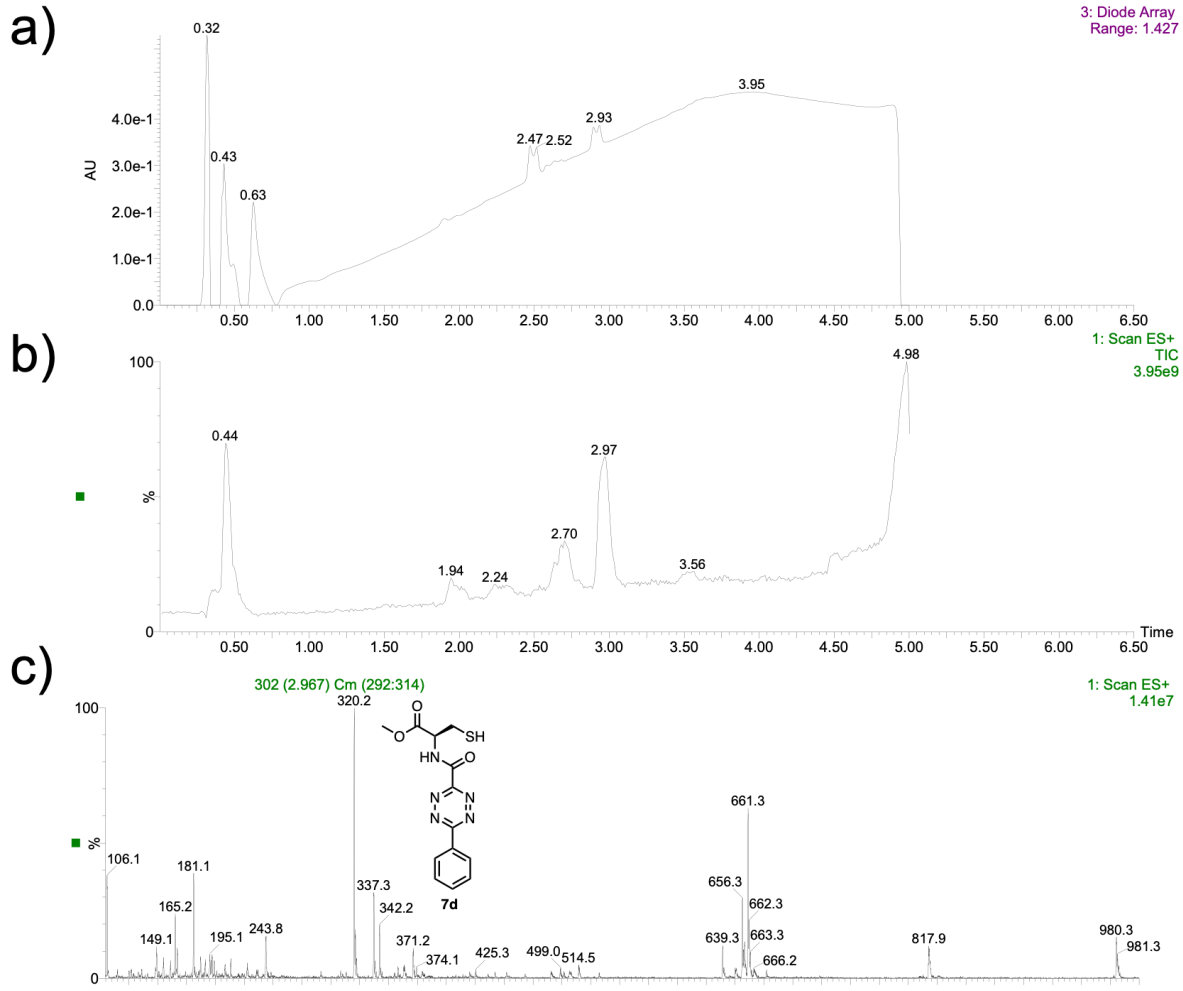


**FIGURE S.95.** Diode array and ES+ scans of *N*-terminal cysteine modification with tetrazine-MPAA thioester **7c**. Tetrazine-MPAA thioester **7c** + *O*-Me-cysteine for synthesis of **7d** is shown. **A)** Diode array. **B)** ES+ scan. **C**) m/z ions of peak at 2.97 min, **7d**. Expected mass of **7d** = 319 Da.

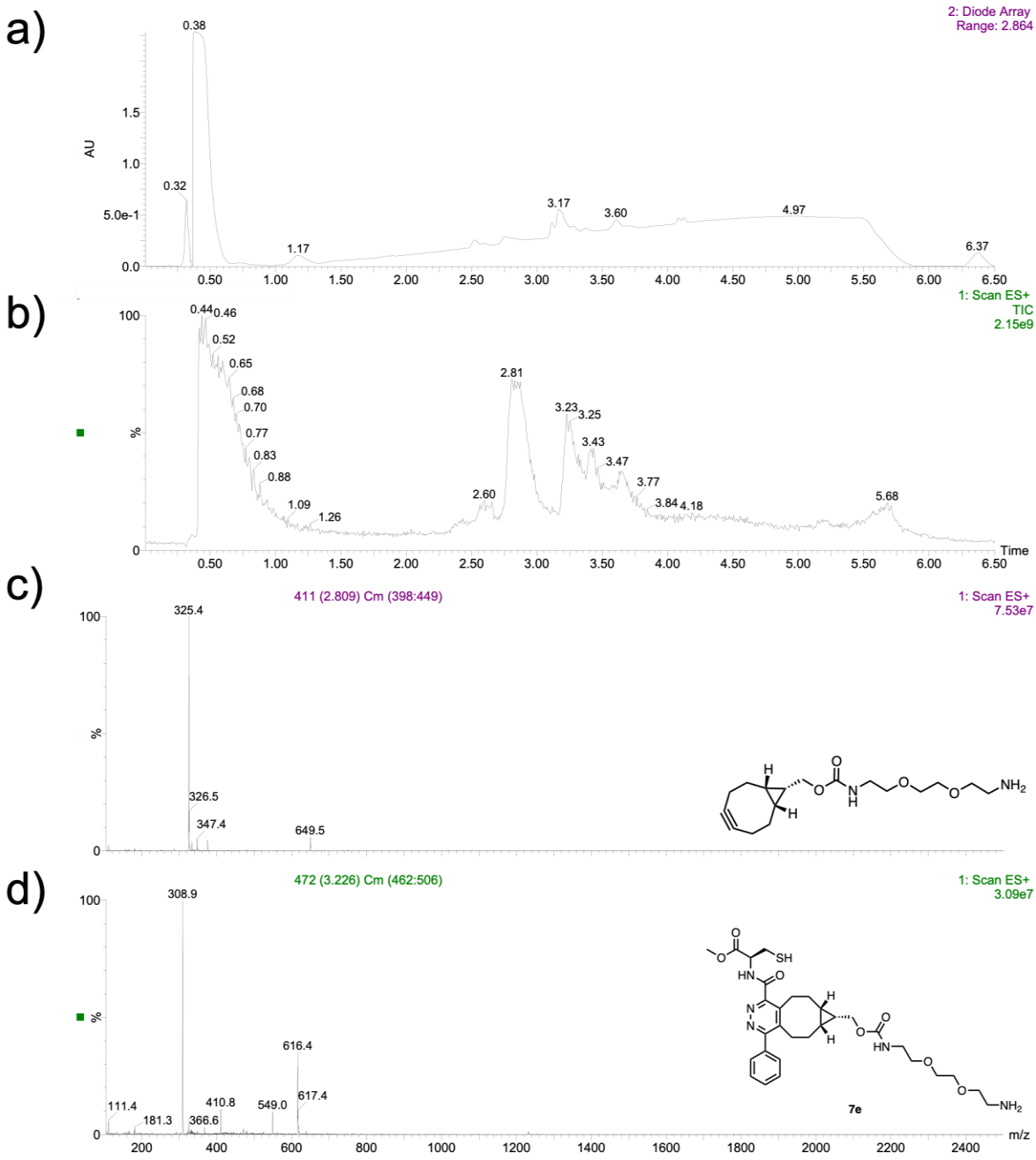


**FIGURE S.96.** Diode array and ES+ scans of *N*-terminal cysteine modification with tetrazine-MPAA thioester **7c**. Tetrazine-MPAA thioester **7c** + *O*-Me-cysteine + BCN-amine for synthesis of **7e** is shown. **A)** Diode array. **B)** ES+ scan. **C)** m/z ions of peak at 2.81 min. **D)** m/z ions of peak at 3.23 min, **7e**. Expected mass of **7e** = 618 Da.

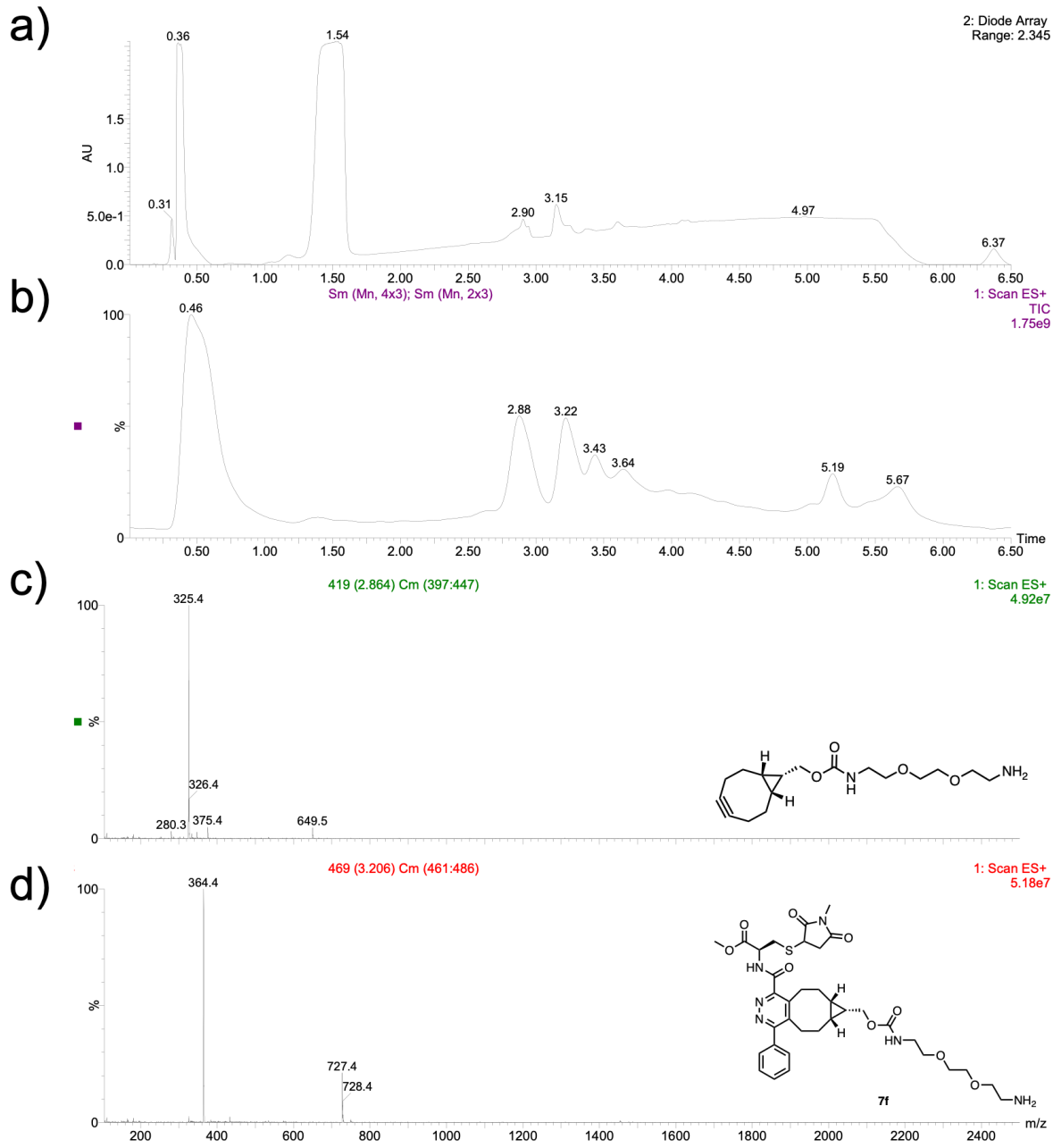


**FIGURE S.97.** Diode array and ES+ scans of *N*-terminal cysteine modification with tetrazine-MPAA thioester **7c**. Tetrazine-MPAA thioester **7c** + *O*-Me-cysteine + BCN-amine for synthesis of **7f** is shown. **A)** Diode array. **B)** ES+ scan. **C)** m/z ions of peak at 2.88 min. **D)** m/z ions of peak at 3.22 min, **7f**. Expected mass of **7f** = 728 Da.